

---

# METAL COMPLEXES WITH SULFUR LIGANDS AS CYTOTOXIC AGENTS

---

## Dissertation

Zur Erlangung des akademischen Grades doctor rerum naturalium  
(Dr. rer. nat.)



---

seit 1558

Vorgelegt dem Rat der Chemisch-Geowissenschaftlichen Fakultät  
der Friedrich-Schiller Universität Jena

**von Diplom-Chemikerin Carolin Mügge**

geboren am 10.12.1985 in Leipzig

Gutachter:

1. Prof. Dr. Wolfgang Weigand, Friedrich-Schiller Universität Jena
2. Prof. Dr. Luigi Messori, Università degli Studi di Firenze
3. Prof. Dr. Bernhard Keppler, Universität Wien

Tag der Verteidigung: 04. Dezember 2015







This monograph contains parts of the following publications and manuscripts:

1. *Novel Platinum(II) Compounds with O,S Bidentate Ligands: Synthesis, Characterisation, Antiproliferative Properties and Biomolecular Interactions*  
  
C. Mügge, R. Liu, H. Görls, C. Gabbiani, E. Michelucci, N. Rüdiger, J. H. Clement, L. Messori, W. Weigand  
  
*Dalton Transactions* **2014**, 43, 3072–3086.
2. *Platinum(II) Complexes with O,S Bidentate Ligands: Biophysical Characterization, Antiproliferative Activity and Crystallographic Evidence of Protein Binding*  
  
C. Mügge, T. Marzo, L. Massai, J. Hildebrandt, N. Metzler-Nolte, L. Messori, W. Weigand  
  
*Inorganic Chemistry* **2015**, accepted.
3. *Elucidating the Reactivity of Pt(II) Complexes with (O,S) Bidentate Ligands Towards DNA Using Various Model Systems and Analytical Techniques*  
  
C. Mügge, D. Musumeci, E. Michelucci, F. Porru, T. Marzo, L. Massai, L. Messori, W. Weigand, D. Montesarchio  
  
*Manuscript in preparation.*



Further publications have appeared in peer-reviewed journals and were prepared during the time of PhD research.

4. *Structure, Solution Chemistry, Antiproliferative Actions and Protein Binding Properties of Non-Conventional Platinum(II) Compounds with Sulfur and Phosphorus Donors*

C. Mügge, C. Rothenburger, A. Beyer, H. Görls, C. Gabbiani, A. Casini,  
E. Michelucci, I. Landini, S. Nobili, E. Mini, L. Messori, W. Weigand,

*Dalton Transactions* **2011**, 40, 2006-2016.

5. *Reactions of Metallodrugs with Proteins: Selective Binding of Phosphane-Based Platinum(II) Dichlorides to Horse Heart Cytochrome c Probed by ESI MS coupled to Enzymatic Cleavage*

C. Mügge, E. Michelucci, F. Boscaro, C. Gabbiani, L. Messori, W. Weigand

*Metallomics* **2011**, 3, 987-990.

6. *Stabilizing Effects of Combined Trifluoromethyl Groups and Semifluorinated Side Chains on the Thermotropic Liquid Crystal Behavior of  $\beta$ -Enaminoketone Ligands and their Bischelate Pd<sup>II</sup>Complexes*

A. Martin, C. Mügge, D. L. Gin, B. Donnio, W. Weigand

*European Journal of Inorganic Chemistry* **2014**, 32, 5609-5617.



# CONTENTS

<b>1</b>	<b>Introduction</b> .....	<b>1</b>
1.1	Cisplatin and analogs: Current clinical status and research focus .....	3
1.2	Chemistry, biological mode of action of Cisplatin and analogs .....	5
1.2.1	Accumulation .....	5
1.2.2	Activation and biomolecule binding .....	6
1.2.3	Cellular Processing .....	9
<b>2</b>	<b>Motivation, Aim of this Work</b> .....	<b>11</b>
<b>PART A</b>	<b>(O,S) CHELATE COMPOUNDS: SYNTHESIS, STRUCTURAL CHARACTERIZATION AND BIOLOGICAL EVALUATION</b> .....	<b>15</b>
<b>3</b>	<b>Compounds Based on <math>\beta</math>-Hydroxydithiocinnamic Ester Derivatives</b> .....	<b>17</b>
3.1	$\beta$ -Hydroxydithiocinnamic esters .....	17
3.1.1	Known synthetic approaches.....	17
3.1.2	Synthesis and characterization of $\beta$ -hydroxydithiocinnamic ester derivatives 7-28.....	18
3.2	Platinum(II) complexes.....	21
3.2.1	Reported metal complexes with ligands based on derivatives of $\beta$ -hydroxydithiocinnamic esters .....	21
3.2.2	Syntheses of the (O,S) bidentate Pt(II) complexes .....	22
3.2.3	Influence of the base .....	24
3.2.4	Bischelates .....	24
3.2.5	Characterization of the complexes .....	25
<b>4</b>	<b>Solution Chemistry of the (O,S) Chelate Compounds</b> .....	<b>27</b>
4.1	Solubility in aqueous medium – determination of $\text{Log}P_{o/w}$ values .....	27
4.2	Behavior in solution – UV-visible spectroscopic experiments .....	31

<b>5</b>	<b>Biological Assays</b> .....	<b>35</b>
5.1	Results of antiproliferative assays.....	35
5.2	Use of DMSO as solvent .....	38
5.3	Influence of incubation time on antiproliferative activity .....	38
5.4	Fluorescence microscopy .....	41
5.5	Comparison of assay methods .....	42
5.6	Possible sources of error .....	45
<b>PART B</b>	<b>INTERACTION WITH BIOMOLECULES</b> .....	<b>49</b>
<b>6</b>	<b>Studying Biomolecule Interactions with ESI Mass Spectrometry</b> .....	<b>51</b>
6.1	Electrospray ionization mass spectrometry .....	52
6.1.1	ESI technique.....	52
6.1.2	The LTQ-Orbitrap device .....	54
<b>7</b>	<b>Studying Metal-Protein Interactions</b> .....	<b>57</b>
7.1	The model proteins .....	57
7.1.1	Cytochrome c .....	57
7.1.2	Lysozyme .....	59
7.1.3	Ribonuclease A .....	60
7.2	Execution, technical considerations.....	61
7.3	Interaction of selected (O,S)Pt complexes with cytochrome c .....	62
7.5	Interaction of selected (O,S)Pt complexes with lysozyme .....	65
7.6	Interaction of selected (O,S)Pt complexes with ribonuclease A .....	67
7.7	UV-visible spectroscopic data .....	68
7.8	Interaction of selected (O,S)Pt complexes with albumin .....	69
<b>8</b>	<b>Studying Metal-DNA Interactions</b> .....	<b>71</b>
8.1	Studies on metal-oligonucleotide adducts: recent developments and practical considerations .....	72
8.2	Interaction of compounds 30, 46 and 48 with 9-methylguanine.....	72
8.2.1	ESI mass spectrometric data .....	73
8.2.2	UV-visible spectroscopic results.....	74
8.3	Selection and preparation of the DNA model systems - Oligonucleotides.....	76
8.4	ESI MS studies of free oligonucleotides .....	77
8.4.1	Optimization of measurement conditions .....	78
8.5	ESI MS of ODN-platinum adducts.....	79

8.5.1	General observations.....	80
8.5.2	Comparison of the compounds' reactivity.....	81
8.5.3	Influence of incubation time.....	82
8.6	MS <sup>2</sup> Experiments of ODN1-platinum adducts.....	83
8.6.1	Typical fragmentation pathways – fragmentation of unplatinated ODN1 .....	83
8.6.2	Fragmentation of adduct peaks – general observations .....	84
8.6.3	Fragmentation of the monoadduct between ODN1 and compound 46 .....	86
8.6.4	Fragmentation of the mono- and bisadducts between ODN1 and compound 30 .....	88
<b>9</b>	<b>Discussion to Biomolecule Interaction Data.....</b>	<b>91</b>
9.1	Interactions of platinum(II) complexes with model proteins .....	91
9.2	Interactions of platinum(II) complexes 30, 46 and 48 with 9-methylguanine and single-stranded ODNs .....	92
9.3	General conclusions .....	94
<b>PART C</b>	<b>BIOCONJUGATES .....</b>	<b>95</b>
<b>10</b>	<b>Background .....</b>	<b>97</b>
10.1	Metal-peptide bioconjugates.....	97
10.2	The model peptide .....	101
10.3	Considerations on different conjugation methods.....	102
10.3.1	Copper(I)-catalyzed alkyne-azide cycloaddition (CuAAC).....	102
10.3.2	Amide bond formation.....	103
<b>11</b>	<b>Bioconjugates via Copper(I)-Catalyzed Alkyne-Azide Cycloaddition (CuAAC) .....</b>	<b>105</b>
11.1	Introducing alkyne functionalities into $\beta$ -hydroxydithiocinnamic esters .....	105
11.1.1	Introducing the alkynyl group at the aromatic subsite.....	105
11.1.2	Introducing the alkynyl group at the dithiocarbonyl site .....	108
11.2	Complexation reactions of alkyne-derived $\beta$ -hydroxydithiocinnamic esters .....	111
11.2.1	Complexation reactions of Ph-O-propargyl compound 54.....	111
11.2.2	Complexation reactions of Ph-O-pentynyl compound 55 .....	112
11.2.3	Complexation reactions of S-propargyl compound 57 .....	114
11.2.4	Complexation reactions with the S-butynyl derived compound 59 .....	115
11.3	Introducing an azide group into $\beta$ -hydroxydithiocinnamic esters .....	116
11.3.1	Synthesis of benzylazide-derived compound 71 .....	117
11.3.2	Reactions of compound 71 with K <sub>2</sub> PtCl <sub>4</sub> .....	118

11.3.3	Stability at HPLC conditions.....	119
11.4	Preparation and derivatization of Leu <sup>5</sup> -Enkephalin .....	120
11.5	Formation of bioconjugates <i>via</i> CuAAC.....	123
11.5.1	Bischelates.....	123
11.5.2	Monochelates.....	124
<b>12</b>	<b>Bioconjugates <i>via</i> Amide Bond Formation .....</b>	<b>127</b>
12.1	Ligand and complex synthesis.....	127
12.2	Formation of amide bonds.....	128
12.2.1	HOBt coordination .....	131
12.3	Analysis of the amide-linked bioconjugates.....	133
<b>13</b>	<b>Bioactivity of the Platinum-Peptide Bioconjugates.....</b>	<b>137</b>
13.1	Triazol-linked compounds .....	137
13.2	Amide-linked compounds .....	138
<b>14</b>	<b>Discussion .....</b>	<b>141</b>
<b>EXPERIMENTAL PART.....</b>		<b>143</b>
<b>15</b>	<b>Syntheses: General Remarks .....</b>	<b>145</b>
15.1	Syntheses of compounds based on the $\beta$ -hydroxydithiocinnamic ester structural motif.....	145
15.2	Peptide syntheses.....	145
15.3	Literature-reported syntheses .....	146
15.4	Analytical methods and devices.....	147
15.5	X-ray data collection and structure solution refinement.....	148
15.6	General synthetic procedures .....	150
15.7	HPLC analysis and purification .....	155
<b>16</b>	<b>Compound Syntheses and Analyses.....</b>	<b>157</b>
16.1	$\beta$ -Hydroxydithiocinnamic esters .....	157
16.2	Pt(II) complexes.....	166
16.3	Alkynyl-functionalized compounds .....	179
16.4	Azide-functionalized compounds.....	189
16.5	Peptide derivatizations.....	193
16.6	Bioconjugates <i>via</i> CuAAC.....	198
16.7	Bioconjugates <i>via</i> amide bonds.....	205
16.8	NMR-based test of stability under cleaving conditions (TFA) .....	212



<b>17</b>	<b>Behavior of the Compounds in Solution .....</b>	<b>213</b>
17.1	UV-visible spectroscopy of compound 30.....	213
17.2	Determination of Log $P_{o/w}$ values through the shake-flask method.....	214
17.3	Determination of extinction coefficients.....	215
<b>18</b>	<b>Biological Studies .....</b>	<b>219</b>
18.1	General information.....	219
18.2	Cell culture conditions .....	222
18.3	Data handling.....	225
18.4	Fluorescence microscopy.....	226
<b>19</b>	<b>Biomolecule Interaction Studies .....</b>	<b>227</b>
19.1	Materials .....	227
19.2	Devices .....	227
19.3	Metal complex - protein interaction studies .....	228
19.4	Reactions with 9-methylguanine .....	229
19.5	Incubation with oligonucleotides.....	230
	<b>SUMMARY.....</b>	<b>231</b>
<b>20</b>	<b>Summary .....</b>	<b>231</b>
<b>21</b>	<b>Zusammenfassung.....</b>	<b>239</b>
	<b>REFERENCES.....</b>	<b>247</b>
	<b>SUPPLEMENT .....</b>	<b>269</b>
	<b>Supplement A: Crystallographic Data.....</b>	<b>271</b>
	<b>Supplement B: Protein Interaction - ESI MS Spectral Data .....</b>	<b>283</b>
	Interaction with horse heart cytochrome c .....	283
	Interaction with hen egg white lysozyme .....	286
	Interaction with ribonuclease A.....	288
	<b>Supplement C: DNA Interaction.....</b>	<b>289</b>
	Positive ESI MS and UV-vis experiments with 9-methyl guanine .....	289
	Negative ESI MS experiments of free ODNs.....	290
	Negative ESI MS of ODN adducts .....	292
	MS <sup>2</sup> of free ODN1 .....	298
	MS <sup>2</sup> of ODN1-46 monoadduct.....	299

MS <sup>2</sup> of ODN1-30 monoadduct.....	301
MS <sup>2</sup> of ODN1-30 bisadduct.....	303
<b>Supplement D: Bioconjugates .....</b>	<b>305</b>
<b>Supplement E: Media Composition .....</b>	<b>307</b>
DPBS .....	307
Trypsin-EDTA .....	307
DMEM .....	308
<b>Supplement F: Abbreviations.....</b>	<b>309</b>
<b>Supplement G: Digital Media .....</b>	<b>313</b>
<b>ACKNOWLEDGEMENT .....</b>	<b>315</b>
<b>CURRICULUM VITAE.....</b>	<b>319</b>
<b>LIST OF CONFERENCE PRESENTATIONS .....</b>	<b>323</b>
<b>LIST OF PUBLICATIONS.....</b>	<b>325</b>
<b>DECLARATION OF AUTHORSHIP.....</b>	<b>327</b>

# 1 INTRODUCTION

When Michel Peyrone (Figure 1) reported on the compound named *cis*-diammine dichlorido platinum(II) in 1844,<sup>4</sup> he could have never envisioned what an important substance he had created for the very first time. It was not until the 1960's, through a serendipitous finding of Barnett Rosenberg (Figure 2), that the potential of this complex gradually became apparent.<sup>5-7</sup> Since then, the story of the discovery of the first platinum-based chemotherapeutic has been told numerous times and thousands of researchers worldwide have dedicated their research to elucidating the chemistry, biochemistry and medicinal properties of the compound which is now widely known as Cisplatin. It has reached such popularity in research and clinical application that it has even been termed "penicillin of cancer drugs",<sup>8</sup> being applied in ca. 50% of all cancer medications with activity against a wide variety of cancers.<sup>9,10</sup>

Cisplatin is not only one of the most "simple" square-planar complexes known, bearing just two types of small donor groups – chloride and ammonia, being bound in *cis* position to a Pt(II) center (Chart 1).<sup>i</sup> It moreover

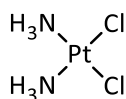


Chart 1 Cisplatin,  
cis-diammine  
dichlorido  
platinum(II).

exhibits a very sophisticated solution chemistry which complexity is greatly enhanced when a biological milieu adds to the conditions it is placed in: platinum-biomolecule interactions in general, platinum-nucleic acid as well as platinum-protein interactions in particular, have received considerable interest over the last 50 years.



Figure 1 Michele Peyrone (1813-1883). Graphic reproduced from ref. 1 as originally taken from ref. 2.



Figure 2 Barnett Rosenberg (1924-2009). Graphic from ref. 3.

<sup>i</sup> The differences in *cis* and *trans* isomers of  $\text{PtCl}_2(\text{NH}_3)_2$ , amongst other metal-ammine complexes, have been investigated by Alfred Werner in great detail. He was awarded the 1913 Nobel Prize in Chemistry "in recognition of his work on the linkage of atoms in molecules by which he has thrown new light on earlier investigations and opened up new fields of research especially in inorganic chemistry".<sup>11</sup>

Bernhard Lippert recently concluded:<sup>12</sup>

*“The impact Cisplatin had on cancer chemotherapy is probably exceeded by the influence its discovery had on fundamental science regarding metal-nucleic acid interactions and on the then (1960s and later) emerging field termed ‘Bioinorganic Chemistry’ in general. There can be no doubt that Rosenberg’s discovery of Cisplatin provided a major boost to this new topic, and it is probably no exaggeration to state that without the interest in understanding Pt-nucleobase chemistry on the molecular level, our present knowledge on metal-DNA and metal-RNA chemistry would be considerably less advanced.”*

With this thesis, an attempt is made to contribute to the wide field of research on platinum(II) based chemotherapeutics by designing new drug candidates with a common ligand structural motif. In particular, the antiproliferative properties of the likely drug candidates will be determined and their interactions with proteins and nucleobases will be tested.

## 1.1 Cisplatin and analogs: Current clinical status and research focus

To date, the panel of platinum-based drugs is comprised of three compounds being approved worldwide for clinical application (Cisplatin/Platinol™, Carboplatin/Paraplatin™ and Oxaliplatin/Eloxatin™, Chart 2 top panel),<sup>13–15</sup> accompanied by some compounds being mainly approved in Asia. These are (Chart 2, middle panel):<sup>16</sup> Nedaplatin (Aqupra™), approved in Japan for the treatment of several tumors<sup>ii</sup> (NSCLC, SCLC, oesophageal cancer and head and neck cancers)<sup>13</sup> and is currently undergoing further clinical trials in China and Japan,<sup>17,18</sup> Lobaplatin, approved in China for different cancers (*e.g.* the treatment of SCLC, chronic myelogenous leukaemia, and inoperable metastatic breast cancer),<sup>13,19</sup> and Heptaplatin, approved for the treatment of gastric cancers in South Korea, and recently reported to undergo further clinical trials for head and neck cancers.<sup>20,21</sup>

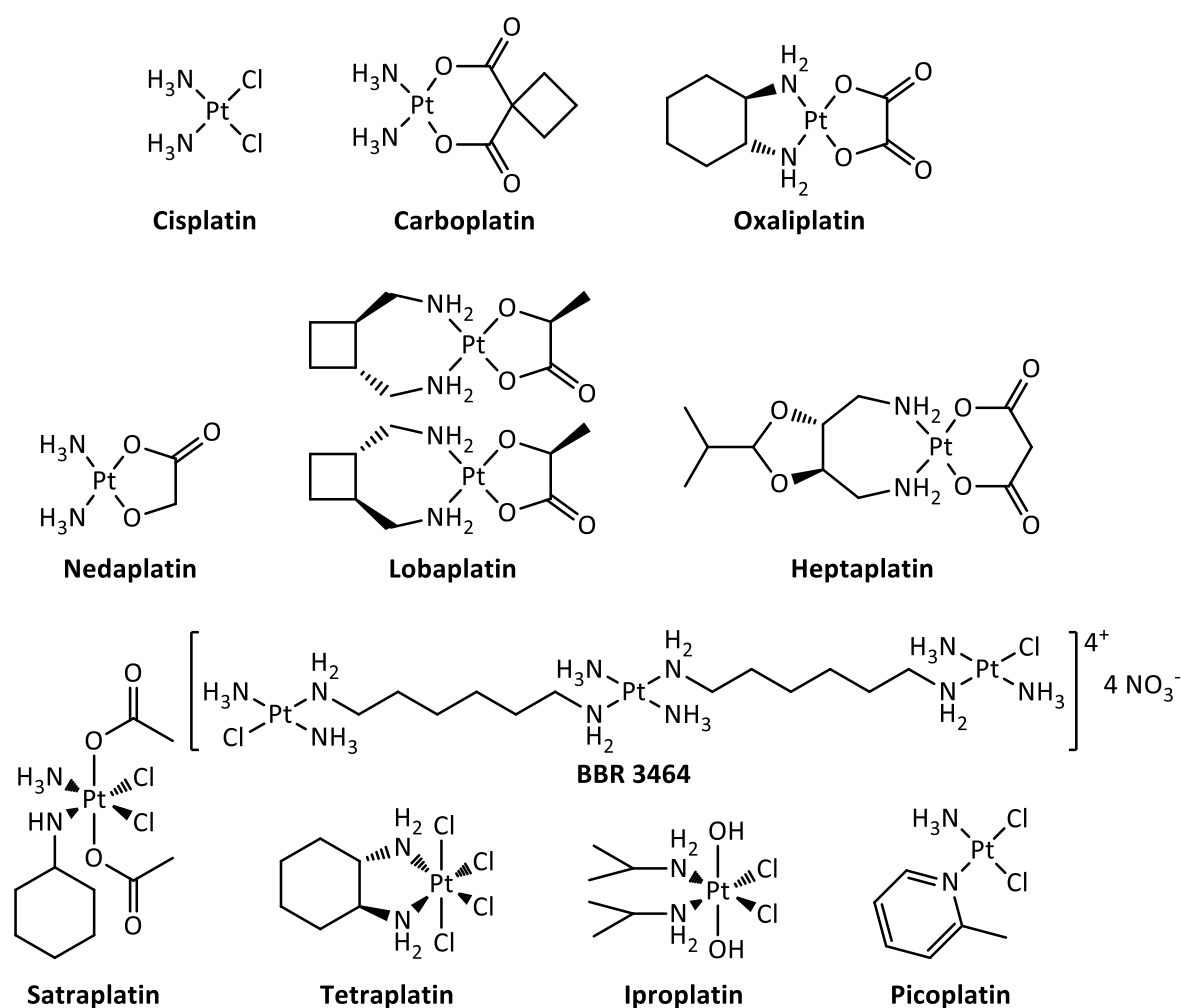


Chart 2 Platinum drugs that are approved worldwide (top panel), locally (middle panel) and such that have recently been evaluated in advanced clinical trials (bottom panel).

<sup>ii</sup> Abbreviations used in this paragraph: NSCLC – non-small cell lung cancer; SCLC – small cell lung cancer.

Satraplatin, the first Pt(IV) complex to enter clinical trials, reached phase III clinical studies.<sup>22</sup> It was, however, not approved<sup>23</sup> because its performance was not superior enough compared to the established drugs and has not yet re-entered clinical trials.<sup>24</sup> Other Pt(IV) compounds that entered clinical evaluation are Tetraplatin (Ormaplatin) and Iproplatin, none of which has reached approval to date.<sup>25</sup> Furthermore, Picoplatin, another Pt(II) drug candidate, has been investigated in phase III clinical trials but failed.<sup>26</sup> Surprisingly, its approval status is currently unknown.<sup>27</sup> Additionally, the multinuclear *trans*-Pt(II) complex BBR 3464 has been investigated in clinical phase II trials, but is not approved.<sup>28,29</sup> All described compounds are comprehensively shown in Chart 2 (bottom panel). Some other Pt(II) compounds have entered clinical phase I studies but never reached advanced stages.<sup>30</sup>

Two more compounds should be mentioned for attempts to bring platinum-based compounds into the clinic: Lipoplatin<sup>TM</sup> and ProLindac<sup>TM</sup>. Both are polymeric formulations of either Cisplatin (Lipoplatin; a liposomal formulation)<sup>31,32</sup> or Carboplatin (ProLindac, incorporated into a polymer based on hydroxypropylmethacrylamide)<sup>33,34</sup> and show promising properties in clinical development.

It is surprising that although numerous platinum-derived potential anticancer therapeutics were reported in literature,<sup>25,35-47</sup> the approval rate of platinum-based chemotherapeutics has somewhat experienced a “stand-still” in recent years. Unfortunately, the transfer of research drugs into clinical trials and eventually to approval is very difficult: the preclinical and clinical testing is exceptionally expensive, and the requirements a drug candidate has to meet have grown more and more over the last years, making it very hard for new compounds to fulfill all criteria.<sup>12,48</sup> It is particularly important to reduce toxic side-effects that come along with most platinum chemotherapeutics, the most severe ones being of nephro- and neurotoxic nature. Furthermore, the selectivity of novel compounds for cancer tissue over normal, “healthy”, tissue marks an important parameter in drug evaluation.<sup>49</sup>

These demanding criteria make research on Pt(II) compounds even more motivating:<sup>50</sup> On the one hand, a thorough understanding of the biological mode of action of metal-based chemotherapeutics is necessary to enable rational drug design. On the other hand, novel, unconventional approaches towards the classical motif of Pt(II) being bound to two am(m)ines (A) and suitable leaving groups (X) are necessary to circumvent some of the problems associated with platinum treatment, such as severe side effects or the occurrence of acquired or intrinsic resistance towards the drugs.<sup>50-52</sup>

Up-to-date developments of metal-based chemotherapeutics include

1. the exploration of alternative amine ligands or leaving groups,
2. changing the geometry from a *cis*-[Pt<sup>II</sup>(A)<sub>2</sub>(X)<sub>2</sub>] to a *trans*-isomer,
3. oxidizing Pt(II) to Pt(IV) to make use of the “activation by reduction” principle,
4. attaching targeting units,
5. or exchanging the metal by others, such as ruthenium, gallium, titanium or gold

and were reviewed in numerous peer-reviewed journals within the last 10 years.<sup>25,35–47,53–58</sup>

## 1.2 Chemistry, biological mode of action of Cisplatin and analogs

In general, the mode of action of Cisplatin can be subdivided into three steps: accumulation, activation and cellular processing,<sup>30</sup> with multi-faceted reaction cascades occurring during each of the three steps.

### 1.2.1 Accumulation

Cisplatin is administered through intravenous injection from saline or dextrose solutions,<sup>59</sup> so that it immediately enters the bloodstream.<sup>60</sup> From there, it rapidly diffuses into tissues and can enter cells (Figure 3).

It is still not entirely clarified whether Cisplatin enters cells through active transport mechanisms or by passive diffusion; most probably both processes contribute to its uptake into the (cancer) cell.<sup>61,62</sup> For active transport, the copper transporter protein Ctr1 has been identified as one of the most probable candidates that is able to enhance Cisplatin uptake into cells.<sup>63–66</sup> Other proteins, such as organic cation transporters, OCTs, or proteins involved in copper homeostasis have been identified to play a significant role in platinum-drug uptake.<sup>67,68</sup>

Contrary, recent studies on Cisplatin-serum protein interactions suggested that passive transport, meaning diffusion through the phospholipid bilayer, mainly contributes to the drugs' uptake into cytoplasm. Furthermore it was proposed that binding to serum proteins results in a drug reservoir for gradual release of the drug inside the cells.<sup>69</sup>

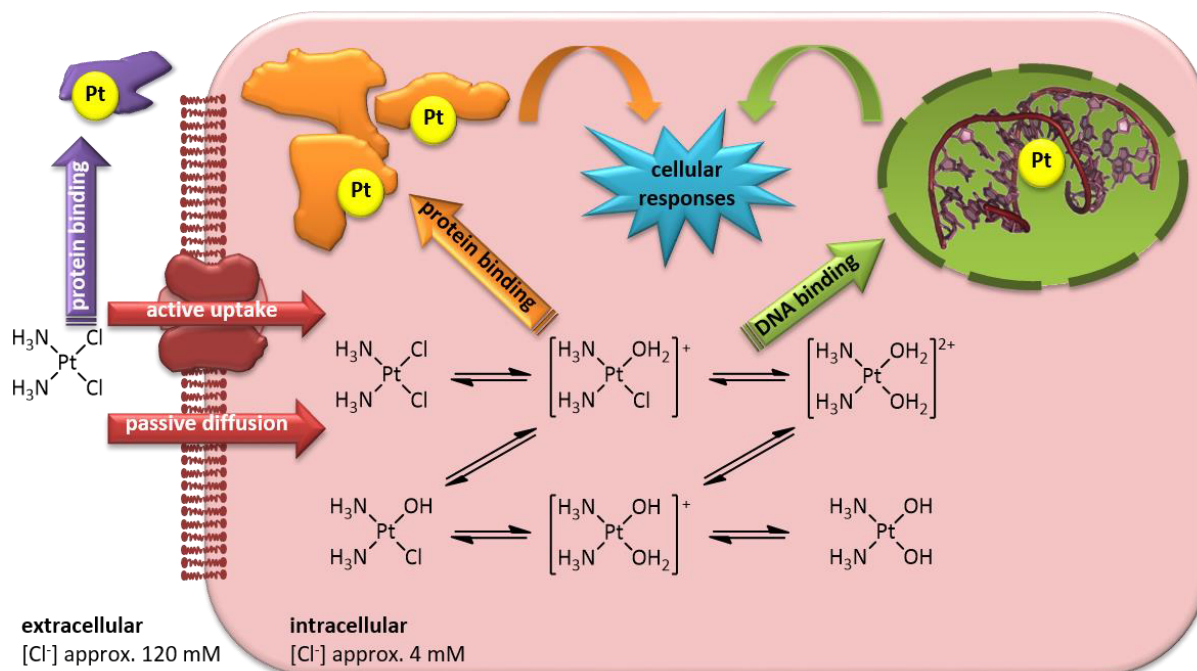


Figure 3 Schematic uptake of Cisplatin into the cell and subsequent cellular processing possibilities. In serum, Cisplatin is already prone to reactions with biomolecules. The drug enters the cell mainly undissociated, either by active uptake through *e.g.* Cu transport proteins or by passive diffusion through the phospholipid bilayer of the cell membrane. Due to a drop in cellular chloride ion concentration, aquation and subsequent biomolecule binding is facilitated. Genomic DNA is considered the main therapeutic target, but binding to proteins and other biomolecules inside the cell also takes place to a large extent. Both result in manifold cellular responses.

A passive diffusion into the cell, however, will only be possible for neutral, rather nonpolar compounds as opposed to highly polar or ionic species. Due to the comparably high chloride ion concentration in the blood (approx. 100-120 mM), most of the administered Cisplatin can remain unchanged and will thus be able to diffuse into the cell.<sup>70</sup>

### 1.2.2 Activation and biomolecule binding

Once inside the cell, a decrease of chloride concentration from high levels in blood and extracellular areas to ca. 4 mM in the cytosol<sup>71</sup> leads to several hydrolysis products to give cationic, aquated species, which are more or less “trapped” inside the cell (Figure 3).<sup>70</sup> Once they reach the nucleus, these aquated species are then capable of DNA platination. As specific binding sites at nuclear DNA, several units have been established, with the N<sup>7</sup> atom of guanines being considered the primary donor atom to bind the Pt(II) center.<sup>72,73</sup> This binding then results in 1,2 or 1,3-intrastrand links as well as interstrand links between nearby guanines (Figure 4). Furthermore, adenine and cytosine can bind platinum through their N<sup>7</sup> and N<sup>3</sup> atoms, respectively – such adducts are however far less frequently observed.<sup>74–77</sup>



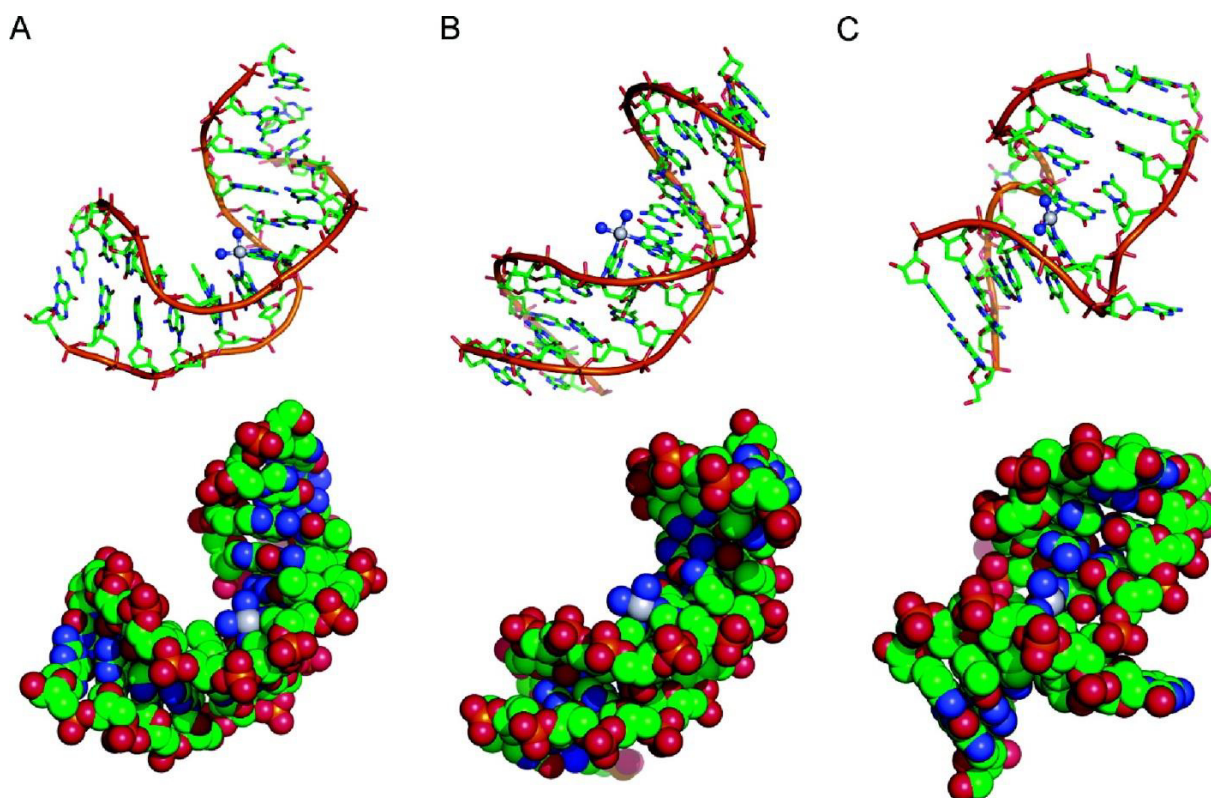


Figure 4 Typical platinum-DNA adduct structures. Duplex DNA containing (A) cisplatin 1,2-d(GpG) (B) 1,3-d(GpTpG) intrastrand, and (C) interstrand cross-links at different representative DNA double strand sequences. Reproduced from ref. 67.

In principle, metal centers could also bind towards other N atoms of the purine (A/G) and pyrimidine (C/T) bases. Some of those are, however, sterically protected or require deprotonation before metal binding (Figure 5).<sup>78</sup>

Apart from DNA as the desired target, other biomolecules are available in the cellular environment which contain preferable binding sites for Cisplatin and analogs. Biomolecules containing sulfur sites have been ascribed to present a central structural target in this context.<sup>79</sup> As an example,  $S^{Cys}$  donors in metallothionein (MT)<sup>80</sup> and glutathione (GSH)<sup>81</sup> have been recognized as very probable targets, and adduct formation with these two compounds is regarded as a main cellular protective response. Acquired resistance to Cisplatin treatment has been closely associated with elevated GSH and MT levels in long-term treated cells.<sup>82</sup> Contrary, NMR-based studies with whole-cell extracts have not been able to identify platinum-GSH adducts and recently, doubt has been shed on this general hypothesis of a principal preferable platinum-GSH binding.<sup>83</sup>

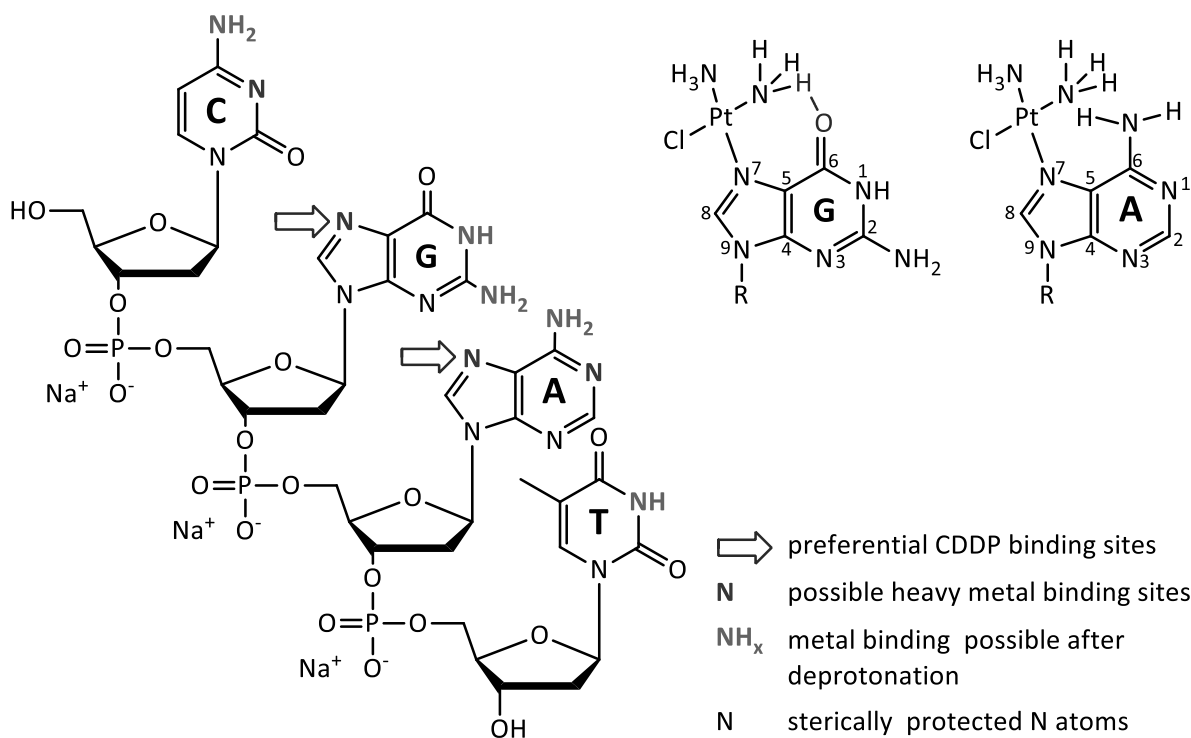


Figure 5 Possible binding sites for heavy metals in a representative tetramer of nucleotides. Stabilization of guanine-N<sup>7</sup> binding through H-bonding in contrast to binding at adenine-N<sup>1</sup> is demonstrated. Adapted from refs. 78,84.

In addition to the two aforementioned sulfur-containing target molecules, MT and GSH, various proteins have been found to bind Cisplatin or analogs in recent times (*cf.* chapter 7). Growing evidence is built towards alternate targets for Cisplatin in the cell which do not necessarily lead to the inactivation of the complexes' pharmacophore.<sup>85</sup>

One example of important metal-biomolecule interactions in chemotherapy are the effects platinum compounds have on serum proteins. Platinum-protein binding can either lead to a simple inactivation of the initial drug or results in toxic effects, *e.g.* through disturbance of crucial protein functions or through transport to healthy tissue which shouldn't be affected by the metal drug. In addition to such unwanted consequences of metal-biomolecule binding, it may well be possible that metal-protein adducts themselves contribute to the desired cytotoxic effects. Furthermore, the protein can serve as a chaperone or drug reservoir to transport the drug into the ("right") cells to be killed.<sup>69,79,86</sup> The overall picture of the consequences that transition metal-protein binding has on cellular processes is by far not yet completely assembled, and multiple research groups strive to contribute to the images' manifold facets.

The question why Cisplatin and analogs are still able to bind DNA despite the vast number of alternate binding sites has been mainly attributed to a thermodynamic stability of platinum-

nucleobase adducts, whereas Cisplatin-protein adducts are rather kinetically stabilized. Thus, eventually a transfer from the kinetically to the thermodynamically preferred biomolecule adduct is feasible.<sup>84,86–88</sup>

### 1.2.3 Cellular Processing

As a consequence of DNA platination, the  $\beta$ -helical structure of DNA is distorted, leading to inhibition of replication and transcription through several cellular pathways.<sup>89,90</sup>

Platinum-DNA adducts can be recognized by different cellular proteins, such as enzymes relevant for DNA repair, histones, high mobility group box (HMGB)-domains, or transcription factors.<sup>51,77</sup> DNA repair occurs mainly through nucleotide excision repair (NER) mechanisms,<sup>91</sup> a process highly dependent on the nature of the adducts and many other factors. Within this repair mechanism, it has been found that *e.g.* HMGB domains can specifically bind 1,2-intrastrand DNA adducts<sup>92</sup> and shield the adduct from being recognized by NER mechanisms.<sup>93,94</sup> The cellular response to Cisplatin-DNA damage is furthermore tightly associated with the activity of the p53 tumor suppressor gene. It can control processing of DNA adducts by activation of various, complex, downstream pathways.<sup>95</sup>

In any case, platinum-DNA binding leads to the onset of multiple direct cellular responses, and the final outcome – cell death through apoptosis or necrosis *or* cell survival depends on many different factors which have to date not been fully understood (Figure 6).<sup>67,96</sup>

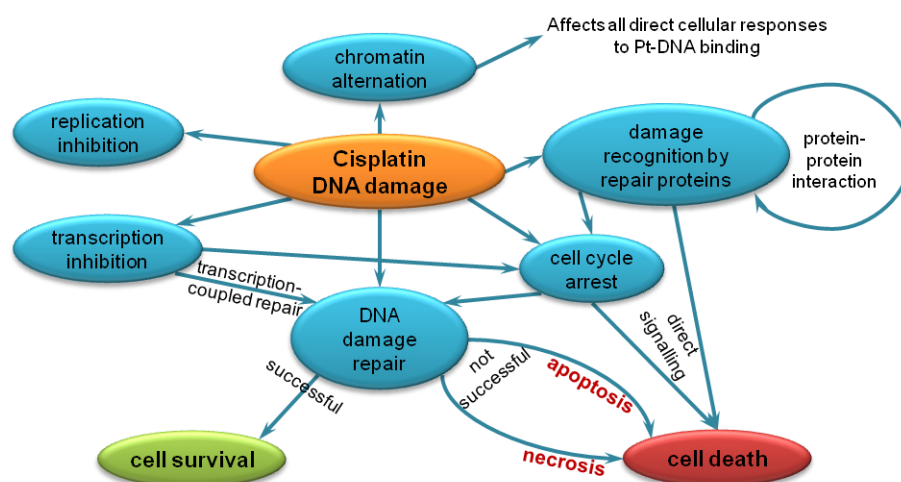


Figure 6 Direct cellular responses to Cisplatin-DNA binding. Adapted from ref. 67.



## 2 MOTIVATION, AIM OF THIS WORK

Cisplatin and its clinically approved analogs are very powerful drugs, able to cure several types of cancer and being applied in many combination therapy schemes. Their major drawback is the large panel of side-effects that are mainly associated with biomolecule binding at the “wrong” sites or unselective accumulation in both cancerous and healthy tissue.

In order to reduce side-effects associated with an unselective binding of the drug towards any available biomolecule, the concepts of hard and soft acids and bases (HSAB) and of the *trans* effect were brought into consideration for this work.

The HSAB concept is a general way of classifying compounds based on their ratio of charge to size, therefore allowing for an assessment of the “hardness” (high charge, low mass/radius) or “softness” (low charge, high mass/radius) of functional groups. It is assumed that chemical bonds between a Lewis acid (here the metal center) and a Lewis base (the ligand) are in principle more stable if the two binding partners are equally hard or soft.<sup>97</sup>

According to the concept of the *trans* effect, the two ligands in *trans* position of square-planar Pt(II) complexes are in competition for the  $\pi$ -electron density contributed by the ligands and the metal center. The ligands therefore have a significant influence on the kinetic lability or inertness of the *trans*-positioned bonds. Pearson precisely stated this circumstance in 1973:<sup>98</sup> “*Two soft ligands in mutual trans position will have a destabilizing effect on each other when attached to class b metal atoms.*”<sup>iii</sup>

Cisplatin, possessing a soft Pt(II) center, has two types of ligands that contribute to the coordination environment: ammonia and chloride. Both ligands can be classified as hard Lewis bases.<sup>99</sup> In this particular case, this binding situation leads to a preferential substitution of chlorido ligands by soft donors, such as biomolecular sulfur atoms, as described above.

---

<sup>iii</sup> A „class b metal atom“ is a soft metal center according to HSAB.

On the contrary, a sulfur atom is a rather soft donor, allowing for a stable binding towards the Pt(II) center with substantial delocalization of  $\pi$  electrons. The soft sulfur donor then induces a preferential binding of “hard” ligands in *trans* position. Therefore, using a soft donor atom set as non-leaving group can reduce a platinum(II) compounds’ affinity towards biological sulfur donor targets.

These considerations represent the basis for the structural rationale that lead to the preparation of the compounds presented in this thesis (Figure 7). The ligands designed as non-leaving groups for Pt(II) complexes are based on the structural motif of  $\beta$ -hydroxydithiocinnamic esters, a compound class which is well-established in the Weigand group and has been gaining growing attention also by others in recent years (*cf.* chapter 3). By forming very stable Pt(II) complexes with this (O,S) bidentate ligand, the resulting compounds’ reactivity towards biological targets should be directed towards a selective interaction pattern rather than a “wild” reactivity towards too many unselective targets. The monodentate ligands designed as leaving groups, chloride and dimethylsulfoxide (DMSO), are conveniently situated in their favored positions relative to O and S of the bidentate unit: The hard chlorido ligand binds platinum *trans* to the soft S donor; and *trans* to the harder O donor, DMSO binds platinum through its sulfur atom. This coordination environment is assumed to afford a specific activity against cancer cell lines, but at the same time to express a more defined interaction pattern with biological targets.

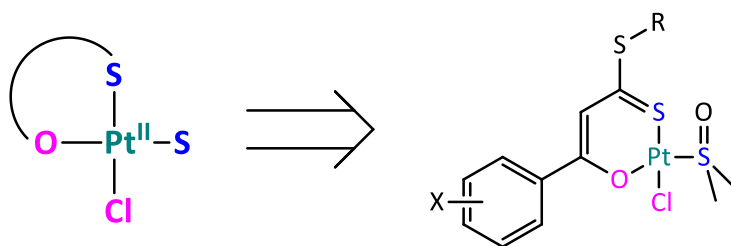


Figure 7 Rationale for the structural motif of Pt(II) complexes used within this thesis. Soft sulfur donors (blue) coordinate in *trans* position to hard O and Cl<sup>-</sup> donors (pink).

All these issues, antiproliferative activity and reactivity towards biomolecules, are addressed within this thesis: The design, synthesis and characterization of a panel of Pt(II) compounds based on the aforementioned structural criteria is reported (chapter 3), alongside with a primary elucidation of the compounds’ behavior in solution (chapter 4) and their activity against selected cell lines (chapter 5). In addition, the interaction of selected model compounds with potential biological targets, namely proteins and DNA, is investigated in detail by applying ESI mass spectrometry as primary

investigational method and UV-visible spectroscopy to corroborate the obtained data (part B, chapters 7 and 8). Furthermore, first steps towards enhanced cellular targeting are made by exploring synthetic methods towards bio-conjugation of the (*O,S*)Pt(II) unit with peptides (part C, chapters 11 and 12).





---

# PART A

## (O,S) CHELATE COMPOUNDS: SYNTHESIS, STRUCTURAL CHARACTERIZATION AND BIOLOGICAL EVALUATION

*Partial results of the chapters within this part have been published in the manuscripts listed below:*

*“Novel Platinum(II) Compounds with O,S Bidentate Ligands: Synthesis, Characterization, Antiproliferative Properties and Biomolecular Interactions”, Dalton Transactions **2014**, 43 (8), 3072-3086,*

*Parts appear in chapter 3*

*and “Platinum(II) Complexes with O,S Bidentate Ligands: Biophysical Characterization, Antiproliferative Activity and Crystallographic Evidence of Protein Binding”, Inorganic Chemistry **2015**, accepted manuscript,*

*Parts appear in chapters 3, 4, and 5.*

*Syntheses of compounds **29**, **30**, **32**, **33**, **34**, and **36** and their corresponding ligands have for the first time been executed within the diploma project.<sup>100</sup> In the course of investigations executed for the PhD project, these compounds have been re-synthesized and their analytical data independently re-evaluated.*

*Compound **50** was prepared by Matthias Hartlieb (FSU Jena) during an advanced practical course, which he conducted under my instruction and supervision of Prof. Dr. Wolfgang Weigand.*



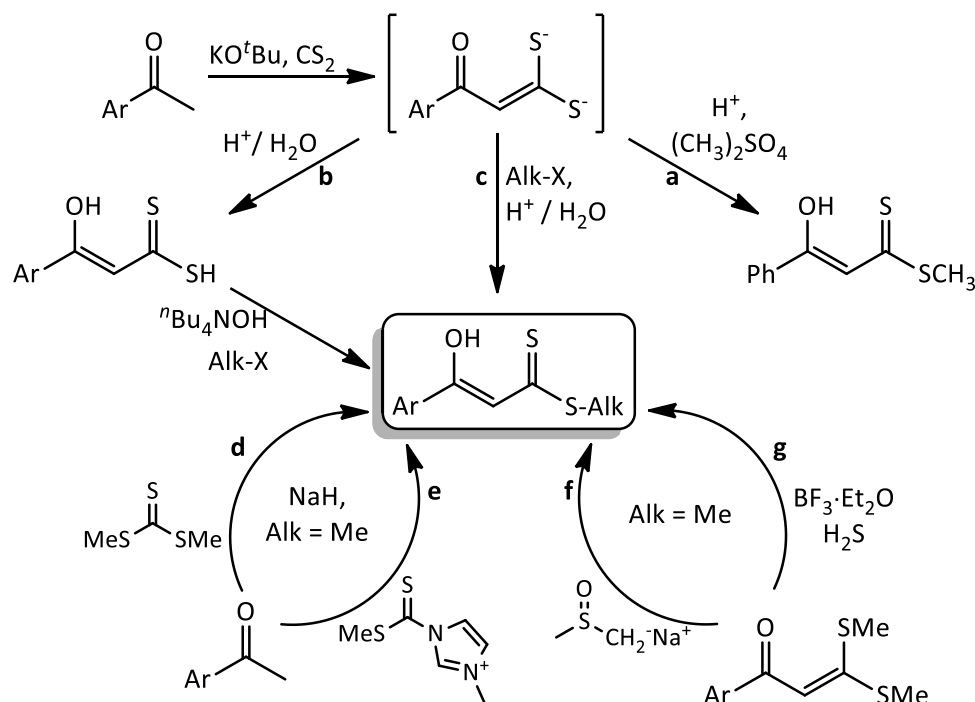
## 3 COMPOUNDS BASED ON $\beta$ -HYDROXYDITHIOGINNAMIC ESTER DERIVATIVES

### 3.1 $\beta$ -Hydroxydithiocinnamic esters

#### 3.1.1 Known synthetic approaches

$\beta$ -Hydroxydithiocinnamic ester derivatives have been used in various synthetic applications for several years.<sup>101</sup> Their syntheses have been described by a number of groups (Scheme 1, Scheme 2). The first reported compound,  $\beta$ -hydroxydithiocinnamic methyl ester, was described in 1967 by Gompper and Schaeffer (Scheme 1a).<sup>102</sup> Later on, Larson and Lawesson reported a two-step-synthesis of various esters *via* isolation of the respective  $\beta$ -hydroxydithiocinnamic acid (Scheme 1b).<sup>103</sup> A one-pot synthesis leading to  $\beta$ -hydroxydithiocinnamic esters with variable alkyl groups was finally described by Saumweber *et al.* in 1998 (Scheme 1c).<sup>104</sup> Since then, the procedure has been refined and well-established in the Weigand group.<sup>105–108</sup> The method conveniently circumvents the isolation of the respective dithiocinnamic acid, which is often associated with purification difficulties. It thus presents the preferred synthesis route applied in this work.

Alternate pathways for the synthesis of methyl esters starting from acetophenone derivatives have been developed (Scheme 1d);<sup>109</sup> optimized<sup>110</sup> and varied (Scheme 1e).<sup>111</sup> Furthermore, methyl esters could also be obtained from the respective ketene mercaptals using different approaches (Scheme 1f and g).<sup>112,113</sup>



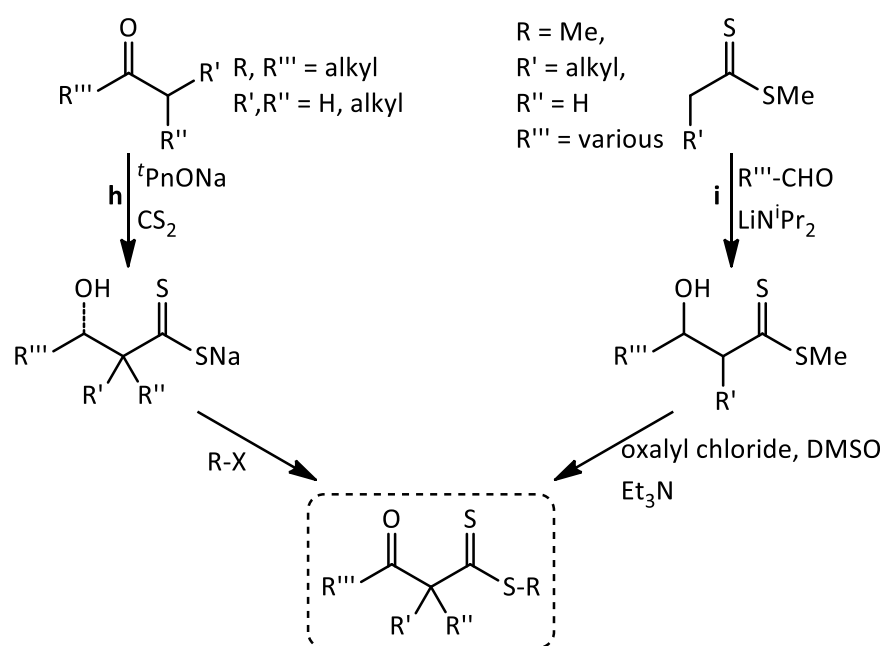
Scheme 1 Synthetic pathways towards  $\beta$ -hydroxydithiocinnamic ester derivatives. **a**, One-pot synthesis affording  $\beta$ -hydroxydithiocinnamic methyl ester. **b**, Two-step synthesis *via* the  $\beta$ -hydroxydithiocinnamic acid. **c**, One-pot synthesis mainly used in this work. **d** and **e**, Syntheses utilizing methyl trithiocarbonate derivatives to give methyl esters. **f** and **g**, Dealkylation of ketene mercaptals.

Additional reports exist on the synthesis of  $\beta$ -oxo dithioesters with various substituents, *e.g.* alkyl groups in  $\alpha$  position. Early reports by Thuillier and Vialle made use of  $\text{CS}_2$  to give dithioacid sodium salts, which were then alkylated (Scheme 2h).<sup>114–116</sup> In another report, lithium diisopropyl amide was used for the conversion of dithioesters with aldehydes to give  $\beta$ -hydroxydithioesters, which were subsequently oxidized (Scheme 2i).<sup>117</sup>

### 3.1.2 Synthesis and characterization of $\beta$ -hydroxydithiocinnamic ester derivatives

#### 7-28

Aliphatic esters of  $\beta$ -hydroxydithiocinnamic ester derivatives were obtained by applying established synthetic procedures (Scheme 3).<sup>118,119</sup> First, the hydroxyl groups of acetophenones **1** and **2** required protection by a *tert*-butyl dimethylsilyl (TBDMS) group, aided by imidazole, to give **3** and **4**.<sup>120</sup> This protection was necessary because such an acidic OH group could easily be activated through the conditions of the following step, namely deprotonation of the CH-active methyl group to enable attack of  $\text{CS}_2$ .

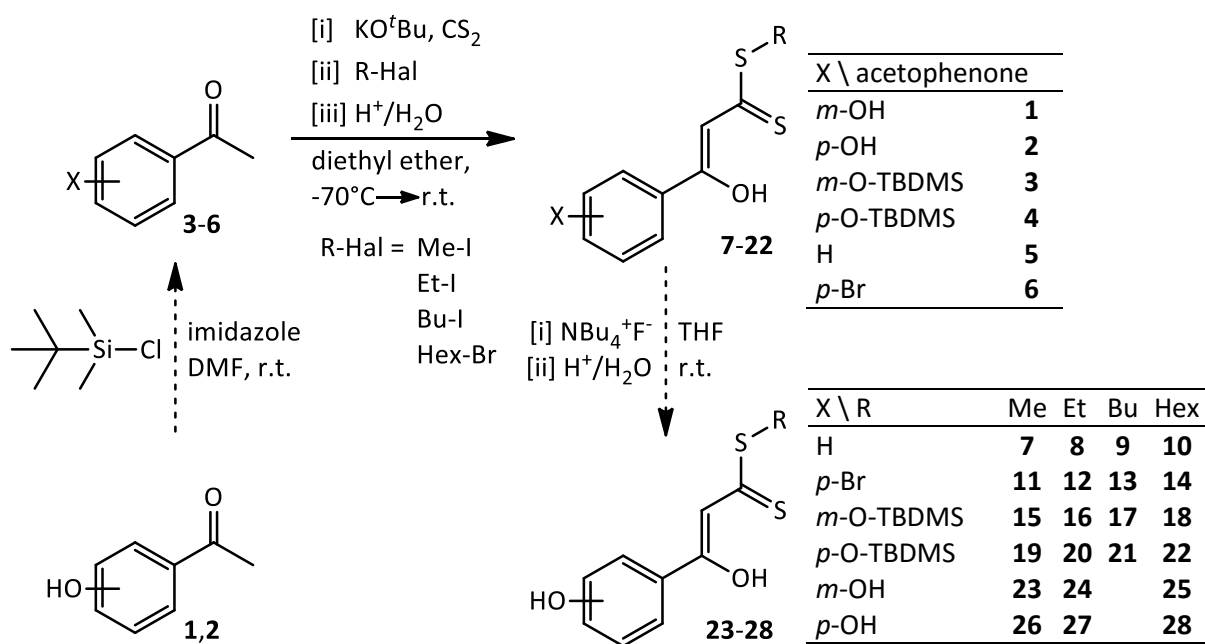


Scheme 2 Further synthetic pathways towards  $\beta$ -oxo dithioesters. Substituents in  $\alpha$  position result in  $\beta$ -oxo forms of the dithiocinnamic esters. **h**, method employing  $\text{CS}_2$ . **i**, derivatization of dithioesters with aldehydes and subsequent oxidation.

Acetophenone derivatives **3**, **4** as well as **5** and **6**, could then be subjected to the previously described one-pot synthesis to afford  $\beta$ -hydroxydithiocinnamic esters **7-22**, bearing H, *p*-Br or *m/p*-O-TBDMS as substituent X. Alkyl chains R of increasing chain length were introduced by proper choice of the alkylating agent. All compounds were obtained in moderate yields which mainly depended on the alkyl group R being introduced.

Notably, yields were generally best for ethyl rests. Obviously, the reactivity of ethyl iodide proved to be both high enough for a high degree of conversion alongside with sufficient inhibition towards the formation of the frequently observed ketene mercaptals. Yields of methyl esters were generally lowered by the preferential double alkylation and reaction towards ketene mercaptals, and butyl iodide resp. hexyl bromide were significantly less reactive, as seen by incomplete conversion in some of the conducted syntheses.

In order to obtain ligands **23-28** with hydroxy groups in *meta* or *para* position of the aromatic unit, O-TBDMS protected compounds **15-22** were subjected to fluoride-based silyl ether cleavage by using tetrabutyl ammonium fluoride (TBAF) as cleavage reagents, followed by acidic work-up to obtain the protonated phenyl-OH group.<sup>105</sup> The conversion usually proceeded smoothly and the desired compounds **23-28** could be isolated in moderate to high yields (Scheme 3).



Scheme 3 Synthetic procedures towards derivatives of  $\beta$ -hydroxydithiocinnamic esters, being varied at the aromatic and dithioester subsite. Reactions with a dashed arrow were only performed for hydroxy-derived compounds.

The compounds were investigated by standard analytical methods ( $^1\text{H}$  and  $^{13}\text{C}$  NMR spectroscopy, IR spectroscopy, mass spectrometry, elemental analysis). A detailed discussion of spectral data can be found in the respective manuscripts<sup>118,119</sup> and earlier work of the Weigand group.<sup>104-107</sup>

The most characteristic signals observed in NMR spectra of  $\beta$ -hydroxydithiocinnamic ester derivatives **7-28**, recorded in  $\text{CDCl}_3$ , include those of the  $\alpha$ -methine group, being observed at 6.8-6.9 and 107-108 ppm in  $^1\text{H}$  and  $^{13}\text{C}$  NMR spectra, respectively.  $^{13}\text{C}$  NMR signals belonging to the quaternary " $\text{CS}_2$ " group are generally observed at 215-217 ppm, those of the  $\beta$ -C-OH group in a range of 168-170 ppm. Furthermore, the  $\beta$ -OH group is commonly observed as a sharp singlet in the range of 15.0-15.3 ppm in  $^1\text{H}$  NMR spectra, indicative for the postulated *cis*-enolic structure of the compounds.

The combined NMR data suggest that an intramolecular hydrogen bonding is an important stabilizing factor for the ligands **7-28**, as has been confirmed by X-ray crystallographic studies by Schubert *et al.* earlier on compound **26**<sup>105</sup> as well as by Mancilla-González *et al.* on compounds **7**, **11** and other derivatives.<sup>121</sup> Other groups have postulated  $\beta$ -oxo dithioester<sup>122,123</sup> or thio-enol structures<sup>124</sup> as possible tautomers, but structural findings for all ligands presented here point towards the postulated  $\beta$ -hydroxydithiolato structure.

Further relevant structural data are given through presence or absence of the silyl-based protection group. In compounds **15-22** with an O-TBDMS group, characteristic NMR signals are observed at 0.2 and 1 ppm (in  $^1\text{H}$ ) as well as at ca. -4 and 26 ppm (in  $^{13}\text{C}$ ) for the methyl and *tert*-butyl groups, respectively. The quarternary  $\text{C}(\text{Me})_3$  carbon exhibits a signal at ca. 18 ppm in  $^{13}\text{C}$  NMR spectra. These signals are diminished upon cleavage of the O-Si bond. NMR spectra of the ligands were typically recorded in  $\text{CDCl}_3$ , so that the formed phenyl-OH group was generally not witnessed in  $^1\text{H}$  NMR spectra of compounds **23-28**.

Mass spectra (EI) of the isolated compounds usually afforded the  $[\text{M}]^+$  or  $[\text{M}+\text{H}]^+$  molecular ion and further characteristic peaks, such as the signal after loss of the S-R group.

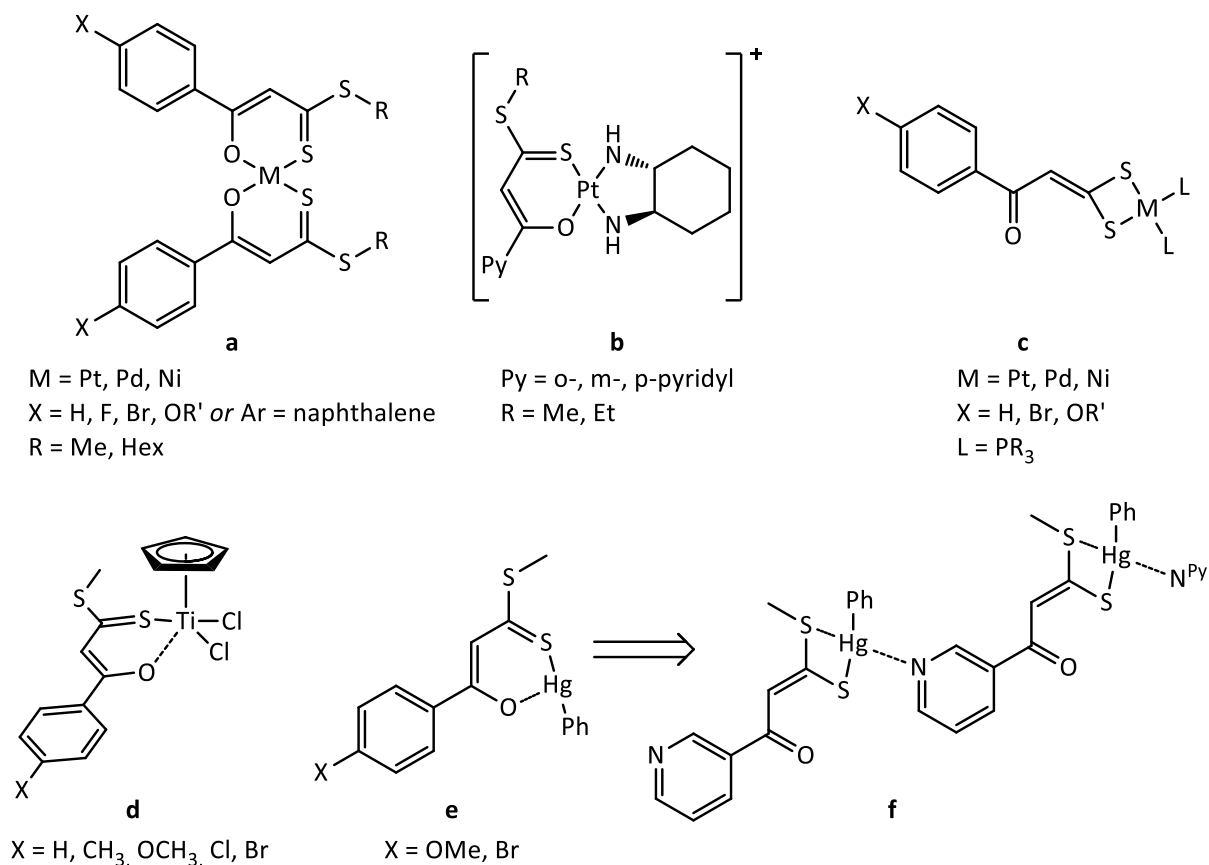
## 3.2 Platinum(II) complexes

### 3.2.1 Reported metal complexes with ligands based on derivatives of $\beta$ -hydroxydithiocinnamic esters

Metal complexes based on the described ligand system have been reported by several groups, mostly affording bis-functional complexes with divalent transition metal centers.<sup>104,105,108,125,126</sup> In principle, coordination of  $\beta$ -hydroxydithiocinnamic esters towards a metal(II) center readily proceeds upon deprotonation of the ligand's hydroxy group, and  $\text{M}^{\text{II}}(\text{O},\text{S})_2$  bischelate complexes are obtained, which form a stable, six-membered chelate unit for each ligand (Chart 3a). As has been reported and demonstrated by X-ray crystallographic methods, transition metal complexes are selectively obtained showing the ligand in *cis* configuration respective to the O and S donor molecules.<sup>104,106,107,125,126</sup>

Furthermore, monocationic complexes have been prepared based on pyridine-derived ligands in combination with a neutral *trans*-(1*R*,2*R*)-diaminocyclohexane (DACH) co-ligand, thus only having one (O,S) binding unit (Chart 3b).<sup>127</sup> Also their incorporation into half-sandwich titanium complexes has been reported (Chart 3d).<sup>121</sup>

Very recently, a report on a selective tuning of the coordination mode from the typical (O,S) to a (S,S) chelate environment was reported with mercury(II) by altering the aromatic substituent of the  $\beta$ -hydroxydithiocinnamic esters: When using pyridine as aromatic substituent (as opposed to *p*-OMe or *p*-Br substituted phenyls, Chart 3e), intermolecular interactions forced the Hg(II) center into a (S,S) $\text{Hg}^{\text{II}}(\text{C}^{\text{Ph}})(\text{N}^{\text{Py}})$  coordination environment (Chart 3f).<sup>128</sup> Such a coordination mode is usually observed for transition metal complexes of the free  $\beta$ -hydroxydithiocinnamic acids (Chart 3c).<sup>106,107</sup>

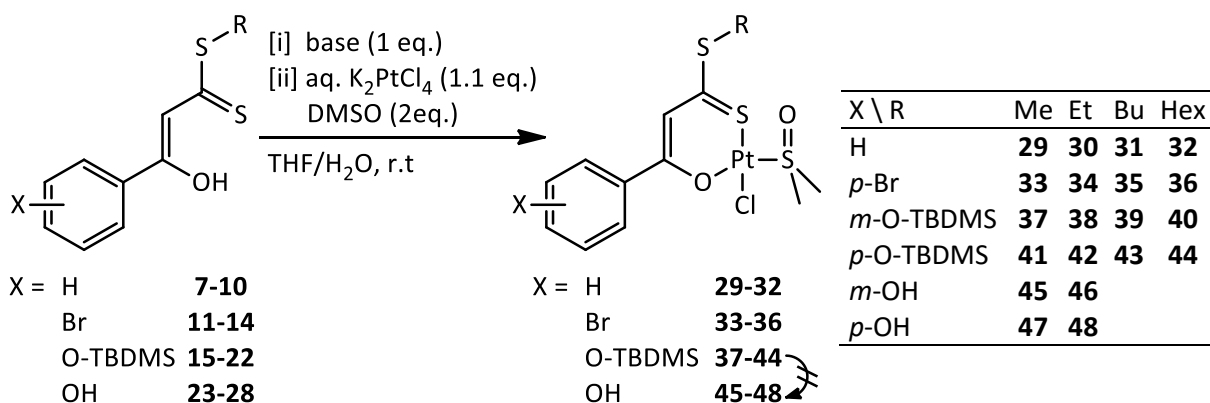
Chart 3 Literature-reported metal complexes based on  $\beta$ -hydroxydithiocinnamic ester derivatives.

### 3.2.2 Syntheses of the (O,S) bidentate Pt(II) complexes

The synthesis of Pt(II) complexes with one (O,S) unit and two monodentate ligands, namely dimethyl sulfoxide (DMSO) as neutral ligand binding *via* its S atom and a chlorido anionic ligand, was reported for the first time in the publication which appeared in Dalton transactions 2014.<sup>118</sup>

To obtain Pt-DMSO species, several approaches have been reported in literature.<sup>129–133</sup> Once “activated” by DMSO coordination, further derivatizations of the coordination environment can be performed, and DMSO can either be substituted by more stable ligands<sup>134</sup> or retained within the coordination sphere.<sup>135–137</sup> For the method described here, a Pt-DMSO species was generated *in situ* and immediately converted with the respective (O,S) ligand, which binds to the Pt(II) center to give the desired (O,S)Pt(DMSO)(Cl) structural motif. This approach avoids tedious and substance-consuming work-up procedures and is thus very efficient from an economical point of view.





Scheme 4 Synthetic procedure towards Pt(II) complexes with an (*O,S*) bidentate ligand based on  $\beta$ -hydroxydithiocinnamic esters, as well as DMSO and chloride as monodentate ligands

For preparation of complexes **29-48**, compounds **7-28** were subjected to the following generalized conditions (Scheme 4): Potassium tetrachloro platinate(II),  $K_2PtCl_4$ , was activated with a slight excess of dimethyl sulfoxide (DMSO) and the ligand, deprotonated through an appropriate base, was added in slightly submolar quantities to suppress the formation of strongly preferred bischelates. The desired compounds **29-48** were obtained in varying yields.<sup>118,119,138</sup>

For compounds with X = O-TBDMS or OH and R = butyl or hexyl group (Scheme 4), the preparation of the desired complexes was only partially successful; not all compounds could be obtained or purified to the desired degree. Interestingly, compounds **43** and **44**, with the substituent in *para* position, were more difficult to obtain than the respective *meta* substituted counterparts (**39/40**). Both species could not be isolated sufficiently. For compounds with a free phenyl-OH group, the synthesis of complexes based on ligands **25** and **28**, bearing hexyl groups, was not successful at all and afforded solely unidentified decomposition products. The alternate approach to obtain the compounds *via* cleavage of the O-TBDMS unit after complexation, *i.e.* from compounds **37-44**, was generally not successful. Again, NMR spectroscopy did not show any sign of the desired complex. Further efforts to obtain these compounds (respectively the butyl compounds) were not undertaken since the main goal of the synthesis of these complexes was to enhance aqueous solubility. The formation of complexes with longer alkylic chains was only of synthetic interest rather than of functional rationale.

### 3.2.3 Influence of the base

To elucidate whether the nature of the base used to deprotonate the  $\beta$ -hydroxydithiocinnamic ester has an influence on the yield of the respective Pt(II) complex and to better be able to adapt the base to the ligands' needs, different bases were used to prepare the *p*-Br/Et substituted model complex **34**. The standard base used in all early experiments was sodium hydride (NaH), which required the deprotonation to be carried out under inert conditions.<sup>118,119</sup> The great advantage of this approach is that evolving H<sub>2</sub> gas can be used to monitor the completion of the reaction and that all acidic protons are removed from the system, thus giving the (*O,S*) compound as a sodium salt. Alternatively, KO<sup>t</sup>Bu was explored as candidate since it was successfully applied for the ligand synthesis and was therefore expected not to induce unwanted side reactions. Third, sodium acetate (NaOAc) was explored as potential base, together with the change from inert to non-inert conditions, thus facilitating the handling of the compounds.

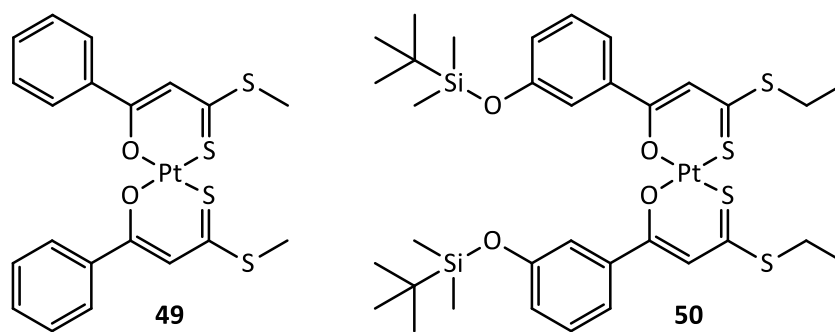
All three approaches lead to the desired complex **34**, but unexpectedly the deprotonation approach with sodium acetate gave the highest yield (66%) of the target compound.<sup>iv</sup> KO<sup>t</sup>Bu proved to be the least effective base (25 % yield) and use of NaH lead to 33 % yield. Therefore, where possible, NaOAc was used as the preferential base in later experiments unless functional groups required otherwise.

### 3.2.4 Bischelates

Typical side products formed during the described procedure are the respective bischelates with two (*O,S*) bidentate units being bound in *cis* configuration. This can be prevented to a large degree by adding the deprotonated ligands to the Pt-DMSO adduct slowly and in sufficient dilution. In some early experiments, still a substantial amount of bischelate was formed during complexation and thus isolated from the mixtures. One representative, compound **49** with H/Me substitution pattern, was chosen as occasional reference for further studies (Scheme 5).

---

<sup>iv</sup> When the synthetic procedure was developed, various approaches had been tested. The compounds could for the first time be obtained when using NaH as base under inert conditions. Attempts to work under air failed in the first experiments, probably due to other parameters that had not been optimized at that point. Later on, it was found that the crucial step for a successful synthesis is the sufficient pre-activation of K<sub>2</sub>PtCl<sub>4</sub> by DMSO rather than the deprotonation of the base. Moreover, the synthesis could even proceed *without* base in special cases, *vide infra*.



Scheme 5 Representative bischelate complexes obtained during the synthesis of compounds **30** and **38**.

Another representative, compound **50** (Scheme 5), was obtained in crystals suitable for X-ray structure determination. *Cis*-coordination of the two (*O,S*) units to give a square-planar coordination environment is clearly demonstrated. The entire molecule, as depicted in Figure 8, is more or less flat and interestingly, the phenyl ring is rotated in such a fashion that the O-TBDMS groups point towards the center of the molecule. This leads to a slight tilting of the phenyl rings to position the silyl units above and below the molecular plane.

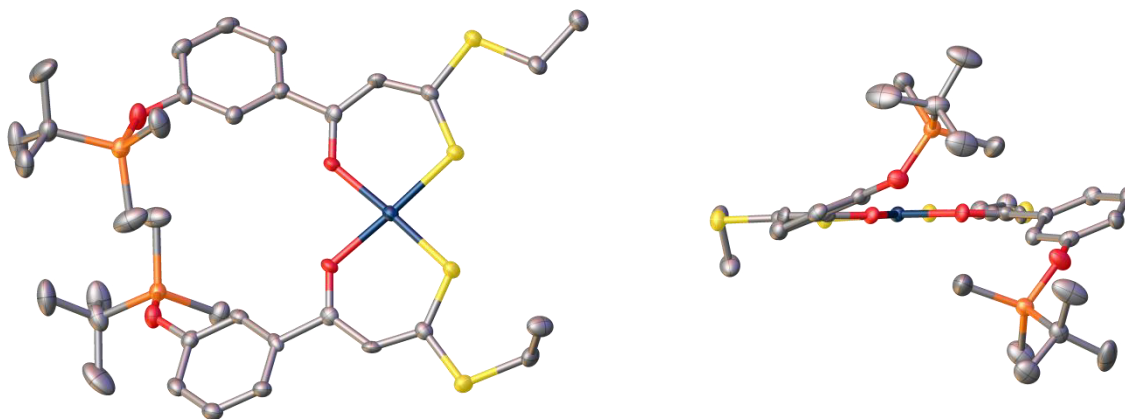


Figure 8 Molecular structure of bischelate **50** (Space group:  $P2_1/c$ ). Left: view onto the molecular plane; right, view along the molecular plane. Thermal ellipsoids are given at 50 % probability level.

### 3.2.5 Characterization of the complexes

All described compounds were characterized by standard analytical methods as described in detail in the respective manuscripts.<sup>118,119</sup> Compounds **32** and **33** were furthermore analyzed by X-ray crystallographic studies as discussed elsewhere.<sup>118</sup>

The most characteristic spectral changes respective to the corresponding ligands are observed in the compounds' NMR spectra, typically recorded in  $\text{CDCl}_3$  (for **29-44**), acetone- $\text{d}_6$  or THF- $\text{d}_8$  (for **45-48**). The loss of the high-frequency  $\beta$ -OH proton signal is generally accompanied by a shift of the binding  $\beta$ -C-OPt carbon signal to higher frequencies by ca. +5 ppm (found at 173-176 ppm in  $^{13}\text{C}$  NMR spectra). Furthermore, the signals belonging to the methine group experience characteristic shifts, *i.e.* by ca. +0.3 ppm to 7.0-7.2 ppm and by ca. +4 ppm to 111-112 ppm in the  $^1\text{H}$  and  $^{13}\text{C}$  NMR spectra, respectively. In addition, the dithiocarbonyl-carbon atom experiences a massive shift to lower frequencies by ca. 35 ppm and can be found at 180-182 ppm when coordinated to the Pt(II) center. A broad singlet belonging to the phenyl-OH group may be witnessed at ca. 8-9 ppm in  $^1\text{H}$  NMR spectra of **45-48** when recorded in acetone- $\text{d}_6$  or THF- $\text{d}_8$ , but not in NMR spectra recorded in  $\text{CDCl}_3$ .

These typical signal sets can be observed in both, the desired monofunctional compounds **29-48**, but very similarly also in the bis-functional side products such as **49** or **50**. An unambiguous proof of the formation of (*O,S*) bidentate compounds with DMSO and chloride being bound towards platinum presents the combination of mass spectrometric data (typically obtained through ESI), which frequently gave signals of the molecular ions or  $\text{Na}^+$  adducts, and the observation of Pt-coordinated DMSO in NMR spectra. In  $^1\text{H}$  NMR spectra, a singlet at ca. 3.6-3.7 ppm with Pt-satellites and a  $^3J_{\text{Pt-H}}$  coupling constant of 23-24 Hz can be assigned to Pt-coordinated DMSO with a shift of ca. +1 ppm compared to free DMSO.<sup>139</sup> In  $^{13}\text{C}$  NMR spectra, Pt-bound DMSO is observed at 46-47 ppm, thus shifted by ca. 6 ppm compared to free DMSO.<sup>139</sup> Under some circumstances (high compound concentration and low magnetic field, typically 200 MHz), even Pt-C coupling could be observed with  $^1J_{\text{Pt-C}} \approx 59$  Hz. In cases where THF- $\text{d}_8$  presented the most suitable deuterated solvent for NMR analyses (as was the case for compounds **45-48**), the proton signal of coordinated DMSO was obscured by intrinsic solvent signals but could typically be detected from cross-peaks in HSQC experiments.

Overall, the spectral data for complexes **29-48** markedly demonstrate that it is possible to alter the structure of the (*O,S*) bidentate ligand in a wide range without significantly affecting the pharmacophore's electronic structure, thus enabling further variations for functional optimization.

## 4 SOLUTION CHEMISTRY OF THE (O,S) CHELATE COMPOUNDS

### 4.1 Solubility in aqueous medium – determination of $\text{Log}P_{o/w}$ values

It is generally a desirable aim to prepare compounds with a defined aqueous solubility which makes the uptake of drug candidates *via* oral administration (for highly water soluble compounds) or the blood stream possible. Highly lipophilic compounds may also be administered by other means, such as oil immersions or emulsions, but some degree of hydrophilicity is in general needed for the application of new drug candidates.<sup>140</sup> A well-defined polarity of a compound can lead to an appreciable degree of aqueous solubility; if aided by H-bonds, this can be significantly enhanced.<sup>141</sup>

The solubility of organic compounds in aqueous or organic medium is frequently quantified by their water/*n*-octanol partition coefficient, given as  $\text{Log}P_{o/w}$  value, which is usually determined through the shake-flask method.<sup>142,143</sup> In recent times, this quantification method has also been introduced in medicinal inorganic research scopes for determining the polarity of metal compounds.<sup>144–147</sup> It appears indeed to be a straight-forward idea since the method is simple and versatile at the same time: essentially, a defined stock solution of the compound in water or *n*-octanol is mixed with the respective complimentary solvent, followed by determination of its concentration in both phases by appropriate quantification methods). Computer programs are nowadays even available which try to predict these values by using different increment methods.<sup>147–149</sup> In addition, alternate methods have been developed, such as HPLC-based regression methods, where the compounds'  $\text{Log}P_{o/w}$  value is extrapolated from its retention time in a water-methanol gradient.<sup>150–153</sup>

However, the shake-flask method will not give reliable results when using metal complexes that are prone to hydrolysis reactions in aqueous medium. As an alternative method to determine the polarity of the compounds discussed here, the HPLC method was tested. However, the compounds under investigation underwent fast solvolysis at conditions appropriate for this approach, thus rendering this method inapplicable for the compounds under investigation.

It is indeed not useful to determine the polarity of the *complexes* in a water/*n*-octanol mixture. If the experiment is planned in a time-frame shorter than needed for full hydrolysis, the system will not be in equilibrium state due to ongoing aquation reactions (even if slowed down by the addition of appropriate salts). If the experiment is performed at true equilibrium state, as required for a correct determination of “Log $P_{o/w}$ ”, there will be two (or more) different components in the mixture.<sup>154</sup> For example, the Log $P_{o/w}$  value of Cisplatin is reported in literature as ranging from -1.7<sup>147</sup> to -2.5<sup>144</sup> and therefore spans almost one order of magnitude of  $P_{o/w}$  ( $P_{o/w} \approx 2 \cdot 10^{-2}$  and  $3 \cdot 10^{-3}$ , respectively). These deviating values may originate from differences in the determination method, but foremost these differences can be ascribed to hydrolysis processes going on during the experiment. Notably, similar variations were observed with the herein described complexes **29-48**, rendering this method unsuitable for determining meaningful data.

To circumvent this predicament, Log $P_{o/w}$  values were determined for the pre-ligands **7-28** presented here and not for their Pt(II) complexes. The decision was based on a simple rationale: the final pharmacophore of the complexes is identical in all cases, only variations of the (O,S) bidentate ligand contribute to changes in the complexes' polarity. It is therefore possible to attribute the complexes' *relative* polarity from their ligands' Log $P_{o/w}$  values. Although the obtained results cannot give exact results for the complexes, they allow for a comparison of the polarity development within this series.

The compounds were subjected to the shake-flask method as described in detail in the experimental section. The relative concentration in both phases was determined by UV-visible spectrophotometry. Log $P_{o/w}$  values were then calculated from the average absorbance in the range of 300 and 500 nm using formula (1). The results are summarized in Figure 9.

$$\text{Log}P_{o/w} = \lg\left(\frac{c_{\text{octanol}}}{c_{\text{water}}}\right) = \lg\left(\frac{A_{\text{octanol}}^{300-500\text{nm}}}{A_{\text{water}}^{300-500\text{nm}}}\right) \quad (1)$$

The Log $P_{o/w}$  values range from 1.71 to 2.72 and hence span one order of magnitude for  $P_{o/w}$ . The lowest values were obtained for the *meta*-hydroxy substituted compounds **23-28**, the highest for the O-silyl protected compounds **15-22**. Unsubstituted or Br-derived compounds **7-14** gave intermediate Log $P_{o/w}$  values.

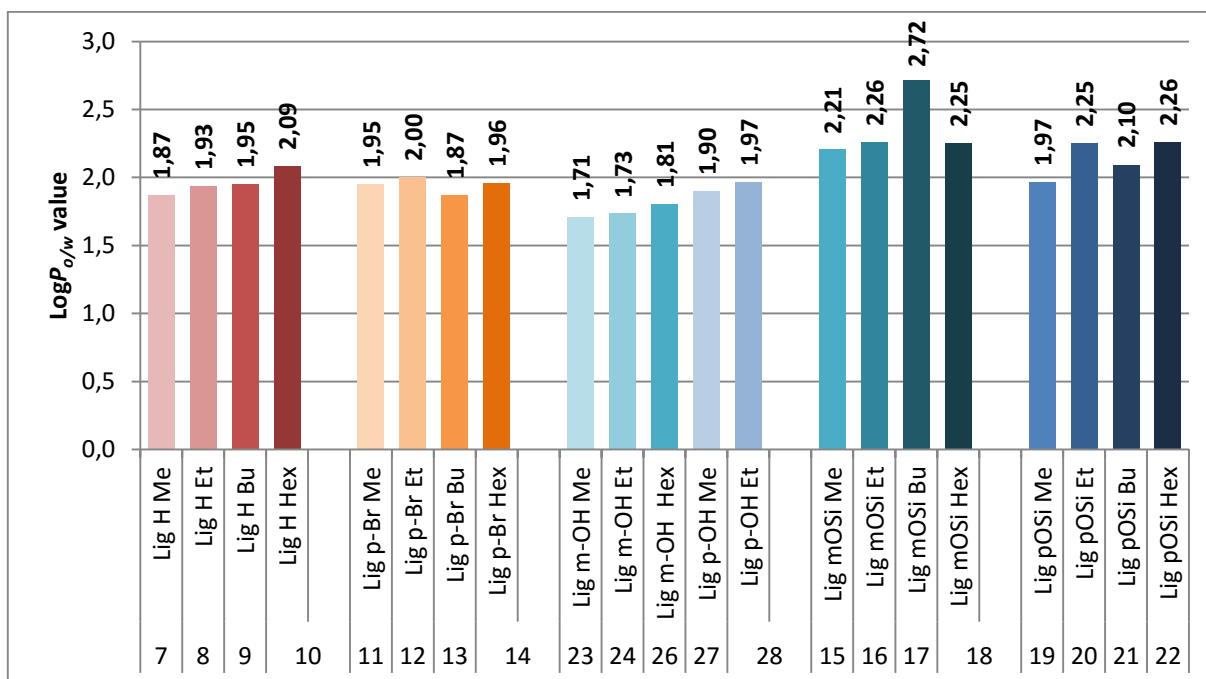


Figure 9 Log $P_{o/w}$  values of  $\beta$ -Hydroxydithiocinnamic acid esters as obtained from the shake-flask method.

The graph in Figure 9 demonstrates that the strongest influence on the compounds' polarity originates from the substitution pattern at the aromatic unit rather than from the length of the alkylic chain at the sulfur moiety. Nevertheless, an overall rising Log $P_{o/w}$  was observed when the thioester chain length was increased. The most significant observation is made within the series of hydroxy-substituted compounds **23-27**: whilst *m*-OH compounds **23/24** exhibit the lowest Log $P_{o/w}$  values, those bearing *p*-OH groups **26/27** are higher and come into the range of unsubstituted and Br-substituted compounds **7-14**. Obviously, the position of the polar group has a significant impact on the final polarity of the compound.

Some technical note should be given on the experimental setup. UV-vis spectroscopy provides a useful tool to determine a compounds' concentration in solution, given a well-defined absorption spectrum and a proper concentration range. The compounds discussed here, both  $\beta$ -hydroxydithiocinnamic esters and their corresponding Pt(II) complexes, give a characteristic absorption spectrum in the visible range of the spectrum. In the aqueous phase however, the signal intensity is very low and noise dominates the spectrum. Several approaches have been employed to circumvent this issue, including the application of smoothing functions or choosing certain singular wavelengths for the determination of the log $P_{o/w}$  value. Furthermore, it was attempted to calculate the absolute concentration of the compounds in each phase through their extinction coefficients  $\epsilon$  (for a detailed description, cf. the experimental part), but since the compounds' solubility in water

without the use of solubility-mediating additives (such as DMSO) is low, no extinction coefficient for the aqueous phase could be calculated, so that this approach also did not lead to reliable results.

Based on these considerations, it was decided to use the average absorbance in the wavelength range of 300-500 nm, as mentioned earlier, for calculating the relative concentration in the aqueous vs. *n*-octanol phase. This range was chosen on the rationale that below 300 nm, absorptions of the solvents could obscure the spectrum even after baseline correction. Above 500 nm, no specific absorptions of any investigated compound were observed. Choosing a 200 nm range furthermore muddled out noise in the water-phase spectra to a large degree. Representative spectra are given in Figure 10.

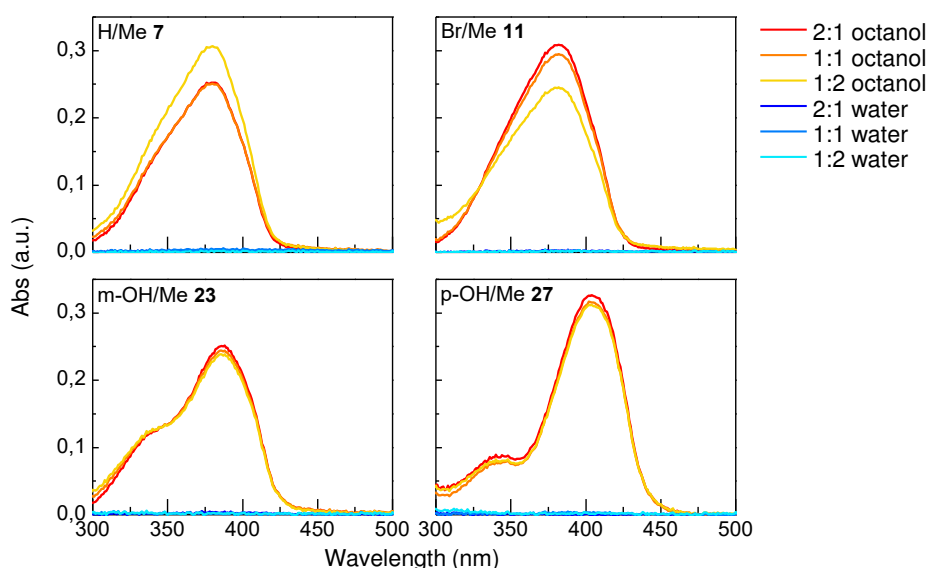


Figure 10 Some representative UV-vis absorption spectra of methyl-dithioesters **7**, **11**, **23** and **26** as used for calculation of  $\text{Log}P_{o/w}$  in the relevant wavelength range 300-500 nm. The three well-defined signals (reds/yellows) originate from the *n*-octanol phase, the spectra close to the baseline (blues) were recorded in water.

In principle, also other methods to determine the compounds' quantity in each phase are thinkable. For experiments that were conducted with the complexes, quantification of Pt content by ICP-OES was attempted;<sup>v</sup> yet the sample preparation failed since it was not possible to mineralize the large quantity of octanol present in the respective phase.

<sup>v</sup> These experiments were carried out by Tiziano Marzo (Firenze, private communication).



## 4.2 Behavior in solution – UV-visible spectroscopic experiments

The investigational compounds' behavior in aqueous solution was also monitored by UV-visible spectroscopic experiments. In-depth discussion of procedures and results can be found in the respective manuscripts.<sup>118,119</sup> Some further details of these investigations are presented in this section.

All metal complex spectra share a very similar chromophore expressed as three absorption bands, centered at about 270-280 nm, 350-370 nm, and at 410-430 nm. The exact position and shape of the spectrum differs with the varying substituents at the (O,S) bidentate ligand. Overall, these bands well represent the yellow color of the solid compounds and solutions. A definite assignment of the three transition bands is purposely not made due to the complexity of influences contributing to the compounds' electronic structure.<sup>vi</sup> Nevertheless, based on spectra obtained from pure ligands (as shown *e.g.* in Figure 10) and the experiments described below, it becomes clear that the electronic transitions must originate from the (O,S) bidentate ligand bound to the Pt(II) center and that the positions of the bands are strongly influenced by the ligands in *trans* position.

In general, it was found that the compounds stay dissolved in 100  $\mu$ M buffered solutions over 24 h when a suitable amount of DMSO (10-25 %) is added to aid dissolution. Some evidence of partial hydrolysis is found from minor spectral changes in the long-wave band at ca. 420-430 nm.

For H and Br compounds, a noticeable dependence of solubility and alkyl chain length was found (*i.e.*, increasing aqueous solubility by shortening the alkyl chain, as would be expected), alongside with an enhanced aqueous solubility for unsubstituted compounds in comparison with their *p*-bromo counterparts.<sup>118</sup> These observations correlate well with the found  $\text{Log}P_{o/w}$  values, even though the mere *observation* of UV-visible spectra suggest much stronger changes in *P* than the determined  $\text{log}P_{o/w}$  values show. This might, however, be an issue of perception.

Similar UV-visible spectra were recorded from buffered solutions of the OH substituted compounds **45-48** and are discussed in detail in the corresponding manuscript.<sup>119</sup> Overall, these compounds present an appreciable solubility in buffered solutions containing 25 % v/v DMSO. Some indications of hydrolysis were found, as expected, and no significant influence of the alkyl group at the dithioester moiety was observed – an expectable result, given the fact that only methyl and ethyl groups were incorporated into the structural motif. Interestingly, the position of the OH group

---

<sup>vi</sup> Initial attempts to simulate the most probable electronic transitions of these UV-vis spectra by DFT methods gave no reliable data due to the presence of Pt as heavy atom. (Pablo Rivera Fuentes / ETH Zürich, private communication)

proved to be relevant for the relative intensity of the long-wave band at ca. 410 nm. It is, in contrast to all other compounds, in *p*-OH complexes **47** and **48** more intensive than the middle band around 350 nm. In addition, a shoulder at about 470 nm could be observed in spectra with 50 % DMSO v/v. This observation is indicative of some mesomeric effects induced by the *para*-position of the hydroxy group.

When kept in pure DMSO, no spectral changes are observed over the course of 96 h for a 1 mM solution of compound **34**, indicating that DMSO stabilizes the compound (Figure 11). Even when kept in mixtures with 50 vol-% water or phosphate buffer (PB, 10 mM) at 1 mM, most of the compound stays dissolved over 96 h. At lower DMSO concentrations, *e.g.* 10 vol-% DMSO, significant precipitation is observed immediately, thus demonstrating the expected low aqueous solubility. Comparable results were obtained when using water instead of PB (data not shown). The spectra depicted here were recorded in pure DMSO to enable direct comparison of the bands' intensity. These conditions, however, will not allow for an assessment of possible hydrolysis processes going on in the aqueous mixtures: Obviously, DMSO is a favorable ligand that may well bind to platinum itself and thus alter the compound's chromophore.

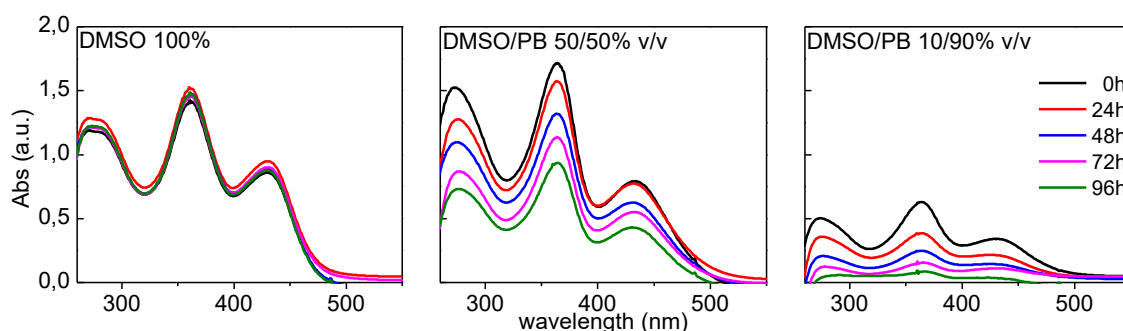


Figure 11 Long-term UV-visible spectra of **34**. 1 mM solutions in the respective solvent combination were kept at r.t. over the period of time. Aliquots were taken periodically and diluted to 100  $\mu$ M in DMSO for measurement.

To monitor the compound's behavior directly in the respective solvent, UV-visible spectra were recorded over the course of 24 h as depicted in Figure 12. Interestingly, some minor spectral changes are observed here even at 100 vol-% DMSO, but to a very low degree. When keeping the solutions in buffered solutions, in addition to effects of precipitation, some variation in the relative band intensity of the bands at ca. 365 and 420-430 nm are observed. Apparently, hydrolysis occurs over time. First spectral evidence for this process is found after ca. 1 h in the spectra recorded from 10 vol-% DMSO solutions in form of a loss of the long-wave bands' intensity. This is accompanied by a slight, gradual blue-shift of the bands' maximum from 413 nm to 409 nm.

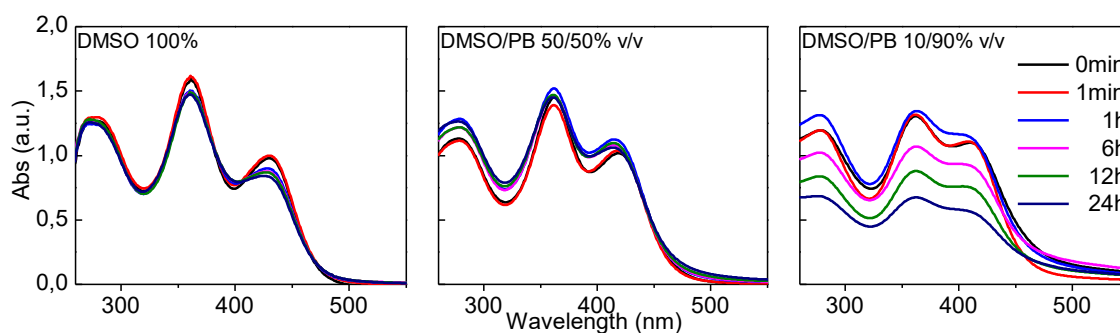


Figure 12 UV-visible spectral development of **34**, dissolved in the indicated solvents, at 100  $\mu\text{M}$  over 24 h. The compound was kept at 100  $\mu\text{M}$  in the respective solvent combination and UV-visible spectra recorded periodically.

It is further interesting to see that the band maximum of the long-wave band at  $t = 0$  is solvent-dependent whilst the other two bands are not: in pure DMSO, the band maximum lies at 430 nm; in 10/90 % v/v DMSO/PB, this maximum is blue-shifted to 413 nm. The other two bands remain fairly stable throughout all experiments. Representative peak data can be found in Table 1.

When the chlorido ligand of compound **34** was abstracted by an excess of silver nitrate, the long-wave band at initially 430 nm experienced a blue-shift of 20 nm towards 410 nm in spectra recorded in pure DMSO (Figure 13). In the spectra recorded in DMSO/H<sub>2</sub>O 50/50 % v/v,<sup>vii</sup> the long-wave band shifts from 418 nm to 410 nm. These results strongly indicate that an exchange of the chlorido ligand results in a shift of the long-wave band, which can be used as an indicator for further UV-vis spectroscopy-based investigations.

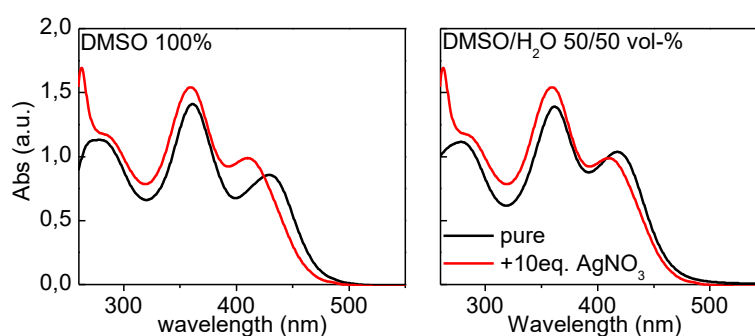


Figure 13 UV-visible spectra of **34** before (black) and after (red) abstraction of the chlorido ligand by AgNO<sub>3</sub>. Precipitation was performed with a 100-fold excess of AgNO<sub>3</sub> (1 M in DMSO) at 1 mM drug concentration, followed by dilution to 100  $\mu\text{M}$  in the respective solvent for spectra recording.

<sup>vii</sup> In this case, the use of PB was impractical due to the formation of Ag<sub>3</sub>PO<sub>4</sub>.

Table 1 Representative UV-visible peak data for compound 34 under different conditions. Wavelengths are given from peak maxima with an accuracy of  $\pm 1$  nm.

Solvent	time / additive	$\lambda_{max}^1$ (nm $\pm 1$ )	$\lambda_{max}^2$ (nm $\pm 1$ )	$\lambda_{max}^3$ (nm $\pm 1$ )
<b>DMSO 100 %</b>	<b>0 h</b>	279	361	430
	<b>24 h</b>	273	360	425
	<b>0 h + AgNO<sub>3</sub></b>	n.o. <sup>a</sup>	360	410
<b>DMSO/PB 50/50 % v/v</b>	<b>0 h</b>	273	363	421
	<b>1 h</b>	274	362	415
	<b>24 h</b>	278	361	414
	<b>0 h + AgNO<sub>3</sub></b>	n.o. <sup>a</sup>	360	410
<b>DMSO/PB 10/90 % v/v</b>	<b>0 h</b>	275	364	413
	<b>1 h</b>	274	366	408
	<b>24 h</b>	274	366	409

<sup>a</sup> n.o. – not observed due to overlay with AgNO<sub>3</sub>-induced signals at short wavelentghs

## 5 BIOLOGICAL ASSAYS

In order to gain insight into the compounds' biological activity, a panel of suitable candidates was selected (Chart 4) and subjected to the resazurin-based PrestoBlue<sup>®</sup> assay. The prepared compounds were tested against a panel of representative cell lines, *i.e.* HeLa (cervical cancer), HT29 (colon carcinoma), MCF7 (female breast cancer), and HEK 293T (kidney) cell lines. The cell lines were incubated with a concentration series of the investigational compounds for 72 h and then their IC<sub>50</sub> values determined from logarithmic regression of the sigmoidal dose-response curves obtained from PrestoBlue<sup>®</sup> assay (*vide infra* for more detailed information).

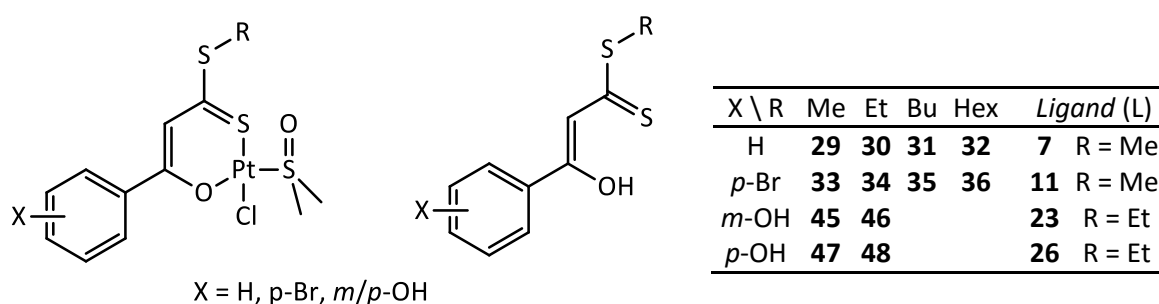


Chart 4 Overview of compounds under investigation for biological assays.

### 5.1 Results of antiproliferative assays

The results of the PrestoBlue<sup>®</sup> assays, executed after 72 h incubation with the platinum compounds, are shown in Table 2 and Figure 14. It can be seen that the determined IC<sub>50</sub> values of the newly synthesized compounds are generally higher than the corresponding reference, Cisplatin (here abbreviated with CDDP). Some further interesting trends can be seen from these studies.

For the unsubstituted compounds **29-32**, a substantial difference in activity is observed for compounds bearing a short alkyl chain (*i.e.*, Me or Et groups), and those bearing longer alkyl chains.

With elongation of the alkyl substituent, the activity against cells is markedly reduced and IC<sub>50</sub> values above 100 μM are obtained.

Curiously, when a *p*-Br substituent is introduced into the same structural motif, compound **36** with R = Hex seems to be the most active compound in this series against all cell lines.

This difference in structure *vs.* activity may be explained through the compounds' differences in lipophilicity, but possibly also by differences in their metabolism. Compounds with less lipophilic character, *i.e.* H/Me or H/Et compounds, may be metabolized more rapidly or easily than the more lipophilic ones, but very lipophilic compounds might preferentially be taken up into the cells by a different pathway, *e.g.* by passive diffusion through the lipophilic cell membrane.

In general, the differences in activity of the single unsubstituted or Br-substituted compounds against the individual cell lines is rather low and no general trend can be deduced from this data, given the high standard deviations of the IC<sub>50</sub> values.

On the contrary, when an OH group is incorporated into the aromatic ring in *meta* or *para* position, marked differences in activity of the resulting complexes are observed. The substances present an antiproliferative activity against HeLa and MCF7 cells, but very low activity against HT29 or 293T HEK cells.<sup>viii</sup>

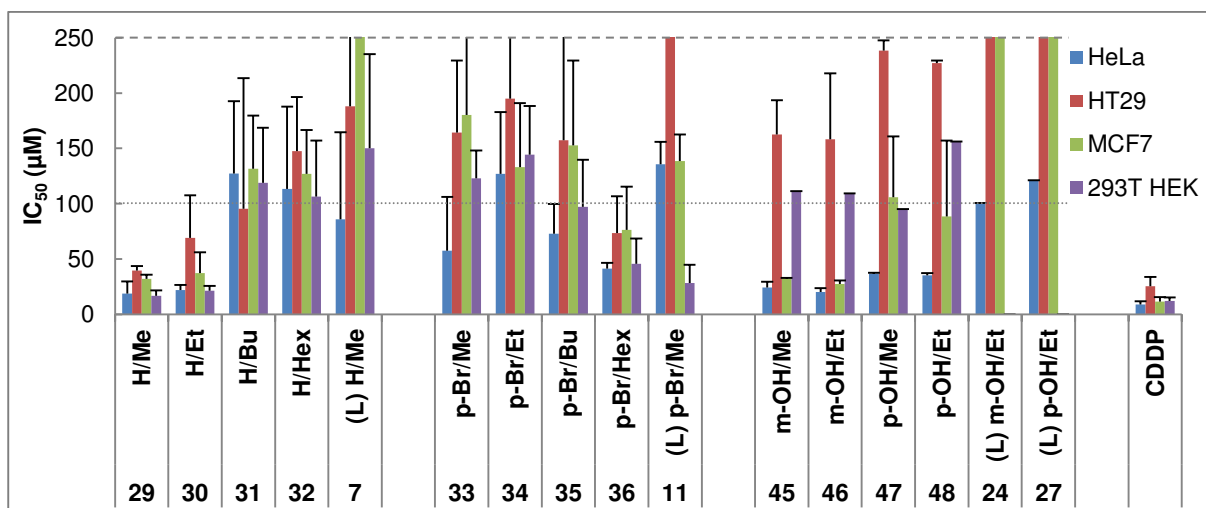


Figure 14 IC<sub>50</sub> values of the Pt(II) compounds and representative ligands against the model cell lines HeLa (blue), HT29 (red), MCF7 (green) and 293T HEK (purple). Compounds with values above 100 μM (dotted line) are considered inactive. Bars crossing the 250 μM scale (dashed line) continue above but are not defined. Error bars are given as biological standard deviation (SD) out of at least two independent experiments.

<sup>viii</sup> The activity of the OH substituted compounds against 293T HEK cells was only assayed once and shall therefore not be discussed in detail.

Table 2 IC<sub>50</sub> values of the compounds under investigation as determined by PrestoBlue® assay. IC<sub>50</sub> values are given as mean out of individual regressions ± biological standard deviation.

Compound			HeLa	HT29	MCF7	293T HEK
Nr.	X	R	IC <sub>50</sub> [μM]	IC <sub>50</sub> [μM]	IC <sub>50</sub> [μM]	IC <sub>50</sub> [μM]
29	H	Me	18.8 ± 11.0	39.5 ± 4.0	31.9 ± 3.8	16.7 ± 4.8
30	H	Et	21.9 ± 4.5	69.1 ± 38.6	37.3 ± 18.8	21.3 ± 4.4
31	H	Bu	127.2 ± 65.5	95.4 ± 118.1	131.5 ± 48.2	118.8 ± 49.7
32	H	Hex	113.2 ± 74.4	147.6 ± 48.7	127.0 ± 39.6	106.3 ± 50.8
7 (L)	H	Me	85.9 ± 78.8	188.2 ± 98.0	>250	150.2 ± 84.9
33	<i>p</i> -Br	Me	57.4 ± 48.7	164.3 ± 65.2	180.3 ± 86.7	122.9 ± 25.3
34	<i>p</i> -Br	Et	127.1 ± 55.6	194.9 ± 82.4	133.2 ± 57.9	144.2 ± 44.0
35	<i>p</i> -Br	Bu	72.9 ± 26.8	157.4 ± 127.4	152.7 ± 76.8	97.1 ± 42.5
36	<i>p</i> -Br	Hex	41.3 ± 5.3	73.3 ± 33.4	76.5 ± 39.0	45.8 ± 22.8
11 (L)	<i>p</i> -Br	Me	135.6 ± 20.4	>250	138.6 ± 23.9	28.3 ± 16.4
45	<i>m</i> -OH	Me	24.3 ± 5.1	162.6 ± 31.1	32.6 ± 0.3	111.2 <sup>a</sup>
46	<i>m</i> -OH	Et	20.3 ± 3.3	158.2 ± 59.7	27.4 ± 3.3	109.3 <sup>a</sup>
47	<i>p</i> -OH	Me	36.7 ± 0.7	238.3 ± 9.3	105.7 ± 55.0	95.2 <sup>a</sup>
48	<i>p</i> -OH	Et	35.3 ± 2.1	227.2 ± 2.2	88.5 ± 68.6	156.2 <sup>a</sup>
24 (L)	<i>m</i> -OH	Et	100.7 <sup>a</sup>	>250	>250	n.d. <sup>b</sup>
27 (L)	<i>p</i> -OH	Et	121.1 <sup>a</sup>	>250	>250	n.d. <sup>b</sup>
CDDP			9.0 ± 2.7	25.4 ± 8.3	11.6 ± 4.0	12.0 ± 3.1

<sup>a</sup> only one reliable value obtained, therefore no biological standard deviation available; <sup>b</sup> n.d. – not determined

Notably, the *meta*-hydroxy complexes **45** and **46** are significantly more active than their *para*-hydroxy counterparts **47** and **48** up to a degree that the *p*-OH compounds can also be considered inactive against MCF7 cells, when taking an IC<sub>50</sub> value of max. 100 μM as a reference. Obviously, introducing an OH group brings forth increased selectivity towards certain cell lines with a marked difference between the two substitution patterns.

To test the activity of the ligands alone, selected reference compounds, *i.e.* the methyl esters of unsubstituted and *p*-Br derived β-hydroxyditiocinnamic acid (**7** resp. **11**) and the ethyl esters of the two OH-derived hydroxyditiocinnamic acids (**24**, **27**) were screened for antiproliferative activity as well. They did show some minor activity, but IC<sub>50</sub> values were generally determined to be above 100 μM and thus no in-depth investigations were conducted on these compounds.

Furthermore, the activity of one bischelate, *i.e.* of **49**, and of the O-TBDMS derived complexes **37**, **38**, **41**, and **42** was also screened. However, the solubility of these compounds in the biological cell culture medium was too low to reliably determine IC<sub>50</sub> values when keeping any influence from an organic solvent at below 2% (data not shown).

## 5.2 Use of DMSO as solvent

It has to be noted that for all the compounds except Cisplatin, DMSO was used as solvent for manufacturing stock solutions.

For compounds that are not well soluble in aqueous medium, it is common practice to use DMSO as initial solvent for stock solutions.<sup>140,155</sup> Still, some drawbacks exist when using this solvent, *e.g.* the occurrence of unwanted side reactions such as ligand exchange<sup>156</sup> or an intrinsic cytotoxic effect of DMSO itself.<sup>157</sup> In the case of the here discussed compounds, the presence of DMSO in stock solutions may even be favorable, because it can actually slow down the solvation process. Nevertheless, stock solutions were always prepared freshly from powder for each assay and the amount of DMSO used was kept at a minimum level. This was achieved by preparing the stock solutions at the highest possible concentrations (min. 10 mM, typically 50 mM) that allowed for the dilution series prepared with the biological cell culture medium to be made without precipitation. More precisely, the amount of DMSO present in all dilutions was max. 1 vol-%, typically lower (0.2 vol-%) at 100  $\mu$ M drug concentration. In separate experiments using only DMSO as additive, cellular activity was found to be only marginally affected by the highest amounts of DMSO present, and thus generally neglected.

In principle, keeping the amount of DMSO constant in every single dilution within an assay is a different approach to equalize the solvent's effect towards the cells at all concentrations. This, however, results in unnecessarily high DMSO concentrations in all samples and might also influence the compounds' hydrolysis behavior. In order to use optimized conditions for all compounds, this approach was therefore evited.

Cisplatin, as reference, was dissolved in phosphate-buffered saline (PBS) to better represent its therapeutic application scheme. The use of DMSO as a solvent for Cisplatin might furthermore lead to various side reactions that could eventually lead to inactivation of the initial drug.<sup>158,159</sup>

## 5.3 Influence of incubation time on antiproliferative activity

In initial experiments on the unsubstituted and *p*-bromo substituted compounds,<sup>118</sup> substantial activity of the (*O,S*) chelate compounds was observed against A549 cell lines upon a short incubation time of 24 h. In an attempt to deeper investigate the compounds' activity against a greater panel of



cell lines and at different time points, further investigations were conducted using the panel of cell lines presented here.

(*O,S*)Pt compounds **33-36**, bearing a bromo substituent at the aromatic moiety, were chosen for a representative time-dependent experiment. Cells were incubated with these drug candidates for 24, 48, and 72 h, and subsequently subjected to the PrestoBlue® assay. Results are summarized in Table 3 and Figure 15. The  $IC_{50}$  values and standard deviations obtained from these experiments are comparably high (many  $IC_{50}$  values are calculated above 100  $\mu\text{M}$ ), so that a precise value comparison is not feasible. However, the cellular response towards the compounds shows an unusual trend: In HeLa and HT29 cells, the compounds seem to be most active after 48 h. After 72 h, the compounds' activity is reduced in HT29 and MCF7 cells (and to some degree in HeLa cells). 293T HEK cells give a cellular response almost as expected, *i.e.* a slightly increased activity with elongated incubation time.

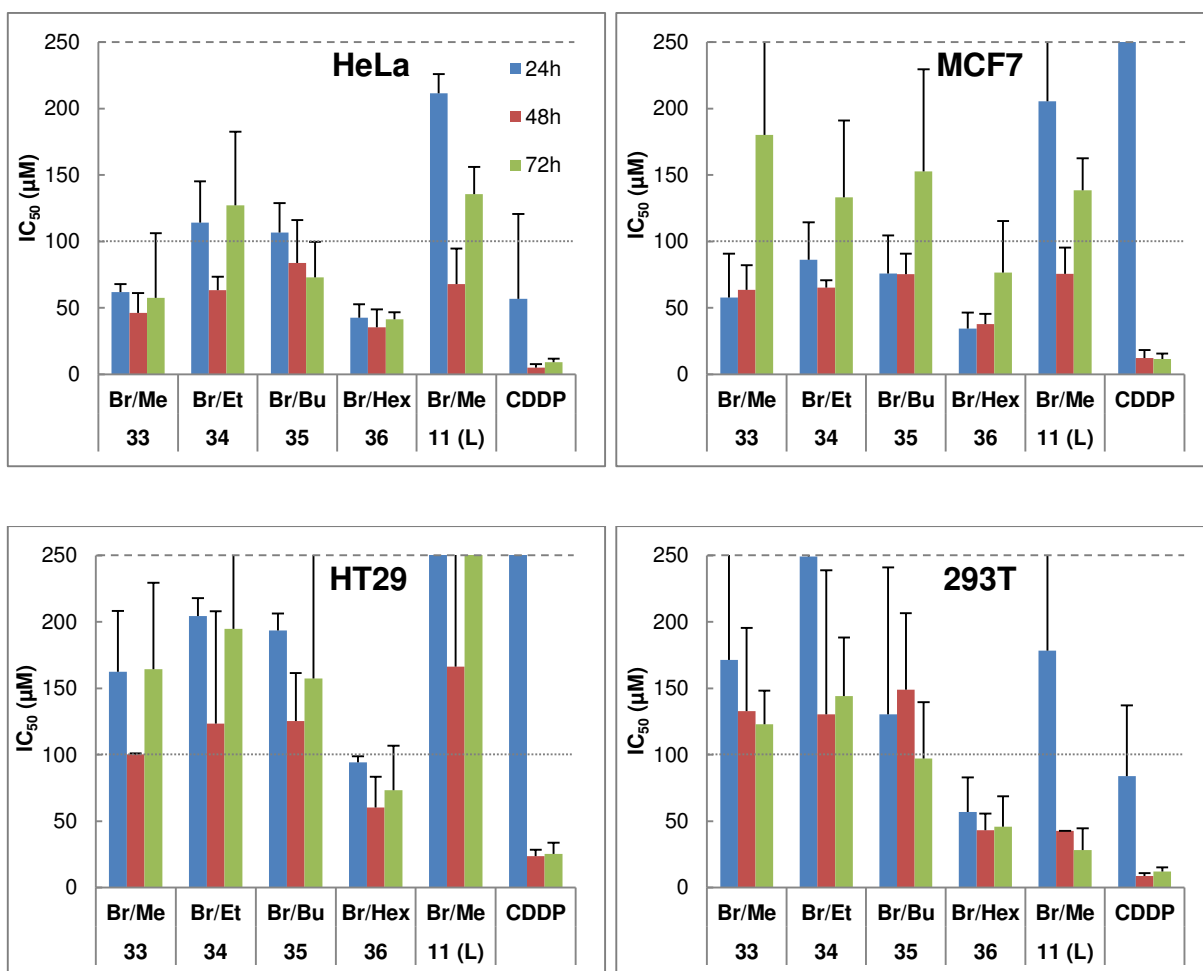


Figure 15  $IC_{50}$  values of Br-substituted compounds and Cisplatin (CDDP) as determined by PrestoBlue® assay after 24 (blue), 48 (red) and 72 h (green bars). Compounds with values above 100  $\mu\text{M}$  (dotted line) are considered inactive. Bars crossing the 250  $\mu\text{M}$  scale (dashed line) continue above but are not defined. Error bars are given as biological standard deviation (SD) out of at least two independent experiments.

Table 3 IC<sub>50</sub> values of the activity of Br substituted compounds against the investigated cell lines. IC<sub>50</sub> values are given as the mean value of at least two experiments ± biological standard deviation out of the individual determinations.

cpd X/R	time	HeLa IC <sub>50</sub> [μM]		HT29 IC <sub>50</sub> [μM]		MCF7 IC <sub>50</sub> [μM]		293T HEK IC <sub>50</sub> [μM]	
<b>33</b> Br/Me	24h	61.8 ±	5.9	162.5 ±	45.8	57.8 ±	33.0	171.3 ±	122.8
	48h	46.2 ±	14.8	100.3 ±	0.6	63.5 ±	18.7	132.9 ±	62.6
	72h	57.4 ±	48.7	164.3 ±	65.2	180.3 ±	86.7	122.9 ±	25.3
<b>34</b> Br/Et	24h	114.1 ±	31.0	204.3 ±	13.6	86.3 ±	28.1	249.3 ±	156.9
	48h	63.4 ±	10.1	123.4 ±	84.7	65.3 ±	5.5	130.3 ±	108.5
	72h	127.1 ±	55.6	194.9 ±	82.4	133.2 ±	57.9	144.2 ±	44.0
<b>35</b> Br/Bu	24h	106.7 ±	22.2	193.6 ±	12.6	75.9 ±	28.7	130.4 ±	110.7
	48h	83.7 ±	32.4	125.3 ±	36.3	75.3 ±	15.4	149.1 ±	57.6
	72h	72.9 ±	26.8	157.4 ±	127.4	152.7 ±	76.8	97.1 ±	42.5
<b>36</b> Br/Hex	24h	42.6 ±	10.1	94.2 ±	4.5	34.4 ±	12.0	56.8 ±	26.1
	48h	35.4 ±	13.4	60.2 ±	23.1	37.6 ±	7.9	43.3 ±	12.5
	72h	41.3 ±	5.3	73.3 ±	33.4	76.5 ±	39.0	45.8 ±	22.8
<b>11 (L)</b> Br/Me	24h	211.4 ±	14.6	>250		205.5 ±	105.4	178.3 ±	131.7
	48h	68.0 ±	26.7	166.3 ±	175.4	75.6 ±	19.7	42.7 <sup>a</sup>	
	72h	135.6 ±	20.4	>250		138.6 ±	23.9	28.3 ±	16.4
<b>CDDP</b>	24h	56.7 ±	63.9	>250		>250		83.9 ±	53.2
	48h	5.0 ±	2.5	23.6 ±	5.0	12.1 ±	6.1	8.6 ±	2.2
	72h	9.0 ±	2.7	25.4 ±	8.3	11.6 ±	4.0	12.0 ±	3.1

<sup>a</sup> only one reliable value obtained, therefore no biological standard deviation available.

In comparison, Cisplatin is least active after 24 h, exerts its highest activity after 48 h and keeps this activity up to 72 h incubation. Remarkably, the IC<sub>50</sub> values after 48 and 72 h are reduced by at least a factor of 10 when compared to their 24 h counterpart in all investigated cell lines. The data obtained for Cisplatin can be well explained by the kinetics of the different hydrolysis and biomolecule binding processes and has been investigated by many researchers.<sup>160</sup>

In general, the compounds' cytotoxic activities are rather comparable over the time scale - albeit generally lower than Cisplatin under the given conditions: As obvious in Figure 15, the order of magnitude of the determined IC<sub>50</sub> values does not change as strongly as for Cisplatin.

For the investigated compounds **33-36** and the ligand **11**, this time-dependent behavior might result from different cellular response processes going on under the influence of these drug candidates. One (unfavorable) effect might be the onset of repair mechanisms, which effectively reduces the compounds' antiproliferative activity.

## 5.4 Fluorescence microscopy

A possibility to visualize the cellular response towards the drug candidates is given by fluorescence microscopy after staining with appropriate fluorescent dyes. For a representative experiment, the m-OH/Et compound **46** was chosen and allowed to react with HeLa and MCF7 cells, followed by staining with 4',6-Diamidin-2-phenylindol (DAPI) and propidium iodide (PI). Their emission was examined using fluorescence microscopy.

DAPI/PI counterstaining is a useful method to easily examine the cells' viability based on morphological features. Both dyes can bind to DNA and produce fluorescence signals at specific wavelengths, which can be excited and detected separately. DAPI is in principle able to penetrate intact cell membranes. It stains virtually all nuclei, living and early apoptotic as well as dead cells.<sup>161-163</sup> PI, on the contrary, stains DNA inside the cell only after loss of membrane integrity. It is therefore only permanent to late apoptotic, necrotic, or dead cells.<sup>164</sup> By selective excitation and detection of both stains and overlaying the resulting micrographs, one is able to distinguish between living/early apoptotic and late apoptotic/necrotic cells.<sup>165-167</sup> The shape of the fluorescent spots can indicate morphologies for the stained cells typical after apoptosis (found as small, round bodies leaving the dish's surface) or necrosis (seen as scattered fragments, swimming cell parts, and indicated by fields of distributed fluorescence through undefined distribution of cellular material in the medium).

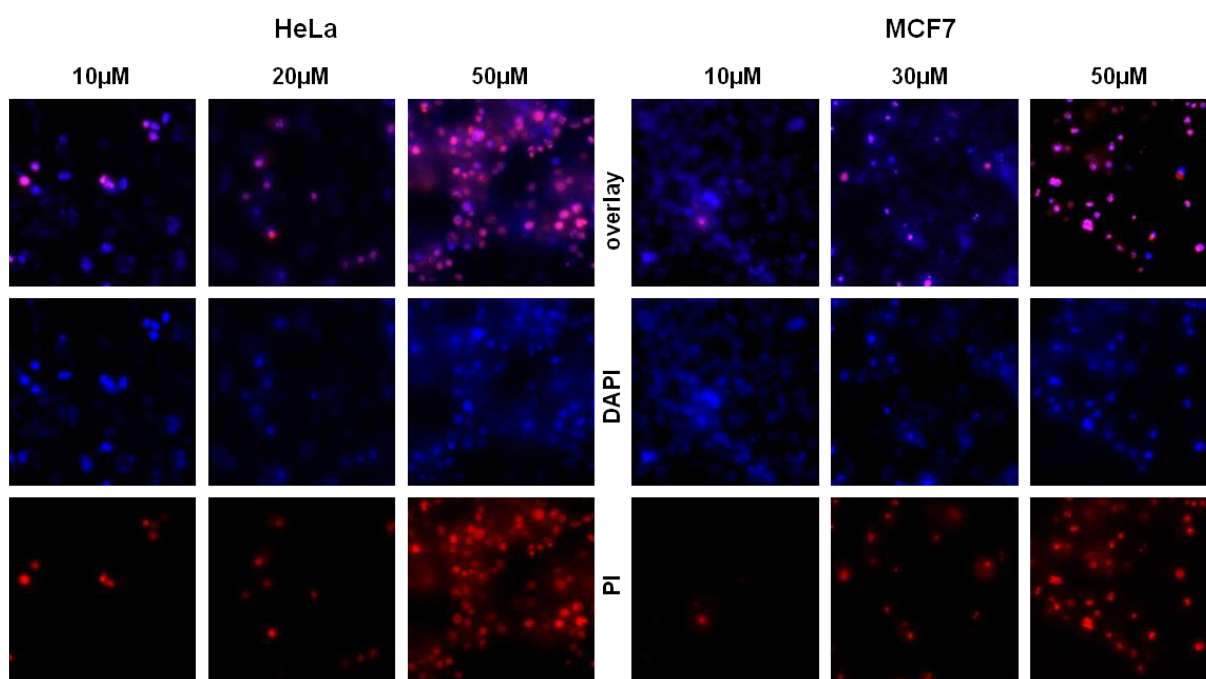


Figure 16 Fluorescence micrographs of HeLa (left) and MCF7 cells (right) exposed to **46** in concentrations below, at, and above the determined  $IC_{50}$  value. Bottom, PI staining; middle, DAPI staining; top, overlay. All pictures were recorded at 200-fold magnification.

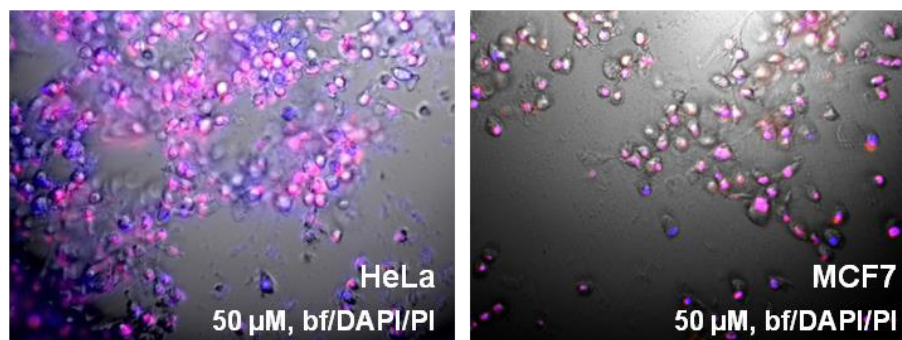


Figure 17 Fluorescence micrographs of HeLa (left) and MCF7 cells (right) at 50  $\mu\text{M}$ . Bright field (bf), DAPI and PI channels are overlaid to demonstrate the aggregates of apoptotic bodies in HeLa cells which may appear as undefined PI staining in fluorescence micrographs. All micrographs were recorded at 200-fold magnification.

HeLa and MCF7 cells were exposed to **46** in concentrations below, at, and above the respective  $\text{IC}_{50}$  value for 72 h and then stained with both dyes. Inspection of the cells by fluorescence microscopy resulted in fluorescence micrographs depicted in Figure 16 and Figure 17.

Both cell lines respond to drug treatment, as can be seen from the formation of condensed nuclei in DAPI-stained pictures in the micrographs of cells below and at the respective  $\text{IC}_{50}$  value. Extensive drug treatment leads to cell death, as visualized by the large number of PI-stained cells at high drug concentration. The earlier mentioned possibility of necrosis was excluded by comparison of the fluorescence images with their bright field (bf) counterpart (Figure 17). The apparently “smeared” labeled DNA in this figure merely originates from the formation of aggregated apoptotic bodies, which cannot be displayed sharply in the short field depth of the microscopic setting needed to visualize staining properly.

It is therefore reasonable to assume that this compound induces substantial cellular reactions in the investigated cell lines, rather inducing apoptosis than necrosis. A further strong indicator for apoptosis induction is provided by activation of the caspase cascade, observed by caspase 3/7 assay, as described in detail elsewhere.<sup>118</sup>

## 5.5 Comparison of assay methods

For the biological assays discussed here, the resazurin-based PrestoBlue<sup>®</sup> assay was used. It is a reliable assay, which monitors the cellular redox potential as a function of viability.<sup>168</sup> Viable cells maintain a reducing environment within their cytosol and lose this environment upon death. Viable cells are therefore able to reduce resazurin to resurofin, whereas dead cells cannot produce

resurofin (Figure 18). The amount of formed resurofin can be monitored quantitatively by absorbance or, more effectively, fluorescence intensity measurements – as was used in this study.

An alternate, well-established assay protocol used in many laboratories investigating metal-based chemotherapeutic agents is the MTT assay. It is based on a colorimetric monitoring of 3-(4,5-dimethylthiazol-2-yl)-2,5-diphenyltetrazolium bromide (MTT) reduction into formazan, which is also only produced in viable cells and accumulates in crystals at the bottom of the assay wells.<sup>169</sup> The factors that determine this reducing environment are manifold and have in the last years been studied and not completely been understood.<sup>170,171</sup>

Generally speaking, both methods reliably produce similar data on cellular viability on various model systems.<sup>172–174</sup> However, the assay protocol used for both assays is substantially different.<sup>175</sup> For the PrestoBlue<sup>®</sup> assay, the protocol used for this work has been established by the supplier, life technologies<sup>™</sup>.<sup>176</sup> On the other hand, the MTT assay protocol, being employed since decades in different laboratories worldwide, has numerous variations and is by far not uniform.<sup>ix</sup> In order to see the effects that these differences may have on the activity data obtained, a one-time representative experiment was carried out by incubating HeLa cells with Cisplatin under the conditions used for PrestoBlue<sup>®</sup> and MTT (internal protocol of Metzler-Nolte and Hahn groups).

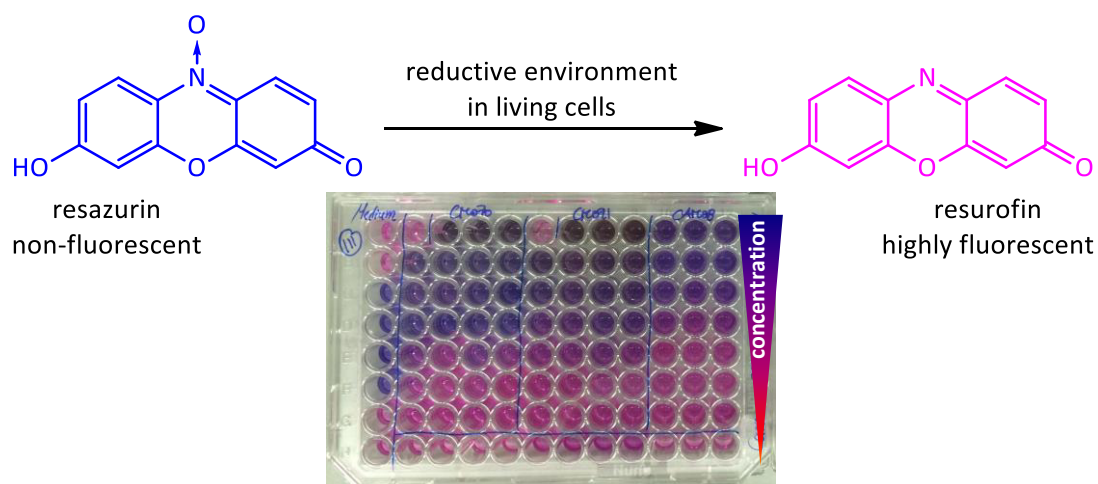


Figure 18 Principle of the resazurin-based PrestoBlue<sup>®</sup> assay. A typical plate protocol of the applied assay is shown with drug concentrations from high (200  $\mu$ M, top rows) to low (1  $\mu$ M, bottom rows).

<sup>ix</sup> A comparison of internal MTT protocols used by *e.g.* the Keppler group (Wien), and the Metzler-Nolte and Hahn groups (Bochum) already surfaces differences in important parameters such as drug incubation volume and incubation time after adding MTT reagent. (Verena Pichler, Wien / Sandra Bobersky, Bochum, private communications)

Different concentrations of Cisplatin in the range of 0.5 to 50  $\mu\text{M}$  were added to HeLa cells and incubated for 48 h; positive and negative controls included. A first substantial difference is the incubation volume: For the PrestoBlue<sup>®</sup> assay, 90  $\mu\text{L}$  drug-containing medium are used, for MTT assay, the final volume is 200  $\mu\text{L}$  at the same concentrations. After 46 h, PrestoBlue<sup>®</sup> reagent was added to the respective wells and after 48 h total incubation time, the cellular viability was read through fluorescence measurement. After these 48 h, MTT reagent solution was also added to the respective wells, the samples incubated for 2 h upon which the medium was removed, the formazan crystals formed by viable cells extracted using DMSO and the absorbance read for the respective wells.

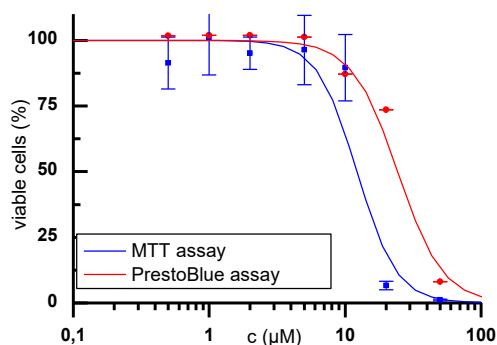


Figure 19 Results of the MTT (blue) and PrestoBlue<sup>®</sup> (red) assays on %viability scale. The regression graphs are for visualization purposes only; regression has been performed from individual values as described in the experimental section.

Data analysis of the obtained results gives some indication on the different outcome that can be obtained just by following different protocols. First, it is obvious that the  $\text{IC}_{50}$  value obtained differs significantly; it is ca. 12  $\mu\text{M}$  for MTT and ca. 26  $\mu\text{M}$  for PrestoBlue<sup>®</sup> assay. This rough doubling of  $\text{IC}_{50}$  values may well be explained by the different volumes of drug-containing medium used in each assay – 200  $\mu\text{L}$  and 90  $\mu\text{L}$  for MTT and PrestoBlue<sup>®</sup>, respectively, resulting in a more than doubled molar amount of substance affecting HeLa cells in the MTT assay protocol. Furthermore, the standard deviation of measurements of each single concentration is substantially higher in MTT assays than it is for PrestoBlue<sup>®</sup>. This may originate from the fact that after incubation with MTT, the medium is decanted from the formazan crystals that have accumulated at the bottom of each well and subsequently the crystals have to be dissolved in DMSO in order to read out the absorbance. Various sources of error are apparent during this process, *e.g.* accidental removal of formazan from the wells or inhomogeneous dissolving of the formazan crystals in DMSO. The process is furthermore more

time-consuming and requires more consumables (solvent, pipette tips, etc) than the PrestoBlue® method – which is albeit more expensive in the initial purchase.<sup>x</sup>

The aim of this short study was not to deeply investigate the effectiveness of either method, determine precise IC<sub>50</sub> values, or judge the methods' applicability. The intention was rather to demonstrate that the experimental conditions strongly affect the outcome of biological assays, even if performed on the same compound, cell line and microwell plate. Both methods have their advantages and disadvantages and can well be used for the assessment of the cytotoxic potential of drug candidates. It has, however, to be strongly emphasized that data obtained from different laboratories or different methods *cannot* be directly compared – it is rather necessary to make use of a standard reference compound towards which a comparison may be conducted and can then enable comparisons of results amongst different experimental settings. The here presented studies use Cisplatin as a reference; a compound which has evolved as the state of the art reference compound in many research scopes investigating metal-based drug candidates.

## 5.6 Possible sources of error

The biological data obtained exhibits quite strong standard deviations, which might necessitate some rationalization.

It is generally accepted amongst scientists that biological assays exhibit large variations due to several factors, such as biological, technical and chemical influences that alter the results of each individual assay.

*Biological* factors may, amongst others, be aging effects of the cells during prolonged passaging, leading to alterations in cellular metabolism and growth. By using cells only up to a certain passage, these effects may be kept low, but can never be evited. Attachment of the cells onto the respective culture or multiwell plate may vary from plate to plate, leading to differences in cellular metabolism. Contamination with bacteria, such as *mycoplasma*, can significantly alter cellular activity and is a common problem in cell culture labs. To circumvent this, antibiotics are generally used as supplement to the cell culture medium (here: Penicillin/Streptomycin), and cells frequently analyzed

---

<sup>x</sup> 100 mL PrestoBlue® assay solution (suitable for the assay of 10 000 wells in a 96-well plate format) cost ca. 330 €, giving a price of ca. 3.3 ct/well. 1 g MTT powder costs ca. 72 € and is suitable for 8 000 wells. When also calculating the price of PBS (ca. 16 €/500 mL) and DMSO (ca. 63 €/1 L), the cost for an MTT assay is at ca. 2.4 ct/well, not considered the need of extra consumables (tips, pipettes) for medium removal and DMSO addition in comparison to the PrestoBlue® assay.

by PCR (polymerase chain reaction) analysis,<sup>177</sup> but contamination can still remain undetected for a certain period of time. Edge growth effects (*i.e.*, different cellular growth on the multiwell plate depending on the wells' position on the plate) can influence the assays' outcome. Here, these effects have been widely avoided by choosing a multiwell plate layout that preferentially places blanks or controls and very high drug concentrations at the plate's outermost positions. The mere choice of supplier and type of all consumables used for cell culture plays another important role in the cellular growth.<sup>xi</sup> Therefore, the consumables (plates, pipettes, containers, etc.) used for the here described assays were kept constant all the time. Such, and other biological factors, contribute most significantly to differences between otherwise identical assays and are the main reason why they are usually repeated in "biological" triplicate.

*Technical* errors may be those produced by pipetting inaccuracies, producing *e.g.* inhomogeneous cell distribution over the entity of the multiwell plate, or leading to deviations in the volume of drug-medium or assay solution being applied. Such errors can be circumvented in most cases by thorough and concentrated working procedures, but may always contribute to the final results. Such errors would often lead to outliers within the replicates produced for each drug concentration and can often be eliminated by outlier detection. Other technical errors, such as variations in the stock solutions' concentrations (and thus all following dilutions), can be caused by weighing or pipetting errors caused by either the analyst or the used devices. Such variations could lead to systematical deviations not necessarily detectable in the experiments' outcome. In order to circumvent such errors, again a most careful working procedure was conducted. Inaccuracies can still not be excluded from any of the experiments, especially since the stock solutions were prepared freshly from powder for each individual assay to prevent long-term storage effects (a possible *chemical* source of error).

The method applied for IC<sub>50</sub> value determination also affects the results. Many different approaches are possible and have been reported in literature, but shall not be discussed in detail here. For regression and IC<sub>50</sub> value determination in the actual work, the procedure is described in detail in the experimental section (chapter 18) and was kept constant throughout all experiments. It should be noted, however, that every IC<sub>50</sub> value determined through regression of the semi-logarithmic growth curves contains a technical standard deviation itself. For the calculation of the biological standard deviation, this SD was generally neglected.

---

<sup>xi</sup> As an example, the IC<sub>50</sub> value of Cisplatin was recently determined on several cell lines, using two different 96-well plates, *i.e.* *ThermoScientific nunc* and *Eppendorf* plates. The determined IC<sub>50</sub> value depended strongly on the used plate. For example, results for MCF7 and HeLa cell lines obtained after 72 h incubation differed in a factor of 2 (MCF7: 1.65 ± 0.72 μM (*nunc*) / 3.12 ± 0.81 μM (*Eppendorf*); HeLa: 4.49 ± 0.89 μM (*nunc*) / 2.57 ± 0.61 μM (*Eppendorf*)). (Sandra Bobersky, RU Bochum, private communication)



Overall, manifold sources of error contribute to the final determinations of  $IC_{50}$  values and their *biological standard deviation*. All values given in this section have been obtained by thorough working procedures to best knowledge and belief and are not manipulated other than as described in the experimental section.



---

# PART B

## INTERACTION WITH BIOMOLECULES

*Partial results of the chapters within this part have been published in the manuscripts listed below:*

*“Novel Platinum(II) Compounds with O,S Bidentate Ligands: Synthesis, Characterization, Antiproliferative Properties and Biomolecular Interactions”, Dalton Transactions **2014**, 43 (8), 3072-3086,*

*Parts appear in chapter 7*

*“Platinum(II) Complexes with O,S Bidentate Ligands: Biophysical Characterization, Antiproliferative Activity and Crystallographic Evidence of Protein Binding”, Inorganic Chemistry **2015**, accepted manuscript,*

*Parts appear in chapter 7*

*“Elucidating the reactivity of Pt(II) complexes with (O,S) bidentate ligands towards DNA using various model systems and analytical techniques”, manuscript in preparation*

*Chapter 8 is part of this manuscript.*

*Incubation with model proteins has been performed by myself, with the exception of mass spectrometry samples **37-48** in combination with cytochrome c. These particular samples were prepared together with Jana Hildebrandt (FSU Jena) during her time as a master student, when she performed a research internship in the laboratory of Prof. Dr. Luigi Messori (Florence) under my instruction and supervision of Prof. Dr. Luigi Messori and Prof. Dr. Wolfgang Weigand. All obtained results have been individually evaluated by myself.*

*Preparation of all DNA-model adducts and data interpretation has been performed by myself.*

*Data acquisition of the ESI mass spectra discussed within these chapters has generally been executed by the mass spectrometer's operator, Elena Michelucci (CISM Florence).*

*X-Ray crystallographic studies on adducts of **46** and **48** with HEWL have been performed by Dr. Antonello Merlino and co-workers (Naples).*

*Oligonucleotide sequences were synthesized by Dr. Domenica Musumeci in the laboratory of Prof. Dr. Daniela Montesarchio (Naples).*



## 6 STUDYING BIOMOLECULE INTERACTIONS WITH ESI MASS SPECTROMETRY

In the last decades, the investigation of drug-biomolecule interaction has attracted growing attention. “Metallomics”, the analysis of metal-biomolecule interactions in particular, has grown to be one of the most useful tools in investigations concerning the mode of action of new metal-drug candidates.<sup>178,179</sup> Such studies can *e.g.* give information on cytotoxic metal compounds’ mode of action, since metal-biomolecule interactions are considered a key factor in both, favorable antiproliferative activities, and also unwanted side effects. At the molecular level, especially mass spectrometry proves to be a versatile and frequently used method to gain valuable insight into such interactions. With the proper experimental setup and in connection with suitable additional techniques to corroborate the data, such as UV-visible (UV-vis) or circular dichroism (CD) spectroscopy, information on metal-biomolecule adducts and also binding sites can be gathered. Mass spectrometry has found widespread application in the investigation of metal-protein as well as metal-nucleic acid interactions by several researchers,<sup>179–183</sup> as described in detail in the following sections.

Electrospray ionization mass spectrometry (ESI MS), coupled to suitable detectors, presents itself as an ideal tool to investigate biomolecules and metals that bind to them. Since it is a “soft” ionization method, protein-coordinated metal fragments can be conserved and obtained as multiply charged ions. In contrast to MALDI-ionization mode (matrix-assisted laser desorption ionization), no matrix is needed and thus a direct detection of the adduct ions under investigation may be afforded.<sup>184</sup> To understand why this is possible, a short introduction into the method is given in the following section.

## 6.1 Electrospray ionization mass spectrometry

### 6.1.1 ESI technique

The electrospray ionization (ESI) technique is one of the most frequently applied ionization techniques when it comes to large molecules, such as biomolecules. Its basic principles in application for mass spectrometry have been developed in the late 1960's by Dole and co-workers,<sup>185</sup> but only the pioneering works by John Fenn and his co-workers, published in the 1980's, made the technique popular and well-accepted in the scientific community.<sup>186,187</sup> For his contributions to "*the development of methods for identification and structure analyses of biological macromolecules*", John B. Fenn was awarded the 2002 Nobel Prize in Chemistry.<sup>188xii</sup>

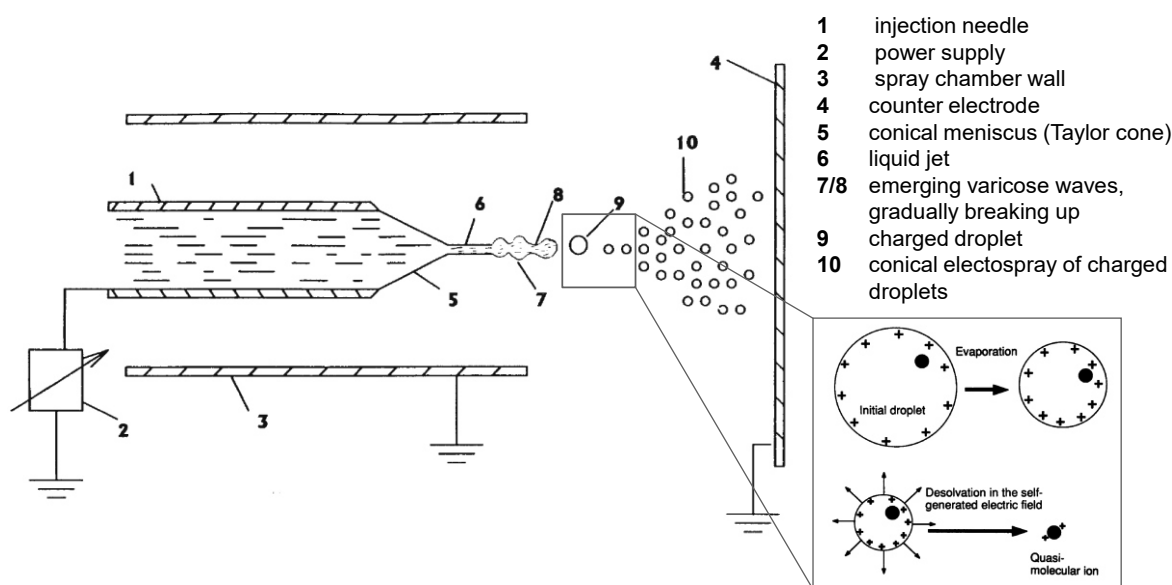


Figure 20 Principle of electrospray ionization. The solubilized analyte is introduced into the injection needle (1) which is maintained at a potential (2) relative to the spray chamber wall (3) and counter electrode (4). Due to the resulting electric double layer at the needle tip, a meniscus (5) forms, resulting in a liquid jet (6). Due to surface tension and viscosity, the liquid forms "varicose waves" (7/8), which eventually cause it to separate into small droplets (9). Due to solvent evaporation and growing coulomb repulsion, these break up further and result in a conical "electrospray" (10). Inset: evolving "quasi-molecular ions" through the electrospray process. Graph derived from literature 187,189.

The technique's principles, as shown in Figure 20, are based on the production of highly charged droplets from solutions of (non-volatile) analytes in volatile solvents due to coulomb repulsion, known as the "Rayleigh instability".<sup>190</sup> First reported by Rayleigh in 1882,<sup>191</sup> this term describes the

<sup>xii</sup> Fenn shared the prize (¼) with Koichi Tanaka (¼), who was rewarded for his development of soft laser desorption (SLD), which later lead to MALDI MS techniques, and with Kurt Wüthrich (½), who received the prize "for his development of nuclear magnetic resonance spectroscopy for determining the three-dimensional structure of biological macromolecules in solution".

processes happening during the evaporation of solvent from a droplet with an electric net charge – induced by the electric field applied to the system. As the droplet becomes smaller, the coulomb repulsion within the droplet increases until it reaches a critical limit, the “Rayleigh limit”, and the repulsion overcomes surface tension. This results in a breaking of the droplet into smaller droplets.<sup>190</sup> This process may be repeated through continuous solvent evaporation until each droplet could contain only one gas-phase molecule which retains some of the droplet’s charge and can then be detected by a suitable mass analyzer.<sup>189,192</sup> The droplet can either be loaded with excess positive or negative charge, depending on the polarization of the electrodes, making the method well- suitable for various applications.

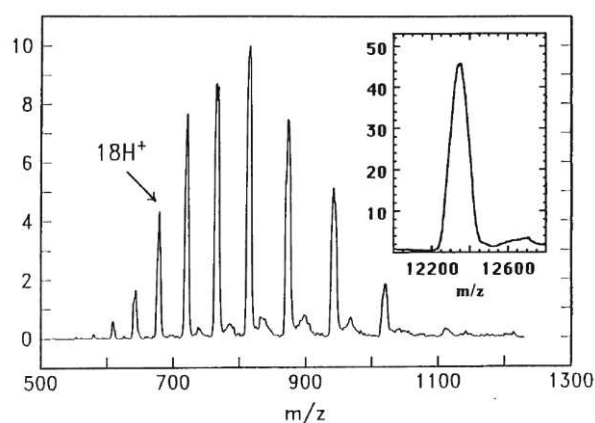


Figure 21 One of the first reported multicharge ESI mass spectra of a whole protein was that of cytochrome c.<sup>187</sup> The deconvolution technique has been successfully applied for the first time to this milestone spectrum.

This principle was fostered by several technical improvements,<sup>189</sup> so that since the first recognized report of mass spectrometry on whole proteins,<sup>187</sup> a vast number of researchers have utilized this technique for various biomolecular research scopes. One major aspect of the technique is the formation of multiply charged ions (cations or anions), which can be transformed (*deconvoluted*) to give averaged signals of the analytes’ relative molecular mass, *i.e.* the  $m/z$  value of a (theoretical) single ion with one massless charge (Figure 21).<sup>187</sup> This bears the great advantage that the mass analyzer only needs to be able to measure  $m/z$  values in a reasonable range, *e.g.* up to 2 000, and still can obtain mass spectra of large biomolecules.

### 6.1.2 The LTQ-Orbitrap device

Given the opportunities to analyze large, multiply charged molecules through the proper ionization method, the analysis method must be able to resolve the complex peak pattern generated by the ions. Nowadays, high-resolution mass spectrometers are available, utilizing different detection techniques. One very recent and powerful mass analyzer is the Orbitrap, allowing for a very high resolution of multicharged mass spectra and a good mass accuracy.<sup>193</sup> The device used for the here presented studies was a *Thermo Finnigan LTQ Orbitrap* mass spectrometer of the type similar to the one depicted in Figure 22.<sup>194</sup>

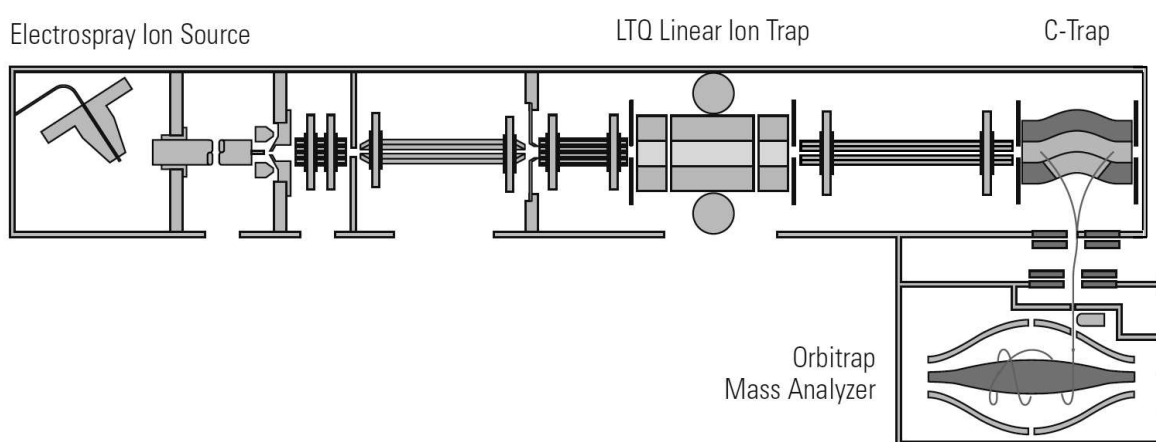


Figure 22 Schematical drawing of an LTQ Orbitrap hybrid FT mass spectrometer from Thermo Scientific. The drawing was modified to meet the used devices' specifications.<sup>194</sup>

The device is basically composed of an ESI source, which introduces the generated ions into a linear ion trap (linear trap quadrupole, LTQ), where they can be subjected to collision-induced ionization (CID) if needed, or directly transferred into the C-trap. The C-trap is a curved radio-frequency only quadrupole ion trap, working as a connection between the ion trap and Orbitrap, where the ions could, in principle, be fragmented further. In the C-trap, the ions are stored and collisionally cooled (through residual nitrogen gas), before they are introduced into the Orbitrap mass analyzer. The detailed working mode of Orbitrap mass analyzers is very complex and has been described in detail by the developers.<sup>195–197</sup> In short, the ions are captured through a rapid increase of the electric field. By introducing ion packets in a slight offset relative to the trap's equator, they gradually spread into thin rings, oscillating along the inner electrode.<sup>195,197</sup> When all ions have entered the trap, the image current from coherent ion packets is detected once the voltage of the inner electrode has been stabilized. The image current is detected at the two halves of the outer electrodes. Signals are amplified and a frequency spectrum is generated through Fourier transformation which is related to



the axial oscillations of the ions along the Orbitrap (equation 2). This frequency spectrum is then converted back into a mass spectrum. Through this method, peak resolutions of up to 100 000 (full-width-half height) are achieved.<sup>196</sup>

axial oscillation frequency

$$\omega = \sqrt{\frac{k}{m/z}}$$

$\omega$  oscillation frequency  
 $k$  instrumental constant  
 $m/z$  mass-to-charge ratio

(2)



## 7 STUDYING METAL-PROTEIN INTERACTIONS

The interactions of various metal-based anticancer agents with proteins have been studied by mass spectrometric techniques in the past, amongst them compounds containing platinum,<sup>198–202</sup> ruthenium,<sup>203,204</sup> or gold.<sup>205–209</sup> Frequently used model proteins for such studies include *e.g.* cytochrome c, lysozyme, albumin, or ubiquitin.<sup>210,211</sup>

To characterize the reactivity of the here discussed platinum compounds with protein targets, their reactions with the model proteins horse heart cytochrome c (cyt c), hen egg white lysozyme (HEWL), and bovine pancreas ribonuclease A (RNase A) were analyzed through ESI MS analysis according to established procedures.<sup>212</sup> Spectral analysis allows determining the nature of the protein-bound metallic species and to define the stoichiometry of the formed adducts. Furthermore, the reactivity of selected compounds towards bovine serum albumin was monitored through inductively coupled plasma optical emission spectrometry (ICP-OES) analysis.

These model proteins were chosen on the basis of several rationales as described below. All proteins have been well-investigated in view of their interaction with platinum-based drugs and some very interesting results have been reported (*cf.* the following sections).

### 7.1 The model proteins

#### 7.1.1 Cytochrome c

Cytochrome c (cyt c, Figure 23) is an electron-carrier protein primarily located in the mitochondria. It is comprised of 104 amino acids in one singular chain. Most of the sequence is identical throughout various vertebrates,<sup>213</sup> which makes it an overall “highly conserved” protein. Cyt c is furthermore found in various plants and microorganisms, such as yeast.<sup>214</sup>

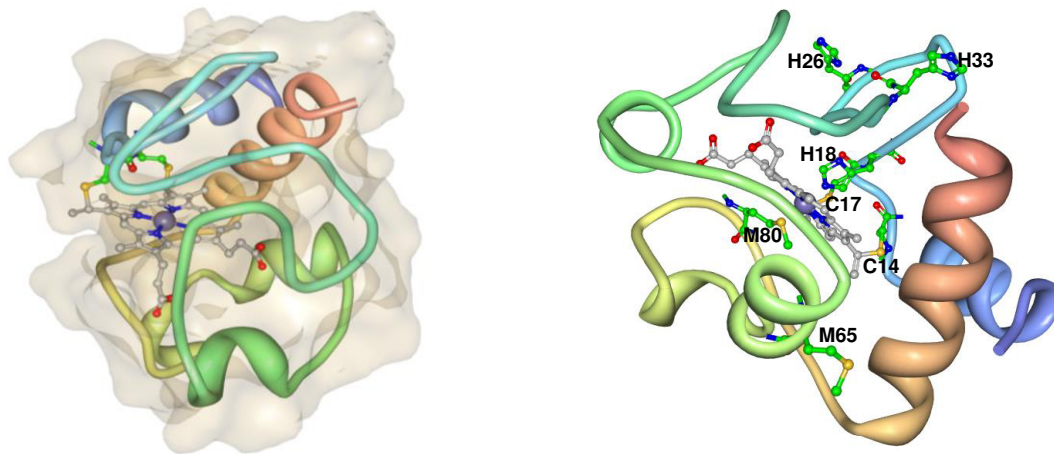


Figure 23 Molecular structure of horse heart cytochrome c, PDB ID: 1HRC.<sup>215</sup> Left, ribbon/band representation with the heme group bound *via* C14 and C17. Right, potential metal binding sites H18, H26, H33, M65 and M80 in the cartoon representation. Graphs were generated with the RCSB PDB protein workshop tool.<sup>216</sup>

The protein carries a heme group which is covalently bound to Cys14 and Cys17. This heme group can interchange between the ferrous ( $\text{Fe}^{\text{II}}$ ) and ferric ( $\text{Fe}^{\text{III}}$ ) state<sup>217,xiii</sup> within the cellular environment and thus enables its function as universal catalyst in cellular respiration: It allows for electron transport between oxygen and respirable substrates such as cytochrome c reductase or cytochrome oxidase.<sup>220</sup>

Moreover, it has been recognized as an important mediator in apoptotic pathways:<sup>221,222</sup> Under proapoptotic conditions, release of cyt c from the intermembrane space of mitochondria into the cytosol can be triggered by proteins of the Bcl-2 family.<sup>xiv</sup> Released cyt c, in course, can then bind to calcium channels (the  $\text{IP}_3$  receptor<sup>xv</sup>) on the outer membrane of the endoplasmic reticulum (ER), resulting in release of  $\text{Ca}^{2+}$  into the cytoplasm and in last consequence, to apoptosis. It furthermore participates in the caspase cascade by association with the apoptotic protease activating factor (Apaf), leading to the formation of the apoptosome complex.<sup>xvi</sup> This leads to downstream activation of caspase 9, which in turn leads to activation of caspases 3 and 7, both hallmark proteases in the apoptotic process.<sup>226,227</sup> The aforementioned release of  $\text{Ca}^{2+}$  from the ER also facilitates activation of caspases 3 and 9, since both processes are Ca-dependent.<sup>228</sup>

<sup>xiii</sup> Unlike other heme proteins like cytochrome P450 or cytochrome c oxidase, which can adapt  $\text{Fe}^{\text{IV}}$  and  $\text{Fe}^{\text{V}}$  oxidation states,<sup>218,219</sup> cyt c only occurs with its heme-iron in oxidation state +II/+III.<sup>217</sup>

<sup>xiv</sup> Bcl-2 proteins play important regulatory roles in cellular apoptosis processes.<sup>223</sup>

<sup>xv</sup> Inositol 1,4,5-trisphosphate ( $\text{IP}_3$ ) is a second messenger that induces the release of  $\text{Ca}^{2+}$  from the endoplasmic reticulum (ER).<sup>224</sup>

<sup>xvi</sup> Apaf-1 oligomerizes in the presence of cytochrome c and dATP to form the very large (700–1400 kDa) apoptosome complex. The apoptosome recruits and processes caspase-9, which in turn recruits and activates the effector caspases.<sup>225</sup>

Due to its ubiquitous abundance and compact size, cyt c is a well-recognized model protein for metal-binding experiments; easily these can be carried out by ESI MS. Preferential binding sites have previously been assigned for Cisplatin and other metallodrugs (Figure 23, right): two methionine sites, Met65 and Met80 as well as three histidine sites, His18, His26 and His33 (Figure 23).<sup>229,230</sup> In earlier studies, Met65, followed by His26 and His33 have been determined to be the most prominent binding sites for Pt drugs since His18 and Met80 are not readily accessible on the protein surface.<sup>199,201,212,231</sup> Recently, the predominant role of Met65 as binding site was also shown in the X-ray structure of a Cisplatin-cyt c adduct; here together with an “assisting” role of Glu residues.<sup>230</sup>

### 7.1.2 Lysozyme

Lysozymes are a class of proteins with glucosaminidase activity, *i.e.* the proteins generally hydrolyze 1,4- $\beta$ -glycosidic bonds of N-actylmuramic acid and N-acetyl-D-glucoseamine residues in peptidoglycans or between N-acetyl-D-glucoseamine residues in chitodextrins.<sup>232,233</sup> It is generally able to degrade bacterial cell walls (through hydrolysis of peptidoglycans) and has been found in various organisms, including birds, humans (in tissues and secretions), various other vertebrates and also invertebrates.<sup>234,235</sup>

Hen egg white lysozyme (HEWL, Figure 24), the protein used for the here presented studies specifically, is a small protein, consisting of a single chain with 129 amino acids and bridged by four S<sup>Cys</sup>-S<sup>Cys</sup> disulfide bridges. Its crystal structure was one of the first whole-peptide structures solved.<sup>236</sup> It is known to crystallize in a number of forms, mainly dependent on the pH and nature of the precipitation salt.<sup>237</sup> This makes lysozyme a well-suitable model protein *e.g.* for crystallography studies.

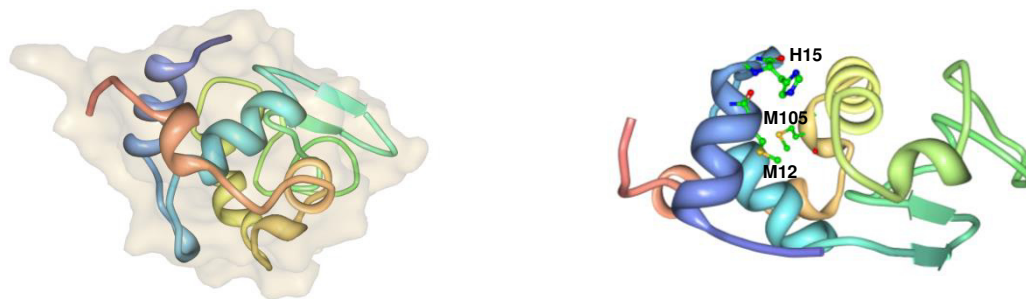


Figure 24 Molecular structure of HEWL, PDB ID: 4J1A.<sup>238</sup> Left, ribbon/band representation with surface structure. Right, potential metal binding sites M12, H15 and M105 in the cartoon representation. Graphs were generated with the RCSB PDB protein workshop tool.<sup>216</sup>

Moreover, it is well-suitable for ESI MS analytic investigation, since ionization occurs well due to the presence of several positively charged groups at its surface. It has, in principle, three possible metal binding sites (Figure 24 right): His15 is the only potential metal-binding site which is located at the surface of the protein. Furthermore, two methionine sites, Met12 and Met105, are theoretically available for metal binding, but difficult to access.<sup>239–241</sup> Thus, a straight-forward interaction pattern is expected in ESI MS spectra of drug-incubated proteins.

Interestingly, in a recent study in the group of Merlino on competitive binding of Cisplatin and Oxaliplatin to HEWL using X-ray crystallography, ESI MS and other methods, two distinct binding positions were found for each metal: Cisplatin was expectedly found at His15, whilst Oxaliplatin was bound to Asp119.<sup>242</sup> Contrary, in a study comparing Cisplatin and Carboplatin, Tanley *et al.* found fragments of both drugs bound to His15.<sup>243</sup>

### 7.1.3 Ribonuclease A

Ribonucleases are a class of nucleases that generally degrade RNA. They can be subdivided into exo- and endonucleases,<sup>xvii</sup> with ribonuclease A (RNase A, Figure 25) being the most prominent representative of the latter type: It is considered as one of the best-investigated proteins of the 20<sup>th</sup> century, with four Nobel prizes being associated with studies on this protein.<sup>244–246</sup> RNase A is found primarily in ruminant pancreas, but RNases in general are abundant also in humans and other mammals and vertebrates in general.<sup>247</sup>

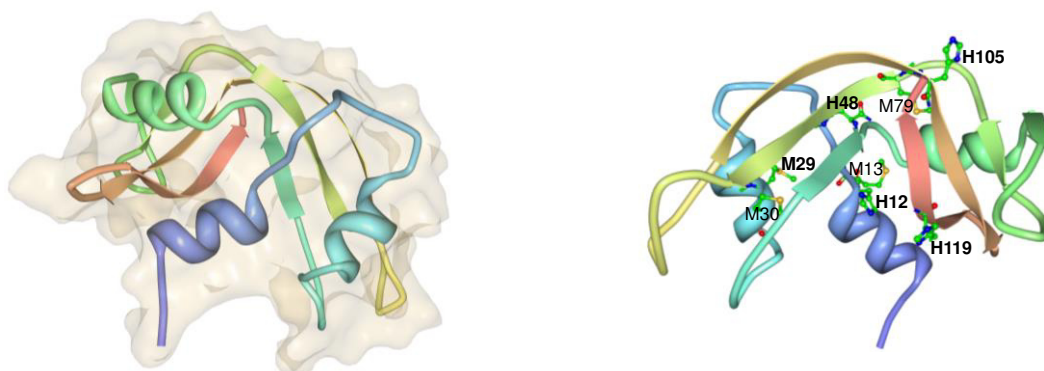


Figure 25 Molecular structure of bovine pancreatic ribonuclease A, PDB ID: 4OT4.<sup>248</sup> Left, ribbon/band representation with surface. Right, potential metal binding methionines and histidines in the cartoon representation. Amino acids that have actually been found involved in metal binding are given in boldface. Graphs were generated with the RCSB PDB protein workshop tool.<sup>216</sup>

<sup>xvii</sup> Exoribonucleases remove terminal nucleotides of RNA, endoribonucleases cleave RNA at internal sites.

RNase A catalyzes the cleavage of the phosphodiester bond between the 5'-ribose of a nucleotide and the phosphate group attached to the 3'-ribose of an adjacent pyrimidine (C or U) nucleotide. This cleavage forms a 2',3'-cyclic phosphate, which is then hydrolyzed to the corresponding 3'-nucleoside phosphate.<sup>249</sup> It consists of 124 amino acids and is stabilized by 4 disulfide bridges,<sup>250</sup> making it a suitable model protein for MS-based or crystallographic investigations of metal-protein adducts.

Recent crystallographic studies of RNase A – metal adducts revealed a high diversity of binding sites depending on the studied compound (Figure 25, right). In some cases, such as a *trans*-amine Pt(II) dichloride,<sup>240</sup> a Au(III)<sup>251</sup> and a Ru(III) compound,<sup>252</sup> metal binding to several histidine side chains (*i.e.* His12, His48, His105, and/or His119) was observed, with His119 being part of the protein active site. Interestingly, the data obtained from crystals of Cisplatin with RNase A revealed selective binding of Cisplatin towards Met29,<sup>248</sup> thus demonstrating its high preference for sulfur donors, even if Cisplatin has been found to preferentially bind histidine side chains in other model proteins, such as cyt c or lysozymes (*vide supra*).

## 7.2 Execution, technical considerations

In order to investigate metal-protein interactions, the compounds were generally incubated with the respective model protein in a 3:1 molecular ratio at 37 °C, using a buffered system (tetramethyl ammonium acetate, TMAA, pH 7.4). After the desired incubation time, the samples were introduced into the ESI source and possible adduct formation monitored from the evolution of peaks assignable to free protein or protein with a metal unit.

After deconvolution, *i.e.* data processing to extract the ion masses from the multicharged spectra,<sup>253</sup>

- a) an assignment of the composition/stoichiometry of formed adducts is possible from the peak position and
- b) an estimation of the amount of Pt being bound towards the protein can be made from comparison of relative peak intensities.

Even though mass spectrometry is not a quantitative method *per se* due to compound-dependent tendencies to ionize, it is still possible to semi-quantitatively characterize metal-protein adducts: In studies where ICP-OES was used for the quantification of platinum-protein adducts, a remarkable correlation was found between peak intensity and adduct quantity.<sup>212,231,239</sup> This may be made

possible by the overall dominant role the biomolecule plays in ionization, which equalizes the ionizability of all compounds to detect in the mixture.

### 7.3 Interaction of selected (O,S)Pt complexes with cytochrome c

Selected Pt(II) compounds were incubated with cyt c for a typical incubation time of 72 h. Representative adduct spectra of S-ethyl compounds **30**, **34**, **41** and **48** are shown in Figure 26, details of the cyt c adducts with **46** are given in Figure 27. All other spectra can be found in supplement B (Figures marked with an S) and supplementary information of the respective manuscript.<sup>118</sup>

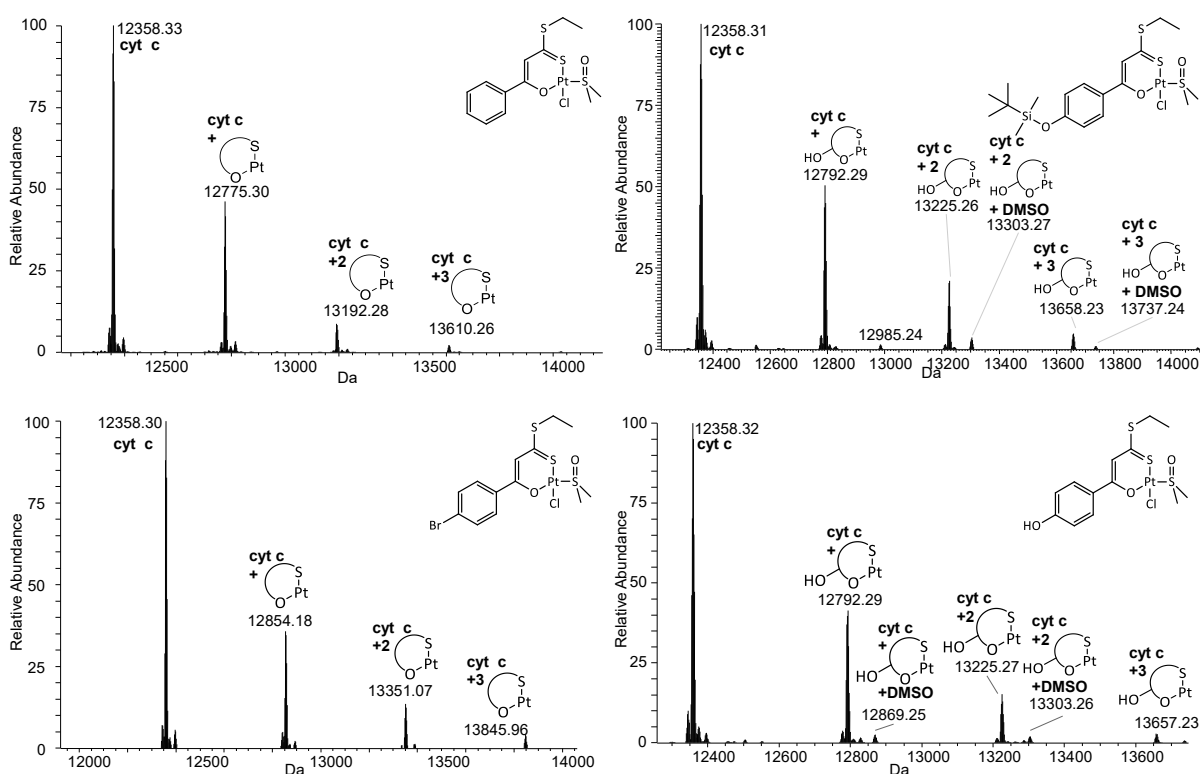


Figure 26 Deconvoluted LTQ-Orbitrap ESI mass spectra of platinum compounds **30** (top left), **34** (bottom left), **41** (top right) and **48** (bottom right) dissolved in 25 mM TMAA buffer, pH 7.4 after 72 h of incubation with cyt c. Protein concentration is 100  $\mu$ M with a metallodrug-protein molar ratio of 3:1 in all cases.

In all spectra, several adduct peaks are witnessed which can be assigned to 1, 2 or 3 (O,S)Pt units bound to the protein. Here, (O,S)Pt refers to the Pt(II) center with the chelating ligand still bound to the metal center. In principle, the adduct stoichiometry is comparable for all depicted compounds, but compound **46**, bearing a *meta*-hydroxy group, seems to bind to protein sites to a larger degree



than the other investigated compounds as seen from the relative peak intensities of free vs. platinated cyt c (Figure 27). In addition, compounds **46** and **48** of the hydroxyl-substituted series show adducts with a DMSO ligand still bound to the (*O,S*)Pt unit, an observation not made with the “H” or “Br” series. For the latter, a good correlation between chain length and adduct formation tendency was found, the S-Me derivative **29** giving the most intense cyt c interaction pattern (up to five (*O,S*)Pt fragments were found at cyt c) and the S-Hex compounds **32** and **36** giving the lowest intensity of adduct peaks (Figure S 1).<sup>118</sup>

When the “precursor” complexes **37**, **38**, **40** and **41**, bearing a O-TBDMS moiety at the aromatic ring, were reacted with cyt c as model protein, the adduct spectra proved protein binding of the complexes, however in all cases the initially applied protecting group was lost and thus confirmed fast hydrolysis of the TBDMS group under physiological conditions (Figure 26, top right, and Figure S 2). These compounds were thus excluded from further testing.

These results indicate that in general, the (*O,S*) moiety is retained with the Pt(II) center, whilst the chlorido ligand is always lost. The fate of the DMSO ligand seems to depend on the substitution pattern of the ligand and the protein binding site.

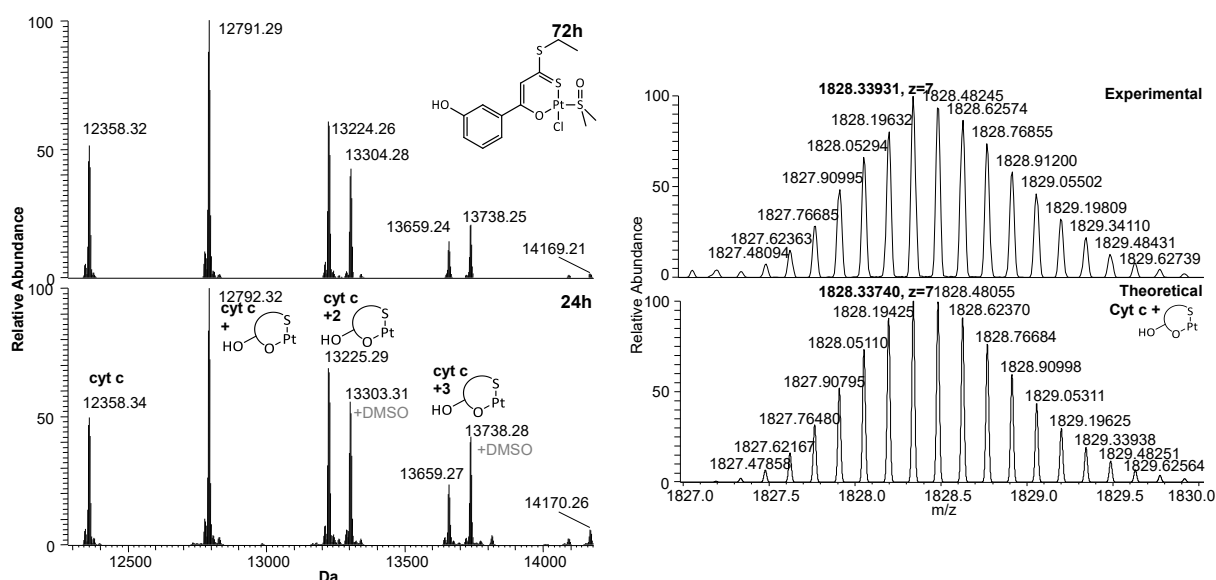


Figure 27 Left, deconvoluted ESI mass spectra of compound **46** after 72 h (top) or 24 h (bottom) hours of incubation with cyt c. Right, comparison of experimental vs. theoretical isotopic pattern of the cyt c-**46** monoadduct at charge state +7.

Some conclusions might be drawn from these observations: Binding of the investigational compounds to the *primary* binding site leads to adducts of the (*O,S*)Pt unit without DMSO in all cases. When two and three Pt units are bound to the protein, two different scenarios emerge for the two

compound series: For the “H” or “Br” complexes, all subsequently binding (O,S)Pt centers can bind to the protein under release of the chlorido and DMSO ligands. For the “OH” series, the second adduct binding to cyt c still contains DMSO whilst the third one seems to resemble another adduct of the (O,S)Pt unit bound after DMSO release, as observed from the fact that only one DMSO molecule is found within the detected adduct. Binding of the (O,S)Pt unit could in principle take place in a bidentate fashion, under assistance of nearby donor atoms such as oxygen or nitrogen of amino acid side chains or the backbone, but the lack of a fourth ligand is not uncommon in Pt(II)-protein adducts.<sup>254,255</sup>

In principle, three amino acid side chains have been identified as most probable Pt(II) binding sites, namely Met65, followed by His26 and His33 (*vide supra*). On the basis of chemical similarity of the binding sites and the resulting coordination environment around Pt(II), one might hypothesize that these findings are an indicator that the two readily available N<sup>His</sup> donors in His26 and His33 represent the first and third binding site, whilst binding to S<sup>Met</sup> in Met65 is not always accompanied by DMSO loss. Most certainly, also contributions of the other possible Pt(II) binding sites, *i.e.* His18 or Met80, are thinkable: In an earlier study concerning the binding of *cis*-bisphosphane platinum(II) dichlorides to cyt c, the histidines H18, H26, H33 were identified as the three primary binding sites.<sup>255</sup> An exact binding mode at defined amino acids can, however, in this case not be determined with certainty by mass spectrometric methods: MS<sup>n</sup> techniques would unequivocally lead to a break of the Pt-DMSO bond, as has been observed in mass spectra with the free compounds. Digestion experiments could also result in fragmentation of the metal adducts bound in monodentate (and thus less stable) fashion.

Experiments with the compounds **45-48** containing a Ph-OH group were also carried out at shorter incubation times, namely 24 h, to elucidate whether this affects the stoichiometry of adduct formation (Figure 27 left, Figure S 3). Almost no difference in the spectral composition in the 24 h vs. 72 h spectra is witnessed; not even when comparing the peak intensities of (cyt c + x(O,S)Pt) vs. (cyt c + x(O,S)Pt(DMSO)) peaks. This indicates that the maximum possible conversion of the metal core with the model protein has occurred within the first 24 hours of incubation and further supports the hypothesis of a defined manner of binding of either (O,S)Pt or (O,S)Pt(DMSO) units towards distinct amino acids.

## 7.5 Interaction of selected (O,S)Pt complexes with lysozyme

Also, incubating the samples with HEWL proved the reactivity of the (O,S)Pt center towards this model protein. Defined adduct formation with one (O,S)Pt unit bound to the intact protein is demonstrated for all compounds, only a very small peak corresponds to a (O,S)Pt-HEWL bisadduct (Figure 28, Figure S 4, Figure S 5). No noteworthy abundance of a (O,S)Pt(DMSO) adduct peak is observed. An apparently less pronounced metalation with respect to cyt c can be well-explained by the fact that in HEWL; less binding sites are available. His15, Met12 and Met105 are in principle able to serve as donors, His15 has been identified as the highly preferred binding site for Cisplatin and analogs earlier, but also a contribution of Asp119 to Oxaliplatin binding has been discussed (*vide supra*).<sup>239–243</sup>

Overall, the reactivity of all investigated complexes towards HEWL is comparable and structural differences lead to almost negligible changes in the intensity of adduct peaks. Furthermore, as demonstrated from 24 and 72 h incubation spectra of compound **46**, elongation of the reaction time to 72 h did not significantly alter the degree of adduct formation (Figure 29).

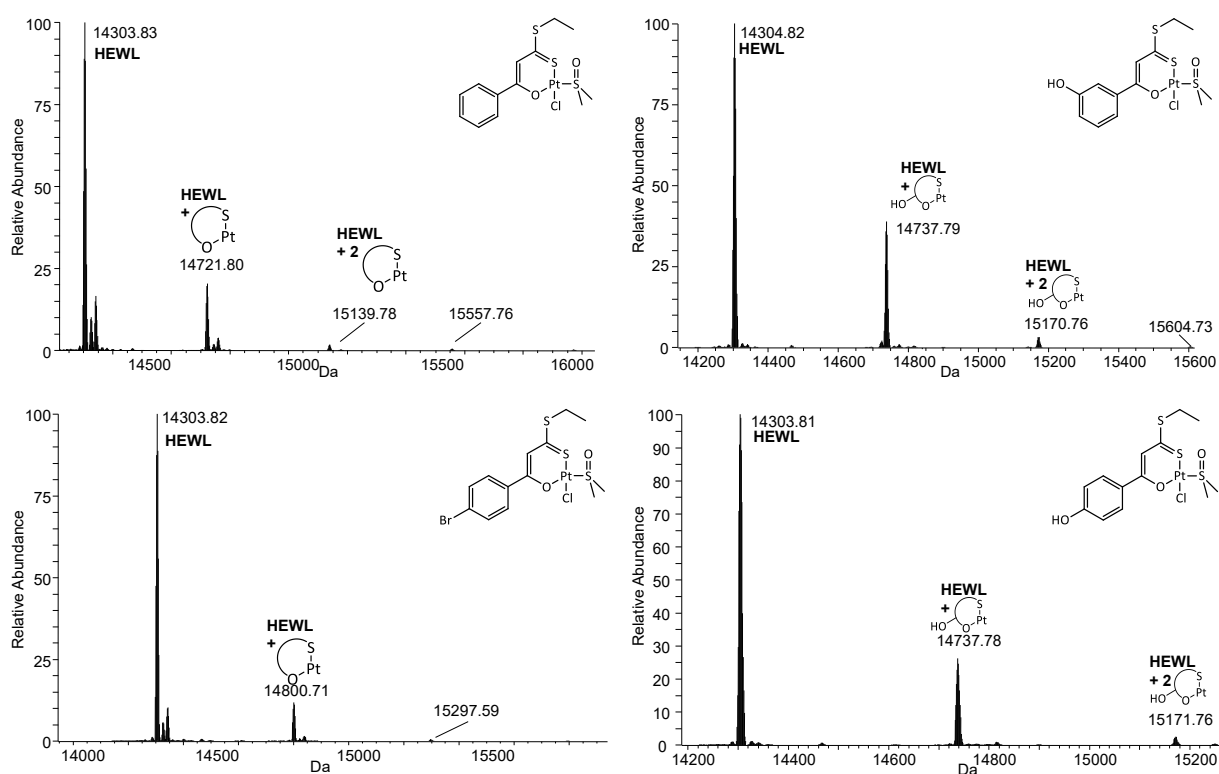


Figure 28 Deconvoluted LTQ-Orbitrap ESI mass spectra of platinum compounds **30** (top left), **34** (bottom left) after 72 h, and of compounds **46** (top right) and **48** (bottom right) after 24 h of incubation with lysozyme. Incubation was performed in 25 mM TMAA buffer, pH 7.4, at a protein concentration of 100  $\mu$ M with a metallodrug-protein molar ratio of 3:1.

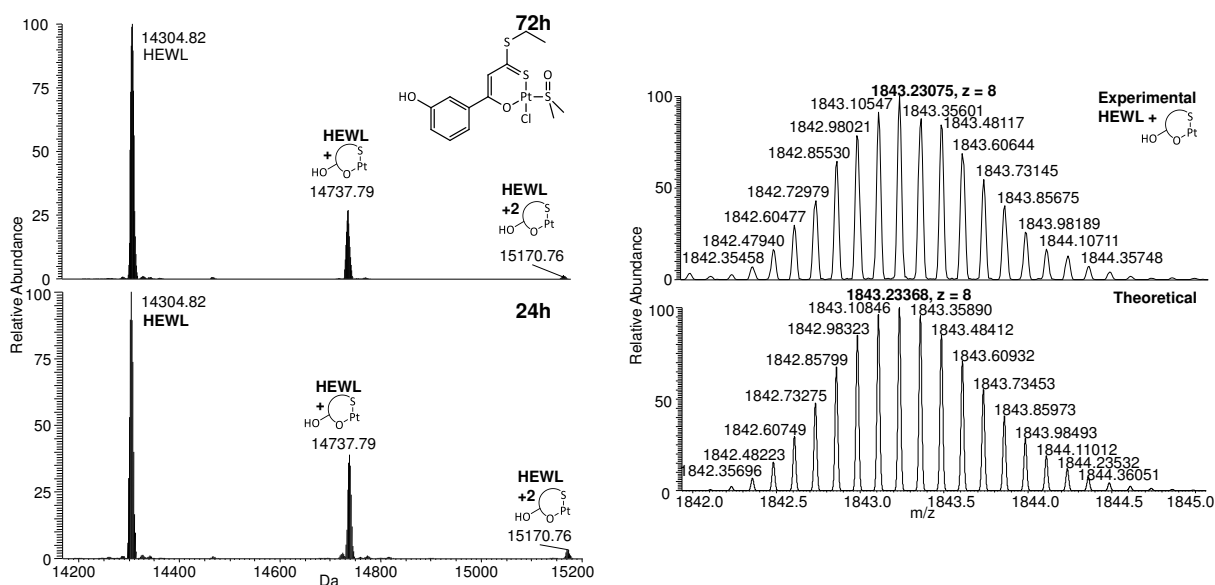


Figure 29 Left, deconvoluted ESI mass spectra of compound **46** after 72 (top) or 24 (bottom) hours of incubation with HEWL. Right, comparison of experimental vs. theoretical isotopic pattern of the HEWL-**46** monoadduct at charge state +8.

In addition to these experiments, crystallization experiments of HEWL with compounds **45** and **46** were performed by Antonello Merlino and co-workers. As a result, molecular structures of HEWL-Pt monoadducts could be solved.<sup>119</sup> The structures obtained unambiguously show the binding of the (O,S)Pt unit under retention of DMSO towards the expected binding site, to ND1 in the side chain of His15. This binding is stabilized by several hydrogen bonds towards the Ph-OH and DMSO units. A detailed discussion on the structural data is given in the respective manuscript.

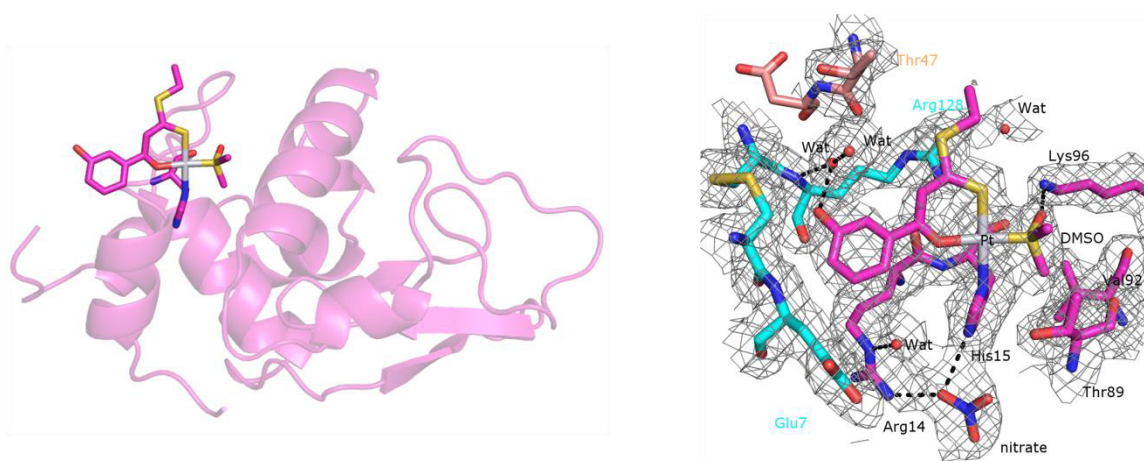


Figure 30 Left, ribbon-and-band representation of HEWL with compound **46** bound to His15 (side chain of His15 and (O,S)Pt(DMSO) unit given in wireframe). Right,  $2F_o - f_c$  electron density map of the binding site in the HEWL-**46** structure with contours given at  $0.6\sigma$  after model building and refinement. Stabilizing hydrogen bonds are depicted through dashed lines.

## 7.6 Interaction of selected (O,S)Pt complexes with ribonuclease A

Adducts of the “OH” compounds **45-48** with bovine pancreatic RNase A further prove the defined interaction of these complexes with model proteins (Figure 31 and Figure S 6, Figure S 7 for simulation). Adducts of RNase A, containing one and two (O,S)Pt units, are witnessed. The reactivity towards RNase A appears to be slightly higher for the *meta*-substituted compounds **45** and **46** than for the *para*-OH compounds **47** and **48**.

Unlike in the case of cyt c or HEWL, a slight increase in the relative signal intensity of adducts formed after 72 h vs. 24 h is witnessed. These findings suggest a slower but progressive binding of one or two (O,S)Pt units towards the model protein. All adduct peaks witnessed originate from metal fragments after loss of both possible leaving groups Cl<sup>-</sup> and DMSO. No higher stoichiometries than bisadducts are observed. These findings again suggest a distinctive selectivity of these compounds for available binding sites. As discussed above, RNase A bears various amino acid side chains which may in principle be available for metal binding. For the here presented compounds, binding to His side chains might be the most reasonable assumption which remains to be clarified in future experiments.

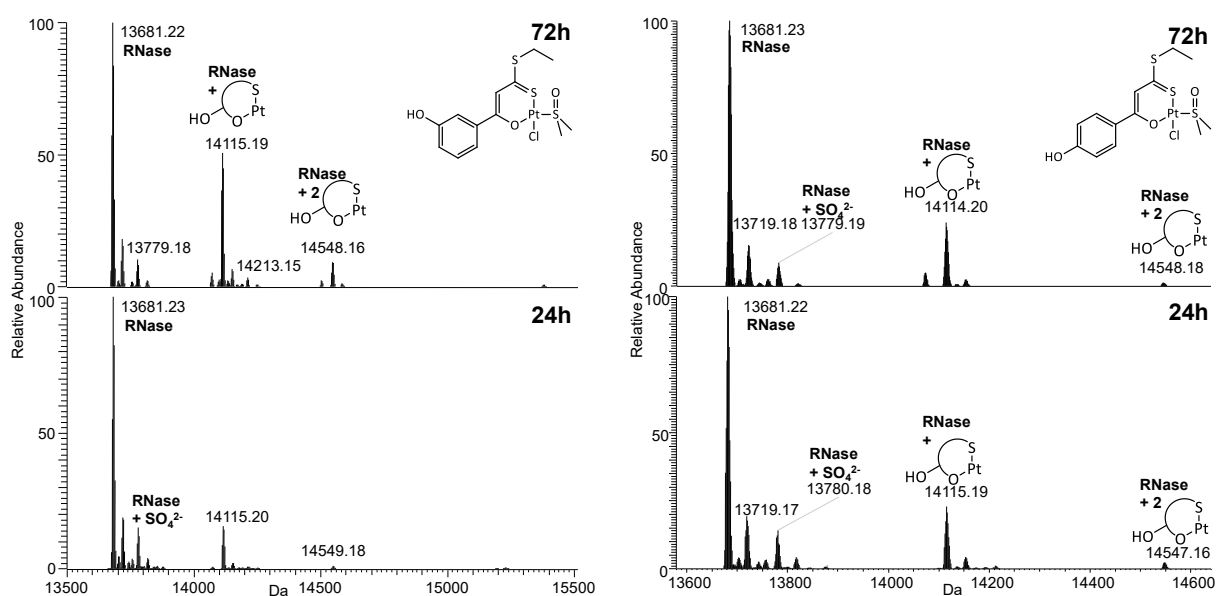


Figure 31 Deconvoluted LTQ-Orbitrap ESI mass spectra of platinum compounds **46** (left) and **48** (right) dissolved in 25 mM TMAA buffer, pH 7.4 after 24 h (bottom) and 72 h (top) of incubation with RNase A. Protein concentration is 10<sup>-4</sup>M with a metallodrug-protein molar ratio of 3:1. Presence of sulfate in the RNase A spectra is intrinsic to the protein and has been observed in other, independent experiments. It does not originate from the actual incubation experiment and was thus neglected.

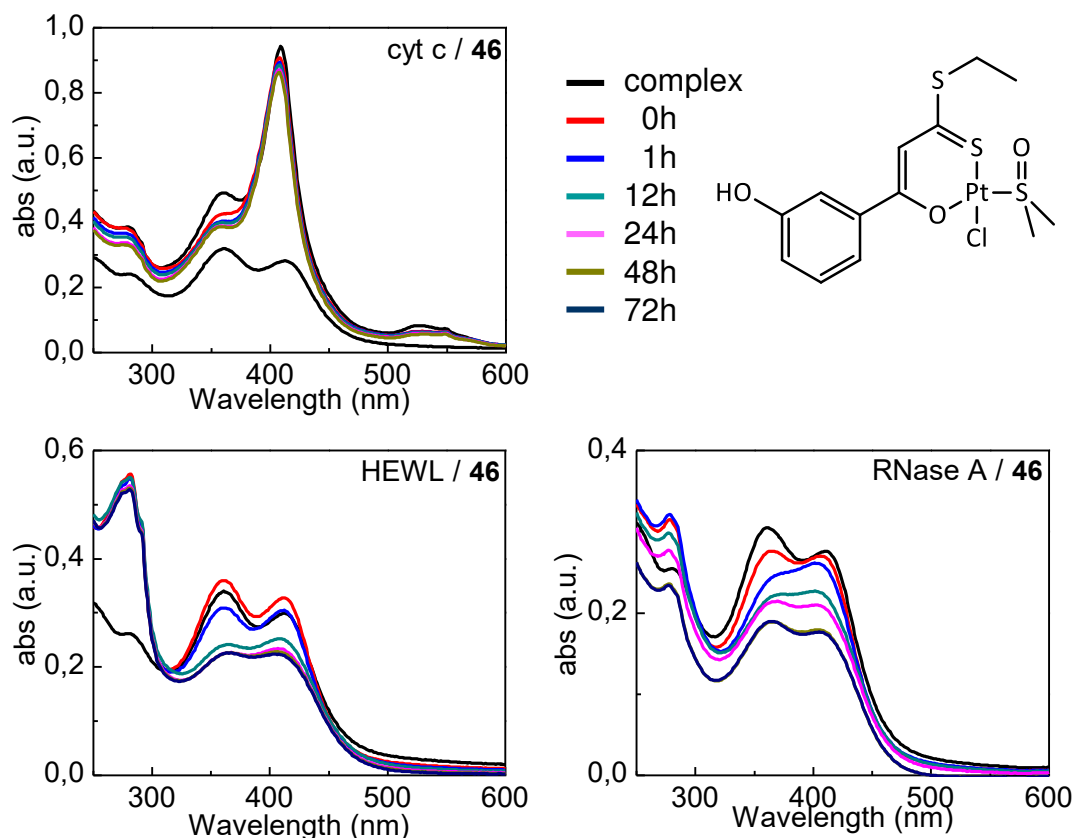


Figure 32 UV-visible time-course spectra of the reaction of compound **46** with the three model proteins over 72 h. Spectra were recorded at a Pt:protein ratio of 3:1;  $c(\text{protein}) = 10 \mu\text{M}$  in TMAA.

## 7.7 UV-visible spectroscopic data

For all described model proteins, analogous binding experiments have been carried out using UV-visible spectroscopy. Representative spectra obtained with compound **46** are given in Figure 32. The so obtained data generally support the observations made by ESI MS experiments through characteristic transformations of the complexes' initial spectral profile. Overall, a similar trend is observed: Bands which are characteristic for the intact  $(O,S)\text{PtCl}(\text{DMSO})$  chromophore gradually lose intensity until they reach a "static" state. When comparing these spectral changes with those observed for the compounds in absence of any biomolecule (*cf.* chapter 4.2), these changes can be attributed to gradual hydrolysis of the chloride ligand and eventually by the DMSO ligand, followed by binding of the respective protein.

The time development of these spectra seems to be in good accordance with the amount and speed of witnessed adduct formation in the ESI data: the conversion seems to be complete after approximately 12 h for the cyt c adduct, after 24 h for HEWL and after about 48 h in the case of the

RNase A adducts. This corroborates the findings of no spectral changes in mass spectra of cyt c or HEWL adducts recorded after 24 h vs. 72 h, and the adduct peak increase for spectra with RNase A.

Through metal binding, the proteins' intrinsic chromophores do not seem to be affected by metal binding. This is an indicator that their overall structure, respective their active center (which gives the predominant signal in the cyt c spectra), is not altered to a large degree and is therefore in good agreement with the ESI measurements, where intact proteins are witnessed rather than protein fragmentation.

## 7.8 Interaction of selected (O,S)Pt complexes with albumin

Furthermore, experiments with H- and *p*-Br substituted compounds were carried out using bovine serum albumin (BSA) as model protein. The binding of numerous drugs towards serum proteins, especially albumin, is well documented.<sup>85</sup> As a consequence of metal-albumin binding, either the concentration of free, available drug which was initially introduced into the blood stream may simply be reduced. Alternately, the protein could serve as a "chaperone"<sup>256,257</sup> to actually aid transportation of the metal-drug towards its final target. Various Cisplatin binding sites towards albumins have been reported.<sup>200,258–260</sup> It is however a rather large protein (of ca. 66 kDa) which is not ideally suited for high-resolution ESI MS of the whole protein. Therefore, experiments with BSA were carried out using ICP-OES as analysis method which gave quantitative feedback on metal-BSA binding. These experiments are in detail discussed in the respective manuscript.<sup>118</sup>

When incubating selected compounds bearing either no or a *p*-Br substituent at the aromatic site with 1 eq. BSA over 96 h, practically complete binding of all added Pt(II) to the protein was found, less than 1 % of unbound Pt was determined.

In addition, detachment experiments, using glutathione (GSH) as competitive ligand, gave no evidence of a release of BSA-bound Pt from the protein. This finding might be considered as a hint that binding of this kind of platinum complexes is not reversible, other than has been discussed for Cisplatin and analogs.<sup>199,211,261</sup>





## 8 STUDYING METAL-DNA INTERACTIONS

It is generally accepted that nuclear DNA is the main therapeutic cellular target of Cisplatin and its analogs. Even though it is today considered that only a small percentage of initially applied Cisplatin reaches this final target and that the level of accumulation is tissue-dependent,<sup>262</sup> the consequences of this biomolecular interaction are crucial for the compound's success as anticancer therapeutic (*cf.* chapter 1.2).

In order to establish the DNA-binding potential of the compounds presented within this thesis, three representative compounds with an S-ethyl group and H or OH substituents, **30**, **46**, and **48** (Chart 5), were selected for an in-depth investigation of their reactivity towards DNA. Two DNA model systems, suitable for investigations through different analytical techniques, were chosen: 9-methylguanine (**9-mg**), and oligonucleotides (**ODNs**). Metallodrug-biomolecule interactions were analyzed through UV-vis and CD spectroscopy, as well as ESI MS methods as described in detail in the respective manuscript.<sup>138</sup> In this chapter, the focus shall be set mainly on the ESI MS based experiments on DNA interaction.

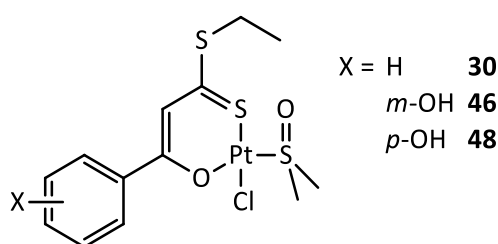


Chart 5 (*O,S*) bidentate Pt(II) complexes used for DNA interaction studies.

## 8.1 Studies on metal-oligonucleotide adducts: recent developments and practical considerations

Several reports exist on MS-based studies of metal-oligonucleotide adducts. Often Na<sup>+</sup> adducts<sup>263</sup> or other alkali/alkaline earth metals<sup>264,265</sup> are investigated, *e.g.* aiming at the elucidation of charge distribution or phosphate backbone binding. Few studies deal with cytotoxic compounds, such as platinum complexes, with the intention to find potential nucleobase binding sites.<sup>266–276</sup> In these studies, different mass spectrometric methods have been applied to obtain information on the metal-ODN composition. Usually, negative ESI in various modifications is used<sup>xviii</sup> (*e.g.* by coupling of the ESI source to LC methods,<sup>267</sup> detecting the signals by FTICR<sup>269–271</sup> or TOF<sup>274,275</sup> detectors or applying different MS<sup>2</sup> ionization methods,<sup>277</sup> including IRMPD<sup>276</sup>), but sometimes also FAB methods,<sup>266</sup> MALDI,<sup>268</sup> or positive ESI<sup>274,278,279</sup> are applied to investigate oligonucleotide adducts.

Especially the use of positive ESI seems quite contradictory since on the one hand, the DNA-binding fragments of Cisplatin and other Pt compounds are expected to bear an intrinsic positive charge. On the other hand, the phosphodiester backbone of DNA is strongly negatively charged. For the biomolecule to become a cation, all phosphodiester groups will need to be protonated up to a neutral state and additional protons will have to bind, eventually, at the nucleobases.<sup>280</sup> In combination with unfavorable effects of the overall charge in the droplets to be ionized, negative ESI methods are suggested to be the superior choice for studying metal-oligonucleotide adducts.<sup>279</sup>

## 8.2 Interaction of compounds 30, 46 and 48 with 9-methylguanine

As a small model for the possible target DNA, 9-methylguanine (**9-mg**) was chosen. It resembles the smallest-possible nucleobase model that still has the binding site which is understood as Cisplatin's preferential binding position at its final target, DNA.<sup>84,86,281</sup> Binding to **9-mg** was monitored with ESI mass spectrometry and with UV-visible spectroscopy. By both methods, the binding of the metal complexes to **9-mg** could be shown.

---

<sup>xviii</sup> Abbreviations in this section: LC – liquid chromatography; FTICR MS – fourier transform ion cyclotron resonance mass spectrometry; IRMPD MS – infrared-multiphoton dissociation mass spectrometry; FAB – fast atom bombardment; MALDI – matrix-assisted laser desorption ionization

### 8.2.1 ESI mass spectrometric data

ESI mass spectra were recorded in positive mode after an incubation period of 24 h or 90 h at 37 °C in a 3:1 metal:nucleobase ratio. The obtained spectra showed that upon platination of **9-mg**, several adducts can be formed. Apart from the signal of free **9-mg** at  $m/z = 166.07$  as dominant peak, two main adduct peaks are observed: those of the  $(O,S)Pt(DMSO)$  and the  $(O,S)Pt$  units bound to one **9-mg** molecule (Figure 33 and Table 4, Figure S 8 for a spectrum of free **9-mg**). In principle, this can be interpreted as monodentate binding of  $(O,S)Pt(DMSO)$  towards  $N^7$  of **9-mg** in the first case, and the formation of a chelate structure between the  $(O,S)Pt$  unit and the  $(N^7,O^6)$  unit of **9-mg** in the second case. Yet, it cannot be ruled out that the latter signals simply originate from the ionization process and not from gradual chelate formation: Frańska recently discussed ESI mass spectra of Pt(II) adducts with DMSO and guanine and found defined DMSO dissociation upon increase of the cone voltage during the ionization process.<sup>282</sup> In combination with the results obtained with oligonucleotides, as discussed below, it is however unlikely that dissociation of DMSO due to the ionization process is the only reason for the appearance of these signals.

In lower abundance, also adduct peaks of the  $(O,S)Pt$  unit and two **9-mg** molecules could be detected in adduct spectra of **30** and **46**. These findings suggest that the here discussed compounds could, under certain circumstances, bind DNA in a comparable manner as Cisplatin and analogs would; namely in a bis-functional manner to give 1,2- or 1,3- intrastrand or interstrand links.

A principal change of spectral composition over time (24 h vs. 90 h) is not observed (Figure 33, left). This is in good accordance with data obtained from UV-vis spectra, which indicate that the reaction reaches equilibrium within the first hour (*vide infra*).

Table 4 Typical ESI MS adduct peaks for the reaction of **30**, **46** and **48** with **9-mg**.

Fragment <sup>a</sup>	<b>30</b>		<b>46</b>	<b>48</b>	<b>46 / 48</b>
	$m/z$ value <sup>b</sup>	calcd. mass <sup>c</sup>	$m/z$ value <sup>b</sup>	$m/z$ value <sup>b</sup>	calcd. mass <sup>c</sup>
$[(O,S)Pt(DMSO)Cl+H]^+$	n.o.	532.98	n.o.	n.o.	547.98
$[(O,S)Pt(9-mg)]^+$	583.05	583.05	599.05	599.05	599.05
$[(O,S)Pt(DMSO)(9-mg)]^+$	661.07	661.07	677.06	677.06	677.06
$[(O,S)Pt(9-mg)_2]^+$	748.12	748.12	764.11	n.o.	764.11
$[9-mg+H]^+$	166.07	166.07	166.07	166.07	166.07

<sup>a</sup>  $(O,S)Pt - Pt(II)$  with the complete  $(O,S)$  bidentate ligand bound; <sup>b</sup> n.o. – not observed; <sup>c</sup> calculated monoisotopic mass

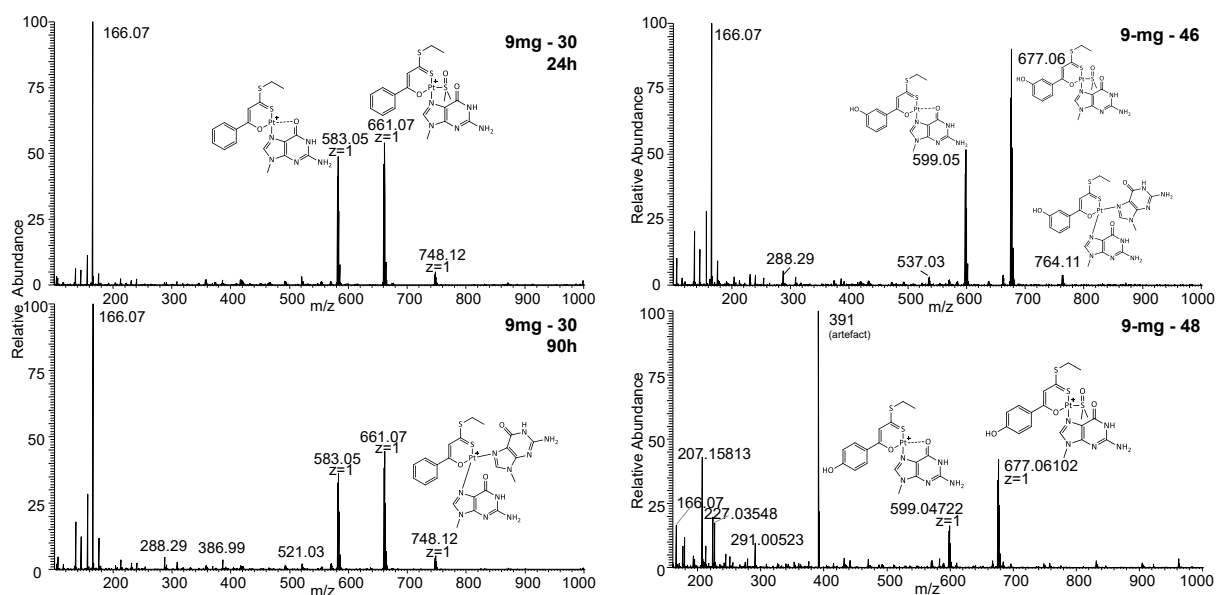


Figure 33 Left, Comparative positive ESI MS spectra of adducts formed between **9-mg** and **30** after incubation for 24 h (top) and 90 h (bottom). Right, spectra of adducts formed between **9-mg** and **46** (top), and **48** (bottom). All spectra were recorded in LC-MS grade water at a 3:1 metal:**9-mg** ratio.

A short note should be given on the incubation conditions. The experiment discussed here was performed in LC-H<sub>2</sub>O instead of in buffered solutions, as would usually be the case. Indeed, experiments were initially performed in ammonium acetate buffer (pH 6.8) in order to represent a more physiological-like environment. In the resulting ESI mass spectra, the same adduct peaks could be found; however the signal intensity was by far decreased under these conditions. Therefore, in order to get a more detailed structural information (*i.e.* on the molecular composition of the adducts), conditions were chosen that allowed to directly obtain signals in an optimal data acquisition setting.

### 8.2.2 UV-visible spectroscopic results

The reaction of the model compounds was also monitored by UV-visible spectrophotometry. Compounds **30** or **46** and **9-mg** were combined in a 1:1 metal:nucleobase ratio in water and the spectral profile recorded at different time points (Figure 34 and Figure S 9). In initial experiments, a screening over 72 h was performed with measurement intervals of 10 min during the first hour. It was found that substantial spectral changes occurred already during the first 10 minutes of the experiment, so that these happenings should be monitored more closely. After shortening the measurement intervals to 30 seconds, two isosbestic points became apparent, indicative of a binuclear reaction such as the substitution of one leaving ligand by **9-mg**. In parallel, the band set at low wavelengths decreases in intensity, which is indicative of a reduction of the amount of free **9-mg**.

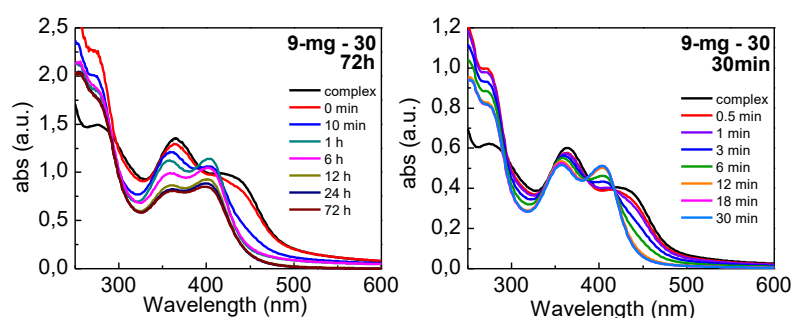


Figure 34 UV-vis spectra of the adduct formation between **30** and **9-mg** ( $c = 50 \mu\text{M}$ , LC-MS  $\text{H}_2\text{O}$ ), recorded without **9-mg** (black line), and after different time intervals up to 72 h (left spectra) and over 30 min in short intervals (right).

It is quite obvious to see that the spectral profiles after 30 min are very similar in both cases of **30** and **46**, as is their time-dependent behavior. For **46**, the band at 403 nm reaches maximum height after ca. 6 min (Figure S 9); for **30** the changes are slightly slower and a maximum height of the 404 nm band seems to be reached after ca. 12 min (Figure 34).

Over the course of the full 72 h, some further spectral changes seem to occur which are less pronounced and overlap with some precipitation of the formed compounds. Wavelengths of the respective absorption maxima are given in Table 5.

The spectral development was also monitored in pure water to compare the compounds' behavior in presence and absence of **9-mg** (Figure 35). It can be clearly seen that without any additives, immediate hydrolysis of the compounds seems to take place, leading to substantial reduction of signal intensity of the long-wave absorption band.

Table 5 Band maxima of the UV-visible spectra of **30** and **46** during the reaction with 1 eq. **9-mg**

Cpd	Time (min)	$\lambda_{max}^1$ (nm)	$\lambda_{max}^2$ (nm) <sup>a</sup>	$\lambda_{max}^3$ (nm)	$\lambda_{max}^4$ (nm)
<b>9-mg</b>		252	275 s	-	-
<b>+ 30</b>	<b>0 / complex</b>	-	-	362	412
	<b>0,5</b>	250	275 s	360	410
	<b>30</b>	254	280 s	356	404
	<b>shift<sup>b</sup></b>	+2	+5	-6	-8
<b>+ 46</b>	<b>0 / complex</b>	-	-	363	420
	<b>0,5</b>	250	275 s	361	414
	<b>30</b>	254	278 s	357	403
	<b>shift<sup>b</sup></b>	+2	+3	-6	-17

<sup>a</sup> s = shoulder; <sup>b</sup> shift reported compared to free **9-mg** ( $\lambda_{max}^{1/2}$ ) resp. **30** or **46** ( $\lambda_{max}^{3/4}$ )

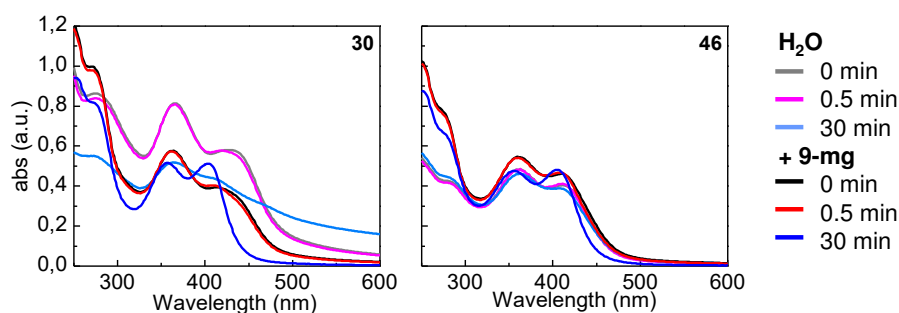


Figure 35 Behavior of **30** (left) and **46** (right) in pure water ( $\text{H}_2\text{O}$ ) and in presence of **9-mg** (intensive-colored lines). Spectra at  $t = 0, 0.5$  min and 30 min are given.

This fast hydrolysis is clearly promoted by the absence of any buffer or other salts, also resulting in a low  $\text{pH}$ ,<sup>xix</sup> which could slow down aquation reactions of the compounds. In contrast, in presence of **9-mg** this band shifts to lower wavelengths and has similar or higher intensity than in the initial spectrum. Together, these data give a good indication that the Pt(II) complexes can react with **9-mg** quickly upon ligand exchange. Both major bands observed in the initial UV-vis spectra are ascribed to the (*O,S*) ligand chromophore bound to Pt(II). As was demonstrated in chapter 4.2, the electronic structure of the (*O,S*) chelating unit and the adjoining moieties are strongly influenced by the nature of the monodentate ligands *trans* to S and O. This is again clearly shown by the here presented data. On the contrary, the free ligand would give a completely different spectral profile (Figure 10) – thus the loss of the bidentate donor molecule can again be ruled out in these investigations.

### 8.3 Selection and preparation of the DNA model systems - Oligonucleotides

The reactivity of compounds **30**, **46** and **48** towards three selected model oligonucleotide sequences was investigated in detail using different spectroscopic (CD, UV-vis) and spectrometric techniques (ESI MS). Results of CD and UV-vis experiments are discussed in detail by Daniela Montesarchio and Domenica Musumenci (University of Naples Federico II).<sup>138,283</sup> The results obtained from mass spectrometric investigations of the interaction with model oligonucleotides are subject of the following chapter.

The choice of oligonucleotide sequences was based on the initial assumption that the DNA binding properties of compounds **30**, **46** and **48** could in principle be similar to those of Cisplatin, which is

<sup>xix</sup> The pH of the used LC-MS grade water was determined to be 3.98.

able to form stable covalent adducts with contiguous guanines in a DNA strand.<sup>281,284–288</sup> Therefore, the following DNA model systems with presence or absence of adjacent guanines (“GG” boxes) have been chosen for the present study (Table 6): a single strand 12-mer oligonucleotide **ODN1**, containing one unit of adjacent guanines in the middle of the sequence; a 12-mer **ODN2**, containing two GG sites at either end of the sequence; and a single strand 24-mer **ODN3** not containing guanines in the sequence. All ODN sequences were synthesized by Domenica Musumeci in solid phase using an automatic DNA synthesizer with the standard phosphoramidite method.<sup>289</sup> For ESI MS studies, representative samples were desalted by dialysis vs. H<sub>2</sub>O and lyophilized.

Table 6 Overview of oligonucleotides (ODNs) used in this study. “GG” boxes are given in boldface.

ODN	sequence	sum formula	M <sub>av</sub> (g/mol) <sup>a</sup>	M <sub>mono</sub> (g/mol) <sup>b</sup>
1	d(5' CCTCT <b>GG</b> TCTCC3')	C <sub>114</sub> H <sub>149</sub> N <sub>36</sub> O <sub>74</sub> P <sub>11</sub>	3548.353	3546.607
2	d(5' <b>GG</b> AGACCAG <b>GG</b> 3')	C <sub>118</sub> H <sub>145</sub> N <sub>56</sub> O <sub>66</sub> P <sub>11</sub>	3744.505	3742.678
3	d(5'TCACACACACACACACACACTT3')	C <sub>229</sub> H <sub>292</sub> N <sub>89</sub> O <sub>135</sub> P <sub>23</sub>	7163.761	7160.260

<sup>a</sup> M<sub>av</sub> – molar mass - average mass, <sup>b</sup> M<sub>mono</sub> – monoisotopic mass

## 8.4 ESI MS studies of free oligonucleotides

First, to establish the measurement conditions for all following experiments, negative ESI mass spectra of the free oligonucleotides were recorded (Figure 36). As medium, LC-MS grade water was chosen in order to reduce oligonucleotide-cation adduct peaks. Such, especially in the presence of sodium, would lead to numerous [M+xNa<sup>+</sup>]<sup>z-</sup> adducts and thus strongly reduce the signal-to-noise ratio in the resulting ESI mass spectra. This was the case *e.g.* in spectra of **ODN3**, where dialysis could not give a completely desalted product (Figure 36, bottom right). Nevertheless, an appreciable signal-to-noise ratio was achieved and experiments on **ODN3**-Pt adduct formation with the model complexes were carried out.

A comparison of theoretical vs. experimental isotopic patterns of the most abundant multicharged peak sets are given in Figure 36, top right, for **ODN1** and Figure S 10 for **ODN2** and **3**. Expected and found masses for the respective oligonucleotide sequences are given in Table 7.

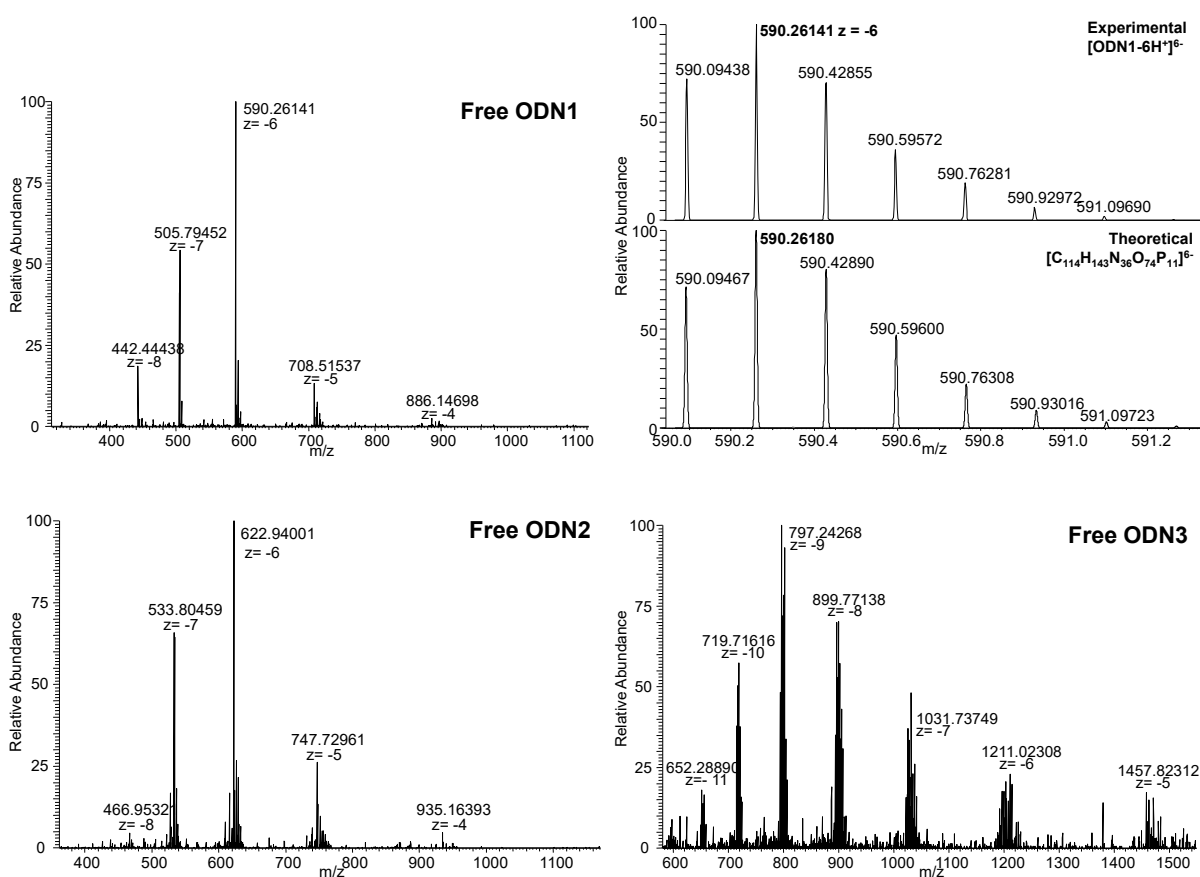


Figure 36 Multicharged negative ESI mass spectra of free **ODN1** (top left) and comparison of theoretical vs. experimental multicharge isotopic patterns at charge state -6 (top right). Bottom, multicharged negative ESI mass spectra of free **ODN2** (left), and **ODN3** (right).

The multicharged spectra of the 12-mers **ODN1** and **2** exhibit signals of the intact ODNs at charge states  $z = -4$  to  $-8$ , with the signal at charge state  $-6$  being the most abundant. Spectra of **ODN3**, owing to the longer sequence, give signals at higher charge states; those at  $z = -5$  to  $-10$  are resolved well enough for charge assignment. For **ODN1** and **2**, only a marginal abundance of sodium adducts was found. In the case of the 24-mer **ODN3**, up to 6  $\text{Na}^+$  ions were found bound to the single strand (Table 7).

#### 8.4.1 Optimization of measurement conditions

Various reports exist describing the use of positive ionization<sup>278,279,274</sup> and also the use of additives such as organic solvents that might facilitate the ionization of the desired molecules. Especially the use of ammonium acetate ( $\text{NH}_4\text{OAc}$ ) buffer was reported in several cases.<sup>267,272,271,274,276</sup>



Table 7 Calculated and observed multicharged peaks of the free oligonucleotides. For **ODN3**, only values of the peak with highest intensity are listed per charge state – multiple signal sets corresponding to different Na<sup>+</sup> adducts are in fact found (signals with maximum intensity given for experimental data).

ODN	<i>m/z</i>							
	-4	-5	-6	-7	-8	-9	-10	
<b>1</b>	calcd <sup>a</sup>	886,14699	708,51562	590,26180	505,79479	442,44453		
	found <sup>b</sup>	886,14698	708,51537	590,26141	505,79452	442,44438	-	-
<b>2</b>	calcd <sup>a</sup>	935,16460	747,72973	622,94023	533,80487	466,95336		
	found <sup>b</sup>	935,16393	747,72961	622,94001	533,80459	466,95321	-	-
<b>3</b>	calcd <sup>a</sup>		1457,82581	1211,02331	1031,73875	899,77243	797,24336	719,71675
	found <sup>b</sup>	-	1457,82312	1211,02308	1031,73749	899,77138	797,24268	719,71616
	x Na		6Na	5Na	3Na	2Na	1Na	2Na

It is discussed that the ammonium ion should substitute all possibly phosphate-bound Na<sup>+</sup> and K<sup>+</sup> cations and then dissociate in the ESI source to release NH<sub>3</sub> and keep the proton residing at the phosphate backbone, thus leading to “cleaner” spectra.<sup>272</sup> In initial experiments to find the optimal experimental setup, oligonucleotide mass spectra were also recorded in ammonium acetate buffer. Albeit the data could be acquired in ammonium acetate, the signal-to-noise ratio was found to be greatly increased when pure water was used (*cf.* Figure S 11 for comparative spectra). The positive effect of slightly reduced Na<sup>+</sup> adduct abundance in spectra of **ODN3** could not compensate the overall low signal-to-noise ratio under these conditions. However, ionization had to be enhanced by adding 50 vol-% MeOH to solutions of **ODN3** directly prior to measurement to acquire a suitable spectrum (Figure 36, bottom). For all experiments except for this singular spectrum, water without any additives was used and the same sample preparation and measurement conditions throughout the experiments were applied.

## 8.5 ESI MS of ODN-platinum adducts

After these initial experiments, conversion with the Pt(II) compounds was pursued. The oligonucleotide sequences were incubated with Pt(II) complexes in a 1:1 and a 3:1 metal:oligonucleotide ratio in water for 24 h and also in a 3:1 ratio for 72 h. Adduct formation was investigated with negative ESI mass spectrometry. Representative results can be seen in Figure 37 and Figure 38, isotopic patterns and detailed peak data can be found in Supplement C.

### 8.5.1 General observations

After 24 h of incubation, Pt-ODN adduct peaks can be observed that correspond to monoadducts with **ODN1**, alongside with free **ODN1** (Figure 37 left). An increased metal:protein ratio also favors the presence of bis- and triple adducts being formed, but unplatinated **ODN1** still is a dominant species (Figure 37 right).

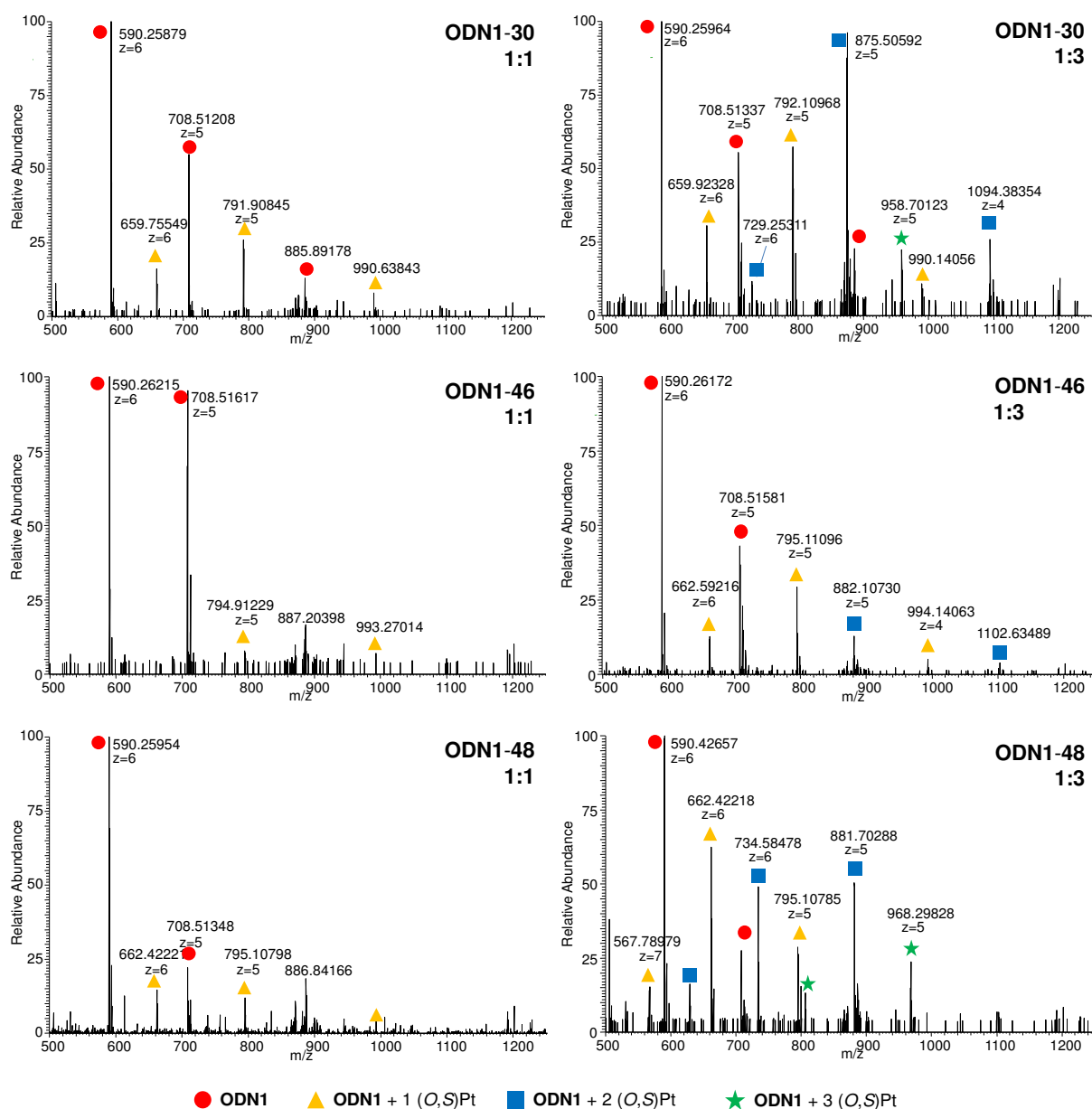


Figure 37. Multicharged negative ESI mass spectra of **1** after incubation with **1** (left) and **3** (right) equivalents of compound **30** (top), **46** (middle) and **48** (bottom) for 24 h at 37 °C. Z values are generally negative.

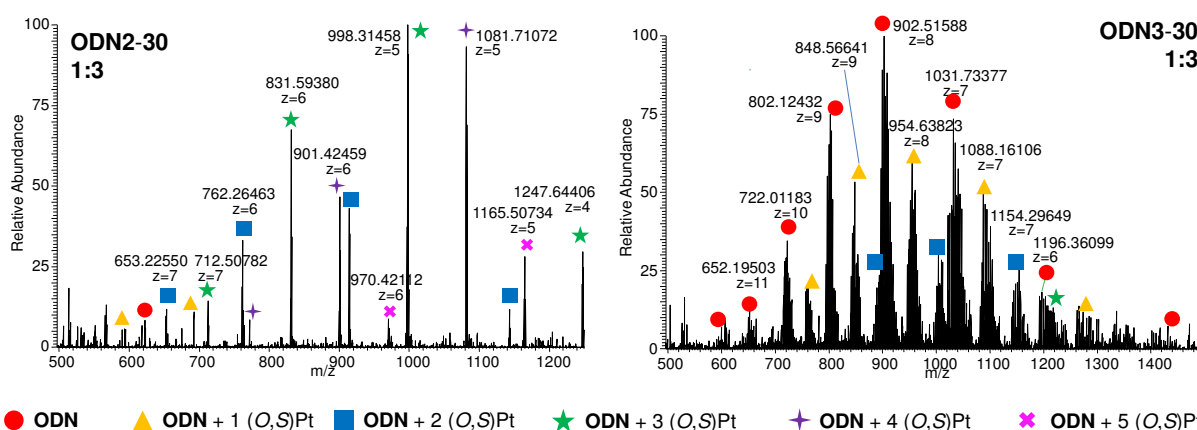


Figure 38 Multicharged negative ESI mass spectra of **ODN2** (left) and **ODN3** (right) after incubation with 3 equivalents of **30** for 24 h at 37 °C. Z values are generally negative.

For the base-complementary strand **ODN2**, bearing two “GG” boxes and thus a greater number of G and GG binding sites, also a significant abundance of higher adduct stoichiometries can be found (Figure 38 left and Figure S 12).

For **ODN3**, having no guanine residues and thus no favorable binding site, platinum adducts are found as well (Figure 38 right and Figure S 12). This indicates that also different binding sites than G are possible for this type of Pt(II) compounds. Binding of the compounds towards **ODN3** has also been witnessed in CD and UV experiments.<sup>138</sup> Overall, **ODN3** still proved to be the least reactive towards the three model Pt(II) compounds discussed here. As expected, the absence of the conceivably favored binding site G considerably reduces adduct formation. Adenine (A) most probably serves as alternative binding site, in analogy to findings for Cisplatin or other drug candidates – but cytosine (C) and after deprotonation of NH even thymine (T) may as well allow Pt binding (*cf.* Figure 5).<sup>290</sup>

As a general observation, signals assigned to platinated ODNs mostly display their peaks with highest intensity at lower charges than those observed for the free ODNs. This is in good accordance with the theory that the (O,S)Pt fragment, after loss of Cl<sup>-</sup> and DMSO, is a monocharged cation which contributes to an overall reduction of the observed adduct ions’ net charge.

### 8.5.2 Comparison of the compounds’ reactivity

In accordance with results from CD and UV-vis data,<sup>138</sup> the reactivity of the unsubstituted compound **30** towards the ODNs appears to be generally higher than that of **46** or **48** with a hydroxy group. Compound **30** is even able to coordinate five (O,S)Pt units towards **ODN2**, which is the highest observed stoichiometry in these experiments. Compounds **46** and **48** seem to have a similar

reactivity towards this sequence with a low abundance of four (*O,S*)Pt units bound (Table S 12). On the contrary, **48** seems to be the most reactive complex towards the 24-mer **ODN3** – up to 4 (*O,S*)Pt units were detected in **ODN3-48** adduct spectra, the same samples with compounds **30** and **46** exhibited a maximum of triple adducts (Table S 13 - Table S 15).

### 8.5.3 Influence of incubation time

When **ODN1** was allowed to react with the metal salts **30** and **46** for a longer time, *i.e.* 72 h, also multiple adducts are found (Figure 39) and unplatinated ODNs are not observed anymore. This again indicates that alternative binding modes, *e.g.* on the phosphate backbone or at C and T bases are in general thinkable. It is however unlikely that these serve as primary binding sites. In that case, a less defined interaction pattern would be observed in adducts with **ODN1** at lower incubation ratio and time.

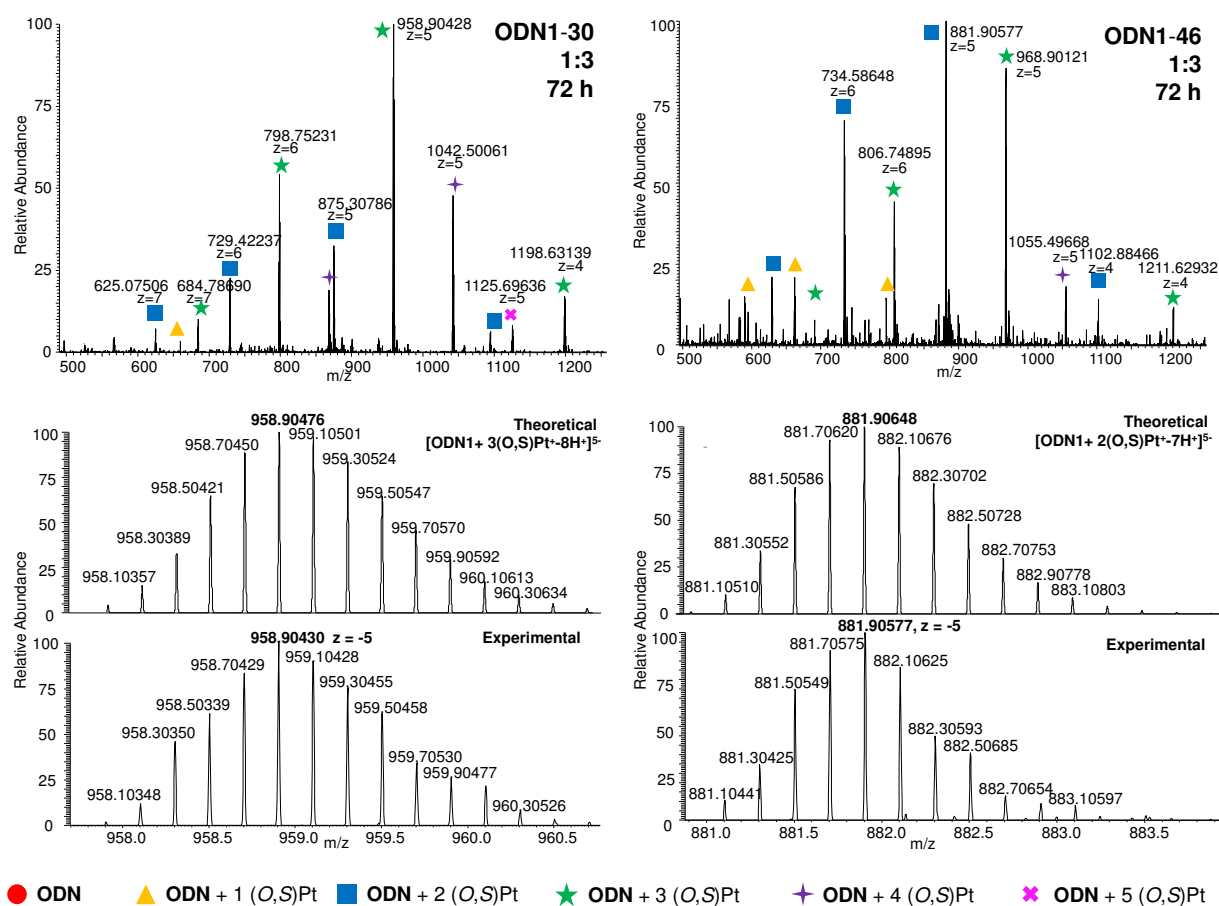


Figure 39 Top, multicharged spectra of **ODN1** incubated with **30** (left) and **46** (right) in a 3:1 metal:ODN ratio for 72 h. Z values are generally negative. Below, comparison of the theoretical vs. experimental multicharge peaks of the **ODN1-30** triple adduct (left) and **ODN1-46** bisadduct (right), both at charge state -5.

Rather could gradual C binding be envisioned with cytosine-N<sup>3</sup> as another potential platinum binding site. It generally has to be kept in mind that the experimental setup provides the oligonucleotide target with a stoichiometric excess (3 eq.) of metallodrug over **ODN1**, which is necessary for the measurement conditions of this proof-of principle experiment. In an actual cellular environment, the ratio of platinum over nucleobase is expected to be much lower: In a recent study by Groessl and co-workers, the concentration of metallated DNA of A2780 cells after treatment with Cisplatin at IC<sub>50</sub> for 24 h was determined to be about 2 nmol/mg DNA.<sup>291</sup>

## 8.6 MS<sup>2</sup> Experiments of ODN1-platinum adducts

For a more precise insight into the binding position of the metal fragments, MS<sup>2</sup> experiments were performed on selected adducts formed with **ODN1**.

### 8.6.1 Typical fragmentation pathways – fragmentation of unplatinated ODN1

First, MS<sup>2</sup> experiments were conducted on free **ODN1** to build a reference library of fragment peaks. The most abundant multicharge peak set was selected for collision-induced dissociation (CID) experiments, *i.e.* the  $z = -6$  signal at  $m/z = 590$  (Figure 41, top). Signal assignment was performed by comparison with theoretical fragmentation data using the web-based Mongo Oligo Mass calculator.<sup>292</sup> Theoretical and identified fragment signals are summarized in Table S 16.

CID ionization of the full strand of **ODN1** at charge state -6 yielded all typical types of fragmentation known for nucleotide strands, *i.e.*  $a_n$ - $B_n$ ,  $w_n$  and  $y_n$  fragments<sup>293</sup> of nearly all positions  $n$  (Figure 41).<sup>xx</sup> Their origin is schematically depicted in Figure 40.  $[a_n-B_n]^x$  ions derive from elimination of the respective nucleobase  $B_n$ , followed by strand breaking at the corresponding 3' C<sup>ribose</sup>-O<sup>phosphate</sup> site  $a_n$ . This in turn results in a further elimination reaction which finally results in a furan ring at the 3'-terminal ribose  $n$ .<sup>294</sup> They thus give fragments of the intact 5' end of the oligonucleotide under investigation.  $[w_n]^x$  ions give information on the intact 3' end of the sequence. They are considered as the complimentary fragments to  $a_n$ - $B_n$  fragments since it is discussed that base elimination is the initial step of CID-induced oligonucleotide fragmentation. Thus, often both types of fragments are observed that originate from strand breaks at the same position.<sup>295,296</sup> At low  $m/z$  ratios (which have

---

<sup>xx</sup> Negative charges of all discussed peaks originate from the loss of a defined number of H<sup>+</sup> ions, typically from Phosphate groups, in the respective fragments. For the sake of better readability, these proton abstractions are not explicitly noted in the discussion of such peaks and will only be given in detailed calculations or where needed for better understanding of the signals.

not been considered here), also ions of the eliminated bases can usually be detected as [B-H]<sup>+</sup>. Further typical fragmentation pathways lead to  $\gamma_n$ -type fragments which occur after strand breaks from the intact 3' end of the oligomer at the P-O bond next to the 5' end of ribose.<sup>297</sup> Interestingly, corresponding  $c_n$  fragments are not observed. Less frequently, internal fragments are described (*i.e.* of breaks at two  $a_n/w_n$  sites after base loss at the 3'-end), but were not observed in these spectra.

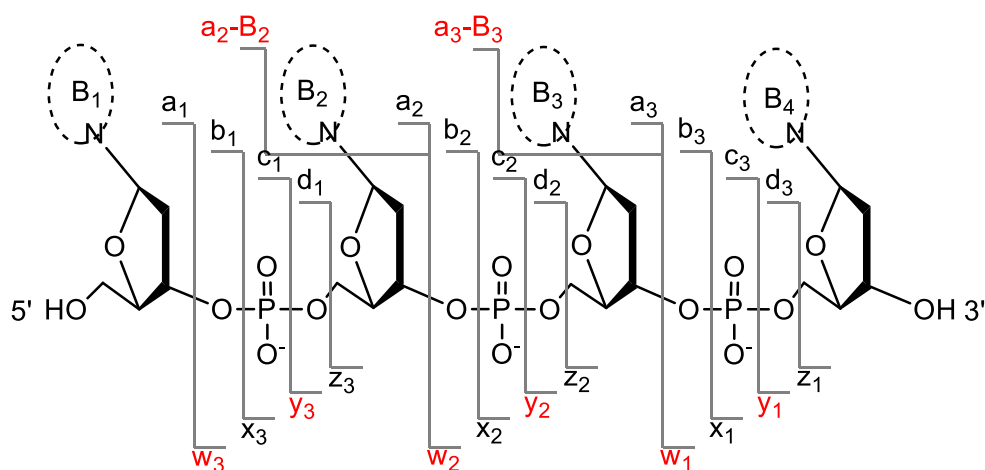


Figure 40 Schematic drawing and nomenclature of the most abundant fragmentation patterns after CID ionization of oligonucleotides according to McLuckey et al.<sup>293–295</sup> fragments marked in red are the most typical observed fragments.

### 8.6.2 Fragmentation of adduct peaks – general observations

MS<sup>2</sup> data was then collected from selected adduct peaks in **ODN1-46** and **ODN1-30** spectra and compared to fragmentation data of unplatinated **ODN1**, as has been reported by others earlier.<sup>271,274</sup> The most abundant peak set of the monoadduct of the *m*-OH substituted compound **46** as well as of mono- and bisadduct peak sets of **30** were subjected to CID ionization. Results are depicted in Figure 41 and listed in Table 8 and Table 9. For more detailed data, *cf.* supplement C.

It is quite obvious to see that in the Pt-adduct MS<sup>2</sup> spectra, only  $a_n$ - $B_n$  signals up to  $a_7$ - $B_7$  and  $w_n$  fragments up to  $w_6$  can be assigned in reasonable abundance. In the MS<sup>2</sup> data of free **ODN1**, the whole range of possible fragments is found – including the typical complementary  $a_n$ - $B_n/w_n$  pairs. This indicates that the initial **ODN1** sequence is unchanged from the 5' end up to position 5 (*i.e.* 5'-OH-CCTCT-) and from the 3' end up to position 8 (*i.e.* -TCTCC-OH<sup>3'</sup>). These findings give a first indication that the primary platinum binding site may be, as expected, at positions 6 and 7, where guanine residues are located.

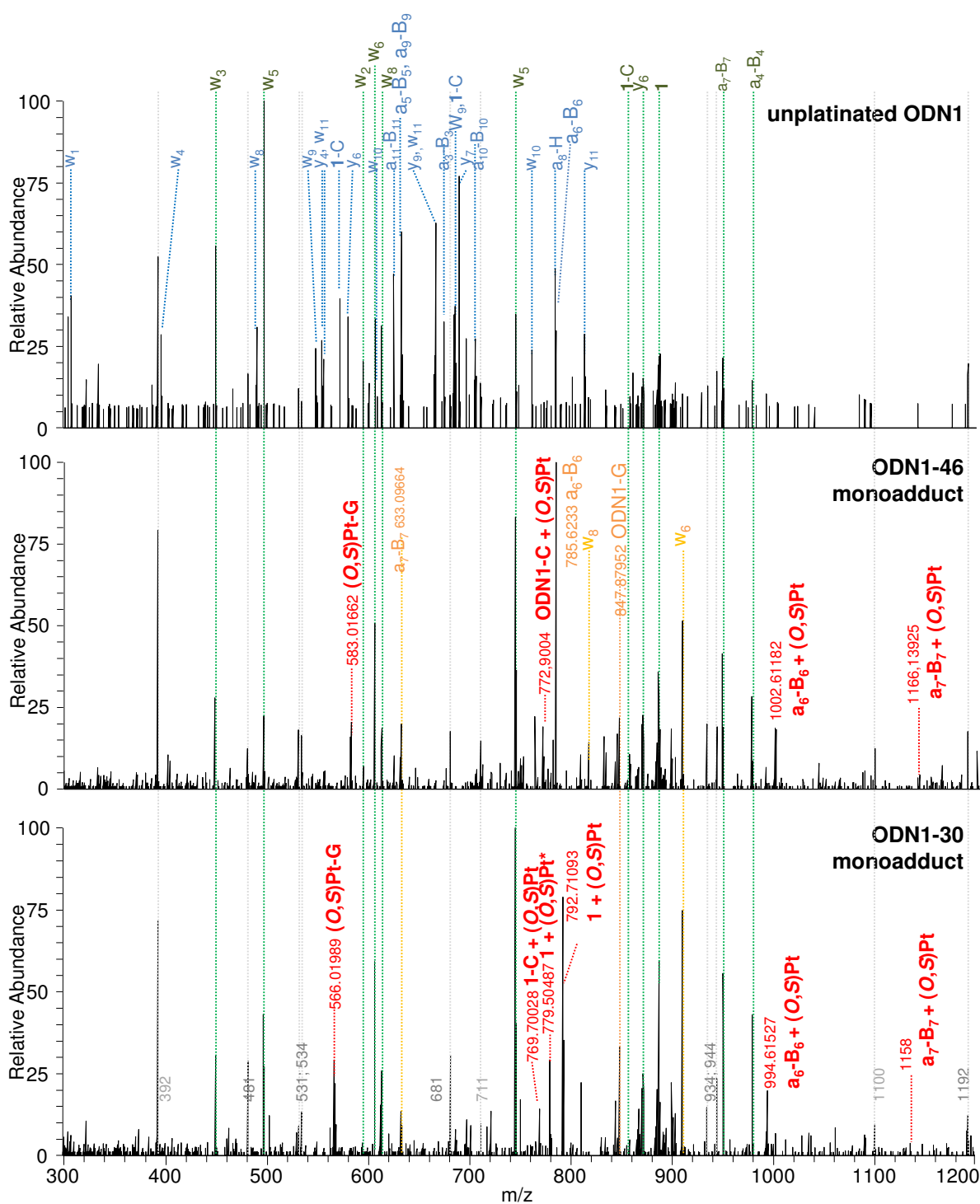


Figure 41 Comparative assignment of MS2 signals of free **ODN1** (top) and the **ODN1-46** (middle) and **ODN1-30** monoadducts (bottom). Green, signals found in all spectra; blue, signals found only in free **ODN1**; orange, signals found only in adduct spectra; red, diagnostic adduct peaks with detected  $(O,S)Pt$  unit; grey, pseudo-signals (noise) due to overall low signal intensity. For the sake of clarity, only one line is used for very close signals.  $m/z$  values given are those of the signal with highest intensity, not necessarily the monoisotopic peak.  $(O,S)Pt^*$  in **ODN1-30** adduct:  $(O,S)Pt$  unit after loss of the S-ethyl fragment.

It should be noted that in general, the signal intensity in these adduct spectra was rather low due to very small sample amounts and a low relative intensity of the mother peaks subjected to CID ionization. As a result, some of the found signals that occurred in all spectra could not be attributed to any of the usually discussed fragmentation pathways; not even to the less common  $b_n/c_n/d_n$ ,  $x_n/z_n$  type or internal fragments. Some of these signals also appeared in MS spectra, even in those of **ODN2** and its adducts. They therefore seem to present non-diagnostic peaks, maybe source impurities, which will not be considered in more detail. Such signals appear at *e.g.*  $m/z = 481, 531, 534, 681, 934, 944$  or  $1192$  and are indicated by grey lines in Figure 41.

### 8.6.3 Fragmentation of the monoadduct between ODN1 and compound 46

In the case of the **ODN1-46** monoadduct, it was possible to identify the Pt(II)-containing  $[(a_7-B_7)+(O,S)Pt]^{2-}$  ion at  $m/z = 1166.64$  (Figure 42, for all relevant adducts *cf.* Figure 41 middle and Table 8). This locates the  $(O,S)Pt$  moiety at base  $G_6$ . Together with the observation that also unplatinated  $[a_7-B_7]^{2-/3-}$  ions are found at  $m/z = 950.15$  and  $633.10$ , Pt could additionally be located at base  $G_7$ .<sup>xxi</sup>

This thesis is further underlined by the identification of a  $[G+(O,S)Pt]^-$  adduct ion at  $m/z = 583.02$  (Figure 43, right), which could originate from a preferred base loss of the platinated base in advance of the typical  $a_n$  strand break. This possibility has been discussed in great detail by Nyakas *et al.*, together with several possible platination-specific fragmentation pathways.<sup>273</sup>

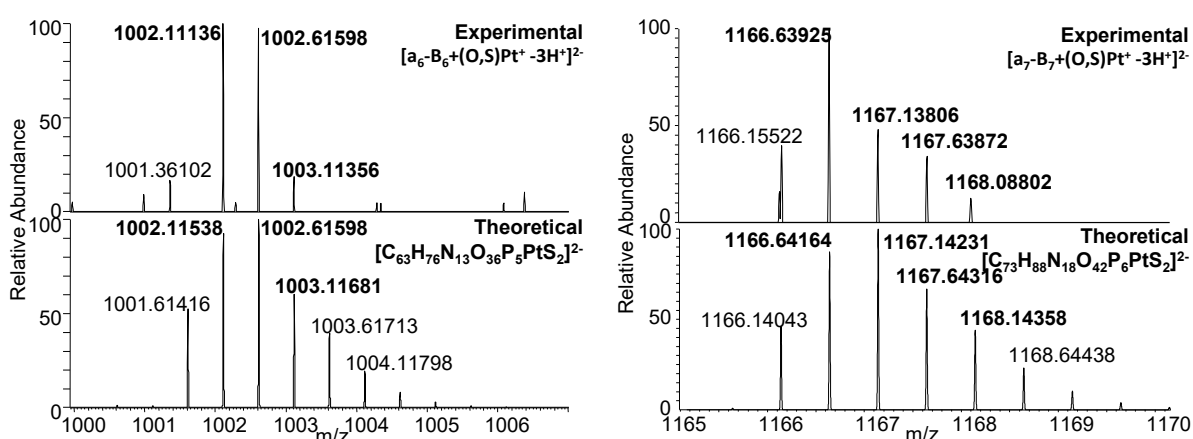


Figure 42 Comparison of the experimental and theoretical isotopic patterns belonging to ODN 1 fragments  $a_6-B_6$  (left) and  $a_7-B_7$  (right) with one  $(O,S)Pt$  unit bound at charge state -2.

<sup>xxi</sup> It cannot be ruled out that fragments such as  $[a_7-B_7]$  originate from adducts of  $(O,S)Pt$  being bound at *e.g.*  $G_6$  in an initial fragment  $[(a_7-B_7)+(O,S)Pt]$  and that the Pt unit is cleaved during CID. All additional spectrometric evidence however fortifies the stated hypothesis and makes the occurrence of such a cleavage unlikely.



Table 8 Relevant fragment peaks of the **ODN1-46** monoplatinated adduct in the MS<sup>2</sup> experiment. identified (O,S)Pt adducts and unplatinated but diagnostic fragment peaks are listed. For found signals, one characteristic peak is listed – typically the first of the pattern. For calculated signals, the corresponding multicharge peak is listed.

found (m/z)	z	calcd (m/z)	error (ppm)	sum formula	fragment
582,01421	-1	582,01701	4,81	C <sub>16</sub> H <sub>14</sub> N <sub>5</sub> O <sub>3</sub> PtS <sub>2</sub>	[G <sup>-</sup> + (O,S)Pt <sup>+</sup> - H <sup>+</sup> ] <sup>-</sup>
772,90004	-5	772,90225	2,86	C <sub>121</sub> H <sub>151</sub> N <sub>33</sub> O <sub>75</sub> P <sub>11</sub> PtS <sub>2</sub>	[ODN1 - C + (O,S)Pt <sup>+</sup> - 6H <sup>+</sup> ] <sup>5-</sup>
785,62387	-2	785,62671	3,61	C <sub>52</sub> H <sub>66</sub> N <sub>13</sub> O <sub>34</sub> P <sub>5</sub>	[a <sub>6</sub> -B <sub>6</sub> - 2H <sup>+</sup> ] <sup>2-</sup>
847,87952	-4	847,88328	4,43	C <sub>109</sub> H <sub>142</sub> N <sub>31</sub> O <sub>73</sub> P <sub>11</sub>	[ODN1 - G - 4H <sup>+</sup> ] <sup>4-</sup>
950,14898	-2	950,15297	4,20	C <sub>62</sub> H <sub>78</sub> N <sub>18</sub> O <sub>40</sub> P <sub>6</sub>	[(a <sub>7</sub> -B <sub>7</sub> ) - 2H <sup>+</sup> ] <sup>2-</sup>
1002,11136	-2	1002,11538	4,01	C <sub>63</sub> H <sub>77</sub> N <sub>13</sub> O <sub>36</sub> P <sub>5</sub> PtS <sub>2</sub>	[(a <sub>6</sub> -B <sub>6</sub> ) + (O,S)Pt <sup>+</sup> - 3H <sup>+</sup> ] <sup>2-</sup>
1166,63925	-2	1166,64164	2,05	C <sub>73</sub> H <sub>88</sub> N <sub>18</sub> O <sub>42</sub> P <sub>6</sub> PtS <sub>2</sub>	[(a <sub>7</sub> -B <sub>7</sub> ) + (O,S)Pt <sup>+</sup> - 3H <sup>+</sup> ] <sup>2-</sup>

Generally, all complimentary ions of a mother fragment should be detectable in oligonucleotide MS<sup>2</sup> experiments.<sup>294</sup> Thus, this fragment could comprise the platinated G<sub>7</sub> ion leading to the occurrence of the unplatinated (a<sub>7</sub>-B<sub>7</sub>) fragment which is also detected as z = -2 and -3 ions (*vide supra*). In good correlation with the observation of unplatinated [a<sub>6</sub>-B<sub>6</sub>]<sup>2-</sup>, it could as well originate from the G<sub>6</sub> ion, as already suggested in combination with the [(a<sub>7</sub>-B<sub>7</sub>)+(O,S)Pt] fragment.

Furthermore the [ODN1-G]<sup>4-</sup> ion was identified (Figure S 13). This is another good indicator that ribose-bound G, upon platination, is destabilized and thus released from ribose easier than unplatinated G: No such fragment can be found in free **ODN1**. The stability of the newly formed (O,S)Pt-G adduct is nicely demonstrated by these findings.

One other diagnostic Pt-containing fragment was identified from the signal at m/z = 1002.61 as the [(a<sub>6</sub>-B<sub>6</sub>)+(O,S)Pt<sup>+</sup>-3H<sup>+</sup>]<sup>2-</sup> ion (Figure S 13). In this segment of **ODN1**, no G is available. Therefore another binding site for Pt must exist in this sequence. A plausible explanation would be C<sub>4</sub> as a secondary binding site: Even though no fragments that give direct evidence for a bisfunctional binding of the (O,S)Pt unit towards one G and one C were found, the presence of a [a<sub>4</sub>-B<sub>4</sub>]<sup>-</sup> ion at m/z = 979.16 together with (low abundance) w<sub>8</sub> fragments at m/z = 612.83 (z = -4) and 817.45 (z = -3) indicate a preferential fragmentation position at the 3' side of ribose 4 and possible release of (platinated) C<sub>4</sub>. One might envision a bisfunctional binding of the (O,S)Pt unit to C<sub>4</sub> and G<sub>6</sub>, which could explain most of the found fragments. This can, however, not be proven solely with the methods provided here. Further, detailed investigations using additional complementary methods might lead to a definite binding site assignment.

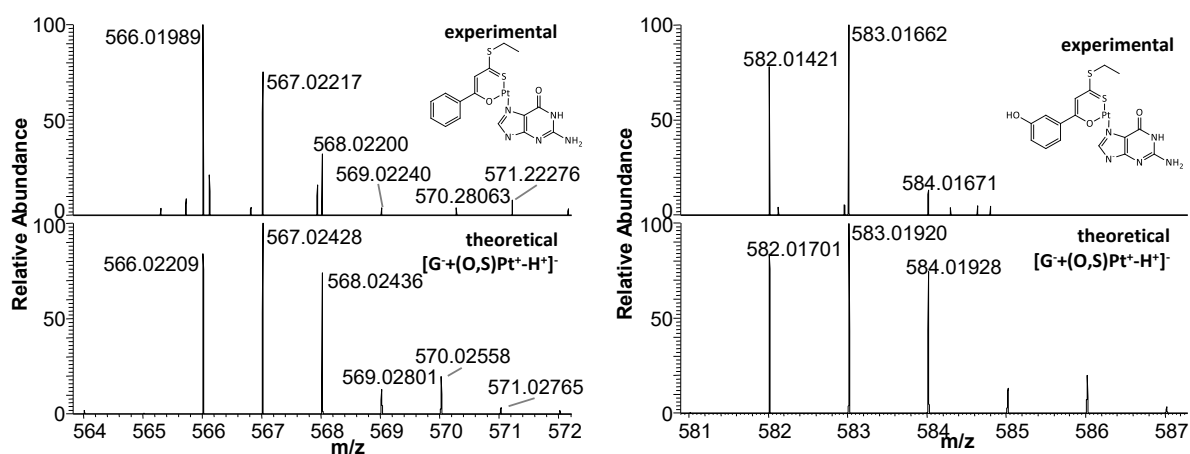


Figure 43 Experimental and theoretical isotopic pattern of the (O,S)Pt-G adducts formed with **30** (left) and **46** (right)

#### 8.6.4 Fragmentation of the mono- and bisadducts between ODN<sub>1</sub> and compound **30**

When evaluating the data obtained from CID ionization of the monoadduct formed between **ODN1** and compound **30**, a similar fragmentation pattern is observed (Figure 41, Table 9, Supplement C). The most important signals are those of  $[G+(O,S)Pt]^-$  at  $m/z = 566.02$  (Figure 43, left) and of  $[(a_6-B_6)+(O,S)Pt^+-3H^+]^{2-}$  and  $[(a_7-B_7)+(O,S)Pt]^{2-}$  at  $m/z = 994.62$  and  $1158.64$ , respectively, which indicate a similar binding mode of the two compounds **30** and **46** (Figure S 14).

Due to the rather high intensity of the mother peak of intact **ODN1+(O,S)Pt** at  $m/z = 792.71$ , less diagnostic fragments are observed in this MS<sup>2</sup> spectrum. Increasing the collision energy to enforce more fragmentation, however, would have led to complete destruction of adduct signals, thus making a definite assignment of adduct sites impossible. This fact is tellingly shown by the signal at  $m/z = 779.50$ ,  $z = -5$ , which is attributed to platinated whole **ODN1** after release of [S-Et] from the bidentate ligand (Figure S 14).

Table 9 Relevant fragment peaks of the A-1 monoplatinated adduct in the MS<sup>2</sup> experiment. Identified (O,S)Pt adducts and unplatinated but diagnostic fragment peaks are listed.

found (m/z)	z	calcd (m/z)	error (ppm)	sum formula	fragment
<b>566,01989</b>	-1	566,02209	3,89	C <sub>16</sub> H <sub>14</sub> N <sub>5</sub> O <sub>2</sub> PtS <sub>2</sub>	$[G^- + (O,S)Pt^+ - H^+]^-$
<b>769,50044</b>	-5	769,50291	3,21	C <sub>121</sub> H <sub>150</sub> N <sub>33</sub> O <sub>75</sub> P <sub>11</sub> PtS <sub>2</sub>	$[1 - 48 + (O,S)Pt^+ - 6H^+]^{5-}$
<b>779,50487</b>	-5	779,50932	5,71	C <sub>123</sub> H <sub>150</sub> N <sub>36</sub> O <sub>75</sub> P <sub>11</sub> PtS	$[1 + \{(O,S)Pt-SEt\}^+ - 6H^+]^{5-}$
<b>847,87996</b>	-4	847,88328	3,92	C <sub>109</sub> H <sub>142</sub> N <sub>31</sub> O <sub>73</sub> P <sub>11</sub>	$[1 - G - 4H^+]^{4-}$
<b>994,11421</b>	-2	994,11792	3,73	C <sub>63</sub> H <sub>76</sub> N <sub>13</sub> O <sub>36</sub> P <sub>5</sub> PtS <sub>2</sub>	$[(a_6-B_6) + (O,S)Pt^+ - 3H^+]^{2-}$
<b>1158,64034</b>	-2	1158,64419	3,32	C <sub>73</sub> H <sub>88</sub> N <sub>18</sub> O <sub>42</sub> P <sub>6</sub> PtS <sub>2</sub>	$[(a_7-B_7) + (O,S)Pt^+ - 3H^+]^{2-}$

In an attempt to identify the second binding site in the observed bisadducts of **ODN1** with **30**, the signal belonging to **ODN1**+2(O,S)Pt at  $m/z = 875.51$ ,  $z = -5$ , was also subjected to CID ionization (Figure S 15). In this case, only few fragment peaks could be assigned, no platinum-containing adduct peaks could be determined due to the low signal intensity. Again, it is striking to see that the most abundant assignable signals belong to  $w_5$ ,  $w_6$ ,  $a_4-B_4$  and  $a_6-B_6$ , thus drawing a similar picture as the monoadduct did. In addition, the appearance of a signal belonging to unplatinated **ODN1** at  $m/z = 886.70$  demonstrates the obvious instability of the bisadduct towards CID ionization. No structural conclusion will therefore be drawn from this data.



## 9 DISCUSSION TO BIOMOLECULE INTERACTION DATA

### 9.1 Interactions of platinum(II) complexes with model proteins

It could be shown through ESI MS and UV-vis spectroscopy that the compound class presented within this thesis is capable of forming adducts with proteins. Detailed studies of the adduct mass spectra reveals that the interaction pattern is distinctive, and that the compounds occupy defined amino acid binding sites within each protein which well correlate with the number of principally available binding sites in each particular sequence. The compounds seem to have a preference for binding N atoms of His side chains as opposed to *e.g.* S atoms at Cys or Met sites, but may possibly also bind these amino acid side chains.

X-ray crystallographic data on the HEWL-**46** and HEWL-**48** adducts tellingly demonstrate the adduct formation between the (O,S)Pt unit and ND1 of a His side chain. Interestingly, DMSO is retained within the coordination sphere and stabilized by hydrogen bonds. In the corresponding ESI mass spectra however, no evidence of DMSO being retained is found. Obviously, the different experimental conditions make the retention in one case and the release of DMSO in the other case possible.

For the hydroxy-substituted complexes **45-48**, adducts formed with cyt c also reveal partial retention of the DMSO ligand within the coordination sphere of the Pt(II) center, a feature that is not observed for the compounds of the unsubstituted or *p*-Bromo substituted series **29-36**. Apart from this difference between the compound subgroups, they generally exhibit a similar adduct formation behavior; with slight differences in adduct quantity depending on the substituent and the length of the alkyl chain. Compounds with a short alkyl chain usually form more adducts than their homologues with longer chains. This behavior can most probably be explained by a better solubility in the buffer medium and by the smaller size of the S-methyl esters, making them easier available and allow them to better access binding sites.

Compound **46**, with a *m*-OH group, generally seems to bind the proteins to the largest extent when comparing all *S*-ethyl esters. This is deduced from the overall higher intensity of adduct peaks compared to the other compounds.

When comparing the reactivity of the compounds towards the different proteins, UV-vis spectra give a good indication that the reactions with the proteins occur on slightly different time scales. Taking as a measure the time needed for the spectrum to equalize (*i.e.* to show no further significant band shifts), the speed of adduct formation by the Pt(II) compounds can be put in the order *cyt c* > HEWL > RNase A; a finding that is also corroborated by ESI MS spectra recorded after 24 vs. 72 h of incubation.

In summary, it can be concluded that a defined interaction pattern of the (*O,S*)PtCl(DMSO) compounds with the model proteins is witnessed, with slight differences arising from the substitution pattern at the (*O,S*) bidentate ligand and the protein used. In all cases, the chlorido ligand is released as a prerequisite for biomolecule binding. Whether DMSO is substituted or retained within the Pt(II) coordination sphere mainly depends on the experimental setup and to some extent on the compound. These findings show, in any case, that DMSO is a ligand that forms a stable and partially inert bond between its sulfur donor atom and the Pt(II) center. This might, in consequence, slow down the general reactivity of the compound class towards biomolecules and might therefore contribute to the goal of this thesis to achieve compounds that do not interact with all biomolecules available in an uncontrolled manner.

## 9.2 Interactions of platinum(II) complexes **30**, **46** and **48** with 9-methylguanine and single-stranded ODNs

ESI MS analyses carried out in negative ion mode show that compounds **30**, **46** and **48** are able to form adducts with the single strand DNA models **ODN1-3**. The resulting metallodrug-DNA adducts contain only (*O,S*)Pt fragments, implying that the loss of both monodentate ligands is a crucial step in the DNA binding mechanism.

The presence of more than one (*O,S*)Pt fragment linked to the model sequences suggests that the selected platinum complexes have an affinity also for sequences different from the “GG-boxes” or, in alternative, form adducts within the same nucleobase involving the participation of *e.g.* the guanine  $O^6$  atom ( $N^7, O^6$ ) chelates,<sup>298</sup> thus leaving the  $N^7$  of the neighboring guanine available for coordination with another metal center.

MS<sup>2</sup> experiments on adducts of **ODN1** with **30** and **46** further confirm that guanine is the primary DNA binding site for these compounds. Direct evidence is given from the detection of [G + (O,S)Pt] fragments in both MS<sup>2</sup> fragmentation spectra, indirect evidence emerges from the combined appearance of characteristic platinated and unplatinated fragments. It was furthermore shown that binding of the (O,S)Pt unit to other nucleobases, perhaps C, is also possible as described above.

As an alternative to nucleobase binding, one might envision the binding of Pt(II) towards the phosphate backbone. This is highly unlikely for several reasons: First, no direct evidence in form of typical small-molecule adducts was found. Secondly, it is generally discussed that transition metals preferentially bind DNA nucleobases while alkali and alkali earth metals generally prefer backbone phosphodiester groups.<sup>264</sup> Thirdly, altered fragmentation pathways have been identified for oligonucleotides with Na<sup>+</sup> bound to the phosphate backbone, none of which are observed here.<sup>264,265</sup> Therefore, phosphate binding can be ruled out.<sup>xxii</sup>

When taking into account the data obtained from experiments with **9-mg**, the following picture emerges: Binding of the investigated Pt(II) compounds occurs fast under the given conditions, **9-mg** replaces the chlorido ligand of the intact Pt(II) compounds and can, to some extent, also substitute the DMSO molecule, possibly leading to the formation of a bischelate structure with platinum coordinated to the (O,S) ligand and to **9-mg** in a (N<sup>7</sup>,O<sup>6</sup>) bidentate manner. Given the fact that not all platinum is bound in that way, it can be concluded that the O<sup>6</sup> atom of **9-mg** is not very efficient in binding the (O,S)Pt unit. This is in good accordance with the initially stated thesis that *trans* to a hard donor atom in Pt(II) complexes – here the β-hydroxy oxygen -, a soft ligand is preferably bound, thus explaining the retention of DMSO in parts of the adducts (*cf.* the HSAB concept in chapter 2).

These results with **9-mg** give further indication that such a monofunctional binding may also be possible within a single strand oligonucleotide. However, when two guanines are spatially adjacent in an ODN sequence, two N-donors (the N<sup>7</sup> positions of the two guanines) can efficiently replace chloride, DMSO or water to give cross-links, as is indicated by the complete absence of (O,S)Pt(DMSO) units in the adduct spectra with **ODNs**. In the presence of excess of platinum, alternate binding sites can then be occupied by the (O,S)Pt units, such as the aforementioned (N<sup>7</sup>,O<sup>6</sup>) bidentate site or alternate nucleobase donor atoms.

---

<sup>xxii</sup> At this point it should be mentioned that attempts to investigate the compounds' reactivity towards 5'-guanosine monophosphate (5'-GMP) as a nucleotide model have also been pursued. However, ESI mass spectrometric studies gave no reliable peak data. Efforts to study the behavior in solution by NMR methods were also inconclusive due to solubility issues and overlay of solvent signals with essential signals of the compounds.

### 9.3 General conclusions

Taken together all the findings of biomolecule binding experiments, it is noteworthy that the extent of reactivity observed for the three compounds is somewhat different when reacting with proteins or ODNs: towards ODNs on the one hand, the unsubstituted complex **30** was found to be most reactive and compounds **46** and **48** behaved more or less similar in ESI MS experiments. In experiments conducted by CD and UV-vis spectroscopy,<sup>138,283</sup> an order of reactivity **30, 46 > 48 (>> CDDP)** was elucidated. On the other hand, ESI MS data of adducts formed with proteins manifested a reactivity order to be set as **46 > 30, 48**. Thus, it can be concluded that the nature and position of the aromatic substituent plays a role when it comes to a defined biomolecule binding and target preferences. Together with the data on antiproliferative assays described in chapter 5, it becomes clear that structure-activity relationships of this series of compounds cannot be broken down to a singular trait or reaction pattern. It is rather the sum of all consequences that derivatizations bring forth with them that contribute to a final biological activity. Nevertheless, compounds **29/30** and **45/46** can be considered to represent the most potential drug candidates within this series.<sup>xxiii</sup>

---

<sup>xxiii</sup> Even though in depth-experiments were only carried out with the S-ethyl compounds **30** and **46** for practical reasons, their S-methyl homologues should be considered as similarly potential compounds as deduced from the overall data.



---

## PART C

# BIOCONJUGATES

*Parts of the here described syntheses on alkynyl group-bearing compounds **51-67** have been carried out by Nora Nowak (FSU Jena) during her bachelors' thesis and advanced practical course, which she conducted under my direct instruction and supervision of Prof. Dr. Wolfgang Weigand. All relevant analytical data has been independently re-evaluated and syntheses repeated when necessary.*



## 10 BACKGROUND

$\beta$ -hydroxyditiocinnamic esters bear several moieties which can, in principle, easily be modified to fine-tune their properties. Incorporation of functional groups that allow for the formation of metal complexes as bioconjugates is therefore a desirable aim. Such bioconjugates could improve *e.g.* the compounds' selectivity towards certain biological targets through specific receptor targeting. They could also lead to "chimeric" compounds that bear several biologically relevant functionalities for complex and directed pharmacological applications.<sup>299,300</sup>

### 10.1 Metal-peptide bioconjugates

The field of bioconjugates is huge, and a plethora of methods and techniques are being applied in the field of forming bioconjugates.<sup>301,302</sup> Metal-complex bioconjugates resemble a small portion of this research, but are nowadays explored for different biological/medical applications.<sup>303,304</sup> Especially metal-peptide bioconjugates have emerged as promising research focus in recent years, several reviews have dealt with this subject.<sup>305-307</sup> As one of the first representatives, ferrocene-derived peptides have been prepared by solid-phase peptide synthesis.<sup>308,309</sup> Other early approaches include those of the group of G. Jaouen, who used *e.g.* Mo and Co  $\pi$ -alkyne organometallic compounds to prepare peptide conjugates.<sup>310</sup>

The concept of metal-peptide bioconjugate formation has been widely extended, especially by the Metzler-Nolte group, to give bioconjugates of various metals and based on very different structural approaches. Some are named here as representatives for the large number of metal-peptide bioconjugates that have been described in the literature by many researchers.

Iron(II), in form of ferrocene carboxylic acids, has been explored in detail and reported frequently as basis for metal-peptide bioconjugates. It is usually bound to model peptides *via* an amide bond (Chart 6a),<sup>311-314</sup> in one case the use of an alkyne spacer was reported (Chart 6b).<sup>315</sup>

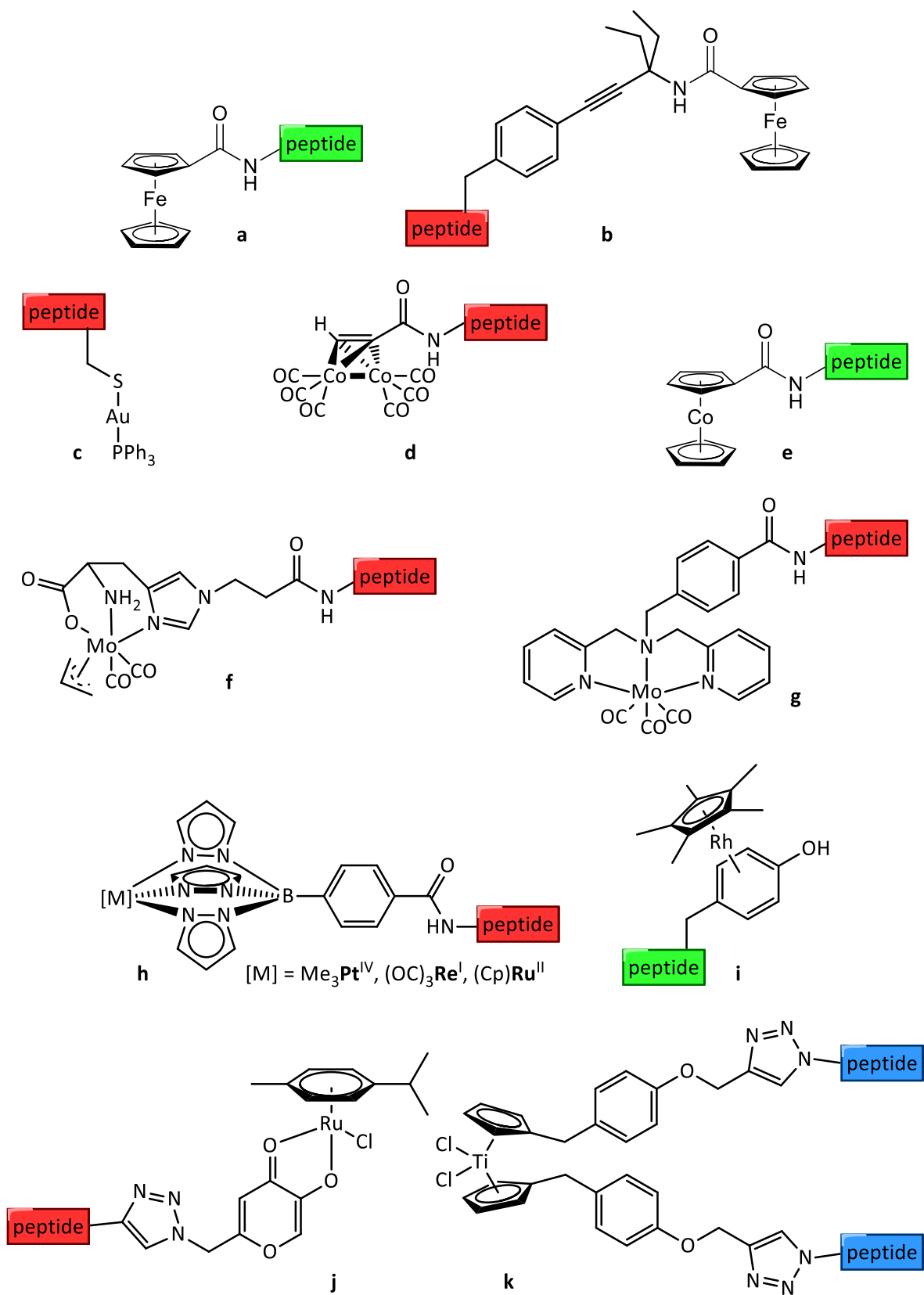


Chart 6 Some coordination environments of transition metal bioconjugates from the Metzler-Nolte group. Green peptide box: various peptides; red peptide box: enkephalin derivatives. Blue peptide box: short sequences. Cf. the text for detailed description.

Other metals have been explored for their applicability in metal-peptide bioconjugates, *e.g.* gold(I), bound to Cys<sup>5</sup>-Enkephalin through S<sup>Cys</sup> (Chart 6c).<sup>316</sup> Cobalt, bound to peptides as Co-carbonyl *via* terminal propionic acid (Chart 6d),<sup>317</sup> or as cobaltocenium carboxylic acid (Chart 6e),<sup>318,319</sup> have been reported. In the latter case, enhanced cellular uptake and delivery to the nuclei was observed by making use of nuclear localization signal (NLS) peptide sequences. Furthermore, molybdenum has been attached to enkephalin *via* nitrogen donors (Chart 6f and g),<sup>320,321</sup> and also Re<sup>I</sup>(CO)<sub>3</sub>, Pt<sup>IV</sup>Me<sub>3</sub>, and ( $\eta^5$ -Cp)Ru<sup>II</sup> units have been bound to this model peptide by making use of the monoanionic tris(pyrazolyl)borate ligand (Chart 6h).<sup>322,323</sup>

Binding of a ( $\eta^5$ -Cp\*)Rh<sup>II</sup> unit was made possible by forming a sandwich complex with Tyrosine, thus giving a ( $\eta^5$ -Cp\*)Rh<sup>II</sup>( $\eta^6$ -Ph<sup>Tyr</sup>) structural motif, incorporated into several peptide sequences (Chart 6i).<sup>324</sup> The binding of the enkephalin derivative of this series towards opioid receptors has been studied in detail by 2D NMR spectroscopy and modeling techniques.<sup>325</sup> Titanocene<sup>326</sup> and Ru-arene units<sup>327</sup> (Chart 6j and k, respectively) have been attached to model peptides through copper(I)-catalyzed alkyne-azide cycloaddition (CuAAC).

The first report on Pt(II)-peptide bioconjugates appeared in the year 2000 by members of Jan Reedijk's group.<sup>328,329</sup> Fully working under solid phase conditions, a tripeptide, tethered to ethylenediamine, was prepared and coordinated towards a Pt<sup>II</sup>Cl<sub>2</sub> unit (Chart 7l). Further derivatives have subsequently been described, all bearing a common (en)PtCl<sub>2</sub> pharmacophore (en = ethylenediamine).<sup>330,331</sup> In DNA binding studies, it was shown that these compounds produce DNA adducts structurally similar to those Cisplatin or free (en)PtCl<sub>2</sub> would.<sup>332</sup> Taking advantage of the newly developed method, the group also prepared a dinuclear Pt(II) complex with two *trans*-(NH<sub>3</sub>)<sub>2</sub>PtCl moieties being bound in monodentate fashion to a short peptide (Chart 7m).<sup>333</sup>

Furthermore, Pt(II) conjugates with octreotide derivatives have been obtained from a solid-phase approach (Chart 7n), and binding of this conjugate towards a short oligonucleotide sequence was demonstrated.<sup>334</sup> An organometallic variant of a Pt-peptide bioconjugate was prepared by using a (*N,C,M*)-binding pincer ligand which was readily attached to different peptide sequences (Chart 7o).<sup>335</sup> In two independent reports, Pt(II) peptide bioconjugates were described utilizing a malonate-based ligand and a long linker to connect the coordination site with a peptide (Chart 7p and q).<sup>336,337</sup> In addition, the variability of the axial position in Pt(IV) complexes was exploited by several research groups (Chart 7r and s).<sup>322,338–340</sup>

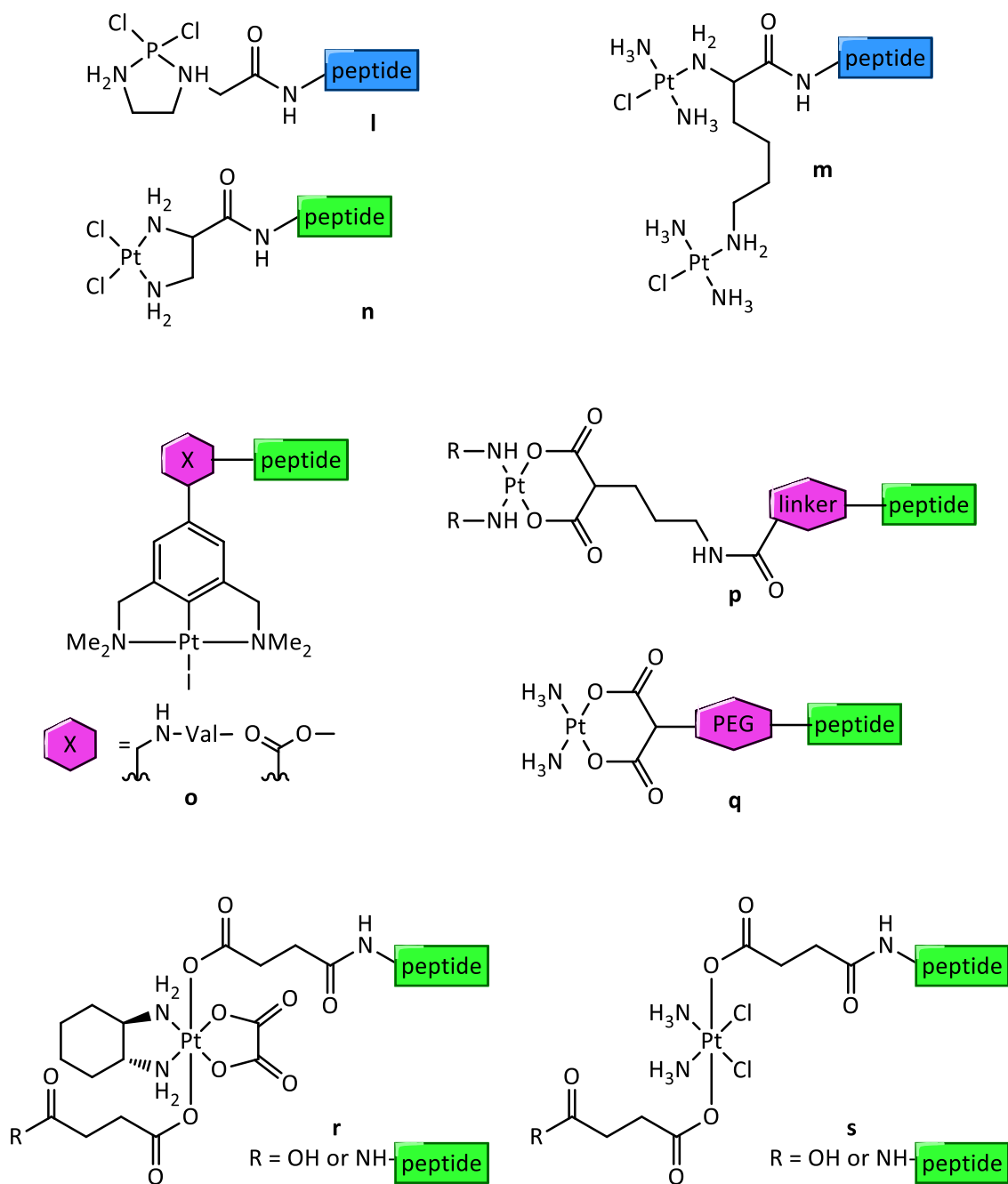


Chart 7 Literature-reported peptide bioconjugates based on Pt(II) and Pt(IV) scaffolds. Green peptide box: various peptides; Blue peptide box: short sequences (3 amino acids); pink box: linker unit. *Cf.* the text for detailed description.

It should be noted that efforts have also been made in attaching Pt(II) or Pt(IV) scaffolds to polymeric nanoparticles or nano-metal organic frameworks.<sup>55,341</sup> Lipoplatin<sup>31</sup> and ProLindac<sup>TM34</sup> are examples of such compounds that have actually reached clinical trials (*cf.* chapter 1.1), the latter being a carboplatin analog which is in fact connected to a polymer backbone *via* short peptide linkers.

In several of these mentioned reports on metal-peptide bioconjugates, enhanced uptake into cells<sup>314,318,336</sup> and/or activity against selected cancer cell lines was reported as compared to their non-conjugated subunits.<sup>317,327,337–340</sup>

These results strikingly demonstrate the effects that conjugation of active metal centers with defined peptide sequences can have and show the great structural versatility of artificial metal-biomolecule conjugates. It is thus only a logical consequence to use the structural motif available from the previous studies and strive to combine (*O,S*) chelating Pt(II) complexes with peptides.

## 10.2 The model peptide

As a model for the here described studies, the pentapeptide Leu<sup>5</sup>-Enkephalin (Leu<sup>5</sup>-Enk) was chosen. Enkephalins are known neurotransmitters and ligands for opiate receptors,<sup>325,342,343</sup> and naturally occur in two forms (Chart 8): Met<sup>5</sup>-Enk, with methionine being bound in position 5, and Leu<sup>5</sup>-Enk with leucine as amino acid in position 5. Enkephalins originate from precursor proteins of the preproenkephalin group and of  $\beta$ -Lipotrophin<sup>344</sup> by proteolytic processes. They were first isolated and characterized from porcine brains in 1975,<sup>345,346</sup> where they are produced in neuronal cells. Molecular structures of both forms were solved,<sup>347–349</sup> but in solution a very flexible secondary structure is assumed<sup>350–352</sup> which allows for the peptides to potentially adapt to several receptor binding sites. Opioid-receptors occur in the brain,<sup>353</sup> but also in the spinal region<sup>354</sup> and colon,<sup>355</sup> and have been found to be overexpressed in small-cell lung carcinoma, neuroblastoma and breast cancer cell types.<sup>356</sup>

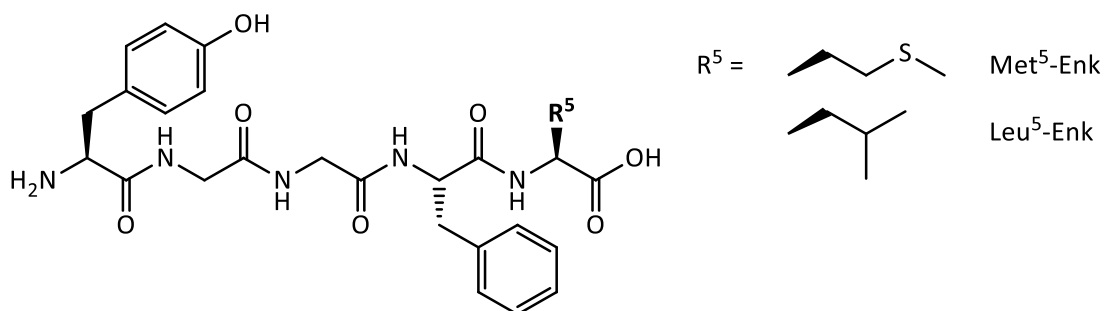


Chart 8 The Enkephalins.

Due to their high potency to bind to opioid receptors and thus induction of analgesic effects, they were initially considered as potential analgetic drug candidates. However, a short life-time in several test systems and evidence for addictive properties have lead to a need for structural modifications of the naturally occurring peptide sequence.<sup>353</sup> Among these, *e.g.* the substitution of amino acids by non-natural derivatives or the introduction of metal centers, may increase the compounds' lifetime and could lead to more favourable properties in such a quest.

Overall, the pentapeptides can be considered suitable model peptides for bioconjugate preparation. Leu<sup>5</sup>-Enk, from here on referred to as Enk, was chosen for the first attempts to form (O,S)Pt –derived bioconjugates on the basis of several considerations: Firstly, Leu<sup>5</sup>-Enk is a readily available model peptide. It is short (5 amino acids) and bears one functional group which requires the application of protective groups, *i.e.* a *tert*-butyl (<sup>t</sup>Bu) group for the Tyr<sup>1</sup>-OH,<sup>357</sup> still making various structural alterations possible. Secondly, is this a well-established model peptide which is known to be a good representative for subsequent experiments with further, larger, peptides – as was demonstrated in the previous section.

### 10.3 Considerations on different conjugation methods

The versatile possibilities of forming metal bioconjugates have just recently been reviewed in great detail<sup>300</sup> and some examples been outlined in the previous chapter. Here, the two methods applied for this project are described briefly.

#### 10.3.1 Copper(I)-catalyzed alkyne-azide cycloaddition (CuAAC)

The use of “click” chemistry as versatile and bioorthogonal approach has attracted growing attention in the last years. The prototype of classical “click” chemistry as established by Kolb, Finn and Sharpless,<sup>358,359</sup> is the linking of two separate “building blocks” *via* Huisgen-type 1-3 dipolar azide-alkyne cycloaddition<sup>360,361</sup> and has become increasingly applied in its Cu(I) mediated application scheme, as independently reported by the groups of Sharpless<sup>362,363</sup> and Meldal<sup>364</sup> and widely applied over the last decade.<sup>365–369</sup>

Azides do not occur in nature,<sup>370</sup> alkynes are very sparse;<sup>371</sup> both do have some biological activity.<sup>372</sup> Nevertheless, terminal alkynes and azides bear a number of structural features which render them important in many synthetic approaches. They are both stable towards nucleophiles, electrophiles



and a variety of standard reaction conditions. Importantly, both are nearly unreactive towards most biological molecules since they are small, relatively unpolar, and do not form hydrogen bonds to a significant degree.<sup>373</sup> These characteristics renders them perfect candidates for bioorthogonal synthetic approaches, also because they are considered to not significantly change the properties of the biomolecules they are attached to.<sup>370</sup> The resulting 1,2,3-triazoles have found wide-spread applications, *e.g.* as pharmacophores<sup>374</sup> or simply as linking function of building blocks.<sup>367</sup>

One aim of this study was thus to explore synthetic approaches towards the incorporation of both functional groups, azides and alkynes, into the main structural unit of (*O,S*)Pt complexes to finally enable bioconjugation with peptides as model compounds. In the here described studies, first the introduction of terminal alkynyl groups at either the aromatic or dithiocarbonyl subsite was explored. Secondly, preparation of an azide-functionalized structure was pursued. In parallel, derivatization of Enk with the respective complementary functional group should be explored.

### 10.3.2 Amide bond formation

Another approach which has frequently found application is the binding of suitable metal units *via* amide bonds. Usually, the metal unit should bear a carboxylic group which can then be coupled *N*-terminally to the desired peptide unit. In this context, both the coupling on solid phase - during peptide synthesis -, or in solution - after synthesis of the whole peptide -, are thinkable and have been utilized earlier (*vide supra* for various examples). Coupling in solid phase or in solution can in principle occur by the same methods,<sup>375-377</sup> and usually typical amino acid coupling methods are applied to the desired system. It is generally considered that coupling in solid phase is more efficient and leads to less unwanted side reactions.<sup>378</sup> However, deprotection and cleavage from resin usually require harsh conditions (*e.g.* high concentrations of TFA) which some target compounds, especially metal complexes with highly functionalized ligands, might not survive. Therefore, it is favorable if the (metal-bound or free) ligand can survive deprotection/cleavage conditions without decomposition (when coupling in solid phase), and is not reactive towards other functionalities present in the peptide (if coupled after deprotection and/or cleavage from resin).

These considerations in mind, a second approach towards metal-peptide bioconjugates was the introduction of a carboxylic group into the overall structure of the  $\beta$ -hydroxy ditiocinnamic ester to enable its coupling towards the model peptide Enk *via* amide bonds.



# 11 BIOCONJUGATES VIA COPPER(I)-CATALYZED ALKYNE-AZIDE CYCLOADDITION (CuAAC)

## 11.1 Introducing alkyne functionalities into $\beta$ -hydroxydithiocinnamic esters

### 11.1.1 Introducing the alkynyl group at the aromatic subsite

For the formation of compounds that bear a phenyl-ether with a terminal  $C\equiv C$  triple bond, it is possible to directly introduce the alkynyl group into hydroxy acetophenones and then attempt ligand synthesis. It may as well be possible to first protect the hydroxy group, *e.g.* by the already discussed silyl-based ethers, commence with building up the (*O,S*) main structure and subsequently deprotect the OH group to then etherificate the resulting phenolate-bearing ligand. This procedure is by far more laborious and since the yields of the first three steps are known to be only moderate (*cf.* chapter 3.1), the first-described pathway was chosen as primary route; knowing that an alternate route would be available.

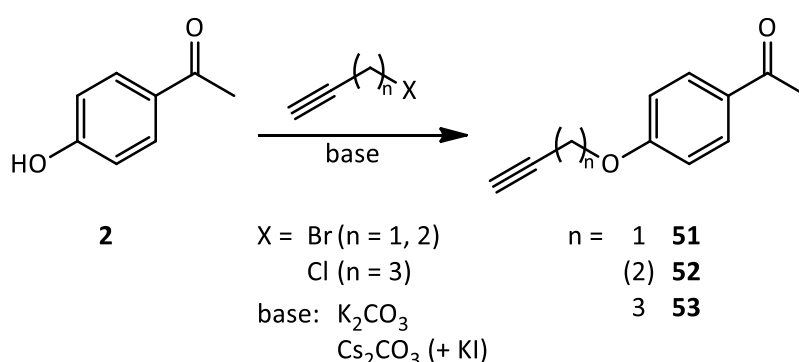
From an economic standpoint, propargyl bromide, a  $C_3$  building block, is the cheapest<sup>xxiv</sup> and most readily available aliphatic alkynyl halide and therefore presented the substrate of choice in initial experiments. Subsequently, also  $C_4$  and  $C_5$  units were used.

---

<sup>xxiv</sup> *e.g.* Costs of propargyl bromide, 80 % solution in toluene: ca. 35 eur/50 mL vs. butynyl bromide or pentynyl chloride: 5 g ca. 65 eur when retrieved from SigmaAldrich

### 11.1.1.1 Derivatization of 4-hydroxy acetophenone

Compound **51** was prepared in good yields (81 %) by a literature-reported Williamson-ether synthesis, using 4-hydroxy acetophenone and propargyl bromide as starting materials and potassium carbonate as base (Scheme 6).<sup>379</sup> In subsequent steps, the propargylic group proved to be prone to rearrangement reactions, mostly due to the acidity of both terminal CH<sup>380</sup> and internal CH<sub>2</sub> groups (*vide infra*). Therefore the elongation of the distance between the two functional groups was pursued. First, one CH<sub>2</sub> group should be added to obtain compound **52**.



Scheme 6 Introduction of a terminal alkyne at the *p*-O-Ph site of acetophenone.

To introduce a butynyl group at the aromatic subsite, 4-hydroxy acetophenone was converted with butynyl bromide according to the same procedure, but no conversion was achieved after 24 h or even 7 days of stirring. As an alternative base with better solubility in organic solvents, caesium carbonate (Cs<sub>2</sub>CO<sub>3</sub>) was applied. Still, merely 4-hydroxyacetophenone was recovered, even after heating at reflux, long-time stirring or addition of KI as activator.<sup>381</sup>

It seems that a Williamson-ether type synthesis of *p*-butynyl-oxy-acetophenone **52** is not possible from butynyl bromide. This might be due to an E<sub>2</sub>-type elimination which may be favoured in butynyl halogenides (Figure 44): the β-CH<sub>2</sub> group respective to the halogenide is CH-acidic due to neighbourhood to the alkynyl group,<sup>382</sup> thus enabling the abstraction of a proton in β position, followed by elimination of the halogenide. This would explain why in most cases, the reagent 4-hydroxyacetophenone was recovered quantitatively. Such a reaction would neither be possible in propargyl halogenides, where no β-CH is available, nor in pentynyl halogenides, where the β-CH is not activated enough for proton abstraction.

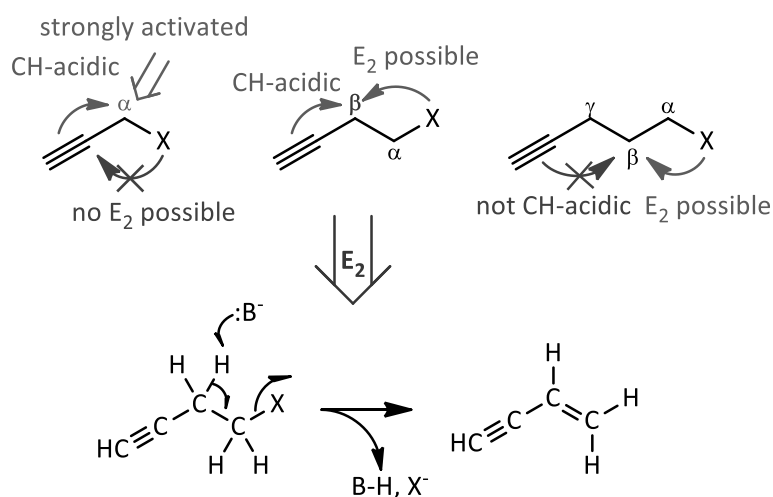
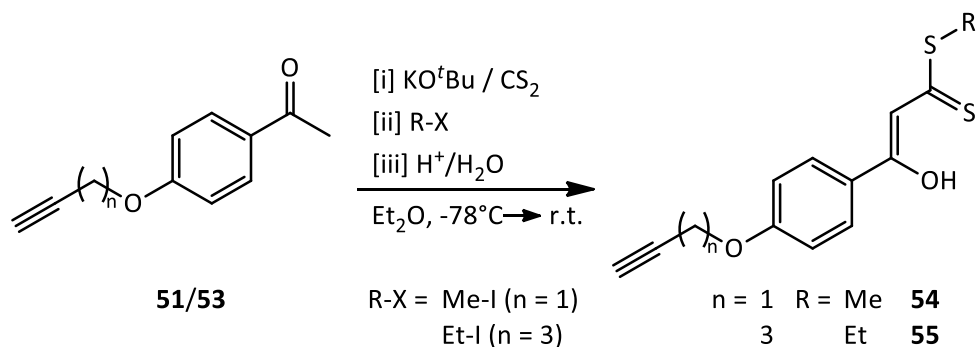


Figure 44 Possible E2-type elimination of the terminal halogenide due to CH-activation of the  $\beta$ -CH<sub>2</sub> in butynyl halogenides. The acidity and activity of the functional groups is schematically depicted.

Based on these considerations, the expected favourable properties of the pentynyl group (*i.e.* no superimposed C-H activating effects due to the increased distance by one CH<sub>2</sub> group) lead to the usage of pentynyl chloride as substrate. Phenol has been described to react with the reactant by usage of Cs<sub>2</sub>CO<sub>3</sub> and KI.<sup>381</sup> With this procedure, the desired product **53** was obtained in excellent yield of 92 % (Scheme 6).

#### 11.1.1.2 Preparation of $\beta$ -hydroxydithiocinnamic esters from acetophenones **51** and **53**

The alkynyl-functionalized acetophenone derivatives were then converted into  $\beta$ -hydroxy dithiocinnamic esters. In principle, it is possible to prepare this substance class in two steps,<sup>103</sup> or by using a one-pot approach.<sup>104,105</sup> The latter is faster and in many cases more efficient, but sometimes reactive intermediates caused by functional groups might require the isolation of the respective dithiocinnamic acid.



Scheme 7  $\beta$ -Hydroxydithiocinnamic esters based on acetophenones **51** and **53**.

Following the one-step approach, compound **51** was converted with CS<sub>2</sub> and methyl iodide (Scheme 7) and gave the desired compound **54** in a low yield (14 %). As a side reaction in this setup, deprotonation of the propargylic group through potassium tert-butoxide (KO<sup>t</sup>Bu) could compete against deprotonation of the acetophenone-methyl group. In a second and third attempt to improve the yield, more equivalents of KO<sup>t</sup>Bu, *i.e.* 2.5 and 3 eq., were therefore used, giving almost no improvement of the reaction's outcome in the first (yield 16 %) and a more than doubled yield of **55** (36 %) in the second case. It appears as if the presence of the alkynyl group requires one additional equivalent of base for complete deprotonation of the terminal alkyne-carbon atom prior to activation of the methyl group in  $\alpha$ -position to the carbonyl group.

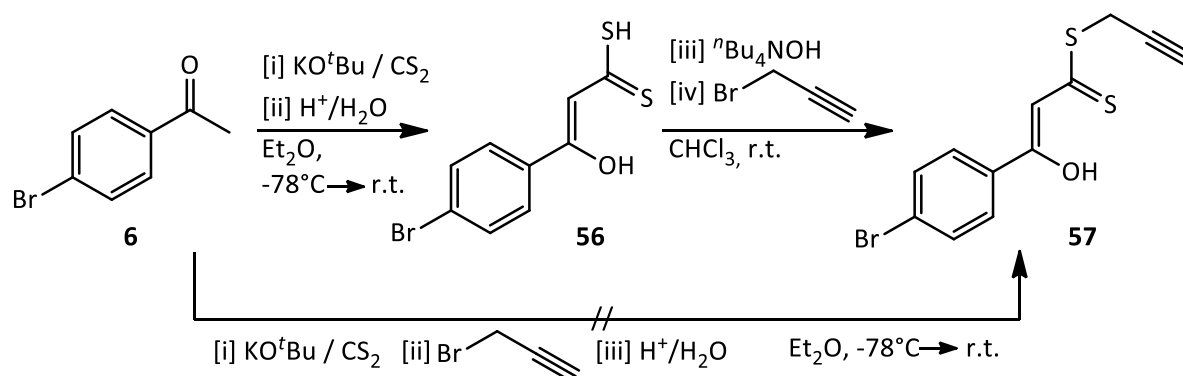
The acetophenone derivative **53** was also successfully converted to the respective  $\beta$ -hydroxydithiocinnamic ester **55** in 42 % yield, using 2.5 eq. of KO<sup>t</sup>Bu and ethyl iodide as alkylating agent. Not only the favourable pentynyl group, but also the use of an ethyl- instead of a methyl group contributed to the markedly increased yield. It has been found in earlier experiments that the use of methyl iodide as alkylating agent lead to an enhanced formation of the respective ketene mercaptal, thus lowering the overall yield.<sup>118</sup> In some cases, the use of substoichiometric amounts (0.9 eq.) of alkylating agent could improve the overall yield by suppressing this unfavourable side reaction.<sup>104,105</sup>

## 11.1.2 Introducing the alkynyl group at the dithiocarbonyl site

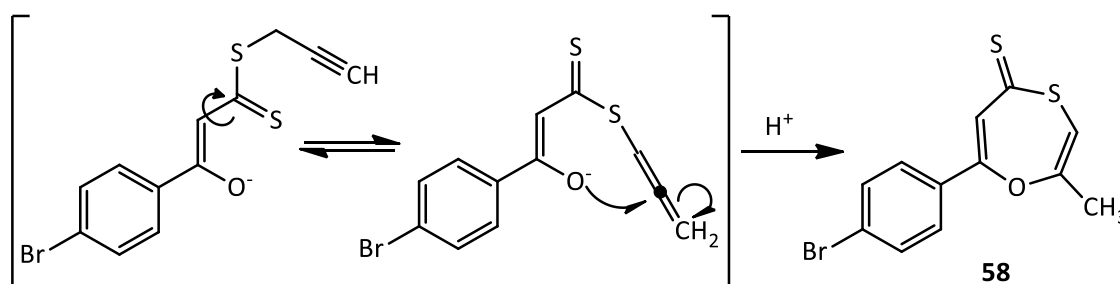
### 11.1.2.1 Introducing a propargyl group

The synthesis of compound **57** in a two-step reaction reported in literature (Scheme 8)<sup>383</sup>. Following this procedure, first the free  $\beta$ -hydroxydithiocinnamic acid **56** was isolated in 56 % yield by recrystallization from *n*-hexane/ethyl acetate. In the second step, the propargylic group was introduced *via* a two-phase reaction in chloroform/water with tetrabutyl ammonium hydroxide (tBu<sub>4</sub>NOH) as base and phase-transfer salt. After recrystallization from ethanol and isopropanol, pure **57** was obtained in 43 % yield (overall yield 24 % in two steps).

In an attempt to optimize the preparation of **57**, the well-established one-pot method was explored as an alternative approach (Scheme 8). However, it was not possible to isolate the desired compound: A yellow solid was recovered which could not be identified as the target molecule. Analysis with NMR, mass spectrometry and IR spectroscopy lead to the assumption that a rearrangement process must have occurred during the reaction.

Scheme 8 Two possible pathways towards compound **57**.

The isolated compound has the identical sum formula as **57**, established from EI-MS data:  $[\text{M}]^+$  and  $[\text{M}+2]^+$  singlets at  $m/z = 312/314$ , characteristic for a Br-containing compound were found, but not the typical fragment after release of S-alkyl (here: S-Propargyl), as was found as dominant fragment peak in the EI mass spectrum of **57**. NMR spectroscopic analyses point towards a cyclization reaction, leading to a compound **58** with a seven-membered heterocycle as outlined in Scheme 9. It is noteworthy that several signals appear to be doubled in both <sup>1</sup>H and <sup>13</sup>C NMR spectra of **58**, indicative of two isomers being present in the CDCl<sub>3</sub> solution (Figure S 17). These could originate from different ring-bent formations of this heterocycle which may be stabilized through lone pair electrons of S and O, leading to diverse electronic effects onto the conformer structures. This rearranged compound may be formed from an allene-propargyl tautomeric intermediate as suggested in Scheme 9.

Scheme 9 Possible rearrangement of compound **57** during conditions of the one-pot reaction to give **58**. The cyclization may occur *via* an allene tautomeric intermediate.

Such a cyclization towards a seven-membered ring has not previously been discussed in literature. Larsson and Lawesson reported on a thio-claisen rearrangement of the homologous ketene mercaptal towards a thiapyran structure (Chart 9a),<sup>383</sup> furthermore a cyclization leading to a 5-membered ring and an exocyclic double bond was reported from cyclization of compounds bearing propargyl thioamide structure (Chart 9b).<sup>384,385</sup> Similar reactions might in principle be thinkable also in this present case, however spectroscopic data point against these structural motifs, *e.g.* by absence of a band of  $\nu(\text{C}=\text{O})$  in the IR spectrum of **58**.

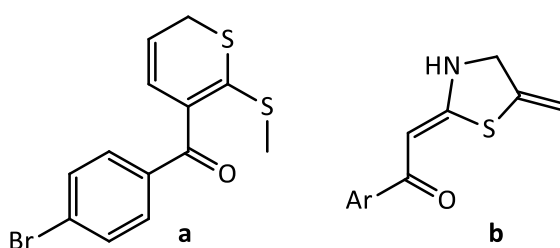


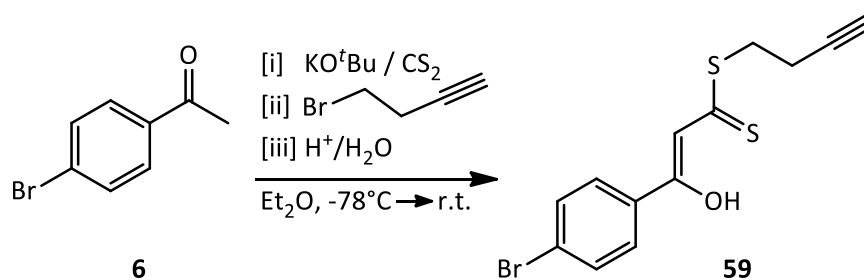
Chart 9 Products of rearrangement processes originating from propargyl-substituted  $\beta$ -oxo thioesters.

In this first one-pot reaction, an instantaneous dark-brown discoloration upon addition of propargyl bromide at room temperature indicated an immediate, probably unwanted, reaction. No such color change was observed in the successful two-step synthesis. Therefore the reaction was repeated and maintained at  $-78\text{ }^\circ\text{C}$  until addition of propargyl bromide and closely monitored by TLC. As soon as the mixture was allowed to warm up to room temperature, the discoloration appeared again but did not manifest itself in a significant change in the TLC pattern. Since column chromatography might present one other source of side reactions, the mixture was subjected to crystallization from isopropanol; however without success. The isolated red-brown oil did include the desired product (as established from NMR and MS data), but a purification was not possible.

#### 11.1.2.2 Introducing a butynyl group

In contrast to the encountered problems with the synthesis of propargyl-derived compound **57**, it was possible to convert 4-bromo acetophenone **6** into the *S*-butynyl derived  $\beta$ -hydroxy dithiocinnamic ester **59** *via* the one-pot synthetic procedure in 22 % yield. No rearrangement or other significant side reactions were observed; even after workup *via* column chromatography (Scheme 10).





Scheme 10 Synthesis of  $\beta$ -hydroxydithiocinnamic ester **59** with a S-butynyl group.

## 11.2 Complexation reactions of alkyne-derived $\beta$ -hydroxydithiocinnamic esters

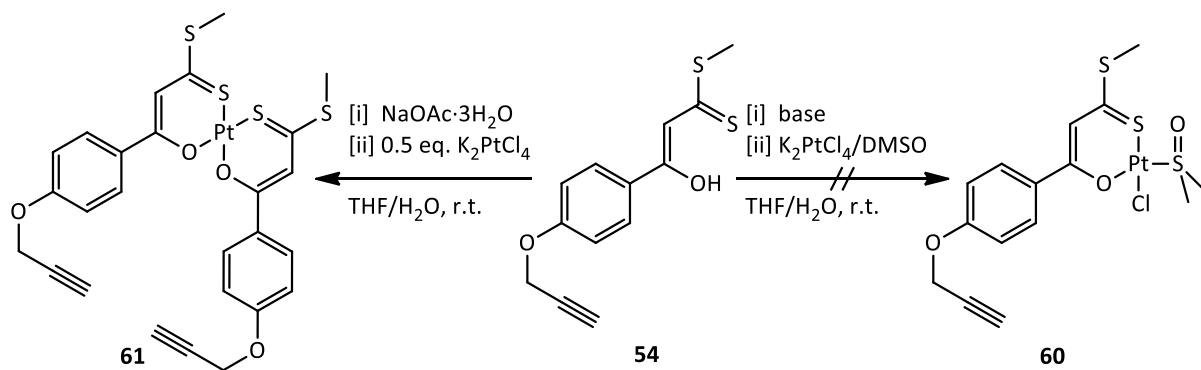
The obtained alkyne-functionalized compounds were subsequently used to prepare the respective (*O,S*) chelate complexes. Since a variety of bases can be used to deprotonate the  $\beta$ -hydroxy group, sodium acetate (NaOAc) was chosen as the preferable base. It is not as acidic as the typically used NaH which is expected to probably also deprotonate the terminal alkynes, thus leading to unwanted side reactions. Table 10 lists  $\text{pK}_a$  and  $\text{pK}_b$  values for representative C-H acidities and relevant bases.

Table 10  $\text{pK}_a$  and  $\text{pK}_b$  values of acid/base combinations relevant for this study.

compound	$\text{pK}_a$	ref.	compound	$\text{pK}_b$	ref.
$\text{CH}_4$	48	380	NaH	ca. -26	386
$\text{H}_2\text{C}=\text{CH}_2$	44	380	KO <sup>t</sup> Bu	ca. -18	387
$\text{HC}\equiv\text{CH}$	24	380	NaOAc	9.24	386

### 11.2.1 Complexation reactions of Ph-O-propargyl compound **54**

Compound **54** was converted with  $\text{K}_2\text{PtCl}_4$  according to the standard procedure, using NaOAc as base. A yellow solid was recovered from recrystallization; purification *via* column chromatography was not attempted due to the previously observed rearrangements under such conditions. Based on MS and NMR data, the isolated compound did neither contain platinum nor did it show the main structural features of compound **54**. Even the use of KO<sup>t</sup>Bu as a base, both under inert and non-inert conditions, did not lead to the desired compound **60** (Scheme 11).



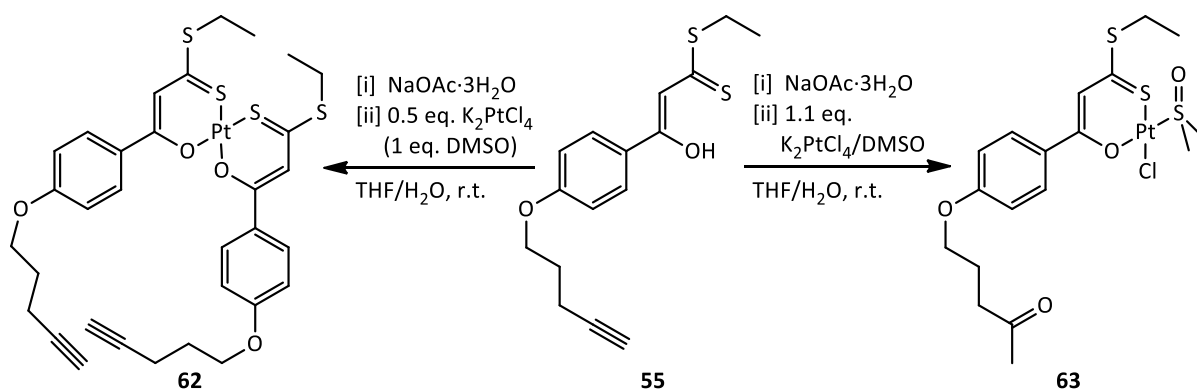
Scheme 11 Attempts to coordinate  $\beta$ -hydroxydithiocinnamic ester **54**, bearing a O-propargyl group, towards a Pt(II) center.

It is generally known that due to the strong delocalization of electron density in the chelate ring, bischelates are very stable and preferably formed.<sup>107</sup> To assess whether the ligand would in principle be capable of forming (*O,S*) bidentate Pt(II) complexes, the synthesis of the respective bischelate **61** was attempted. It was possible to isolate the desired compound, however in low yield (10 %) and not to an appreciable degree of purity. This is mostly due to decomposition during the reaction and work-up processes.

### 11.2.2 Complexation reactions of Ph-O-pentynyl compound **55**

To establish whether the pentynyl-functionalized substance **55** would in principle be capable of forming Pt(II) complexes, the synthesis of the corresponding bischelate was attempted (Scheme 12). Deprotonation was achieved using sodium acetate, followed by conversion with an aqueous solution of potassium tetrachloroplatinate. After work-up by filtration through silica, the red, pure bischelate was obtained in 28 % yield. Analytical data proved the formation of the desired compound **62**.

After the successful conversion of **55** into **62**, synthesis of the respective monochelate was attempted. NMR spectra gave characteristic signals indicating the formation of an (*O,S*) chelate with DMSO as co-ligand, however the pentynyl group was not retained (Scheme 12).



Scheme 12 Conversion of pentynyl-derived  $\beta$ -hydroxythiocinnamic ethyl ester **55** to mono- and bisfunctional Pt(II) complexes.

Instead, the triple bond had been hydrated and a methyl ketone was formed, as indicated by the analytical data of **63**: <sup>1</sup>H and <sup>13</sup>C NMR spectroscopy (Table 11) showed the loss of signals belonging to the alkynyl group, whilst the newly formed –COCH<sub>3</sub> unit gave characteristic signals for the methyl group at 2.2 ppm and 29.8 ppm in <sup>1</sup>H and <sup>13</sup>C NMR spectra, respectively, as well as at high frequency for the carbonyl-C at 208.9 ppm in <sup>13</sup>C NMR spectra. Mass spectrometry gave the [M+Na]<sup>+</sup> peak with matching isotopic pattern at *m/z* = 653. In the IR spectrum, C≡C stretching vibrations were lost and a new band at 1705 cm<sup>-1</sup> was assigned to a C=O stretching vibration. Finally, elemental analysis proved the composition of the formed compound.

Table 11 NMR spectroscopic data of **55** and the resulting Pt(II) complexes **62** and **63**. All spectra were recorded in CDCl<sub>3</sub>.

	<sup>1</sup> H NMR data [ppm]				<sup>13</sup> C NMR data [ppm]		
	<b>55</b>	<b>62</b>	<b>63</b>		<b>55</b>	<b>62</b>	<b>63</b>
≡CH	1.98	1.99	2.18 (CO-CH <sub>3</sub> )	≡CH	69.2	69.2	29.85 (CO-CH <sub>3</sub> )
CH <sub>2</sub> <sup>γ</sup>	2.42	2.43	--	≡C-	83.3	83.4	208.9 (C=O)
CH <sub>2</sub> <sup>β</sup>	2.03	2.04	2.06	CH <sub>2</sub> <sup>γ</sup>	14.9	14.9	39.6
CH <sub>2</sub> <sup>α</sup>	4.14	4.15	4.01	CH <sub>2</sub> <sup>β</sup>	27.8	28.3	20.8
C-OH	15.23	--	--	CH <sub>2</sub> <sup>α</sup>	66.4	66.4	67.1
=CH-	6.88	7.08	7.09	C-OX	170.7	174.6	174.8
DMSO	--	--	3.65	=CH-	107.7	112.6	111.3
			<sup>3</sup> J <sub>PtH</sub> = 23.4 Hz	CS <sub>2</sub>	215.88	175.9	178.6
				DMSO			46.7

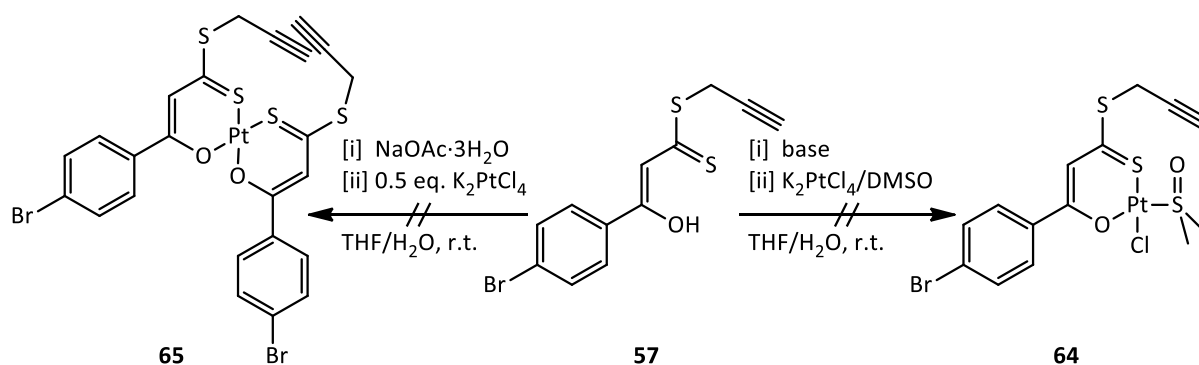
Platinum-catalyzed alkyne hydration has been known since the early 1960's<sup>388</sup> but not investigated until the 1990's, when the hydration of terminal and internal  $C\equiv C$  triple bonds through Zeise's dimer was first described.<sup>389</sup> This concept was quickly expanded to other Pt(II) salts.<sup>390,391</sup> Today, a great variety of alkyne-hydrating catalysts from platinum or other metals is known that efficiently and regioselectively hydrate terminal and internal alkynes.<sup>392</sup>

With this information in mind, the conversion of *two* equivalents **55** with  $K_2PtCl_4$  was repeated, also in presence and absence of DMSO to rule out any influence from that additive. NMR data of the crude material gave no evidence for a hydration of the alkyne functionality. Obviously, the fast and stable formation of the bischelate structure prevents the Pt(II) center from attacking an alkyne functionality in that case. When preparing monochelate complexes, usually a slight stoichiometric excess of aqueous potassium tetrachloroplatinate (1.1 eq.) is used to prevent the formation of bischelates. Therefore some unchelated  $K_2PtCl_4$  might remain in solution which could act as catalyst. In addition, in monochelate complexes, two binding sites are available that can easily bind and substitute available donor atoms. It is unlikely that Pt(II) exerts its catalytic properties on alkynes that are directly (*O,S*) chelate-bound to the same metal center: The ligand's steric features do not allow for the pentynyl group to bind to the same Pt(II) center. Instead, an intermolecular pathway may be envisioned where the alkyne group of a (*O,S*) ligand bound to a different Pt(II) center or of unbound ligands is attacked.

Detailed clarification of the possible reaction mechanism has not been pursued since catalysis of triple bond reactions is not within the scope of these studies. Future investigations might elucidate if it is possible to prevent this side-reaction by substituting water as solvent for the pre-activation of  $K_2PtCl_4$ , working completely water-free and at the same time avoiding an excess of  $K_2PtCl_4$ . For the further development of this research scope, using alkyne functionalities at the Pt(II) unit was proven to be not favourable and alternative lead structures should be found.

### 11.2.3 Complexation reactions of S-propargyl compound **57**

Despite the aforementioned difficulties, the prepared S-Alkynyl functionalized ligands **57** and **59** should be converted into the respective complexes to see whether this altered position of the alkyne function might lead to a different outcome (Scheme 13).

Scheme 13 Attempts to coordinate compound **57** to a Pt(II) center.

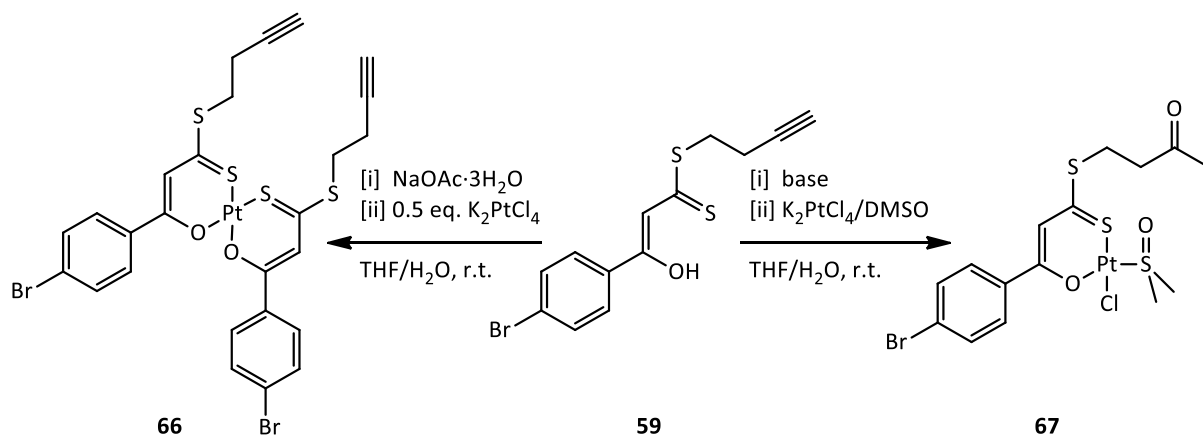
Compound **57**, with the propargyl group at the sulfur site, was converted with K<sub>2</sub>PtCl<sub>4</sub> under various conditions. Neither the use of NaOAc nor of KO<sup>t</sup>Bu as base lead to the desired product **64**, even though analytical data hint towards the formation of the same product mixture in both cases. Isolated solids did, however, neither contain platinum (established from the missing characteristic isotopic pattern in MS spectra) nor the main structural features of the ligands in NMR data.

It was not even possible to isolate the respective bischelate **65** under the conditions which proved to be successful in attempts with the other ligands. Strikingly, structural features of the rearranged compound **58** from ligand synthesis were observed in MS and NMR spectra, thus indicating that the same reaction that was induced earlier had now also occurred under the complexation conditions.

#### 11.2.4 Complexation reactions with the S-butynyl derived compound **59**

The butynyl-derived ligand **59** was successfully converted to give the bischelate **66** upon deprotonation with sodium acetate as red solid (Scheme 14). Although mass spectra did not give signals of the whole molecule, NMR (Table 12) and IR spectroscopic data as well as elemental analysis proved the formation of compound **66**.

After the confirmation that this ligand is able to form Pt(II) bischelate complexes, preparation of the monochelate **67** was attempted. Similar to **63**, spectroscopic data gives evidence for the formation of a monochelated (*O,S*) bidentate complex with assisting coordination of DMSO, however again hydration of the triple bond occurred, as observed in NMR spectroscopic data (Table 12).

Scheme 14 Conversion of S-butynyl-derived  $\beta$ -hydroxydithiocinnamic ester **59** to mono- and bisfunctional Pt(II) complexes.Table 12 NMR spectroscopic data of **59** and the resulting Pt(II) complexes **66** and **67**. All spectra were recorded in CDCl<sub>3</sub>.

	<sup>1</sup> H NMR data [ppm]				<sup>13</sup> C NMR data [ppm]		
	<b>59</b>	<b>66</b>	<b>67</b>		<b>59</b>	<b>66</b>	<b>67</b>
<b>≡CH</b>	2.07	2.11	2.20 (CO-CH <sub>3</sub> )	<b>≡CH</b>	70.06	70.56	29.53 (CO-CH <sub>3</sub> )
<b>CH<sub>2</sub><sup>β</sup></b>	2.65	2.74	3.00	<b>≡C-</b>	81.97	81.67	206.36 (C=O)
<b>S-CH<sub>2</sub><sup>α</sup></b>	3.46	3.40	3.45	<b>CH<sub>2</sub><sup>β</sup></b>	17.91	18.64	42.12
<b>C-OH</b>	14.10			<b>S-CH<sub>2</sub><sup>α</sup></b>	32.01	32.70	27.56
<b>=CH-</b>	6.88	7.05	7.02	<b>C-OX</b>	169.49	174.07	174.17
<b>CS<sub>2</sub></b>				<b>=CH-</b>	108.18	113.22	111.8
<b>DMSO</b>	--	--	3.66	<b>CS<sub>2</sub></b>	216.57	177.01	180.88
				<b>DMSO</b>	--	--	46.81

### 11.3 Introducing an azide group into $\beta$ -hydroxydithiocinnamic esters

In parallel to the above-mentioned efforts, the preparation of a  $\beta$ -hydroxydithiocinnamic ester with an azide group at the aromatic subsite was attempted. Introducing a N<sub>3</sub> group in aryl or benzylic positions is a widely applied methodology and well documented. Phenyl azides could be introduced from amino acetophenones,<sup>393,394</sup> azidomethyl groups could be formed from methyl acetophenones.<sup>395,396</sup>

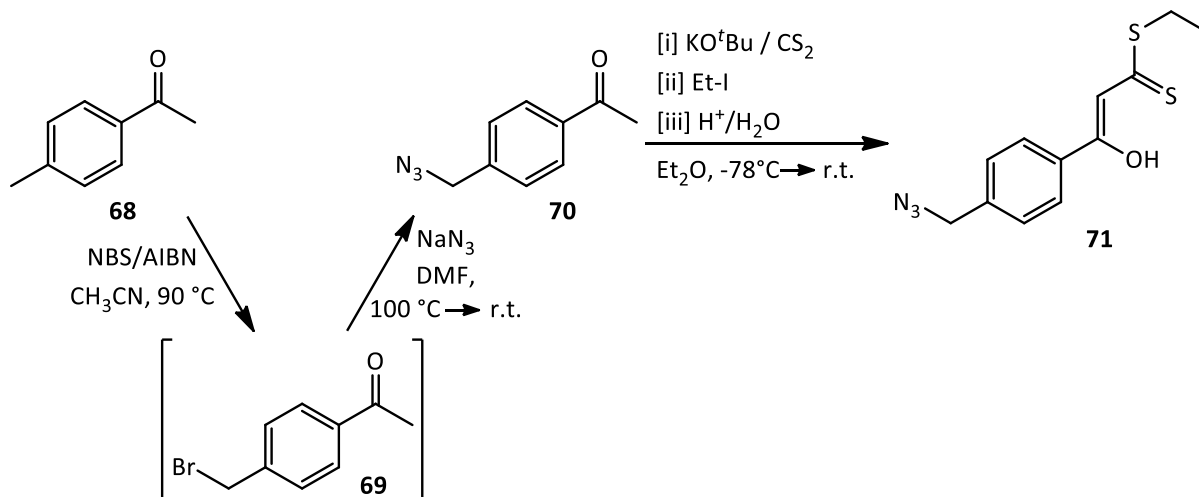
In this work, the azidomethyl group was chosen as preferential lead structure. The azide group itself can be considered as a pseudo-halogenide, inducing (-I) and (+M) effects onto an aromatic ring quite

similar to a bromo substituent.<sup>372</sup> In the final “clicked” products, delocalization of  $\pi$ -electrons in the triazol ring might also lead to – at this point unwanted – additional electronic influences to the chelating system (*e.g.* by mesomeric effects), thus adding more variables to the coordination environment than wanted for these first proof-of-principle experiments.

### 11.3.1 Synthesis of benzylazide-derived compound **71**

The preparation of 4-(azidomethyl) acetophenone **70** in two steps was achieved in good yields from 4-methyl acetophenone **68** *via* 4-(bromomethyl) acetophenone **69** by modified literature procedures.<sup>395,396</sup> It was then used to prepare  $\beta$ -hydroxydithiocinnamic ester derivative **71** in moderate yield (33 %) through the one-pot synthetic approach. By IR spectroscopy, the presence of the intact azido group could be proven by a strong band at  $\tilde{\nu} = 2098 \text{ cm}^{-1}$  which represents the asymmetric stretching bond of the azide group and has since decades been used as a reliable identifier for the presence of such groups.<sup>397</sup> The symmetric stretching bond, generally more variable in position (ca.  $1250\text{-}1300 \text{ cm}^{-1}$ ), is overlaid by a strong, broad band of the C=S stretching vibration at  $1228 \text{ cm}^{-1}$ .

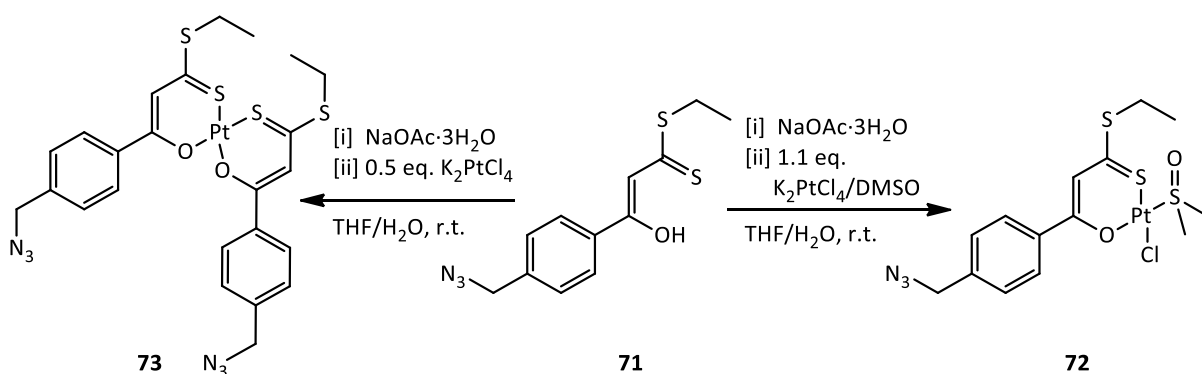
In contrast to experiences with alkynyl-derived compounds, this synthetic route proved to yield the target compounds without rearrangement processes or major impeding side-products.



Scheme 15 Sequential synthesis of Compound **71** with a benzyl-azide functionality.

### 11.3.2 Reactions of compound **71** with $K_2PtCl_4$

Preparation of the corresponding Pt(II) complexes was successful for both mono- and bis-functional complex types (Scheme 16).



Scheme 16 Coordination reactions of of compound **71** towards platinum.

The monochelate **72** was initially isolated with a crude yield of 53 %, but decomposition was witnessed during final purification processes (*i.e.* crystallization from DCM/*n*-hexane and further column chromatographic work-up) so that the final yield was significantly lowered (33 %). In a second attempt, by slightly altering the work-up procedure, an appreciably increased yield (82 %) of the product as orange needles was achieved. The molecular structure of **72** was confirmed by single-crystal X-ray analysis (Figure 45, left). Single crystals, despite having an appreciable appearance at macroscopic scale, showed substantial twinning. In several crystallization attempts, this could not be circumvented – therefore no bond lengths or –angles are discussed in detail. Still, all desired functional groups, especially the intact benzyl-azide unit and the monodentate chlorido and DMSO ligands, the latter binding *via* its sulfur atom, were found and the typical square-planar coordination environment clearly demonstrated.

It was unfortunately not possible to obtain MS data that corresponds to the compound or to characteristic fragments. The presence of the N<sub>3</sub> group might account for this problem, or the complexes' generally low tendency to ionize under the applied conditions.



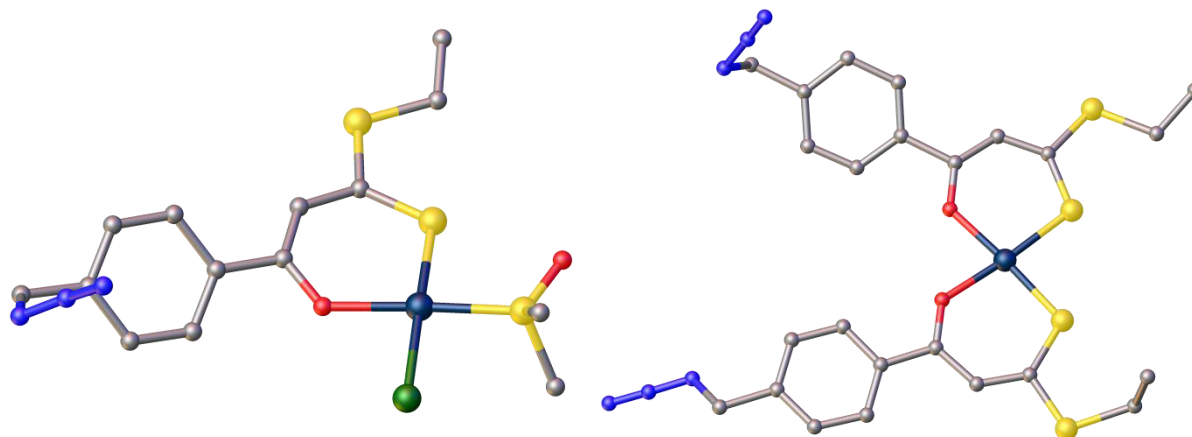


Figure 45 Molecular structures of Pt(II) complexes **72** (space group  $P2_1/n$ , left) and **73** (space group  $P-1$ , right) obtained on the basis of benzylazide-based ligand **71**. Structural motifs are given by ball and stick models.

Furthermore, it was possible to isolate the respective bischelate **73** from the conversion of two equivalents **71** with  $K_2PtCl_4$ . Crystals suitable for X-ray structure analysis were obtained from crystallization in DCM/*n*-hexane (Figure 45, right). Again due to twinning effects and the flexibility of the azido unit, no detailed discussion of bond lengths and –angles is possible. The square-planar coordination environment with the (*O,S*) units in *cis* position and the intact benzyl-azide units are still unambiguously shown within the structural motif.

During the course of various syntheses of this compound **73**, it was noted that addition of DMSO, as is usually done for the synthesis of monochelates, leads to strongly raised yields also of the bischelate (*O,S*)Pt(II) complexes: Low yields of ca. 12 % were obtained without DMSO, and ca. 70 % of **73** could be isolated when  $K_2PtCl_4$  was pre-activated with 2 eq. of DMSO. Even though the formation of bis-functional (*O,S*)<sub>2</sub>Pt(II) complexes is strongly favored (which can be seen *e.g.* by the fact that bischelates are frequently formed as a side product in monochelate syntheses), incomplete conversion alongside with decomposition have been a problem in purposeful bischelate syntheses. DMSO obviously accelerates  $PtCl_4^{2-}$  solvolysis and thus leads to neater conversion with subsequently offered donors.

### 11.3.3 Stability at HPLC conditions

Both products, **72** and **73**, were thoroughly characterized by analytical methods and their stability towards typical *rp*-HPLC conditions tested. This presents a key prerequisite for subsequent bioconjugation and purification of such compounds.

When **72** and **73** were eluted in a typical water-acetonitrile buffer gradient (*i.e.* 100/0 to 0/100 % v/v water/acetonitrile) on a C8 *rp* column, it became apparent from their retention time that these compounds are significantly more soluble in the organic phase than in water (both eluted at 95-100 % acetonitrile). Furthermore it was found that the monofunctional complex is prone to ligand substitution under the given conditions: additional peaks occurred in the HPLC chromatogram of **72** at earlier retention times, *i.e.* more polar solvent conditions. By ESI MS analysis, these were assigned to species where one and two monodentate ligands had been exchanged by acetonitrile. Since it is assumed that this solvolysis takes place gradually during the complexes' contact with acetonitrile in the buffer mixture, it cannot be excluded that the newly formed species' peaks tailed into the peak of the initial complex; thus no baseline separated peaks could be obtained in the HPLC chromatograms and HPLC stability of monodentate (*O,S*) compounds can generally not be established.

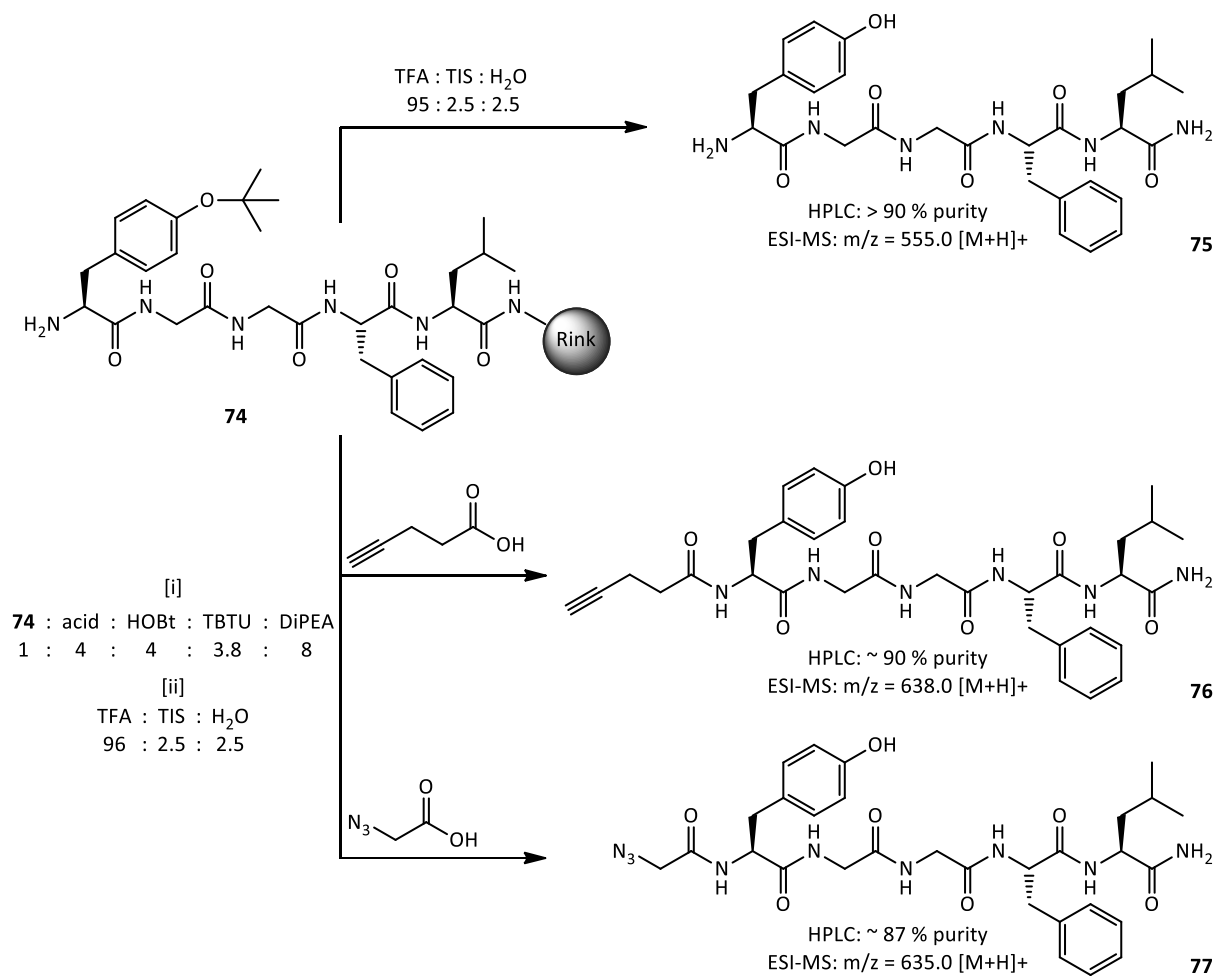
#### 11.4 Preparation and derivatization of Leu<sup>5</sup>-Enkephalin

In addition to the (*O,S*) units, the model peptide Enk required suitable derivatization prior to CuAAC reactions. The peptide was prepared by Fmoc-based solid phase peptide synthesis (SPPS) on Rink amide resin,<sup>317,320,322</sup> using an automated peptide synthesizer (Scheme 17). As activator, the TBTU/HOBt/DiPEA method was applied.<sup>xxv</sup> Before deprotection of the Tyr<sup>1</sup>-OH group and cleavage from the resin, **74** was further derivatized using either pentynoic acid or azido-acetic acid to introduce a terminal alkyne or azide, respectively (Scheme 17). Both acids were coupled manually to H-Enk-Rink **74** on solid phase using the same standard coupling procedures, upon which the functionalized peptide was deprotected and cleaved from the resin to give C-terminal amides. The functionalized peptides were obtained in good yields (59 % and 84 % for **76** and **77**, respectively) and were used for further reactions without HPLC purification since analytical HPLC proved the purity of the compounds to be greater than 85 %, a sufficiently high level for further reactions.

The identity of the functionalized peptides was established from their ESI MS data, in all cases yielding the [M+H]<sup>+</sup> signal. Furthermore, signals in <sup>1</sup>H and <sup>13</sup>C NMR spectra could, assisted by HSQC and HMBC experiments, unambiguously be identified.

---

<sup>xxv</sup> Abbreviations in this paragraph: TBTU: *N,N,N',N'*-tetramethyl-*O*-(benzotriazol-1-yl)uronium tetrafluoroborate, HOBt: 1-hydroxybenzotriazol, DiPEA: diisopropylethylamine

Scheme 17 Solid-phase peptide syntheses of Leu<sup>5</sup>-Enk derivatives **75-77**.

Upon binding of either azidoacetic or pentynoic acid, some significant shifts are induced onto signals belonging to adjoining units (see Figure 46 for comparative <sup>1</sup>H NMR data). The *N*-terminal NH<sub>2</sub> of **75** is converted to an amide-NH (*a* in Figure 46) and results in a slight shift to higher frequencies in both **76** and **77** (by ca. +0.25 and +0.08 ppm, respectively). The NH<sup>α</sup> of Gly<sup>2</sup> (*g* in Figure 46) experiences a substantial shift to lower frequencies by -0.34 and -0.51 ppm in **76** and **77**, respectively. The Phe<sup>1</sup>-OH (*f* in Figure 46), giving a sharp signal at 9.32 ppm in **75**, is broadened and shifted by ca. -0.20 ppm when a terminal acid is conjugated. The H<sup>α</sup> of Phe<sup>1</sup> (*b* in Figure 46) also experiences a substantial shift to higher frequencies by ca. +0.5 and by +0.43 ppm in **76** and **77**, respectively. Signals of conjugated azido acetic acid and pentynoic acid could be witnessed and are assigned as indicated in Figure 46 (*u*, *v*, *w*). It should be noted that signal assignment of N-H and H<sup>α</sup> signals deviates from data found for Leu<sup>5</sup>-Enk in literature.<sup>322</sup> The here presented assignment is however strongly fortified by HSQC and HMBC experiments; in the latter a defined <sup>2</sup>J<sub>CH</sub> coupling of the -C(=O)-NH- groups was witnessed, alongside with other strongly indicative cross-peaks of H/C couplings.

In  $^{13}\text{C}$  NMR spectra of the two Enk-derivatives **76** and **77**, only negligible signal shift differences are observed. All carbon atoms belonging to conjugated azidoacetic and pentynoic acid were identified.

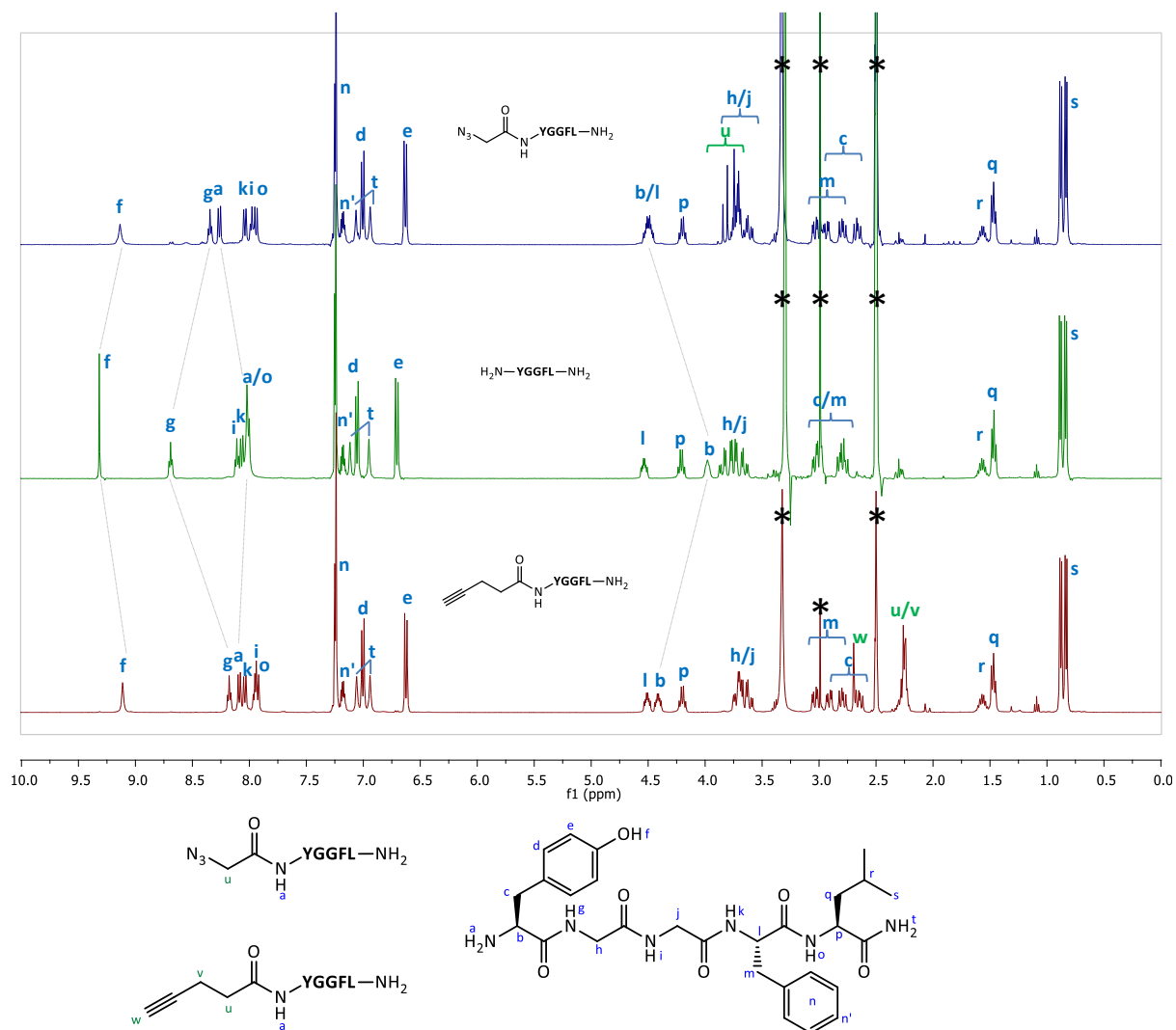
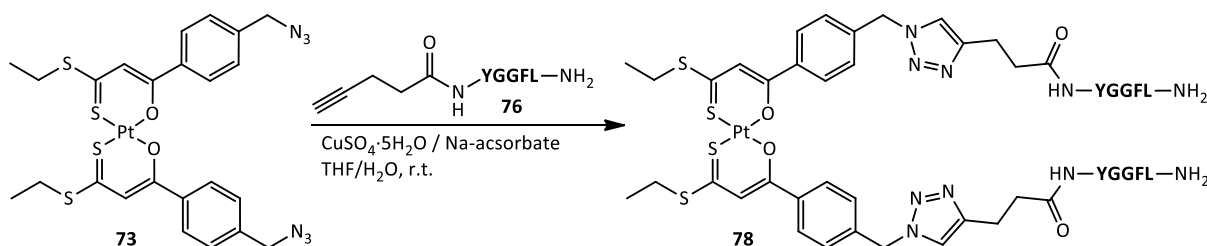


Figure 46  $^1\text{H}$  NMR spectra (400 MHz,  $\text{DMSO-d}_6$ ) of azido-functionalized **77** (top), unfunctionalized Enk-amide **75** (middle) and alkyne-functionalized **76** (bottom). Significant signal shifts in **76/77** relative to **75** are marked by grey lines. \* represents solvent residual signals.  $^1\text{H}$  NMR spectra were recorded from peptides not subjected to HPLC purification.

## 11.5 Formation of bioconjugates via CuAAC

### 11.5.1 Bischelates

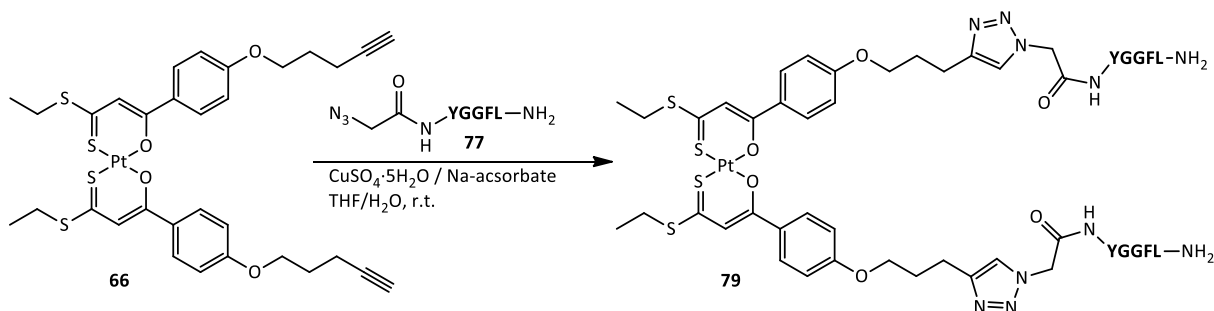
In initial experiments to form enkephalin bioconjugates *via* CuAAC, the  $(O,S)_2Pt$  bischelate compounds **66** and **73** were used to establish whether a Cu(I)-catalyzed formation of triazol rings would in principle be possible in the presence of the essential functional groups of the  $(O,S)$  unit.



Scheme 18 Combination of compounds **72** and **76** by CuAAC to give bioconjugate **78**.

First, compounds **73** and **76** were linked under Cu(I) catalysis (Scheme 18), using the combination of copper(II) sulfate (CuSO<sub>4</sub>) and sodium ascorbate to generate the Cu(I) species *in situ*, as was introduced by Sharpless and coworkers.<sup>362</sup> The course of the reaction was monitored by analytical HPLC; the degree of conversion was indicated by reducing signal intensity of the starting material **76** and increasing intensity of the product peak. Conversion was complete after two days of stirring at room temperature. Work-up included removal of all water-soluble byproducts and precipitation, the pre-purified adduct was then subjected to preparative HPLC to give pure **78** in 31 % yield. When copper(I) iodide was used as catalyst for the reaction, the yield was lower and more side products were formed (based on *rp*-HPLC of the crude material), so that the CuSO<sub>4</sub>/ascorbate combination was used in subsequent experiments.

Furthermore, compounds **66** and **79** were successfully combined under similar conditions to give **79** (Scheme 19). The conversion was, however, markedly lower and more side products were formed, as was established from analytical HPLC of the crude material. This combination was, not only because of the lower yields but also due to the above-described difficulties with alkyne-derived  $(O,S)$  compounds, not used in following experiments.



Scheme 19 Combination of compounds **66** and **77** by CuAAC to give bioconjugate **79**.

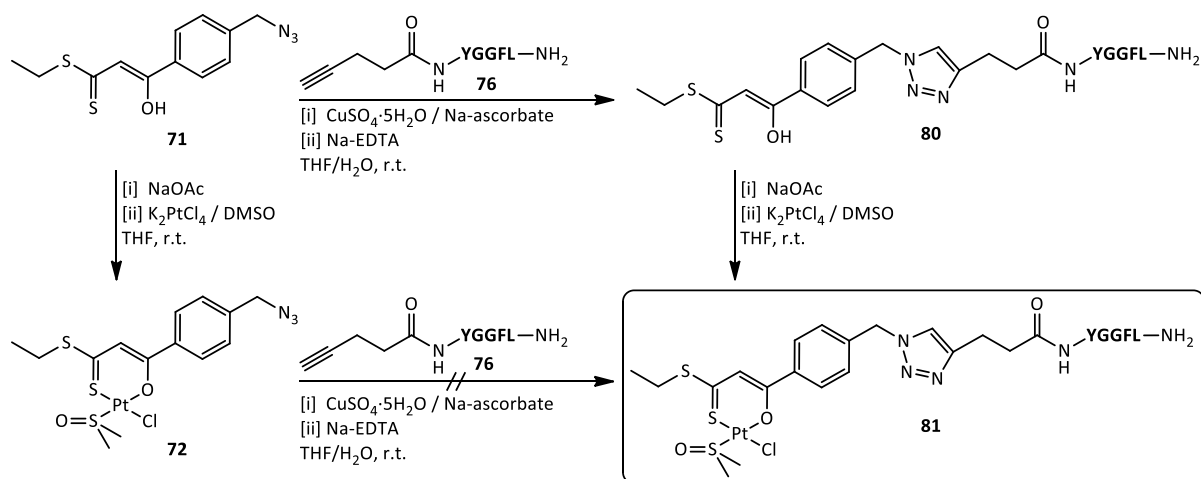
### 11.5.2 Monochelates

Subsequently, the bioconjugation of the monofunctional Pt(II) complex **81** was attempted. Two pathways are in principle thinkable for this endeavour (Scheme 20):

- linking of a monofunctional Pt(II) complex towards the Enk derivative, and
- linking of the respective ligand by CuAAC, followed by coordination towards the Pt(II) center.

The first-mentioned option was found to be less promising, since Cu(I/II) could partially stand in concurrence to Pt(II) coordination. Furthermore could the HPLC-chromatographic work-up lead to ligand substitution of the monodentate ligands, leading to various solvolysis products. The second option, on the contrary, was expected to also lead to possible copper complexes, which might albeit be cleavable by addition of proper copper chelators. Subsequent Pt(II) coordination could lead to monofunctional Pt(II) complexes with a defined set of monodentate ligands which could either be conserved by circumventing HPLC workup through alternative work-up techniques or could selectively be exchanged by HPLC-stable ligands.

Indeed, when the monofunctional Pt(II) complex **72** was combined with **76** under influence of CuSO<sub>4</sub> and ascorbate, it was not possible to isolate a pure compound. A plethora of signals was observed in HPLC chromatograms of the reaction mixture, and the main peaks that were isolated could not be identified as Pt(II) containing bioconjugates. In fact, the isotopic pattern which was observed in ESI mass spectra of several peaks rather pointed to copper-containing adducts than towards the presence of Pt(II) in these samples. It was not possible to clearly identify the formed products, but obviously this approach was not going to lead to the desired bioconjugates.

Scheme 20 Pathways towards bioconjugate **81** via CuAAC.

When following the second approach, *i.e.* linking of **76** with the azide-derived ligand **71** through CuAAC, it was necessary to use more than 1 mol-eq. of  $\text{CuSO}_4$  for a successful conversion of the reactants – the usage of the typical 0.2 eq. (or less) of  $\text{CuSO}_4$  did not lead to sufficient conversion of the starting materials. Obviously, one eq. of copper was indeed consumed through coordination towards the (O,S) chelating unit. The starting materials were consumed after two days, and the addition of excess  $\text{Na}_2\text{EDTA}$  (disodium ethylenediamine tetraacetate) lead to reversal of Cu-(O,S) chelation. The water-soluble Cu-EDTA complex was conveniently removed from the mixture through liquid-liquid extraction. Purification by *rp*-HPLC lead to pure bioconjugated  $\beta$ -hydroxydithiocinnamic ester **80** in appreciable yields (42 %).

Purified **80** was then used to prepare **81** by conversion with  $\text{K}_2\text{PtCl}_4$  and DMSO by adapting the established protocol for small-molecule complex formation. After a reaction time of one day, crude **81** was obtained and purified by repeated extraction and precipitation steps. According to ESI MS analysis, the presence of DMSO and chloride as monodentate ligands was confirmed.

$^1\text{H}$  NMR spectra of **80** and **81** were recorded in  $\text{DMSO-d}_6$  and are shown comparatively in Figure 47 with the starting material **76** as reference. Signal assignment was confirmed through HSQC and HMBC experiments. Upon formation of the triazole by CuAAC, the signals belonging to pentynoic acid in **76** are shifted in **80**, its  $\beta$ - $\text{CH}_2$  group appearing at 2.76 ppm, thus shifted by ca. +0.5 ppm to higher fields. The newly formed methine group of the triazol linker (*w* in Figure 47) appears at 7.79 ppm. The OH proton of the free  $\beta$ -hydroxydithiocinnamic unit is clearly observable at high field (15.15 ppm). Upon coordination towards the Pt(II) unit, this signal is lost and a typical shift of the methine proton belonging to the (O,S) unit (*4* in Figure 47) by ca. +0.05 ppm is witnessed so that it

appears together with aromatic signals of Phe<sup>4</sup>. Even though ESI mass spectral data proved the sum formula to include DMSO and chloride, the signal of Pt-coordinated DMSO is not detected in the <sup>1</sup>H NMR spectrum of **81** due to gradual exchange with its deuterated equivalent.<sup>xxvi</sup>

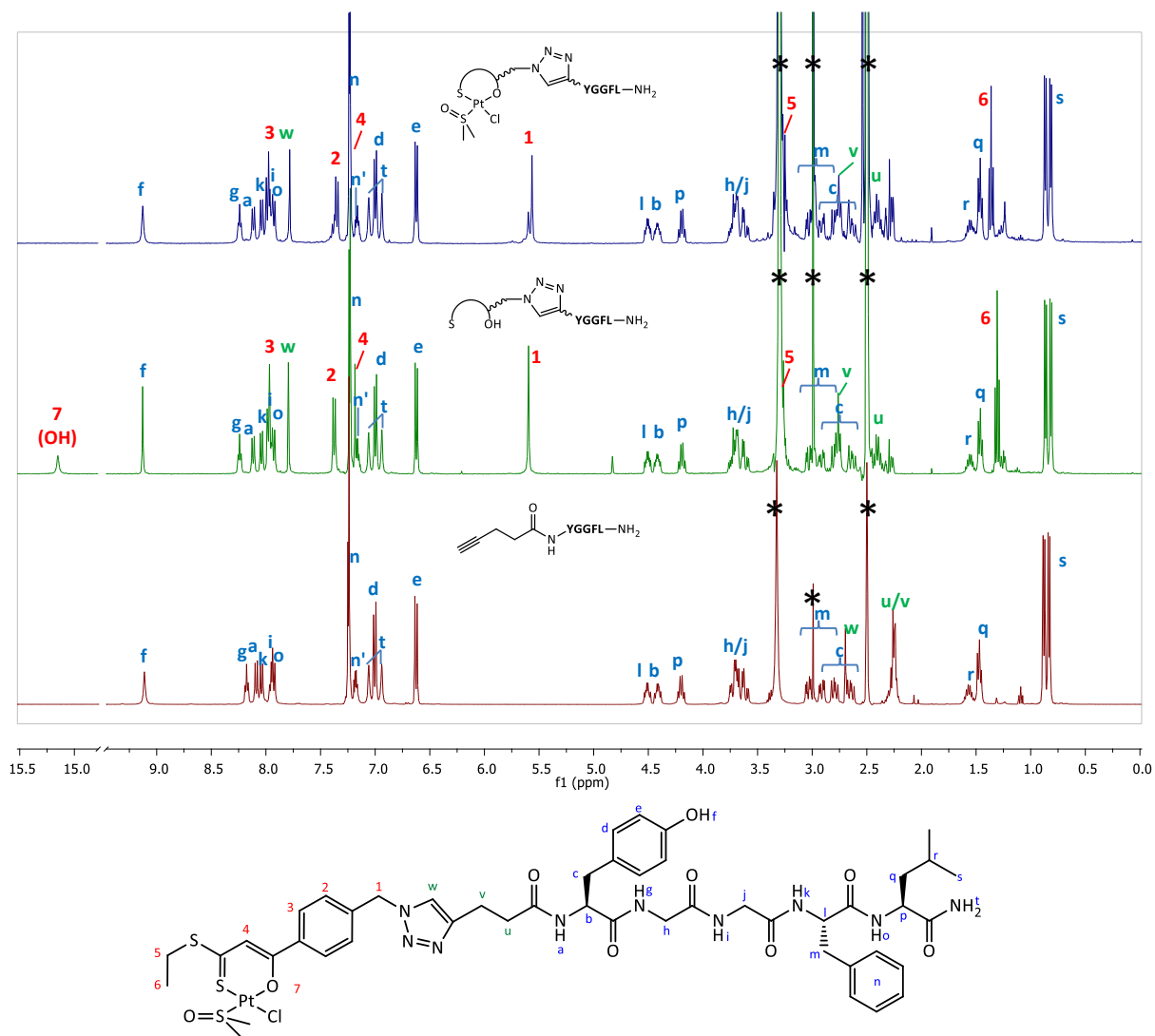


Figure 47 <sup>1</sup>H NMR spectra (400 MHz, DMSO-d<sub>6</sub>) of Pt(II) complex **81** (top), the ligand with triazole linker **80** (middle) and the starting material, alkyne-derived Leu<sup>5</sup>-Enk **76** (bottom). The signal of Pt-coordinated DMSO is not witnessed in the spectrum of **81** due to a gradual exchange by DMSO-d<sub>6</sub>.

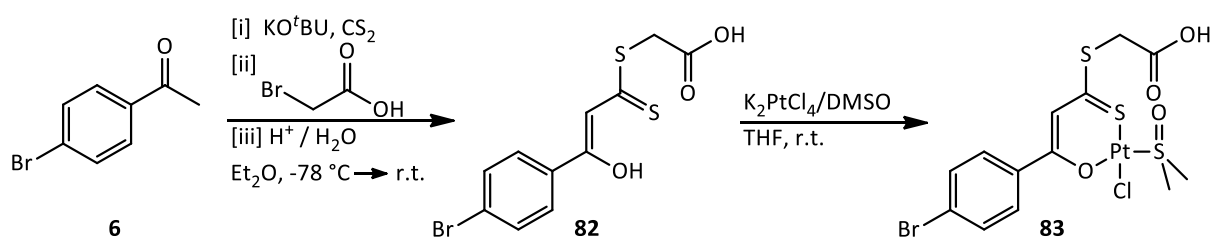
<sup>xxvi</sup> Data recording in an alternate solvent, such as THF-d<sub>8</sub>, would have been favourable. Unfortunately, compounds **76** and **80** were not soluble in THF-d<sub>8</sub> enough for appreciable signal intensity. For the sake of better comparability, spectra of **81** were therefore also recorded in DMSO-d<sub>6</sub>.



## 12 BIOCONJUGATES VIA AMIDE BOND FORMATION

### 12.1 Ligand and complex synthesis

As described above, incorporation of a carboxy group into subunits of the chelating ligand might enable bioconjugation through formation of amide bonds.



Scheme 21 Preparation of compounds **82** and **83** with a carboxylic group at the dithioester unit.

For that reason, 4-bromo acetophenone was converted with CS<sub>2</sub> and bromoacetic acid to form the β'-carboxyethane derived β-hydroxy dithiocinnamic ester **82** in good yields *via* the one-pot approach (Scheme 21). The successful synthesis of this compound was proven by standard analytical methods as well as by X-ray crystallographic data.

In crystals of **82**, the molecules are arranged in a catamer-type<sup>398</sup> array through intermolecular hydrogen bonds of the molecules' carboxy groups ( $d(\text{O}\cdots\text{O}) = 2.675 \text{ \AA}$ ), leading to band-like secondary structures in the unit cell. The molecule is flat, with only the carboxy function protruding from the molecular plane. The stabilization of the *cis*-conformation in the (*O,S*) unit through intramolecular hydrogen bonding is clearly demonstrated by the structural data. Furthermore, the β-hydroxy / dithiolato structural motif is undoubtedly shown from the bond lengths of the O3-C5=C4-C3=S2 unit, which are typical for O-C<sup>sp2</sup> and C<sup>sp2</sup>-C<sup>sp2</sup> single bonds ( $d(\text{O3-C5}) = 1.323(3) \text{ \AA}$ ;  $d(\text{C4-C3}) = 1.431(3) \text{ \AA}$ ) and C<sup>sp2</sup>=S and C<sup>sp2</sup>=C<sup>sp2</sup> double bonds ( $d(\text{C3-S2}) = 1.671(2) \text{ \AA}$ ;  $d(\text{C5-C4}) = 1.375(3) \text{ \AA}$ ) in the expected

positions. This structural feature is furthermore confirmed by the sharp singlet signal at 15.02 ppm in the compound's  $^1\text{H}$  NMR spectrum which can be attributed to the  $\beta$ -OH proton being involved in intramolecular hydrogen bonding.<sup>105,399</sup>

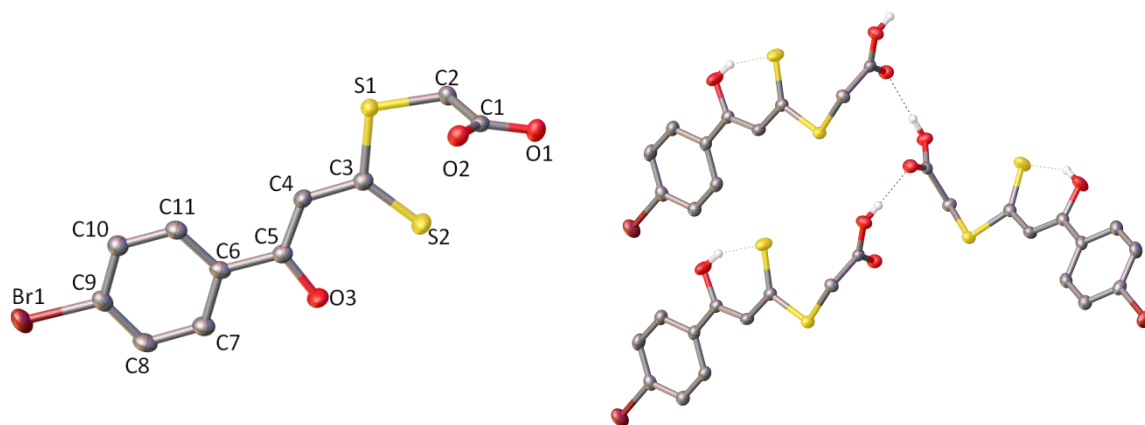
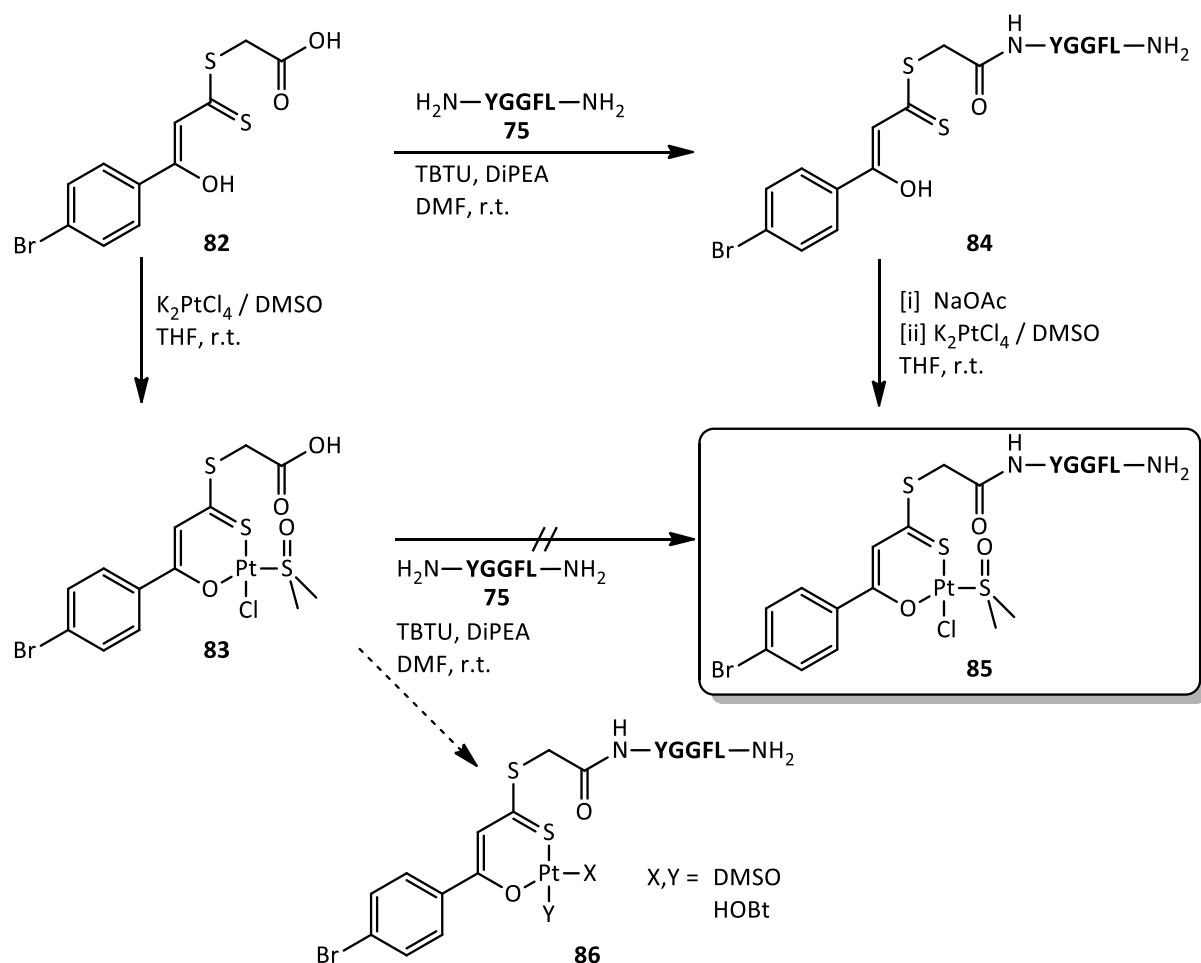


Figure 48. Molecular structure (left) and catamer-type arrangement (right) in single crystals of carboxy-derived compound **82**. The Structure is depicted in thermal ellipsoids at 50 % probability level. Space group:  $P2_12_12_1$ .

Also the respective monofunctional (*O,S*) complex **83** (Scheme 21) was successfully prepared by slightly modifying the coordination protocol: no base was used for deprotonation of the  $\beta$ -hydroxy group, since this was expected to preferentially deprotonate the  $\beta'$ -carboxy group, thus enabling unforeseeable side reactions. Analytical data of the isolated product proved the selective coordination of the ligand *via* the (*O,S*) unit and not through atoms of the newly introduced carboxy function. NMR spectroscopic and mass spectrometric data showed the chloride and DMSO ligands to be bound according to the established binding mode.

## 12.2 Formation of amide bonds

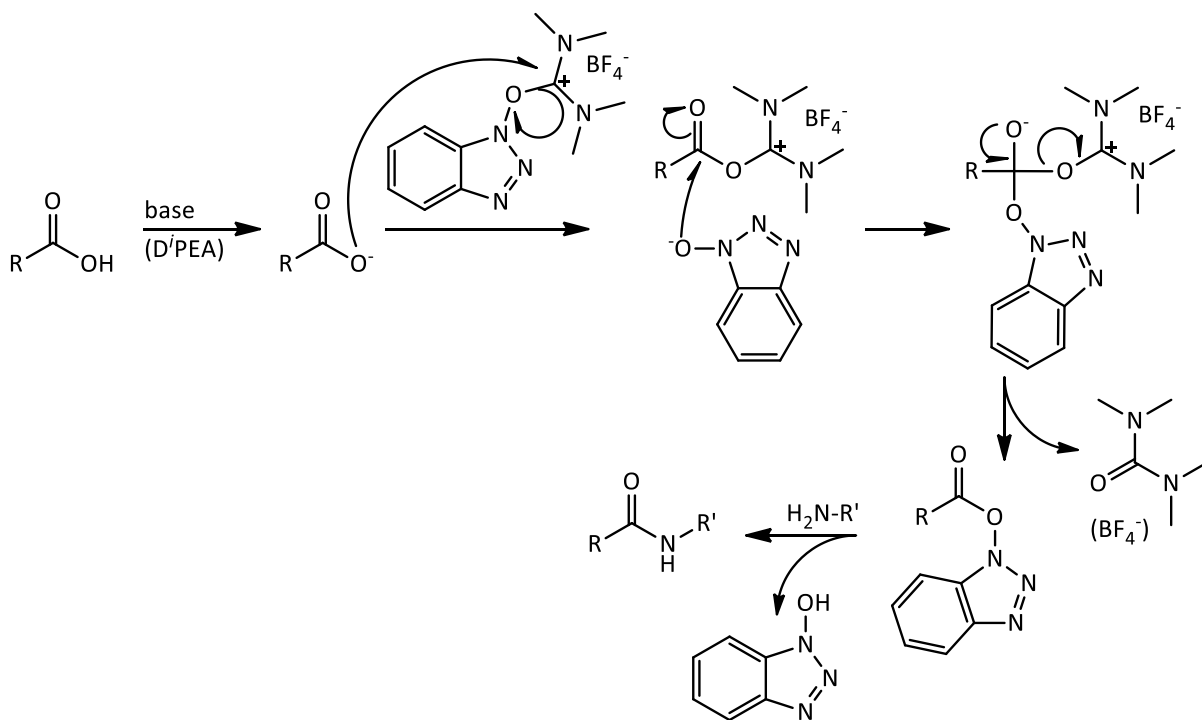
Subsequently, the formation of amide bonds was attempted for both **82** and the respective complex **83** by coupling in solution (Scheme 22). A slight excess (1.1 eq.) of the carboxy-functionalized monomer was used. TBTU<sup>400</sup> and DiPEA were used as coupling reagents, no HOBt was applied – as would usually be the case in solid phase coupling: Compound **82** does not contain a stereo center and thus does not require the racemization-suppressing additive HOBt.<sup>401</sup> Amide bonds were successfully formed within 2 h of coupling.



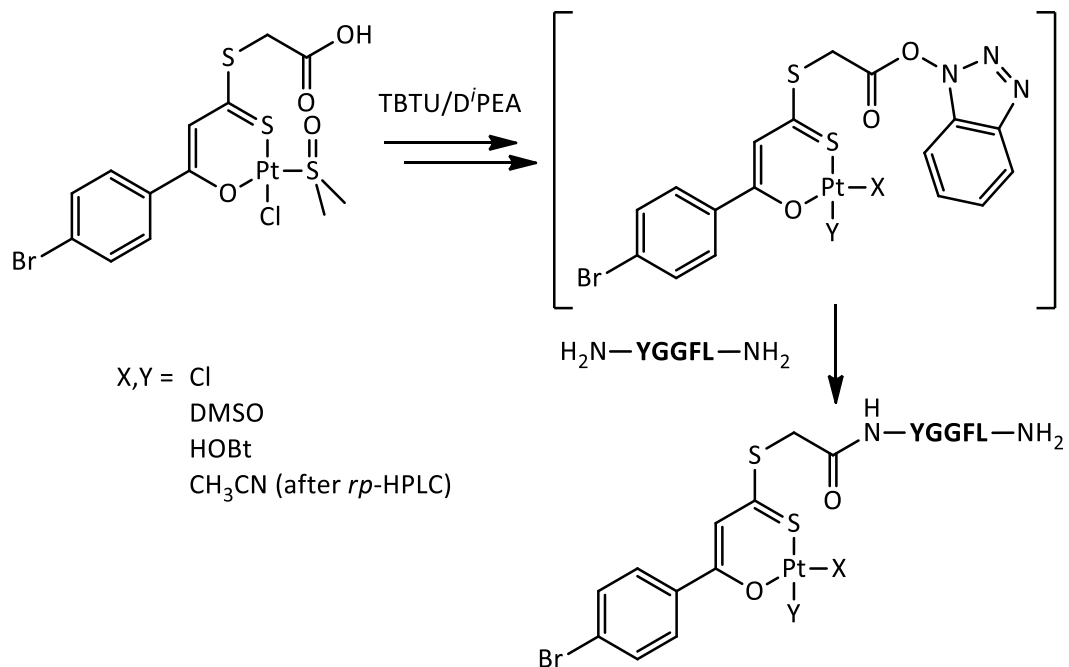
Scheme 22 Synthetic approaches towards (O,S)Pt bioconjugates through amide bond formation. When subjecting **83** to standard coupling conditions, **85** could not be isolated. Instead, **86** is formed with a mixture of monodentate ligands X/Y; amongst them HOBT which is formed from TBTU under coupling conditions (*vide infra*).

By this method, compound **84** was isolated in good yields (38 %) and purity (>95 %) after preparative *rp*-HPLC. Its identity, purity and structure could be established through ESI MS and  $^1\text{H}$  NMR analysis (*vide infra*).

Coupling of the complex **83** by the same method was successful in retaining the Pt(II) center within the coordination sphere (**86**, Scheme 22). The monodentate ligands DMSO and chloride, however, were partially substituted by HOBT, a side product which is released from the coupling reagent TBTU during the coupling reaction (Scheme 23).<sup>375–377</sup> A mixture of different substitution products was obtained as crude material, HPLC-based analysis of **86** revealed several fractions of complexes containing DMSO, HOBT or  $\text{CH}_3\text{CN}$  (from HPLC) as monodentate ligands (Scheme 24).



Scheme 23 Mechanism of activation of carboxylic acids through TBTU for the formation of amide bonds. Upon amide bond formation, HOBT is liberated.



Scheme 24 Possible formation of HOBT complexes by the applied coupling procedure.

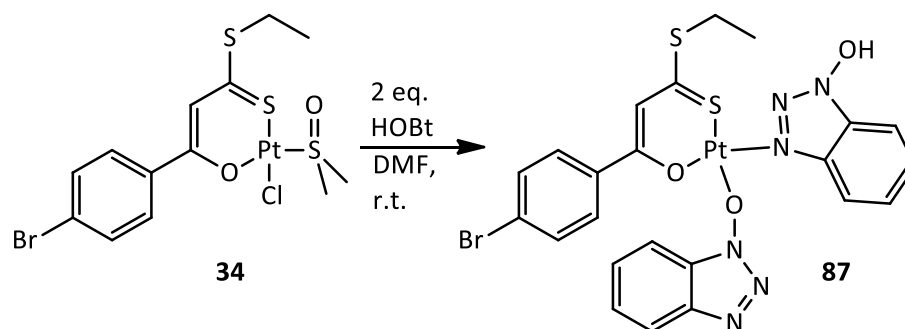
In an alternate approach to isolate the desired Enk-derived (*O,S*) bidentate Pt(II) complex with DMSO and chlorido ligands, **84** was converted with  $K_2PtCl_4$ /DMSO under the same conditions as used for the “clicked” bioconjugate system (Scheme 22). By precipitation from water and applying repeated steps of washing with water and diethyl ether, the desired complex **85** was successfully isolated.

Coupling in solid phase was not attempted after these positive findings, since the necessary cleavage step, involving the use of TFA, was expected to lead to decomposition of the chelating unit resp. the resulting complexes. Indications for such an outcome had been observed in an initial NMR-based study on the stability of a model compound in presence of 50 vol-% TFA: the half-life of the complexes was found to be about 2 h, with first indications of decomposition appearing already after 40 min (*cf.* experimental section).

### 12.2.1 HOBt coordination

HOBt has been found to coordinate transition metals in various models, however these usually involved Ni(II), Cu(II) and other early transition metals.<sup>402–404</sup> There is only one Pt-HOBt complex reported in literature to date.<sup>405</sup> In these reports, it was demonstrated from X-ray crystallographic studies that both O- and N- coordination can occur at the same time.

To check if a ligand exchange of chloride and/or DMSO by HOBt would take place also under non-coupling conditions, simply through the presence of HOBt, a model reaction was performed (Scheme 25). Compound **34**, the homologous monochelate to **83** without the carboxy functionality, was stirred in DMF in presence of two equivalents of HOBt. Subsequent column chromatographic work-up and analysis by ESI mass spectrometry and  $^1H$  NMR spectroscopy (Figure 49) showed that both monodentate ligands had been replaced by HOBt in **87**.



Scheme 25 Substitution of the monodentate chlorido and DMSO ligands by HOBt to give a (*O,S*)Pt(HOBt)<sub>2</sub> compound with a proposed coordination environment as given for **87**.

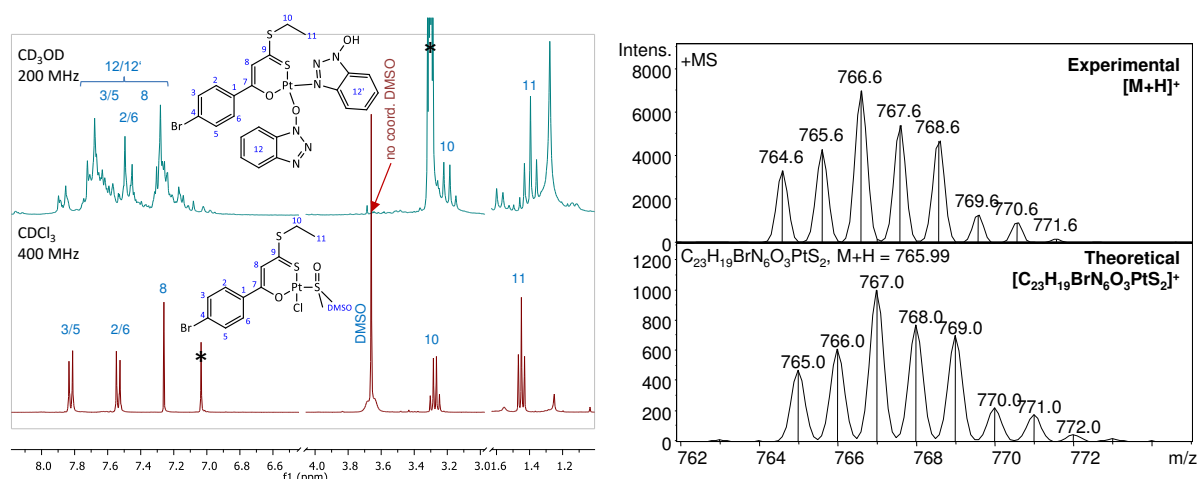


Figure 49 Left, selected regions of the  $^1\text{H}$  NMR spectra of **87** (in  $\text{CD}_3\text{OD}$ , 200 MHz) in comparison with the starting compound **34** (in  $\text{CDCl}_3$ , 400 MHz). Loss of DMSO is clearly demonstrated; detailed analysis of the aromatic region is not possible due to the complexity of the compound's structural features. \* mark solvent residual signals. Right, comparison of the experimental vs. theoretical ESI MS signal of the  $[\text{M}+\text{H}]^+$  signal of  $(O,S)\text{Pt}(\text{HOBt})_2$  compound **87**.

Signals in  $^1\text{H}$  NMR spectra were, however, not clearly assignable since in the aromatic region multiple signals overlay. It is on the contrary obvious that DMSO has been released from the system. Even though no crystals suitable for X-ray crystallography were obtained, it can be assumed that HOBt coordinates towards Pt(II) in two different modes when presupposing the formation of an overall neutral complex: Since the  $(O,S)$  unit is negatively charged, one excess positive charge has to be neutralized by the newly introduced ligands. HOBt itself bears three possible donor sites, namely two N and one OH group. It is thus reasonable to assume that one HOBt is coordinated through oxygen after deprotonation of the same, and the other HOBt molecule should bind *via* a nitrogen atom; most probably  $\text{N}^3$ . This versatile coordination behavior certainly contributes to the complex signal pattern in  $^1\text{H}$  NMR spectra.

A short note should be given on the used deuterated NMR solvent: the isolated compound was readily soluble in ethanol but only moderately soluble in methanol- $\text{d}_4$ . Even though it should be well-soluble in acetonitrile or DMSO, use of these solvents was avoided due to the known coordinating properties of both towards the Pt(II) center in this peculiar system. Therefore signal intensity in the NMR spectra of **87** is low and intrinsic impurities of the solvent obscure the signals.

### 12.3 Analysis of the amide-linked bioconjugates

Compounds **84** and **85** were analyzed by ESI MS analysis and NMR spectroscopy. The resulting data can be found in Figure 50 and Figure 51.

ESI MS analysis provided evidence for the sum formulae of both compounds, the isotopic patterns matched the calculated ones well: For **84**, the  $[M+H]^+$  ion was found at  $m/z = 868.8$ , and for **85**, the  $[M+K]^+$  ion was detected at  $m/z = 1214.9$  (Figure 50).<sup>xxvii</sup>

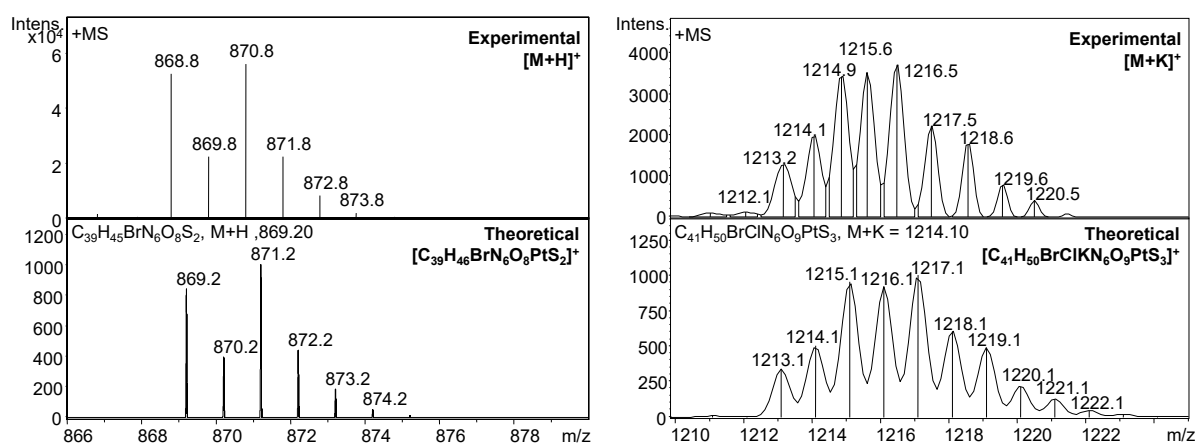


Figure 50 Comparison of ESI+ MS spectral profiles of **84** (left) and **85** (right). Top, experimental data, bottom, simulated pattern.

Furthermore,  $^1\text{H}$  NMR spectra of **84** and **85** were recorded in  $\text{THF-d}_8$  and gave all expected signals of  $\text{Leu}^5\text{-Enk}$ . Comparative NMR spectra are given in Figure 51.

A  $^1\text{H}$  NMR spectrum of **Enk 75** was also recorded in  $\text{THF-d}_8$  to enable a direct comparison between the compounds in the same solvent. Solubility of unfunctionalized **Enk** is, however, very low in  $\text{THF-d}_8$  so that only signals in the aromatic region can be clearly seen in this experimental setup; signals in the aliphatic region are in part obscured by solvent signals. When comparing the  $^1\text{H}$  NMR spectrum of **75** in  $\text{THF-d}_8$  towards the one recorded in  $\text{DMSO-d}_6$  (*vide supra*) or other solvents,<sup>351,320,317,322</sup> it becomes apparent that the solvents' influence on chemical shifts and visibility of acidic protons is substantial.

<sup>xxvii</sup> The peak positions of the MS signals discussed in this chapter generally deviate from the theoretical values since the used ESI MS device is not laid out for high-resolution ESI MS data collection. Still, the isotopic profiles are clearly indicative of the proposed sum formulae.

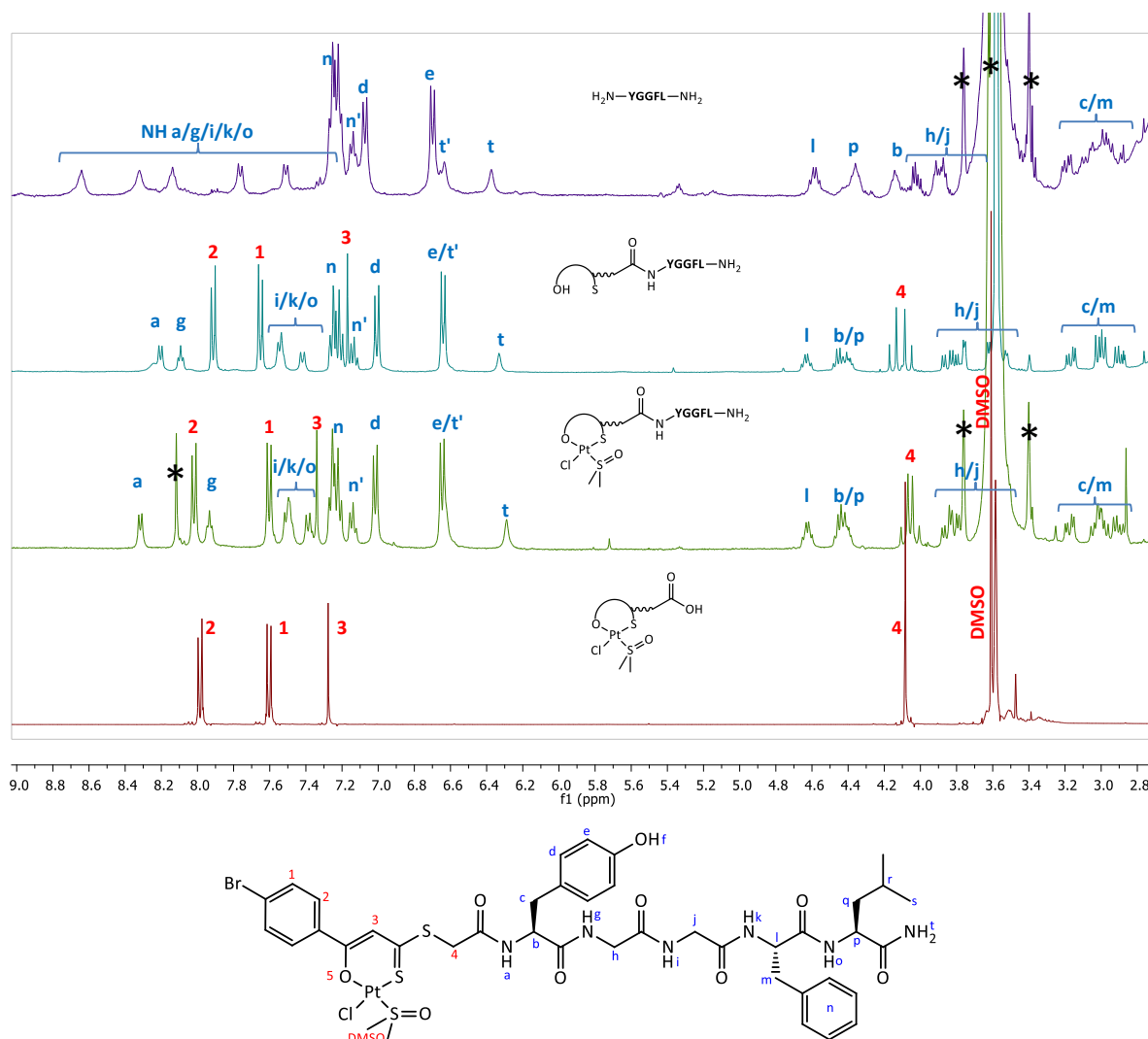


Figure 51 Comparison of <sup>1</sup>H NMR spectra of Leu<sup>5</sup>-Enk **75** (top/violet), ligand **84** (second, petrol), complex **85** (third, green) and complex **83** (bottom, red). Spectral range of 3–9 ppm given, the full spectral range can be found in Figure S 16. All spectra were recorded in THF-d<sub>8</sub>. Asterisks mark residual signals. Below: representative signal assignment, demonstrated on compound **85**.

Massive shifts of the amide protons are observed by the change of solvents, and a definite assignment of all NH protons was not feasible for the <sup>1</sup>H NMR spectrum of free Enk **75** in THF-d<sub>8</sub>.

Amide bond formation of the initially terminal NH<sub>2</sub> group was still demonstrated by appearance of a sharp doublet assignable to the Leu<sup>5</sup>-NH signal at 8.20 ppm in spectra of **84** (*a* in Figure 51), together with massive shifts of all other NH protons compared to those in **75**. Furthermore, all characteristic signals for the β-hydroxydithiocinnamic unit were found, alongside with a splitting of the S-CH<sub>2</sub> signal at 4.11 ppm into a doublet of doublets (*4* in Figure 51), indicative of



- a) the formation of an amide bond in close proximity to this CH<sub>2</sub> group, and
- b) of a significant sterical crowding around this group, inhibiting rotation and therefore creating diastereotopic effects.

Upon binding of **84** towards the Pt(II) center to give **85**, the signal belonging to the methine proton experiences the typical shift to higher frequencies (+0.17 ppm from 7.17 in **84** to 7.34 ppm in **85**, 3 in Figure 51). From HSQC experiments, the presence of Pt-bound DMSO could also be proven from the characteristic  $^1J_{\text{CH}}$  cross-peak at 3.63/46.4 ppm. This signal was not directly witnessed in the  $^1\text{H}$  NMR spectrum due to an overlay with the intrinsic THF-d<sub>8</sub> signal.

Recording of  $^{13}\text{C}$  NMR spectra was not possible due to the low quantities available, but indirect measurement through HSQC experiments gave the signal positions of the most important characteristic peaks.



## 13 BIOACTIVITY OF THE PLATINUM-PEPTIDE BIOCONJUGATES

### BIOCONJUGATES

#### 13.1 Triazol-linked compounds

The prepared “click” compounds were examined for their biological activity towards selected cancer cell lines. A first screening of the compounds in this series showed that  $IC_{50}$  values of bioconjugates and precursor molecules were in most cases too high to be considered bioactive; only the monochelate **72** and the corresponding “small-molecule” ligand **71** showed antiproliferative activity with some  $IC_{50}$  values determined below 100  $\mu M$  (Figure 52). For this reason, the cell tests on these compounds were only carried out once; the depicted values merely embody an orientation and do not represent statistically verified  $IC_{50}$  values.

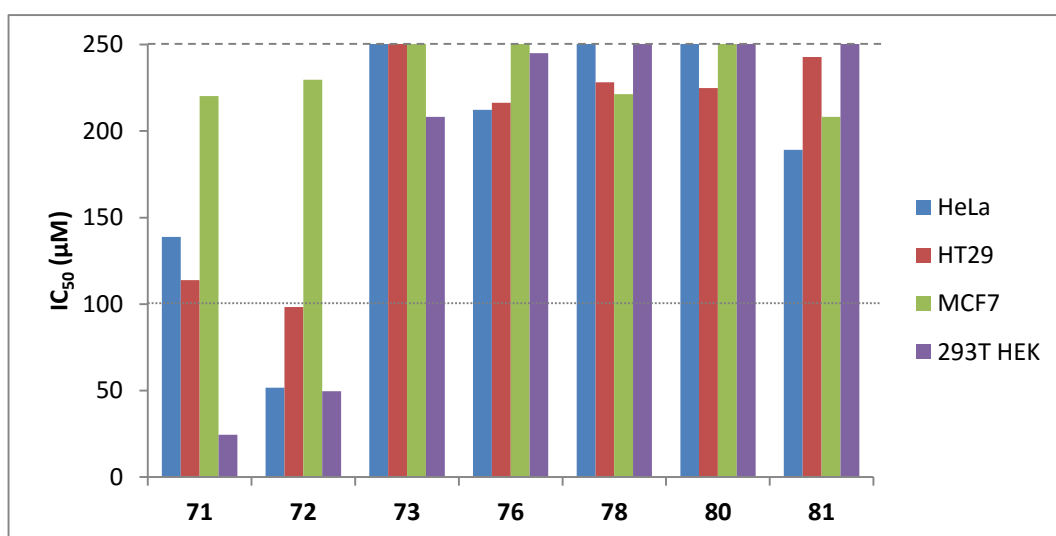


Figure 52 Preliminary  $IC_{50}$  values of the bioconjugates obtained from CuAAC and their precursor compounds. Bars are cut off above a determinable  $IC_{50}$  of 250  $\mu M$ . A biological standard deviation is not available.

The apparent lack of biological activity of these compounds could be explained by the choice of peptide vs. the investigated cell lines: Enk **75**, being a ligand for opioid receptors, may be selectively taken up by cells expressing those receptors, and might be excluded from other cells. The cell lines that were available for the here described studies, however, are not known to express this receptor.

Since the aim of this study was to establish the possibility of bioconjugation of Pt(II) compounds with ligands based on  $\beta$ -hydroxydithiocinnamic esters in principle, these data do not necessarily represent a draw-back. They merely demonstrate that for these cell lines, the proper chaperone is not Enkephalin.

### 13.2 Amide-linked compounds

The amide-linked compounds were also screened once for their potential cytotoxic properties (Figure 53). The obtained preliminary  $IC_{50}$  values of **84** and **85**, albeit lower than those of the triazol-linked compounds, are still too high to consider them cytotoxic.

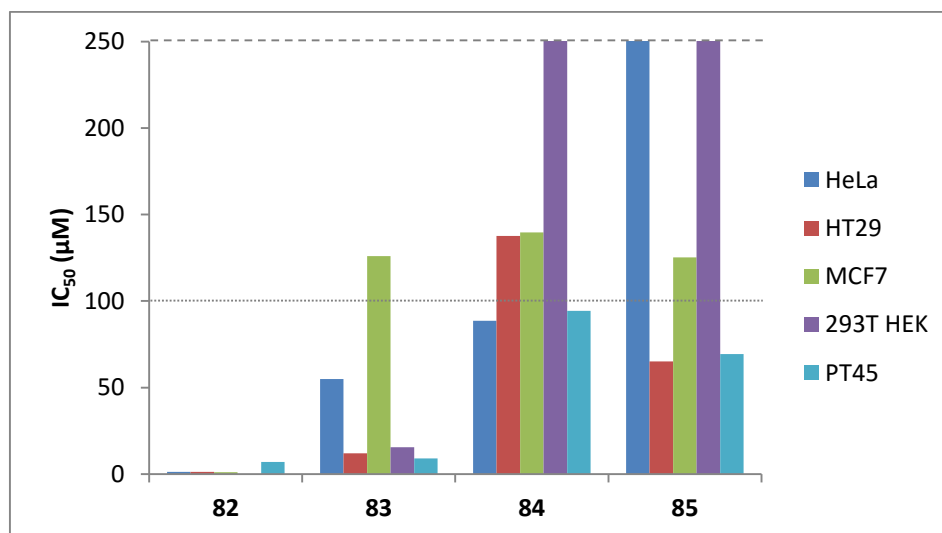


Figure 53 Preliminary  $IC_{50}$  values of the bioconjugates **84** and **85** obtained through amide bond formation and their precursor compounds **82** and **83**. Bars are cut off above a determinable  $IC_{50}$  of 250  $\mu$ M. A biological standard deviation is not available.

Interestingly, very low concentrations of **82** were found to be effective against the tested cell lines. This might in part be associated with the enhanced hydrophilicity of this compound – the  $\log P_{o/w}$  value of its ligand **82**, determined alongside with the earlier discussed compounds **7-28**, was found to

be the lowest in the series ( $\log P_{o/w} = 1.11$ ). Compound **82** produced the strongest cellular response, irrespective of the used cell line, with preliminary  $IC_{50}$  values of 1-6  $\mu$ M. This interesting finding indicates that the structure of this purely organic unit might represent a potent substrate for a vital cellular target and might be investigated in more detail in future experiments.



## 14 DISCUSSION

It was shown that the formation of bioconjugates through CuAAC is in principle possible by utilization of both azide/alkyne combinations by the successful preparation of peptide-conjugated (*O,S*)<sub>2</sub>Pt(II) bischelates **78** and **79**. One approach should however be preferred: When introducing the azide group into the (*O,S*) unit (**73**) and deriving the peptide with pentynoic acid to give a terminal alkyne (**76**), far less synthetic obstacles were encountered along the way to compound **78** as opposed to the complimentary combination to give **79**: Alkyne-derived  $\beta$ -hydroxydithiocinnamic esters **54**, **55**, **57**, and **59** could be isolated but coordination towards platinum resulted in a variety of side reactions such as hydrogenation of the C $\equiv$ C triple bond or uncontrolled rearrangements. Only bischelates of compounds **54**, **55** and **59** were obtained, no monochelate complex was isolated that still contained the alkynyl group. On the contrary, the synthesis of the benzylazide-derived series **71**, **72** and **73** was straight-forward and yields were generally higher than for the alkyne series. CuAAC of the two units **73** and **76** furthermore lead to a cleaner reaction (less side products were formed) and a higher yield of purified bioconjugate **78** than the opposite combination (*i.e.* **66+75** to give **79**). It is therefore the preferred set-up for further experiments.

In efforts to obtain the respective monochelate **81**, first CuAAC was performed with the ligand **71** and Enk derivative **76** using the classical CuSO<sub>4</sub>/ascorbate catalyst combination, followed by quantitative removal of copper through addition of EDTA. Subsequently, the Pt(II) unit could be introduced into the system by an adaption of the complexation procedure frequently used for small-molecule complexations. Since the resulting product is not stable to classical *rp*-HPLC conditions, it was purified by repeated precipitation. NMR- and ESI MS analysis could however prove the identity of the compound and also showed that the compound was sufficiently pure.

Furthermore, it was found that a direct conjugation of the (*O,S*) chelating unit through an amide bond is possible. Carboxy-derived precursor molecules were prepared and both the ligand **82** and the (*O,S*)Pt monochelate **83** were coupled to Leu<sup>5</sup>-Enk in solution. Since coupling of **83** under standard TBTU-based coupling conditions resulted in a ligand exchange of chloride and DMSO by intermediately formed HOBT in **86**, the desired Pt(II) complex was prepared by introduction of the Pt

center *after* bioconjugation. Also in this case, NMR and ESI mass spectroscopic methods proved the formation of the desired compound.

Preliminary results of the compounds' cytotoxic potential were obtained from the resazurin-based PrestoBlue® assay. It was found that the bioconjugates are not active towards the selected cancer cell lines in a measure to consider them cytotoxic. The small units proved to be more active than the bioconjugated structures, with the purely organic **82** being the most cytotoxic compound measured under these experimental conditions. This overall finding is not considered a negative result *per se*, since none of the used cell lines overexpress a receptor for Enk: The rationale for the use of this model peptide laid in its function as a well-established and –understood model peptide rather than in its potential targeting abilities.



---

## EXPERIMENTAL PART

*Experimental work presented in this thesis has been carried out in different laboratories in Jena (D), Bochum (D) and Florence (IT):*

**Syntheses** of “small-molecule”  $\beta$ -hydroxydithiocinnamic esters and their corresponding (O,S)Pt complexes were carried out at Friedrich-Schiller Universität Jena, IAAC (Institut für Anorganische und Analytische Chemie), under supervision of Prof. Dr. W. Weigand.

*Syntheses of peptides and bioconjugates, including selected precursors, were executed at Ruhr-Universität Bochum, LS AC1 (Lehrstuhl für Anorganische Chemie I - Bioanorganische Chemie), under supervision of Prof. Dr. N. Metzler-Nolte.*

**Biological assays** were carried out at FSU Jena, IZKF (Interdisziplinäres Zentrum für Klinische Forschung), under supervision of Dr. J. Clement (2009-2013) and at RU Bochum, LS AC1, under supervision of Prof. Dr. N. Metzler-Nolte (2014-2015).

**Biomolecule interactions** were investigated at Università degli Studi di Firenze, Laboratory of metals in medicine, under supervision of Prof. Dr. L. Messori.



## 15 SYNTHESSES: GENERAL REMARKS

### 15.1 Syntheses of compounds based on the $\beta$ -hydroxydithiocinnamic ester structural motif

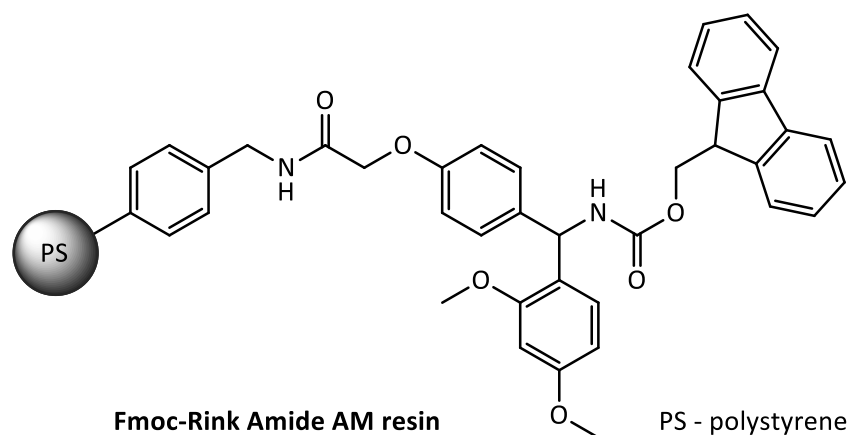
**Syntheses** were carried out under argon or nitrogen atmosphere using conventional Schlenk techniques when stated in the general procedures, otherwise standard air-exposed methods were used.

Most **starting materials and solvents** were purchased from common suppliers (*ABCR, Acros, Aldrich, Fluka, Merck, SigmaAldrich, and TCI*). Starting materials were usually obtained in the highest available purity grade (analytical or ACS grade). Solvents were of technical grade or higher and were dried according to known procedures<sup>406</sup> and distilled prior to use when required. For air-exposed syntheses, they were used as received. For column chromatography, Silica gel of the type *VWR Kieselgel 60* was used.

### 15.2 Peptide syntheses

All chemicals and solvents used for **peptide syntheses** were of analytical reagent grade or better and purchased from *Novabiochem* (Bad Soden, Germany), *Iris Biotech* (Marktredwitz, Germany). Dimethyl formamide (DMF) was purchased from *Biosolve* (Valkenswaard, NL) or *Fisher scientific* (Schwerte, D) and of peptide synthesis grade. HPLC-grade acetonitrile was purchased from *VWR* or *Fisher Scientific*. Water was purified by a milliQ purification system.

A Fmoc-Rink-Amid AM **resin**<sup>407</sup> (*Iris Biotech* Br-1330.0025, in 100-200mesh) was used with loadings of 0.59 or 0.71 mmol/g.



All **solid phase syntheses** were carried out according to standard solid phase peptide synthesis procedures (SPPS, **GP12**) using the Fmoc- protection approach with HOBT/TBTU as coupling reagents.<sup>400,401,408,409</sup> Leu<sup>5</sup>-Enk was synthesized using an automated peptide synthesizer (*CEM Liberty* microwave assisted peptide synthesizer) in a 250  $\mu$ mol scale. Further derivatization was performed manually using plastic syringes with a filter disc made of polypropylene as reaction vessels following **GP12**.

**NMR signal assignment** of peptide data was based on HSQC and HMBC experiments. In some cases, direct measuring of <sup>13</sup>C NMR data was not possible due to low available sample quantity, but <sup>13</sup>C NMR data could be deduced from cross-peaks of HSQC and HMBC experiments.

### 15.3 Literature-reported syntheses

Acetophenone derivatives **1**, **2**, **5** and **6** were obtained from commercial suppliers. Derivatives **3** and **4** were prepared according to literature procedures.<sup>105,106</sup>

$\beta$ -Hydroxydithiocinnamic esters **7**,<sup>103</sup> **11**,<sup>102</sup> **14**,<sup>107</sup> **15**,<sup>106</sup> **19**,<sup>105</sup> **23**,<sup>106</sup> **26**<sup>105</sup> have been reported in literature. Syntheses and characterizations of compounds **8**, **10**, and **12**, have for the first time been executed during the diploma project and are reported in the corresponding publication.<sup>118</sup> For this research project, all syntheses of previously reported  $\beta$ -hydroxydithiocinnamic esters were repeated following **GP3**.

The preparation of Pt(II) complexes **29**, **30**, **32-34**, **36**, and **49** has been performed for the first time during the diploma project. Details are reported in the corresponding publication.<sup>118</sup> Syntheses have been repeated for this project by following **GP5** or **GP7**.

4-(Prop-2-inyloxy)acetophenone **51** was prepared according to literature procedures<sup>379</sup> following **GP1**.

Azidoacetic acid was kindly provided by Martin Strack (Bochum) and has been prepared according to literature procedures.<sup>410</sup>

## 15.4 Analytical methods and devices

**Melting points** were determined on a *Stuart melting point SMP3* or using a polarization microscope *Axiolab (Zeiss Jena GmbH)* equipped with a heating plate *THMS 600* and control devices *LNP* and *CI 93 (Linkam)*. All values are uncorrected.

**Elemental analyses** (C, H, N, S) were carried out on a *LECO CHNS-931* instrument (Jena) or a *Elementar Hanau vario EL* device (Bochum). Obtaining proper elemental analyses of (O,S)Pt complexes proved to be difficult since the simultaneous presence of the elements Pt, S (and Si in some cases) lead to the formation of various undetectable or false-detected combustion products.

Results are represented in the form:

Sum formula (molar weight in g/mol): element, percentage (in %).

**NMR-Spectra** (<sup>1</sup>H-, <sup>13</sup>C{<sup>1</sup>H}-, <sup>31</sup>P{<sup>1</sup>H}-, H,H-COSY, HSQC, HMBC) were recorded on different devices and operating at different frequencies as listed below.

	<b>Spectrometer</b>	<b><sup>1</sup>H</b>	<b><sup>13</sup>C</b>
Jena	<i>Bruker AVANCE 200</i>	200.13 MHz	50.33 MHz
	<i>Bruker AVANCE 400</i>	400.00 MHz	100.63 MHz
	<i>Brukere ultrashield+ AVANCE 600</i>	600.13 MHz	150.94 MHz
Bochum	<i>Bruker DPX200</i>	200.13 MHz	50.32 MHz
	<i>Bruker DPX250</i>	250.13 MHz	62.9 MHz
	<i>Bruker DRX400</i>	400.13 MHz	100.61 MHz

Chemical shifts  $\delta$  are given in ppm relative to TMS. The undeuterated residues of the deuterated solvent served as an internal standard in <sup>1</sup>H and <sup>13</sup>C{<sup>1</sup>H} NMR spectra.

In some cases, signals are obscured by solvent residual signals (SRS). Signal assignment was confirmed by H,H COSY, HMBC and HSQC experiments. Signals are given in the following form:

$^1\text{H}$  NMR spectra: chemical shift  $\delta$  in ppm (multiplicity, coupling constant, number of hydrogen atoms, assignment).

$^{13}\text{C}\{^1\text{H}\}$  NMR spectra: chemical shift  $\delta$  in ppm (multiplicity, coupling constant, assignment).

**Mass spectra** were recorded on different instruments listed below.

	<b>device</b>	<b>ionization source</b>	<b>notes</b>
<b>Jena</b>	<i>Finnigan MAT SSQ 710</i>	FAB / DEI	
	<i>Finnigan MAT95XL</i>	ESI	high-res
<b>Bochum</b>	<i>Bruker Esquire 6000</i>	ESI	

Peaks are given in the form:

fragment  $m/z$  [assignment].

**FT-IR spectra** were measured on different devices listed below

	<b>device</b>		<b>form</b>
<b>Jena</b>	<i>Perkin-Elmer 2000</i>		pressed discs (KBr)
	<i>Bruker Equinox 55 FRA 106/5</i>	<i>Specac Golden ATR unit</i>	ATR
<b>Bochum</b>	<i>Bruker Tensor 27</i>	<i>Pike MIRacle micro ATR unit</i>	ATR

Signals are given in the form:

Wave number  $\tilde{\nu}$  in  $\text{cm}^{-1}$  (intensity).

## 15.5 X-ray data collection and structure solution refinement

Crystals of **50** were obtained by Matthias Hartlieb by evaporation of the solvents used for column chromatography, dichloromethane and hexane.

Crystals of **72**, **73** and **82** were grown by slow diffusion of hexane into solutions of the compounds dissolved in chloroform or dichloromethane.

Crystal structure collection and data refinement of compound **50** was executed by Helmar Görls (University Jena); for **72**, **73** and **82** samples were processed by Ulf-Peter Apfel (University Bochum).

Detailed crystallographic data is given in Supplement A.

### Data collection and refinement of compound 50

The intensity data were collected on a Nonius KappaCCD diffractometer using graphite-monochromated Mo-K $\alpha$  radiation. Data were corrected for Lorentz effects, polarization effects and for absorption effects.<sup>411–413</sup> The structure was solved by direct methods (SHELXS)<sup>414</sup> and refined by full-matrix least squares techniques against  $F_o^2$  (SHELXL-97).<sup>414</sup> All hydrogen atoms were included at calculated positions with fixed thermal parameters. All non-disordered, non-hydrogen atoms were refined anisotropically.<sup>414</sup>

### Data collection and refinement of compounds 72, 73 and 82

Single crystals suitable for X-ray analysis were coated with Paratone-N oil, mounted on a fiber loop, and placed in a cold, gaseous N<sub>2</sub> stream on a Rigaku XtlabMini diffractometer performing  $\phi$  and  $\omega$  scans at 170(2) K. Diffraction intensities were measured using graphite-monochromatic Mo K $\alpha$  radiation ( $\lambda = 0.71073$  Å). Data collection, indexing, initial cell refinements, frame integration, final cell refinements, and absorption corrections were accomplished with the program CrystalClear.<sup>415</sup> Space groups were assigned by analysis of the metric symmetry and systematic absences (determined by XPREP) and were further checked by PLATON<sup>416,417</sup> for additional symmetry. Structures were solved by direct methods and refined against all data in the reported  $2\theta$  ranges by full-matrix least squares on  $F^2$  with the SHELXL program suite<sup>414</sup> using the OLEX2 interface.<sup>418</sup>

## 15.6 General synthetic procedures

### General procedure 1 (GP1):

#### Williamson ether synthesis of alkinyl-derived acetophenones

4-Hydroxyacetophenone (1 eq., typically 2 g) and potassium carbonate ( $K_2CO_3$ , 1.5 eq.) or caesium carbonate ( $Cs_2CO_3$ , 1.5 eq.) are suspended in 10 mL anhydrous DMF and stirred at r.t. for 10 minutes. Subsequently, the alkinyl halide (1.2 eq.) is added and the mixture stirred at room temperature for at least 24 h. The suspension is treated with 5-10 mL ice-cold water and the white precipitate washed with ice-water. Purification is achieved by crystallization from methanol.

### General procedure 2 (GP2):

#### Williamson ether synthesis of alkinyl-derived acetophenones

4-Hydroxy acetophenone (1 eq., typically 1 g),  $Cs_2CO_3$  (1.5 eq.), potassium iodide (KI; 0.1 eq.) and butinyl bromide (1.1 eq.) are suspended in 30 mL acetonitrile and stirred at reflux for 20 h. After cooling to room temperature, 10 mL water and 10 mL ethyl acetate are added. The phases are separated, extracted with ethyl acetate (3 x 5 mL) and the combined organic phases washed with water (2 x 5 mL). The organic solvents are dried over sodium sulfate and then evaporated.

### General procedure 3 (GP3):

#### Synthesis of $\beta$ -hydroxydithiocinnamic acid esters

The synthesis requires inert working conditions. The desired acetophenone derivative (ca. 2 g, 1 eq.) is dissolved in dry diethyl ether (40 mL) and transferred into a precooled suspension of potassium-*tert*-butoxylate ( $KO^tBu$ , 2 eq.) in dry diethyl ether (40 mL) at  $-78\text{ }^\circ\text{C}$ . Carbon disulfide ( $CS_2$ , 1.4 eq.) is added dropwise to the solution under vigorous stirring, the mixture maintained at  $-78\text{ }^\circ\text{C}$  for 3 hours and allowed to warm up to room temperature. After adding the alkyl halide (0.9-1 eq.), the mixture is stirred protected from light at room temperature for further 15 hours.

Subsequently, the suspension is acidified with sulfuric acid (50 mL 2 M aqueous solution), leading to a two-phased system of an organic and aqueous phase which are then separated. The aqueous phase is extracted with dichloromethane (3 x 5 mL), the combined organic solutions washed with water (3 x 5 mL), and dried with sodium sulfate.



After filtration, the crude product is obtained which is usually purified by column chromatography on silica gel (eluent: dichloromethane/*n*-hexane in varying ratios).

#### General procedure 4 (GP4):

##### Cleavage of the O-TBDMS group

The reaction is performed under inert conditions. The O-TBDMS protected compound (1 eq, 3 mmol) is brought to reaction with tetrabutyl ammonium fluoride (TBAF, 2 eq., 1 M in THF) in THF (ca. 50 mL) and stirred for several days until TLC control shows consumption of the starting material (usually 5 to 6 days). Then, the mixture is acidified using H<sub>2</sub>SO<sub>4</sub> (2 M aqueous solution) and stirred for 3 h. The evolving two-phased system is separated, the aqueous phase extracted with chloroform (3 × 10 mL), the combined organic phases washed with water (3 × 10 mL) and dried with sodium sulfate. The crude material is further purified as described separately for each compound.

#### General procedure 5 (GP5):

##### Monofunctional complexes using NaOAc as base

The  $\beta$ -hydroxydithiocinnamic acid ester (1 eq., dissolved in 30-50 mL THF), is stirred for 30 min with sodium acetate (1 eq. in ca. 9 mL THF/water (7:2)). Potassium tetrachloro platinate (K<sub>2</sub>PtCl<sub>4</sub>; 1.1 eq., typically 200 mg) is dissolved in 2 mL water and dimethyl sulfoxide (DMSO; 2 eq.) is added. Within 30 minutes, a white precipitate is formed. The solution of the deprotonated  $\beta$ -hydroxydithiocinnamic acid ester is slowly added and the mixture and stirred at room temperature overnight. The resulting red-orange solution is concentrated and extracted with DCM (3 × 4 mL). The combined organic phases are washed with water (2 × 3 mL) and dried over sodium sulfate. Purification is typically performed *via* column chromatography on silica gel as described individually for each compound.

#### General procedure 6 (GP6):

##### Monofunctional complexes using KO<sup>t</sup>Bu as base

The synthesis is conducted in analogy to **GP5** under usage of potassium *tert*-butoxide (KO<sup>t</sup>Bu) as base. The reaction was either carried out under normal atmosphere, using standard solvents or under nitrogen atmosphere and usage of dry/degassed THF as well as degassed water as stated individually.

**General procedure 7 (GP7):****Monofunctional complexes using NaH as base**

Working in analogy to **GP5**, the synthesis is carried out under argon or nitrogen atmosphere. NaH (60 % susp. In mineral oil, 1 eq) is used as a base. Deprotonation takes place in dry THF, degassed water is used to dissolve  $K_2PtCl_4$ .

**General procedure 8 (GP8):****Synthesis of bischelate complexes**

$\beta$ -Hydroxydithiocinnamic acid ester (2 eq., in 30 mL THF), is deprotonated by addition of NaOAc (1 eq. in 7 mL THF and 2 mL water). After 30 min of stirring at room temperature,  $K_2PtCl_4$  (1 eq., typically 100 mg dissolved in 2 mL water) is added and the mixture stirred overnight. The crude product is obtained by evaporation of the solvent *in vacuo*, followed by extraction with DCM (3 × 4 mL), washing with water (3 × 3 mL) and drying with sodium sulfate.

**General procedure 9 (GP9):****Copper-catalyzed 1,3-dipolar azide-alkyne cycloaddition (CuAAC) of (O,S)Pt(II) complexes and Enk derivatives**

The complimentary compounds, one containing the alkyne and one containing the azide group (1:1 ratio of functional groups, 1 eq. = 1 functional group pair; FGP), are dissolved in a THF / water mixture (ca. 7 mL 5:2 ratio) and degassed for at least 30 min by an Ar-stream. Sodium ascorbate (0.4 eq./FGP, 0.1 or 1 M aqueous solution) and  $CuSO_4 \cdot 5 H_2O$  (0.2 eq./FGP, 0.1 M aqueous solution) are added to initiate the reaction. The mixture is stirred at r.t. until no further conversion of the starting materials was observed according to HPLC analysis. Work-up is performed individually for each compound and includes precipitation from diethyl ether and / or preparative HPLC.

**General procedure 10 (GP10):****Copper-catalyzed 1,3-dipolar azide-alkyne cycloaddition (CuAAC) of  $\beta$ -hydroxydithiocinnamic esters and Enk derivatives**

The complimentary compounds, one containing the alkyne and one containing the azide group (1:1 ratio of functional groups, 1 eq. = 1 FGP), are dissolved in a THF / water mixture (ca. 7 mL 5:2 ratio)

and degassed for at least 30 min by an Ar-stream. Sodium ascorbate (2.4 eq./FGP, 1 M aqueous solution) and  $\text{CuSO}_4 \cdot 5 \text{H}_2\text{O}$  (1.2 eq./FGP, 0.5 M aqueous solution) are added to initiate the reaction. The mixture is stirred at r.t. until HPLC control shows consumption of the starting materials. To remove the copper salts, sodium ethylenediamine tetraacetate ( $\text{Na}_2\text{EDTA}$ , 2.5 eq./FGP, 0.1 M aqueous solution) is added and the mixture stirred overnight. Work-up is performed individually for each compound and includes removal of  $\text{Cu}(\text{EDTA})$ , precipitation from diethyl ether and / or preparative HPLC.

### General procedure 11 (GP11):

#### Complexation of bioconjugates

In a microreaction tube,  $\text{K}_2\text{PtCl}_4$  (2eq. 0.1 M aqueous solution) is activated by addition of an excess of DMSO (50  $\mu\text{L}$ ). In parallel, the Enk-conjugated  $\beta$ -hydroxydithiocinnamic ester (1 eq., dissolved in 600  $\mu\text{L}$  THF) is deprotonated by NaOAc (10 eq., 0.1 M aqueous solution) and added to the Pt-mixture in portions of 50  $\mu\text{L}$ ; 100  $\mu\text{L}$  water are added to facilitate mixing of the solvents. After over-night shaking on a laboratory shaker, water and THF are removed *in vacuo*. By addition of 500  $\mu\text{L}$  water the compound is precipitated, then centrifugated and the solvents decanted. The solid residue is washed repeatedly with water and  $\text{Et}_2\text{O}$  and dried under vacuum to give the desired complex.

### General procedure 12 (GP12):

#### Solid Phase Peptide Synthesis (SPPS)

In general, peptide synthesis consists of the following steps irrespective of manual or microwave-assisted coupling ( $\mu\text{W}$ ):

**Swelling:** Before synthesis, the resin is swollen in DMF or DCM for at least 30 min.

**Deprotection:** N-terminal Fmoc protection groups are removed by a solution of 20 % piperidine in DMF ( $\mu\text{W}$ : (i) P = 30 W, t = 35 s, T = 38 °C; (ii) P = 50 W, t = 180 s, T = 77 °C).

**Washing:** After each deprotection and each coupling step, the resin is washed excessively with DMF to remove any residual activation or deprotection reagents.

**Coupling:** Fmoc protected amino acids (4 eq., 0.2 mmol/mL in DMF) resp. functionalized acids (4 eq., 0.1 mmol/mL in DMF) are mixed with 1-Hydroxybenzotriazol (HOBt, 4 eq. 0.5 M in DMF) and *N,N,N',N'*-Tetramethyl-*O*-(benzotriazol-1-yl)uronium tetrafluoroborate (TBTU, 3.8 eq. 0.5 M in DMF).

Coupling is initiated by addition of diisopropylethylamine (D'PEA, 8 eq. 2 M in DMF). Conditions for manual coupling reactions: shaking at r.t. on a laboratory shaker (350 rpm); for  $\mu$ W-assisted coupling: P = 24 W, t = 300 s, T = 78 °C.

**Ninhydrin test:** For manual coupling reactions, a ninhydrin test is performed to ensure complete conversion of all terminal amines. For that, few resin beads are soaked with a solution of ninhydrin (2 mg/mL) in 2-butanol/H<sub>2</sub>O/acetic acid (95:4.5:0.5 v/v) and heated to 100 °C for 5 min. A purple color would indicate the presence of amines and thus incomplete conversion; no color change indicates complete conversion of all terminal amines.

**Workup after automated synthesis:** After deprotection of the last amino acid, the peptide-loaded resin is transferred into a filter syringe, washed with DMF and DCM (3 × 5 mL, 1-2 min each) and dried *in vacuo*. When needed, the dried resin is split into smaller portions at this point and manual coupling performed equally as described above.

**Cleavage:** After coupling of all (amino) acids, the peptidyl resin is treated with a mixture of TFA/H<sub>2</sub>O/TES (trifluoroacetic acid/water/triethylsilane) (95:2.5:2.5 v/v; 1200  $\mu$ L / 100  $\mu$ M peptide on resin) and shaken on a laboratory shaker at r.t. for approx. 2 h.

**Purification:** The cleaved peptide is precipitated by introduction into ca. 80 mL of a 1:1 mixture of *n*-hexane and diethyl ether at -80 °C and the resin washed with a minimum amount of cleavage mixture. The precipitate is centrifuged (8000 rpm, 10 min, r.t.), decanted and washed with diethyl ether (2-3 × 5-10 mL). When needed, the peptide is purified by HPLC as described for the individual compounds. Purified peptides are lyophilized from H<sub>2</sub>O/CH<sub>3</sub>CN solutions and obtained as amorphous solids.

### General procedure 13 (GP13):

#### Coupling in solution– liquid phase peptide synthesis (LPPS)

In a microreaction tube, the free carboxylic acid (1.1 eq.) and peptide (Enk, 1 eq.) are mixed with TBTU (1.1 eq.) in DMF (600  $\mu$ L). Coupling is initiated by addition of D'PEA (2.3 eq.) which can be seen through a dark discoloration of the reaction mixture. The mixture is vigorously shaken for 30 sec, centrifuged to collect all solvents and then continuously shaken on a laboratory shaker (350 rpm) at r.t. for 2 h. Workup is performed individually for the respective compounds.

## 15.7 HPLC analysis and purification

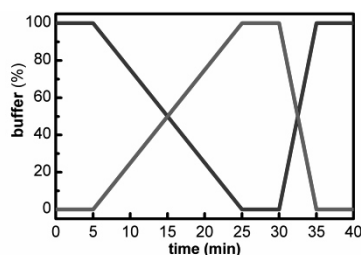
High Performance Liquid Chromatography (HPLC) was performed by using reversed phase (*rp*) columns of the type *Knauer EurospherII* 100-5 C18A (5  $\mu$ m, 250  $\times$  4 mm), or *Dr. Maisch Reprosil-Pur* 120 C8 (5  $\mu$ m, 250  $\times$  4.6 mm) for analytical and *Dr. Maisch Reprosil-Pur* C18-AQ (5  $\mu$ m, 250  $\times$  10 mm) for preparative runs. Millipore Water (mQ-H<sub>2</sub>O) and HPLC-grade acetonitrile (CH<sub>3</sub>CN), both containing 0.1 vol-% trifluoroacetic acid (TFA), were used as eluents. All analytical measurements were performed at a flow rate of 1 mL/min, semi-preparative HPLC was performed at a flow rate of 5 mL/min using different gradient setups:

Buffer A: mQ-H<sub>2</sub>O / 0.1 %TFA

Buffer B: CH<sub>3</sub>CN / 0.1 % TFA

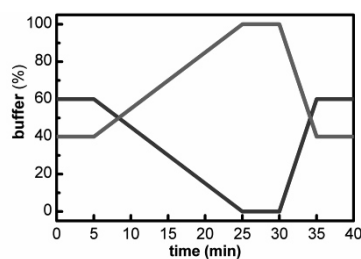
**Gradient 1** used for analytical (1 mL/min) and semi-preparative (5 mL/min) applications:

time	A [%]	B [%]
0	100	0
5	100	0
25	0	100
30	0	100
35	100	0
40	100	0



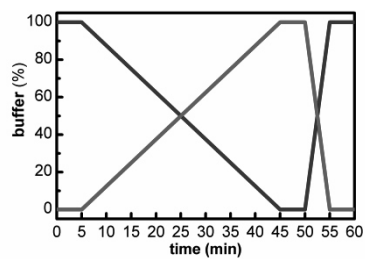
**Gradient 2** used for semi-preparative (5 mL/min) applications:

time	A [%]	B [%]
0	60	40
5	60	40
20	0	100
30	0	100
35	60	40
40	60	40



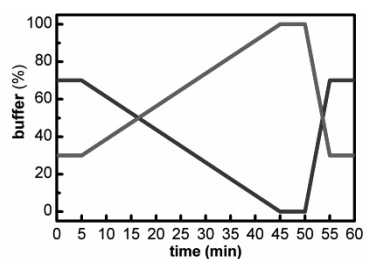
**Gradient 3** used for semi-preparative (5 mL/min) applications:

time	A [%]	B [%]
0	100	0
5	100	0
45	0	100
50	0	100
55	100	0
60	100	0



**Gradient 4** used for semi-preparative (5 mL/min) applications:

time	A [%]	B [%]
0	70	30
5	70	30
45	0	100
50	0	100
55	70	30
60	70	30

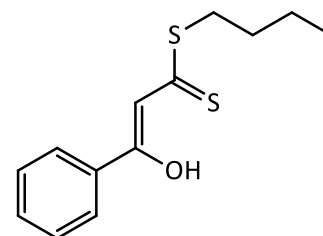


## 16 COMPOUND SYNTHESSES AND ANALYSES

### 16.1 $\beta$ -Hydroxydithiocinnamic esters

#### $\beta$ -Hydroxydithiocinnamic acid butyl ester (**9**)

Using acetophenone **5** (2 g, 20 mmol), KO<sup>t</sup>Bu (4.5 g, 40 mmol), CS<sub>2</sub> (1.7 mL, 28 mmol), and butyl iodide (2.3 mL, 20 mmol), the synthesis was carried out according to **GP3**. Column chromatography was accomplished with *n*-hexane/DCM 1:1 as mobile phase (*R<sub>f</sub>* ≈ 0.7) and yielded **9** (3.48 g, 69 %) as yellow oil.



**<sup>1</sup>H NMR** (400 MHz, CDCl<sub>3</sub>)  $\delta$  =15.17 (s, 1H, OH), 7.92 – 7.84 (m, 2H, Ar-H<sub>2</sub>, Ar-H<sub>6</sub>), 7.58 – 7.40 (m, 3H, Ar-H<sub>3</sub>, Ar-H<sub>4</sub>, Ar-H<sub>5</sub>), 6.93 (s, 1H, =CH-), 3.28 (t, <sup>3</sup>*J*<sub>HH</sub> = 7.4 Hz, 2H, S-CH<sub>2</sub>-), 1.80 – 1.61 (m, 2H, SCH<sub>2</sub>-CH<sub>2</sub>-), 1.49 (m, 2H, SCH<sub>2</sub>CH<sub>2</sub>-CH<sub>2</sub>-), 0.98 (t, *J* = 7.3 Hz, 3H, -CH<sub>3</sub>) ppm.

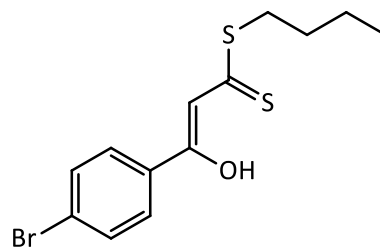
**<sup>13</sup>C{<sup>1</sup>H} NMR** (101 MHz, CDCl<sub>3</sub>)  $\delta$  =216.7 (CS<sub>2</sub>), 169.5 (COH), 134.4 (Ar-C<sub>1</sub>), 131.9 (Ar-C<sub>4</sub>), 128.8 (2C, Ar-C<sub>3</sub>, Ar-C<sub>5</sub>), 126.7 (2C, Ar-C<sub>2</sub>, Ar-C<sub>6</sub>), 108.0 (=CH-), 33.4 (S-CH<sub>2</sub>-), 30.0 (SCH<sub>2</sub>-CH<sub>2</sub>-), 22.3 (SCH<sub>2</sub>CH<sub>2</sub>-CH<sub>2</sub>-), 13.8 (-CH<sub>3</sub>) ppm.

**MS (EI+)** *m/z* = 253 [M+H]<sup>+</sup>, 196 [M-Bu+H]<sup>+</sup>, 163 [M-SBu]<sup>+</sup>, 105, 85, 77.

**FTIR (ATR)**  $\tilde{\nu}$  = 3062 (w), 2957 (w), 2928 (w), 2871 (w), 1588 (s), 1554 (vs), 1491 (s), 1451 (s), 1396 (m), 1279 (w), 1233 (vs, b), 1053 (s), 947 (vs), 826 (s), 759(s) cm<sup>-1</sup>.

**4-Bromo- $\beta$ -hydroxydithiocinnamic acid butyl ester (13)**

Using 4-bromo-acetophenone **6** (3.98 g, 20 mmol), KO<sup>t</sup>Bu (4.5 g, 40 mmol), CS<sub>2</sub> (1.7 mL, 1.4 mmol), and butyl iodide (2.3 mL, 20 mmol), the synthesis was carried out according to **GP3**. Column chromatography was accomplished with *n*-hexane/DCM 1:1 as mobile phase (*R<sub>f</sub>* ≈ 0.7) and yielded **13** (3.04 g, 46 %) as an orange solid.



**<sup>1</sup>H NMR** (400 MHz, CDCl<sub>3</sub>)  $\delta$  = 15.08 (s, 1H, OH), 7.73 (d, <sup>3</sup>*J*<sub>HH</sub> = 8.7 Hz, 2H, Ar-H3, Ar-H5), 7.57 (d, <sup>3</sup>*J*<sub>HH</sub> = 8.7 Hz, 2H, Ar-H2, Ar-H6), 6.85 (s, 1H, =CH-), 3.27 (t, <sup>3</sup>*J*<sub>HH</sub> = 7.4 Hz, 2H, S-CH<sub>2</sub>-), 1.84 – 1.59 (m, 2H, SCH<sub>2</sub>-CH<sub>2</sub>-), 1.48 (m, 2H, SCH<sub>2</sub>CH<sub>2</sub>-CH<sub>2</sub>-), 0.97 (t, <sup>3</sup>*J*<sub>HH</sub> = 7.3 Hz, 3H, -CH<sub>3</sub>) ppm.

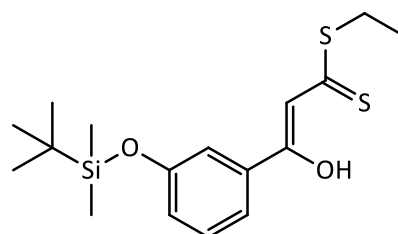
**<sup>13</sup>C{<sup>1</sup>H} NMR** (50 MHz, CDCl<sub>3</sub>)  $\delta$  = 217.3 (CS<sub>2</sub>), 168.1 (COH), 133.4 (Ar-C1), 132.2 (2C, Ar-C3, Ar-C5), 128.2 (2C, Ar-C2, Ar-C6), 126.6 (Ar-C4), 107.9 (=CH-), 33.6 (S-CH<sub>2</sub>-), 30.0 (SCH<sub>2</sub>-CH<sub>2</sub>-), 22.3 (SCH<sub>2</sub>CH<sub>2</sub>-CH<sub>2</sub>-), 13.8 (-CH<sub>3</sub>) ppm.

**MS (EI+)** *m/z* = 331/333 [M+H]<sup>+</sup>/[M+2+H]<sup>+</sup>, 274/276 [M-C<sub>4</sub>H<sub>8</sub>]<sup>+</sup>, 241/243 [M-SBu]<sup>+</sup>, 183/185, 162, 85.

**FTIR (ATR)**  $\tilde{\nu}$  = 2947 (w), 2923 (w), 2864 (w), 1679 (m), 1580 (vs), 1556 (vs), 1484 (s), 1410 (s), 1376 (m), 1303 (m), 1230 (vs), 1213 (m), 1074 (m), 1073 (s), 1045 (s), 1008 (m), 958 (s), 839 (m), 828 (m), 816 (m), 795 (m), 765 (m) cm<sup>-1</sup>.

**3'-(tert-butyl dimethylsilyloxy)- $\beta$ -hydroxydithiocinnamic acid ethyl ester (16)**

Using 3-(*tert*-butyl dimethylsilyloxy) acetophenone **3** (5.00 g, 20 mmol), KO<sup>t</sup>Bu (4.5 g, 40 mmol), CS<sub>2</sub> (1.7 mL, 1.4 mmol), and ethyl iodide (1.6 mL, 20 mmol), synthesis was carried out according to **GP3**. Column chromatography, using *n*-hexane/DCM 1:1 as mobile phase (*R<sub>f</sub>* ≈ 0.8), yielded **16** (1.2 g, 17 %) as orange oil.



**Analysis** calcd. for C<sub>17</sub>H<sub>26</sub>O<sub>2</sub>S<sub>2</sub>Si·0.1 hexane: C 58.20; H 7.60 %; found C 58.13; H 7.74 %



$^1\text{H NMR}$  (200 MHz,  $\text{CDCl}_3$ )  $\delta$  = 15.04 (s, 1H, OH), 7.43 – 7.33 (m, 1H, Ar-H6), 7.30 – 7.24 (m, 1H, Ar-H2), 7.24 – 7.16 (m, 1H, Ar-H5), 6.90 (m, 1H, Ar-H4), 6.78 (s, 1H, =CH-), 3.21 (q,  $^3J_{\text{HH}}$  = 7.4 Hz, 2H, S-CH<sub>2</sub>-), 1.31 (t,  $^3J_{\text{HH}}$  = 7.4 Hz, 3H, SCH<sub>2</sub>-CH<sub>3</sub>), 0.93 (s, 9H, SiC(CH<sub>3</sub>)<sub>3</sub>), 0.16 (s, 6H, Si(CH<sub>3</sub>)<sub>2</sub>).

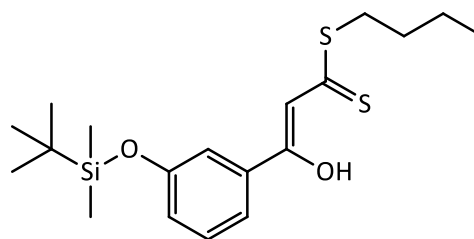
$^{13}\text{C}\{^1\text{H}\}$  NMR (101 MHz,  $\text{CDCl}_3$ )  $\delta$  = 216.6 (CS<sub>2</sub>), 169.6 (COH), 156.2 (Ar-C3), 135.9 (Ar-C1), 129.8 (Ar-C5), 123.8 (Ar-C6), 119.7 (Ar-C4), 118.4 (Ar-C2), 108.11 (=CH-), 28.0 (S-CH<sub>2</sub>-), 25.8 (3C, SiC(CH<sub>3</sub>)<sub>3</sub>), 18.4 (SiC<sub>q</sub>), 13.0 (SCH<sub>2</sub>-CH<sub>3</sub>), -4.2 (2C, Si(CH<sub>3</sub>)<sub>2</sub>).

**MS (EI+)**  $m/z$  = 354 [M]<sup>+</sup>, 293 [M-SEt]<sup>+</sup>, 235.

**FTIR (ATR)**  $\tilde{\nu}$  = 2955 (w), 2929 (w), 2858 (w), 1587 (m), 1562 (vs), 1478 (m), 1446 (m), 1283 (s), 1253 (s), 1230 (s), 1197 (vs), 1165 (w), 1083 (w), 1064 (w), 1038 (w), 1000 (w), 974 (s), 934 (s), 835 (vs), 803 (m), 776 (vs) cm<sup>-1</sup>.

### 3'-(Tert-butyltrimethylsilyloxy)-6-hydroxydithiocinnamic acid butyl ester (17)

Using 3-(tert-butyltrimethylsilyloxy) acetophenone **3** (5.00 g, 20 mmol), KO<sup>t</sup>Bu (4.5 g, 40 mmol), CS<sub>2</sub> (1.7 mL, 1.4 mmol), and butyl iodide (2.3 mL, 20 mmol), synthesis was carried out according to **GP3**. Column chromatography, using *n*-hexane/DCM 1:1 as mobile phase ( $R_f \approx 0.5$ ), yielded **17** (1.6 g, 21 %) as orange oil.



$^1\text{H NMR}$  (400 MHz,  $\text{CDCl}_3$ )  $\delta$  = 15.12 (s, 1H, OH), 7.45 (d,  $J$  = 7.8 Hz, 1H, Ar-H6), 7.35 (s, 1H, Ar-H2), 7.29 (t,  $J$  = 7.9 Hz, 1H, Ar-H5), 6.98 (dd,  $J$  = 8.0, 2.3 Hz, 1H, Ar-H4), 6.87 (s, 1H, =CH-), 3.27 (t,  $^3J_{\text{HH}}$  = 7.4 Hz, 2H, S-CH<sub>2</sub>-), 1.77 – 1.54 (m, 2H, SCH<sub>2</sub>-CH<sub>2</sub>-), 1.54-1.37 (m, 2H, SCH<sub>2</sub>CH<sub>2</sub>-CH<sub>2</sub>-), 1.03 – 0.92 (m, 12H, SiC(CH<sub>3</sub>)<sub>3</sub>, SCH<sub>2</sub>CH<sub>2</sub>CH<sub>2</sub>-CH<sub>3</sub>), 0.23 (s,  $J$  = 3.4 Hz, 6H, Si(CH<sub>3</sub>)<sub>2</sub>) ppm.

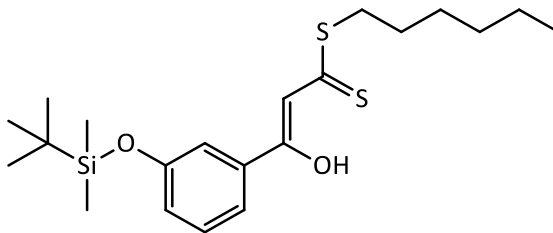
$^{13}\text{C}\{^1\text{H}\}$  NMR (101 MHz,  $\text{CDCl}_3$ )  $\delta$  = 216.8 (CS<sub>2</sub>), 169.4 (COH), 156.2 (Ar-C3), 135.9 (Ar-C1), 129.8 (Ar-C5), 123.7 (Ar-C6), 119.7 (Ar-C4), 118.4 (Ar-C2), 108.2 (=CH-), 33.4 (S-CH<sub>2</sub>-), 30.1 (SCH<sub>2</sub>-CH<sub>2</sub>-), 25.8 (SiC(CH<sub>3</sub>)<sub>3</sub>), 22.3 (SCH<sub>2</sub>CH<sub>2</sub>-CH<sub>2</sub>-), 18.4 (SiC<sub>q</sub>), 13.8 (SCH<sub>2</sub>CH<sub>2</sub>CH<sub>2</sub>-CH<sub>3</sub>), -4.3 (Si(CH<sub>3</sub>)<sub>2</sub>) ppm.

**MS (EI+)**  $m/z$  = 382 [M]<sup>+</sup>, 326 [M-C<sub>4</sub>H<sub>8</sub>]<sup>+</sup>, 293 [M-SBu]<sup>+</sup>, 269, 235, 85, 73, 57.

**FTIR (ATR)**  $\tilde{\nu}$  = 2956 (w), 2929 (w), 2858 (w), 1587 (m), 1562 (vs), 1478 (m), 1446 (m), 1283 (s), 1253 (s), 1235 (s), 1197 (vs), 1165 (w), 1083 (w), 1057 (m), 1000 (w), 976 (s), 935 (s), 835 (vs), 804 (m), 777 (vs) cm<sup>-1</sup>.

### 3'-(*Tert*-butyldimethylsilyloxy)- $\beta$ -hydroxydithiocinnamic acid hexyl ester (**18**)

The synthesis of **18** was carried out according to **GP3**, using 3-(*tert*-butyldimethylsilyloxy) acetophenone **3** (5.00 g, 20 mmol), KO<sup>t</sup>Bu (4.5 g, 40 mmol), CS<sub>2</sub> (1.7 mL, 1.4 mmol), and hexyl bromide (2.8 mL, 20 mmol). Column chromatography, using *n*-hexane as mobile phase ( $R_f \approx 0.5$ ), yielded **18** (3.4 g, 28 %) as orange oil.



<sup>1</sup>H NMR (200 MHz, CDCl<sub>3</sub>)  $\delta$  = 15.08 (s, 1H, OH), 7.48 – 7.38 (m, 1H, Ar-H<sub>6</sub>), 7.34-7.17 (m, 2H, Ar-H<sub>2</sub>, Ar-H<sub>5</sub>), 6.94 (m, 1H, Ar-H<sub>4</sub>), 6.83 (s, 1H, =CH-), 3.23 (t, <sup>3</sup>J<sub>HH</sub> = 7.2 Hz, 2H, S-CH<sub>2</sub>-), 1.79 – 1.57 (m, 2H, SCH<sub>2</sub>-CH<sub>2</sub>-), 1.51-1.17 (m, 6H, SCH<sub>2</sub>CH<sub>2</sub>-CH<sub>2</sub>-CH<sub>2</sub>-CH<sub>2</sub>-), 1.08 – 0.95 (m, 9H, SiC(CH<sub>3</sub>)<sub>3</sub>), 0.95 – 0.79 (m, 3H, -CH<sub>3</sub>), 0.20 (s, 6H, Si(CH<sub>3</sub>)<sub>2</sub>) ppm.

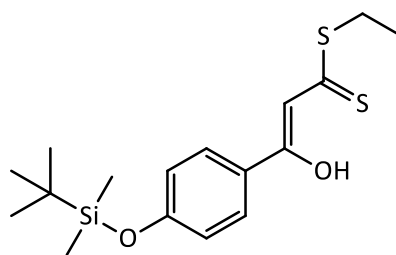
<sup>13</sup>C{<sup>1</sup>H} NMR (50 MHz, CDCl<sub>3</sub>)  $\delta$  = 216.9 (CS<sub>2</sub>), 169.5 (COH), 156.2 (Ar-C<sub>3</sub>), 136.0 (Ar-C<sub>1</sub>), 129.9 (Ar-C<sub>5</sub>), 123.8 (Ar-C<sub>6</sub>), 119.8 (Ar-C<sub>4</sub>), 118.5 (Ar-C<sub>2</sub>), 108.2 (=CH-), 33.8 (S-CH<sub>2</sub>-), 31.5 (SCH<sub>2</sub>-CH<sub>2</sub>-), 28.9 (SCH<sub>2</sub>CH<sub>2</sub>-CH<sub>2</sub>-), 28.0 (SCH<sub>2</sub>CH<sub>2</sub>CH<sub>2</sub>-CH<sub>2</sub>-), 25.8 (SiC(CH<sub>3</sub>)<sub>3</sub>), 22.7 (SCH<sub>2</sub>CH<sub>2</sub>CH<sub>2</sub>CH<sub>2</sub>-CH<sub>2</sub>-), 18.4 (SiC<sub>q</sub>), 14.1 (-CH<sub>3</sub>), -4.2 (Si(CH<sub>3</sub>)<sub>2</sub>) ppm.

**MS (EI+)**  $m/z$  = 410 [M]<sup>+</sup>, 326 [M-C<sub>6</sub>H<sub>12</sub>]<sup>+</sup>, 293 [M-SHex]<sup>+</sup>, 269, 235, 85, 73, 57.

**FTIR (ATR)**  $\tilde{\nu}$  = 2955 (w), 2928 (w), 2857 (w), 1587 (m), 1563 (vs), 1489 (m), 1478 (m), 1457 (m), 1284 (s), 1254 (s), 1232 (s), 1197 (vs), 1165 (w), 1083 (w), 1058 (m), 1000 (w), 975 (s), 934 (s), 836 (vs), 804 (m), 777 (vs) cm<sup>-1</sup>.

### 4'-(*tert*-butyldimethylsilyloxy)- $\beta$ -hydroxydithiocinnamic acid ethyl ester (**20**)

Using 4-(*tert*-butyldimethylsilyloxy) acetophenone **4** (5.00 g, 20 mmol), KO<sup>t</sup>Bu (4.5 g, 40 mmol), CS<sub>2</sub> (1.7 mL, 1.4 mmol), and ethyl iodide (1.6 mL, 20 mmol), synthesis was carried out according to **GP3**. Column chromatography, using *n*-hexane/DCM 1:1 as mobile phase ( $R_f \approx 0.8$ ), yielded **20** (1.4 g, 19 %) as orange oil.



**Analysis** calcd. for  $C_{17}H_{26}O_2S_2Si \cdot 0.25$  hexane: C 59.07, H 7.90 %; found C 59.06; H 7.72 %

**$^1H$  NMR** (200 MHz,  $CDCl_3$ )  $\delta$  = 15.21 (s, 1H, OH), 7.80 (d,  $^3J_{HH}$  = 8.9 Hz, 2H, Ar-H2, Ar-H6), 6.92 – 6.84 (m, 3H, Ar-H3, Ar-H5, =CH-), 3.27 (q,  $^3J_{HH}$  = 7.4 Hz, 2H, S- $CH_2$ -), 1.38 (t,  $^3J_{HH}$  = 7.4 Hz, 3H,  $SCH_2CH_3$ ), 1.00 (s, 9H,  $SiC(CH_3)_3$ ), 0.24 (s, 6H,  $Si(CH_3)_2$ ).

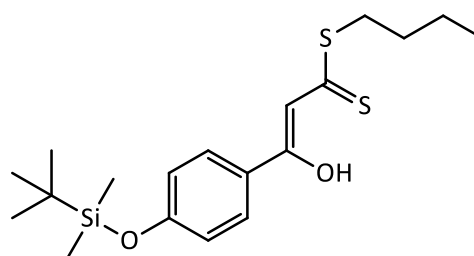
**$^{13}C\{^1H\}$  NMR** (50 MHz,  $CDCl_3$ )  $\delta$  = 215.2 ( $CS_2$ ), 170.1 (COH), 159.6 (Ar-C4), 128.7 (2C, Ar-C2, Ar-C6), 127.1 (Ar-C1), 120.5 (2C, Ar-C3, Ar-C5), 107.4 (=CH-), 27.8 (S- $CH_2$ -), 25.7 (3C,  $SiC(CH_3)_3$ ), 18.4 ( $SiC_q$ ), 13.2 ( $SCH_2CH_3$ ), -4.2 (2C,  $Si(CH_3)_2$ ).

**MS (EI+)**  $m/z$  = 354  $[M]^+$ , 293  $[M-SEt]^+$ , 235.

**FTIR (ATR)**  $\tilde{\nu}$  = 2955 (w), 2929 (w), 2885 (w), 2857 (w), 1600 (m), 1582 (s), 1563 (m), 1498 (vs), 1471 (w), 1427 (m), 1254 (s, b), 1223 (vs, b), 1169 (s), 1111 (w), 1062 (w), 1035 (w), 945 (s), 905 (vs), 834 (vs), 801 (s), 778 (vs)  $cm^{-1}$ .

#### 4'-(Tert-butyldimethylsilyloxy)- $\beta$ -hydroxydithiocinnamic acid butyl ester (**21**)

Using 4-(*tert*-butyldimethylsilyloxy) acetophenone **4** (5.00 g, 20 mmol),  $KO^tBu$  (4.5 g, 40 mmol),  $CS_2$  (1.7 mL, 1.4 mmol), and butyl iodide (1.7 mL, 15 mmol), the synthesis of **21** was carried out according to **GP3**. Column chromatography, using *n*-hexane/DCM 1:1 as mobile phase ( $R_f \approx 0.5$ ), yielded **21** (1.85g, 32 %) as orange oil.



**$^1H$  NMR** (400 MHz,  $CDCl_3$ )  $\delta$  = 15.21 (s, 1H, OH), 7.80 (d,  $^3J_{HH}$  = 8.8 Hz, 2H, Ar-H2, Ar-H6), 6.92 – 6.84 (m, 3H, Ar-H3, Ar-H5, =CH-), 3.27 (d,  $^3J_{HH}$  = 7.4 Hz, 1H, S- $CH_2$ -), 1.75 – 1.62 (m, 2H,  $SCH_2-CH_2$ -), 1.54 – 1.36 (m, 2H,  $SCH_2CH_2-CH_2$ -), 1.04 – 0.92 (m, 12H,  $SiC(CH_3)_3$ ,  $SCH_2CH_2CH_2-CH_3$ ), 0.24 (s, 6H,  $Si(CH_3)_2$ ) ppm.

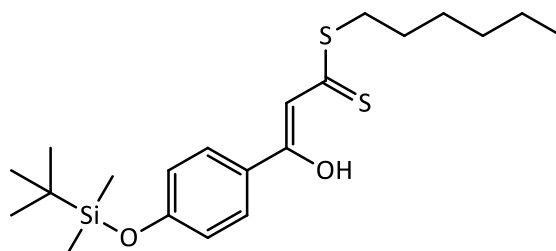
**$^{13}C\{^1H\}$  NMR** (101 MHz,  $CDCl_3$ )  $\delta$  = 215.3 ( $CS_2$ ), 170.0 (COH), 159.6 (Ar-C4), 128.7 (2C, Ar-C2, Ar-C6), 127.1 (Ar-C1), 120.5 (2C, Ar-C3, Ar-C5), 107.4 (=CH-), 33.3 (S- $CH_2$ -), 30.2 ( $SCH_2-CH_2$ -), 25.8 (3C,  $SiC(CH_3)_3$ ), 22.4 ( $SCH_2CH_2-CH_2$ -), 18.4 ( $SiC_q$ ), 13.8 ( $SCH_2CH_2CH_2-CH_3$ ), -4.2 (2C,  $Si(CH_3)_2$ ) ppm.

**MS (EI+)**  $m/z$  = 382  $[M]^+$ , 326  $[M-C_4H_8]^+$ , 293  $[M-SBu]^+$ , 235, 85, 73, 57.

**FTIR (ATR)**  $\tilde{\nu}$  = 2956 (w), 2929 (w), 2858 (w), 1601 (m), 1583 (s), 1563 (m), 1499 (vs), 1463 (m), 1427 (m), 1391 (m), 1274 (s), 1254 (s), 1232 (vs, b), 1169 (s), 1111 (w), 1052 (m), 1006 (w), 948 (s), 906 (vs), 834 (vs), 801 (s), 779 (vs)  $\text{cm}^{-1}$ .

#### 4'-(Tert-butyldimethylsilyloxy)- $\beta$ -hydroxydithiocinnamic acid hexyl ester (**22**)

Synthesis was carried out following **GP3** by using 4-(tert-butyldimethylsilyloxy) acetophenone **4** (5.00 g, 20 mmol),  $\text{KO}^t\text{Bu}$  (4.5 g, 40 mmol),  $\text{CS}_2$  (1.7 mL, 1.4 mmol), and hexyl bromide (2.8 mL, 20 mmol). Column chromatography was performed with *n*-hexane/DCM 1:1 as mobile phase ( $R_f \approx 0.7$ ), yielded **22** (2.6g, 31 %) as orange oil.



**$^1\text{H NMR}$**  (200 MHz,  $\text{CDCl}_3$ )  $\delta$  =15.20 (s, 1H, OH), 7.80 (d,  $^3J_{\text{HH}} = 8.9$  Hz, 2H, Ar-H2, Ar-H6), 6.96 – 6.81 (m, 3H, Ar-H3, Ar-H5, =CH-), 3.26 (t,  $^3J_{\text{HH}} = 7.2$  Hz, 1H, S- $\text{CH}_2$ -), 1.76 – 1.65 (m, 2H, S $\text{CH}_2$ - $\text{CH}_2$ -), 1.65 – 1.19 (m, 6H, S $\text{CH}_2$ CH $_2$ -CH $_2$ -CH $_2$ -CH $_2$ -), 1.07 – 0.82 (m, 12H, SiC(CH $_3$ ) $_3$ , S $\text{CH}_2$ CH $_2$ CH $_2$ CH $_2$ CH $_2$ -CH $_3$ ), 0.24 (s, 6H, Si(CH $_3$ ) $_2$ ) ppm.

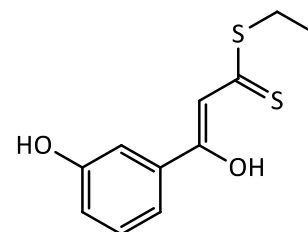
**$^{13}\text{C}\{^1\text{H}\}$  NMR** (50 MHz,  $\text{CDCl}_3$ )  $\delta$  =215.2 ( $\text{CS}_2$ ), 170.0 (COH), 159.6 (Ar-C4), 128.7 (2C, Ar-C2, Ar-C6), 127.1 (Ar-C1), 120.5 (2C, Ar-C3, Ar-C5), 107.5 (=CH-), 33.6 (S- $\text{CH}_2$ -), 31.5 (S $\text{CH}_2$ - $\text{CH}_2$ -), 28.9 (S $\text{CH}_2$ CH $_2$ - $\text{CH}_2$ -), 28.1 (S $\text{CH}_2$ CH $_2$ CH $_2$ - $\text{CH}_2$ -), 25.7 (3C, SiC(CH $_3$ ) $_3$ ), 22.7 (S $\text{CH}_2$ CH $_2$ CH $_2$ CH $_2$ - $\text{CH}_2$ -), 18.4 (SiC $_q$ ), 14.1 (S $\text{CH}_2$ CH $_2$ CH $_2$ CH $_2$ CH $_2$ -CH $_3$ ), -4.2 (2C, Si(CH $_3$ ) $_2$ ) ppm.

**MS (EI+)**  $m/z$  = 410 [M] $^+$ , 326 [M-C $_6$ H $_{12}$ ] $^+$ , 293 [M-SHex] $^+$ , 235.

**FTIR (ATR)**  $\tilde{\nu}$  = 2955 (w), 2928 (w), 2857 (w), 1601 (m), 1583 (s), 1563 (m), 1499 (vs), 1470 (m), 1427 (m), 1391 (w), 1275 (s), 1254 (s), 1227 (vs, b), 1169 (s), 1111 (w), 1054 (m), 1007 (w), 946 (m), 906 (vs), 835 (vs), 801 (s), 779 (vs)  $\text{cm}^{-1}$ .

### 3'-hydroxo- $\beta$ -hydroxydithiocinnamic acid ethyl ester (24)

The TBDMS group in precursor compound **16** (709 mg, 2 mmol) was cleaved according to **GP4** by using TBAF (4 mL 1 M soln. in THF) and stirred for 5 days before acidification (35 mL 2 M aq. H<sub>2</sub>SO<sub>4</sub>). The crude material was purified by column chromatography (mobile phase: CDM .  $R_f \approx 0.7$ ) and pure **24** (347 mg, 72 %) obtained as orange solid.



**Analysis** calcd. for C<sub>11</sub>H<sub>12</sub>O<sub>2</sub>S<sub>2</sub>: C 54.97, H 5.03 %; found C 54.92; H 5.06 %

**<sup>1</sup>H NMR** (200 MHz, CDCl<sub>3</sub>)  $\delta$  = 15.09 (s, 1H, C(OH)CHCS<sub>2</sub>), 7.47 – 7.18 (m, 3H, Ar-H2, Ar-H5, Ar-H6), 7.03 – 6.90 (m, 1H, Ar-H4), 6.82 (s, 1H, =CH-), 3.24 (d, <sup>3</sup>J<sub>HH</sub> = 7.4 Hz, 2H, S-CH<sub>2</sub>-), 1.35 (t, <sup>3</sup>J<sub>HH</sub> = 7.4 Hz, 3H, SCH<sub>2</sub>-CH<sub>3</sub>).

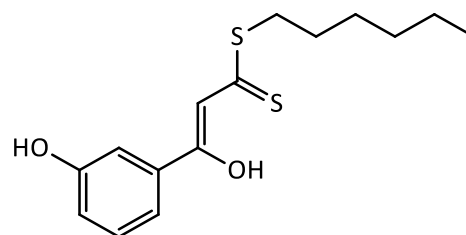
**<sup>13</sup>C{<sup>1</sup>H} NMR** (50 MHz, CDCl<sub>3</sub>)  $\delta$  = 216.7 (CS<sub>2</sub>), 169.1 (C(OH)CHCS<sub>2</sub>), 155.9 (Ar-C3), 135.9 (Ar-C1), 130.1 (Ar-C5), 119.2 (2C, Ar-C4, Ar-C6), 113.6 (Ar-C2), 108.1 (=CH-), 28.0 (S-CH<sub>2</sub>-), 12.9 (SCH<sub>2</sub>-CH<sub>3</sub>).

**MS (EI+)**  $m/z$  = 240 [M]<sup>+</sup>, 179 [M-SEt]<sup>+</sup>, 121.

**FTIR (ATR)**  $\tilde{\nu}$  = 3302 (w, b), 2975 (w), 2964 (w), 2924 (w), 2866 (w), 1587 (m), 1558 (vs), 1488 (m), 1469 (m), 1404 (m, b), 1360 (w), 1310 (w), 1263 (s), 1246 (m), 1233 (s), 1176 (s), 1085 (m), 1048 (m), 1033 (m), 998 (m), 961 (m), 900 (vs), 863 (s), 807 (m), 783 (m), 758 (s) cm<sup>-1</sup>.

### 3'-Hydroxy- $\beta$ -hydroxydithiocinnamic acid hexyl ester (25)

The TBDMS group in precursor compound **18** (1.23 g, 3mmol) was cleaved according to **GP4** by using TBAF (6 mL 1 M soln. in THF) and stirred for 6 days before acidification (100 mL 2 M aq. H<sub>2</sub>SO<sub>4</sub>). The crude material was flushed over a plug of silica gel using chloroform as solvent and thus **25** (795 mg, 89 %) obtained as orange oil.



**<sup>1</sup>H NMR** (200 MHz, CDCl<sub>3</sub>)  $\delta$  =15.06 (s, 1H, C(OH)CHCS<sub>2</sub>), 7.42 – 7.18 (m, 3H, Ar-H2, Ar-H5, Ar-H6), 7.04 – 6.88 (m, 1H, Ar-H4), 6.82 (s, 1H, =CH-), 3.22 (d, <sup>3</sup>J<sub>HH</sub> = 7.2 Hz, 2H, S-CH<sub>2</sub>-), 1.80-1.49 (m, 2H, SCH<sub>2</sub>-CH<sub>2</sub>-), 1.49 – 1.14 (m, 6H, SCH<sub>2</sub>CH<sub>2</sub>-CH<sub>2</sub>-CH<sub>2</sub>-CH<sub>2</sub>-), 0.90-0.85 (m, 3H, SCH<sub>2</sub>CH<sub>2</sub>CH<sub>2</sub>CH<sub>2</sub>CH<sub>2</sub>-CH<sub>3</sub>) ppm.

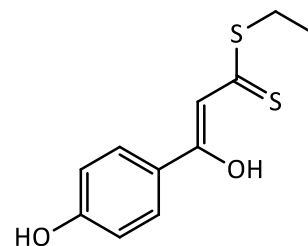
**$^{13}\text{C}\{^1\text{H}\}$  NMR** (50 MHz,  $\text{CDCl}_3$ )  $\delta$  = 216.9 ( $\text{CS}_2$ ), 169.1 ( $\text{C}(\text{OH})\text{CHCS}_2$ ), 156.1 (Ar-C3), 136.0 (Ar-C1), 130.1 (Ar-C5), 119.2, 119.1 (2C, Ar-C4, Ar-C6), 113.7 (Ar-C2), 108.2 (=CH-), 33.8 (S- $\text{CH}_2$ -), 31.4 ( $\text{SCH}_2$ - $\text{CH}_2$ -), 28.8 ( $\text{SCH}_2\text{CH}_2$ - $\text{CH}_2$ -), 27.9 ( $\text{SCH}_2\text{CH}_2\text{CH}_2$ - $\text{CH}_2$ -), 22.6 ( $\text{SCH}_2\text{CH}_2\text{CH}_2\text{CH}_2$ - $\text{CH}_2$ -), 14.1 ( $\text{SCH}_2\text{CH}_2\text{CH}_2\text{CH}_2\text{CH}_2$ - $\text{CH}_3$ ) ppm.

**MS (EI+)**  $m/z$  = 296  $[\text{M}]^+$ , 212  $[\text{M}-\text{C}_6\text{H}_{12}]^+$ , 179  $[\text{M}-\text{SEt}]^+$ , 121.

**FTIR (ATR)**  $\tilde{\nu}$  = 3377 (w, b), 2954 (w), 2927 (w), 2855 (w), 1564 (vs,b), 1490 (m), 1455 (m), 1401 (w), 1310 (w), 1281 (m), 1231 (s), 1188 (s), 1057 (s), 997 (w), 965 (m), 905 (s), 836 (w), 802 (w), 774 (vs)  $\text{cm}^{-1}$ .

#### 4'-hydroxo- $\beta$ -hydroxydithiocinnamic acid ethyl ester (27)

The TBDMS group in precursor compound **20** (709 mg, 2 mmol) was cleaved according to **GP4** by using TBAF (4 mL 1 M soln. in THF) and stirred for 4 days before acidification (35 mL 2 M aq.  $\text{H}_2\text{SO}_4$ ). The crude material was purified by column chromatography (mobile phase: CDM .  $R_f \approx 0.7$ ) and pure **24** (217 mg, 45 %) obtained as orange solid.



**Analysis** calcd. for  $\text{C}_{11}\text{H}_{12}\text{O}_2\text{S}_2 \cdot 0.02$  dichloromethane: C 54.68, H 5.01 %; found C 54.38; H 5.38 %

**$^1\text{H}$  NMR** (400 MHz,  $\text{CDCl}_3$ )  $\delta$  = 15.22 (s, 1H,  $\text{C}(\text{OH})\text{CHCS}_2$ ), 7.87 – 7.67 (m, 2H, Ar-H2, Ar-H6), 6.96 – 6.79 (m, 3H, Ar-H3, Ar-H5,  $\text{CHCS}_2$ ), 3.27 (d,  $^3J_{\text{HH}} = 7.4$  Hz, 2H,  $\text{SCH}_2$ ), 1.37 (t,  $^3J_{\text{HH}} = 7.4$  Hz, 3H,  $\text{SCH}_2\text{CH}_3$ ).

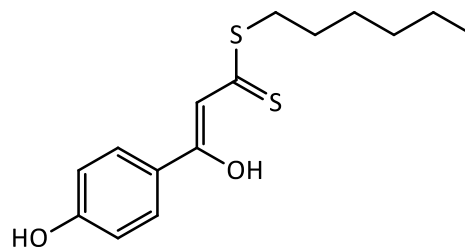
**$^{13}\text{C}\{^1\text{H}\}$  NMR** (101 MHz,  $\text{CDCl}_3$ )  $\delta$  = 215.2 ( $\text{CS}_2$ ), 169.9 ( $\text{C}(\text{OH})\text{CHCS}_2$ ), 159.3 (Ar-C4), 129.1 (2C, Ar-C2, Ar-C6), 126.7 (Ar-C1), 115.9 (2C, Ar-C3, Ar-C5), 107.2 (=CH-), 27.8 ( $\text{SCH}_2$ ), 13.2 ( $\text{SCH}_2\text{CH}_3$ ).

**MS (EI+)**  $m/z$  = 240  $[\text{M}]^+$ , 179  $[\text{M}-\text{SEt}]^+$ , 121.

**FTIR (ATR)**  $\tilde{\nu}$  = 3421 (w, b), 2972 (w), 2964 (w), 2927 (w), 2852 (w), 1593 (s), 1568 (vs), 1504 (s), 1445 (s, b), 1390 (m), 1371 (m), 1227 (vs, b), 1178 (m), 1116 (m), 1060 (m), 1043 (m), 953 (s), 838 (vs), 815 (s), 770 (vs)  $\text{cm}^{-1}$ .

#### 4'-Hydroxy- $\beta$ -hydroxydithiocinnamic acid hexyl ester (**28**)

The precursor compound **22** (1.23 g, 3mmol) was deprotected according to **GP4** by using TBAF (6 mL 1 M soln. in THF) and stirred for 5 days before acidification (50 mL 2M H<sub>2</sub>SO<sub>4</sub>). The crude material was subjected to a short column chromatographic workup on silica gel using DCM as solvent and thus **28** (568 mg, 64 %) obtained as orange solid.



<sup>1</sup>H NMR (200 MHz, CDCl<sub>3</sub>)  $\delta$  =15.21 (s, 1H, C(OH)CHCS<sub>2</sub>), 7.80 (d, <sup>3</sup>J<sub>HH</sub> = 8.8 Hz, 2H, Ar-H2, Ar-H6), 6.96 – 6.79 (m, 3H, Ar-H3, Ar-H5, CHCS<sub>2</sub>), 3.27 (t, <sup>3</sup>J<sub>HH</sub> = 7.2 Hz, 2H, S-CH<sub>2</sub>-), 1.88 – 1.57 (m, 2H, SCH<sub>2</sub>-CH<sub>2</sub>-), 1.54 – 1.19 (m, 6H, SCH<sub>2</sub>CH<sub>2</sub>-CH<sub>2</sub>-CH<sub>2</sub>-CH<sub>2</sub>-), 0.98 – 0.77 (m, 3H, SCH<sub>2</sub>CH<sub>2</sub>CH<sub>2</sub>CH<sub>2</sub>CH<sub>2</sub>-CH<sub>3</sub>) ppm.

<sup>13</sup>C{<sup>1</sup>H} NMR (50 MHz, CDCl<sub>3</sub>)  $\delta$  =215.4 (CS<sub>2</sub>), 169.8 (COH), 159.3 (Ar-C4), 129.1 (2C, Ar-C2, Ar-C6), 126.7 (Ar-C1), 115.9 (2C, Ar-C3, Ar-C5), 107.34 (CHCS<sub>2</sub>), 33.6 (S-CH<sub>2</sub>-), 31.48 (SCH<sub>2</sub>-CH<sub>2</sub>-), 28.9 (SCH<sub>2</sub>CH<sub>2</sub>-CH<sub>2</sub>-), 28.1 (SCH<sub>2</sub>CH<sub>2</sub>CH<sub>2</sub>-CH<sub>2</sub>-), 22.7 (SCH<sub>2</sub>CH<sub>2</sub>CH<sub>2</sub>CH<sub>2</sub>-CH<sub>2</sub>-), 14.1 (SCH<sub>2</sub>CH<sub>2</sub>CH<sub>2</sub>CH<sub>2</sub>CH<sub>2</sub>-CH<sub>3</sub>) ppm.

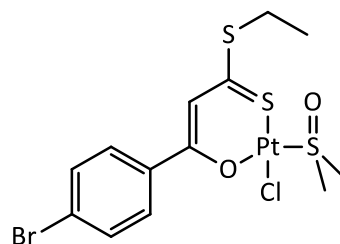
MS (EI+)  $m/z$  = 296 [M]<sup>+</sup>, 212 [M-C<sub>6</sub>H<sub>12</sub>]<sup>+</sup>, 179 [M-SEt]<sup>+</sup>, 121.

FTIR (ATR)  $\tilde{\nu}$  = 3538 (w), 3273 (w, b), 2955 (w), 2926 (w), 2854 (w), 1593 (s), 1562 (s, b), 15505 (s), 1445 (s), 1391 (m), 1298 (w), 1256 (m), 1227 (vs, b), 1171 (s), 1113 (m), 1051 (m), 940 (vs), 845 (s), 839 (s), (w), 793 (s), 774 (vs) cm<sup>-1</sup>.

## 16.2 Pt(II) complexes

### Chloro-(1-(4-bromophenyl)-3-(ethylthio)-3-thioxo-prop-1-en-1-olate-O,S)-(dimethylsulfoxide-S)-platinum(II) (**34**) - Effect of base

**Method 1: NaH as base.** The compound was prepared according to **GP7** as described in detail in the respective publication.<sup>118</sup> Based on 200 mg (0.482 mmol)  $K_2PtCl_4$ , the yield of **34** after repeated column chromatography was 89 mg (33 %).

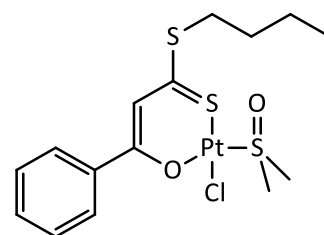


**Method 2: KO<sup>t</sup>Bu as base.** 4-Bromo- $\beta$ -hydroxydithiocinnamic ethyl ester **12** (118.8 mg, 0.391 mmol),  $K_2PtCl_4$  (200 mg, 0.482 mmol), DMSO (62  $\mu$ L, 0.876 mmol) and KO<sup>t</sup>Bu (49.15 mg, 0.438 mmol) were reacted following **GP6**. The crude material was purified by column chromatography using a gradient (mobile phase: DCM/*n*-hexane 2 : 1 to 1 : 0,  $R_f \approx 0.3$ ) affording **34** in 25 % yield (61 mg).

**Method 3: NaOAc as base.** 4-Bromo- $\beta$ -hydroxydithiocinnamic ethyl ester **12** (133 mg, 0.438 mmol),  $K_2PtCl_4$  (200 mg, 0.482 mmol), DMSO (62  $\mu$ L, 0.876 mmol) and NaOAc (36 mg, 0.438 mmol) were reacted following **GP5**. The crude material was purified by column chromatography using a gradient (mobile phase: DCM/*n*-hexane 2 : 1 to 1 : 0,  $R_f \approx 0.3$ ) to give **34** in 67 % yield (179 mg).

### Chloro-(1-phenyl-3-(butylthio)-3-thioxo-prop-1-en-1-olate-O,S)-(dimethylsulfoxide-S)-platinum(II) (**31**)

Following **GP5**,  $K_2PtCl_4$  (400 mg, 0.96 mmol) was reacted with **9** (221 mg, 0.88 mmol), using NaOAc $\cdot$ 3H<sub>2</sub>O (119 mg, 0.88 mmol) as base and 125  $\mu$ L (1.76 mmol) DMSO. The mixture was stirred for 2 days and the crude product purified *via* column chromatography on silica gel using a gradient (DCM/*n*-hexane 3:2 to 1:0;  $R_f \approx 0.1$ ) and crystallized from DCM/*n*-hexane to afford **31** (160 mg, 33 %) as orange powder.



<sup>1</sup>H NMR (200 MHz, CDCl<sub>3</sub>)  $\delta$  = 8.13 – 7.81 (m, 2H, Ar-H2, Ar-H6), 7.47 (dt,  $J$  = 14.7, 7.2 Hz, 3H, Ar-H3, Ar-H4, Ar-H5), 7.11 (s, 1H, =CH-), 3.66 (s, <sup>3</sup> $J_{PtH}$  = 23.5 Hz, 6H, CH<sub>3</sub>(DMSO)), 3.25 (t, <sup>3</sup> $J_{HH}$  = 7.3 Hz, 2H, S-CH<sub>2</sub>-), 1.94 – 1.61 (m, 2H, SCH<sub>2</sub>-CH<sub>2</sub>-), 1.49 (m, 2H, SCH<sub>2</sub>CH<sub>2</sub>-CH<sub>2</sub>-), 0.96 (t, <sup>3</sup> $J_{HH}$  = 7.2 Hz, 3H, -CH<sub>3</sub>) ppm.



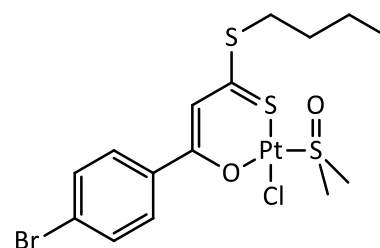
$^{13}\text{C}\{^1\text{H}\}$  NMR (50 MHz,  $\text{CDCl}_3$ )  $\delta$  =180.6 ( $\text{CS}_2$ ), 174.7 (C-OPt), 137.3 (Ar-C1), 132.1 (Ar-C4), 128.9 (2C, Ar-C3, Ar-C5), 128.1 (2C, Ar-C2, Ar-C6), 111.7 (=CH-), 47.0 (s,  $^2J_{\text{PtC}}$  = 59.9 Hz,  $\text{CH}_3(\text{DMSO})$ ), 34.2 (S- $\text{CH}_2$ -), 30.1 (S $\text{CH}_2$ - $\text{CH}_2$ -), 22.2 (S $\text{CH}_2\text{CH}_2$ - $\text{CH}_2$ -), 13.8 (- $\text{CH}_3$ ) ppm.

**MS (EI+)**  $m/z$  =560  $[\text{M}+\text{H}]^+$ .

**FTIR (ATR)**  $\tilde{\nu}$  = 3008 (w), 2957 (w), 2929 (w), 2874 (w), 1503 (s), 1475 (s), 1432 (m), 1287 (m), 1271 (m), 1219 (w), 1182 (w), 1130 (m), 1033 (m), 975 (m), 944 (w), 925 (w), 834 (m), 764(s), 689 (vs)  $\text{cm}^{-1}$ .

### Chloro-(1-(4-bromophenyl)-3-(butylthio)-3-thioxo-prop-1-en-1-olate-O,S)- (dimethylsulfoxide-S)-platinum(II) (35)

According to **GP5**, the synthesis was performed by reaction of **13** (290 mg, 0.88 mmol) and NaOAc·3H<sub>2</sub>O (128 mg, 0.94 mmol) with DMSO (130  $\mu\text{L}$ , 1.83 mmol) overnight. The crude product was purified *via* column chromatography on silica gel (mobile phase: DCM/*n*-hexane 3:2,  $R_f \approx 0.1$ ). The product **35** (340 mg, 61 %) was obtained as yellow solid.



$^1\text{H}$  NMR (200 MHz,  $\text{CDCl}_3$ )  $\delta$  =7.82 (d,  $^3J_{\text{HH}}$  = 8.7 Hz, 2H, Ar-H3, Ar-H5), 7.53 (d,  $^3J_{\text{HH}}$  = 8.7 Hz, 2H, Ar-H2, Ar-H6), 7.03 (s, 1H, =CH-), 3.66 (s,  $^3J_{\text{PtH}}$  = 23.4 Hz,  $\text{CH}_3(\text{DMSO})$ ), 3.25 (t,  $J$  = 7.3 Hz, 2H, S- $\text{CH}_2$ -), 1.86 – 1.68 (m, 2H, S $\text{CH}_2$ - $\text{CH}_2$ -), 1.49 (m, 2H, S $\text{CH}_2\text{CH}_2$ - $\text{CH}_2$ -), 0.93 (s, 2H, - $\text{CH}_3$ ) ppm.

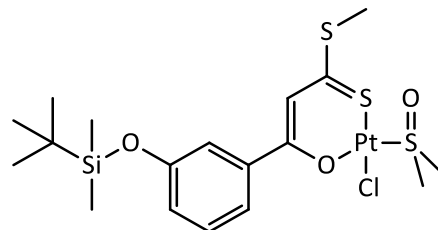
$^{13}\text{C}\{^1\text{H}\}$  NMR (150 MHz,  $\text{CDCl}_3$ )  $\delta$  =182.3 ( $\text{CS}_2$ ), 173.6 (C-OPt), 136.5 (Ar-C1), 132.5 (2C, Ar-C3, Ar-C5), 129.8 (2C, Ar-C2, Ar-C6), 127.3 (Ar-C4), 111.5 (CH $\text{CS}_2$ ), 46.8 (( $\text{CH}_3(\text{DMSO})$ ), 34.1 (S- $\text{CH}_2$ -), 29.8 (S $\text{CH}_2$ - $\text{CH}_2$ -), 21.8 (S $\text{CH}_2\text{CH}_2$ - $\text{CH}_2$ -), 13.3 (- $\text{CH}_3$ ) ppm.

**MS (EI+)**  $m/z$  =638  $[\text{M}]^+$

**FTIR (ATR)**  $\tilde{\nu}$  3016 (w), 2928 (w), 2860 (w), 1583 (w), 1502, 1474 (vs), 1307 (m), 1285 (m), 1222 (m), 1140, 1130 (m), 1086 (w), 1070 (w), 1035 (m), 1006 (s), 978 (m), 9223 (w), 852 (m), 837 (s), 783 (m)  $\text{cm}^{-1}$ .

**Chlorido-(1-(3'-tert-butyl dimethylsilyloxy)-3-(methylthio)-3-thioxo-prop-1-en-1-olate-O,S)-(dimethylsulfoxide-S)-platinum(II) (37)**

Compound **15** (149 mg, 0.44 mmol) was reacted with  $K_2PtCl_4$  (200 mg, 0.48 mmol), NaH (20 mg, 0.5 mmol 60 % in mineral oil), and DMSO (70  $\mu$ L, 0.99 mmol) according to **GP7**. The mixture was stirred overnight. The crude material obtained after workup was subjected to column chromatography (mobile phase: DCM/*n*-hexane 2:1,  $R_f \approx 0.1$ ). Compound **37** (124 mg, 52 %) was obtained as orange powder.



**Analysis** calcd. for  $C_{18}H_{29}ClO_3PtS_3Si \cdot 0.25$  pentane: C 34.89, H 4.84 %; found C 34.89, H 4.57 %.

**$^1H$  NMR** (200 MHz,  $CDCl_3$ )  $\delta$  = 7.65 – 7.36 (m, 2H, Ar-H2, Ar-H6), 7.36 – 7.13 (m, 1H, Ar-H5, overlaid by SRS), 7.08 (s, 1H,  $CHCS_2$ ), 7.01 (d,  $J$  = 8.1 Hz, 1H Ar-H4), 3.66 (s w/ Pt satellites,  $^3J_{Pt-H}$  = 23.3 Hz, 6H,  $CH_3$ (DMSO)), 2.67 (s, 3H,  $SCH_3$ ), 0.99 (s, 9H  $SiC(CH_3)_3$ ), 0.24 (s, 6H,  $Si(CH_3)_2$ ).

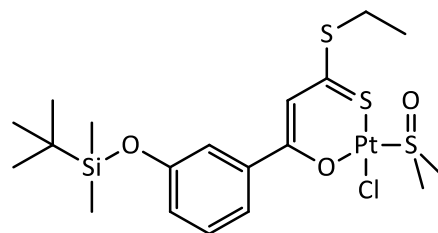
**$^{13}C\{^1H\}$  NMR** (151 MHz,  $CDCl_3$ )  $\delta$  = 180.9 ( $CS_2$ ), 174.5 (COPt), 156.3 (Ar-C3), 138.8 (Ar-C1), 129.8 (Ar-C5), 124.1 (Ar-C4), 120.9 (Ar-C6), 119.6 (Ar-C2), 111.7 ( $CHCS_2$ ), 47.0 (2C,  $CH_3$ (DMSO)), 25.9 (3C,  $SiC(CH_3)_3$ ), 18.4 ( $SiC_q$ ), 17.7 ( $SCH_3$ ), -4.2 ( $Si(CH_3)_2$ ).

**MS (EI+)**  $m/z$  = 648  $[M]^+$ , 612  $[M-Cl-H]^+$ , 235.

**FTIR (ATR)**  $\tilde{\nu}$  = 3013 (w), 2950 (w), 2929 (w), 2887 (w), 2856 (w), 1596 (w), 1584 (w), 1488 (vs), 1474 (vs), 1406 (m), 1362 (w), 1312 (m), 1285 (m), 1275 (s), 1252 (m), 1222 (s), 1142 (m), 1029 (m), 1005 (m), 976 (m), 963 (m), 938 (w), 887 (w), 849 (vs), 840 (vs), 811 (m), 789 (vs), 780 (vs)  $cm^{-1}$ .

**Chlorido-(1-(3'-tert-butyl dimethylsilyloxy)-3-(ethylthio)-3-thioxo-prop-1-en-1-olate-O,S)-(dimethylsulfoxide-S)-platinum(II) (38)**

Compound **16** (155 mg, 0.44 mmol) was brought to reaction with  $K_2PtCl_4$  (200 mg, 0.48 mmol), NaH (20 mg, 0.5 mmol 60 % in mineral oil), and DMSO (70  $\mu$ L, 0.99 mmol) according to **GP7**. The mixture was stirred overnight. The crude material obtained after workup was subjected to column chromatography (mobile phase: DCM,  $R_f \approx 0.5$ ).



Compound **38** (93 mg, 32 %) was obtained as orange powder.

**Analysis** calcd. for  $C_{19}H_{31}ClO_3PtS_3Si \cdot 0.1$  pentane: C 34.98; H 4.85 %; found C 35.36, H 4.85 %.

**$^1H$  NMR** (200 MHz,  $CDCl_3$ )  $\delta$  = 7.58 – 7.42 (m, 2H, Ar-H2, Ar-H6), 7.34 – 7.19 (m, 1H overlaid by SRS, Ar-H5), 7.11 – 6.95 (m, 2H, Ar-H4,  $CHCS_2$ ), 3.66 (s w/ Pt satellites,  $^3J_{Pt-H}$  = 23.4 Hz, 6H,  $CH_3(DMSO)$ ), 3.27 (q,  $^3J_{HH}$  = 7.4 Hz, 2H,  $SCH_2$ ), 1.44 (t,  $^3J_{HH}$  = 7.4 Hz, 3H,  $SCH_2CH_3$ ), 0.99 (s, 9H,  $SiC(CH_3)_3$ ), 0.23 (s, 6H,  $Si(CH_3)_2$ ).

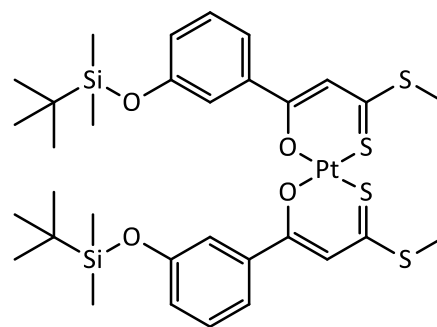
**$^{13}C\{^1H\}$  NMR** (50 MHz,  $CDCl_3$ )  $\delta$  = 180.2 ( $CS_2$ ), 174.7 (COPt), 156.3 (Ar-C3), 138.8 (Ar-C1), 129.8 (Ar-C5), 124.1 (Ar-C4), 120.9 (Ar-C6), 119.5 (Ar-C2), 111.8 ( $CHCS_2$ ), 47.0 (2C, s w/ Pt satellites,  $^2J_{Pt-C}$  = 59.3 Hz,  $CH_3(DMSO)$ ), 28.9 ( $SCH_2$ ), 25.8 (3C,  $SiC(CH_3)_3$ ), 18.4 ( $SiC_q$ ), 13.3 ( $SCH_2CH_3$ ), -4.2 (2C,  $Si(CH_3)_2$ ).

**MS (FAB+ in nba)**  $m/z$  = 662  $[M]^+$ , 626  $[M-Cl]^+$ .

**FTIR (ATR)**  $\tilde{\nu}$  = 2955 (w), 2929 (w), 2858 (w), 1590 (w), 1582 (w), 1489 (s, b), 1459 (s, b), 1416 (w), 1283 (s), 1252 (m), 1205 (m), 1138 (m), 1091 (w), 1073 (w), 1032 (w), 999 (w), 938 (m), 883 (w), 840 (vs), 806 (m), 782 (vs)  $cm^{-1}$ .

### Bis-(1-(4'-tert-butyltrimethylsilyloxy)-3-(methylthio)-3-thioxo-prop-1-en-1-olate-O,S)-platinum(II) (**50**)

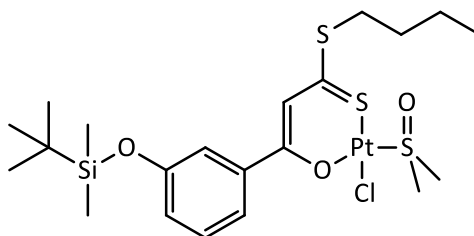
As a side product of the synthesis of compound **38**, compound **50** was isolated by column chromatography. Crystals suitable for X-Ray structure determination were obtained by evaporation of the solvents used for column chromatography (DCM/*n*-hexane). Due to the low quantity (few crystals were obtained), no further analysis was performed.



**MS (EI+):**  $m/z$  = 902  $[M]^+$ , 679, 663, 221, 111, 97, 71, 57.

**Chlorido-(1-(3'-tert-butyltrimethylsilyloxy)-3-(butylthio)-3-thioxo-prop-1-en-1-olate-O,S)-(dimethylsulfoxide-S)-platinum(II) (39)**

Compound **17** (169 mg, 0.44 mmol) was reacted with  $K_2PtCl_4$  (200 mg, 0.48 mmol), NaH (30 mg, 0.76 mmol 60 % in mineral oil), and DMSO (70  $\mu$ L, 0.99 mmol) according to **GP7**. The mixture was stirred overnight and the crude material was subjected to column chromatography (mobile phase: DCM,  $R_f \approx 0.3$ ). Compound **39** (50 mg, 17 %) was obtained as orange solid.



**$^1H$  NMR** (600 MHz,  $CDCl_3$ )  $\delta$  = 7.52 (d,  $^3J_{HH} = 8.1$  Hz, 1H, Ar-H6), 7.47 – 7.43 (m, 1H, Ar-H2), 7.24 (m, 1H, Ar-H5), 7.06 (s, 1H, =CH-), 7.01 (dd,  $^3J_{HH} = 7.9, 2.4$  Hz, 1H, Ar-H4), 3.66 (s, 6H,  $CH_3$ (DMSO)), 3.25 (t,  $^3J_{HH} = 7.3$  Hz, 2H, S- $CH_2$ -), 1.81 – 1.72 (m, 2H,  $SCH_2-CH_2$ -), 1.50 (m, 2H,  $SCH_2CH_2-CH_2$ -), 1.01 – 0.93 (m, 12H,  $Si(CH_3)_3$ ,  $SCH_2CH_2CH_2-CH_3$ ), 0.23 (s, 6H,  $Si(CH_3)_2$ ) ppm.

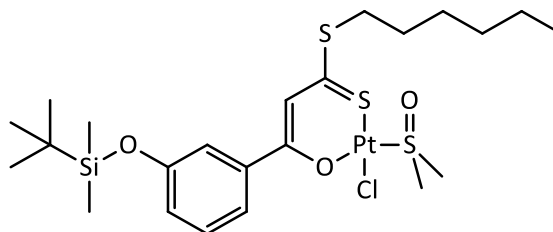
**$^{13}C\{^1H\}$  NMR** (151 MHz,  $CDCl_3$ )  $\delta$  = 180.5 ( $CS_2$ ), 174.5 (COPt), 156.3 (Ar-C3), 138.8 (Ar-C1), 129.9 (Ar-C5), 124.1 (Ar-C4), 120.9 (Ar-C6), 119.5 (Ar-C2), 111.8 ( $CHCS_2$ ), 47.0 (2C,  $CH_3$ (DMSO)), 34.3 (S- $CH_2$ -), 30.2 ( $SCH_2-CH_2$ -), 25.9 (3C,  $Si(CH_3)_3$ ), 22.2 ( $SCH_2CH_2-CH_2$ -), 18.4 ( $SiC_q$ ), 13.8 ( $SCH_2CH_2CH_2-CH_3$ ), -4.2 (2C,  $Si(CH_3)_2$ ) ppm.

**MS (EI+)**  $m/z = 689$  [M] $^+$ .

**FTIR (ATR)**  $\tilde{\nu} = 3013$  (w), 2951 (w), 2929 (w), 2857 (w), 1599 (w), 1581 (w), 1488 (s), 1460 (s), 1418 (w), 1361 (w), 1281 (s), 1250 (m), 1206 (m), 1147 (w), 1130 (m), 1090 (w), 1072 (w), 1035 (m), 1001 (m), 940 (s), 840 (vs), 806 (w), 781 (vs)  $cm^{-1}$ .

**Chlorido-(1-(3'-tert-butyl(dimethylsilyloxy)-3-(hexylthio)-3-thioxo-prop-1-en-1-olate-O,S)-  
(dimethylsulfoxide-S)-platinum(II) (40)**

The reaction was performed following **GP7**.  $K_2PtCl_4$  (200 mg, 0.48 mmol), DMSO (62  $\mu$ L, 0.88 mmol), **18** (180 mg, 0.44 mmol) and NaH (18 mg, 0.44 mmol (60 % in mineral oil) were stirred for 2 d and workup was performed by column chromatography on silica gel (mobile phase: gradient DCM/*n*-hexane 1:1 to 1:0,  $R_f \approx 0.2$ ), followed by repeated crystallization from DCM/pentane. This process afforded **40** (81 mg, 26 %) as orange solid.



**$^1H$  NMR** (200 MHz,  $CDCl_3$ )  $\delta$  = 7.52 (d,  $^3J_{HH} = 7.9$  Hz, 1H, Ar-H6), 7.48 – 7.38 (m, 1H, Ar-H2), 7.25 (t,  $J = 7.9$  Hz, 1H, Ar-H5), 7.06 (s, 1H, =CH-), 7.01 (dd,  $^3J_{HH} = 7.6, 2.0$  Hz, 1H, Ar-H4), 3.66 (s,  $^3J_{PtH} = 23.3$  Hz, 6H,  $CH_3$  (DMSO)), 3.24 (t,  $^3J_{HH} = 7.3$  Hz, 2H, S- $CH_2$ -), 1.92 – 1.60 (m, 2H,  $SCH_2$ - $CH_2$ -), 1.40 – 1.07 (m, 6H,  $SCH_2CH_2$ - $CH_2$ - $CH_2$ -), 1.04 – 0.77 (m, 12H,  $SiC(CH_3)_3$ , - $CH_3$ ), 0.24 (s, 6H,  $Si(CH_3)_2$ ) ppm.

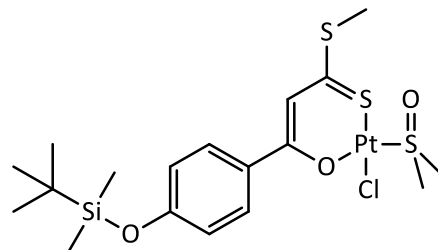
**$^{13}C\{^1H\}$  NMR** (50 MHz,  $CDCl_3$ )  $\delta$  = 189.3 ( $CS_2$ ), 174.5 (COPt), 156.3 (Ar-C3), 138.9 (Ar-C1), 129.9 (Ar-C5), 124.0 (Ar-C4), 120.9 (Ar-C6), 119.5 (Ar-C2), 111.8 ( $CHCS_2$ ), 47.0 (2C,  $CH_3$  (DMSO)), 34.6 (S- $CH_2$ -), 31.4 ( $SCH_2$ - $CH_2$ -), 28.7 ( $SCH_2CH_2$ - $CH_2$ -), 28.1 ( $SCH_2CH_2CH_2$ - $CH_2$ -), 25.9 (3C,  $SiC(CH_3)_3$ ), 22.6 ( $SCH_2CH_2CH_2CH_2$ - $CH_2$ -), 18.4 ( $SiC_q$ ), 14.1 ( $SCH_2CH_2CH_2CH_2CH_2$ - $CH_3$ ), -4.2 (2C,  $Si(CH_3)_2$ ) ppm.

**MS (FAB+ in nba)**  $m/z = 718$   $[M+H]^+$ .

**FTIR (ATR)**  $\tilde{\nu} = 3019$  (w), 2954 (w), 2928 (w), 2855 (w), 1599 (w), 1581 (w), 1488 (s), 1464 (s), 1405 (w), 1361 (w), 1282 (s), 1252 (m), 1205 (m), 1145 (w), 1091 (w), 1072 (w), 1031 (m), 1000 (m), 984 (w), 940 (s), 882 (w), 840 (vs), 806 (m), 781 (vs)  $cm^{-1}$ .

**Chlorido-(1-(4'-tert-butyl(dimethylsilyloxy))-3-(methylthio)-3-thioxo-prop-1-en-1-olate-O,S)-(dimethylsulfoxide-S)-platinum(II) (41)**

Following **GP7**, the reaction was conducted based on 200 mg (0.48 mmol)  $K_2PtCl_4$ , compound **19** (149 mg, 0.44 mmol), NaH (20 mg, 0.5 mmol 60 % in mineral oil), and DMSO (70  $\mu$ L, 0.99 mmol). After 2 days of stirring, workup afforded the crude material which was subjected to column chromatography using a gradient (mobile phase: DCM:acetone 1:0 to 1:1). Pure **41** (137 mg, 58 %) was obtained as orange powder.



**Analysis** calcd. for  $C_{18}H_{29}ClO_3PtS_3Si \cdot 0.15$  pentane: C 34.17, H 4.71 %; found C 34.27, H 4.60 %.

**$^1H$  NMR** (200 MHz,  $CDCl_3$ )  $\delta$  = 7.87 (d,  $^3J_{HH}$  = 8.9 Hz, 2H, Ar-H2, Ar-H6), 7.06 (s, 1H,  $CHCS_2$ ), 6.80 (d,  $^3J_{HH}$  = 8.8 Hz, 2H, Ar-H3, Ar-H5), 3.63 (s w/ Pt satellites,  $^3J_{Pt-H}$  = 23.4 Hz, 6H,  $CH_3$ (DMSO)), 2.63 (s, 3H,  $SCH_3$ ), 0.94 (s, 9H,  $Si(CH_3)_3$ ), 0.19 (s, 6H,  $Si(CH_3)_2$ ).

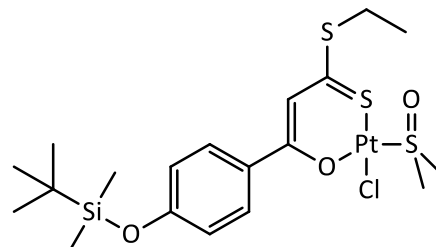
**$^{13}C\{^1H\}$  NMR** (50 MHz,  $CDCl_3$ )  $\delta$  = 178.9 ( $CS_2$ ), 174.3 (COPt), 159.9 (Ar-C4), 130.3 (2C, Ar-C2, Ar-C6), 120.5 (2C, Ar-C3, Ar-C5), 111.1 ( $CHCS_2$ ), 47.0 (2C,  $CH_3$ (DMSO)), 25.7 (3C,  $Si(CH_3)_2$ ), 18.4 ( $SiC_q$ ), 17.63 ( $SCH_3$ ), -4.2 (2C,  $Si(CH_3)_2$ ).

**MS (FAB+ in nba)**  $m/z$  = 648  $[M]^+$ .

**FTIR (ATR)**  $\tilde{\nu}$  = 3007 (w), 2955 (w), 2928 (w), 2885 (w), 2856 (w), 1598 (m), 1576 (w), 1488 (s), 1467 (vs, b), 1404 (m), 1362 (w), 1313 (m), 1249 (vs), 1168 (m), 1142 (m), 1130 (m), 1113 (m), 1037 (w), 1008 (w), 984 (w), 960 (w), 911 (s), 900 (s), 836 (s), 802 (s), 786 (s)  $cm^{-1}$ .

**Chlorido-(1-(4'-tert-butyl dimethylsilyloxy)-3-(ethylthio)-3-thioxo-prop-1-en-1-olate-O,S)-(dimethylsulfoxide-S)-platinum(II) (42)**

The reaction was performed following **GP7**.  $K_2PtCl_4$  (200 mg, 0.48 mmol), DMSO (70  $\mu$ L, 0.99 mmol), **20** (155 mg, 0.44 mmol) and NaH (23 mg, 0.58 mmol 60 % in mineral oil) were stirred overnight. Workup included column chromatography on silica gel (mobile phase: DCM,  $R_f \approx 0.3$ ), followed by repeated crystallization from DCM/pentane. This process afforded **42** (104 mg, 36 %) as orange powder.



**Analysis** calcd. for  $C_{19}H_{31}ClO_3PtS_3Si$ : C 34.46; H 4.72 %; found C 34.70, H 4.63 %.

**$^1H$  NMR** (200 MHz,  $CDCl_3$ )  $\delta$  = 8.03 – 7.74 (m, 2H, Ar-H2, Ar-H6), 7.08 (s, 1H,  $CHCS_2$ ), 6.92 – 6.74 (m, 2H, Ar-H3, Ar-H5), 3.65 (s w/ Pt satellites,  $^3J_{Pt-H} = 23.4$  Hz, 6H,  $CH_3$ (DMSO)), 3.26 (q,  $J = 7.4$  Hz, 2H,  $SCH_2$ ), 1.44 (t,  $J = 7.4$  Hz, 3H,  $SCH_2CH_3$ ), 0.97 (s, 9H,  $SiC(CH_3)_3$ ), 0.22 (s, 6H,  $Si(CH_3)_2$ ).

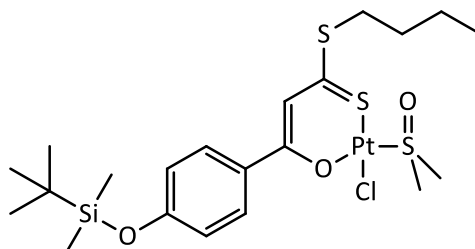
**$^{13}C\{^1H\}$  NMR** (50 MHz,  $CDCl_3$ )  $\delta$  = 182.6 ( $CS_2$ ), 174.6 (COPt), 159.9 (Ar-C4), 130.3 (2C, Ar-C2, Ar-C6), 120.5 (2C, Ar-C3, Ar-C5), 111.3 ( $CHCS_2$ ), 47.0 (2C,  $CH_3$ (DMSO)), 28.8 ( $SCH_2$ ), 25.7 (3C,  $SiC(CH_3)_3$ ), 18.4 ( $SiC_q$ ), 13.5 ( $(SCH_2CH_3)$ ), -4.2 (2C,  $Si(CH_3)_2$ ).

**MS** (ESI)  $m/z = 626$   $[M-Cl]^+$ .

**FTIR (ATR)**  $\tilde{\nu} = 3005$  (w), 2953 (w), 2929 (w), 2858 (w), 1598 (m), 1491 (s), 1468 (s, b), 1404 (w), 1314 (w), 1256 (vs), 1169 (m), 1131 (m), 1113 (w), 1037 (w), 975 (w), 909 (s), 837 (s), 803 (m), 783 (s)  $cm^{-1}$ .

**Chlorido-(1-(4'-tert-butyl dimethylsilyloxy)-3-(butylthio)-3-thioxo-prop-1-en-1-olate-O,S)-(dimethylsulfoxide-S)-platinum(II) (43)**

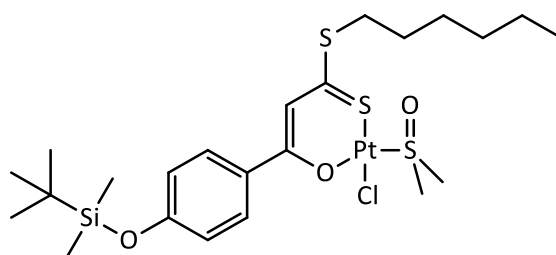
The reaction proceeded according to **GP5**.  $K_2PtCl_4$  (400 mg, 0.96 mmol), DMSO (140  $\mu$ L, 1.97 mmol), NaOAc $\cdot$ 3H $_2$ O (119 mg, 0.88 mmol), and **21** (335 mg, 0.88 mmol) were stirred overnight. The crude material was subjected to column chromatography on silica gel (eluent as gradient: DCM/*n*-hexane 2:1 to 1:0). Evidence of the formed product **43** ( $R_f \approx 0.5$ ) was found, but the compound was obtained as oil and could not be obtained as analytically pure material.



$^1H$  NMR (200 MHz,  $CDCl_3$ )  $\delta$  = 7.86 (d,  $^3J_{HH} = 8.7$  Hz, 2H, Ar-H2, Ar-H6), 7.02 (s, 1H,  $CHCS_2$ ), 6.80 (d,  $^3J_{HH} = 8.7$  Hz, 2H, Ar-H3, Ar-H5), 3.62 (s,  $^3J_{PtH} = 20.5$  Hz, 6H,  $CH_3$ (DMSO)) 3.20 (t,  $^3J_{HH} = 7.3$  Hz, 2H, S- $CH_2$ -), 2.00 – 1.59 (m, 2H,  $SCH_2-CH_2$ -), 1.45 (dd,  $J = 15.1, 7.5$  Hz, 2H,  $SCH_2CH_2-CH_2$ -), 1.12 – 0.44 (m, 12H,  $Si(CH_3)_3$ ,  $SCH_2CH_2CH_2-CH_3$ ), 0.19 (s, 6H,  $Si(CH_3)_2$ ) ppm.

**Chlorido-(1-(4'-tert-butyl dimethylsilyloxy)-3-(hexylthio)-3-thioxo-prop-1-en-1-olate-O,S)-(dimethylsulfoxide-S)-platinum(II) (44)**

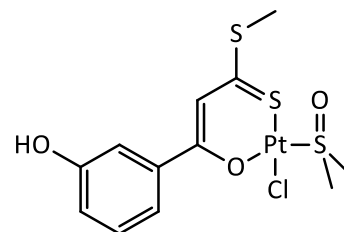
Following **GP7**, the reaction was conducted based on 200 mg (0.48 mmol)  $K_2PtCl_4$ . After 4 days of stirring, workup included column chromatography on silica gel (mobile phase: DCM:THF 10:0 to 10:0.5,  $R_f \approx 0.1$ ) but could not afford the desired product **44**.





**Chlorido-(1-(3'-hydroxy)-3-(methylthio)-3-thioxo-prop-1-en-1-olate-O,S)-  
(dimethylsulfoxide-S)-platinum(II) (45)**

Following **GP7**, the reaction was conducted based on 200 mg (0.48 mmol)  $K_2PtCl_4$ , compound **23** (99 mg, 0.44 mmol), NaH (20 mg, 0.5 mmol 60 % in mineral oil), and DMSO (70  $\mu$ L, 0.99 mmol). After overnight stirring, workup afforded the crude material which was subjected to column chromatography (mobile phase: DCM:acetone 10:1,  $R_f \approx 0.6$ ). Pure **45** (132 mg, 51 %) was obtained as orange powder.



**Analysis** calcd. for  $C_{12}H_{15}ClO_3PtS_3 \cdot 0.4$  pentane: C 29.88, H 3.55, S 17.09 %; found C 30.29, H 3.18, S 16.40 %.

**$^1H$  NMR** (600 MHz, Acetone- $d_6$ )  $\delta$  = 8.82 (s, 1H, Ar-OH), 7.64 – 7.50 (m, 2H, Ar-H2, Ar-H6), 7.30 (m, 1H, Ar-H5), 7.22 (s, 1H,  $CHCS_2$ ), 7.12 – 7.02 (m, 1H, Ar-H4), 3.68 (s,  $^3J_{Pt-H} = 24.3$  Hz, 6H,  $CH_3(DMSO)$ ), 2.70 (s, 3H,  $SCH_3$ ).

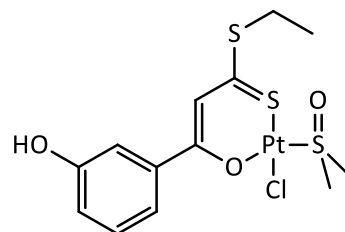
**$^{13}C\{^1H\}$  NMR** (151 MHz, Acetone- $d_6$ )  $\delta$  = 182.3 ( $CS_2$ ), 175.3 (COPt), 159.0 (s, Ar-C3), 139.7 (Ar-C1), 131.0 (Ar-C5), 120.3 (Ar-C4), 120.0 (Ar-C6), 115.7 (Ar-C2), 111.8 ( $CHCS_2$ ), 47.0 (2C,  $^2J_{Pt-C} = 56.2$  Hz,  $CH_3(DMSO)$ ), 17.9 ( $SCH_3$ ).

**MS (FAB+ in nba)**  $m/z = 534 [M]^+$ , 498  $[M-Cl]^+$ .

**FTIR (ATR)**  $\tilde{\nu} = 3302$  (m, b), 3024 (w), 3007 (w), 2954 (w), 2921 (m), 2853 (w), 1662 (w), 1611 (w), 1583 (m), 1511 (s), 1491 (s), 1472 (s), 1445 (s), 1426 (s), 1402 (s), 1366 (w), 1329 (m), 1291 (s), 1248 (m), 1210 (m), 1092 (vs), 1069 (m), 1029 (m), 997 (m), 973 (m), 962 (w), 933 (w), 910 (s), 865 (m), 796 (m), 778 (s)  $cm^{-1}$ .

**Chlorido-(1-(3'-hydroxy)-3-(ethylthio)-3-thioxo-prop-1-en-1-olate-O,S)-  
(dimethylsulfoxide-S)-platinum(II) (46)**

The reaction was performed following **GP7**.  $K_2PtCl_4$  (200 mg, 0.48 mmol), DMSO (70  $\mu$ L, 0.99 mmol), **24** (105 mg, 0.44 mmol) and NaH (20 mg, 0.5 mmol 60 % in mineral oil) were stirred overnight. Workup included column chromatography on silica gel (mobile phase: DCM:acetone 10 : 1,  $R_f \approx 0.5$ ), upon which **46** (132 mg, 55 %) was obtained as orange powder.



**Analysis** calcd. for  $C_{13}H_{17}ClO_3PtS_3 \cdot 0.15$  pentane: C 29.55; H 3.39; S 17.21 %; found C 29.48, H 3.37, S 17.20 %.

**$^1H$  NMR** (200 MHz, THF- $d_8$ )  $\delta$  = 8.72 (s, 1H, Ar-OH), 7.59 – 7.33 (m, 2H, Ar-H2, Ar-H6), 7.33 – 7.03 (m, 2H, Ar-H5, CHCS<sub>2</sub>), 7.03 – 6.79 (m, 1H, Ar-H4), 3.60 (s,  $^3J_{Pt-H} = 23.7$  Hz, 6H, CH<sub>3</sub>(DMSO), overlaid by THF), 3.25 (q,  $^3J_{H-H} = 7.4$  Hz, 2H, SCH<sub>2</sub>), 1.42 (t,  $^3J_{H-H} = 7.4$  Hz, 3H, SCH<sub>2</sub>CH<sub>3</sub>).

**$^1H$  NMR** (250 MHz, Acetone- $d_6$ )  $\delta$  = 8.80 (s, 1H, Ar-OH), 7.59 – 7.46 (m, 2H, Ar-H2, Ar-H6), 7.31 (t,  $^3J_{H-H} = 8.1$  Hz, 1H, Ar-H5), 7.21 (s, 1H, CHCS<sub>2</sub>), 7.16 – 7.01 (m, 1H, Ar-H4), 3.68 (s,  $^3J_{Pt-H} = 24.1$  Hz, 6H, CH<sub>3</sub>(DMSO)), 3.29 (q,  $^3J_{H-H} = 7.4$  Hz, 2H, SCH<sub>2</sub>), 1.44 (t,  $^3J_{H-H} = 7.4$  Hz, 3H, SCH<sub>2</sub>CH<sub>3</sub>).

**$^{13}C\{^1H\}$  NMR** (50 MHz, THF- $d_8$ )  $\delta$  = 180.7 (CS<sub>2</sub>), 175.6 (COPt), 159.4 (Ar-C3), 139.8 (Ar-C1), 130.5 (Ar-C5), 120.3 (Ar-C6), 119.51 (Ar-C4), 115.7 (Ar-C2), 112.1 (s), 111.3 (CHCS<sub>2</sub>), 46.7 (2C, CH<sub>3</sub>(DMSO)), 29.3 (SCH<sub>2</sub>), 13.9 (SCH<sub>2</sub>CH<sub>3</sub>).

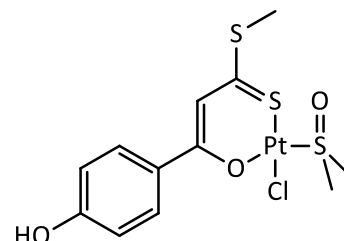
**$^{13}C\{^1H\}$  NMR** (63 MHz, Acetone- $d_6$ )  $\delta$  = 181.15 (CS<sub>2</sub>), 175.46 (COPt), 158.86 (Ar-C3), 139.58 (Ar-C1), 130.83 (Ar-C5), 120.26 (Ar-C6), 119.86 (Ar-C4), 115.55 (Ar-C2), 111.93 (CHCS<sub>2</sub>), 46.85 (2C, CH<sub>3</sub>(DMSO)), 13.63 (SCH<sub>2</sub>CH<sub>3</sub>). Signal of SCH<sub>2</sub> overlaid by solvent signal

**MS (ESI+)**  $m/z$  = 571 [M+Na]<sup>+</sup>, 512 [M-Cl-H]<sup>+</sup>.

**FTIR (ATR)**  $\tilde{\nu}$  = 3335 (m, b), 3005 (w), 2981 (w), 2921 (m), 2853 (w), 1609 (w), 1581 (m), 1507 (s), 1490 (s), 1466 (s), 1441 (s), 1429 (s), 1402 (s), 1311 (m), 1288 (m, b), 1255 (m), 1237 (m), 1198 (m), 1138 (w), 1098 (vs), 1069 (m), 1028 (s), 997 (m), 972 (m), 931 (w), 911 (s), 884 (m), 796 (m), 779 (vs)  $cm^{-1}$ .

**Chlorido-(1-(4'-hydroxy)-3-(methylthio)-3-thioxo-prop-1-en-1-olate-O,S)-  
(dimethylsulfoxide-S)-platinum(II) (47)**

Following **GP7**, the reaction was conducted using 200 mg (0.48 mmol)  $K_2PtCl_4$ , compound **26** (99 mg, 0.44 mmol), NaH (20 mg, 0.5 mmol) 60 % in mineral oil), and DMSO (70  $\mu$ L, 0.99 mmol). After stirring for 5 days, workup afforded the crude material which was subjected to column chromatography (mobile phase: DCM:acetone 10:1,  $R_f \approx 0.6$ ). Pure **47** (136 mg, 58 %) was obtained as orange powder.



**Analysis** calcd. for  $C_{12}H_{15}ClO_3PtS_3 \cdot 0.35$  pentane: C 29.53; H 3.46; S 17.20 %; found C 29.56, H 3.33, S 16.49 %.

$^1H$  NMR (200 MHz, Acetone- $d_6$ )  $\delta$  = 9.28 (s, 1H, Ar-OH), 8.03 (d,  $^3J_{H-H} = 8.9$  Hz, 2H, Ar-H2, Ar-H6), 7.23 (s, 1H,  $CHCS_2$ ), 6.92 (d,  $^3J_{H-H} = 8.8$  Hz, 2H, Ar-H3, Ar-H5), 3.66 (s,  $^3J_{Pt-H} = 24.3$  Hz, 6H,  $CH_3$ (DMSO)), 2.68 (s, 3H,  $SCH_3$ ).

$^{13}C\{^1H\}$  NMR (50 MHz, Acetone- $d_6$ )  $\delta$  = 179.64 ( $CS_2$ ), 175.0 (COPt), 162.4 (Ar-C4), 131.4 (2C, Ar-C2, Ar-C6), 129.3 (Ar-C1), 116.5 (2C, Ar-C3, Ar-C5), 110.8 ( $CHCS_2$ ), 46.8 (2C,  $CH_3$ (DMSO)), 17.6 ( $SCH_3$ ).

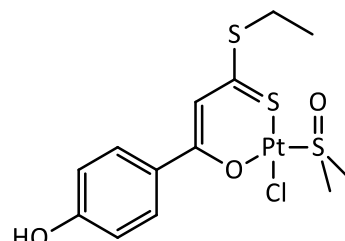
$^{195}Pt$  NMR (128 MHz, DMSO- $d_6$ )  $\delta$  = -3082 ppm.

**MS (FAB+ in nba)**  $m/z$  = 534  $[M]^+$ , 498  $[M-Cl]^+$ .

**FTIR (ATR)**  $\tilde{\nu}$  = 3320 (m, b), 2999 (w), 2912 (w), 2854 (w), 1602 (m), 1585 (m), 1520 (w), 1490 (s), 1454 (vs), 1416 (s), 1358 (w), 1313 (w), 1281 (m), 1265 (m), 1212 (m), 1169 (m), 1122 (vs, b), 1026 (s), 980 (m), 952 (m), 934 (m), 925 (w), 842 (s), 794 (vs)  $cm^{-1}$ .

**Chlorido-(1-(4'-hydroxy)-3-(ethylthio)-3-thioxo-prop-1-en-1-olate-O,S)-  
(dimethylsulfoxide-S)-platinum(II) (48)**

The reaction was performed following **GP7**.  $K_2PtCl_4$  (200 mg, 0.48 mmol), DMSO (70  $\mu$ L, 0.99 mmol), **27** (105 mg, 0.44 mmol) and NaH (20 mg, 0.5 mmol 60 % in mineral oil) were stirred overnight. Workup included column chromatography on silica gel (mobile phase: DCM:THF 10 : 0.5,  $R_f \approx 0.5$ ), upon which **48** (31 mg, 13 %) was obtained.



When the reaction was repeated following **GP5** (base: NaOAc 58 mg, 0.71 mmol) and column chromatography was performed using DCM:acetone 10 : 1 as mobile phase, the compound was obtained in improved yield and purity (175 mg, 73 %) as orange powder.

**Analysis** could not be obtained. NMR data suggest a pure compound.

**$^1H$  NMR** (400 MHz, THF- $d_8$ )  $\delta$  = 9.10 (s, 1H, Ar-OH), 7.96 (d,  $^3J_{H-H}$  = 8.8 Hz, 2H, Ar-H2, Ar-H6), 7.15 (s, 1H, CHCS<sub>2</sub>), 6.78 (d,  $^3J_{H-H}$  = 8.8 Hz, 2H, Ar-H3, Ar-H5), 3.59 (s, 6H, CH<sub>3</sub>(DMSO) overlaid by THF), 3.24 (q,  $^3J_{H-H}$  = 7.4 Hz, 2H, SCH<sub>2</sub>), 1.40 (t,  $^3J_{H-H}$  = 7.4 Hz, 3H, SCH<sub>2</sub>CH<sub>3</sub>).

**$^1H$  NMR** (200 MHz, Acetone- $d_6$ )  $\delta$  = 9.29 (s, 1H, Ar-OH), 8.02 (d,  $^3J_{H-H}$  = 8.9 Hz, 2H, Ar-H2, Ar-H6), 7.23 (s, 1H, CHCS<sub>2</sub>), 6.93 (d,  $^3J_{H-H}$  = 8.9 Hz, 2H, Ar-H3, Ar-H5), 3.66 (s,  $^3J_{Pt-H}$  = 24.2 Hz, 6H, CH<sub>3</sub>(DMSO)), 3.28 (q,  $^3J_{H-H}$  = 7.4 Hz, 2H, SCH<sub>2</sub>), 1.41 (t,  $^3J_{H-H}$  = 7.4 Hz, 3H, SCH<sub>2</sub>CH<sub>3</sub>).

**$^{13}C\{^1H\}$  NMR** (101 MHz, THF- $d_8$ )  $\delta$  = 178.03 (CS<sub>2</sub>), 175.37 (COPt), 162.84 (Ar-C4), 131.36 (2C, Ar-C2, Ar-C6), 129.32 (Ar-C1), 116.39 (2C, Ar-C3, Ar-C5), 111.23 (CHCS<sub>2</sub>), 46.70 (2C, CH<sub>3</sub>(DMSO)), 29.05 (SCH<sub>2</sub>), 13.97 (SCH<sub>2</sub>CH<sub>3</sub>).

**$^{13}C\{^1H\}$  NMR** (63 MHz, Acetone- $d_6$ )  $\delta$  = 175.41 (COPt), 162.46 (Ar-C4), 131.45 (2C, Ar-C2, Ar-C6), 129.33 (Ar-C1), 116.54 (2C, Ar-C3, Ar-C5), 111.19 (CHCS<sub>2</sub>), 46.87 (2C, CH<sub>3</sub>(DMSO)), 13.78 (SCH<sub>2</sub>CH<sub>3</sub>). Signal of SCH<sub>2</sub> overlaid by solvent signal; quaternary CS<sub>2</sub> not observed.

**MS (ESI+)**  $m/z$  = 570 [M+Na]<sup>+</sup>, 512 [M-Cl-H]<sup>+</sup>, 235.

**FTIR (ATR)**  $\tilde{\nu}$  = 3326 (m, b), 2999 (w), 2963 (w), 2924 (w), 2865 (w), 1602 (m), 1584 (m), 1522 (w), 1490 (s), 1460 (vs), 1449 (vs), 1417 (s), 1360 (m), 1346 (m), 1308 (w), 1281 (m), 1260 (s), 1208 (s), 1170 (s), 1121 (vs), 1025 (s), 971 (m), 850 (m), 842 (m), 793 (vs)  $cm^{-1}$ .

### 16.3 Alkynyl-functionalized compounds

#### Conversion of 4-hydroxy acetophenone **2** with butynyl bromide

Following **GP1**, 4-hydroxy acetophenone (2 g; 14.69 mmol; 1 eq.),  $K_2CO_3$  (3.05 g; 22.03 mmol; 1.5 eq.) and butynyl bromide (1.65 mL; 17.63 mmol; 1.2 eq.) were stirred for 24 h or 7 d.

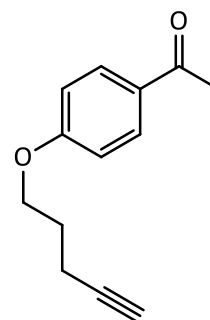
The same reaction was repeated using 4-hydroxy acetophenone (2 g; 14.69 mmol; 1 eq.),  $Cs_2CO_3$  (7.18 g; 22.03 mmol; 1.5 eq.) and butynyl bromide (1.65 mL; 17.63 mmol; 1.2 eq.). The mixture was stirred for 44 h at r.t.

Furthermore, the reaction was carried out by following **GP2**, using 4-hydroxy acetophenone (1 g, 7.34 mmol, 1 eq.),  $Cs_2CO_3$  (3.57 g, 11.02 mmol, 1.5 eq.), butynyl bromide (1.11 mL, 8.08 mmol, 1.1 eq.) and KI (0.15 g, 0.734 mmol, 0.1 eq.).

In all cases, the starting material 4-hydroxy acetophenone was recovered in almost quantitative yields, thus indicating that no conversion had occurred due to decomposition of butynyl bromide.

#### 4-(Pent-4-in-1-yloxy)acetophenone (**53**)

4-Hydroxy acetophenone (1 g, 7.39 mmol), was converted with pentynyl chloride (856  $\mu$ L, 8.08 mmol) according to **GP2**, using  $Cs_2CO_3$  (3.59 g, 11.02 mmol), and KI (0.12 g, 0.7 mmol). The product **53** was obtained as white crystals (1.37 g; 91.9 %).



**Analysis** calcd. for  $C_{13}H_{14}O_2$  (M = 202,25 g/mol): C, 77.20; H, 6.98; found: C, 76.82; H, 6.92.

**m.p.:** 60,4 - 61,2 °C

**$^1H$  NMR** (400 MHz,  $CDCl_3$ ):  $\delta$  = 7.92 (d,  $^3J_{HH}$  = 8.9 Hz, 2H, Ar-H2, Ar-H6), 6.93 (d,  $^3J_{HH}$  = 8.9 Hz, 2H, Ar-H3, Ar-H5), 4.13 (t,  $^3J_{HH}$  = 6.11 Hz, 2H, O- $CH_2^\alpha$ ), 2.55 (s, 3H,  $CH_3$ ), 2.41 (td,  $^3J_{HH}$  = 6.93 Hz,  $^4J_{HH}$  = 2.63 Hz, 2H,  $CH_2^\gamma$ ), 2.02 (m, 2H,  $CH_2^\beta$ ), 1.98 (t,  $^4J_{HH}$  = 2.7 Hz, 1H,  $\equiv CH$ ) ppm.

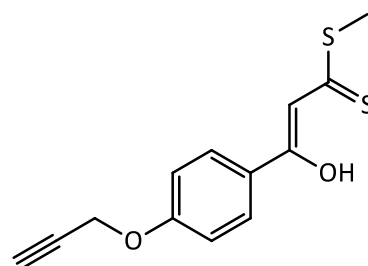
**$^{13}C\{^1H\}$  NMR** (100 MHz,  $CDCl_3$ ):  $\delta$  = 197.7 (Ar-C1), 163.5 (Ar-C4), 131.1 (Ar-C2, Ar-C6), 130.8 (C=O), 114.50 (Ar-C3, Ar-C5), 82.3 ( $\equiv C-$ ), 69.2 ( $\equiv CH$ ), 66.4 (O- $CH_2^\alpha$ ), 27.8 ( $CH_2^\beta$ ), 26.2 (S- $CH_3$ ), 14.9 ( $CH_2^\gamma$ ) ppm.

**MS(EI+)**  $m/z = 202 [M]^+$ ,  $187 [M-Me]^+$ ,  $121 [M-Me-pentynyl+H]^+$ .

**FTIR (ATR)**  $\tilde{\nu} = 3234$  (m),  $2998$  (w),  $2957$  (w),  $2938$ ,  $2880$  (w),  $1665$  (s),  $1597$  (vs),  $1511$  (s),  $1465$  (m),  $1422$  (m),  $1359$  (s),  $1306$  (m),  $1254$  (vs),  $1171$  (vs),  $1120$  (m),  $1041$  (s),  $959$  (m),  $931$  (m),  $827$  (vs),  $704$  (s,b),  $588$  (vs)  $\text{cm}^{-1}$ .

#### 4-(Prop-2-inyloxy)-6-hydroxydithiocinnamic acid methyl ester (54)

Compound **51** (494.9 mg, 2.87 mmol),  $\text{KO}^t\text{Bu}$  (651.2 mg, 5.74 mmol),  $\text{CS}_2$  (0.23 mL, 4.018 mmol) and methyl iodide (0.18 mL, 2.87 mmol) were reacted according to **GP3**. Column chromatography was performed using dichloromethane as mobile phase ( $R_f \approx 0.9$ ). **54** was obtained as yellow solid (108 mg, 14.2 %).



Compound **51** (1.0 g, 5.74 mmol) was furthermore converted using 2.5 eq. (1.61 g, 14.35 mmol) or 3 eq. of  $\text{KO}^t\text{Bu}$  (1.93 g; 17.22 mmol),  $\text{CS}_2$  (0.48 mL, 8.036 mmol) and methyl iodide (0.36 mL; 5.74 mmol). Column chromatography using dichloromethane/*n*-hexane (2 : 1,  $R_f \approx 0.7$ ; or 3 : 2,  $R_f \approx 0.6$ ) yielded **54** as yellow solid. When 3 eq. of  $\text{KO}^t\text{Bu}$  were used, the yield was significantly enhanced (550 mg, 36.2 % / 3 eq. vs. 237 mg, 15.6 % / 2.5 eq.).

**Analysis** calcd. for  $\text{C}_{13}\text{H}_{12}\text{O}_2\text{S}_2$  ( $M = 264.36$  g/mol): C, 59.06; H, 4.58; S, 24.26; found: C, 59.36; H, 4.56; S, 24.80.

**m.p.:** 109.7-113.1 °C

**$^1\text{H}$  NMR** (400 MHz,  $\text{CDCl}_3$ )  $\delta = 15.16$  (s, 1H, OH), 7.77 (d,  $^3J_{\text{HH}} = 9.0$  Hz, 2H, Ar-H2, Ar-H6), 7.03 (d,  $^3J_{\text{HH}} = 9.0$  Hz, 2H, Ar-H3, Ar-H6), 6.93 (s, 1H, =CH-), 4.76 (d,  $^4J_{\text{HH}} = 2.4$  Hz, 2H, O- $\text{CH}_2^\alpha$ ), 2.65 (s, 3H, S- $\text{CH}_3$ ), 2.56 (t,  $^4J_{\text{HH}} = 2.4$  Hz, 1H,  $\equiv\text{CH}$ ) ppm.

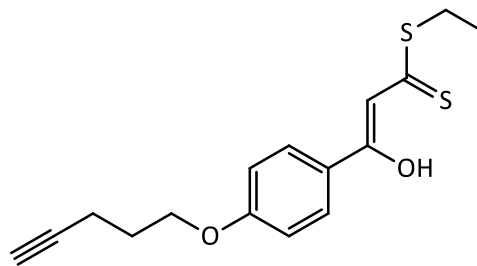
**$^{13}\text{C}\{^1\text{H}\}$  NMR** (100 MHz,  $\text{CDCl}_3$ )  $\delta = 216.2$  ( $\text{CS}_2$ ), 169.4 (C-OH), 160.7 (Ar-C4), 128.8 (Ar-C2, Ar-C6), 127.1 (Ar-C1), 115.2 (Ar-C3, Ar-C5), 107.4 (=CH-), 77.9 ( $\equiv\text{C}$ -), 76.3 ( $\equiv\text{CH}$ ), 65.0 (O- $\text{CH}_2^\alpha$ ), 17.2 (S- $\text{CH}_3$ ) ppm.

**MS (EI+)**  $m/z = 264 [M]^+$ ,  $217 [M-\text{SMe}]^+$ ,  $178 [M-\text{SMe-Propargyl}]^+$

**FTIR (ATR)**  $\tilde{\nu} = 3273$  (m),  $2912$  (w),  $2859$  (w),  $1603$  (m),  $1580$ ,  $1551$  (m),  $1501$ (m),  $1427$ (m),  $1374$  (m),  $1295$  (w),  $1230$  (vs),  $1183$  (s),  $1120$  (m),  $1020$  (m),  $937$  (vs),  $841$  (m),  $808$  (m),  $788$  (m)  $\text{cm}^{-1}$ .

#### 4-(Pent-4-in-1-yloxy)- $\beta$ -hydroxydithiocinnamic acid ethylester (55)

**53** (1 g, 4.94 mmol), CS<sub>2</sub> (0.41 mL, 6.914 mmol), ethyl iodide (0.4 mL, 4.94 mmol) and KO<sup>t</sup>Bu (1.39 g, 12.35 mmol, 2.5 eq) were converted following **GP3** in slightly altered reactant ratios. Column chromatography with dichloromethane/*n*-hexane (2 : 1; R<sub>f</sub> ≈ 0.7) as mobile phase yielded **55** (638 mg; 42.3 %) as yellow solid.



**Analysis** calcd. for C<sub>16</sub>H<sub>18</sub>O<sub>2</sub>S<sub>2</sub> (M = 306.44 g/mol): C, 62.71; H, 5.92, S, 20.93; found: C, 63.09; H, 6.08; S, 20.98.

**m.p.:** 64.0 °C

**<sup>1</sup>H NMR** (400 MHz, CDCl<sub>3</sub>)  $\delta$  = 15.23 (s, 1H, OH), 7.85 (d, <sup>3</sup>J<sub>HH</sub> = 9.1 Hz, 2H, Ar-H2, Ar-H6), 6.95 (d, <sup>3</sup>J<sub>HH</sub> = 9.1 Hz, 2H, Ar-H3, Ar-H6), 6.88 (s, 1H, =CH-), 4.14 (t, <sup>3</sup>J<sub>HH</sub> = 6.1 Hz, 2H, O-CH<sub>2</sub> <sup>$\alpha$</sup> ), 3.27 (q, <sup>3</sup>J<sub>HH</sub> = 7.4 Hz, 2H, S-CH<sub>2</sub>), 2.42 (td, <sup>3</sup>J<sub>HH</sub> = 6.9 Hz, <sup>4</sup>J<sub>HH</sub> = 2,7 Hz, 2H, CH<sub>2</sub> <sup>$\beta$</sup> ), 2.03 (p, <sup>3</sup>J<sub>HH</sub> = 6.5 Hz, 2H, CH<sub>2</sub> <sup>$\beta$</sup> ), 1.98 (t, 1H, <sup>4</sup>J<sub>H1-H3</sub> = 2.7 Hz,  $\equiv$ CH), 1.38 (t, <sup>3</sup>J<sub>HH</sub> = 7.4 Hz, 3H, CH<sub>3</sub>) ppm.

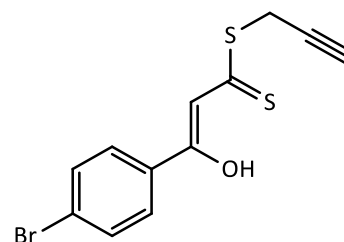
**<sup>13</sup>C{<sup>1</sup>H}-NMR** (100 MHz, CDCl<sub>3</sub>)  $\delta$  = 215.9 (CS<sub>2</sub>), 170.7 (C-OH), 162.9 (Ar-C4), 129.1 (Ar-C2, Ar-C6), 126.8 (Ar-C1), 115.0 (Ar-C3, Ar-C5), 107.5 (=CH-), 83.35 ( $\equiv$ C-), 69.2 ( $\equiv$ CH), 66.4 (O-CH<sub>2</sub> <sup>$\alpha$</sup> ), 27.8 (CH<sub>2</sub> <sup>$\beta$</sup> ), 27.5 (S-CH<sub>2</sub>), 14.9 (CH<sub>2</sub> <sup>$\gamma$</sup> ), 12.8 (CH<sub>3</sub>) ppm.

**MS (EI+)** *m/z* = 306 [M]<sup>+</sup>, 245 [M-SEt]<sup>+</sup>, 187 [M-SEt-(CH<sub>2</sub>=C=S)]<sup>+</sup>, 121.

**FTIR (ATR)**  $\tilde{\nu}$  = 3261 (m), 2971 (w), 2954 (w), 2925 (w), 2869 (w), 1605 (m), 1581 (vs), 1545 (s), 1502 (vs), 1461 (m), 1430 (s), 1400 (m), 1385 (m), 1368 (m), 1298 (w), 1228 (vs), 1176 (s), 1118 (m), 1046 (s), 950 (s), 932 (s), 837 (s), 806 (w), 778 (vs), 643 (m), 607 (m), 529 (m) cm<sup>-1</sup>.

#### Synthesis of 4-Bromo- $\beta$ -hydroxydithiocinnamic acid propargylic ester (57)<sup>103</sup>

4-Brom- $\beta$ -hydroxydithiocinnamic acid **56** was prepared according to literature procedures and could be obtained in 56 % yield after recrystallization from *n*-hexane/ethyl acetate (4:1). Further following the literature procedure, **57** (43 %) was then isolated after crystallization from ethanol and isopropanol as yellow-orange solid.



The overall yield of this reaction was 24 % over two steps.

**$^1\text{H}$  NMR** (400 MHz,  $\text{CDCl}_3$ )  $\delta$  = 14.93 (s, 1H, OH), 7.74 (d,  $^3J_{\text{HH}}$  = 8.8 Hz, 2H, Ar-H3, Ar-H5), 7.59 (d,  $^3J_{\text{HH}}$  = 8.8 Hz, 2H, Ar-H2, Ar-H6), 6.87 (s, 1H, =CH-), 4.02 (d,  $^4J_{\text{HH}}$  = 2.7 Hz, 2H, S-CH $_2^\alpha$ ), 2.25 (t,  $^4J_{\text{HH}}$  = 2.7 Hz, 1H,  $\equiv\text{CH}$ ) ppm.

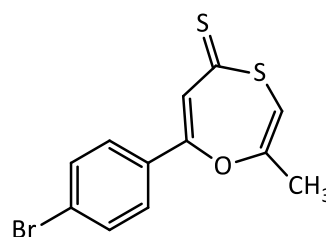
**$^{13}\text{C}\{^1\text{H}\}$  NMR** (100 MHz,  $\text{CDCl}_3$ )  $\delta$  = 213.8 ( $\text{CS}_2$ ), 169.3 (C-OH), 133.0 (Ar-C1), 132.3 (2C, Ar-C2, Ar-C6), 128.3 (2C, Ar-C3, Ar-C5), 127.1 (Ar-C4), 107.4 (=CH-), 77.3 ( $\equiv\text{C}$ -), 72.1 ( $\equiv\text{CH}$ ), 22.3 (S-CH $_2^\alpha$ ) ppm.

**MS (EI+)**  $m/z$  = 312/314 [ $\text{M}/\text{M}+2$ ] $^+$ , 274/276 [ $\text{M}-\text{C}_3\text{H}_2$ ] $^+$ , 241 [ $\text{M}$ -Spropargyl] $^+$ , 183, 162, 155, 85.

**FTIR (ATR)**  $\tilde{\nu}$  = 3294 (m), 2961 (w), 2873 (w), 1582, 1559 (m), 1478 (m), 1415 (m), 1238 (m), 1218 (m), 1069, 1052 (m), 1007 (m), 961 (m), 831 (m), 785 (m), 761 (m), 667 (m), 639 (m), 459 (m)  $\text{cm}^{-1}$ .

### Conversion of 4-bromo-acetophenone with $\text{CS}_2$ and propargyl bromide (58)

Furthermore, preparation of **57** was attempted by following **GP3**. 4-bromo acetophenone (0.99 g, 5 mmol),  $\text{KO}^t\text{Bu}$  (1.12 g, 10 mmol),  $\text{CS}_2$  (0.42 mL, 7 mmol) and propargyl bromide (0.54 mL, 5 mmol, 80 % in toluene) were used. When the alkynyl halogenide was added at room temperature, an immediate brown discoloration appeared. Column chromatography with a gradient of dichloromethane/hexanes (1:3 to 1:0,  $R_f \approx 0,5$ ) afforded a yellow solid (785.2 mg) which was identified as rearrangement product.



**$^1\text{H}$  NMR** (600 MHz,  $\text{CDCl}_3$ )  $\delta$  = 7.82 (dd,  $J_{\text{HH}}$  = 8.5, 2.6 Hz, 2H, Ar-H3, Ar-H5), 7.57 (dd,  $J_{\text{HH}}$  = 8.5, 1.9 Hz, 2H, Ar-H2, Ar-H6), 7.34/7.33 (d,  $J_{\text{HH}}$  = 1.1 Hz / s, 1H, C(O)=CH- $\text{CS}_2$ ), 6.46/6.39 (m / d,  $J_{\text{HH}}$  = 1.1 Hz, 1H, S-CH=C(CH $_3$ )), 2.31 (d,  $^4J_{\text{HH}}$  = 0.9 Hz, 3H, CH $_3$ ).

**$^{13}\text{C}\{^1\text{H}\}$  NMR** (151 MHz,  $\text{CDCl}_3$ )  $\delta$  = 182.7/182.4 ( $\text{CS}_2$ ), 168.8/168.4 (Ar-C(-O)=), 137.39/137.36 (Ar-C1), 136.8/131.6 (=C(CH $_3$ )-), 131.9 (2C, Ar-C2, Ar-C6), 129.3/129.2 (2C, Ar-C3, Ar-C5), 126.46/126.45 (Ar-C4), 118.8/112.2 (=CH- $\text{CS}_2$ ), 103.4/102.6 (=CH-S), 16.1/15.8 (CH $_3$ ).

**MS (EI+)**  $m/z$  = 312/314 [ $\text{M}/\text{M}+2$ ] $^+$ ; 284/286 [ $\text{M}-\text{CHCH}_3$ ] $^+$ , 279/281 [ $\text{M}-\text{SH}$ ] $^+$ ; 183/185; 157, 155.

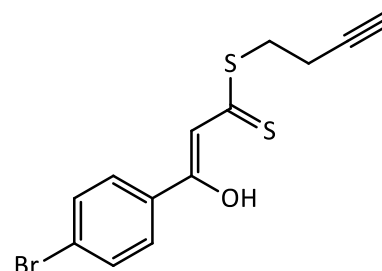
**FTIR (ATR)**  $\tilde{\nu}$  = 3083, 3054 (w), 2913 (w), 1584, 1557 (m), 1489 (m), ca. 1450 (vs), 1388 (m), 1231 (s), 1179 (m), 1067 (s), 1052 (s), 1006 (m), 977 (m), 848 (m), 815 (m), 769 (m), 641 (m)  $\text{cm}^{-1}$ .



In a second attempt to circumvent the brown discoloration assumed to indicate the cyclization reaction, 4-bromo acetophenone (1.99 g, 10 mmol), KO<sup>t</sup>Bu (2.24 g, 20 mmol) and CS<sub>2</sub> (1.08 mL, 14 mmol) were reacted. After 3.5 h of stirring at -78 °C, propargyl bromide (1.08 mL, 10 mmol, 80 % in toluene) was added. TLC control immediately after addition of the alkynyl halogenide indicated the formation of two new products ( $R_{f1} \approx 0.3$  und  $R_{f2} \approx 0.7$  in DCM). After 1.5 h of no visible conversion, the suspension was slowly allowed to warm to room temperature, which quickly lead to the occurrence of a dark-brown discoloration, barely indicated in TLC controls. Thus, the suspension was quickly cooled again and stirred for another hour upon which sulfuric acid (35 mL, 0.5 M aqueous solution) was added. The phases were separated, extracted with DCM (3 × 5 mL), washed with water (2 × 5 mL) and dried over sodium sulfate. After evaporation of the solvents, an oily residue was obtained. NMR analysis indicated the presence of the desired product **57**, but purification by crystallization methods was not possible.

#### 4-Bromo-*β*-hydroxydithiocinnamic acid butynyl ester (**59**)

Preparation of **59** was achieved by slightly modifying the reactant ratios in **GP3**. By using 4-Bromo acetophenone (3.98 g, 20 mmol), CS<sub>2</sub> (1.7 mL, 28 mmol), butynyl bromide (1.7 mL, 18 mmol, 0.9 eq.) and KO<sup>t</sup>Bu (4.51 g, 40 mmol), crude **59** was obtained which was purified by column chromatography with dichloromethane/*n*-hexane (3 : 2,  $R_f \approx 0,6$ ) as mobile phase. **59** (1.46 g, 22.3 %) was obtained as yellow solid.



**m.p.:** 66,4 °C

**Analysis** calcd. for C<sub>12</sub>H<sub>11</sub>BrOS<sub>2</sub> (M = 327,24 g/mol): C, 47.71; H, 3.39; S, 19.60; found C, 48.19; H, 3.50; S, 19.41.

**<sup>1</sup>H NMR** (600 MHz, CDCl<sub>3</sub>): δ = 15.00 (s, 1H, OH); 7.74 (d, <sup>3</sup>J<sub>HH</sub> = 8.8 Hz, 2H, Ar-H3, Ar-H5); 7.59 (d, <sup>3</sup>J<sub>HH</sub> = 8.8 Hz, 2H, Ar-H2, Ar-H6); 6.88 (s, 1H, =CH-); 3.46 (t, <sup>3</sup>J<sub>HH</sub> = 7.1 Hz, 2H, S-CH<sub>2</sub><sup>α</sup>); 2.65 (td, <sup>3</sup>J<sub>HH</sub> = 7.1, <sup>4</sup>J<sub>HH</sub> = 2.7 Hz, 2H, CH<sub>2</sub><sup>β</sup>); 2.07 (1H, t, <sup>4</sup>J<sub>HH</sub> = 2,6 Hz, ≡CH) ppm.

**<sup>13</sup>C{<sup>1</sup>H} NMR** (150 MHz, CDCl<sub>3</sub>): δ = 216.6 (CS<sub>2</sub>); 169.5 (C-OH); 133.5 (Ar-C1); 132.6 (2C, Ar-C2, Ar-C6); 128.6 (2C, Ar-C3, Ar-C5); 127.2 (Ar-C4); 108.2 (=CH-); 81.97 (≡C-); 70.0 (≡CH); 32.0 (S-CH<sub>2</sub><sup>α</sup>); 17.9 (CH<sub>2</sub><sup>β</sup>) ppm.

**MS (EI+)**  $m/z = 326/328$   $[M/M+2]^+$ , 274/276  $[M-C_4H_4]^+$ , 241/243  $[M-Sbutinyl]^+$ , 183/185, 162, 155/157, 85.

**FTIR (ATR)**  $\tilde{\nu} = 3283$  (m), 2961, 2927 (w), 2851 (w), 1578 (s), 1553 (m), 1481 (s), 1414 (s), 1379 (m), 1232 (vs), 1206 (s), 1074 (m), 1052 (m), 1007 (m), 953 (vs), 830 (vs), 797 (vs), 750 (vs), 666 (vs), 641 (vs), 544 (s)  $cm^{-1}$ .

### Conversion of **54** with one equivalent of $K_2PtCl_4$ and DMSO

**54** (108 mg; 0,409 mmol),  $K_2PtCl_4$  (200 mg; 0,482 mmol), DMSO (0,06 mL; 0,876 mmol) and NaOAc·3H<sub>2</sub>O (56 mg; 0,409 mmol) converted following **GP5**. Repeated crystallization from DCM/*n*-hexane did not yield the desired complex **60**.

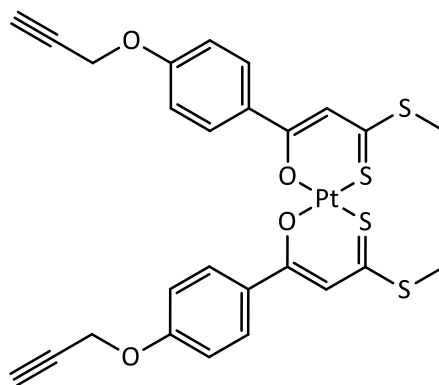
Preparation of **60** was further attempted by using **54** (62,6mg; 0,237mmol),  $K_2PtCl_4$  (108,2 mg; 0,261 mmol), DMSO (0,03 mL; 0,474 mmol) and KO<sup>t</sup>Bu (26,6 mg; 0,237 mmol) according to **GP6**. Repeated crystallization from DCM/*n*-hexane did not yield the desired complex.

The same base/reactant combination was also used in an approach using inert conditions (**GP6**), again without success.

### Bis(4-( Prop-2-inyloxy)- $\beta$ -hydroxydithiocinnamic acid ethyl ester-*O,S*)-platinum(II)

(**61**)

Following **GP8**, **54** (127.4 mg; 0.482 mmol),  $K_2PtCl_4$  (100 mg; 0.241 mmol) und NaOAc·3H<sub>2</sub>O (66 mg, 0.482 mmol) were converted to give a dark-red crude material. This was precipitated from DCM/hexane, followed by flushing through a short plug of silica gel using DCM and traces of hexane when crystallization did not afford a pure compound. The target complex was isolated as dark-red solid (18.5 mg, 10.6 %)



**Analysis** calcd. for  $C_{26}H_{22}O_4PtS_4$ : C, 43.26; H, 3.03; S, 17.77; found C, 43.19; H, 2.84; S, 17.36.

$^1H$  NMR (400 MHz,  $CDCl_3$ )  $\delta$  = 8.02 (d,  $^3J_{HH}$  = 9.0 Hz, 4H, Ar-H2, Ar-H6), 7.09 (s, 2H, =CH-), 7.02 (d,  $^3J_{HH}$  = 9.0 Hz, 4H, Ar-H3, Ar-H5), 4.77 (d,  $^4J_{HH}$  = 2.4 Hz, 4H, O-CH<sub>2</sub>), 2.63 (s, 6H, S-CH<sub>3</sub>), 2.56 (t,  $^4J_{HH}$  = 2.4 Hz, 2H,  $\equiv$ CH) ppm.

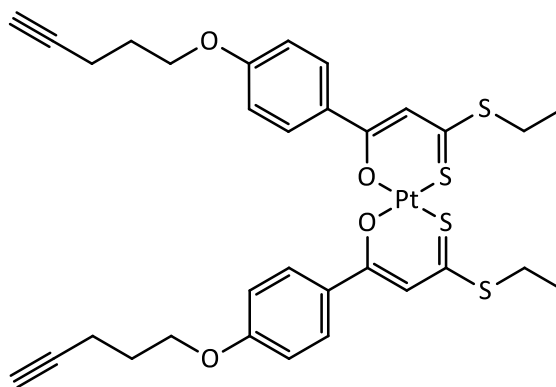
$^{13}C\{^1H\}$  NMR (100 MHz,  $CDCl_3$ )  $\delta$  = 177.3 (CS<sub>2</sub>), 174.2 (C-OPt), 160.7 (Ar-C4), 132.7 (Ar-C1), 129.7 (2C, Ar-C2, Ar-C6), 115.4 (2C, Ar-C3, Ar-C5), 112.4 (=CH-), 78.1 ( $\equiv$ C-), 76.2 ( $\equiv$ CH), 55.9 (O-CH<sub>2</sub>), 17.3 (S-CH<sub>3</sub>) ppm.

**MS (ESI+)**  $m/z$  = 744.8 [M+Na]<sup>+</sup>.

**FTIR (ATR)**  $\tilde{\nu}$  = 3278 (m), 2918 (w), 2851 (w), 1602 (s), 1582 (m), 1495 (m), 1449 (vs), 1405 (m), 1308 (s), 1290 (s), 1259 (s), 1242 (s), 1219 (s), 1177 (m), 1020 (w), 1030 (m), 979 (m), 954 (m), 836 (m), 808 (m), 784 (m)  $cm^{-1}$ .

### Bis(4-(Pent-4-yn-1-yloxy)-6-hydroxydithiocinnamic acid ethyl ester-O,S)-platinum(II) (62)

**55** (147.7 mg; 0.482 mmol),  $K_2PtCl_4$  (100 mg; 0.241 mmol) und  $NaOAc \cdot 3H_2O$  (65.6 mg, 0.482 mmol) were reacted following **GP8** and stirred for 4 days. For purification, the crude solid was first precipitated from DCM/*n*-hexane, the precipitate filtered and then flushed through a plug of silica gel using DCM as solvent. The pure product (54 mg; 28 %) was obtained as red solid.



**Analysis** calcd. for  $C_{32}H_{34}O_4PtS_4$  (M = 805,95 g/mol): C, 47.69; H, 4.25; S, 15.91; C, 47.38; H, 4.21; S, 15.41.

$^1H$  NMR (400 MHz,  $CDCl_3$ )  $\delta$  = 8.00 (d,  $^3J_{HH}$  = 9.0 Hz, 2H, Ar-H2, Ar-H6); 7.08 (s, 1H, =CH-); 6.94 (d,  $^3J_{HH}$  = 9.0 Hz, 2H, Ar-H3, Ar-H6); 4.15 (t,  $^3J_{HH}$  = 6.1 Hz, 2H, O-CH<sub>2</sub><sup>a</sup>); 3.22 (q,  $^3J_{HH}$  = 7.4 Hz, 2H, S-CH<sub>2</sub>); 2.43 (td,  $^3J_{HH}$  = 7.0 Hz,  $^4J_{HH}$  = 2.7 Hz, 2H, CH<sub>2</sub><sup>b</sup>); 2.04 (m, 2H, CH<sub>2</sub><sup>b</sup>); 1.99 (t,  $^4J_{HH}$  = 2.6 Hz, 1H,  $\equiv$ CH); 1.44 (t,  $^3J_{HH}$  = 7.4 Hz; 3H, CH<sub>3</sub>) ppm.

**$^{13}\text{C}\{^1\text{H}\}$  NMR** (100 MHz,  $\text{CDCl}_3$ )  $\delta$  = 175.9 ( $\text{CS}_2$ ), 174.6 (C-OPt), 162.3 (Ar-C4), 131.9 (Ar-C1), 129.8 (Ar-C2, Ar-C6), 114.9 (Ar-C3, Ar-C5), 112.6 (=CH-), 83.4 ( $\equiv\text{C}$ -), 69.2 ( $\equiv\text{CH}$ ), 66.4 ( $\text{O}-\text{CH}_2^\alpha$ ), 28.3 ( $\text{CH}_2^\beta$ ), 27.9 ( $\text{S}-\text{CH}_2$ ), 14.9 ( $\text{CH}_2^\gamma$ ), 13.4 ( $\text{CH}_3$ ) ppm.

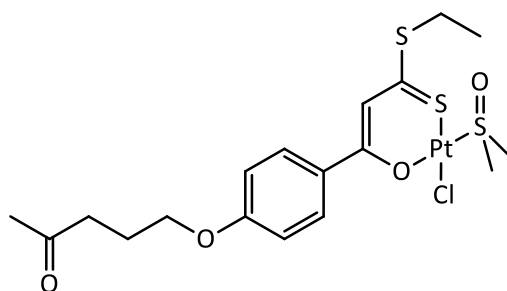
**MS (DEI+)**  $m/z$  = 805  $[\text{M}]^+$ .

**MS(ESI+)**  $m/z$  = 828  $[\text{M}+\text{Na}]^+$ , 685  $[\text{M}-2\text{SEt}+2\text{H}]^+$ .

**FTIR (ATR)**  $\tilde{\nu}$  = 3270 (w), 3254 (w), 2956 (w), 2924 (w), 2873 (w), 1601 (w), 1578 (m), 1493 (m), 1447 (vs), 1405 (m), 1311 (m), 1290 (m), 1244 (vs), 1223 (s), 1175 (s), 1044 (m), 960 (m), 837 (m), 808 (m), 785 (s), 655 (m), 533 (m)  $\text{cm}^{-1}$ .

### Conversion of 55 with one equivalent of $\text{K}_2\text{PtCl}_4$ and DMSO (63)

**55** (119 mg, 0.388 mmol)  $\text{K}_2\text{PtCl}_4$  (200 mg, 0.482 mmol), DMSO (62  $\mu\text{L}$ , 0.876 mmol) and NaOAc (36 mg, 0.438 mmol) were converted according to **GP5**. After 4 days of stirring, the crude product was purified by column chromatography on silica gel using a gradient (mobile phase DCM/acetone 100 : 2.5 to 100 : 10,  $R_f \approx 0.4$ ), upon which an orange crystalline solid was isolated. This was characterized as the triple-bond hydrated compound (48 mg, 19 % based on amount of **55** used).



**Analysis** calcd for  $\text{C}_{18}\text{H}_{25}\text{ClO}_4\text{PtS}_3 \cdot 0.2 \text{CH}_2\text{Cl}_2$ : C, 34.20; H, 3.99; S, 15.22; found C, 33.51, H 3.90, S, 14.76.

**$^1\text{H}$  NMR** (200 MHz,  $\text{CDCl}_3$ )  $\delta$  = 7.95 (d,  $^3J_{\text{HH}} = 8.9$  Hz, 2H, Ar-H2, Ar-H6), 7.09 (s, 1H, =CH-), 6.87 (d,  $^3J_{\text{HH}} = 8.9$  Hz, 2H, Ar-H3, Ar-H6), 4.02 (t,  $^3J_{\text{HH}} = 6.0$  Hz, 2H,  $\text{O}-\text{CH}_2^\alpha$ ), 3.65 (s,  $^3J_{\text{PtH}} = 23.4$  Hz, 6H,  $\text{CH}_3$  (DMSO)), 3.26 (q,  $^3J_{\text{HH}} = 7.5$  Hz, 2H, S- $\text{CH}_2$ ), 2.66 (t,  $^3J_{\text{HH}} = 7.5$  Hz, 3H,  $\text{CH}_2^\gamma$ ), 2.18 (s, 3H,  $\text{COCH}_3$ ), 2.13-2.00 (m, 2H,  $\text{CH}_2^\beta$ ), 1.44 (t,  $^3J_{\text{HH}} = 7.4$  Hz, 3H,  $\text{CH}_3$ ) ppm.

**$^{13}\text{C}\{^1\text{H}\}$  NMR** (50 MHz,  $\text{CDCl}_3$ )  $\delta$  = 208.9 (C=O), 178.6 ( $\text{CS}_2$ ), 174.8 (C-OPt), 162.9 (Ar-C4), 130.7/130.4 (Ar-C2, Ar-C6), 129.8 (Ar-C1), 114.8 (2C, Ar-C3, Ar-C5), 111.2 (=CH-), 67.08 ( $\text{O}-\text{CH}_2^\alpha$ ), 46.7 ( $\text{CH}_3$  (DMSO)), 39.6 ( $\text{CH}_2^\gamma$ ), 29.9 (C(O)- $\text{CH}_3$ ), 28.4 (S- $\text{CH}_2$ ), 22.9 ( $\text{CH}_2^\beta$ ), 13.0 ( $\text{CH}_3$ ) ppm.

**FTIR (ATR)**  $\tilde{\nu}$  = 3013 (w), 2963 (w), 2928 (w), 2917 (w), 2870 (w), 1705 (s), 1600 (s), 1573 (m), 1493 (s), 1453 (vs), 1405 (s), 1352 (m), 1309 (m), 1247 (vs), 1220 (m), 1175 (s), 1047 (m), 1020 (s), 966 (m), 845 (m), 796 (m)  $\text{cm}^{-1}$ .

**MS (ESI+)**  $m/z$  = 652.8  $[\text{M}+\text{Na}]^+$ .

### Conversion of 57 with one equivalent of $\text{K}_2\text{PtCl}_4$ and DMSO

Following **GP5**, **57** (137.2 mg, 0.438 mmol),  $\text{K}_2\text{PtCl}_4$  (200 mg, 0.482 mmol), DMSO (60  $\mu\text{L}$ ; 0.876 mmol) and  $\text{NaOAc} \cdot 3\text{H}_2\text{O}$  (59.6 mg, 438  $\mu\text{mol}$ ) converted. Purification was attempted through crystallization from DCM/*n*-hexane. Despite evidence of the formation of the desired product in NMR spectra, it was not possible to isolate pure **64**.

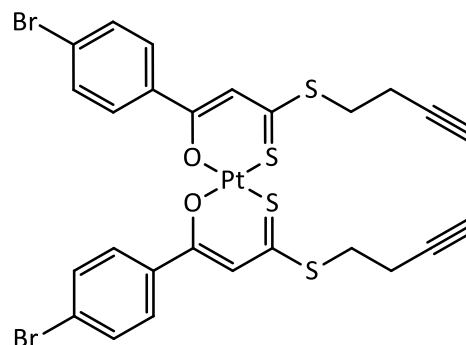
Further attempts to isolate desired complex **64** by using  $\text{KO}^t\text{Bu}$  (49.15 mg, 0.438 mmol) as a base according to **GP6** were also not successful.

### Conversion of two equivalents 57 with $\text{K}_2\text{PtCl}_4$

**57** (156.8 mg; 0.501 mmol) was reacted with  $\text{K}_2\text{PtCl}_4$  (103.9 mg; 0.250 mmol) following **GP8**, using  $\text{NaAc} \cdot 3\text{H}_2\text{O}$  (68.1 mg; 0.501 mmol) as a base. Precipitation from *n*-hexane yielded a brown solid which could not be identified as the target compound **65**.

### Bis(4-Brom- $\beta$ -hydroxydithiocinnamic butynylester-*O,S*)-platin(II) (**66**)

**59** (157.7 mg; 0.482 mmol) was brought to reaction with  $\text{K}_2\text{PtCl}_4$  (100 mg; 0.241 mmol) and  $\text{NaOAc} \cdot 3\text{H}_2\text{O}$  (65.59 mg, 0.482 mmol) according to **GP8**. The crude material was flushed through a short plug of silica using DCM as solvent, upon which the pure compound **66** (25.2 mg; 12 % yield) was isolated as red solid.



**Smp.:** 175.8 °C (decomp.)

**Analysis** calcd. for C<sub>26</sub>H<sub>20</sub>Br<sub>2</sub>O<sub>2</sub>PtS<sub>4</sub> (M = 847,59 g/mol): C, 36.84; H, 2.38; S, 15.13; found: C, 36.82; H, 2.74; S, 12.28.

**<sup>1</sup>H NMR** (400 MHz, CDCl<sub>3</sub>) δ = 7.85 (d, <sup>3</sup>J<sub>HH</sub> = 8.8 Hz, 2H, Ar-H2, Ar-H5), 7.58 (d, <sup>3</sup>J<sub>HH</sub> = 8.8 Hz, 2H, Ar-H2, Ar-H6), 7.06 (s, 1H, =CH-), 3.40 (t, <sup>3</sup>J<sub>HH</sub> = 7.1 Hz, 2H, S-CH<sub>2</sub><sup>α</sup>), 2.74 (td, <sup>3</sup>J<sub>HH</sub> = 7.1, <sup>4</sup>J<sub>HH</sub> = 2.7 Hz, 2H, CH<sub>2</sub><sup>β</sup>), 2.11 (t, <sup>4</sup>J<sub>HH</sub> = 2,6 Hz, 1H, ≡CH) ppm.

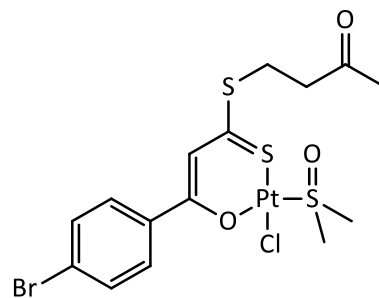
**<sup>13</sup>C{<sup>1</sup>H} NMR** (100 MHz, CDCl<sub>3</sub>): δ = 177.0 (CS<sub>2</sub>), 174.1 (C-OPt), 138.1 (Ar-C1), 132.6 (Ar-C2, Ar-C6), 129.2 (Ar-C3, Ar-C5), 126.8 (Ar-C4), 113.2 (=CH-), 81.7 (≡C-), 70.6 (≡CH), 32.7 (S-CH<sub>2</sub><sup>α</sup>), 18.6 (CH<sub>2</sub><sup>β</sup>) ppm.

**FTIR (ATR)**  $\tilde{\nu}$  = 3282 (w), 3269 (w), 2953, 2918 (s), 2850 (s), 1584 (m), 1506 (m), 1491 (m), 1453 (vs), 1384 (m), 1306 (m), 1288 (m), 1258 (m), 1216 (m), 1178 (m), 1072 (m), 1009 (s), 972 (m), 829 (m), 777(s), 643 (m) cm<sup>-1</sup>.

**MS** data could not be obtained in EI, FAB or ESI-based measurements.

### Conversion of **59** with one equivalent of K<sub>2</sub>PtCl<sub>4</sub> and DMSO (**67**)

**59** (143.33 mg; 0.438 mmol), K<sub>2</sub>PtCl<sub>4</sub> (200 mg; 0.482 mmol.), DMSO (62 μL; 0.876 mmol) and NaOAc·3H<sub>2</sub>O (59.60 mg, 0.438 mmol) were converted according to **GP5**. Column chromatography on silica gel using a gradient (mobile phase DCM/ethyl acetate 100 : 0 to 100 : 5) afforded a brown solid (*R*<sub>f</sub> ≈ 0,3), which could not be identified as the target compound. Instead, one isolated fraction was identified as the hydrated homolog **67**.



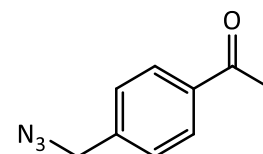
**<sup>1</sup>H NMR** (600 MHz, CDCl<sub>3</sub>) δ = 7.80 (d, <sup>3</sup>J<sub>HH</sub> = 8.7 Hz, 2H, Ar-H2, Ar-H5), 7.52 (d, <sup>3</sup>J<sub>HH</sub> = 8.7 Hz, 2H, Ar-H2, Ar-H6), 7.02 (s, 1H, =CH-), 3.65 (s, 6H, CH<sub>3</sub>(DMSO)), 3.44 (t, <sup>3</sup>J<sub>HH</sub> = 6.6 Hz, 2H, S-CH<sub>2</sub><sup>α</sup>), 3.00 (t, <sup>3</sup>J<sub>HH</sub> = 6.6 Hz, 2H, CH<sub>2</sub><sup>β</sup>), 2.19 (s, 3H, C(O)-CH<sub>3</sub>) ppm.

**<sup>13</sup>C{<sup>1</sup>H} NMR** (150 MHz, CDCl<sub>3</sub>) δ = 206.4 (C=O), 180.9 (CS<sub>2</sub>), 174.2 (C-OPt), 136.4 (Ar-C1), 132.6 (2C, Ar-C2, Ar-C6), 129.9 (2C, Ar-C3, Ar-C5), 127.5 (Ar-C4), 111.8 (=CH-), 46.8 (CH<sub>3</sub> (DMSO)), 42.1 (CH<sub>2</sub><sup>β</sup>), 29.5 (C(O)-CH<sub>3</sub>), 27.6 (S-CH<sub>2</sub><sup>α</sup>) ppm.

## 16.4 Azide-functionalized compounds

### *p*-(Azidomethyl) acetophenone (**70**)

*p*-(azidomethyl) acetophenone was prepared in two steps,<sup>395,396</sup> starting with the literature-reported synthesis of *p*-bromomethyl acetophenone **69** from *p*-methyl acetophenone (5 g, 37.5 mmol). The crude material obtained after extraction from Et<sub>2</sub>O/water, which still contained ca. 10 mol-% methyl acetophenone **68** (6.95 g, ca. 28 mmol), was then dissolved in dimethylformamide (DMF, 30 mL) and cooled to 0 °C.

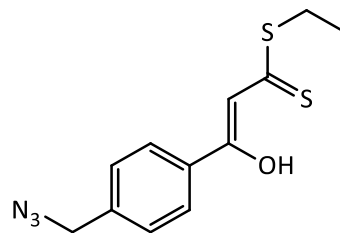


A suspension of NaN<sub>3</sub> (1.84 g, 28.3 mmol) in DMF (40 mL) was added and the mixture stirred at 0 °C for 4 h, upon which no conversion was visible by TLC control. The mixture was thus heated up to 90 °C for 1.5 h, allowed to cool down and stirred overnight. To the resulting yellow solution, water and ethyl acetate (50/50 mL) were added and the evolving two-phased system separated. The aqueous phase was extracted with ethyl acetate (3 × 20 mL), the combined organic phases washed with brine (2 × 10 mL) and dried over sodium sulfate. The crude material was purified by column chromatography (mobile phase: ethyl acetate/*n*-hexane 1:2, R<sub>f</sub> ≈ 0,3) and **70** obtained as pale yellow oil in 97 % yield (4.77 g, overall yield 73 %)

<sup>1</sup>H NMR (400 MHz, CDCl<sub>3</sub>) δ = 7.94 (d, <sup>3</sup>J<sub>HH</sub> = 8.0 Hz, 2H, Ar-H3, Ar-H5), 7.39 (d, <sup>3</sup>J<sub>HH</sub> = 8.0 Hz, 2H, Ar-H2, Ar-H6), 4.39 (s, 2H, Ph-CH<sub>2</sub>-), 2.57 (s, 3H, CO-CH<sub>3</sub>).

***p*-(Azidomethyl)  $\beta$ -hydroxydithiocinnamic acid ethyl ester (71)**

Compound **71** was prepared following **GP3**, using **70** (1.75 g; 10 mmol), KO<sup>t</sup>Bu (2.23 g; 20 mmol), CS<sub>2</sub> (850  $\mu$ L; 14 mmol), and ethyl iodide (800  $\mu$ L; 10 mmol). For purification, the crude material was subjected to column chromatography using a gradient (mobile phase: DCM/hexanes 1:2 to 1:1;  $R_f \approx 0.5$ ).



**Analysis** calcd. for C<sub>12</sub>H<sub>13</sub>N<sub>3</sub>OS<sub>2</sub> (M = 279.38 g/mol): C, 51.59; H, 4.69; N, 15.04; S, 22.95; found: C, 51.61, H, 4.84, N, 14.72, S, 22.87.

**<sup>1</sup>H NMR** (200 MHz, CDCl<sub>3</sub>)  $\delta$  = 15.12 (s, 1H, OH), 7.89 (d, <sup>3</sup>J<sub>HH</sub> = 8.3 Hz, 2H, Ar-H2, Ar-H6), 7.40 (d, <sup>3</sup>J<sub>HH</sub> = 8.2 Hz, 2H, Ar-H3, Ar-H5), 6.89 (s, 1H, =CH-), 4.40 (s, 2H, Ph-CH<sub>2</sub>-), 3.28 (q, <sup>3</sup>J<sub>HH</sub> = 7.4 Hz, 2H, S-CH<sub>2</sub>), 1.38 (t, *J* = 7.4 Hz, 3H, CH<sub>3</sub>) ppm.

**<sup>13</sup>C{<sup>1</sup>H} NMR** (50 MHz, CDCl<sub>3</sub>)  $\delta$  = 217.8 (CS<sub>2</sub>), 169.4 (C-OH), 139.8 (Ar-C4), 134.7 (Ar-C1), 128.8 (2C, Ar-C3, Ar-C5), 127.6 (2C, Ar-C2, Ar-C6), 108.2 (=CH-), 54.3 (Ph-CH<sub>2</sub>-), 27.7 (S-CH<sub>2</sub>-), 12.6 (-CH<sub>3</sub>) ppm.

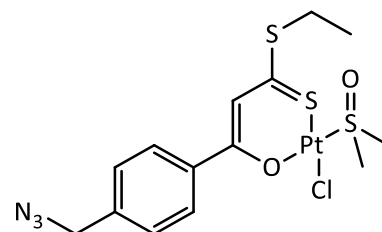
**MS (EI+)** *m/z* = 280 [M+H]<sup>+</sup>, 237 [M-N<sub>3</sub>]<sup>+</sup>; 218 [M-SEt]<sup>+</sup>.

**FTIR (ATR)**  $\tilde{\nu}$  = 2974, 2925 (w), 2870 (w), 2098 (s), 1583 (vs), 1556 (vs), 1501 (s), 1416 (s), 1228 (s), 1118 (w), 1062 (m), 1037 (m), 949 (s), 774 (s) cm<sup>-1</sup>.



**Chloro-(4-(azidomethyl)- $\beta$ -hydroxydithiocinnamic acid ethyl ester-O,S)-  
(dimethylsulfoxide-S)- platinum(II) (72)**

Compound **72** was prepared from **71** following **GP5**, using **71** (122.3 mg; 0,438 mmol),  $K_2PtCl_4$  (200 mg; 0.482 mmol.), DMSO (62  $\mu$ L; 0,876 mmol) and NaOAc (36 mg, 0,438 mmol). In a first attempt, column chromatography on silica gel using a gradient (mobile phase: DCM/hexanes 2 : 1 to DCM to DCM/acetone 10 : 1) yielded 53 % semi-pure product.



Attempts to further purify the complex by crystallization from DCM/hexane and subsequent column chromatography (gradient: DCM/acetone 10 : 0 to 10 : 1) lead to partial decomposition and resulted in a final yield of 83.7 mg (33 %) pure product **72**.

In a second attempt, column chromatography on silica gel (mobile phase: DCM/acetone 50 : 1 to 10 : 1) was performed and lead to 82 % (211 mg) yellow crystalline **72** after partial evaporation of the mobile phase and allowing for the left-over acetone to slowly evaporate from the solution.

**Analysis** calcd. for  $C_{14}H_{18}ClN_3O_2PtS_3$  (M = 587.04 g/mol): C, 28.64; H, 3.09; N, 7.16; S, 16.39; calcd. for  $C_{14}H_{18}ClN_3O_2PtS_3 \cdot 0.5$  acetone C, 30.22; H, 3.44; N, 6.82; S, 15.61; found C, 30.29, H, 3.22, N, 6.77, S, 15.79.

**$^1H$  NMR** (200 MHz,  $CDCl_3$ )  $\delta$  = 7.97 (d,  $^3J_{HH}$  = 8.3 Hz, 2H, Ar-H2, Ar-H6), 7.35 (d,  $^3J_{HH}$  = 8.3 Hz, 2H, Ar-H3, Ar-H5), 7.08 (s, 1H, =CH-), 4.37 (s, 2H, Ph-CH<sub>2</sub>-), 3.66 (s w/ Pt satellites,  $^3J_{PtH}$  = 23.5 Hz, 6H, CH<sub>3</sub> (DMSO)), 3.27 (q,  $^3J_{HH}$  = 7.4 Hz, 2H, S-CH<sub>2</sub>), 1.45 (t,  $J$  = 7.4 Hz, 3H, CH<sub>3</sub>) ppm.

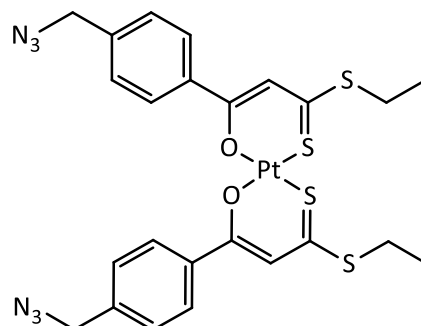
**$^{13}C\{^1H\}$  NMR** (50 MHz,  $CDCl_3$ )  $\delta$  = 180.9 (CS<sub>2</sub>), 173.9 (C-OPt), 139.5 (Ar-C4), 137.2 (Ar-C1), 128.6 (2C, Ar-C2, Ar-C6), 128.5 (2C, Ar-C3, Ar-C5), 111.6 (=CH-), 54.5 (Ph-CH<sub>2</sub>-), 47.0 (2C, CH<sub>3</sub> (DMSO)), 28.92 (S-CH<sub>2</sub>), 13.3 (CH<sub>3</sub>) ppm.

**MS** data could not be obtained in ESI measurement.

**FTIR (ATR)**  $\tilde{\nu}$  = 2962 (w), 2926 (m), 2853 (w), 2095 (s), 1517 (w), 1461 (vs), 1406 (w), 1288 (s), 1256 (s), 1146 (s), 1029 (s), 978 (m), 841 (m), 810 (s), 689 (m)  $cm^{-1}$ .

**Bis(4-(azidomethyl)- $\beta$ -hydroxydithiocinnamic acid ethyl ester-*O,S*)-platinum(II) (**73**)**

Following **GP8**, **71** (268.3 mg; 0.964 mmol),  $K_2PtCl_4$  (200 mg; 0.482 mmol.), and NaOAc (79 mg, 0,964 mmol) were used to prepare compound **73** in 12 % final yield (45.8 mg) after repeated column chromatographic purification on silica gel using DCM/hexanes 2 : 1 and 1 : 1 as mobile phase.



**71** (67.3 mg; 0.241 mmol) was further converted with  $K_2PtCl_4$  (50 mg; 0.120 mmol.), DMSO (17  $\mu$ L, 0.241 mmol) and NaOAc (20 mg, 0,241 mmol) according to **GP5**. Column chromatography using a gradient (mobile phase: DCM/hexanes 1:1 to 1:0) yielded **73** (63 mg, 70 % yield) as red crystalline material.

**Analysis** calcd. for  $C_{24}H_{24}N_6O_2PtS_4$  ( $M = 751,83$  g/mol): C, 38.34; H, 3.22; N, 11.18; S, 17.06; calcd. for  $C_{24}H_{24}N_6O_2PtS_4 \cdot 0.1$  acetone: C, 38.52; H, 3.27; N, 11.09; S, 16.93; found C, 38.34, H, 3.27, N, 10.73, S, 16.98.

**$^1H$  NMR** (400 MHz,  $CDCl_3$ )  $\delta$  8.02 (d,  $J = 8.1$  Hz, 2H, Ar-H2, Ar-H6), 7.39 (d,  $J = 8.1$  Hz, 2H, Ar-H3, Ar-H5), 7.07 (s, 1H, =CH-), 4.39 (s, 2H, Ph- $CH_2$ -), 3.24 (q,  $^3J_{HH} = 7.4$  Hz, 2H, S- $CH_2$ ), 1.45 (t,  $^3J_{HH} = 7.4$  Hz, 3H,  $CH_3$ ) ppm.

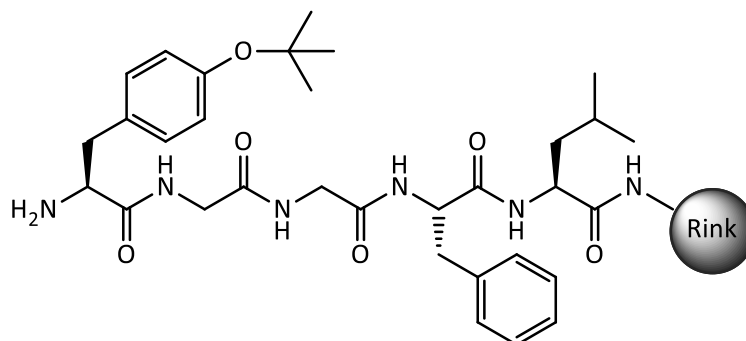
**$^{13}C\{^1H\}$  NMR** (50 MHz,  $CDCl_3$ )  $\delta$  178.3 ( $CS_2$ ), 174.2 (C-OPt), 139.5 (Ar-C4), 139.1 (Ar-C1), 128.9 (2C, Ar-C3, Ar-C5), 128.2 (2C, Ar-C2, Ar-C6), 113.0 (=CH-), 54.5 (Ph- $CH_2$ -), 28.4 (S- $CH_2$ ), 13.2 ( $CH_3$ ) ppm.

**MS (ESI+)**  $m/z = 774$   $[M+Na]^+$

**FTIR (ATR)**  $\tilde{\nu} = 2959$  (vs), 2921(vs), 2850 (s), 2094 (s), 1510 (w), 1461 (vs), 1374 (w), 1285 (s), 1257 (s), 1176 (s), 1096 (m), 1018 (m), 966 (w), 780 (s)  $cm^{-1}$ .

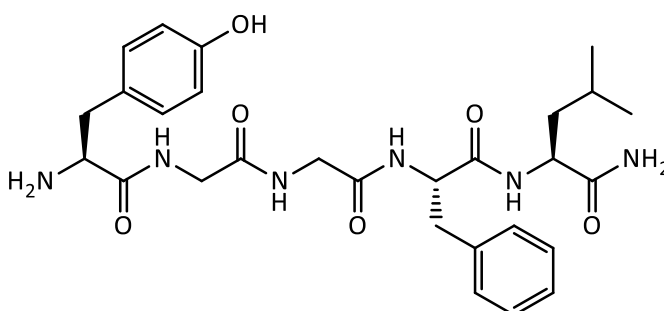
## 16.5 Peptide derivatizations

### Leu<sup>5</sup>-Enkephalin bound to Rink Amide AM Resin (**74**)



Leu<sup>5</sup>-Enkephalin bound to Rink Amide AM Resin **74** was prepared by automated SPPS (**GP12**) in a 250  $\mu\text{mol}$  scale according to the described procedure, using Rink resin with 0.59 or 0.71 mmol/g loading. Fmoc-protected amino acids (Fmoc-Leu-OH, Fmoc-Phe-OH, 2  $\times$  Fmoc-Gly-OH, Fmoc-Tyr(<sup>t</sup>Bu)-OH) were used in 4-fold excess (1 mmol). After drying of the peptidized resin, it was split into two equal portions equivalent to 125 mmol peptide and treated separately for further reactions.

### Free Leu<sup>5</sup>-Enkephalin amide (**75**)



One 125  $\mu\text{mol}$  equivalent of **74** was cleaved (90 min/r.t.) and precipitated from Et<sub>2</sub>O/*n*-hexane. Repeated washing and lyophilization according to the described protocol for SPPS (**GP12**) yielded Leu<sup>5</sup>-Enk **75** as C-terminal amide (58 mg; 84 %) in >90 % purity.

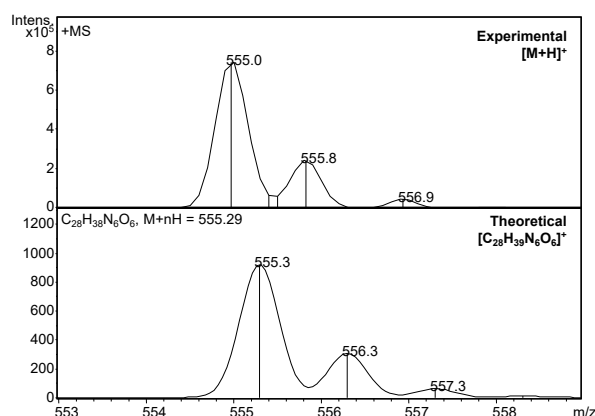
*rp*-HPLC (gradient1):  $t_R = 13.7$  min (>90 %)

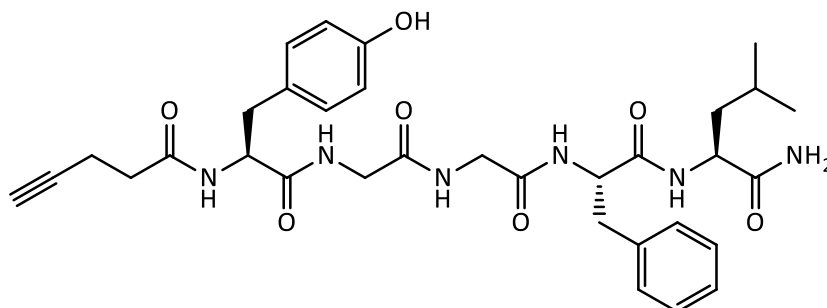
MS (ESI+):  $m/z = 555.0$  [M+H]<sup>+</sup> (calcd. for C<sub>28</sub>H<sub>39</sub>N<sub>6</sub>O<sub>6</sub>: 555.3).

**<sup>1</sup>H NMR** (400 MHz, THF-*d*<sub>8</sub>)  $\delta$  = 10.82 (s, 1H, Y<sup>1</sup>: Ar-OH), 8.64 (m, 1H, -NH-), 8.32 (m, 1H, -NH-), 8.14 (m, 1H, -NH-), 7.76 (d, <sup>3</sup>J<sub>HH</sub> = 8.1 Hz, -NH-), 7.51 (d, <sup>3</sup>J<sub>HH</sub> = 8.1 Hz, -NH-), 7.24 (m, 5H, F<sup>4</sup>: Ar-H<sub>2,3,5,6</sub>, -NH-), 7.14 (m, 1H, F<sup>4</sup>: Ar-H<sub>4</sub>), 7.07 (d, <sup>3</sup>J<sub>HH</sub> = 8.2 Hz, 2H, Y<sup>1</sup>: Ar-H<sub>2,6</sub>), 6.70 (d, <sup>3</sup>J<sub>HH</sub> = 8.3 Hz, 2H, Y<sup>1</sup>: Ar-H<sub>3,5</sub>), 6.50 (d, <sup>2</sup>J<sub>HH</sub> = 104.4 Hz, 2H, L<sup>5</sup>: -NH<sub>2</sub>), 4.59 (m, 1H, F<sup>4</sup>: CH <sup>$\alpha$</sup> ), 4.36 (m, 1H, L<sup>5</sup>: CH <sup>$\alpha$</sup> ), 4.14 (m, 1H, Y<sup>1</sup>: CH <sup>$\alpha$</sup> ), 4.06-3.84 (m, 2H, G<sup>2</sup>/G<sup>3</sup>: -CH<sub>2</sub> <sup>$\beta$</sup> -; additional signals obscured by SRS), 3.20-2.88 (m, 4H, Y<sup>1</sup>/F<sup>4</sup>: -CH<sub>2</sub> <sup>$\beta$</sup> -Ar + SRS), 1.58 (m, L<sup>5</sup>: -CH<sub>2</sub> <sup>$\beta$</sup> -CH <sup>$\nu$</sup> Me<sub>2</sub> + SRS), 0.89-0.85 (m, L<sup>5</sup>: 2  $\times$  -CH<sub>3</sub> + SRS) ppm. Parts of the signal sets are obscured by solvent residual signals (SRS)

**<sup>1</sup>H NMR** (400 MHz, DMSO-*d*<sub>6</sub>)  $\delta$  = 9.32 (s, 1H, Y<sup>1</sup>: Ar-OH), 8.69 (t, <sup>3</sup>J<sub>HH</sub> = 5.5 Hz, 1H, G<sup>2</sup>: -NH-), 8.11 (t, <sup>3</sup>J<sub>HH</sub> = 5.7 Hz, 1H, G<sup>3</sup>: -NH-), 8.07 (d, <sup>3</sup>J<sub>HH</sub> = 8.2 Hz, 1H, F<sup>4</sup>: -NH-), 8.01 (m, 3H, Y<sup>1</sup>: -NH<sub>2</sub>, L<sup>5</sup>: -NH-), 7.25 (m, 4H, F<sup>4</sup>: Ar-H<sub>2,3,5,6</sub>), 7.18 (m, 1H, F<sup>4</sup>: Ar-H<sub>4</sub>), 7.06 (d, <sup>3</sup>J<sub>HH</sub> = 8.4 Hz, 2H, Y<sup>1</sup>: Ar-H<sub>2,6</sub>), 7.03 (d, <sup>2</sup>J<sub>HH</sub> = 66.5 Hz, 2H, L<sup>5</sup>: -NH<sub>2</sub>), 6.70 (d, <sup>3</sup>J<sub>HH</sub> = 8.4 Hz, 2H, Y<sup>1</sup>: Ar-H<sub>3,5</sub>), 4.54 (dt, <sup>3</sup>J<sub>HH</sub> = 9.0, 4.5 Hz, 1H, F<sup>4</sup>: CH <sup>$\alpha$</sup> ), 4.21 (dt, <sup>3</sup>J<sub>HH</sub> = 15.4, 7.7 Hz, 1H, L<sup>5</sup>: CH <sup>$\alpha$</sup> ), 3.98 (m, 1H, Y<sup>1</sup>: CH <sup>$\alpha$</sup> ), 3.87-3.62 (m, 4H, G<sup>2</sup>/G<sup>3</sup>: -CH<sub>2</sub> <sup>$\alpha$</sup> -), 3.05-2.98, 2.84-2.27 (2 m, 4H, Y<sup>1</sup>/F<sup>4</sup>: -CH<sub>2</sub> <sup>$\beta$</sup> -Ar), 1.61-1.52 (m, 1H, L<sup>5</sup>: -CH <sup>$\nu$</sup> Me<sub>2</sub>), 1.46 (m, 2H, L<sup>5</sup>: -CH<sub>2</sub> <sup>$\beta$</sup> -), 0.89-0.83 (m, 6H, L<sup>5</sup>: 2  $\times$  -CH<sub>3</sub>) ppm.

**<sup>13</sup>C NMR** (100 MHz, DMSO-*d*<sub>6</sub>)  $\delta$  = 173.7 (L<sup>5</sup>: C=O), 171.0 (F<sup>4</sup>: C=O), 168.7 (Y<sup>1</sup>: C=O), 168.5 (G<sup>2</sup>: C=O), 168.3 (G<sup>3</sup>: C=O), 156.5 (Y<sup>1</sup>: Ar-C<sub>4</sub>), 137.7 (F<sup>4</sup>: Ar-C<sub>1</sub>), 130.3 (2C, Y<sup>1</sup>: Ar<sub>2,6</sub>), 130.2 (Y<sup>1</sup>: Ar-C<sub>1</sub>), 129.0, 127.8 (4C, F<sup>4</sup>: Ar), 126.2 (F<sup>4</sup>: Ar-C<sub>4</sub>), 115.2 (2C, Y<sup>1</sup>: Ar-C<sub>3,5</sub>), 53.5 (Y<sup>1</sup>: CH <sup>$\alpha$</sup> ), 53.6 (F<sup>4</sup>: CH <sup>$\alpha$</sup> ), 50.7 (L<sup>5</sup>: CH <sup>$\alpha$</sup> ), 41.6 (G: CH <sup>$\alpha$</sup> ), 41.4. (G: CH <sup>$\alpha$</sup> ), 40.8 (L<sup>5</sup>: CH<sub>2</sub> <sup>$\beta$</sup> ), 37.3 (F<sup>4</sup>: CH<sub>2</sub> <sup>$\beta$</sup> -Ar), 35.3 (Y<sup>1</sup>: CH<sub>2</sub> <sup>$\beta$</sup> -Ar), 24.0 (L<sup>5</sup>: CH <sup>$\nu$</sup> ), 22.90 (L<sup>5</sup>: CH<sub>3</sub>), 21.6 (L<sup>5</sup>: CH<sub>3</sub>) ppm. Data of <sup>13</sup>C NMR obtained indirectly from HSQC and HMBC experiments.



Alkyne-functionalized Leu<sup>5</sup>-Enkephalin (**76**)

Peptide-loaded rink resin **74**, equivalent to 125  $\mu\text{mol}$ , was coupled with pentynoic acid (PA, 49 mg, 0.5 mmol) under addition of HOBT/TBTU (4/3.8 eq) and D'PEA (8 eq.) at room temperature for 2 h by SPPS (following **GP13**). After cleavage and precipitation, a white powder of **76** (50 mg; 63 % yield) was obtained which was > 85 % purity according to analyt. HPLC and thus used without further purification.

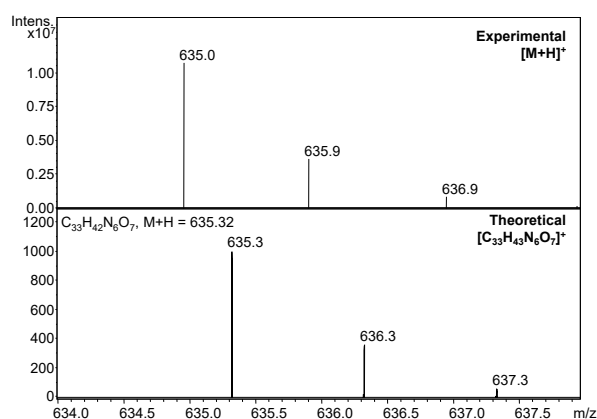
**rp-HPLC** (C8, gradient 1):  $t_R = 16.05$  min (82 %).

**rp-HPLC** (C18, gradient 1):  $t_R = 16.35$  min (>85 %).

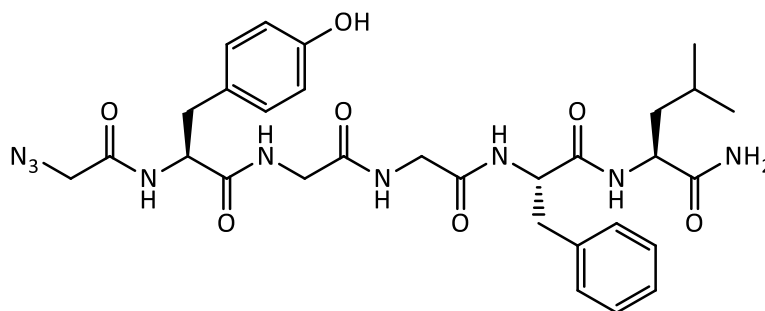
**MS** (ESI+):  $m/z = 635.0$  [M+H]<sup>+</sup> (calcd for C<sub>33</sub>H<sub>43</sub>N<sub>6</sub>O<sub>7</sub>: 635.3).

**<sup>1</sup>H NMR** (400 MHz, DMSO-d<sub>6</sub>)  $\delta = 9.11$  (s, 1H, Y<sup>1</sup>: Ar-OH), 8.18 (t, <sup>3</sup>J<sub>HH</sub> = 5.6 Hz, 1H, G<sup>2</sup>: -NH-), 8.09 (d, <sup>3</sup>J<sub>HH</sub> = 8.1 Hz, 1H, Y<sup>1</sup>: -NH-), 8.04 (d, <sup>3</sup>J<sub>HH</sub> = 8.1 Hz, 1H, F<sup>4</sup>: -NH-), 7.94 (m, 2H, G<sup>3</sup>: -NH-, L<sup>5</sup>: -NH-), 7.24 (m, 4H, F<sup>4</sup>: Ar-H<sub>2,3,5,6</sub>), 7.18 (m, 1H, F<sup>4</sup>: Ar-H<sub>4</sub>), 7.00 (d, <sup>3</sup>J<sub>HH</sub> = 8.4 Hz, 2H, Y<sup>1</sup>: Ar-H<sub>2,6</sub>), 7.00 (d, <sup>2</sup>J<sub>HH</sub> = 47.3 Hz, 2H, L<sup>5</sup>: -NH<sub>2</sub>), 6.63 (d, <sup>3</sup>J<sub>HH</sub> = 8.4 Hz, 2H, Y<sup>1</sup>: Ar-H<sub>3,5</sub>), 4.51 (dt, <sup>3</sup>J<sub>HH</sub> = 8.9, 4.6 Hz, 1H, F<sup>4</sup>: CH <sup>$\alpha$</sup> ), 4.41 (dt, <sup>3</sup>J<sub>HH</sub> = 9.0, 4.8 Hz, 1H, Y<sup>1</sup>: CH <sup>$\alpha$</sup> ), 4.21 (dt, <sup>3</sup>J<sub>HH</sub> = 15.2, 7.9 Hz, 1H, L<sup>5</sup>: CH <sup>$\alpha$</sup> ), 3.80-3.52 (m, 4H, G<sup>2</sup>/G<sup>3</sup>: -CH<sub>2</sub> <sup>$\alpha$</sup> -), 3.04/2.79 (2m, 2H, F<sup>4</sup>: -CH<sub>2</sub> <sup>$\beta$</sup> -Ar), 2.91/2.65 (2 m, 2H, Y<sup>1</sup>: -CH<sub>2</sub> <sup>$\beta$</sup> -Ar), 2.70 (t, <sup>3</sup>J<sub>HH</sub> = 2.1 Hz, PA<sup>0</sup>:  $\equiv\text{CH}$ ), 2.31-2.23 (m, 4H, PA<sup>0</sup>: CH<sub>2</sub> <sup>$\alpha,\beta$</sup> ), 1.61-1.52 (m, 1H, L<sup>5</sup>: -CH <sup>$\nu$</sup> Me<sub>2</sub>), 1.47 (m, 2H, L<sup>5</sup>: -CH<sub>2</sub> <sup>$\beta$</sup> -), 0.89-0.82 (m, 6H, L<sup>5</sup>: 2  $\times$  -CH<sub>3</sub>) ppm.

**<sup>13</sup>C NMR** (100 MHz, DMSO-d<sub>6</sub>)  $\delta = 173.9$  (L<sup>5</sup>: C=O), 171.7 (Y<sup>1</sup>: C=O), 170.6 (F<sup>4</sup>: C=O), 170.3 (PA<sup>0</sup>: C=O), 169.0 (G<sup>2</sup>: C=O), 168.6 (G<sup>3</sup>: C=O), 155.7 (Y<sup>1</sup>: Ar-C<sub>4</sub>), 137.7 (F<sup>4</sup>: Ar-C<sub>1</sub>), 130.0 (2C, Y<sup>1</sup>: Ar-C<sub>2,6</sub>), 129.2 (2C, F<sup>4</sup>: Ar-C<sub>3,5</sub>), 128.0 (2C, F<sup>4</sup>: Ar-C<sub>2,6</sub>), 127.9 (Y<sup>1</sup>: Ar-C<sub>1</sub>), 126.2 (F<sup>4</sup>: Ar-C<sub>4</sub>), 114.8 (2C, Y<sup>1</sup>: Ar-C<sub>3,5</sub>), 83.7 (PA<sup>0</sup>: -C $\equiv$ ), 71.2 (PA<sup>0</sup>:  $\equiv\text{CH}\delta$ ), 54.4 (Y<sup>1</sup>: CH <sup>$\alpha$</sup> ), 54.0 (F<sup>4</sup>: CH <sup>$\alpha$</sup> ), 51.0 (L<sup>5</sup>: CH <sup>$\alpha$</sup> ), 42.0 (G: CH <sup>$\alpha$</sup> ), 41.9 (G: CH <sup>$\alpha$</sup> ), 40.8 (L<sup>5</sup>: CH<sub>2</sub> <sup>$\beta$</sup> ), 37.3 (F<sup>4</sup>: CH<sub>2</sub> <sup>$\beta$</sup> -Ar), 36.6 (Y<sup>1</sup>: CH<sub>2</sub> <sup>$\beta$</sup> -Ar), 34.0 (PA<sup>0</sup>: -CH <sup>$\alpha$</sup> -), 24.2 (L<sup>5</sup>: CH <sup>$\nu$</sup> ), 23.0 (L<sup>5</sup>: CH<sub>3</sub>), 21.6 (L<sup>5</sup>: CH<sub>3</sub>), 14.0 (PA<sup>0</sup>: -CH<sub>2</sub> <sup>$\beta$</sup> -) ppm.



### Azide-functionalized Leu<sup>5</sup>-Enkephalin (**77**)



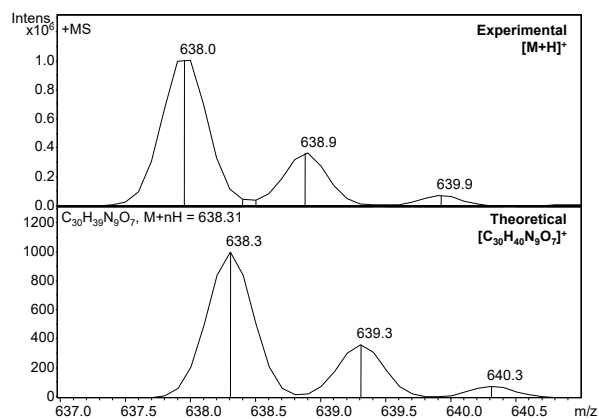
Peptide-loaded rink resin **74**, equivalent to 125  $\mu\text{mol}$ , was coupled with azidoacetic acid (AA, 50.5 mg, 0.5 mmol) under addition of HOBt/TBTU (4/3.8 eq) and *D*'PEA (8 eq.) at room temperature for 2 h by SPPS, following **GP12**. After cleavage and precipitation, a white powder of **77** (47 mg, 59 %) was obtained which was of 90 % purity according to analyt. HPLC and thus used without further purification.

**rp-HPLC** (C18, gradient1):  $t_R = 16.3$  min (90 %).

**MS** (ESI+):  $m/z = 638.0$   $[\text{M}+\text{H}]^+$  (calcd. for  $\text{C}_{30}\text{H}_{40}\text{N}_9\text{O}_7$ : 638.3).

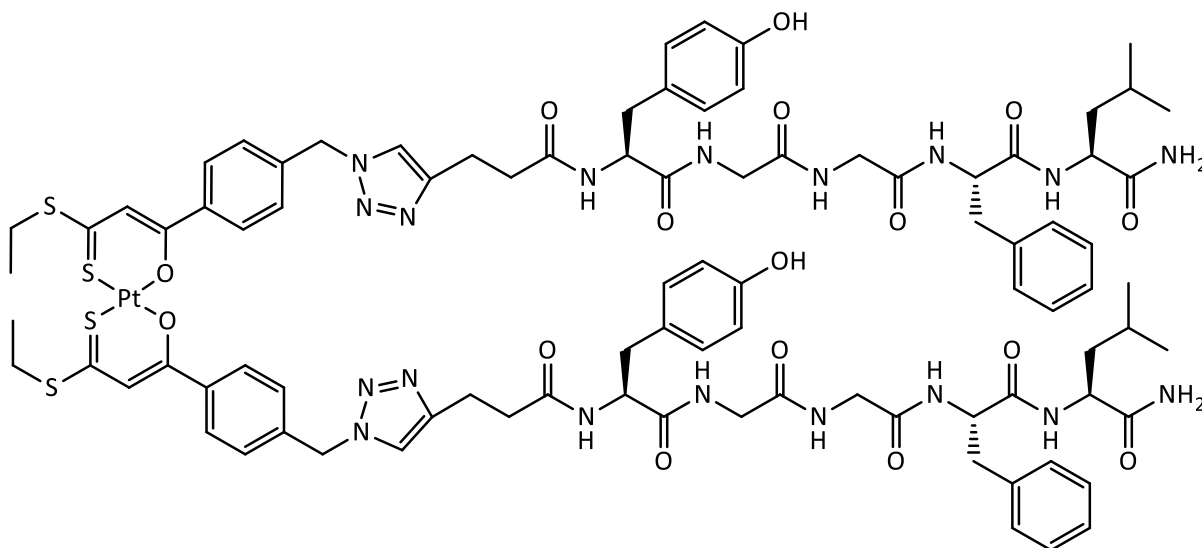
**<sup>1</sup>H NMR** (400 MHz,  $\text{DMSO-d}_6$ )  $\delta = 9.14$  (s, 1H, Y<sup>1</sup>: Ar-OH), 8.35 (t,  $^3J_{\text{HH}} = 5.7$  Hz, 1H, G<sup>2</sup>: -NH-), 8.26 (d,  $^3J_{\text{HH}} = 8.2$  Hz, 1H, Y<sup>1</sup>: -NH-), 8.04 (d,  $^3J_{\text{HH}} = 8.1$  Hz, 1H, F<sup>4</sup>: -NH-), 7.98 (t,  $^3J_{\text{HH}} = 5.7$  Hz, 1H, G<sup>3</sup>: -NH-), 7.94 (d,  $^3J_{\text{HH}} = 8.3$  Hz, 1H, L<sup>5</sup>: -NH-), 7.24 (m, 4H, F<sup>4</sup>: Ar-H<sub>2,3,5,6</sub>), 7.18 (m, 1H, F<sup>4</sup>: Ar-H<sub>4</sub>), 7.01 (d,  $^3J_{\text{HH}} = 8.5$  Hz, 2H, Y<sup>1</sup>: Ar-H<sub>2,6</sub>), 7.00 (d,  $^2J_{\text{HH}} = 50$  Hz, 2H, L<sup>5</sup>: -NH<sub>2</sub>), 6.63 (d,  $^3J_{\text{HH}} = 8.5$  Hz, 2H, Y<sup>1</sup>: Ar-H<sub>3,5</sub>), 4.61-4.40 (m, 2H, Y<sup>1</sup>/F<sup>4</sup>: CH <sup>$\alpha$</sup> ), 4.20 (dt,  $^3J_{\text{HH}} = 15.1, 8.0$  Hz, 1H, L<sup>5</sup>: CH <sup>$\alpha$</sup> ), 3.84-3.58 (m, 6H, AA<sup>0</sup>/G<sup>2</sup>/G<sup>3</sup>: -CH<sub>2</sub> <sup>$\alpha$</sup> -), 3.03/2.79 (2m, 2H, F<sup>4</sup>: -CH<sub>2</sub> <sup>$\beta$</sup> -Ar), 2.93/2.65 (2 m, 2H, Y<sup>1</sup>: -CH<sub>2</sub> <sup>$\beta$</sup> -Ar), 1.62-1.52 (m, 1H, L<sup>5</sup>: -CH <sup>$\gamma$</sup> Me<sub>2</sub>), 1.47 (m, 2H, L<sup>5</sup>: -CH<sub>2</sub> <sup>$\beta$</sup> -), 0.89-0.82 (m, 6H, L<sup>5</sup>: 2  $\times$  -CH<sub>3</sub>) ppm.

$^{13}\text{C}$  NMR (100 MHz, DMSO- $d_6$ )  $\delta$  = 173.8 ( $\text{L}^5$ : C=O), 171.3 ( $\text{Y}^1$ : C=O), 170.6 ( $\text{F}^4$ : C=O), 168.9 ( $\text{G}^2$ : C=O), 168.6 ( $\text{G}^3$ : C=O), 167.2 ( $\text{AA}^0$ : C=O), 155.8 ( $\text{Y}^1$ : Ar-C4), 137.7 ( $\text{F}^4$ : Ar-C1), 130.0 (2C,  $\text{Y}^1$ : Ar-C2,6), 129.2 (2C,  $\text{F}^4$ : Ar-C3,5), 128.0 (2C,  $\text{F}^4$ : Ar-C2,6), 127.6 ( $\text{Y}^1$ : Ar-C1), 126.2 ( $\text{F}^4$ : Ar-C4), 114.9 (2C,  $\text{Y}^1$ : Ar-C3,5), 54.3 ( $\text{Y}^1$ :  $\text{CH}^\alpha$ ), 54.0 ( $\text{F}^4$ :  $\text{CH}^\alpha$ ), 51.0 ( $\text{L}^5$ :  $\text{CH}^\alpha$ ), 50.5 ( $\text{AA}^0$ :  $\text{CH}^\alpha$ ), 42.1 (G:  $\text{CH}^\alpha$ ), 41.9 (G:  $\text{CH}^\alpha$ ), 40.8 ( $\text{L}^5$ :  $\text{CH}_2^\beta$ ), 37.3 ( $\text{F}^4$ :  $\text{CH}_2^\beta$ -Ar), 36.7 ( $\text{Y}^1$ :  $\text{CH}_2^\beta$ -Ar), 24.2 ( $\text{L}^5$ :  $\text{CH}^\gamma$ ), 23.0 ( $\text{L}^5$ :  $\text{CH}_3$ ), 21.6 ( $\text{L}^5$ :  $\text{CH}_3$ ) ppm.



## 16.6 Bioconjugates via CuAAC

### Enkephalin-modified bischelate of azide-(O,S)<sub>2</sub>Pt (**78**)



**Method 1:** The reaction was carried out according to **GP9**, using **76** (10 mg, 15.7  $\mu\text{mol}$ ) and **73** (5.92 mg, 7.88 mmol).  $\text{CuSO}_4 \cdot 5 \text{H}_2\text{O}$  (31  $\mu\text{L}$  0.1 M soln.) and sodium ascorbate (63  $\mu\text{L}$  0.1 M soln) was used to enable the conversion. After 3 days of stirring, THF was removed *in vacuo*, water decanted. The residue was re-dissolved in THF/water, precipitation achieved with cold  $\text{Et}_2\text{O}$ . After centrifugation, the water phase was removed and the precipitate repeatedly washed with  $\text{Et}_2\text{O}$ . After lyophilization, 22 mg of crude material were obtained which were purified in several fractions by semiprep. *rp*-HPLC using gradient3. Pure (> 95 %) **78** was obtained in 31 % yield (5 mg).

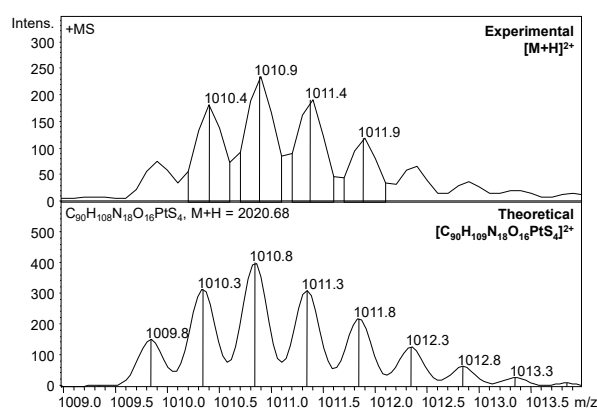
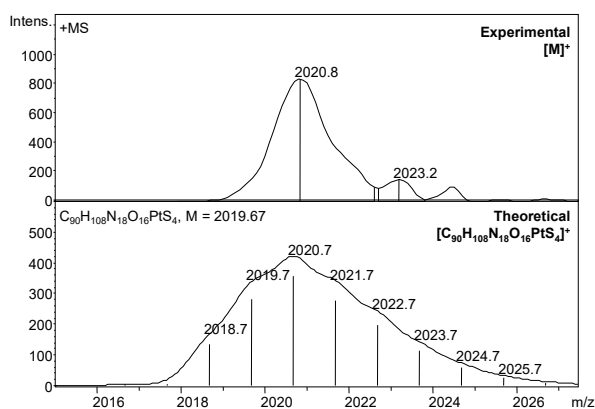
**Method 2:** In a second approach, the reaction was carried out using **76** (5 mg, 7.9  $\mu\text{mol}$ ) and **73** (2.9 mg, 3.9 mmol). *D*'PEA (1.4  $\mu\text{L}$ ) as well as  $\text{CuI}$  (2 mg) was used to enable the conversion. After 5 days of stirring, the solution was liberated of THF and precipitation enforced through addition of ice-cold  $\text{Et}_2\text{O}$ . The mixture was centrifuged, the solvents removed, the red solid repeatedly washed with  $\text{Et}_2\text{O}$  and lyophilized. After prep. HPLC (gradient1), the desired complex was obtained, but a significantly increased abundance of several side products showed that this method is less effective than the usage of  $\text{CuSO}_4/\text{Na-ascorbate}$ .



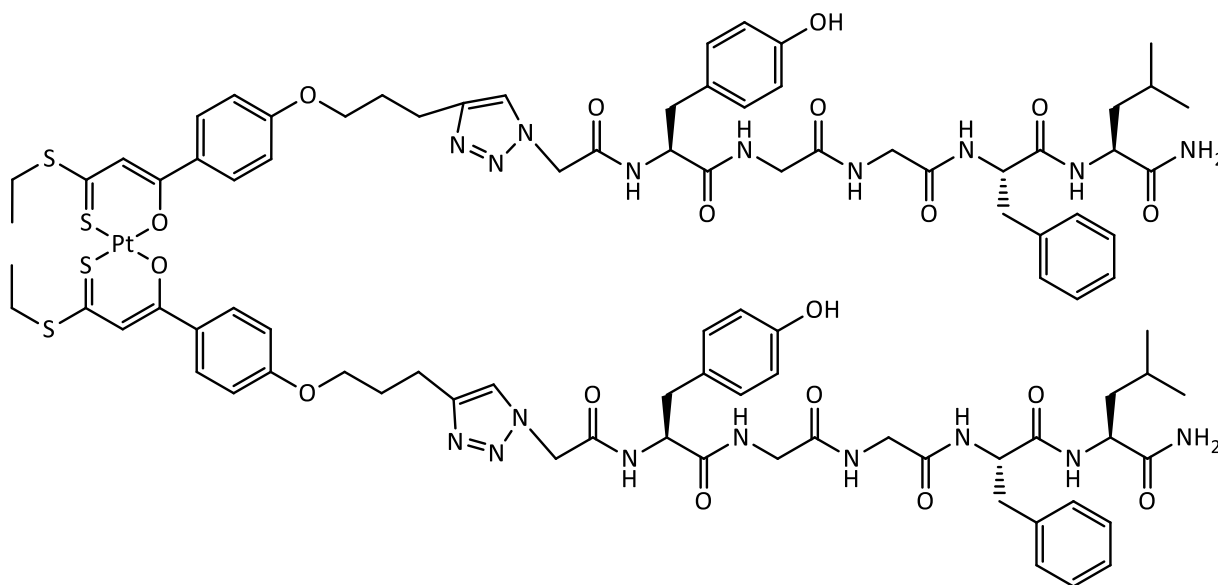
**rp-HPLC** (C18, gradient1):  $t_R = 23.6$  min (> 95 %).

**MS** (ESI+):  $m/z = 2020.8$   $[M]^+$  (calcd. for  $[C_{90}H_{108}N_{18}O_{16}PtS_4]^+$ : 2020.7 / highest peak), 1010.9  $[M+H]^{2+}$  (calcd. for  $[C_{90}H_{109}N_{18}O_{16}PtS_4]^+$ : 1010.8 / highest peak).

**$^1H$  NMR** (400 MHz, DMSO- $d_6$ )  $\delta = 9.13$  (s, 1H,  $Y^1$ : Ar-OH), 8.25 (t,  $^3J_{HH} = 5.5$  Hz, 1H,  $G^2$ : -NH-), 8.12 (d,  $^3J_{HH} = 8.0$  Hz, 1H,  $Y^1$ : -NH-), 8.08-7.92 (m, 2H,  $F^4$ : -NH-,  $G^3$ : -NH-,  $L^5$ : -NH-, (O,S): Ar-H2,6), 7.81 (s, 1H,  $PA^0$ : ta-CH=), 7.41 (d,  $^3J_{HH} = 8.4$  Hz, (O,S): Ar-H3,5), 7.23-7.22 (m, 4H,  $F^4$ : Ar-H2,3,5,6) 7.21 (s, 1H, (O,S): =CH-), 7.17-7.14 (m, 1H,  $F^4$ : Ar-H4), 7.00 (d,  $^3J_{HH} = 8.4$  Hz, 2H,  $Y^1$ : Ar-H2,6), 7.00 (d,  $^2J_{HH} = 47.7$  Hz, 2H,  $L^5$ : -NH $_2$ ), 6.62 (d,  $^3J_{HH} = 8.3$  Hz, 2H,  $Y^1$ : Ar-H3,5), 5.58 (s, 2H, (O,S): Ph-CH $_2$ -N $^{ta}$ ), 4.51 (dt,  $^3J_{HH} = 8.8$ , 4.7 Hz, 1H,  $F^4$ : CH $^\alpha$ ), 4.45-4.40 (m, 1H,  $Y^1$ : CH $^\alpha$ ), 4.19 (dt,  $^3J_{HH} = 15.3$ , 7.8 Hz, 1H,  $L^5$ : CH $^\alpha$ ), 3.77-3.58 (m, 4H,  $G^2/G^3$ : -CH $_2$  $^\alpha$ -), 3.25 (m, 2H, (O,S): S-CH $_2$ -, obscured by SRS), 3.03/2.79 (2m, 2H,  $F^4$ : -CH $_2$  $^\beta$ -Ar), 2.92/2.65 (2 m, 2H,  $Y^1$ : -CH $_2$  $^\beta$ -Ar), 2.77 (m, 2H,  $PA^0$ : -CH $_2$  $^\beta$ -), 2.44-2.37 (m, 4H,  $PA^0$ : -CH $_2$  $^\alpha$ -), 1.59-1.51 (m, 1H,  $L^5$ : -CH $^\nu$ Me $_2$ ), 1.46 (m, 2H,  $L^5$ : -CH $_2$  $^\beta$ -), 1.35 (t,  $^3J_{HH} = 7.3$  Hz, 3H, (O,S): -CH $_3$ ), 0.87-0.80 (m, 6H,  $L^5$ : 2  $\times$  -CH $_3$ ) ppm. Some signals are partially obscured by solvent residual signals (SRS).



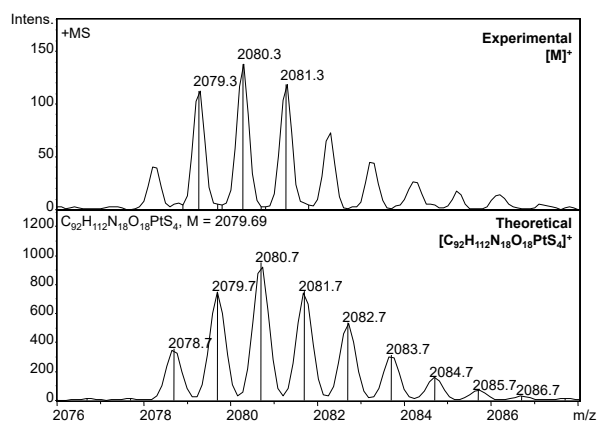
### Enkephalin-modified bischelate of alkyne-(O,S)<sub>2</sub>Pt (79)



The reaction was carried out according to **GP9**, using **77** (10 mg, 7.8  $\mu\text{mol}$ ) and **66** (3.2 mg, 3.9  $\mu\text{mol}$ ).  $\text{CuSO}_4 \cdot 5 \text{H}_2\text{O}$  (16  $\mu\text{L}$  0.1 M soln.) and sodium ascorbate (31  $\mu\text{L}$  0.1 M soln.) was used to enable the conversion. The mixture was stirred for 5 days, upon which the THF was removed *in vacuo*, water decanted, the solid re-dissolved in THF/water, precipitated from ice-cold  $\text{Et}_2\text{O}$  and washed. Preparative *rp*-HPLC (gradient4) yielded **79** (2 mg, 24 % yield).

*rp*-HPLC (C18, gradient1):  $t_R = 25.9$  min (>90%).

**MS** (ESI+):  $m/z = 2080.3$   $[\text{M}]^+$  (calcd. for  $[\text{C}_{92}\text{H}_{112}\text{N}_{18}\text{O}_{18}\text{PtS}_4]^+$ : 2080.7 / highest peak).

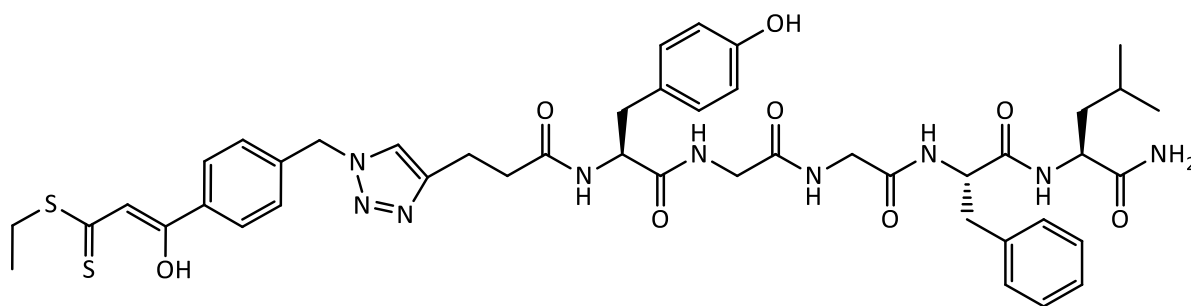


### Conversion of azide-(*O,S*)Pt(DMSO)Cl **72** with alkyne-Enk **76**

Following **GP9**, **76** (5 mg, 7.9  $\mu\text{mol}$ ) and **72** (4.63 mg, 7.9  $\mu\text{mol}$ ) were brought to reaction under addition of sodium ascorbate (4  $\mu\text{L}$  1 M soln.) and  $\text{CuSO}_4 \cdot 5 \text{H}_2\text{O}$  (16  $\mu\text{L}$  0.1 M soln.) and stirred for 4 days. The solvent was reduced *in vacuo*, the red solid re-dissolved in THF/water, precipitated from  $\text{Et}_2\text{O}$  and washed.

Analytical HPLC indicated consumption of the starting material to multiple products. ESI mass spectrometry of the most abundant peaks gave no indication of the desired product, but the isotopic pattern of the obtained signal sets indicated possible formation of a copper-containing compound. The nature of the actually obtained compound could be identified.

### Enkephalin-modified triazol-(*O,S*) ligand (**80**)



The reaction was carried out with **76** (10 mg, 15.8  $\mu\text{mol}$ ), **71** (4.4 mg, 15.8  $\mu\text{mol}$ ), sodium ascorbate (38  $\mu\text{L}$  1 M soln) and  $\text{CuSO}_4 \cdot 5 \text{H}_2\text{O}$  (35  $\mu\text{L}$  0.5 M soln) according to **GP10**. After stirring for 24 h,  $\text{Na}_2\text{EDTA}$  (435  $\mu\text{L}$  0.1 M soln.) was added and the mixture stirred overnight. THF was removed *in vacuo* upon which a brownish oil was formed. Cu-EDTA containing water was decanted, the residue washed with water and  $\text{Et}_2\text{O}$ . The oil was dissolved in acetonitrile/water and lyophilized to give ca. 13 mg of crude material. This was purified by prep. *rp*-HPLC (gradient 3) to give pure **80** (6 mg, 42 %; >95 %purity) as yellow amorphous solid after lyophilization.

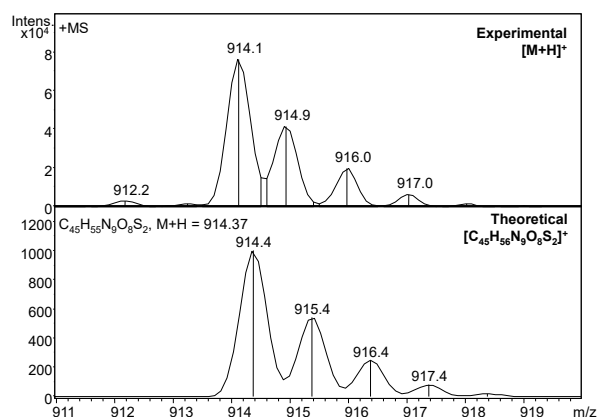
**rp-HPLC** (C18, gradient1):  $t_R = 20.4$  min (> 95 %).

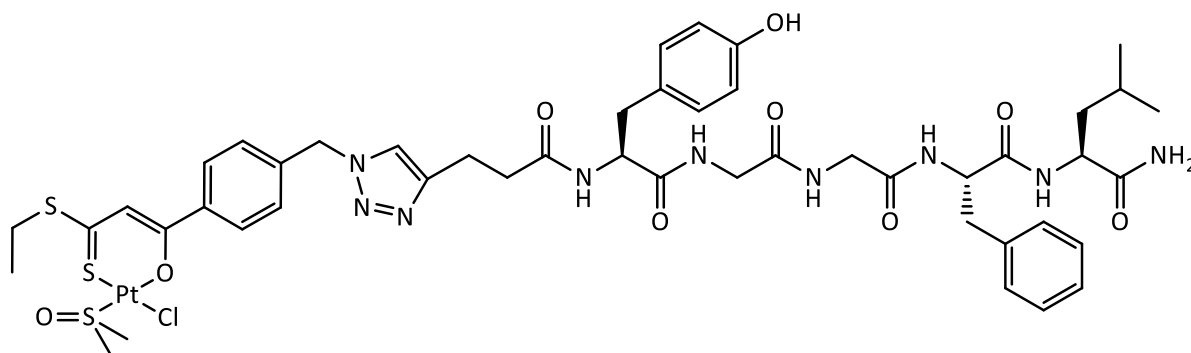
**MS** (ESI+):  $m/z = 914.1$   $[\text{M}+\text{H}]^+$  (calcd. for  $[\text{C}_{45}\text{H}_{56}\text{N}_9\text{O}_8\text{S}_2]^+$ : 914.4).

**$^1\text{H}$  NMR** (400 MHz,  $\text{DMSO-d}_6$ )  $\delta = 15.15$  (s, 1H, (*O,S*): C-OH), 9.13 (s, 1H,  $\text{Y}^1$ : Ar-OH), 8.24 (t,  $^3J_{\text{HH}} = 5.6$  Hz, 1H,  $\text{G}^2$ : -NH-), 8.12 (d,  $^3J_{\text{HH}} = 8.1$  Hz, 1H,  $\text{Y}^1$ : -NH-), 8.04 (d,  $^3J_{\text{HH}} = 8.1$  Hz, 1H,  $\text{F}^4$ : -NH-), 7.99-7.95 (m, 3H,  $\text{G}^3$ : -NH-, (*O,S*): Ar-H2,6), 7.93 (d,  $^3J_{\text{HH}} = 8.4$  Hz, 1H,  $\text{L}^5$ : -NH-), 7.79 (s, 1H,  $\text{PA}^0$ : ta-CH=), 7.38 (d,  $^3J_{\text{HH}} = 8.4$  Hz, (*O,S*): Ar-H3,5), 7.23 (m, 4H,  $\text{F}^4$ : Ar-H2,3,5,6), 7.18 (m, 2H,  $\text{F}^4$ : Ar-H4, (*O,S*): =CH-), 7.00 (d,

$^3J_{HH} = 8.4$  Hz, 2H,  $Y^1$ : Ar-H2,6), 7.00 (d,  $^2J_{HH} = 48.3$  Hz, 2H,  $L^5$ : -NH<sub>2</sub>), 6.62 (d,  $^3J_{HH} = 8.4$  Hz, 2H,  $Y^1$ : Ar-H3,5), 5.60 (s, 2H, (O,S): Ph-CH<sub>2</sub>-N<sup>ta</sup>), 4.51 (dt,  $^3J_{HH} = 8.9$ , 4.6 Hz, 1H,  $F^4$ : CH<sup>α</sup>), 4.42 (dt,  $^3J_{HH} = 9.5$ , 4.7 Hz, 1H,  $Y^1$ : CH<sup>α</sup>), 4.19 (dt,  $^3J_{HH} = 15.2$ , 7.9 Hz, 1H,  $L^5$ : CH<sup>α</sup>), 3.82-3.54 (m, 4H,  $G^2/G^3$ : -CH<sub>2</sub><sup>α</sup>-), 3.27 (m, 2H, (O,S): S-CH<sub>2</sub>-, obscured by SRS), 3.03/2.81 (2m, 2H,  $F^4$ : -CH<sub>2</sub><sup>β</sup>-Ar), 2.92/2.63 (2 m, 2H,  $Y^1$ : -CH<sub>2</sub><sup>β</sup>-Ar), 2.78 (t,  $^3J_{HH} = 8.2$  Hz,  $PA^0$ : -CH<sub>2</sub><sup>β</sup>-), 2.46-2.35 (m, 2H,  $PA^0$ : -CH<sub>2</sub><sup>α</sup>-), 1.63-1.50 (m, 1H,  $L^5$ : -CH<sup>γ</sup>Me<sub>2</sub>), 1.46 (m, 2H,  $L^5$ : -CH<sub>2</sub><sup>β</sup>-), 1.32 (t,  $^3J_{HH} = 7.4$  Hz, 3H, (O,S): -CH<sub>3</sub>), 0.89-0.82 (m, 6H,  $L^5$ : 2 × -CH<sub>3</sub>) ppm. Some signals are partially obscured by solvent residual signals (SRS).

**<sup>13</sup>C NMR** (100 MHz, DMSO-d<sub>6</sub>)  $\delta = 174.4$  ( $L^5$ : C=O), 171.7 ( $Y^1$ : C=O), 170.6 ( $F^4$ : C=O), 171.4 ( $PA^0$ : C=O), 168.8 ( $G^3$ : C=O), 168.7 ( $G^2$ : C=O), 168.5 ((O,S): C-OH), 155.7 ( $Y^1$ : Ar-C4), 146.4 ( $PA^0$ : ta-C<sup>α</sup>), 140.6 ((O,S): Ar-C4), 137.7 ( $F^4$ : Ar-C1), 129.8 (2C,  $Y^1$ : Ar-C2,6), 129.0 ( $PA^0$ : C<sub>q</sub> $\delta =$ ), 128.8 (2C,  $F^4$ : Ar-C3,5), 128.2 ( $Y^1$ : Ar-C1), 128.0 (2C, (O,S): Ar-C3,5), 127.7 (2C,  $F^4$ : Ar-C2,6), 127.1 (2C, (O,S): Ar-C2,6), 125.9 ( $F^4$ : Ar-C4), 122.3 ( $PA^0$ : N-CH=), 121.9 ( $PA^0$ : ta-CH=), 114.6 (2C,  $Y^1$ : Ar-C3,5), 107.4 ((O,S): =CH-), 54.1 ( $Y^1$ : CH<sup>α</sup>), 53.8 ( $F^4$ : CH<sup>α</sup>), 52.1 ((O,S): Ph-CH<sub>2</sub>-N<sup>ta</sup>), 50.7 ( $L^5$ : CH<sup>α</sup>), 42.1 ( $G^2$ : CH<sup>α</sup>), 41.7 ( $G^3$ : CH<sup>α</sup>), 40.7 ( $L^5$ : CH<sub>2</sub><sup>β</sup>), 37.1 ( $F^4$ : CH<sub>2</sub><sup>β</sup>-Ar), 36.3 ( $Y^1$ : CH<sub>2</sub><sup>β</sup>-Ar), 34.3 ( $PA^0$ : -CH<sup>α</sup>-), 27.1 ((O,S): S-CH<sub>2</sub>-), 23.9 ( $L^5$ : CH<sup>γ</sup>), 22.9 ( $L^5$ : CH<sub>3</sub>), 21.4 ( $L^5$ : CH<sub>3</sub>), 21.0 ( $PA^0$ : -CH<sub>2</sub><sup>β</sup>-), 12.6 ((O,S): -CH<sub>3</sub>) ppm. Data of <sup>13</sup>C NMR obtained indirectly from HSQC and HMBC experiments. Expected signal of (O,S)-CS<sub>2</sub> (above 200 ppm) not within spectral range.



Enk-(O,S)Pt(DMSO)Cl from **80** (**81**)

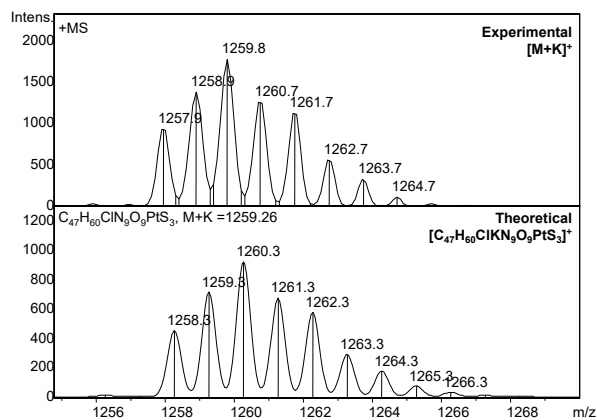
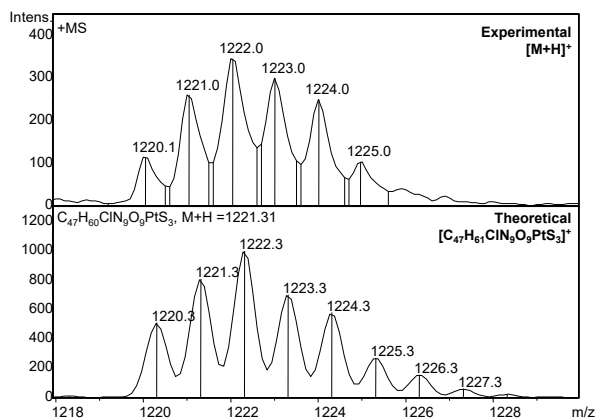
**80** (1.3 mg, 1.4  $\mu\text{mol}$ ) was reacted with  $\text{K}_2\text{PtCl}_4$  (28  $\mu\text{L}$  0.1 M soln.) in presence of DMSO (50  $\mu\text{L}$ ) and NaOAc (14  $\mu\text{L}$  0.1 M soln.) according to **GP11**. The desired compound was obtained as yellow-orange solid (1.8 mg, 100 %).

**MS** (ESI+):  $m/z = 1259.8$   $[\text{M}+\text{K}]^+$  (calcd. for  $[\text{C}_{47}\text{H}_{60}\text{ClKN}_9\text{O}_9\text{PtS}_3]^+$ : 1260.3 / highest peak), 1243.9  $[\text{M}+\text{Na}]^+$  (calcd. for  $[\text{C}_{47}\text{H}_{60}\text{ClN}_9\text{O}_9\text{PtS}_3]^+$ : 1244.3 / highest peak), 1222.0  $[\text{M}+\text{H}]^+$  (calcd. for  $[\text{C}_{47}\text{H}_{61}\text{ClN}_9\text{O}_9\text{PtS}_3]^+$ : 1222.3 / highest peak).

**$^1\text{H}$  NMR** (400 MHz, DMSO- $d_6$ )  $\delta = 9.13$  (s, 1H,  $\text{Y}^1$ : Ar-OH), 8.24 (t,  $^3J_{\text{HH}} = 5.5$  Hz, 1H,  $\text{G}^2$ : -NH-), 8.12 (d,  $^3J_{\text{HH}} = 8.1$  Hz, 1H,  $\text{Y}^1$ : -NH-), 8.05 (d,  $^3J_{\text{HH}} = 8.1$  Hz, 1H,  $\text{F}^4$ : -NH-), 8.00-7.95 (m, 4H,  $\text{G}^3$ : -NH-,  $\text{L}^5$ : -NH-, (O,S): Ar-H<sub>2,6</sub>), 7.78 (s, 1H,  $\text{PA}^0$ : ta-CH=), 7.35 (d,  $^3J_{\text{HH}} = 8.3$  Hz, (O,S): Ar-H<sub>3,5</sub>), 7.24-7.23 (m, 5H,  $\text{F}^4$ : Ar-H<sub>2,3,5,6</sub>, (O,S): =CH-), 7.17 (m, 1H,  $\text{F}^4$ : Ar-H<sub>4</sub>), 7.00 (d,  $^3J_{\text{HH}} = 8.4$  Hz, 2H,  $\text{Y}^1$ : Ar-H<sub>2,6</sub>), 7.00 (d,  $^2J_{\text{HH}} = 48.0$  Hz, 2H,  $\text{L}^5$ : -NH<sub>2</sub>), 6.62 (d,  $^3J_{\text{HH}} = 8.3$  Hz, 2H,  $\text{Y}^1$ : Ar-H<sub>3,5</sub>), 5.56 (s, 2H, (O,S): Ph-CH<sub>2</sub>-N<sup>ta</sup>), 4.51 (dt,  $^3J_{\text{HH}} = 8.9$ , 4.7 Hz, 1H,  $\text{F}^4$ : CH $^\alpha$ ), 4.42 (dt,  $^3J_{\text{HH}} = 9.3$ , 4.6 Hz, 1H,  $\text{Y}^1$ : CH $^\alpha$ ), 4.19 (dt,  $^3J_{\text{HH}} = 15.2$ , 7.8 Hz, 1H,  $\text{L}^5$ : CH $^\alpha$ ), 3.77-3.49 (m, 4H,  $\text{G}^2/\text{G}^3$ : -CH<sub>2</sub> $^\alpha$ -), 3.26 (m, 2H, (O,S): S-CH<sub>2</sub>-, obscured by SRS), 3.03/2.79 (2m, 2H,  $\text{F}^4$ : -CH<sub>2</sub> $^\beta$ -Ar), 2.92/2.65 (2 m, 2H,  $\text{Y}^1$ : -CH<sub>2</sub> $^\beta$ -Ar), 2.76 (m, 2H,  $\text{PA}^0$ : -CH<sub>2</sub> $^\beta$ -), 2.46-2.35 (m, 4H,  $\text{PA}^0$ : -CH<sub>2</sub> $^\alpha$ -), 1.60-1.50 (m, 1H,  $\text{L}^5$ : -CH $^\gamma$ Me<sub>2</sub>), 1.46 (m, 2H,  $\text{L}^5$ : -CH<sub>2</sub> $^\beta$ -), 1.32 (t,  $^3J_{\text{HH}} = 7.3$  Hz, 3H, (O,S): -CH<sub>3</sub>), 0.87-0.81 (m, 6H,  $\text{L}^5$ : 2  $\times$  -CH<sub>3</sub>) ppm. Some signals are partially obscured by solvent residual signals (SRS). DMSO signal not detected due to substitution by DMSO- $d_6$ .

**$^{13}\text{C}$  NMR** (100 MHz, DMSO- $d_6$ )  $\delta = 180.0$  ((O,S): CS<sub>2</sub>), 173.5 ( $\text{L}^5$ : C=O), 173.2 ((O,S): C-O<sub>2</sub>), 171.9 ( $\text{Y}^1$ : C=O), 170.7 ( $\text{F}^4$ : C=O), 171.5 ( $\text{PA}^0$ : C=O), 168.9 ( $\text{G}^2$ : C=O), 168.4 ( $\text{G}^3$ : C=O), 155.6 ( $\text{Y}^1$ : Ar-C<sub>4</sub>), 146.4 ( $\text{PA}^0$ : ta-C $^\alpha$ ), 140.9 ((O,S): Ar-C<sub>4</sub>), 137.7 ( $\text{F}^4$ : Ar-C<sub>1</sub>), 129.8 (2C,  $\text{Y}^1$ : Ar-C<sub>2,6</sub>), 129.1 ( $\text{PA}^0$ : C $^\alpha$ ), 128.8 (2C,  $\text{F}^4$ : Ar-C<sub>3,5</sub>), 128.0 (2C, (O,S): Ar-C<sub>3,5</sub>), 128.0 ( $\text{Y}^1$ : Ar-C<sub>1</sub>), 127.7 (2C,  $\text{F}^4$ : Ar-C<sub>2,6</sub>), 127.1 ((O,S): Ar-C<sub>2,6</sub>), 126.1 ( $\text{F}^4$ : Ar-C<sub>4</sub>), 122.3 ( $\text{PA}^0$ : N-CH=), 121.8 ( $\text{PA}^0$ : ta-CH=), 114.6 (2C,  $\text{Y}^1$ : Ar-C<sub>3,5</sub>), 110.7 ((O,S): =CH-), 54.1 ( $\text{Y}^1$ : CH $^\alpha$ ), 53.7 ( $\text{F}^4$ : CH $^\alpha$ ), 52.1 ((O,S): Ph-CH<sub>2</sub>-N<sup>ta</sup>), 50.7 ( $\text{L}^5$ : CH $^\alpha$ ), 41.7 ( $\text{G}^2$ : CH $^\alpha$ ), 41.6 ( $\text{G}^3$ : CH $^\alpha$ ), 40.7 ( $\text{L}^5$ : CH<sub>2</sub> $^\beta$ ), 37.1 ( $\text{F}^4$ : CH<sub>2</sub> $^\beta$ -Ar), 36.3 ( $\text{Y}^1$ : CH<sub>2</sub> $^\beta$ -Ar), 34.4 ( $\text{PA}^0$ : -CH $^\alpha$ -), 27.9 ((O,S): S-CH<sub>2</sub>-), 23.9

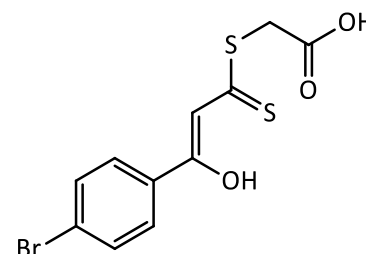
(L<sup>5</sup>: CH<sup>v</sup>), 22.0 (L<sup>5</sup>: CH<sub>3</sub>), 21.4 (L<sup>5</sup>: CH<sub>3</sub>), 21.0 (PA<sup>0</sup>: -CH<sub>2</sub><sup>θ</sup>-), 13.0 ((O,S): -CH<sub>3</sub>) ppm. Data of <sup>13</sup>C NMR obtained indirectly from HSQC and HMBC experiments.



## 16.7 Bioconjugates via amide bonds

### 4-Bromo- $\beta$ -hydroxydithiocinnamic acid $\beta'$ -carboxyethane (**82**)

The reaction was carried out by following **GP3** and using 4-Bromo acetophenone **6** (1.99g; 10 mmol), CS<sub>2</sub> (844  $\mu$ L; 14 mmol), KO<sup>t</sup>Bu (2.24 g; 20 mmol), and bromoacetic acid (1.25 g, 9 mmol). After phase separation of the reaction mixture, extraction with dichloromethane and drying over NaSO<sub>4</sub>, the crude product was recrystallized from chloroform and **82** (1.6 g, 53 %) obtained as yellow crystalline material.



Crystals suitable for X-ray characterization were obtained by slow evaporation of acetone from the NMR sample.

**Analysis** calcd. for C<sub>11</sub>H<sub>9</sub>BrO<sub>3</sub>S<sub>2</sub>: C, 39.65; H, 2.72; S, 19.25; found C, 39.57; H, 2.72; S 19.19 %.

**<sup>1</sup>H NMR** (200 MHz, Acetone-d<sub>6</sub>)  $\delta$  = 15.02 (s, 1H, OH), 7.98 (d, <sup>3</sup>J<sub>HH</sub> = 8.9 Hz, 2H, Ar-H3, Ar-H3), 7.73 (d, <sup>3</sup>J<sub>HH</sub> = 8.9 Hz, 2H, Ar-H2, Ar-H6), 7.26 (s, 1H, =CH-), 4.22 (s, 2H, S-CH<sub>2</sub>-) ppm.

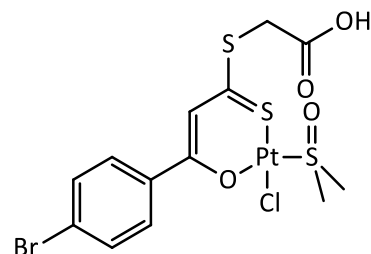
**<sup>13</sup>C NMR** (63 MHz, Acetone-d<sub>6</sub>)  $\delta$  = 217.10 (CS<sub>2</sub>), 169.82 (COH), 168.68 (COOH), 133.87 (Ar-C1), 133.10 (2C, Ar-C3, Ar-C5), 129.57 (2C, Ar-C2, Ar-C4), 127.40 (Ar-C4), 108.35 (=CH-), 36.44 (S-CH<sub>2</sub>-) ppm.

**MS** (DEI):  $m/z$  = 332/334 [M/M+2]<sup>+</sup>, 241/243 [M-SCH<sub>2</sub>COOH]<sup>+</sup>, 183/185.

**IR** (ATR):  $\tilde{\nu}$  = 2916 (w), 1715 (m), 1578 (m), 1553 (m), 1515 (w), 1481 (m), 1415 (m), 1353 (w), 1275 (m), 1234 (s), 1160 (s), 1110 (w), 1073 (m), 1056 (m), 1007 (m), 948 (vs), 867 (m), 824 (vs), 762 (vs) cm<sup>-1</sup>.

**Chloro-(4-(bromo)- $\beta$ -hydroxydithiocinnamic acid  $\beta'$ -carboxyethane-O,S)-  
(dimethylsulfoxide-S)- platinum(II) (83)**

$K_2PtCl_4$  (130 mg, 0.31 mmol) was dissolved in water (2 mL) stirred for 30 min in presence of DMSO (60  $\mu$ L, 0.84 mmol). **82** (80 mg, 0.24 mmol), dissolved in THF (40 mL), was added slowly and the mixture stirred at r.t. for 2 days. THF was removed and an orange precipitate formed. Extraction from DCM was not completely able to dissolve all precipitate.



Solids were filtered, dissolved in acetone and the combined organic solutions concentrated *in vacuo*. The residue was carefully dissolved in a minimum amount of acetone/water and lyophilized to give an orange powder alongside with a dark residue. This was removed manually and the desired complex (109 mg, 70 %) isolated.

$^1H$  NMR (200 MHz, Acetone- $d_6$ )  $\delta$  = 8.05 (d,  $^3J_{HH}$  = 8.9 Hz, 2H, Ar-H3, Ar-H3), 7.71 (d,  $^3J_{HH}$  = 8.9 Hz, 2H, Ar-H2, Ar-H6), 7.38 (s, 1H, =CH-), 4.20 (s, 2H, SCH<sub>2</sub>), 3.68 (s,  $^3J_{HH}$  = 24.6 Hz, 6H, CH<sub>3</sub> (DMSO)) ppm.

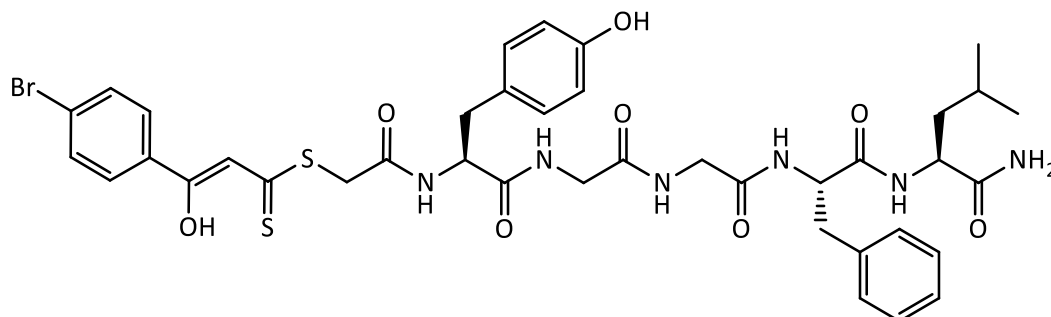
$^1H$  NMR (400 MHz, THF- $d_8$ )  $\delta$  = 7.99 (d,  $^3J_{HH}$  = 8.7 Hz, 2H, Ar-H3, Ar-H3), 7.60 (d,  $^3J_{HH}$  = 8.7 Hz, 2H, Ar-H3, Ar-H3), 7.28 (s, 1H, =CH-), 4.08 (s, 2H, SCH<sub>2</sub>), 3.61 (s, 6H, CH<sub>3</sub> (DMSO)) ppm.

$^{13}C$  NMR (101 MHz, THF)  $\delta$  = 180.53 (CS<sub>2</sub>), 174.35 (COPt), 168.81 (COOH), 137.40 (Ar-C1), 132.89 (2C, Ar-C2, Ar-C6), 130.65 (2C, Ar-C3, Ar-C5), 127.50 (Ar-C4), 111.86 (=CH-), 46.70 (2C, CH<sub>3</sub>(DMSO)), 37.19 (S-CH<sub>2</sub>-) ppm.

**MS** (ESI+): could not be obtained.

**IR** (ATR):  $\tilde{\nu}$  = 3013 (w), 2965 (w) 2927 (w), 1725 (m), 1680 (m), 1583 (m), 1507 (s), 1481 (s), 1458 (s), 1407 (m), 1385 (m), 1280 (m), 1258 (m), 1246 (m), 1168 (s), 1142 (s), 1113 (s), 1071 (s), 1010 (vs), 978 (s), 892 (m), 832 (s), 784 (vs)  $cm^{-1}$ .



Coupling of **82** with Enk **75** in solution (**84**)

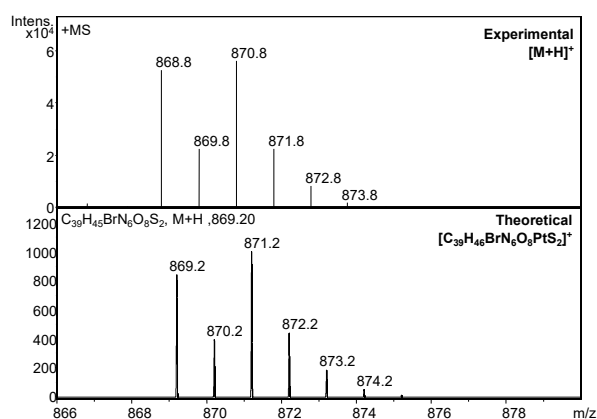
By LPSS following **GP13**, compound **82** (6.6 mg, 19.8  $\mu\text{mol}$ ) and Enk **75** (10 mg, 18.0  $\mu\text{mol}$ ) were coupled using TBTU (6.3 mg, 19.8  $\mu\text{mol}$ ) and *D*'PEA (6.7  $\mu\text{L}$ , 41  $\mu\text{mol}$ ) in DMF (600  $\mu\text{L}$ ). The reaction mixture was diluted with  $\text{CH}_3\text{CN}$ /water and directly subjected to semiprep. HPLC (gradient 1) in several portions. Pure **84** was obtained as yellow powder (6 mg, 38 %).

**rp-HPLC** (C8, gradient1):  $t_R = 18.9$  min (>95 %).

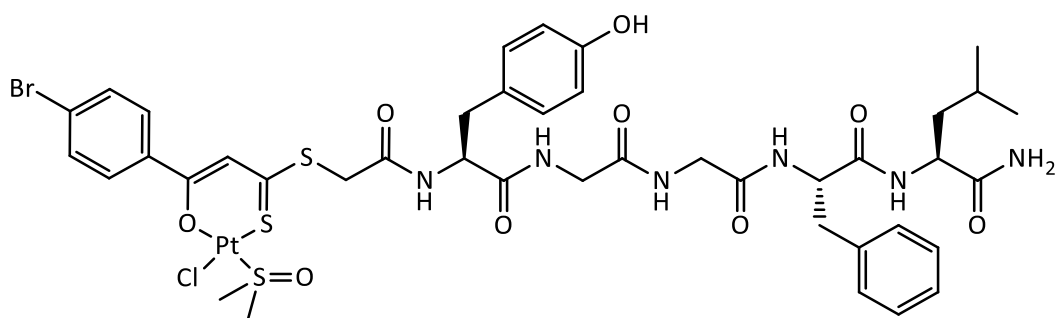
**rp-HPLC** (C18, gradient1):  $t_R = 20.5$  min (> 95%).

**MS** (ESI+):  $m/z = 906.7/908.7$   $[\text{M}+\text{K}]^+$ ,  $890.8/892.8$   $[\text{M}+\text{Na}]^+$ ,  $868.8/870.8$   $[\text{M}+\text{H}]^+$  (calcd. for  $[\text{C}_{39}\text{H}_{46}\text{BrN}_6\text{O}_8\text{PtS}_2]^+$ : 869.2),  $851.8/853.8$   $[\text{M}-\text{NH}_2]$ .

**$^1\text{H}$  NMR** (400 MHz,  $\text{THF-d}_8$ )  $\delta = 14.97$  (s, 1H, (O,S): C-OH), 10.74 (s, 1H,  $\text{Y}^1$ : Ar-OH), 8.20 (d,  $^3J_{\text{HH}} = 6.9$  Hz,  $\text{Y}^1$ : -NH-), 8.09 (t,  $^3J_{\text{HH}} = 5.5$  Hz,  $\text{G}^2$ : -NH-), 7.91 (d,  $^3J_{\text{HH}} = 8.7$  Hz, 2H, (O,S): Ar-H2,6), 7.65 (d,  $^3J_{\text{HH}} = 8.7$  Hz, 2H, (S,O): Ar-H3,5), 7.54 (m, 2H,  $\text{G}^3/\text{F}^4$ : -NH-), 7.42 (d,  $^3J_{\text{HH}} = 7.3$  Hz,  $\text{L}^5$ : -NH-), 7.23 (m, 4H,  $\text{F}^4$ : Ar-H1,2,4,5), 7.17 (s, 1H, (O,S): =CH-), 7.13 (m, 1H,  $\text{F}^4$ : Ar-H3), 7.01 (d,  $^3J_{\text{HH}} = 8.4$  Hz, 2H,  $\text{Y}^1$ : Ar-H2,6), 6.64 (d+s,  $^3J_{\text{HH}} = 8.4$  Hz, 3H,  $\text{Y}^1$ : Ar-H3,5,  $\text{L}^5$ : -NH<sub>2</sub>), 6.33 (s, 1H,  $\text{L}^5$ : -NH<sub>2</sub>), 4.63 (dd,  $^3J_{\text{HH}} = 13.5$ , 7.9 Hz, 1H,  $\text{F}^4$ : CH), 4.43 (m, 2H,  $\text{Y}^1/\text{L}^5$ : CH); 4.11 (dd, 2H,  $^1J_{\text{HH}} = 34.0$  Hz,  $^3J_{\text{HH}} = 15.2$  Hz, (O,S): S-CH<sub>2</sub>-), 3.88-3.62 (m, 4H,  $\text{G}^2/\text{G}^3$ : -CH<sub>2</sub>-), 3.17, 3.00, 2.89 (m, 4 H,  $\text{Y}^1/\text{F}^4$ : -CH<sub>2</sub>-Ar), 1.59 (m, 3H,  $\text{L}^5$ : -CH<sub>2</sub>-CHMe<sub>2</sub>), 0.88 (m, 6H,  $\text{L}^5$ : 2  $\times$  -CH<sub>3</sub>) ppm.



### Enk-(O,S)Pt(DMSO)Cl from 84 (85)

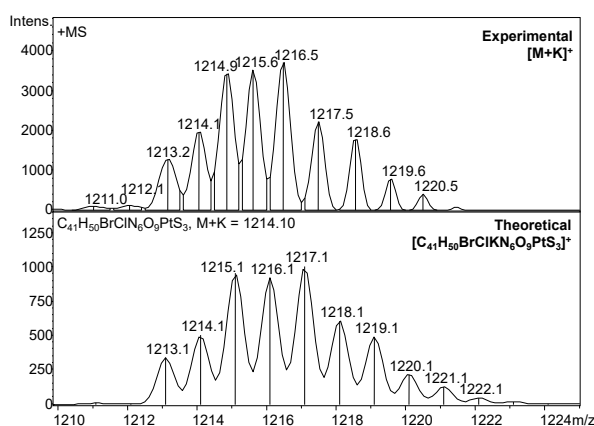


**CM159** (2 mg, 2.3  $\mu\text{mol}$ ) was reacted with  $\text{K}_2\text{PtCl}_4$  (46  $\mu\text{L}$  0.1 M soln.) in presence of DMSO (50  $\mu\text{L}$ ) and NaOAc (23  $\mu\text{L}$  0.1 M soln.) according to **GP11**. The desired compound was obtained as orange solid (1.4 mg, 52 %).

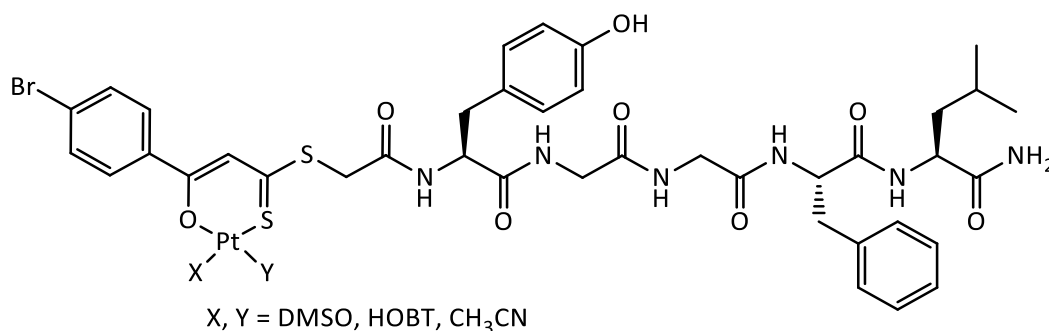
**rp-HPLC** (C18, gradient1):  $t_r = 18.9$  min (under solvolysis of Cl/DMSO ligands).

**MS** (ESI+):  $m/z = 1214.9$   $[\text{M}+\text{K}]^+$  (calcd. for  $[\text{C}_{41}\text{H}_{50}\text{BrClKN}_6\text{O}_9\text{PtS}_3]^+$ : 1215.1 / first high peak), 1198.8  $[\text{M}+\text{Na}]^+$  (calcd. for  $[\text{C}_{41}\text{H}_{50}\text{BrClNaN}_6\text{O}_9\text{PtS}_3]^+$ : 1199.1 / first high peak).

**$^1\text{H NMR}$**  (400 MHz,  $\text{THF-d}_8$ )  $\delta = 10.80$  (s, 1H,  $\text{Y}^1$ : Ar-OH), 8.32 (d, 1H,  $^3J_{\text{HH}} = 6.9$  Hz,  $\text{Y}^1$ : -NH-), 8.02 (d,  $^3J_{\text{HH}} = 8.6$  Hz, 2H, (O,S): Ar-H2,6), 7.93 (t,  $^3J_{\text{HH}} = 5.6$  Hz,  $\text{G}^2$ : -NH-), 7.60 (d,  $^3J_{\text{HH}} = 8.6$  Hz, 2H, (O,S): Ar-H3,5), 7.50 (m, 2H,  $\text{G}^3/\text{F}^4$ : -NH-), 7.39 (d,  $^3J_{\text{HH}} = 7.3$  Hz,  $\text{L}^5$ : -NH-), 7.34 (s, 1H, (O,S): =CH-), 7.24 (m, 4H,  $\text{F}^4$ : Ar-H1,2,4,5), 7.14 (m, 1H,  $\text{F}^4$ : Ar-H3), 7.02 (d,  $^3J_{\text{HH}} = 8.3$  Hz, 2H,  $\text{Y}^1$ : Ar-H2,6), 6.65 (d+s,  $^3J_{\text{HH}} = 8.4$  Hz, 3H,  $\text{Y}^1$ : Ar-H3,5,  $\text{L}^5$ : -NH<sub>2</sub>), 6.29 (s, 1H,  $\text{L}^5$ : -NH<sub>2</sub>), 4.63 (dd,  $^3J_{\text{HH}} = 13.4, 7.9$  Hz, 1H,  $\text{F}^4$ : CH), 4.43 (m, 2H,  $\text{Y}^1/\text{L}^5$ : CH); 4.06 (dd, 2H,  $^1J_{\text{HH}} = 28.0$  Hz,  $^3J_{\text{HH}} = 16.0$  Hz, (O,S): S-CH<sub>2</sub>-), 3.83 (m, 4H,  $\text{G}^2/\text{G}^3$ : -CH<sub>2</sub>-), 3.76, 3.62 (CH<sub>3</sub> (DMSO), obscured by SRS but observed through HSQC) 3.17, 3.12-2.87 (m, 4 H,  $\text{Y}^1/\text{F}^4$ : -CH<sub>2</sub>-Ar), 1.62 ( $\text{L}^5$ : -CH<sub>2</sub>-CHMe<sub>2</sub>, obscured by SRS), 0.89 (m, 6H,  $\text{L}^5$ : 2  $\times$  -CH<sub>3</sub>) ppm.



### Coupling of **83** with Enk **75** in solution (**86**)



**83** (12.7 mg, 19.8  $\mu\text{mol}$ ) and Enk **75** (10 mg, 18  $\mu\text{mol}$ ) were coupled using TBTU (6.3 mg, 19.8  $\mu\text{mol}$ ) and D'PEA (6.7  $\mu\text{L}$ , 41  $\mu\text{mol}$ ) in DMF (600  $\mu\text{L}$ ) by LPSS, following **GP13**. Precipitation from Et<sub>2</sub>O/*n*-hexane merely gave a turbid solution and an orange slurry, therefore the volatile solvents were removed *in vacuo*, precipitation achieved by addition of 4 mL water. After centrifugation, repeated washing and lyophilization, an oily residue was obtained which could, as such, not be analyzed through ESI mass spectrometry. It was therefore subjected to repeated semiprep. HPLC (gradient 3, gradient 4) and the resulting fractions lyophilized. Due to partial solvolysis during HPLC runs, no pure fractions were obtained. The components of the two main fractions were identified by their ESI mass spectral profile and were found to contain the Enk-bound (O,S) unit coordinated towards Pt(II) with varying combinations of the monodentate ligands DMSO, Cl, CH<sub>3</sub>CN and HOBT.

**rp-HPLC** (C8, gradient1):  $t_R = 19.0$  min:

**MS** (ESI+): (19.0 min)  $m/z = 1197.6$  [(O,S)Pt(HOBT)]<sup>+</sup>, 1140.9 [(O,S)Pt(DMSO)]<sup>+</sup>, 1103.7 [(O,S)Pt(CH<sub>3</sub>CN)]<sup>+</sup>, 1063.0 [(O,S)Pt]<sup>+</sup>. Selected simulations below.

**rp-HPLC** (C8, gradient1):  $t_R = 19.8$  min:

**MS (ESI+):** (19.8 min)  $m/z = 1275$  [(O,S)Pt(DMSO)(HOBT)]<sup>+</sup>, 1238 [(O,S)Pt(CH<sub>3</sub>CN)(HOBT)]<sup>+</sup>, 1197 [(O,S)Pt(HOBT)]<sup>+</sup>, 1140[(O,S)Pt(DMSO)]<sup>+</sup>, 1103[(O,S)Pt(CH<sub>3</sub>CN)]<sup>+</sup>, 1063[(O,S)Pt]<sup>+</sup>. Selected simulations below.

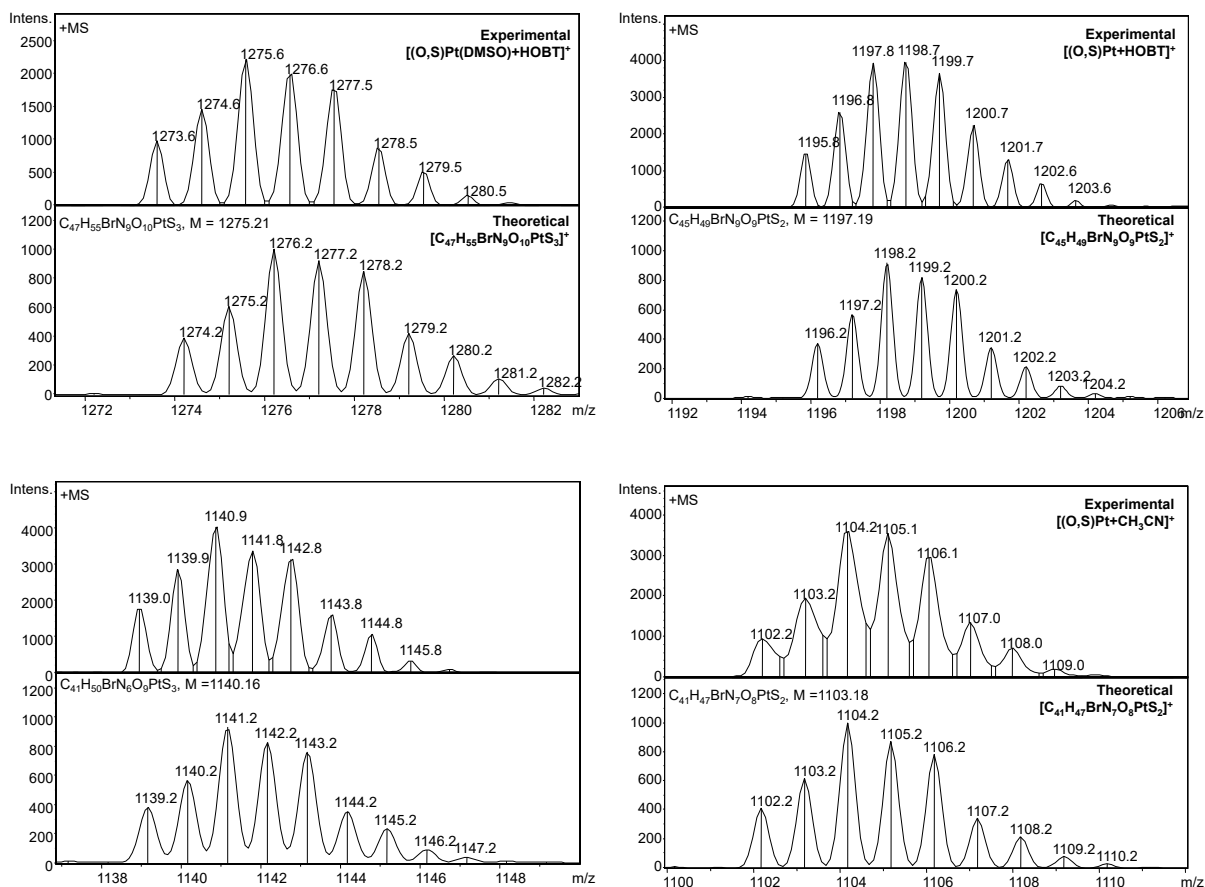
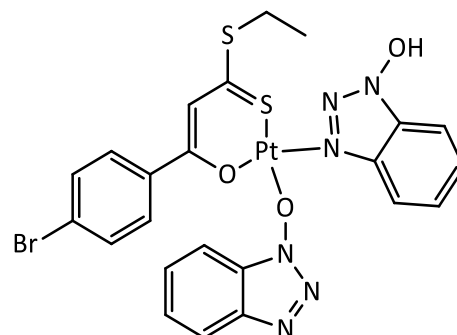


Figure 54 representative ESI+ MS spectra of fractions of compound 86.

### Conversion of **34** with HOBt: (O,S)Pt(HOBt)<sub>2</sub> (**87**)

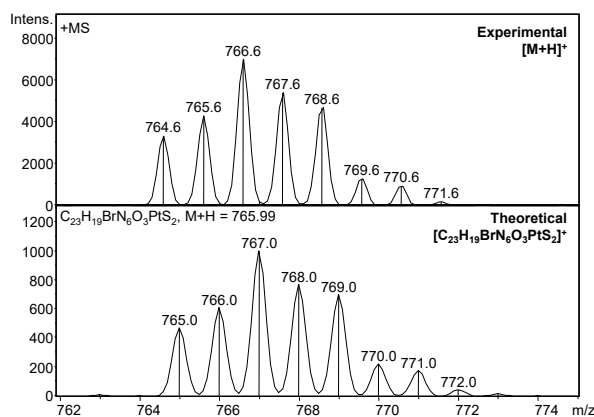
Compound **34** (20 mg, 32.7 μmol) was stirred in DMF (2 mL) in presence of HOBt (8.9 mg, 65.5 μmol) at r.t. for 3 days. The solvent was removed *in vacuo*, and the crude material purified *via* column chromatography on silica gel using a gradient (mobile phase: DCM – acetone – EtOH). The fraction collected in pure ethanol was crystallized from DCM/*n*-hexane to obtain a yellow precipitate.



**MS** (ESI-pos):  $m/z = 766.6$  [M+H]<sup>+</sup> (calcd. for [C<sub>23</sub>H<sub>20</sub>BrN<sub>6</sub>O<sub>3</sub>PtS<sub>2</sub>]<sup>+</sup>: 767.0 / highest peak), 631.6 [M-HOBt]<sup>+</sup> (calcd. for [C<sub>17</sub>H<sub>15</sub>BrN<sub>3</sub>O<sub>2</sub>PtS<sub>2</sub>]<sup>+</sup>: 631.9 / highest peak).

**MS** (ESI-neg):  $m/z = 764.6$  [M-H]<sup>-</sup> (calcd. for [C<sub>23</sub>H<sub>18</sub>BrN<sub>6</sub>O<sub>3</sub>PtS<sub>2</sub>]<sup>-</sup>: 764.9 / highest peak).

**<sup>1</sup>H NMR** (200 MHz, MeOD)  $\delta = 8.03 - 7.79$  (m, 1H, Ar-H), 7.79 – 7.38 (m, 8H, Ar-H), 7.36 – 7.09 (m, 4H, Ar-H, =CH-), 3.20 (q, <sup>3</sup>J<sub>HH</sub> = 7.4 Hz, 2H, S-CH<sub>2</sub>-), 1.39 (t, <sup>3</sup>J<sub>HH</sub> = 7.4 Hz, 3H, -CH<sub>3</sub>) ppm.



## 16.8 NMR-based test of stability under cleaving conditions (TFA)

For peptide cleavage from resin, 95 % TFA is frequently used as reagent. It is not possible to collect well-resolved  $^1\text{H}$  NMR spectra under these conditions, thus a lower concentration of TFA was chosen for overview spectra. **34** (10 mg), as a representative compound, was dissolved in  $\text{CD}_2\text{Cl}_2$  (450  $\mu\text{L}$ ) and the  $^1\text{H}$  NMR spectrum (200 MHz, NS = 128) recorded at room temperature. TFA (500  $\mu\text{L}$ ) was added and after short mixing, the  $^1\text{H}$  NMR spectrum was recorded again. In a series of measurements,  $^1\text{H}$  NMR spectra were then recorded at r.t. over the course of 20 h in 10 min intervals, starting from 40 min after TFA addition (instrumental problems prevented an earlier start of data recording).

Decomposition set in after a short period, visible *e.g.* by loss of the Pt-DMSO signal, shift of the S-CH<sub>3</sub> signal and loss of Ar-H and =CH- signals. A half-life of max. 2 h in presence of ca. 50 % TFA can be assumed.

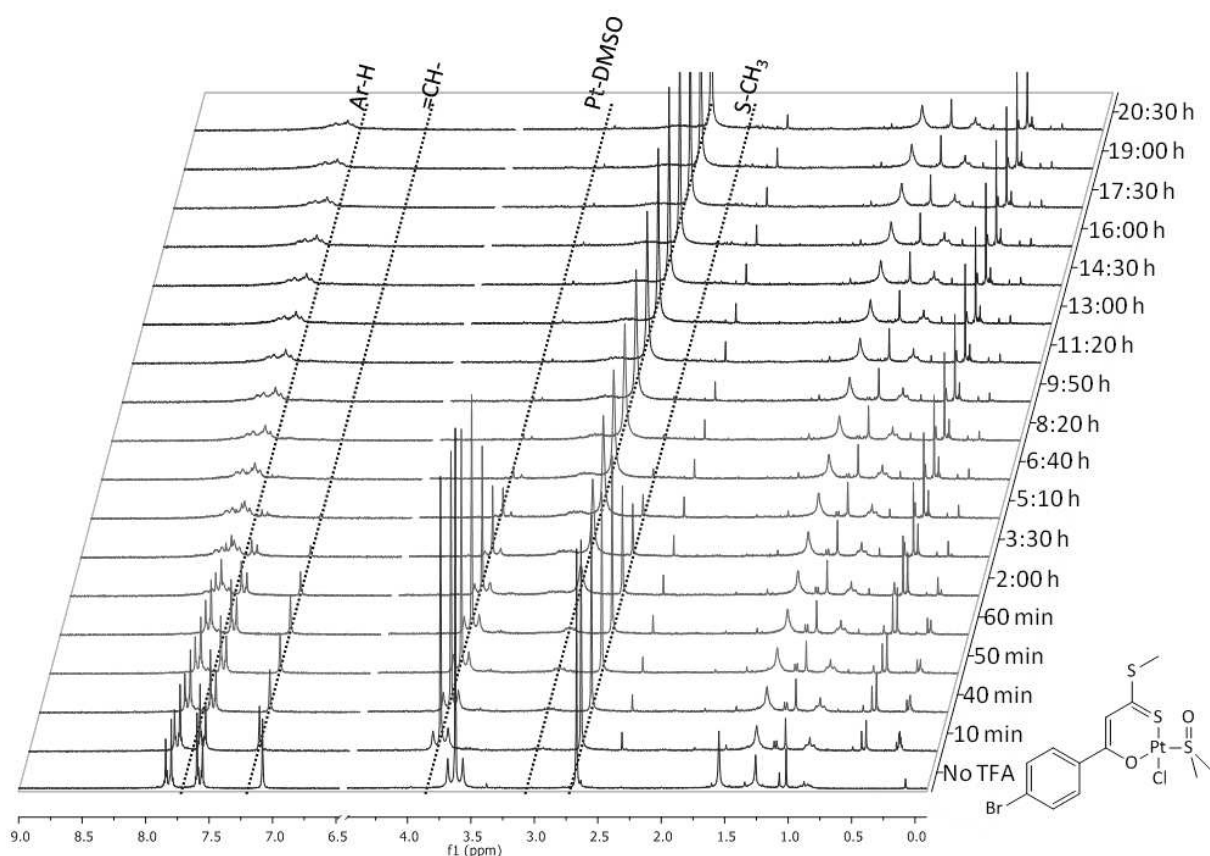


Figure 55 Time development of the  $^1\text{H}$  NMR spectrum of **34** in the presence of 50 % TFA. First spectrum (red), no TFA added; second spectrum (dark orange), recorded after addition of TFA and short shaking,  $t = 10$  min. third (light orange) and following spectra, time series started 40 min after addition of TFA. Every 10<sup>th</sup> recorded spectrum is given up to a final recording time of 20 h. Cut-out: intrinsic signal of  $\text{CD}_2\text{Cl}_2$  was cut out for better visibility (range: 4.5 – 6.5 ppm).

## 17 BEHAVIOR OF THE COMPOUNDS IN SOLUTION

### 17.1 UV-visible spectroscopy of compound 30

#### Stability studies

Buffered solutions used were: phosphate buffer (PB, 10 mM or 50 mM, pH 7.4), tetramethyl ammonium acetate (TMAA, 25 mM, pH 7.4), or sodium acetate (AmAc, 20 mM, pH 6.8)

#### Long-term solubility

Compound **30**, selected as a reference compound, was subjected to UV-visible spectrophotometry in different solvent combinations. The stock solution was prepared at 10 mM in DMSO. 100  $\mu$ L aliquots were added to different solvent combinations to give a final drug concentration of 1 mM in pure DMSO, DMSO/water (10/90 % v/v and 50/50 % v/v) and DMSO/PB (10/90 % v/v and 50/50 % v/v). The samples were kept at room temperature and UV-vis spectra periodically recorded at the indicated times (*i.e.*, 0 h, 24 h, 48 h, 72 h, 96 h). For this, 100  $\mu$ L aliquots were diluted to 100  $\mu$ M in DMSO in 10 mm quartz cuvettes. Data acquisition was performed in the range of 200-800 nm.

#### Hydrolysis studies

A stock solution of **30** (10 mM in DMSO) was diluted to 1 mM in DMSO or DMSO/water 50/50 % v/v. A 100-fold excess of AgNO<sub>3</sub> (1 M in DMSO) was added, the mixture diluted to 100  $\mu$ M in the respective solvent combination and UV-vis spectra recorded in the range of 200-800 nm before AgNO<sub>3</sub> addition and immediately afterwards.

### Hydrolysis studies over 24 h

A Stock solution of **30** (10 mM in DMSO) was diluted to 100  $\mu\text{M}$  in DMSO or DMSO/PB (50/50 resp. 10/90 % v/v). UV-visible spectra were recorded over a period of 24 h at r.t. in 10 mm quartz cuvettes in the range of 200-800 nm, using 1 min intervals during the first 10 min, 10 min intervals up to 1 h and hourly intervals afterwards.

## 17.2 Determination of $\text{Log}P_{o/w}$ values through the shake-flask method

For determination of  $\text{Log}P$  values by the shake-flask method, mQ water and *n*-octanol (ACS reagent grade, Acros) were presaturated through vigorous stirring for a minimum time of 48 h and the phases allowed to separate for at least 24 h to ensure complete phase separation.

Stock **solutions** of the compounds under investigation were prepared at 500  $\mu\text{M}$  in presaturated *n*-octanol and diluted to a final concentration of 50  $\mu\text{M}$  in the same solvent. The solutions were then combined with presaturated water in 1500  $\mu\text{L}$  micro reaction tubes. Three mixtures for each compound were prepared with *n*-octanol/water ratios of 2:1, 1:1 and 1:2 (v/v) at a final volume of 1200  $\mu\text{L}$  (*i.e.*, 800/400, 600/600 and 400/800  $\mu\text{L}$  *n*-octanol/water volumes). The mixtures were rigorously mixed ("vortexed", 10 s) and then vigorously shaken on a laboratory shaker for 60 min to enable saturation of both phases with substance, and subsequently centrifugated (10 min at 10.300 g) to separate the phases. Of each sample, both phases were then sampled carefully to avoid cross-contamination and triplicate 100  $\mu\text{L}$  aliquots of each phase transferred onto a 96-well plate. In addition, blanks of water and *n*-octanol were always included.

Samples were generally transferred using manual pipettes and 200  $\mu\text{L}$  tips. *n*-Octanol presents enhanced adhesion towards standard tips and therefore, uptake and release of sample was performed slowly and the sample volume was released several times into the respective new container. For each sample and phase, a new tip was used to avoid cross-contamination of the phases or compounds.

**UV-visible spectra** were recorded between 230 and 600 nm using a plate reader. Spectra were recorded three times and averaged. Spectral data of the triplicate aliquots was then averaged and baseline corrected.  $P_{o/w}$  values were then calculated from the three individual volume ratio experiments, using the average absorbance values of the *n*-octanol and water phases from 300-



500 nm. The overall  $\log P_{o/w}$  value was then calculated from the average out of three individual  $P_{o/w}$  values using equation 3.

$$\begin{aligned} \log P_{o/w} \text{ value} &= \lg \left( \frac{c_{oct}}{c_{water}} \right) \\ &= \lg \left( \frac{A_{oct}^{300-500nm}}{A_{water}^{300-500nm}} \right) \end{aligned}$$

$P_{o/w}$	octanol-water partition coefficient
$c_x$	concentration resp. phase
$A_x^{300-500nm}$	average of abs. values between 300-500 nm in resp. phase

(3)

### 17.3 Determination of extinction coefficients

For all compounds, the stock solution, prepared in pre-saturated *n*-octanol with  $c = 500 \mu\text{M}$ , was subjected to serial dilution to give solutions of 500, 200, 100, 50, 20, 10, and 5  $\mu\text{M}$  concentrations. 100  $\mu\text{L}$  of each solution were transferred in duplicates onto a UV-star 96-well plate, including blanks (pre-saturated *n*-octanol). Absorption was read in the range of 230-600 nm using a plate reader. After executing a baseline correction using the blank absorbance values, band maxima were determined and  $\varepsilon$  calculated for each maximum at all concentrations from the *Lambert-Beer* law (equations 4/5):

<i>Lambert-Beer</i> law	$A = \log \frac{I}{I_0} = \varepsilon \cdot c \cdot d$	A	absorbance [a.u.]	
		ε	molar extinction coefficient [Lmol <sup>-1</sup> cm <sup>-1</sup> ]	(4)
	$\varepsilon = \frac{A}{c \cdot d}$	c	concentration [mol L <sup>-1</sup> ]	
		d	pathlength [cm]	(5)

After plotting the data, **average ε values** were calculated for each maximum in the linear range of results, typically using 20-500  $\mu\text{M}$  data; in some cases 50-500  $\mu\text{M}$ . The defined concentrations and separately determined pathlength of  $d(100\mu\text{L}) = 0.218 \text{ cm}$  were used for calculation (*vide infra*).

## Pathlength determination

**Pathlength determination** of the octanol solutions in micro wells was performed by adapting the established method for water.<sup>419</sup> Solutions of **26** and **47** as representative compounds were used at  $c = 125 \mu\text{M}$  in *n*-octanol. Sample volumes of 225, 200, 175, 150, 125, 100, 75, and 50  $\mu\text{L}$  were pipetted in triplicates into 96 well plates and their UV-vis spectra recorded in the range of 230-1000 nm. Parallel, spectra of the same solutions were measured in a 1 cm quartz cuvette on the same plate reader, using an inset for cuvettes. All spectra were recorded 3 times.

Wavelengths of maximum absorption (350 and 430 nm for **47**, 344 and 404 nm for **26**) were chosen for extrapolation, the absorbance at 600 nm served as reference value (no specific absorption of the investigational compounds at this wavelength).

Pathlengths were calculated for individual filling values using equation 6:

$$\text{Pathlength} \quad d = \frac{A_{max}^V - A_{600}^V}{(A_{max}^{1cm} - A_{600}^{1cm})cm^{-1}} \quad (6)$$

$A_{max}^V$	abs. at maximum of absorption band for respective volume V in well
$A_{600}^V$	abs. at 600 nm for respective volume V in well
$A_{max}^{1cm}$	abs. at maximum of absorption band in 1 cm cuvette
$A_{600}^{1cm}$	abs at at 600nm in 1 cm cuvette

Plotting of  $d$  vs.  $V$  and linear regression afforded the pathlength equation 7)

$$\text{pathlength equation} \quad d = a \cdot V + d_0 \quad (7)$$

$d$	pathlength [cm]
$a$	slope [ $\text{cm } \mu\text{L}^{-1}$ ]
$V$	volume [ $\mu\text{L}$ ]
$d_0$	intrinsic pathlength

The regression equation was nearly identical in all determined maxima (Figure 56). For 100  $\mu\text{L}$  filling volume, as was used in all subsequent experiments, the pathlength of *n*-octanol solutions was found to be **0.218 cm**.

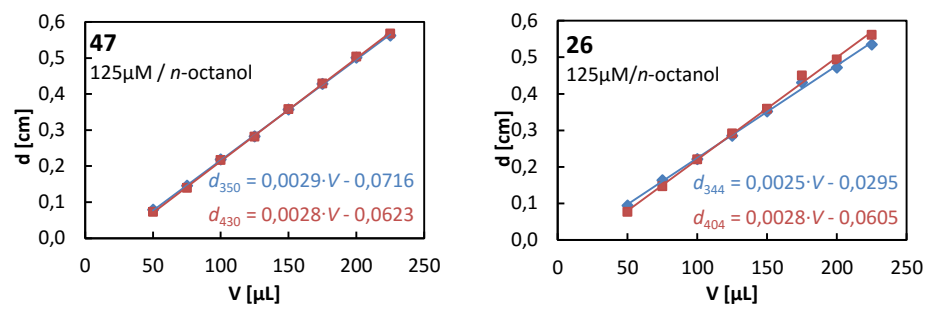


Figure 56 Regressions for pathlength determinations of *n*-octanol solutions using two representative compounds.



## 18 BIOLOGICAL STUDIES

### 18.1 General information

#### Cell lines

Cell lines were kindly provided by Prof. Dr. Stephan Hahn (Molecular gastrointestinal oncology, Medical Faculty, Ruhr University Bochum) and frequently STR analyzed.<sup>xxviii</sup> The following adherent human epithelial cell lines were used in this study (information on characteristics obtained from the ATCC<sup>421</sup> and DSMZ<sup>422</sup> databases):

Table 13 Main characteristics of the used cell lines.

	<b>MCF-7</b>	<b>HeLa</b>	<b>HT-29</b>	<b>HEK 293T</b>
<b>Tissue</b>	<i>mammary gland/breast;</i> derived from metastatic site: pleural effusion	<i>cervix</i>	<i>colon</i>	<i>human embryonal kidney</i>
<b>Disease</b>	adenocarcinoma	cervix adeno- carcinoma	colorectal adeno- carcinoma	
<b>Age</b>	69 years	31 years	44 years	fetus
<b>Gender</b>	female	female	female	n/k <sup>a</sup>
<b>Ethnicity</b>	Caucasian	black	Caucasian	n/k <sup>a</sup>

<sup>a</sup> n/k – not known

---

<sup>xxviii</sup> STR (short tandem repeat) analysis is a frequently applied method to establish the cell lines' identity and exclude possible cross contaminations.<sup>420</sup>

## Equipment

Cell culture and testing was performed using various standard laboratory equipment listed below.

Device	Type	Manufacturer
Laminar flow benches	<i>Msc-Advantage 1.2</i>	Thermo Scientific
Incubators	<i>HeraCell 150 / HeraCell 150i</i>	Thermo Scientific
Cell counter	<i>TC10™ Automated cell counter</i>	BIO-RAD
Centrifuges	<i>Universal 320R</i> <i>5417R</i>	Hettich Zentrifugen Eppendorf
Microplate reader	<i>Sapphire<sup>2</sup></i>	Tecan
Optical microscope		Hund Wetzlar
Fluorescence microscope	<i>IX-81</i>	Olympus
Autoclave	<i>VX-96</i>	Systec
plate shaker	<i>TIMIX</i>	Edmund Bühler GmbH

## Consumables

Type and manufacturer of the containers and transfer devices used for cell culture were kept constant during the investigations and are listed below.

Item	Type	Supplier
Cell culture dishes	10 cm Ø	Sarstedt Ref. 83.3902
Multiwell plates (96-well)	Nunclon DeltaSurface, flat bottom UV Star, flat bottom plates	Nunc / ThermoScientific cat. 167008 Greiner Bio-One, ref. 655081
Microscopic slides	8-well µ-slide ibiTreat	IBIDI GmbH
Falcon™ tubes	15 and 50 mL, sterile	Sarstedt
Microreactor tubes	1.5, 2 mL 5 mL	Sarstedt Eppendorf
Pipettes	2, 5, 10, 25 mL Sarstedt serological pipettes, sterile	Sarstedt
Pipette filter tips	10/20, 200, 1000 µL, graduated, sterile	tipOne / Star lab
Ritips	0.5, 2.5 mL	Ritter
Counting slides	dual chamber counting slides	BIO-RAD

## Chemicals

The following media, additives and reagents were used for biological applications:

chemical	description	supplier	
Dulbecco's Modified Eagle's Medium (DMEM)*	high glucose (4.5 g), GlutaMAX™ supplement, phenol red	Gibco®	61965-026
	high glucose (4.5 g), no phenol red	Gibco®	31053-028
Sodium Pyruvate	100 mM Solution; 11 g/L (100 × concentrated)	Gibco®	11360-039
L-glutamine	GlutaMAX 200 mM (100 × concentrated)	Gibco®	25030-038
Penicillin-Streptomycin	PenStrep 5000 u/mL penicillin; 5000 µg/mL streptomycin (100 × concentrated)	Gibco®	15070-063
Dulbecco's Phosphate-Buffered Saline (DPBS)*	without calcium, magnesium, phenol red	Gibco®	14190-086
Trypsin-EDTA*	0.05% EDTA, phenol red	Gibco®	25300-054
Fetal Bovine Serum (FBS)	FBS Superior, standardized, heat inactivated	Biochrom AG®	S0615
PrestoBlue® Cell Viability Reagent	10 × concentrated resazurin-based fluorescence dye	Molecular Probes™	A-13261
Propidium Iodide (PI)		Molecular Probes™	P1304MP
DAPI	4',6-Diamidino-2-phenylindole, dihydrochloride	Molecular Probes™	D1306
Dimethyl sulfoxide (DMSO)	analytical reagent grade	VWR	23500.297
MTT reagent	thiazolyl blue tetrazolium bromide	Sigma	M5655
Cisplatin (CDDP)	<i>cis</i> -diammineplatinum(II) dichloride	Sigma	P4394

\*Formulation of DMEM, DPBS, trypsin-EDTA is given in the appendix.

## 18.2 Cell culture conditions

### General conditions

Cells were generally handled under sterile conditions in a laminar airflow cabinet. Sterile conditions were ensured by using sterilized consumables (purchased sterile or autoclaved) and applying 70 % ethanol as superficial disinfectant towards surfaces prior to usage.

The cells were maintained in 10 cm  $\emptyset$  cell culture dishes at 37 °C in a humidified incubator under an atmosphere containing 10 % CO<sub>2</sub>.

Cells were cultured in Dulbecco's Modified Eagle's Medium (DMEM, high glucose, with phenol red), which was supplemented with 10 % (v/v) fetal bovine serum (FCS), 1 % sodium pyruvate, 1 % L-glutamine, and 100 units·mL<sup>-1</sup> PenStrep. For microscopy applications, an equally supplemented DMEM without phenol red was used.

Cell passaging was usually performed at 80-90 % cell confluence by standard procedures and until the 50<sup>th</sup> passage at most.

### Cell passage

For **cell passaging**, the medium was removed and cells washed with 5 mL of PBS. Cells were harvested by adding Trypsin-EDTA (3 mL) and incubation for ca. 3 min, until they detached from the culture dish surface as witnessed by microscopic inspection. Subsequently, DMEM (7 mL) was added and the cell suspension transferred into a 50 mL Falcon tube. After centrifugation (300 g, 2 min, r.t.), the supernatant was removed and the cell sediment suspended in 10 mL fresh DMEM. Cells were counted using an automated system.

For all **assays**, an aliquot of cell suspension with the defined number of cells was diluted to 100.000 cells/mL or 60.000 cells/mL in DMEM. 100  $\mu$ L aliquots were transferred into 96-well *nunc*lon plates, yielding 10.000 or 6.000 cells/well, respectively, depending on cell line and experiment. Blank wells were filled with medium without cells. The plates were incubated for one day prior to drug treatment to allow cell attachment.

For **fluorescence microscopy**, HeLa and MCF7 cell sediments obtained by centrifugation were carefully washed with 1 $\times$  PBS once to remove remaining medium with phenol red, and resuspended



in 5 mL DMEM without phenol red. After counting, cells were seeded onto 8-well microscopy slides at a final concentration of 25,000 cells/well in 250  $\mu$ L DMEM (without phenol red) and incubated for one day prior to drug treatment.

For **cell line maintenance**, an adequate aliquot of cell suspension (cell line dependent) was transferred to a new cell culture dish containing DMEM to give a total volume of 10 mL.

## Drug treatment

**Stock solutions** of all samples were prepared at the highest possible concentration in DMSO (typically 10-50 mM) to keep the amount of DMSO in final samples as low as possible. Stock solutions of Cisplatin were prepared at 3.33 mM in PBS. For each independent experiment, fresh stock solutions of all compounds were prepared from powder. All samples were diluted to the desired concentration in DMEM immediately prior to their application to treat cells in a concentration range between 500 and 1  $\mu$ M. By microscopic inspection of the plates after the desired incubation time, it was ensured that no precipitate had formed during incubation. In cases where precipitates were formed (in some cases at approx. 500  $\mu$ M), either the drug concentration surely lead to 0 % viability or the concentration was deleted from the evaluation range.

In separate control experiments, the **effect of DMSO** present in the different sample concentrations was tested by adding DMSO in representative quantities (0-5 % v/v). No significant effect on cell growth at drug concentrations close to respective  $IC_{50}$  values was witnessed (typically with max. 0.5 % DMSO). Therefore, the effect of DMSO was generally neglected.

## PrestoBlue<sup>®</sup> Assay

Medium was removed from the preincubated wells and 90  $\mu$ L fresh drug-containing medium or pure medium (for controls and blanks) was added in triplicates or quadruplicates for each concentration. After an incubation time of 22, 46, or 70 h, 10  $\mu$ L PrestoBlue<sup>®</sup> cell viability agent<sup>176</sup> was added and the plate quickly shaken on a laboratory shaker to ensure homogenous distribution of reagent throughout the well (ca. 10 sec). The cells were then further incubated up to 24, 48 or 72 h, after which the fluorescence intensities were read on a Tecan Sapphire<sup>2</sup> plate reader with the following read-out settings: excitation  $\lambda_{Ex}$  = 560 nm (bandwidth 10 nm); emission  $\lambda_{Em}$  = 590 nm (bandwidth 10 nm); 3 reads/well at 40  $\mu$ s integration time, room temperature.

	1	2	3	4	5	6	7	8	9	10	11	12
A		500	200 $\mu$ M			500	200 $\mu$ M			200 $\mu$ M		
B			100 $\mu$ M				100 $\mu$ M			100 $\mu$ M		
C			50 $\mu$ M				50 $\mu$ M			Reference sample	50 $\mu$ M	
D	Blank – no cells	Sample 1	20 $\mu$ M			Sample 2	20 $\mu$ M				20 $\mu$ M	
E			10 $\mu$ M				10 $\mu$ M				10 $\mu$ M	
F			5 $\mu$ M				5 $\mu$ M				5 $\mu$ M	
G			1 $\mu$ M				1 $\mu$ M			1 $\mu$ M		
H		Control – no drug										

Figure 57 Representative 96-well layout for PrestoBlue® assay. The exact dilution scheme was adjusted to the compounds' requirements in the individual experiments. In wells reserved for "reference samples", CDDP, DMSO or ligand compounds were plated. For investigational drugs, one sample at maximum possible concentration was plated to determine 0 % viability and to check solubility behavior.

## MTT Assay

For comparative MTT assays, sample dilution was performed with double concentrations. 100  $\mu$ L drug-containing medium or pure medium (for controls) was added to the pre-incubated cells (in 100  $\mu$ L DMEM), giving a final volume of 200  $\mu$ L at the desired drug concentrations. After 48 h of incubation at 37  $^{\circ}$ C, 50  $\mu$ L of MTT solution (prepared from 2.5 mg/mL thiazolyl blue tetrazolium bromide in 1 $\times$  PBS or mQ water and filter sterilized) was added and the samples incubated for 2 h. Then, the medium was carefully removed and the formed formazan crystals dissolved in DMSO (200  $\mu$ L/well). The resulting solution was homogenized by repeated up-and-down pipetting of the solutions, after which the absorbance intensities were read on a *Tecan Sapphire*<sup>2</sup> plate reader with the following settings: measurement  $\lambda_{\text{meas}} = 550$  nm, reference  $\lambda_{\text{ref}} = 620$  nm, 3 reads/well, room temperature.

### 18.3 Data handling

Data obtained from the *in vitro* assays were evaluated with Microsoft Office Excel 2007 and OriginPro 8. Fluorescence intensity was determined in arbitrary units (a.u.) and corrected by blanks without cells as determined separately for each plate. Quadruple values for each drug concentration were averaged, standard deviations (*SD*, equation 8) determined and possible outliers elucidated by *Grubbs'* test at a significance level of  $\alpha = 0.05$  using equation 9:

standard deviation  $SD = \sqrt{\frac{\sum_{i=1}^n (x_i - \bar{x})^2}{n - 1}}$   $SD$  standard deviation  
 $n$  number of samples  
 $x_i$  value of individual sample  
 $\bar{x}$  mean of  $n$  samples (8)

*Grubbs'* outlier test  $Z = \frac{|\bar{x} - x_i|}{SD}$

N	Critical Z ( $\alpha = 0.05$ )
3	1.15
4	1.48

(9)

**Dose-response curves** were plotted using the semi-logarithmic scale, *i.e.* fluorescence intensity [a.u.] (resp. absorbance value for MTT) vs. decadic logarithm of final drug concentration [ $\mu\text{M}$ ].

For **IC<sub>50</sub> value determination**, the original, uncorrected data were applied. Single fluorescence intensities (outlier depleted) were used for dose-response curve plotting instead of their mean values. Fluorescence values of positive and negative controls were included for a better definition of  $A_1$  and  $A_2$  at a virtual drug concentration of  $10^{-6}$  resp.  $10^6 \mu\text{M}$ . IC<sub>50</sub> values were then calculated from the inflection point of the sigmoidal curve fit function of *OriginPro 8*. The regression was based on the following equation 10:

sigmoidal curve fit  $f(x) = A_2 + \frac{A_1 - A_2}{1 + \left(\frac{x}{x_0}\right)^p}$   $A_1$  lower asymptote  
 $A_2$  upper asymptote  
 $p$  power / slope  
 $x_0$  inflection point / IC<sub>50</sub> value [ $\mu\text{M}$ ] (10)

The dose-response curves were obtained from at least two, typically three, independent experiments and the singular IC<sub>50</sub> values averaged. Results are given as average IC<sub>50</sub> values  $\pm$  biological SD out of the independent experiments.

## 18.4 Fluorescence microscopy

Sample solutions of compound **46** were prepared from DMSO stock solutions as stated above for the PrestoBlue® assay, using DMEM without phenol red. Medium from the preincubated microscopy slides was replaced by 250  $\mu\text{L}$  drug-containing medium at concentrations above the determined  $\text{IC}_{50}$  (50  $\mu\text{M}$ ), around the  $\text{IC}_{50}$  (20  $\mu\text{M}$  for HeLa and 30  $\mu\text{M}$  for MCF7), and below the  $\text{IC}_{50}$  value (10  $\mu\text{M}$ ). Slides were then incubated for 72 h to achieve the desired cellular reactions.

4',6-Diamidin-2-phenylindol (DAPI) and propidium iodide (PI) were stored as separate stock solutions in 1 $\times$  PBS. Immediately prior to the experiment, a 10 $\times$  concentrated DAPI/PI staining solution was prepared and 27.8  $\mu\text{L}$  directly added to the incubated cells to give final concentrations of 50  $\mu\text{g}/\text{mL}$  DAPI and 20  $\mu\text{g}/\text{mL}$  PI. The medium was not substituted in order to retain all, living and dead, cells in the microscopy wells. Stained cells were preincubated for 1 h before microscopy.

Fluorescence micrographs were collected on an *Olympus* IX-81 fluorescence microscope. The device is equipped with an *XM10* monochrome CCD camera and various filter sets. Filter cubes with  $\lambda_{\text{Ex}} = 330\text{-}385$  nm,  $\lambda_{\text{Em}} = 420+$  nm (for DAPI-stained cells) and with  $\lambda_{\text{Ex}} = 530\text{-}550$  nm,  $\lambda_{\text{Em}} = 590+$  nm (for PI-stained cells) were used to record the micrographs at 200-fold magnification. Fluorescence micrographs of the individual records were colorized with symbolic colors after data collection and overlays generated using the integrated *CellM* software.

## 19 BIOMOLECULE INTERACTION STUDIES

### 19.1 Materials

All proteins used for these studies were purchased from commercial suppliers. Stock solutions of proteins, *i.e.* horse heart cytochrome c (Sigma C7752), chicken egg white lysozyme (Sigma L7651), and bovine pancreas RNase A (Sigma R5500), were prepared in Millipore water at 1 mM and stored at -20 °C until usage.

9-Methylguanine (**9-mg**) was kindly provided by Markus Galanski (University of Vienna).

Oligonucleotides (**ODNs**) were prepared by Domenica Musumenci (University of Naples). The sequences were synthesized in solid phase with the standard phosphoramidite method by using an automatic synthesizer. Detachment from the solid support was enabled with ammonia solution.<sup>289</sup>

Stock solutions (10 mM) of each of the individual Pt(II) compounds were prepared by dissolving the complex under investigation in DMSO.

### 19.2 Devices

UV-Vis absorption spectra were recorded on a Varian Cary 50 UV-Vis spectrophotometer in the range of 200-800 nm.

ESI mass spectra were recorded on a *ThermoFinnigan LTQ Orbitrap* high-resolution mass spectrometer (Thermo, San Jose, CA, USA), equipped with a conventional ESI source by direct introduction of the sample. The instrumental settings were adapted according to the experimental requirements as listed in the individual sections.

Data was acquired and processed with a nominal resolution of 100 000 (at  $m/z$  400), using Xcalibur 2.0 software (Thermo). For spectra in positive mode, monoisotopic and average deconvoluted masses were obtained with the integrated Xtract tool.

### 19.3 Metal complex - protein interaction studies

#### UV-vis spectroscopic experiments on protein interaction

UV-vis measurements with proteins were carried out by diluting the compounds' stock solutions to 30  $\mu\text{M}$  in TMAA. After recording the initial spectrum without protein, the desired model protein was added at 10  $\mu\text{M}$  to yield a final metal:protein ratio of 3:1. Spectra were recorded over 72 h at r.t., operating in 10 min intervals during the first hour, in 1 h intervals up to 24 h and finally in 3 h intervals up to 72 h.

#### ESI MS on Pt-protein adducts

DMSO stock solutions (10 mM) of the investigational complexes were prepared and introduced into tetramethylammonium acetate buffer (TMAA, 25 mM, pH 7.4) at 300  $\mu\text{M}$ , containing 100  $\mu\text{M}$  protein to give a final metal:protein molecular ratio of 3:1. Samples were incubated at 37 °C for 24 h or 72 h.

ESI mass spectra of the metal-protein mixtures were recorded from samples generated through 20-fold dilution with water. The following standardized working conditions were applied: Direct introduction, flow rate 5  $\mu\text{L}/\text{min}$ ; spray voltage 3.1 kV, tube lens voltage 230V, capillary voltage 45 V and capillary temperature 220 °C. Sheath and auxiliary gases were set at 17 a.u. and 1 a.u., respectively.

## 19.4 Reactions with 9-methylguanine

Stock solutions of **9-mg** and the complexes were prepared at 10 mM in DMSO.

### ESI MS of adducts with 9-mg

For adduct formation, samples were diluted in LC-MS grade water or in ammonium acetate buffer (AmAc 20mM, pH = 6.8) to give a final metal:**9-mg** ratio of 3:1,  $c(\mathbf{9-mg}) = 100 \mu\text{M}$ . Samples were then incubated at 37 °C for 24 h, ESI mass spectra recorded, and re-incubated further to a final incubation time of 90 h.

To record the positive ESI mass spectra, the incubated samples were diluted 20-fold in water before injection into the instrument. For recording of free **9-mg**, the stock solution was diluted 100-fold in water. Spectra were recorded on an LTQ-Orbitrap high-resolution mass spectrometer (Thermo, San Jose, CA, USA), equipped with a conventional ESI source (direct introduction, 7  $\mu\text{L}/\text{min}$ ) in the range of 100-1000  $m/z$  values. The following standardized working conditions were applied: spray voltage 3.1 kV, tube lens voltage 230V, capillary voltage 45 V and capillary temperature 220 °C. Sheath and auxiliary gases were set at 17 a.u. and 1 a.u., respectively.

### UV-vis spectroscopy of adducts with 9-mg

All dilutions were performed from 10 mM stock solutions in DMSO. After recording the baseline, a UV-vis spectrum the Pt(II) complex of interest was collected. Then, **9-mg** was added in a 1:1 ratio where appropriate and UV-vis spectra collected over a defined period of time. For long-term reactivity, spectra were recorded at a concentration of 100  $\mu\text{M}$  for both compounds in 10 min intervals during the first hour and hourly up to 72 h. Data was collected in the range of 200-800 nm. For short-term reactivity, spectra were recorded at 50 mM final concentration, scanning the range of 200-600 nm to reduce scanning time.

## 19.5 Incubation with oligonucleotides

### Sample preparation

Stock solutions of the platinum compounds were prepared at 10 mM concentration in DMSO. Stock solutions of oligonucleotides were prepared at 100  $\mu$ M in LC-MS grade water.

For adduct formation of the Pt complexes with oligonucleotides, the substances were combined in a 1:1 or 3:1 metal:oligonucleotide ratio in LC-MS grade water to give a final c(**ODN**) of 20  $\mu$ M. The samples were kept at 37 °C for 24 or 72 h before measurement.

### ODN data recording: ESI MS in negative mode

For recording of the ESI mass spectra, the incubated samples or free oligonucleotides were diluted to 10  $\mu$ M in LC-MS grade water. Unplatinated **ODN3** was diluted in MeOH/water to give a 50/50 vol-% mixture of both solvents immediately prior to data recording.

Spectra were recorded in negative mode (direct introduction, 7  $\mu$ L/min) in the range of -300 to -2000  $m/z$  values. The following standardized working conditions were applied: spray voltage 2.7 kV, tube lens voltage -113 V, capillary voltage -20 V and capillary temperature 280 °C. Sheath and auxiliary gases were set at 23 a.u. and 4 a.u., respectively.

For MS<sup>2</sup> experiments, selected isolated multicharge peaks were subjected to collision induced dissociation (CID); usually those at  $m/z = -5$  or  $-6$  were selected. The normalized collision energy (NCE) was adjusted manually; usually an intensity of 17-19 a.u. was chosen.

Data simulation of fragment peaks was performed using the Mongo Oligo mass calculator tool<sup>292</sup> and the isotope simulation tool of Xcalibur software.



---

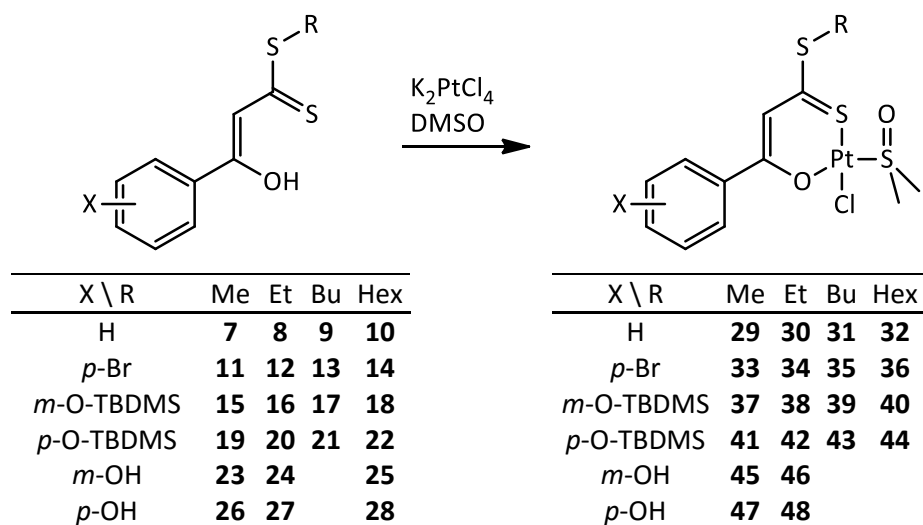
# SUMMARY

## 20 SUMMARY

In the herein presented work, a series of platinum(II) complexes as potential cytotoxic agents is described. They all share a common pharmacophore of an (*O,S*) bidentate ligand based on the structural motif of  $\beta$ -hydroxydithiocinnamic esters. Numerous modifications are possible at this ligand, some of which have been explored within this thesis.

First, a panel of  $\beta$ -hydroxydithiocinnamic esters **7-28** (Scheme 26) was prepared with varying substituents at the aromatic moiety (H, *p*-Br, *m*- and *p*-OX where X = H or TBDMS) and different alkyl chain lengths at the dithioester unit (to give dithio-methyl, -ethyl, -butyl, or -hexyl esters, respectively). Subsequently, they were coordinated towards a platinum(II) center to afford neutral (*O,S*) bidentate complexes **29-48** where the ligand sphere is completed by a chlorido ligand and DMSO which coordinates *via* its sulfur atom (Scheme 26). In addition, two representative (*O,S*)<sub>2</sub>Pt bischelate complexes **49** and **50** are reported as reference compounds for this substance class which is very stable and preferentially formed during the synthesis of the monofunctional compounds **29-48**. The overall aim of synthesizing such a panel of compounds was to achieve different polarities and hence degrees of aqueous solubility of the compounds and to see what effects the different substituents might have on the biological activity of Pt(II) compounds with this particular pharmacophore (chapter 3).

All compounds were analyzed by means of standard analytical methods. The metal complexes' behavior in aqueous solution was assessed by carrying out UV-visible spectroscopic experiments aimed at elucidating the solubility of these compounds and hydrolysis processes occurring when the compounds are placed in buffered medium. These studies presented the prerequisite for further studies on the compounds' interaction with biomolecules. It was found that as a first aquation step, the chlorido ligand is released, whilst the DMSO ligand may be retained within the system (chapter 4).



Scheme 26 Compounds discussed in the first part of this work.

In an attempt to quantify the compounds' aqueous solubility, the  $\text{Log}P_{o/w}$  value of the corresponding ligands was determined by the shake-flask method. This allowed for an indirect assessment of the Pt(II) compounds' relative hydro- or lipophilicity and proved that the incorporation of a hydroxy group at the phenyl ring in *meta* position results in the lowest  $\text{Log}P_{o/w}$  values and hence in the highest polarity. Overall, the compounds are rather unpolar, as shown by generally positive  $\text{Log}P_{o/w}$  values, which means that more compound is found in the octanol- than in the aqueous phase (chapter 4).

Furthermore, the biological activity of compounds **29-36** of the H- and *p*-Br substituted series as well as of compounds **45-46** of the hydroxy-substituted series was assayed against four representative cancer cell lines (HeLa, HT29, MCF7, 293T HEK) by means of the resazurin-based PrestoBlue® assay. Albeit the compounds generally seem to be less cytotoxic than the reference compound, Cisplatin, they manifest an interesting activity pattern: There seems to be a two-sided activity profile depending on the compounds' lipophilicity: on the one hand, the most polar compounds, *i.e.* those with a methyl- or ethyl group at the dithioester subsite, are the most active in compound series with a Ph-H or Ph-OH group (**29, 30, 43-46**). On the other hand, in the series with *p*-Br-Ph, the opposite trend seems to appear, with an increasing cytotoxicity upon elongation of the alkyl chain. This finding could be an indicator for a different cellular accumulation or processing of more polar vs. very lipophilic compounds.

Notably, varying the position of the Ph-OH group to give *meta*- or *para*-OH compounds (**45/46** and **47/48**, respectively) brings forth a significant difference in antiproliferative activity. The origin of this functional difference might lay in different polarities or, maybe additionally, in differences in cellular processing. Future experiments might be able to shed light on this interesting finding.

In general, the compounds seem to exert their highest activity against most model cell lines when incubated for 48 h, as was assessed by a time-line of three different incubation times, 24, 48, and 72 h. Fluorescence microscopy on HeLa and MCF7 cell lines incubated with **46** furthermore gave a first visual impression of the cellular response to drug treatment: the compounds induce cellular death, very probably by apoptosis in favor of necrosis (chapter 5).

Selected compounds of the series presented in this thesis have furthermore been challenged against a panel of three model proteins (cytochrome c, lysozyme, ribonuclease A) and adduct formation monitored by ESI mass spectrometry and UV-vis spectroscopy. One model protein, albumin, was used to quantify the compounds' interaction with a serum protein by means of ICP-OES. It was shown that the compounds are able to form stable covalent bonds with specific amino acid side chains. As potential binding sites, especially His and to some extent also Met side chains are considered, an assumption based on a comparison with similar experiments on Cisplatin and analogs and the finding of a His15-bound Pt(II) complex fragment in the crystal structure of HEWL-**46** and HEWL-**48** adducts (chapter 7).

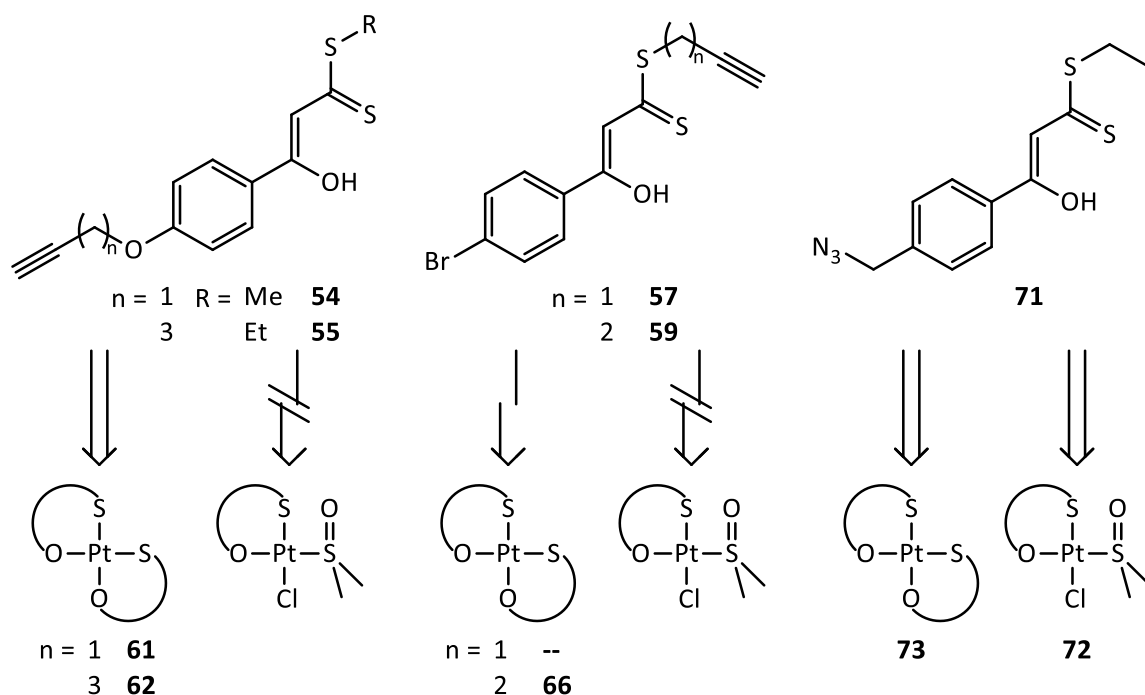
Furthermore, the binding ability of three selected representatives, **30**, **46**, and **48**, towards DNA was probed by making use of two model systems, namely 9-methylguanine (**9-mg**) and single-strand oligonucleotides **ODNs** with a defined sequence containing adjacent guanines as potential binding sites (**ODN1**, **ODN2**) or not containing any guanine binding sites (**ODN3**). Binding of the compounds to **9-mg** was found to occur within minutes, as observed in UV-vis spectra, and several adduct compositions were found in the ESI MS spectra. The (*O,S*)Pt unit can bind **9-mg** either under retention or release of DMSO, in the latter case probably a bidentate binding of Pt to N<sup>7</sup> and O<sup>6</sup> of **9-mg** occurs. Furthermore, adducts of the (*O,S*)Pt unit with two **9-mg** molecules were witnessed (chapter 8).

In adduct spectra of the compounds with the oligonucleotide models, a multifaceted adduct formation behavior was found. MS<sup>2</sup> experiments of adducts formed with **ODN1** suggest a preferential binding of the (*O,S*)Pt unit to guanine, as expected. But in addition to this stable binding, additional binding sites must exist that allow for multiple metal centers to bind to the oligonucleotide single strands. This becomes especially apparent from the observation that multiple (*O,S*)Pt units can bind to **ODN3**, which basically consists of a C-A tandem sequence without any guanine. Phosphate backbone binding is highly improbable, so that alternate nucleobase binding sites must exist. In this case, adenine, and possibly even cytosine, present probable targets (chapter 8).

Overall, it was shown that the panel of investigated compounds is able to bind various biomolecules in a defined manner. Together with the biological and biophysical data acquired within this thesis, it becomes clear that many factors contribute to the final antiproliferative activity of these complexes. Compounds **29/30** and **45/46**, bearing a methyl/ethyl substituent at the dithioester and no substituent resp. a *m*-OH group at the phenyl ring were identified as the most potential drug candidates worthy of further, detailed investigation.

It is by far not yet clear how these compounds could possibly work *in vivo*, yet some important contributions to a first understanding of the compounds' mode of action have been made. Future investigations might elucidate the cellular response in detail, so that the compound class could be further optimized and a lead structure may be identified.

In efforts to enable an enhanced drug targeting towards cancer cells, synthetic pathways towards the formation of bioconjugates have furthermore been reported. Two general methods to link the (*O,S*)Pt pharmacophore to a model peptide, Leu<sup>5</sup>-enkephalin, have been applied, namely the most prominent "click" reaction, CuAAC, and the linking *via* amide bonds. To make CuAAC possible, the  $\beta$ -hydroxydithiocinnamic ester motif was derivatized with alkyne- and azide- functional groups (compounds **54-59** and **71**, respectively, Scheme 27). The first approach, introducing alkyne groups into the structure, resulted in numerous synthetic obstacles such as uncontrolled rearrangement processes or hydration of the triple bonds during ligand and complex syntheses, thus making the isolation of monofunctional compounds with the desired (*O,S*)PtCl(DMSO) coordination environment impossible. Merely (*O,S*)<sub>2</sub>Pt bischelate structures (**61**, **62**, **66**, Scheme 27) were obtained with a preserved alkyne group. On the contrary, synthesis of azidomethyl-derived complexes **72** and **73** proceeded readily and in good yields (Scheme 27, chapter 11).



Scheme 27 Derivatives of  $\beta$ -hydroxydithiocinnamic esters with alkyne and azide functional groups; accessibility of the respective Pt(II) complexes.

After deriving Leu<sup>5</sup>-Enkephalin (Leu<sup>5</sup>-Enk) with carboxylic acids bearing either a terminal alkyne (**76**) or azide (**77**), the linking of the two units was pursued. It was possible to obtain bioconjugates of bischelates with both functional groups (**78** and **79**). The synthesis of **78**, based on the azide- $(O,S)$  compound **73**, proceeded better and gave less side products as well as an increased yield of pure compound. The isolation of the respective monofunctional complex **81** was then possible by first linking the ligand **71** with alkyne-functionalized Enk **76** by CuAAC, followed by coordination to the Pt(II) center (chapter 11). The three relevant bioconjugates are summarized in Chart 10.

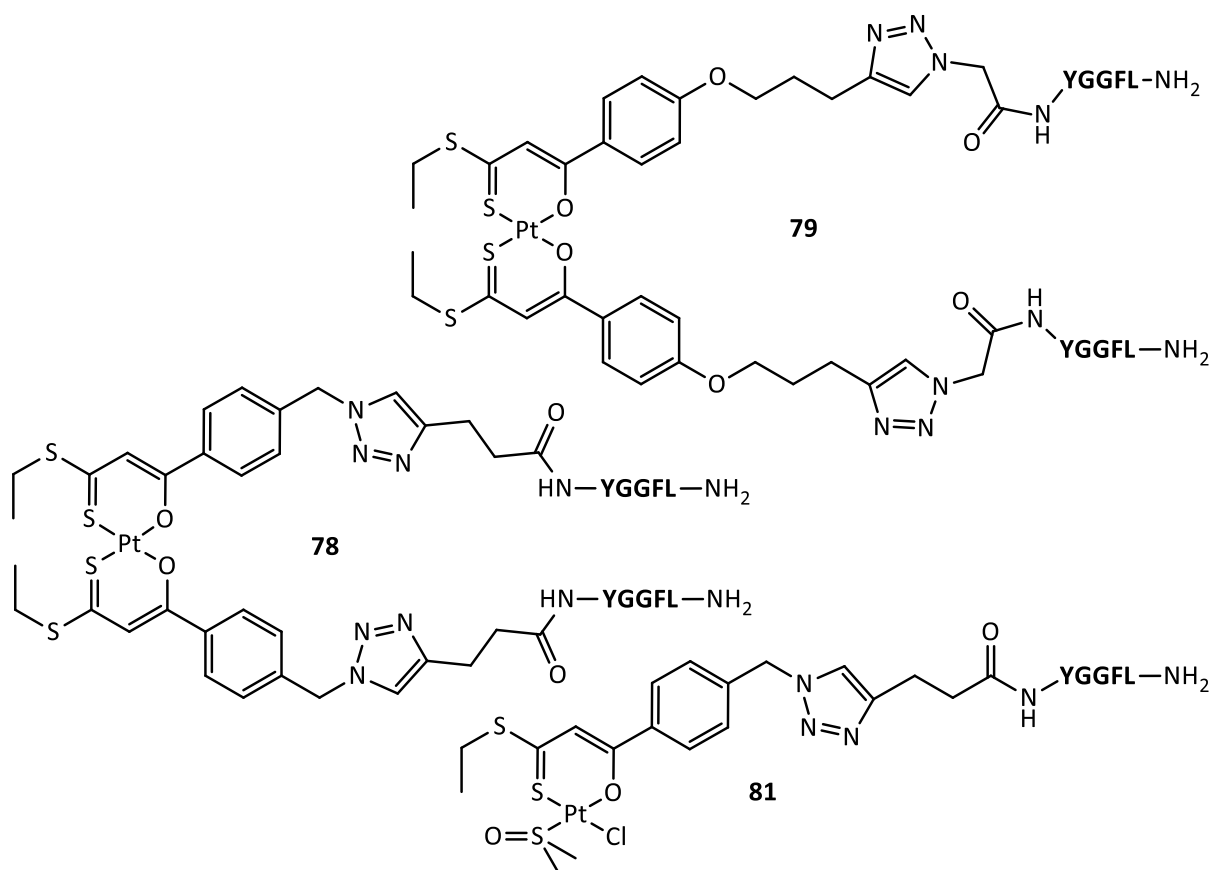


Chart 10 Metal-peptide bioconjugates isolated by CuAAC.

As an alternative route towards bioconjugates with the two desired units, the coupling through an amide bond was also feasible. After preparing compound **82** with a carboxymethyl group bound to the dithiocarbonyl unit, the coupling to Leu<sup>5</sup>-Enk **75** in solution was successfully performed (**84**). It was then possible to generate the monofunctional compound **85** with DMSO and Cl<sup>-</sup> as monodentate ligands (Chart 11). All described compounds were identified by their mass spectrometric profile and NMR spectroscopic data (chapter 12).

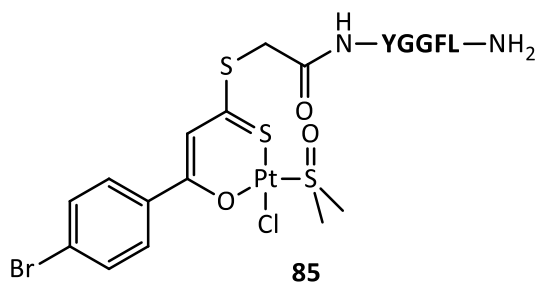


Chart 11 Metal-peptide bioconjugate obtained from amide bond formation

Overall, it could be shown that the basic structural motif of the compounds presented in this thesis offers multiple possibilities to derivatize and optimize the biological relevant properties of the (O,S)Pt pharmacophore. Several synthetic approaches have been demonstrated and diverse methods to explore the functional consequences of such variations applied. This work may thus present a first step into the direction of new, promising drug candidates with an optimized biological profile.



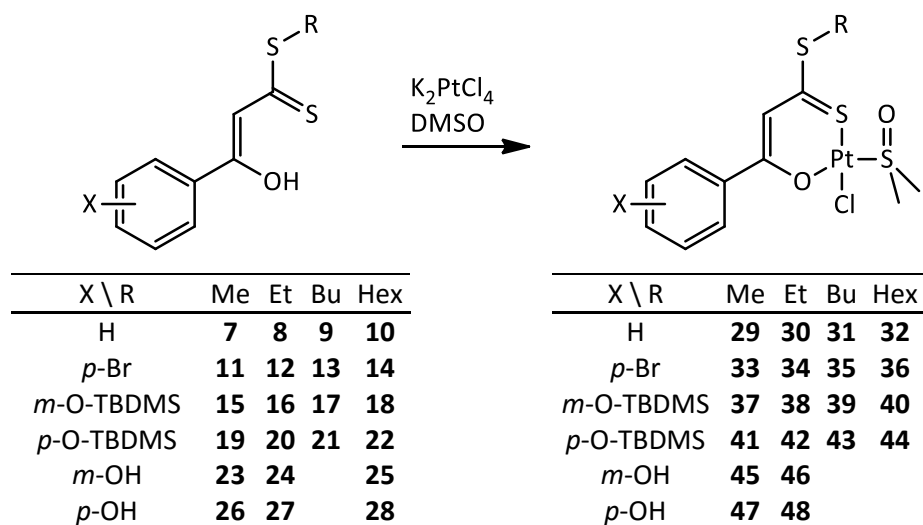


## 21 ZUSAMMENFASSUNG

In der hier vorgestellten Arbeit wird eine Serie von Platin(II) Komplexen beschrieben, welche potentiell als zytotoxische Substanzen dienen können. Sie alle besitzen (*O,S*) bidentate Liganden als gemeinsames Pharmakophor welches auf  $\beta$ -Hydroxydithiozimtsäureestern basiert. Diese Grundstruktur erlaubt verschiedene Modifizierungen, von denen einige in dieser Arbeit untersucht wurden.

Zuerst wurde eine Reihe von  $\beta$ -Hydroxydithiozimtsäureestern (**7-28**, Scheme 26) hergestellt, welche verschiedene Substituenten am Phenylring tragen (H, *p*-Br, *m*- und *p*-OX, mit X = H oder TBDMS) und außerdem verschieden lange Alkylketten an der Dithioestereinheit gebunden sind, um die entsprechende Dithio-methyl, -ethyl, -butyl, oder -hexylester zu erhalten. Durch Koordination an das Platin(II) Zentrum entstanden neutrale Komplexe **29-48** mit den  $\beta$ -Hydroxydithiozimtsäureester-Derivaten als (*O,S*)-chelatisierende Einheit (Scheme 26). Die Koordinationssphäre wird abgesättigt durch einen Chloridoliganden und durch DMSO, welches als *S*-Donor fungiert. Des Weiteren wurden zwei repräsentative Bischelatkomplexe, **49** und **50**, hergestellt welche als Vertreter der sehr stabilen (*O,S*)<sub>2</sub>Pt Komplexe dienen. Das übergeordnete Ziel der Herstellung dieser Substanzreihe bestand darin, verschieden polare und damit unterschiedlich stark wasserlösliche Komplexe zu erhalten. Darüber hinaus sollte ermittelt werden, wie die unterschiedlichen Substituenten am Pharmakophor die biologische Aktivität der Pt(II) Komplexe beeinflussen (Kapitel 3).

Alle Substanzen wurden vollständig mittels Standard-Analysemethoden untersucht. Unter Anwendung von UV-Vis Spektroskopie wurde das Verhalten der Metallkomplexe im wässrigen Medium untersucht, um Informationen über die Löslichkeit und das Hydrolyseverhalten dieser Verbindungen in Pufferlösungen zu erhalten. Diese Untersuchungen bildeten eine Grundlage für weitere Untersuchungen zur Interaktion der Verbindungen mit Biomolekülen. Es konnte gezeigt werden, dass als erster Hydrolyseschritt der Chloridoligand abgespalten wird, während der DMSO-Ligand unter bestimmten Messbedingungen in der Koordinationssphäre erhalten bleiben kann (Kapitel 4).



Scheme 26 Verbindungen, die im ersten Teil der Arbeit hergestellt und untersucht wurden.

Um die Löslichkeit der Komplexe in Wasser zu quantifizieren, wurden die  $\text{Log}P_{o/w}$  Werte der entsprechenden Liganden mithilfe der „Shake-Flask“-Methode ermittelt. Dies ermöglichte eine indirekte Messung der relativen Hydro- oder Lipophilie für die Komplexe **29-48**. Es konnte gezeigt werden, dass das Einbringen einer Hydroxygruppe in *meta*-Position zu den niedrigsten  $\text{Log}P_{o/w}$ -Werten, und damit zur größten Polarität, in dieser Serie führt. Im Allgemeinen sind die Verbindungen wenig polar, was sich in positiven  $\text{Log}P_{o/w}$  Werten äußert, welche wiederum auf eine bevorzugte Anreicherung der Substanzen in der Oktanol- und nicht in der Wasserphase hindeuten (Kapitel 4).

Des Weiteren wurde die biologische Aktivität der Verbindungen **29-36** mit H- und *p*-Br Substituenten und von Verbindungen **45-46** mit hydroxy-Substituenten gegenüber vier repräsentativen Zelllinien (HeLa, HT29, MCF7, 293T HEK) untersucht. Als Assaymethode wurde der auf Resazurin basierende PrestoBlue® Assay verwendet. Obwohl die Substanzen generell weniger toxisch auf die Zelllinien wirken als die Referenzsubstanz Cisplatin, zeigen sie dennoch ein sehr interessantes Aktivitätsspektrum, welches von der Lipophilie der Verbindungen abzuhängen scheint: Auf der einen Seite sind die polarsten Verbindungen (solche mit Methyl- bzw. Ethylgruppen an der Dithioesterfunktion und einem unsubstituierten oder *m*-OH-Phenylring, **29, 30**, und **43-46**) am zytotoxisch aktivsten gegenüber den Zelllinien: In dieser Reihe nimmt die Aktivität bei zunehmender Kettenlänge (C<sub>4</sub>- oder C<sub>6</sub>-Ketten) ab. Auf der anderen Seite aber zeigt sich bei den Verbindungen mit einem *p*-Br Substituenten (**33-36**) ein entgegengesetzter Trend: Hier erhöht sich die Zytotoxizität mit länger werdender Alkylkette. Diese Beobachtungen könnten ein Hinweis darauf sein, dass eher polare bzw. sehr unpolare Verbindungen unterschiedlichen Akkumulations- und Verarbeitungsmechanismen in der Zelle ausgesetzt sind. Wenn die Position der OH-Gruppe am

Phenylring verändert wird (*m*-OH in **45/46** vs. *p*-OH in **47/48**), ergeben sich interessanter Weise signifikante Unterschiede in der zytotoxischen Wirkung der Substanzen. Die Ursache für diese Unterschiede kann einerseits in der abweichenden Polarität der Verbindungen liegen, und/oder in Unterschieden in der zellulären Verarbeitung beider Substanzgruppen. Zukünftige, weiterführende Untersuchungen könnten hier Aufschluss geben (Kapitel 5).

Generell scheinen die Substanzen ihre größte Aktivität gegenüber der Modellzelllinien bei einer Inkubationszeit von 48 h zu zeigen. Dies wurde in einer Serie zeitabhängiger Experimente gefunden, in denen die IC<sub>50</sub> Werte nach 24, 48, und 72 h bestimmt wurden. Fluoreszenzmikroskopische Aufnahmen von HeLa und MCF7-Zellen nach Inkubation mit Verbindung **46** gaben außerdem Aufschluss über die Zellantwort auf Behandlung mit dieser Substanz: Der Zelltod, sehr wahrscheinlich durch Apoptose, tritt ein.

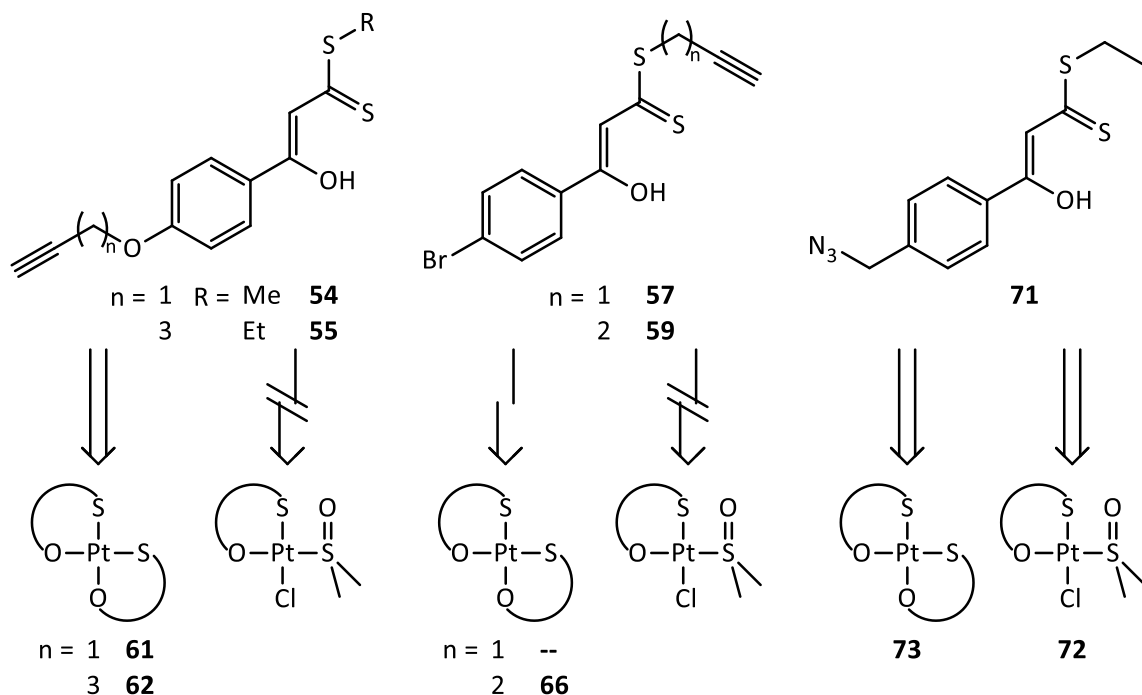
Ausgewählte Vertreter der hier vorgestellten Substanzklasse wurden außerdem auf ihre Reaktivität gegenüber Modellproteinen (Cytochrom c, Lysozym, Ribonuklease A) mittels ESI-Massenspektrometrie untersucht. Ein weiteres Modellprotein, Albumin, wurde verwendet um die Serumprotein-Interaktion der Substanzen mithilfe von ICP-OES zu charakterisieren. Es konnte generell gezeigt werden, dass die Verbindungen stabile kovalente Bindungen mit spezifischen Aminosäure-Seitenketten eingehen können. Als potentielle Bindungsstellen gelten vor allem Histidine, auch Methionine könnten eine Rolle bei der Anbindung von (*O,S*)Pt-Einheiten spielen. Diese Mutmaßung basiert im Wesentlichen auf Erkenntnissen aus ähnlichen Untersuchungen mit Cisplatin und dessen Analoga sowie den Strukturdaten aus Lysozym-Addukten mit den Verbindungen **46** und **48**, in denen beide Male das ND1-Atom von His15 als Bindungsstelle identifiziert wurde (Kapitel 7).

Des Weiteren wurde die Fähigkeit der Substanzen, DNA zu binden, mithilfe von drei Modellkomplexen (**30**, **46**, und **48**) untersucht. Dabei wurden zwei Modellsysteme verwendet: 9-Methylguanin (**9-mg**) und einzelsträngige Oligonukleotide (**ODNs**) mit definierten Sequenzen, welche einerseits benachbarte Guanine (**ODN1**, **ODN2**), oder gar keine Guanine (**ODN3**) enthalten. Wie aus den UV-Vis spektroskopischen Untersuchungen hervor geht, reagieren die Komplexe in Minutenschnelle mit der Modellnukleobase **9-mg**. Außerdem konnten verschiedene Addukte in den dazugehörigen ESI massenpektrometrischen Daten gefunden werden. Die (*O,S*)Pt Einheit kann **9-mg** entweder unter Verlust oder Erhalt des DMSO-Liganden binden; im ersteren Fall wird wahrscheinlich eine bidentate Bindungsweise an N<sup>7</sup> und O<sup>6</sup> des **9-mg** ermöglicht. Zusätzlich wurden auch Bisaddukte von einer (*O,S*)Pt-Einheit mit zwei **9-mg** Molekülen gefunden (Kapitel 8).

In den Adduktspektren der Substanzen mit den ODN-Sequenzen wurde ein vielschichtiges Bindungsverhalten der Platinverbindungen beobachtet. Anhand von MS<sup>2</sup>-Experimenten mit Addukten der Verbindungen mit **ODN1** konnte wie erwartet die bevorzugte Bindung der (O,S)Pt-Einheit an Guanin nachgewiesen werden. Zusätzlich zu dieser stabilen Bindung müssen jedoch auch andere Bindungsstellen existieren, welche das Anbinden mehrerer Metallzentren an die Oligonukleotid-Einzelstränge ermöglichen. Dies wird besonders deutlich anhand der Adduktspektren mit **ODN3**, welches im Wesentlichen aus einer C-A Tandemsequenz besteht. In diesen wurden trotz Abwesenheit von Guanin mehrere an **ODN3** koordinierte (O,S)Pt-Einheiten gefunden. Eine Bindung über das Phosphodiester-Grundgerüst ist sehr unwahrscheinlich, so dass neben Guanin auch noch andere potentielle Bindungsstellen, wie Adenin oder auch Cytosin, für die (O,S)Pt-Einheit vorhanden sein sollten (Kapitel 8).

Generell konnte anhand der Biomolekül-Interaktionsstudien gezeigt werden, dass die untersuchten Substanzen ein definiertes Reaktivitätsspektrum gegenüber verschiedenen Biomolekülen aufweisen. Zusammen mit den biologischen und biophysikalischen Daten die im Rahmen dieser Arbeit erhoben wurden, konnte gezeigt werden dass viele verschiedene Faktoren zur finalen zellwachstumshemmenden Wirkung der Verbindungen beitragen. Verbindungen **29/30** und **45/46** mit Methyl-/Ethylgruppen am Dithioester-Schwefel und Phenyl- bzw. *meta*-Hydroxyphenylgruppen als aromatische Einheit konnten als viel versprechende Kandidaten für weitere detaillierte Untersuchungen identifiziert werden.

Es ist bei Weitem noch nicht geklärt wie diese Verbindungen *in vivo* agieren könnten. Die Ergebnisse dieser Arbeit leisten einen wichtigen Beitrag zu einem ersten Verständnis der Wirkungsweise dieser Substanzklasse. Zukünftige Untersuchungen könnten die Zellantwort auf eine Behandlung mit den potentiellen Cytostatika detaillierter erkunden, so dass eine Leitstruktur für die weitere Entwicklung identifiziert werden kann.



Scheme 27 Organische Precursorverbindungen zur Herstellung von Biokonjugaten mittels CuAAC und Zugänglichkeit der entsprechenden Platinkomplexe.

Um eine verbesserte Selektivität der Substanzen gegenüber Krebszellen zu ermöglichen, wurden Synthesewege zur Anbindung von Biomolekülen erkundet, welche dann als Targeting-Einheit fungieren können. Zwei generelle, bekannte Methoden wurden zu diesem Zweck angewendet: Der prominenteste Vertreter der „Click“-Chemie, die Kupfer(Cu)-katalysierte Azid-Alkin-Cycloaddition (CuAAC) und das Verbinden mittels Amidbindungen. Um eine CuAAC zu ermöglichen wurde das Grundgerüst der  $\beta$ -Hydroxydithiozimtsäureester mit terminalen Alkin- und Azidgruppen funktionalisiert (Verbindungen **54-59** und **71**, Scheme 27). Das Einbringen von terminalen Alkinen in das Grundgerüst erwies sich als äußerst umständlich und ging mit vielen unkontrollierten Umlagerungsreaktionen sowie Hydratationsreaktionen an der Dreifachbindung während der Komplex- und Ligandensynthesen einher. Aufgrund dessen war es nicht möglich, monofunktionale Komplexe mit der gewünschten (O,S)PtCl(DMSO) Koordinationsumgebung zu isolieren; lediglich Bischelate (**61**, **62**, **66**, Scheme 27) wurden erhalten in denen die terminale Alkingruppe bewahrt blieb. Im Gegensatz dazu verlief die Synthese der Benzylazid-funktionalisierten Verbindungen reibungslos und mit guten Ausbeuten (Kapitel 11).

Nachdem Leu<sup>5</sup>-Enkephalin mittels Carbonsäuren die entweder eine Alkin- (**76**) oder eine Azidgruppe (**77**) tragen derivatisiert wurde, sollte die Verlinkung durch CuAAC durchgeführt werden. Es war möglich, Bischelate mit beiden funktionellen Gruppen, einem terminalen Alkin (**62**) oder Azid (**73**), an

das entsprechend komplementäre Enkephalin-Derivat zu koppeln (**78** und **79**). Dabei verlief aber die Synthese von **78** wesentlich effektiver; es wurden weniger Nebenprodukte erhalten und die Ausbeute an reinem Metall-Peptid-Konjugat war dadurch höher. Es war weiterhin möglich, den monofunktionalen Komplex **81** zu erhalten indem zuerst CuAAC am Liganden **71** durchgeführt wurde und anschließend das Pt(II) Zentrum eingeführt wurde (Kapitel 11). Die drei relevanten Metall-Biokonjugate sind in Chart 10 abgebildet.

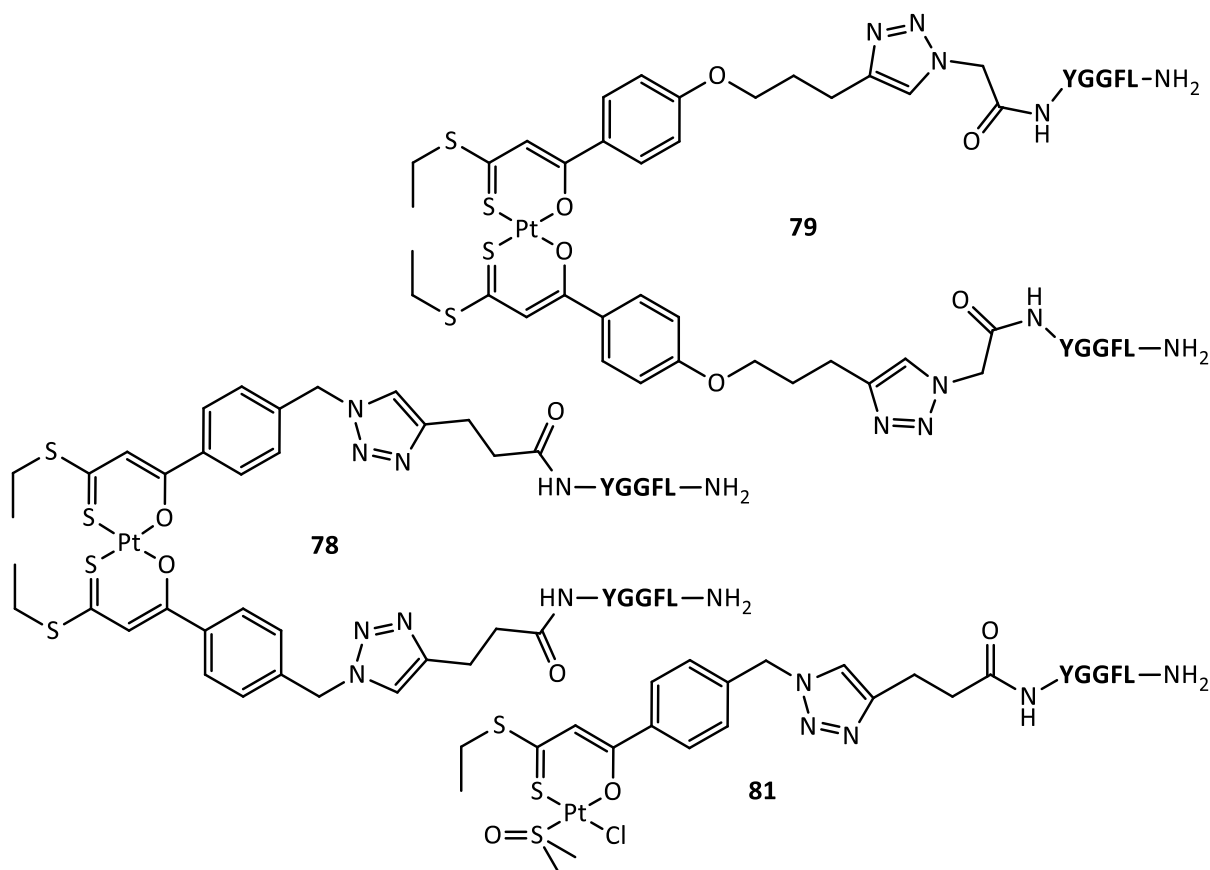


Chart 10 Isolierte Metall-Biokonjugate nach CuAAC.

Als alternative Zugangsmöglichkeit zu Biokonjugaten mit den gewünschten Einheiten (*O,S*)Pt und Enk wurde die Ausbildung von Peptidbindungen untersucht. Nachdem in Verbindung **82** eine Carboxymethyl-Gruppe am Dithioester-Schwefel eingebracht wurde konnte sie erfolgreich in Lösung an Leu<sup>5</sup>-Enk **75** gekoppelt werden. Anschließend wurde der Platin-Komplex generiert der wie gewünscht die monodentaten Chlorido- und DMSO-Liganden trug (Chart 11). Alle isolierten Verbindungen wurden mithilfe ihrer massenspektrometrischen Isotopenprofile und anhand von NMR-Spektren identifiziert (Kapitel 12).

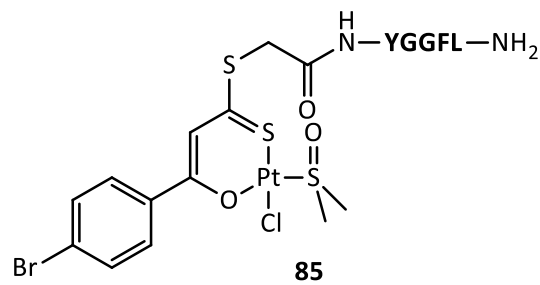


Chart 11 Metall-Biokonjugat nach Verknüpfung durch eine Peptidbindung.

Im Rahmen dieser Arbeit konnte gezeigt werden, dass das grundlegende Strukturmotiv der hier vorgestellten Verbindungen eine Vielzahl von Modifizierungsmöglichkeiten bietet, welche den Zugang zu Verbindungen mit optimierten biologisch-relevanten Eigenschaften des (O,S)Pt Pharmakophors ermöglichen. Mehrere synthetische Ansätze hierzu wurden in dieser Arbeit vorgestellt und verschiedene Methoden zur Untersuchung der funktionellen Konsequenzen angewendet. Diese Arbeit leistet somit einen ersten Beitrag zur Entwicklung neuer, vielversprechender Medikamente mit optimiertem biologischen Profil.





---

## REFERENCES

- (1) Kaufmann, G. B.; Pentimalli, R.; Doldi, S.; Hall, M. D. Michele Peyrone (1813–1883), Discoverer of Cisplatin. *Platinum Met. Rev.* **2010**, *54* (4), 250–256.
- (2) Strucchi, A. Michele Peyrone. *Giornale di Agricoltura, Industria e Commercio del regno d'Italia* **1885**, *22*, 263.
- (3) Amos, J. L. Barnett Rosenberg <http://www.natgeocreative.com/photography/423263>.
- (4) Peyrone, M. Über Die Einwirkung Des Ammoniaks Auf Platinchlorür. *Annalen der Chemie und Pharmacie* **1844**, *51*, 1–29.
- (5) Rosenberg, B.; Van Camp, L.; Krigas, T. Inhibition of Cell Division in Escherichia Coli by Electrolysis Products from a Platinum Electrode. *Nature* **1965**, *205* (4972), 698–699.
- (6) Rosenberg, B. Some Biological Effects of Platinum Compounds. *Platinum Met. Rev.* **1971**, *15* (2), 42–51.
- (7) Rosenberg, B. Platinum Complexes for the Treatment of Cancer. *Interdiscip. Sci. Rev.* **1978**, *3* (2), 134–147.
- (8) Trzaska, S. Cisplatin. *Chem. Eng. News* **2005**, *83* (25), 52.
- (9) O'Dwyer, P. J.; Stevenson, J. P.; Johnson, S. W. Clinical Status of Cisplatin, Carboplatin, and Other Platinum-Based Antitumor Drugs. In *Cisplatin*; Lippert, B., Ed.; Verlag Helvetica Chimica Acta: Zürich, 1999; pp 29–69.
- (10) Galanski, M.; Keppler, B. K. Tumorhemmende Metallverbindungen: Entwicklung, Bedeutung Und Perspektiven. *Pharm. Unserer Zeit* **2006**, *35* (2), 118–123.
- (11) The Nobel Prize in Chemistry 1913 [http://www.nobelprize.org/nobel\\_prizes/chemistry/laureates/1913/](http://www.nobelprize.org/nobel_prizes/chemistry/laureates/1913/) (accessed Jun 18, 2015).
- (12) Lippert, B. Uses of Metal Compounds in Medicine. In *Reference Module in Chemistry, Molecular Sciences and Chemical Engineering*; Elsevier, 2013; Current as of 23 October 2014.
- (13) Wheate, N. J.; Walker, S.; Craig, G. E.; Oun, R. The Status of Platinum Anticancer Drugs in the Clinic and in Clinical Trials. *Dalton Trans.* **2010**, *39* (35), 8113–8127.
- (14) Thayer, A. M. Collaboration Yielded A New Class Of Cancer Drugs. *Chem. Eng. News* **2010**, *88* (26), online exclusive.
- (15) Thayer, A. M. Pedagogy On Platinum Drugs. *Chem. Eng. News* **2010**, *88* (26), online exclusive.
- (16) Buß, I.; Jaehde, U. Platinum Complexes. In *Encyclopedia of Cancer*; Schwab, M., Ed.; Springer: Berlin, Heidelberg, 2008; pp 2358–2363.
- (17) Shukuya, T.; Yamanaka, T.; Seto, T.; Daga, H.; Goto, K.; Saka, H.; Sugawara, S.; Takahashi, T.; Yokota, S.; Kaneda, H.; Kawaguchi, T.; Nagase, S.; Oguri, T.; Iwamoto, Y.; Nishimura, T.; Hattori, Y.; Nakagawa, K.; Nakanishi, Y.; Yamamoto, N. Randomized Phase III Study of Nedaplatin (N) plus Docetaxel (D) versus Cisplatin (C) plus D for Advanced or Relapsed Squamous Cell Carcinoma of the Lung (SqLC): WJOG5208L. *J. Clin. Oncol., ASCO Meet. Abstr.* **2015**, *33* (15\_suppl), 8004.
- (18) U.S. National Library of Medicine. Search of: Nedaplatin - ClinicalTrials.gov <https://clinicaltrials.gov/ct2/results?term=nedaplatin&Search=Search> (accessed Jun 18, 2015).
- (19) U.S. National Library of Medicine. Search of: Lobaplatin - ClinicalTrials.gov <https://clinicaltrials.gov/ct2/results?term=lobaplatin&Search=Search> (accessed Jun 18, 2015).
- (20) Kang, J.-H.; Kuh, H.-J.; Lee, J.-H.; Shin, J.-Y.; Lee, K.-S.; Jung, J.-A.; Chang, D.-Y. Phase I/II Clinical and Pharmacokinetic Trial of Heptaplatin and 5-FU Combination Treatment in Advanced Head and Neck Cancer. *J. Clin. Oncol., ASCO Meet. Abstr.* **2005**, *23* (16\_suppl), 5550.
- (21) Lee, J.-W.; Park, J.-K.; Lee, S.-H.; Kim, S.-Y.; Cho, Y.-B.; Kuh, H.-J. Anti-Tumor Activity of Heptaplatin in Combination with 5-Fluorouracil or Paclitaxel against Human Head and Neck Cancer Cells in Vitro. *Anticancer Drugs* **2006**, *17* (4), 377–384.

- (22) Sternberg, C. N.; Petrylak, D. P.; Sartor, O.; Witjes, J. A.; Demkow, T.; Ferrero, J.-M.; Eymard, J.-C.; Falcon, S.; Calabrò, F.; James, N.; Bodrogi, I.; Harper, P.; Wirth, M.; Berry, W.; Petrone, M. E.; McKearn, T. J.; Noursalehi, M.; George, M.; Rozenzweig, M. Multinational, Double-Blind, Phase III Study of Prednisone and Either Satraplatin or Placebo in Patients With Castrate-Refractory Prostate Cancer Progressing After Prior Chemotherapy: The SPARC Trial. *JCO* **2009**, *27* (32), 5431–5438.
- (23) GPC Biotech Withdraws Satraplatin NDA for Accelerated Approval; Plans to Resubmit With Survival Analysis [http://www.drugs.com/nda/satraplatin\\_070730.html](http://www.drugs.com/nda/satraplatin_070730.html) (accessed Jun 18, 2015).
- (24) U.S. National Library of Medicine. Search of: Satraplatin - ClinicalTrials.gov <https://clinicaltrials.gov/ct2/results?term=satraplatin&Search=Search> (accessed Jun 18, 2015).
- (25) Lovejoy, K. S.; Lippard, S. J. Non-Traditional Platinum Compounds for Improved Accumulation, Oral Bioavailability, and Tumor Targeting. *Dalton Trans.* **2009**, No. 48, 10651–10659.
- (26) Poniard Pharmaceuticals Announces Pivotal Phase 3 SPEAR Trial of Picoplatin in Small Cell Lung Cancer Did Not Meet Primary Endpoint <http://www.fiercebiotech.com/press-releases/poniard-pharmaceuticals-announces-pivotal-phase-3-spear-trial-picoplatin-small-cell-l> (accessed Jun 18, 2015).
- (27) U.S. National Library of Medicine. Search of: Picoplatin - ClinicalTrials.gov <https://clinicaltrials.gov/ct2/results?term=picoplatin&Search=Search> (accessed Jun 18, 2015).
- (28) Hensing, T. A.; Hanna, N. H.; Gillenwater, H. H.; Gabriella Camboni, M.; Allievi, C.; Socinski, M. A. Phase II Study of BBR 3464 as Treatment in Patients with Sensitive or Refractory Small Cell Lung Cancer. *Anticancer Drugs* **2006**, *17* (6), 697–704.
- (29) U.S. National Library of Medicine. Search of: BBR3464 - ClinicalTrials.gov <https://clinicaltrials.gov/ct2/results?term=BBR3464&Search=Search> (accessed Jun 18, 2015).
- (30) Dhar, S.; Lippard, S. J. Current Status and Mechanism of Action of Platinum-Based Anticancer Drugs. In *Bioinorganic Medicinal Chemistry*; Alessio, E., Ed.; Wiley-VCH Verlag GmbH & Co. KGaA: Weinheim, Germany, 2011; pp 79–95.
- (31) Stathopoulos, G. P.; Boulikas, T. Lipoplatin Formulation Review Article. *J. Drug Delivery* **2012**, *2012*, e581363.
- (32) Stathopoulos, G. P.; Antoniou, D.; Dimitroulis, J.; Stathopoulos, J.; Marosis, K.; Michalopoulou, P. Comparison of Liposomal Cisplatin versus Cisplatin in Non-Squamous Cell Non-Small-Cell Lung Cancer. *Cancer Chemother. Pharmacol.* **2011**, *68* (4), 945–950.
- (33) Serova, M.; Ghoul, A.; Rezaï, K.; Lokiec, F.; Cvitkovic, E.; Nowotnik, D.; Faivre, S.; Raymond, E. In Vitro Anti-Proliferative Effects of ProLindac<sup>TM</sup>, a Novel Dach-Platinum-Linked Polymer Compound, as a Single Agent and in Combination with Other Anti-Cancer Drugs. In *Platinum and Other Heavy Metal Compounds in Cancer Chemotherapy*; Cancer Drug Discovery and Development; Humana Press, 2009; pp 41–47.
- (34) Nowotnik, D. P.; Cvitkovic, E. ProLindac<sup>TM</sup> (AP5346): A Review of the Development of an HPMA DACH Platinum Polymer Therapeutic. *Adv. Drug Delivery Rev.* **2009**, *61* (13), 1214–1219.
- (35) Hannon, M. J. Metal-Based Anticancer Drugs: From a Past Anchored in Platinum Chemistry to a Post-Genomic Future of Diverse Chemistry and Biology. *Pure Appl. Chem.* **2007**, *79* (12), 2243–2262.
- (36) Bruijninx, P. C.; Sadler, P. J. New Trends for Metal Complexes with Anticancer Activity. *Current Opinion in Chemical Biology* **2008**, *12* (2), 197–206.
- (37) Jakupec, M. A.; Galanski, M.; Arion, V. B.; Hartinger, C. G.; Keppler, B. K. Antitumour Metal Compounds: More than Theme and Variations. *Dalton Trans.* **2008**, No. 2, 183–194.
- (38) Montaña, A. M.; Batalla, C. The Rational Design of Anticancer Platinum Complexes: The Importance of the Structure-Activity Relationship. *Curr. Med. Chem.* **2009**, *16* (18), 2235–2260.
- (39) Hartinger, C. G.; Dyson, P. J. Bioorganometallic Chemistry—from Teaching Paradigms to Medicinal Applications. *Chem. Soc. Rev.* **2009**, *38* (2), 391–401.

- (40) Aris, S. M.; Farrell, N. P. Towards Antitumor Active Trans-Platinum Compounds. *Eur. J. Inorg. Chem.* **2009**, 2009 (10), 1293–1302.
- (41) Gianferrara, T.; Bratsos, I.; Alessio, E. A Categorization of Metal Anticancer Compounds Based on Their Mode of Action. *Dalton Trans.* **2009**, No. 37, 7588.
- (42) Harper, B.; Krause-Heuer, A.; Grant, M.; Manohar, M.; Garbutcheon-Singh, K. B.; Aldrich-Wright, J. Advances in Platinum Chemotherapeutics. *Chem. - Eur. J.* **2010**, 16 (24), 7064–7077.
- (43) Gasser, G.; Ott, I.; Metzler-Nolte, N. Organometallic Anticancer Compounds. *J. Med. Chem.* **2011**, 54 (1), 3–25.
- (44) Komeda, S.; Casini, A. Next-Generation Anticancer Metallodrugs. *Curr. Top. Med. Chem.* **2012**, 12 (3), 219–235.
- (45) Wang, X.; Guo, Z. Targeting and Delivery of Platinum-Based Anticancer Drugs. *Chem. Soc. Rev.* **2013**, 42 (1), 202–224.
- (46) Mjos, K. D.; Orvig, C. Metallodrugs in Medicinal Inorganic Chemistry. *Chem. Rev.* **2014**, 114 (8), 4540–4563.
- (47) Medici, S.; Peana, M.; Nurchi, V. M.; Lachowicz, J. I.; Crisponi, G.; Zoroddu, M. A. Noble Metals in Medicine: Latest Advances. *Coord. Chem. Rev.* **2015**, 284, 329–350.
- (48) Thayer, A. M. Platinum Drugs Take Their Toll. *Chem. Eng. News* **2010**, 88 (26), 24–28.
- (49) Galanski, M. Editorial [Hot Topic: Anticancer Platinum Complexes - State of the Art and Future Prospects (Guest Editor: Markus Galanski)]. *Anti-Cancer Agents Med. Chem.* **2007**, 7, 1–2.
- (50) Kelland, L. The Resurgence of Platinum-Based Cancer Chemotherapy. *Nat. Rev. Cancer* **2007**, 7 (8), 573–584.
- (51) Wang, D.; Lippard, S. J. Cellular Processing of Platinum Anticancer Drugs. *Nat. Rev. Drug Discovery* **2005**, 4 (4), 307–320.
- (52) Stewart, D. J. Mechanisms of Resistance to Cisplatin and Carboplatin. *Crit. Rev. Oncol. Hematol.* **2007**, 63 (1), 12–31.
- (53) Hartinger, C. G.; Metzler-Nolte, N.; Dyson, P. J. Challenges and Opportunities in the Development of Organometallic Anticancer Drugs. *Organometallics* **2012**, 31 (16), 5677–5685.
- (54) Hartinger, C. G.; Zorbas-Seifried, S.; Jakupec, M. A.; Kynast, B.; Zorbas, H.; Keppler, B. K. From Bench to Bedside – Preclinical and Early Clinical Development of the Anticancer Agent Indazolium Trans-[tetrachlorobis(1H-indazole)ruthenate(III)] (KP1019 or FFC14A). *J. Inorg. Biochem.* **2006**, 100 (5–6), 891–904.
- (55) Graf, N.; Lippard, S. J. Redox Activation of Metal-Based Prodrugs as a Strategy for Drug Delivery. *Adv. Drug Delivery Rev.* **2012**, 64 (11), 993–1004.
- (56) Wilson, J. J.; Lippard, S. J. Synthetic Methods for the Preparation of Platinum Anticancer Complexes. *Chem. Rev.* **2014**, 114 (8), 4470–4495.
- (57) Barry, N. P. E.; Sadler, P. J. Exploration of the Medical Periodic Table: Towards New Targets. *Chem. Commun.* **2013**, 49 (45), 5106–5131.
- (58) Kilpin, K. J.; Dyson, P. J. Enzyme Inhibition by Metal Complexes: Concepts, Strategies and Applications. *Chem. Sci.* **2013**, 4 (4), 1410–1419.
- (59) Cisplatin - FDA prescribing information, side effects and uses [http://www.drugs.com/pro/cisplatin.html#i4i\\_section\\_id\\_8f9578d8-5de6-4e92-90e8-4b7d5ee14154](http://www.drugs.com/pro/cisplatin.html#i4i_section_id_8f9578d8-5de6-4e92-90e8-4b7d5ee14154) (accessed Jun 22, 2015).
- (60) Arnesano, F.; Natile, G. Mechanistic Insight into the Cellular Uptake and Processing of Cisplatin 30 Years after Its Approval by FDA. *Coord. Chem. Rev.* **2009**, 253 (15-16), 2070–2081.
- (61) Hall, M. D.; Okabe, M.; Shen, D.-W.; Liang, X.-J.; Gottesman, M. M. The Role of Cellular Accumulation in Determining Sensitivity to Platinum-Based Chemotherapy. *Annu. Rev. Pharmacol. Toxicol.* **2008**, 48 (1), 495–535.
- (62) Arnesano, F.; Losacco, M.; Natile, G. An Updated View of Cisplatin Transport. *European Journal of Inorganic Chemistry* **2013**, 2013 (15), 2701–2711.

- (63) Ishida, S.; Lee, J.; Thiele, D. J.; Herskowitz, I. Uptake of the Anticancer Drug Cisplatin Mediated by the Copper Transporter Ctr1 in Yeast and Mammals. *Proc. Natl. Acad. Sci.* **2002**, *99* (22), 14298–14302.
- (64) Arnesano, F.; Scintilla, S.; Natile, G. Interaction between Platinum Complexes and a Methionine Motif Found in Copper Transport Proteins. *Angew. Chem.* **2007**, *119* (47), 9220–9222.
- (65) Arnesano, F.; Scintilla, S.; Natile, G. Interaction between Platinum Complexes and a Methionine Motif Found in Copper Transport Proteins. *Angew. Chem., Int. Ed.* **2007**, *46* (47), 9062–9064.
- (66) Safaei, R. Role of Copper Transporters in the Uptake and Efflux of Platinum Containing Drugs. *Cancer Lett.* **2006**, *234* (1), 34–39.
- (67) Jung, Y.; Lippard, S. J. Direct Cellular Responses to Platinum-Induced DNA Damage. *Chem. Rev.* **2007**, *107* (5), 1387–1407.
- (68) Zhang, S.; Lovejoy, K. S.; Shima, J. E.; Lagpacan, L. L.; Shu, Y.; Lapuk, A.; Chen, Y.; Komori, T.; Gray, J. W.; Chen, X.; Lippard, S. J.; Giacomini, K. M. Organic Cation Transporters Are Determinants of Oxaliplatin Cytotoxicity. *Cancer Res.* **2006**, *66* (17), 8847–8857.
- (69) Hermann, G.; Heffeter, P.; Falta, T.; Berger, W.; Hann, S.; Koellensperger, G. In Vitro Studies on Cisplatin Focusing on Kinetic Aspects of Intracellular Chemistry by LC-ICP-MS. *Metallomics* **2013**, *5* (6), 636–647.
- (70) Eljack, N. D.; Ma, H.-Y. M.; Drucker, J.; Shen, C.; Hambley, T. W.; New, E. J.; Friedrich, T.; Clarke, R. J. Mechanisms of Cell Uptake and Toxicity of the Anticancer Drug Cisplatin. *Metallomics* **2014**, *6* (11), 2126–2133.
- (71) Clarke, R. J.; Fan, X. Pumping Ions. *Clin. Exp. Pharmacol. Physiol.* **2011**, *38* (11), 726–733.
- (72) Marcelis, A. T. M.; Erkelens, C.; Reedijk, J. The Interaction of Aquated platinum(II) Compounds with Purine Mononucleotides. *Inorg. Chim. Acta* **1984**, *91* (2), 129–135.
- (73) Fichtinger-Schepman, A. M. J.; Van der Veer, J. L.; Den Hartog, J. H. J.; Lohman, P. H. M.; Reedijk, J. Adducts of the Antitumor Drug Cis-diamminedichloroplatinum(II) with DNA: Formation, Identification, and Quantitation. *Biochemistry* **1985**, *24* (3), 707–713.
- (74) Davies, M. S.; Berners-Price, S. J.; Hambley, T. W. Rates of Platination of AG and GA Containing Double-Stranded Oligonucleotides: Insights into Why Cisplatin Binds to GG and AG but Not GA Sequences in DNA. *J. Am. Chem. Soc.* **1998**, *120* (44), 11380–11390.
- (75) Davies, M. S.; Berners-Price, S. J.; Hambley, T. W. Slowing of Cisplatin Aquation in the Presence of DNA but Not in the Presence of Phosphate: Improved Understanding of Sequence Selectivity and the Roles of Monoaquated and Diaquated Species in the Binding of Cisplatin to DNA. *Inorg. Chem.* **2000**, *39* (25), 5603–5613.
- (76) Fichtinger-Schepman, A. M. J.; Lohman, P. H. M.; Reedijk, J. Detection and Quantification of Adducts Formed upon Interaction of Diamminedichloroplatinum (II) with DNA, by Anion-Exchange Chromatography after Enzymatic Degradation. *Nucleic Acids Res.* **1982**, *10* (17), 5345–5356.
- (77) Jamieson, E. R.; Lippard, S. J. Structure, Recognition, and Processing of Cisplatin–DNA Adducts. *Chem. Rev.* **1999**, *99* (9), 2467–2498.
- (78) Reedijk, J. Platinum Anticancer Coordination Compounds: Study of DNA Binding Inspires New Drug Design. *Eur. J. Inorg. Chem.* **2009**, *2009* (10), 1303–1312.
- (79) Wang, X.; Guo, Z. The Role of Sulfur in Platinum Anticancer Chemotherapy. *Anti-Cancer Agents Med. Chem.* **2007**, *7*, 19–34.
- (80) Kraker, A.; Schmidt, J.; Krezoski, S.; Petering, D. H. Binding of Cis-Dichlorodiammine platinum(II) to Metallothionein in Ehrlich Cells. *Biochem. Biophys. Res. Commun.* **1985**, *130* (2), 786–792.
- (81) Ishikawa, T.; Ali-Osman, F. Glutathione-Associated Cis-diamminedichloroplatinum(II) Metabolism and ATP-Dependent Efflux from Leukemia Cells. Molecular Characterization of

- Glutathione-Platinum Complex and Its Biological Significance. *J. Biol. Chem.* **1993**, *268* (27), 20116–20125.
- (82) Gibson, D. The Mechanism of Action of Platinum Anticancer Agents - What Do We Really Know about It? *Dalton Trans.* **2009**, No. 48, 10681–10689.
- (83) Kasherman, Y.; Sturup, S.; Gibson, D. Is Glutathione the Major Cellular Target of Cisplatin? A Study of the Interactions of Cisplatin with Cancer Cell Extracts. *J. Med. Chem.* **2009**, *52* (14), 4319–4328.
- (84) Reedijk, J. The Relevance of Hydrogen Bonding in the Mechanism of Action of Platinum Antitumor Compounds. *Inorg. Chim. Acta* **1992**, *198*, 873–881.
- (85) Casini, A.; Reedijk, J. Interactions of Anticancer Pt Compounds with Proteins: An Overlooked Topic in Medicinal Inorganic Chemistry? *Chem. Sci.* **2012**, *3* (11), 3135–3144.
- (86) Reedijk, J. Why Does Cisplatin Reach Guanine-N7 with Competing S-Donor Ligands Available in the Cell? *Chem. Rev.* **1999**, *99* (9), 2499–2510.
- (87) Reedijk, J. New Clues for Platinum Antitumor Chemistry: Kinetically Controlled Metal Binding to DNA. *Proc. Natl. Acad. Sci.* **2003**, *100* (7), 3611.
- (88) Reedijk, J. Fast and Slow versus Strong and Weak Metal-DNA Binding: Consequences for Anti-Cancer Activity. *Metallomics* **2012**, *4* (7), 628–632.
- (89) Eastman, A. The Mechanism of Action of Cisplatin: From Adducts to Apoptosis. In *Cisplatin*; Lippert, B., Ed.; Verlag Helvetica Chimica Acta: Zürich, 1999; pp 111–134.
- (90) Todd, R. C.; Lippard, S. J. Inhibition of Transcription by Platinum Antitumor Compounds. *Metallomics* **2009**, *1* (4), 280–291.
- (91) Bowden, N. A. Nucleotide Excision Repair: Why Is It Not Used to Predict Response to Platinum-Based Chemotherapy? *Cancer Lett.* **2014**, *346* (2), 163–171.
- (92) Park, S.; Lippard, S. J. Binding Interaction of HMGB4 with Cisplatin-Modified DNA. *Biochemistry* **2012**, *51* (34), 6728–6737.
- (93) Huang, J. C.; Zamble, D. B.; Reardon, J. T.; Lippard, S. J.; Sancar, A. HMG-Domain Proteins Specifically Inhibit the Repair of the Major DNA Adduct of the Anticancer Drug Cisplatin by Human Excision Nuclease. *Proc. Natl. Acad. Sci.* **1994**, *91* (22), 10394–10398.
- (94) Ohndorf, U.-M.; Rould, M. A.; He, Q.; Pabo, C. O.; Lippard, S. J. Basis for Recognition of Cisplatin-Modified DNA by High-Mobility-Group Proteins. *Nature* **1999**, *399* (6737), 708–712.
- (95) Zamble, D. B.; Lippard, S. J. The Response of Cellular Proteins to Cisplatin-Damaged DNA. In *Cisplatin*; Lippert, B., Ed.; Verlag Helvetica Chimica Acta: Zürich, 1999; pp 71–110.
- (96) Tan, C.-P.; Lu, Y.-Y.; Ji, L.-N.; Mao, Z.-W. Metallomics Insights into the Programmed Cell Death Induced by Metal-Based Anticancer Compounds. *Metallomics* **2014**, *6* (5), 978–995.
- (97) Pearson, R. G. Hard and Soft Acids and Bases. *J. Am. Chem. Soc.* **1963**, *85* (22), 3533–3539.
- (98) Pearson, R. G. Antisymbiosis and the Trans Effect. *Inorg. Chem.* **1973**, *12* (3), 712–713.
- (99) Janiak, C. Kapitel 2: Komplex- Und Koordinationschemie. In *Moderne Anorganische Chemie*; Riedel, E., Ed.; de Gruyter: Berlin, New York, 1999; pp 155–328.
- (100) Mügge, C. Platinum(II) Complexes with Sulfur-Containing Ligands as Possible Cytotoxic Substances, 2009.
- (101) Singh, M. S.; Nandi, G. C.; Chanda, T. Beta-Oxodithioesters: A New Frontier for Diverse Heterocyclic Architectures. *RSC Adv.* **2013**, *3* (34), 14183–14198.
- (102) Gompper, R.; Schaefer, H. Ketenderivate, XII. Beiträge Zur Chemie Der Dithiocarbonsäureester Und Ketenmercaptale. *Chem. Ber.* **1967**, *100* (2), 591–604.
- (103) Larsson, F. C. V.; Lawesson, S. O. Preparation and Alkylation of Substituted B-Hydroxydithiocinnamic Acids. *Tetrahedron* **1972**, *28* (21), 5341–5357.
- (104) Saumweber, R.; Robl, C.; Weigand, W. Synthesis and Coordination Properties of Amphiphilic 3-Oxodithiocarboxylic Esters. *Inorg. Chim. Acta* **1998**, *269* (1), 83–90.
- (105) Schubert, K.; Saumweber, R.; Görls, H.; Weigand, W. Funktionalisierte Beta-Hydroxydithiozimtsäurederivate Als Liganden. Kristallstrukturanalyse von 4'-Hydroxy-Beta-Hydroxydithiozimtsäuremethylester. *Z. Anorg. Allg. Chem.* **2003**, *629* (12-13), 2091–2096.

- (106) Schubert, K.; Alpermann, T.; Nicksch, T.; Görls, H.; Weigand, W. Synthese Und Charakterisierung Funktionalisierter Beta-Hydroxydithiozimsäuren Und Deren Ester. Komplexchemisches Verhalten Gegenüber Nickel(II), Palladium(II) Und Platin(II). *Z. Anorg. Allg. Chem.* **2006**, *632* (6), 1033–1042.
- (107) Schubert, K.; Görls, H.; Weigand, W. Derivatives of Beta-Hydroxydithiocinnamic Acids as Ligands. Syntheses and Characterisation of Novel 1,1-Ethenedithiolato and O,S-Chelate Complexes. *Z. Naturforsch.* **2007**, *62b*, 475–482.
- (108) Schubert, K.; Görls, H.; Weigand, W. Synthesis and Analytical Characterization of Novel Pyridyl-Substituted 1, 1'-Ethenedithiolato Complexes. *Heteroat. Chem.* **2005**, *16* (5), 369–378.
- (109) Singh, G.; Bhattacharjee, S. S.; Ila, H.; Junjappa, H. A Facile One-Step Synthesis of Methyl Beta-Oxodithiocarboxylates. *Synthesis* **1982**, *1982* (08), 693–694.
- (110) Samuel, R.; Asokan, C. V.; Suma, S.; Chandran, P.; Retnamma, S.; Anabha, E. R. A Facile Method for the Synthesis of Substituted 2-Ylidene-1,3-Oxathioles from Acetophenones. *Tetrahedron Lett.* **2007**, *48* (47), 8376–8378.
- (111) Junjappa, H.; Ila, H.; Nandi, S. A Method for Producing Diverse Set of Dithioate Compounds. WO2004101530, November 26, 2004.
- (112) Nair, S. K.; Asokan, C. V. Sulphydrolysis of Acyl Ketene Dithioacetals: A Convenient Synthesis of Beta-Oxodithioesters. *Synth. Commun.* **1999**, *29* (5), 791–798.
- (113) Nair, S. K.; Samuel, R.; Asokan, C. V. Dimethyl Anion Induced Demethylation and Fragmentation Reactions of Alpha-Oxoketenedithioacetals. *Synthesis* **2001**, *2001* (04), 0573–0576.
- (114) Thuillier, A.; Vialle, J. *Bull. Soc. Chim. Fr.* **1962**, 2182–2186.
- (115) Thuillier, A.; Vialle, J. *Bull. Soc. Chim. Fr.* **1962**, 2187–2193.
- (116) Thuillier, A.; Vialle, J. *Bull. Soc. Chim. Fr.* **1962**, 2194–2198.
- (117) P. Beslin; M. C. Houtteville. *Bull. Soc. Chim. Fr.* **1989**, 413–418.
- (118) Mügge, C.; Liu, R.; Görls, H.; Gabbiani, C.; Michelucci, E.; Rüdiger, N.; Clement, J. H.; Messori, L.; Weigand, W. Novel Platinum(II) Compounds with O,S Bidentate Ligands: Synthesis, Characterization, Antiproliferative Properties and Biomolecular Interactions. *Dalton Trans.* **2014**, *43* (8), 3072–3086.
- (119) Mügge, C.; Marzo, T.; Massai, L.; Hildebrandt, J.; Ferraro, G.; Merlino, A.; Metzler-Nolte, N.; Messori, L.; Weigand, W. Platinum(II) Complexes with O,S Bidentate Ligands: Biophysical Characterization, Antiproliferative Activity and Crystallographic Evidence of Protein Binding. *Inorg. Chem.* **accepted manuscript**.
- (120) Corey, E. J.; Venkateswarlu, A. Protection of Hydroxyl Groups as Tert-Butyldimethylsilyl Derivatives. *J. Am. Chem. Soc.* **1972**, *94* (17), 6190–6191.
- (121) Mancilla-González, M. del C.; Jancik, V.; Martínez-Otero, D.; Moya-Cabrera, M.; García-Orozco, I. Half-Sandwich Titanium Complexes with Beta-Oxodithioester Ligands. *J. Organomet. Chem.* **2014**, *770*, 35–41.
- (122) Nandi, G. C.; Singh, M. S.; Ila, H.; Junjappa, H. Highly Regioselective One-Pot, Three-Component Synthesis of 1-Aryl-3,4-Substituted/Annulated-5-(Cycloamino)/(Alkylamino)pyrazoles from Beta-Oxodithioesters. *Eur. J. Org. Chem.* **2012**, *2012* (5), 967–974.
- (123) Koley, S.; Chowdhury, S.; Chanda, T.; Ramulu, B. J.; Singh, M. S. Diversity Oriented Catalyst-Free and Solvent-Free One-Pot MCR at Room Temperature: Rapid and Regioselective Convergent Approach to Highly Functionalized Dihydro-4H-Thiopyrans. *Tetrahedron* **2013**, *69* (37), 8013–8018.
- (124) Chowdhury, S.; Chanda, T.; Koley, S.; Ramulu, B. J.; Jones, R. C. F.; Singh, M. S. Palladium Catalyzed Oxidative Coupling of Alpha-Enolic Dithioesters: A New Entry to 3,4,5-Trisubstituted 1,2-Dithioles via a Double Activation Strategy. *Org. Lett.* **2013**, *15* (20), 5386–5389.
- (125) Beyer, L.; Kirmse, R.; Stach, J.; Szargan, R.; Hoyer, E. Metallkomplexe Des Benzoyldithioessigsäuremethylesters Und Des N-Benzoylamino-Dithiokohlensäureethylesters:

- Darstellung Und Charakterisierung, ESCA-Und EPR-Untersuchungen. *Z. Anorg. Allg. Chem.* **1981**, 476 (5), 7–15.
- (126) Yadav, M. K.; Rajput, G.; Srivastava, K.; Singh, R.; Mishra, R.; Drew, M. G. B.; Singh, N. Anti-Leishmanial Activity of Ni(II), Pd(II) and Pt(II) Beta-Oxodithioester Complexes. *New J. Chem.* **2015**.
- (127) Rothenburger, C. Synthese und Charakterisierung schwefelhaltiger Platin(II)-Komplexe und ihre zytotoxischen Eigenschaften, Dissertation, Friedrich-Schiller Universität Jena: Jena, 2008.
- (128) Rajput, G.; Yadav, M. K.; Drew, M. G. B.; Singh, N. Influence of the Ligand Frameworks on the Coordination Environment and Properties of New phenylmercury(II) Beta-Oxodithioester Complexes. *Dalton Trans.* **2015**, 44 (12), 5909–5916.
- (129) Kukushkin, Y. N.; Vyazmenskii, Y. E.; Zorina, L. I. The Trans Influence of Dimethyl Sulphoxide in platinum(II) Compounds. *Russ. J. Inorg. Chem.* **1968**, 13, 1573–1576.
- (130) Price, J. H.; Williamson, A. N.; Schramm, R. F.; Wayland, B. B. Palladium(II) and platinum(II) Alkyl Sulfoxide Complexes. Examples of Sulfur-Bonded, Mixed Sulfur- and Oxygen-Bonded, and Totally Oxygen-Bonded Complexes. *Inorg. Chem.* **1972**, 11 (6), 1280–1284.
- (131) Melanson, R.; Rochon, F. D. The Crystal Structure of Cis-Dichlorobis(dimethylsulfoxide)platinum(II). *Can. J. Chem.* **1975**, 53 (16), 2371–2374.
- (132) Melanson, R.; Hubert, J.; Rochon, F. D. Potassium Trichloro (dimethyl Sulphoxide) Platinite (II). *Acta Crystallogr., Sect. B: Struct. Crystallogr. Cryst. Chem.* **1976**, 32 (6), 1914–1916.
- (133) Rochon, F. D.; Bensimon, C.; Tessier, C. Multinuclear Magnetic Resonance Study of Pt (II) Compounds with Sulfoxide Ligands and Crystal Structures of Complexes of the Types [Pt(R<sub>2</sub>SO)<sub>3</sub>]-and Pt(R<sub>2</sub>SO)<sub>2</sub>Cl<sub>2</sub>. *Inorg. Chim. Acta* **2008**, 361 (1), 16–28.
- (134) Motschi, H.; Pregosin, P. S.; Ruegger, H. Synthesis of a New Class of Acylplatinum Complexes Derived from Salicylaldehyde. *J. Organomet. Chem.* **1980**, 193 (3), 397–405.
- (135) Farrell, N. WO 8909598: Platinum-Amine-Sulfoxides as Anti-Tumor Agents. *WO 8909598* **1989**.
- (136) Kaplan, S. F.; Kukushkin, V. Y.; Pombeiro, A. J. L. Metal-Mediated and Solvent Dependent Chlorination of the Nitrosonaphtholato Ligand. *J. Chem. Soc., Dalton Trans.* **2001**, No. 22, 3279–3284.
- (137) Aitken, D. J.; Albinati, A.; Gautier, A.; Husson, H.-P.; Morgant, G.; Nguyen-Huy, D.; Kozelka, J.; Lemoine, P.; Ongeri, S.; Rizzato, S.; Viossat, B. Platinum(II) and Palladium(II) Complexes with N-Aminoguanidine. *Eur. J. Inorg. Chem.* **2007**, 2007 (21), 3327–3334.
- (138) Mügge, C.; Musumeci, D.; Michelucci, E.; Porru, F.; Marzo, T.; Massai, L.; Messori, L.; Weigand, W.; Montesarchio, D. Elucidating the Reactivity of Pt(II) Complexes with (O,S) Bidentate Ligands towards DNA Using Various Model Systems and Analytical Techniques. **manuscript in preparation**.
- (139) Fulmer, G. R.; Miller, A. J. M.; Sherden, N. H.; Gottlieb, H. E.; Nudelman, A.; Stoltz, B. M.; Bercaw, J. E.; Goldberg, K. I. NMR Chemical Shifts of Trace Impurities: Common Laboratory Solvents, Organics, and Gases in Deuterated Solvents Relevant to the Organometallic Chemist. *Organometallics* **2010**, 29 (9), 2176–2179.
- (140) Lipinski, C. Drug Solubility in Water and Dimethylsulfoxide. In *Molecular Drug Properties: Measurement and Prediction*; Mannhold, R., Ed.; Kubinyi, H., Folkers, G., Series Eds.; Methods and Principles in Medicinal Chemistry; Wiley-VCH & Co. KGaA: Weinheim, 2008; Vol. 37, pp 257–282.
- (141) Caron, G.; Ermondi, G. Lipophilicity: Chemical Nature and Biological Relevance. In *Molecular Drug Properties. Measurement and Prediction.*; Mannhold, R., Ed.; Kubinyi, H., Folkers, G., Series Eds.; Methods and Principles in Medicinal Chemistry; Wiley-VCH & Co. KGaA: Weinheim, 2008; Vol. 37, pp 315–329.
- (142) Berthod, A.; Carda-Broch, S. Determination of Liquid–liquid Partition Coefficients by Separation Methods. *J. Chromatogr. A* **2004**, 1037 (1–2), 3–14.
- (143) Annex to Commission Directive 92/69/EEC of 31 July 1992 Adapting to Technical Progress for the Seventeenth Time Council Directive 67/548/EEC on the Approximation of Laws,

- Regulations and Administrative Provisions Relating to the Classification, Packaging and Labelling of Dangerous Substances. *Off. J. Eur. Communities: Legis.* **1992**, L383 A, 63–73.
- (144) Screnci, D.; McKeage, M. J.; Galettis, P.; Hambley, T. W.; Palmer, B. D.; Baguley, B. C. Relationships between Hydrophobicity, Reactivity, Accumulation and Peripheral Nerve Toxicity of a Series of Platinum Drugs. *Br. J. Cancer* **2000**, *82* (4), 966–972.
- (145) Baker, M. V.; Barnard, P. J.; Berners-Price, S. J.; Brayshaw, S. K.; Hickey, J. L.; Skelton, B. W.; White, A. H. Cationic, Linear Au(I) N-Heterocyclic Carbene Complexes: Synthesis, Structure and Anti-Mitochondrial Activity. *Dalton Trans.* **2006**, No. 30, 3708–3715.
- (146) Kunz, P. C.; Huber, W.; Rojas, A.; Schatzschneider, U.; Spingler, B. Tricarbonylmanganese(I) and –rhenium(I) Complexes of Imidazol-Based Phosphane Ligands: Influence of the Substitution Pattern on the CO Release Properties. *Eur. J. Inorg. Chem.* **2009**, *2009* (35), 5358–5366.
- (147) Tetko, I. V.; Jaroszewicz, I.; Platts, J. A.; Kuduk-Jaworska, J. Calculation of Lipophilicity for Pt(II) Complexes: Experimental Comparison of Several Methods. *J. Inorg. Biochem.* **2008**, *102* (7), 1424–1437.
- (148) Mannhold, R.; Ostermann, C. Prediction of Log P with Substructure-Based Methods. In *Molecular Drug Properties. Measurement and Prediction.*; Mannhold, R., Ed.; Kubinyi, H., Folkers, G., Series Eds.; Methods and Principles in Medicinal Chemistry; Wiley-VCH & Co. KGaA: Weinheim, 2008; Vol. 37, pp 357–379.
- (149) Tetko, I. V.; Poda, G. I. Prediction of Log P with Property-Based Methods. In *Molecular Drug Properties. Measurement and Prediction.*; Mannhold, R., Ed.; Kubinyi, H., Folkers, G., Series Eds.; Methods and Principles in Medicinal Chemistry; Wiley-VCH & Co. KGaA: Weinheim, 2008; pp 381–406.
- (150) Minick, D. J.; Frenz, J. H.; Patrick, M. A.; Brent, D. A. A Comprehensive Method for Determining Hydrophobicity Constants by Reversed-Phase High-Performance Liquid Chromatography. *J. Med. Chem.* **1988**, *31* (10), 1923–1933.
- (151) Platts, J. A.; Oldfield, S. P.; Reif, M. M.; Palmucci, A.; Gabano, E.; Osella, D. The RP-HPLC Measurement and QSPR Analysis of Log Po/w Values of Several Pt(II) Complexes. *J. Inorg. Biochem.* **2006**, *100* (7), 1199–1207.
- (152) Martel, S.; Guillarme, D.; Henchoz, Y.; Galland, A.; Veuthey, J.-L.; Rudaz, S.; Carrupt, P.-A. Chromatographic Approaches for Measuring Log P. In *Molecular Drug Properties. Measurement and Prediction.*; Mannhold, R., Ed.; Kubinyi, H., Folkers, G., Series Eds.; Methods and Principles in Medicinal Chemistry; Wiley-VCH & Co. KGaA: Weinheim, 2008; Vol. 37, pp 331–355.
- (153) Maschke, M.; Lieb, M.; Metzler-Nolte, N. Biologically Active Trifluoromethyl-Substituted Metallocene Triazoles: Characterization, Electrochemistry, Lipophilicity, and Cytotoxicity. *Eur. J. Inorg. Chem.* **2012**, *2012* (36), 5953–5959.
- (154) Souchard, J. P.; Ha, T. T. B.; Cros, S.; Johnson, N. P. Hydrophobicity Parameters for Platinum Complexes. *J. Med. Chem.* **1991**, *34* (2), 863–864.
- (155) Di, L.; Kerns, E. H. Biological Assay Challenges from Compound Solubility: Strategies for Bioassay Optimization. *Drug Discovery Today* **2006**, *11* (9–10), 446–451.
- (156) Yousef, R. I.; Bette, M.; Kaluđerović, G. N.; Paschke, R.; Yiran, C.; Steinborn, D.; Schmidt, H. Structure Determination and Investigation on Cytotoxicity of Potassium dichlorido(L-prolinato)platinate(II) versus chlorido(dimethylsulfoxide)(L-prolinato)platinum(II) Complex – In Vitro Antitumor Deactivation by Cl–/dmsO Ligand Exchange. *Polyhedron* **2011**, *30* (12), 1990–1996.
- (157) Da Violante, G.; Zerrouk, N.; Richard, I.; Provot, G.; Chaumeil, J. C.; Arnaud, P. Evaluation of the Cytotoxicity Effect of Dimethyl Sulfoxide (DMSO) on Caco2/TC7 Colon Tumor Cell Cultures. *Biol. Pharm. Bull.* **2002**, *25* (12), 1600–1603.
- (158) Sundquist, W. I.; Ahmed, K. J.; Hollis, L. S.; Lippard, S. J. Solvolysis Reactions of Cis- and Trans-diamminedichloroplatinum(II) in Dimethyl Sulfoxide. Structural Characterization and DNA



- Binding of Trans-bis(ammine)chloro(DMSO)platinum(1+). *Inorg. Chem.* **1987**, *26* (10), 1524–1528.
- (159) Fischer, S. J.; Benson, L. M.; Fauq, A.; Naylor, S.; Windebank, A. J. Cisplatin and Dimethyl Sulfoxide React to Form an Adducted Compound with Reduced Cytotoxicity and Neurotoxicity. *NeuroToxicology* **2008**, *29* (3), 444–452.
- (160) Reedijk, J. Metal-Ligand Exchange Kinetics in Platinum and Ruthenium Complexes. *Platinum Met. Rev.* **2008**, *52* (1), 2–11.
- (161) Otto, F. J. Chapter 14: High-Resolution Analysis of Nuclear DNA Employing the Fluorochrome DAPI. In *Methods in Cell Biology*; Zbigniew Darzynkiewicz, J. P. R. and H. A. C., Ed.; Flow Cytometry Second Edition, Part A; Academic Press, 1994; Vol. 41, pp 211–217.
- (162) Kapuscinski, J. DAPI: A DNA-Specific Fluorescent Probe. *Biotech. Histochem.* **1995**, *70* (5), 220–233.
- (163) Zink, D.; Sadoni, N.; Stelzer, E. Visualizing Chromatin and Chromosomes in Living Cells. *Methods* **2003**, *29* (1), 42–50.
- (164) Crissman, H. A.; Hirons, G. T. Chapter 13: Staining of DNA in Live and Fixed Cells. In *Methods in Cell Biology*; Zbigniew Darzynkiewicz, J. P. R. and H. A. C., Ed.; Flow Cytometry Second Edition, Part A; Academic Press, 1994; Vol. 41, pp 195–209.
- (165) Williams, S. C.; Hong, Y.; Danavall, D. C. A.; Howard-Jones, M. H.; Gibson, D.; Frischer, M. E.; Verity, P. G. Distinguishing between Living and Nonliving Bacteria: Evaluation of the Vital Stain Propidium Iodide and Its Combined Use with Molecular Probes in Aquatic Samples. *J. Microbiol. Methods* **1998**, *32* (3), 225–236.
- (166) Pablos, C.; van Grieken, R.; Marugán, J.; Moreno, B. Photocatalytic Inactivation of Bacteria in a Fixed-Bed Reactor: Mechanistic Insights by Epifluorescence Microscopy. *Catal. Today* **2011**, *161* (1), 133–139.
- (167) Darzynkiewicz, Z.; Bruno, S.; Del Bino, G.; Gorczyca, W.; Hotz, M. A.; Lassota, P.; Traganos, F. Features of Apoptotic Cells Measured by Flow Cytometry. *Cytometry* **1992**, *13* (8), 795–808.
- (168) Life Technologies Corporation. PrestoBlue™ Cell Viability Reagent Documentation. 2010.
- (169) Mosmann, T. Rapid Colorimetric Assay for Cellular Growth and Survival: Application to Proliferation and Cytotoxicity Assays. *J. Immunol. Methods* **1983**, *65* (1–2), 55–63.
- (170) Marshall, N. J.; Goodwin, C. J.; Holt, S. J. A Critical Assessment of the Use of Microculture Tetrazolium Assays to Measure Cell Growth and Function. *Growth Regul.* **1995**, *5* (2), 69–84.
- (171) Berridge, M. V.; Herst, P. M.; Tan, A. S. Tetrazolium Dyes as Tools in Cell Biology: New Insights into Their Cellular Reduction. In *Biotechnology Annual Review*; El-Gewely, M. R., Ed.; Elsevier, 2005; Vol. 11, pp 127–152.
- (172) Lall, N.; Henley-Smith, C. J.; De Canha, M. N.; Oosthuizen, C. B.; Berrington, D. Viability Reagent, PrestoBlue, in Comparison with Other Available Reagents, Utilized in Cytotoxicity and Antimicrobial Assays. *Int. J. Microbiol.* **2013**, *2013*, 1–5.
- (173) Boncler, M.; Różalski, M.; Krajewska, U.; Podśędek, A.; Watała, C. Comparison of PrestoBlue and MTT Assays of Cellular Viability in the Assessment of Anti-Proliferative Effects of Plant Extracts on Human Endothelial Cells. *J. Pharmacol. Toxicol. Methods* **2014**, *69* (1), 9–16.
- (174) Xu, M.; McCanna, D. J.; Sivak, J. G. Use of the Viability Reagent PrestoBlue in Comparison with alamarBlue and MTT to Assess the Viability of Human Corneal Epithelial Cells. *J. Pharmacol. Toxicol. Methods* **2015**, *71*, 1–7.
- (175) Riss, T. L.; Moravec, R. A.; Niles, A. L.; Benink, H. A.; Worzella, T. J.; Minor, L. Cell Viability Assays. In *Assay Guidance Manual*; Sittampalam, G. S., Gal-Edd, N., Arkin, M., Auld, D., Austin, C., Bejcek, B., Glicksman, M., Inglese, J., Lemmon, V., Li, Z., McGee, J., McManus, O., Minor, L., Napper, A., Riss, T., Trask, O. J., Weidner, J., Eds.; Eli Lilly & Company and the National Center for Advancing Translational Sciences: Bethesda (MD), 2004.
- (176) Life Technologies Corporation. PrestoBlue™ Cell Viability Reagent Protocol. 2010.
- (177) Uphoff, C. C.; Drexler, H. G. Detecting Mycoplasma Contamination in Cell Cultures by Polymerase Chain Reaction. *Methods Mol. Biol.* **2011**, *731*, 93–103.

- (178) Mounicou, S.; Szpunar, J.; Lobinski, R. Metallomics: The Concept and Methodology. *Chem. Soc. Rev.* **2009**, *38* (4), 1119–1138.
- (179) Groessl, M.; Hartinger, C. G. Anticancer Metallodrug Research Analytically Painting the “omics” Picture—current Developments and Future Trends. *Anal. Bioanal. Chem.* **2013**, *405* (6), 1791–1808.
- (180) Beck, J. L.; Colgrave, M. L.; Ralph, S. F.; Sheil, M. M. Electrospray Ionization Mass Spectrometry of Oligonucleotide Complexes with Drugs, Metals, and Proteins. *Mass Spectrom. Rev.* **2001**, *20* (2), 61–87.
- (181) Brodbelt, J. S. Evaluation of DNA/Ligand Interactions by Electrospray Ionization Mass Spectrometry. *Annu. Rev. Anal. Chem.* **2010**, *3* (1), 67–87.
- (182) Carlton Jr., D. D.; Schug, K. A. A Review on the Interrogation of Peptide–metal Interactions Using Electrospray Ionization–Mass Spectrometry. *Anal. Chim. Acta* **2011**, *686* (1–2), 19–39.
- (183) Barnett, J. P.; Scanlan, D. J.; Blindauer, C. A. Protein Fractionation and Detection for Metalloproteomics: Challenges and Approaches. *Anal. Bioanal. Chem.* **2012**, *402* (10), 3311–3322.
- (184) Hartinger, C. G.; Ang, W. H.; Casini, A.; Messori, L.; Keppler, B. K.; Dyson, P. J. Mass Spectrometric Analysis of Ubiquitin–Platinum Interactions of Leading Anticancer Drugs: MALDI versus ESI. *J. Anal. At. Spectrom.* **2007**, *22* (8), 960.
- (185) Dole, M.; Mack, L. L.; Hines, R. L.; Mobley, R. C.; Ferguson, L. D.; Alice, M. B. Molecular Beams of Macroions. *The Journal of Chemical Physics* **1968**, *49* (5), 2240–2249.
- (186) Yamashita, M.; Fenn, J. B. Electrospray Ion Source. Another Variation on the Free-Jet Theme. *J. Phys. Chem.* **1984**, *88* (20), 4451–4459.
- (187) Fenn, J. B.; Mann, M.; Meng, C. K.; Wong, S. F.; Whitehouse, C. M. Electrospray Ionization for Mass Spectrometry of Large Biomolecules. *Science* **1989**, *246* (4926), 64–71.
- (188) The Nobel Prize in Chemistry 2002 [http://www.nobelprize.org/nobel\\_prizes/chemistry/laureates/2002/](http://www.nobelprize.org/nobel_prizes/chemistry/laureates/2002/) (accessed Jul 5, 2015).
- (189) Fenn, J. Electrospray Ionization Mass Spectrometry: How It All Began. *J. Biomol. Tech.* **2002**, *13* (3), 101–118.
- (190) Zeleny, J. The Electrical Discharge from Liquid Points, and a Hydrostatic Method of Measuring the Electric Intensity at Their Surfaces. *Phys. Rev.* **1914**, *3* (2), 69–91.
- (191) Lord Rayleigh, F. R. S. XX. On the Equilibrium of Liquid Conducting Masses Charged with Electricity. *Philos. Mag. Series 5* **1882**, *14* (87), 184–186.
- (192) Kebarle, P.; Verkerk, U. H. On the Mechanism of Electrospray Ionization Mass Spectrometry (ESIMS). In *Electrospray and MALDI Mass Spectrometry*; Cole, R. B., Ed.; John Wiley & Sons, Inc., 2010; pp 1–48.
- (193) Perry, R. H.; Cooks, R. G.; Noll, R. J. Orbitrap Mass Spectrometry: Instrumentation, Ion Motion and Applications. *Mass Spectrom. Rev.* **2008**, *27* (6), 661–699.
- (194) Thermo Scientific. Thermo Scientific LTQ Orbitrap XL specification sheet [http://www.thermoscientific.com/content/dam/tfs/ATG/CMD/CMD%20Documents/Product%20Manuals%20&%20Specifications/Mass%20Spectrometry/LC%20MS/LC%20MS%20for%20Endocrine%20Analysis/PS30133-LTQ-Orbitrap-XL\\_SpecSheet.pdf](http://www.thermoscientific.com/content/dam/tfs/ATG/CMD/CMD%20Documents/Product%20Manuals%20&%20Specifications/Mass%20Spectrometry/LC%20MS/LC%20MS%20for%20Endocrine%20Analysis/PS30133-LTQ-Orbitrap-XL_SpecSheet.pdf) (accessed Jun 15, 2015).
- (195) Hu, Q.; Noll, R. J.; Li, H.; Makarov, A.; Hardman, M.; Graham Cooks, R. The Orbitrap: A New Mass Spectrometer. *J. Mass Spectrom.* **2005**, *40* (4), 430–443.
- (196) Olsen, J. V.; Godoy, L. M. F. de; Li, G.; Macek, B.; Mortensen, P.; Pesch, R.; Makarov, A.; Lange, O.; Horning, S.; Mann, M. Parts per Million Mass Accuracy on an Orbitrap Mass Spectrometer via Lock Mass Injection into a C-Trap. *Mol. Cell. Proteomics* **2005**, *4* (12), 2010–2021.
- (197) Makarov, A.; Denisov, E.; Kholomeev, A.; Balschun, W.; Lange, O.; Strupat, K.; Horning, S. Performance Evaluation of a Hybrid Linear Ion Trap/Orbitrap Mass Spectrometer. *Anal. Chem.* **2006**, *78* (7), 2113–2120.
- (198) Weidt, S. K.; Mackay, C. L.; Langridge-Smith, P. R. R.; Sadler, P. J. Platination of Superoxide Dismutase with Cisplatin: Tracking the Ammonia Ligands Using Fourier Transform Ion

- Cyclotron Resonance Mass Spectrometry (FT-ICR MS). *Chem. Commun.* **2007**, No. 17, 1719–1721.
- (199) Gabbiani, C.; Casini, A.; Mastrobuoni, G.; Kirshenbaum, N.; Moshel, O.; Pieraccini, G.; Moneti, G.; Messori, L.; Gibson, D. Peculiar Mechanistic and Structural Features of the Carboplatin–cytochrome c System Revealed by ESI-MS Analysis. *J. Biol. Inorg. Chem.* **2008**, *13* (5), 755–764.
- (200) Will, J.; Wolters, D. A.; Sheldrick, W. S. Characterisation of Cisplatin Binding Sites in Human Serum Proteins Using Hyphenated Multidimensional Liquid Chromatography and ESI Tandem Mass Spectrometry. *ChemMedChem* **2008**, *3* (11), 1696–1707.
- (201) Zhao, T.; King, F. L. Direct Determination of the Primary Binding Site of Cisplatin on Cytochrome c by Mass Spectrometry. *J. Am. Soc. Mass Spectrom.* **2009**, *20* (6), 1141–1147.
- (202) Williams, J. P.; Phillips, H. I. A.; Campuzano, I.; Sadler, P. J. Shape Changes Induced by N-Terminal Platination of Ubiquitin by Cisplatin. *J. Am. Soc. Mass Spectrom.* **2010**, *21* (7), 1097–1106.
- (203) Casini, A.; Mastrobuoni, G.; Terenghi, M.; Gabbiani, C.; Monzani, E.; Moneti, G.; Casella, L.; Messori, L. Ruthenium Anticancer Drugs and Proteins: A Study of the Interactions of the ruthenium(III) Complex Imidazolium *trans*-[tetrachloro(dimethyl sulfoxide)(imidazole)ruthenate(III)] with Hen Egg White Lysozyme and Horse Heart Cytochrome c. *J. Biol. Inorg. Chem.* **2007**, *12* (8), 1107–1117.
- (204) Hartinger, C. G.; Casini, A.; Duhot, C.; Tsybin, Y. O.; Messori, L.; Dyson, P. J. Stability of an Organometallic Ruthenium-Ubiquitin Adduct in the Presence of Glutathione: Relevance to Antitumour Activity. *J. Inorg. Biochem.* **2008**, *102* (12), 2136–2141.
- (205) Zou, J.; Taylor, P.; Dornan, J.; Robinson, S. P.; Walkinshaw, M. D.; Sadler, P. J. First Crystal Structure of a Medicinally Relevant Gold Protein Complex: Unexpected Binding of [Au(PEt<sub>3</sub>)]<sup>+</sup> to Histidine. *Angew. Chem. Int. Ed.* **2000**, *39* (16), 2931–2934.
- (206) Zou, J.; Taylor, P.; Dornan, J.; Robinson, S. P.; Walkinshaw, M. D.; Sadler, P. J. Die Erste Kristallstruktur Eines Medizinisch Relevanten Gold-Protein-Komplexes: Unerwartete Koordination von [Au(PEt<sub>3</sub>)]<sup>+</sup> an Histidin. *Angew. Chem.* **2000**, *112* (16), 3054–3057.
- (207) Casini, A.; Hartinger, C.; Gabbiani, C.; Mini, E.; Dyson, P. J.; Keppler, B. K.; Messori, L. Gold (III) Compounds as Anticancer Agents: Relevance of Gold-Protein Interactions for Their Mechanism of Action. *J. Inorg. Biochem.* **2008**, *102* (3), 564–575.
- (208) Gabbiani, C.; Scaletti, F.; Massai, L.; Michelucci, E.; Cinellu, M. A.; Messori, L. Medicinal Gold Compounds Form Tight Adducts with the Copper Chaperone Atox-1: Biological and Pharmacological Implications. *Chem. Commun.* **2012**, *48* (95), 11623–11625.
- (209) Gabbiani, C.; Massai, L.; Scaletti, F.; Michelucci, E.; Maiore, L.; Cinellu, M. A.; Messori, L. Protein Metalation by Metal-Based Drugs: Reactions of Cytotoxic Gold Compounds with Cytochrome c and Lysozyme. *J. Biol. Inorg. Chem.* **2012**.
- (210) Casini, A.; Guerri, A.; Gabbiani, C.; Messori, L. Biophysical Characterisation of Adducts Formed between Anticancer Metallodrugs and Selected Proteins: New Insights from X-Ray Diffraction and Mass Spectrometry Studies. *J. Inorg. Biochem.* **2008**, *102* (5-6), 995–1006.
- (211) Timerbaev, A. R.; Hartinger, C. G.; Aleksenko, S. S.; Keppler, B. K. Interactions of Antitumor Metallodrugs with Serum Proteins: Advances in Characterization Using Modern Analytical Methodology. *Chem. Rev.* **2006**, *106* (6), 2224–2248.
- (212) Casini, A.; Gabbiani, C.; Mastrobuoni, G.; Messori, L.; Moneti, G.; Pieraccini, G. Exploring Metallodrug–Protein Interactions by ESI Mass Spectrometry: The Reaction of Anticancer Platinum Drugs with Horse Heart Cytochrome c. *ChemMedChem* **2006**, *1* (4), 413–417.
- (213) Margoliash, E. Primary Structure and Evolution of Cytochrome C. *Proc Natl Acad Sci U S A* **1963**, *50* (4), 672–679.
- (214) Atlas, S. M.; Farber, E. On the Molecular Weight of Cytochrome c from Mammalian Heart Muscle. *J. Biol. Chem.* **1956**, *219* (1), 031.
- (215) Bushnell, G. W.; Louie, G. V.; Brayer, G. D. High-Resolution Three-Dimensional Structure of Horse Heart Cytochrome c. *J. Mol. Biol.* **1990**, *214* (2), 585–595.

- (216) Berman, H. M.; Westbrook, J.; Feng, Z.; Gilliland, G.; Bhat, T. N.; Weissig, H.; Shindyalov, I. N.; Bourne, P. E. The Protein Data Bank. *Nucleic Acids Res.* **2000**, *28* (1), 235–242.
- (217) Brown, G. C.; Borutaite, V. Regulation of Apoptosis by the Redox State of Cytochrome c. *Biochimica et Biophysica Acta (BBA) - Bioenergetics* **2008**, *1777* (7-8), 877–881.
- (218) Yoshikawa, S.; Shinzawa-Itoh, K.; Nakashima, R.; Yaono, R.; Yamashita, E.; Inoue, N.; Yao, M.; Fei, M. J.; Libeu, C. P.; Mizushima, T.; Yamaguchi, H.; Tomizaki, T.; Tsukihara, T. Redox-Coupled Crystal Structural Changes in Bovine Heart Cytochrome c Oxidase. *Science* **1998**, *280* (5370), 1723–1729.
- (219) Lippard, S. J.; Berg, J. M. 11.2: Sauerstoffübertragungsreaktionen: Fe. In *Bioanorganische Chemie*; Müller-Becker, S., Keppler, B. K., Translators; Spektrum Akademischer Verlag: Heidelberg, Berlin, Oxford, 1995; pp 323–339.
- (220) Cytochrome - Kompaktlexikon der Biologie <http://www.spektrum.de/lexikon/biologie-kompakt/cytochrome/2817> (accessed Jun 16, 2015).
- (221) Liu, X.; Kim, C. N.; Yang, J.; Jemmerson, R.; Wang, X. Induction of Apoptotic Program in Cell-Free Extracts: Requirement for dATP and Cytochrome c. *Cell* **1996**, *86* (1), 147–157.
- (222) Skulachev, V. P. Cytochrome c in the Apoptotic and Antioxidant Cascades. *FEBS Lett.* **1998**, *423* (3), 275–280.
- (223) Czabotar, P. E.; Lessene, G.; Strasser, A.; Adams, J. M. Control of Apoptosis by the BCL-2 Protein Family: Implications for Physiology and Therapy. *Nat. Rev. Mol. Cell Biol.* **2014**, *15* (1), 49–63.
- (224) Mikoshiba, K. IP3 receptor/Ca<sup>2+</sup> Channel: From Discovery to New Signaling Concepts. *J. Neurochem.* **2007**, *102* (5), 1426–1446.
- (225) Cain, K.; Bratton, S. B.; Cohen, G. M. The Apaf-1 Apoptosome: A Large Caspase-Activating Complex. *Biochimie* **2002**, *84* (2–3), 203–214.
- (226) Degterev, A.; Boyce, M.; Yuan, J. A Decade of Caspases. *Oncogene* **2003**, *22* (53), 8543–8567.
- (227) McIlwain, D. R.; Berger, T.; Mak, T. W. Caspase Functions in Cell Death and Disease. *Cold Spring Harbor Perspect. Biol.* **2013**, *5* (4), a008656.
- (228) Tantral, L.; Malathi, K.; Kohyama, S.; Silane, M.; Berenstein, A.; Jayaraman, T. Intracellular Calcium Release Is Required for Caspase-3 and -9 Activation. *Cell Biochem. Funct.* **2004**, *22* (1), 35–40.
- (229) Esteban-Fernández, D.; Moreno-Gordaliza, E.; Canas, B.; Palacios, M. A.; Gómez-Gómez, M. M. Analytical Methodologies for Metallomics Studies of Antitumor Pt-Containing Drugs. *Metallomics* **2010**, *2* (1), 19–38.
- (230) Ferraro, G.; Messori, L.; Merlino, A. The X-Ray Structure of the Primary Adducts Formed in the Reaction between Cisplatin and Cytochrome c. *Chem. Commun.* **2015**, *51* (13), 2559–2561.
- (231) Casini, A.; Gabbiani, C.; Mastrobuoni, G.; Pellicani, R. Z.; Intini, F. P.; Arnesano, F.; Natile, G.; Moneti, G.; Francese, S.; Messori, L. Insights into the Molecular Mechanisms of Protein Platination from a Case Study: The Reaction of Anticancer Platinum(II) Iminoethers with Horse Heart Cytochrome c. *Biochemistry* **2007**, *46* (43), 12220–12230.
- (232) Rupley, J. A. The Hydrolysis of Chitin by Concentrated Hydrochloric Acid, and the Preparation of Low-Molecular-Weight Substrates for Lysozyme. *Biochim. Biophys. Acta* **1964**, *83*, 245–255.
- (233) Holler, E.; Rupley, J. A.; Hess, G. P. Productive and Unproductive Lysozyme-Chitosaccharide Complexes. Kinetic Investigations. *Biochemistry* **1975**, *14* (11), 2377–2385.
- (234) Jollès, P. Lysozymes: A Chapter of Molecular Biology. *Angew. Chem., Int. Ed.* **1969**, *8* (4), 227–239.
- (235) Jollès, P. Lysozyme: Ein Kapitel Molekularbiologie. *Angewandte Chemie* **1969**, *81* (7), 244–256.
- (236) Blake, C. C. F.; Koenig, D. F.; Mair, G. A.; North, A. C. T.; Phillips, D. C.; Sarma, V. R. Structure of Hen Egg-White Lysozyme: A Three-Dimensional Fourier Synthesis at 2 Å Resolution. *Nature* **1965**, *206* (4986), 757–761.
- (237) Jollès, P.; Jollès, J. What's New in Lysozyme Research? *Mol. Cell. Biochem.* **1984**, *63* (2), 165–189.

- (238) Vergara, A.; D'Errico, G.; Montesarchio, D.; Mangiapia, G.; Paduano, L.; Merlino, A. Interaction of Anticancer Ruthenium Compounds with Proteins: High-Resolution X-Ray Structures and Raman Microscopy Studies of the Adduct between Hen Egg White Lysozyme and AziRu. *Inorg. Chem.* **2013**, *52* (8), 4157–4159.
- (239) Casini, A.; Mastrobuoni, G.; Temperini, C.; Gabbiani, C.; Francese, S.; Moneti, G.; Supuran, C. T.; Scozzafava, A.; Messori, L. ESI Mass Spectrometry and X-Ray Diffraction Studies of Adducts between Anticancer Platinum Drugs and Hen Egg White Lysozyme. *Chem. Commun.* **2007**, No. 2, 156–158.
- (240) Messori, L.; Marzo, T.; Michelucci, E.; Russo Krauss, I.; Navarro-Ranninger, C.; Quiroga, A. G.; Merlino, A. Interactions between Anticancer Trans-Platinum Compounds and Proteins: Crystal Structures and ESI-MS Spectra of Two Protein Adducts of Trans-(Dimethylamino)(methylamino)dichloridoplatinum(II). *Inorg. Chem.* **2014**, *53* (15), 7806–7808.
- (241) Tanley, S. W. M.; Diederichs, K.; Kroon-Batenburg, L. M. J.; Levy, C.; Schreurs, A. M. M.; Helliwell, J. R. Carboplatin Binding to Histidine. *Acta Crystallogr., Sect. F: Struct. Biol. Commun.* **2014**, *70* (Pt 9), 1135–1142.
- (242) Marasco, D.; Messori, L.; Marzo, T.; Merlino, A. Oxaliplatin vs. Cisplatin: Competition Experiments on Their Binding to Lysozyme. *Dalton Trans.* **2015**, *44* (22), 10392–10398.
- (243) Helliwell, J. R.; Tanley, S. W. M. The Crystal Structure Analysis of the Relative Binding of Cisplatin and Carboplatin in a Mixture with Histidine in a Protein Studied at 100 and 300 K with Repeated X-Ray Irradiation. *Acta Crystallogr., Sect. D: Biol. Crystallogr.* **2012**, *69* (1), 121–125.
- (244) Raines, R. T. Ribonuclease A. *Chem. Rev.* **1998**, *98* (3), 1045–1066.
- (245) Marshall, G. R.; Feng, J. A.; Kuster, D. J. Back to the Future: Ribonuclease A. *Biopolymers* **2008**, *90* (3), 259–277.
- (246) Cuchillo, C. M.; Nogués, M. V.; Raines, R. T. Bovine Pancreatic Ribonuclease: Fifty Years of the First Enzymatic Reaction Mechanism. *Biochemistry* **2011**, *50* (37), 7835–7841.
- (247) Sorrentino, S. The Eight Human “canonical” Ribonucleases: Molecular Diversity, Catalytic Properties, and Special Biological Actions of the Enzyme Proteins. *FEBS Lett.* **2010**, *584* (11), 2194–2200.
- (248) Messori, L.; Merlino, A. Cisplatin Binding to Proteins: Molecular Structure of the Ribonuclease A Adduct. *Inorg. Chem.* **2014**, *53* (8), 3929–3931.
- (249) Findly, D.; Herries, D. G.; Mathias, A. P.; Rabin, B. R.; Ross, C. A. The Active Site and Mechanism of Action of Bovine Pancreatic Ribonuclease. *Nature* **1961**, *190* (4778), 781–784.
- (250) Moore, S.; Stein, W. H. Chemical Structures of Pancreatic Ribonuclease and Deoxyribonuclease. *Science* **1973**, *180* (4085), 458–464.
- (251) Messori, L.; Scaletti, F.; Massai, L.; Cinellu, M. A.; Krauss, I. R.; Martino, G. di; Vergara, A.; Paduano, L.; Merlino, A. Interactions of Gold-Based Drugs with Proteins: Crystal Structure of the Adduct Formed between Ribonuclease A and a Cytotoxic gold(III) Compound. *Metallomics* **2014**, *6* (2), 233–236.
- (252) Vergara, A.; Russo Krauss, I.; Montesarchio, D.; Paduano, L.; Merlino, A. Investigating the Ruthenium Metalation of Proteins: X-Ray Structure and Raman Microspectroscopy of the Complex between RNase A and AziRu. *Inorg. Chem.* **2013**, *52* (19), 10714–10716.
- (253) Murray, K. K.; Boyd, R. K.; Eberlin, M. N.; Langley, G. J.; Li, L.; Naito, Y. Definitions of Terms Relating to Mass Spectrometry (IUPAC Recommendations 2013). *Pure Appl. Chem.* **2013**, *85* (7), 1515–1609.
- (254) Arnesano, F.; Belviso, B. D.; Caliandro, R.; Falini, G.; Fermani, S.; Natile, G.; Siliqi, D. Crystallographic Analysis of Metal-Ion Binding to Human Ubiquitin. *Chem. - Eur. J.* **2011**, *17* (5), 1569–1578.
- (255) Mügge, C.; Micheucci, E.; Boscaro, F.; Gabbiani, C.; Messori, L.; Weigand, W. Reactions of Metallodrugs with Proteins: Selective Binding of Phosphane-Based Platinum(II) Dichlorides to

- Horse Heart Cytochrome c Probed by ESI MS Coupled to Enzymatic Cleavage. *Metallomics* **2011**, *3* (10), 987–990.
- (256) Ghuman, J.; Zunszain, P. A.; Petitpas, I.; Bhattacharya, A. A.; Otagiri, M.; Curry, S. Structural Basis of the Drug-Binding Specificity of Human Serum Albumin. *J. Mol. Biol.* **2005**, *353* (1), 38–52.
- (257) Kratz, F. Albumin as a Drug Carrier: Design of Prodrugs, Drug Conjugates and Nanoparticles. *J. Controlled Release* **2008**, *132* (3), 171–183.
- (258) Ivanov, A. I.; Christodoulou, J.; Parkinson, J. A.; Barnham, K. J.; Tucker, A.; Woodrow, J.; Sadler, P. J. Cisplatin Binding Sites on Human Albumin. *J. Biol. Chem.* **1998**, *273* (24), 14721–14730.
- (259) Timerbaev, A. R.; Aleksenko, S. S.; Polec-Pawlak, K.; Ruzik, R.; Semenova, O.; Hartinger, C. G.; Oszwaldowski, S.; Galanski, M.; Jarosz, M.; Keppler, B. K. Platinum Metallodrug-Protein Binding Studies by Capillary Electrophoresis-Inductively Coupled Plasma-Mass Spectrometry: Characterization of Interactions between Pt(II) Complexes and Human Serum Albumin. *Electrophoresis* **2004**, *25* (13), 1988–1995.
- (260) Brauckmann, C.; Wehe, C. A.; Kieshauer, M.; Lanvers-Kaminsky, C.; Sperling, M.; Karst, U. The Interaction of Platinum-Based Drugs with Native Biologically Relevant Proteins. *Anal. Bioanal. Chem.* **2013**, *405* (6), 1855–1864.
- (261) Peleg-Shulman, T.; Najajreh, Y.; Gibson, D. Interactions of Cisplatin and Transplatin with Proteins: Comparison of Binding Kinetics, Binding Sites and Reactivity of the Pt-Protein Adducts of Cisplatin and Transplatin towards Biological Nucleophiles. *J. Inorg. Biochem.* **2002**, *91* (1), 306–311.
- (262) Fichtinger-Schepman, A. M. J.; Vendrik, C. P. J.; van Dijk-Knijnenburg, W. C. M.; de Jong, W. H.; van der Minnen, A. C. E.; Claessen, A. M. E.; van der Velde-Visser, S. D.; de Groot, G.; Wubs, K. L.; Steerenberg, P. A.; Schornagel, J. H.; Berends, F. Platinum Concentrations and DNA Adduct Levels in Tumors and Organs of Cisplatin-Treated LOU/M Rats Inoculated with Cisplatin-Sensitive or -Resistant Immunoglobulin M Immunocytoma. *Cancer Res.* **1989**, *49* (11), 2862–2867.
- (263) Favre, A.; Gonnet, F.; Tabet, J.-C. Location of the Na<sup>+</sup> Cation in Negative Ions of DNA Evidenced by Using MS<sup>2</sup> Experiments in Ion Trap Mass Spectrometry. *Int. J. Mass Spectrom.* **1999**, *190–191*, 303–312.
- (264) Keller, K. M.; Brodbelt, J. S. Charge State-Dependent Fragmentation of Oligonucleotide/metal Complexes. *J. Am. Soc. Mass Spectrom.* **2005**, *16* (1), 28–37.
- (265) Wang, Y.; Taylor, J.-S.; Gross, M. L. Fragmentation of Electrospray-Produced Oligodeoxynucleotide Ions Adducted to Metal Ions. *J. Am. Soc. Mass Spectrom.* **2001**, *12* (5), 550–556.
- (266) Martin III, L. B.; Schreiner, A. F.; van Breemen, R. B. Characterization of Cisplatin Adducts of Oligonucleotides by Fast Atom Bombardment Mass Spectrometry. *Anal. Biochem.* **1991**, *193* (1), 6–15.
- (267) Lowe, G.; McCloskey, J. A.; Ni, J.; Vilaivan, T. A Mass Spectrometric Investigation of the Reaction between 4,4'-Vinylenedipyridine bis[2,2' : 6',2''-Terpyridine Platinum (II)] and the Self-Complementary Oligonucleotide d(CpGpTpApCpG). *Bioorg. Med. Chem.* **1996**, *4* (7), 1007–1013.
- (268) Gonnet, F.; Kocher, F.; Blais, J. C.; Bolbach, G.; Tabet, J. C.; Chottard, J. C. Kinetic Analysis of the Reaction Between d(TTGGCCAA) and [Pt(NH<sub>3</sub>)<sub>3</sub>(H<sub>2</sub>O)]<sup>2+</sup> by Enzymatic Degradation of the Products and ESI and MALDI Mass Spectrometries. *J. Mass Spectrom.* **1996**, *31* (7), 802–809.
- (269) Kloster, M. B. G.; Hannis, J. C.; Muddiman, D. C.; Farrell, N. Consequences of Nucleic Acid Conformation on the Binding of a Trinuclear Platinum Drug. *Biochemistry* **1999**, *38* (45), 14731–14737.
- (270) Xu, N.; Paša-Tolić, L.; Smith, R. D.; Ni, S.; Thrall, B. D. Electrospray Ionization–Mass Spectrometry Study of the Interaction of Cisplatin-Adducted Oligonucleotides with Human XPA Minimal Binding Domain Protein. *Anal. Biochem.* **1999**, *272* (1), 26–33.

- (271) Egger, A. E.; Hartinger, C. G.; Hamidane, H. B.; Tsybin, Y. O.; Keppler, B. K.; Dyson, P. J. High Resolution Mass Spectrometry for Studying the Interactions of Cisplatin with Oligonucleotides. *Inorg. Chem.* **2008**, *47* (22), 10626–10633.
- (272) Carte, N.; Legendre, F.; Leize, E.; Potier, N.; Reeder, F.; Chottard, J.-C.; Van Dorselaer, A. Determination by Electrospray Mass Spectrometry of the Outersphere Association Constants of DNA/Platinum Complexes Using 20-Mer Oligonucleotides and  $[\text{Pt}(\text{NH}_3)_4]^{2+}$ ,  $2\text{Cl}^-$  or  $[\text{Pt}(\text{py})_4]^{2+}$ ,  $2\text{Cl}^-$ . *Anal. Biochem.* **2000**, *284* (1), 77–86.
- (273) Nyakas, A.; Eymann, M.; Schürch, S. The Influence of Cisplatin on the Gas-Phase Dissociation of Oligonucleotides Studied by Electrospray Ionization Tandem Mass Spectrometry. *J. Am. Soc. Mass Spectrom.* **2009**, *20* (5), 792–804.
- (274) Groessel, M.; Tsybin, Y.; Hartinger, C.; Keppler, B.; Dyson, P. Ruthenium versus Platinum: Interactions of Anticancer Metallodrugs with Duplex Oligonucleotides Characterised by Electrospray Ionisation Mass Spectrometry. *J. Biol. Inorg. Chem.* **2010**, *15* (5), 677–688.
- (275) Iannitti-Tito, P.; Weimann, A.; Wickham, G.; Sheil, M. M. Structural Analysis of drug–DNA Adducts by Tandemmass Spectrometry. *Analyst* **2000**, *125* (4), 627–634.
- (276) Xu, Z.; Brodbelt, J. S. Differentiation and Distributions of DNA/Cisplatin Crosslinks by Liquid Chromatography-Electrospray Ionization-Infrared Multiphoton Dissociation Mass Spectrometry. *J. Am. Soc. Mass Spectrom.* **2014**, *25* (1), 71–79.
- (277) Xu, Z.; Shaw, J. B.; Brodbelt, J. S. Comparison of MS/MS Methods for Characterization of DNA/Cisplatin Adducts. *J. Am. Soc. Mass Spectrom.* **2012**, *24* (2), 265–273.
- (278) Gupta, R.; Kapur, A.; Beck, J. L.; Sheil, M. M. Positive Ion Electrospray Ionization Mass Spectrometry of Double-Stranded DNA/drug Complexes. *Rapid Commun. Mass Spectrom.* **2001**, *15* (24), 2472–2480.
- (279) Rosu, F.; Pirotte, S.; Pauw, E. D.; Gabelica, V. Positive and Negative Ion Mode ESI-MS and MS/MS for Studying drug–DNA Complexes. *Int. J. Mass Spectrom.* **2006**, *253* (3), 156–171.
- (280) Green-Church, K. B.; Limbach, P. A. Mononucleotide Gas-Phase Proton Affinities as Determined by the Kinetic Method. *J. Am. Soc. Mass Spectrom.* **2000**, *11* (1), 24–32.
- (281) Sherman, S. E.; Lippard, S. J. Structural Aspects of Platinum Anticancer Drug Interactions with DNA. *Chem. Rev.* **1987**, *87* (5), 1153–1181.
- (282) Frańska, M. Electrospray Ionization Mass Spectrometric Study of platinum(II) Complexes with Nucleobases and Dimethyl Sulfoxide. *Int. J. Mass Spectrom.* **2007**, *261* (1), 86–90.
- (283) Montesarchio, D.; Musumeci, D. CD- and UV-Vis Spectroscopic Investigations of Pt-Oligonucleotide Interactions. *private communication* **2015**.
- (284) Iwamoto, M.; Mukundan, S.; Marzilli, L. G. DNA Adduct Formation by Platinum Anticancer Drugs. Insight into an Unusual GpG Intrastrand Cross-Link in a Hairpin-like DNA Oligonucleotide Using NMR and Distance Geometry Methods. *J. Am. Chem. Soc.* **1994**, *116* (14), 6238–6244.
- (285) Hořr, C.; Farrell, N.; Brabec, V. Thermodynamic Properties of Duplex DNA Containing a Site-Specific d(GpG) Intrastrand Crosslink Formed by an Antitumor Dinuclear Platinum Complex. *Nucleic Acids Res.* **2001**, *29* (10), 2034–2040.
- (286) Stehlikova, K.; Kostrhunova, H.; Kasparkova, J.; Brabec, V. DNA Bending and Unwinding due to the Major 1,2-GG Intrastrand Cross-Link Formed by Antitumor Cis-diamminedichloroplatinum(II) Are Flanking-Base Independent. *Nucleic Acids Res.* **2002**, *30* (13), 2894–2898.
- (287) Faivre, S.; Chan, D.; Salinas, R.; Woynarowska, B.; Woynarowski, J. M. DNA Strand Breaks and Apoptosis Induced by Oxaliplatin in Cancer Cells. *Biochem. Pharmacol.* **2003**, *66* (2), 225–237.
- (288) Vrána, O.; Mašek, V.; Dražan, V.; Brabec, V. Raman Spectroscopy of DNA Modified by Intrastrand Cross-Links of Antitumor Cisplatin. *J. Struct. Biol.* **2007**, *159* (1), 1–8.
- (289) Musumeci, D.; Rozza, L.; Merlino, A.; Paduano, L.; Marzo, T.; Massai, L.; Messori, L.; Montesarchio, D. Interaction of Anticancer Ru(III) Complexes with Single Strand and Duplex DNA Model Systems. *Dalton Trans.* **2015**.

- (290) Reedijk, J. Platinum Anticancer Coordination Compounds: Study of DNA Binding Inspires New Drug Design. *Eur. J. Inorg. Chem.* **2009**, 2009 (10), 1303–1312.
- (291) Groessl, M.; Zava, O.; Dyson, P. J. Cellular Uptake and Subcellular Distribution of Ruthenium-Based Metallodrugs under Clinical Investigation versus Cisplatin. *Metallomics* **2011**.
- (292) Jef Rozenski. Mongo Oligo Mass Calculator v2.06  
<http://mods.rna.albany.edu/masspec/Mongo-Oligo>.
- (293) Wu, J.; McLuckey, S. A. Gas-Phase Fragmentation of Oligonucleotide Ions. *Int. J. Mass Spectrom.* **2004**, 237 (2–3), 197–241.
- (294) McLuckey, S. A.; Habibi-Goudarzi, S. Decompositions of Multiply Charged Oligonucleotide Anions. *J. Am. Chem. Soc.* **1993**, 115 (25), 12085–12095.
- (295) McLuckey, S. A.; Berkel, G. J. V.; Glish, G. L. Tandem Mass Spectrometry of Small, Multiply Charged Oligonucleotides. *J. Am. Soc. Mass Spectrom.* **1992**, 3 (1), 60–70.
- (296) Little, D. P.; Chorush, R. A.; Speir, J. P.; Senko, M. W.; Kelleher, N. L.; McLafferty, F. W. Rapid Sequencing of Oligonucleotides by High-Resolution Mass Spectrometry. *J. Am. Chem. Soc.* **1994**, 116 (11), 4893–4897.
- (297) Barry, J. P.; Vouros, P.; Van Schepdael, A.; Law, S.-J. Mass and Sequence Verification of Modified Oligonucleotides Using Electrospray Tandem Mass Spectrometry. *J. Mass Spectrom.* **1995**, 30 (7), 993–1006.
- (298) Warnke, U.; Rappel, C.; Meier, H.; Kloft, C.; Galanski, M.; Hartinger, C. G.; Keppler, B. K.; Jaehde, U. Analysis of Platinum Adducts with DNA Nucleotides and Nucleosides by Capillary Electrophoresis Coupled to ESI-MS: Indications of Guanosine 5'-Monophosphate O6–N7 Chelation. *ChemBioChem* **2004**, 5 (11), 1543–1549.
- (299) Norman, J. F.; Hambley, T. W. Targeting Strategies for Metal-Based Therapeutics. In *Bioinorganic Medicinal Chemistry*; Alessio, E., Ed.; Wiley-VCH Verlag GmbH & Co. KGaA: Weinheim, Germany, 2011; pp 49–78.
- (300) Sista, P.; Ghosh, K.; Martinez, J. S.; Rocha, R. C. Metallo-Biopolymers: Conjugation Strategies and Applications. *Polym. Rev.* **2014**, 54 (4), 627–676.
- (301) *Bioconjugate Techniques*, 2nd ed.; Hermanson, G. T., Ed.; Academic Press: New York, 2008.
- (302) Virta, P.; Katajisto, J.; Niittymäki, T.; Lönnberg, H. Solid-Supported Synthesis of Oligomeric Bioconjugates. *Tetrahedron* **2003**, 59 (28), 5137–5174.
- (303) Van Zutphen, S.; Reedijk, J. Targeting Platinum Anti-Tumour Drugs: Overview of Strategies Employed to Reduce Systemic Toxicity. *Coord. Chem. Rev.* **2005**, 249 (24), 2845–2853.
- (304) Hillard, E. A.; Jaouen, G. Bioorganometallics: Future Trends in Drug Discovery, Analytical Chemistry, and Catalysis. *Organometallics* **2011**, 30 (1), 20–27.
- (305) Metzler-Nolte, N. Medicinal Applications of Metal–Peptide Bioconjugates. *Chimia* **2007**, 61 (11), 736–741.
- (306) Heinze, K.; Beckmann, M.; Hempel, K. Solid-Phase Synthesis of Transition-Metal Complexes. *Chem. - Eur. J.* **2008**, 14 (31), 9468–9480.
- (307) Dirscherl, G.; König, B. The Use of Solid-Phase Synthesis Techniques for the Preparation of Peptide–Metal Complex Conjugates. *Eur. J. Org. Chem.* **2008**, 2008 (4), 597–634.
- (308) Cuingnet, E.; Sergheraert, C.; Tartar, A.; Dautrevaux, M. B-Ferrocenylalanyl Peptides : I. Synthesis of [Fer4, Leu5] Enkephalin. *J. Organomet. Chem.* **1980**, 195 (3), 325–329.
- (309) Brunet, J. C.; Cuingnet, E.; Gras, H.; Marcincal, P.; Mocz, A.; Sergheraert, C.; Tartar, A. New Metallocenic Phenylalanine Analogs. *J. Organomet. Chem.* **1981**, 216 (1), 73–77.
- (310) Sasaki, N. A.; Potier, P.; Savignac, M.; Jaouen, G. Organometallic Derivatives of Peptides: Application to Peptide Receptor Analysis. *Tetrahedron Letters* **1988**, 29 (45), 5759–5762.
- (311) Kirin, S. I.; Noor, F.; Metzler-Nolte, N.; Mier, W. Manual Solid–Phase Peptide Synthesis of Metallocene–Peptide Bioconjugates. *J. Chem. Educ.* **2007**, 84 (1), 108–111.
- (312) Chantson, J. T.; Falzacappa, M. V. V.; Crovella, S.; Metzler-Nolte, N. Antibacterial Activities of Ferrocenoyl- and Cobaltocenium-Peptide Bioconjugates. *J. Organomet. Chem.* **2005**, 690 (21–22), 4564–4572.



- (313) Chantson, J. T.; Vittoria Verga Falzacappa, M.; Crovella, S.; Metzler-Nolte, N. Solid-Phase Synthesis, Characterization, and Antibacterial Activities of Metallocene–Peptide Bioconjugates. *ChemMedChem* **2006**, *1* (11), 1268–1274.
- (314) Pinto, A.; Hoffmanns, U.; Ott, M.; Fricker, G.; Metzler-Nolte, N. Modification with Organometallic Compounds Improves Crossing of the Blood–Brain Barrier of [Leu5]-Enkephalin Derivatives in an In Vitro Model System. *ChemBioChem* **2009**, *10* (11), 1852–1860.
- (315) Hoffmanns, U.; Metzler-Nolte, N. Use of the Sonogashira Coupling Reaction for the “Two-Step” Labeling of Phenylalanine Peptide Side Chains with Organometallic Compounds. *Bioconjugate Chem.* **2006**, *17* (1), 204–213.
- (316) Caddy, J.; Hoffmanns, U.; Metzler-Nolte, N. Introduction of Phosphine-Gold (I) Precursors into a Cys-Modified Enkephalin Neuropeptide as Part of Solid Phase Peptide Synthesis. *Z. Naturforsch., B: J. Chem. Sci.* **2007**, *62* (3), 460.
- (317) Neukamm, M. A.; Pinto, A.; Metzler-Nolte, N. Synthesis and Cytotoxicity of a Cobaltcarbonyl-alkyne Enkephalin Bioconjugate. *Chem. Commun.* **2007**, No. 2, 232–234.
- (318) Noor, F.; Wüstholtz, A.; Kinscherf, R.; Metzler-Nolte, N. A Cobaltocenium–Peptide Bioconjugate Shows Enhanced Cellular Uptake and Directed Nuclear Delivery. *Angew. Chem., Int. Ed.* **2005**, *44* (16), 2429–2432.
- (319) Noor, F.; Wüstholtz, A.; Kinscherf, R.; Metzler-Nolte, N. Ein Peptid-Cobaltocenium-Biokonjugat mit verbesserter Aufnahme in Zellen und Anreicherung im Zellkern. *Angew. Chem.* **2005**, *117* (16), 2481–2485.
- (320) Van Staveren, D. R.; Metzler-Nolte, N. Labelling of [Leu5]-Enkephalin with Organometallic Mo Complexes by Solid-Phase Synthesis. *Chem. Commun.* **2002**, No. 13, 1406–1407.
- (321) Van Staveren, D. R.; Bothe, E.; Metzler-Nolte, N. Circular Dichroism Spectroelectrochemical Investigations on the Fluxional Diamagnetic and Paramagnetic Organometallic Complexes [Mo(His-N $\epsilon$ -C<sub>2</sub>H<sub>4</sub>COOCH<sub>3</sub>)(2-R-allyl)(CO)<sub>2</sub>]<sub>n</sub> (R = H, Me; His = O,N,N $\delta$ -L-Histidinate; N = 0, 1). *Organometallics* **2003**, *22* (15), 3102–3106.
- (322) Kuchta, M. C.; Gross, A.; Pinto, A.; Metzler-Nolte, N. Labeling of the Neuropeptide Enkephalin with Functionalized Tris(pyrazolyl)borate Complexes: Solid-Phase Synthesis and Characterization of P-[Enk-OH]COC<sub>6</sub>H<sub>4</sub>TpPtMe<sub>3</sub> and P-[Enk-OH]COC<sub>6</sub>H<sub>4</sub>TpMeRe(CO)<sub>3</sub>. *Inorg. Chem.* **2007**, *46* (22), 9400–9404.
- (323) Zagermann, J.; Kuchta, M. C.; Merz, K.; Metzler-Nolte, N. Ruthenium-Based Bioconjugates: Synthesis and X-Ray Structure of the Mixed Ligand Sandwich Compound RuCpiPr(p-(CO<sub>2</sub>H)C<sub>6</sub>H<sub>4</sub>Tp) and Labelling of Amino Acids and the Neuropeptide Enkephalin. *J. Organomet. Chem.* **2009**, *694* (6), 862–867.
- (324) Albada, H. B.; Wieberneit, F.; Dijkgraaf, I.; Harvey, J. H.; Whistler, J. L.; Stoll, R.; Metzler-Nolte, N.; Fish, R. H. The Chemoselective Reactions of Tyrosine-Containing G-Protein-Coupled Receptor Peptides with [Cp\*Rh(H<sub>2</sub>O)<sub>3</sub>](OTf)<sub>2</sub>, Including 2D NMR Structures and the Biological Consequences. *J. Am. Chem. Soc.* **2012**, *134* (25), 10321–10324.
- (325) Wieberneit, F.; Korste, A.; Albada, H. B.; Metzler-Nolte, N.; Stoll, R. Structural and Biological Implications of the Binding of Leu-Enkephalin and Its Metal Derivatives to Opioid Receptors. *Dalton Trans.* **2013**, *42* (27), 9799–9802.
- (326) Zagermann, J.; Deally, A.; Metzler-Nolte, N.; Müller-Bunz, H.; Wallis, D.; Tacke, M. Towards Peptide-Substituted Titanocene Anticancer Drugs. *Polyhedron* **2011**, *30* (14), 2387–2390.
- (327) Meier, S. M.; Novak, M.; Kandioller, W.; Jakupec, M. A.; Arion, V. B.; Metzler-Nolte, N.; Keppler, B. K.; Hartinger, C. G. Identification of the Structural Determinants for Anticancer Activity of a Ruthenium Arene Peptide Conjugate. *Chem. - Eur. J.* **2013**, *19* (28), 9297–9307.
- (328) Robillard, M. S.; Valentijn, A. R. P. M.; Meeuwenoord, N. J.; van der Marel, G. A.; van Boom, J. H.; Reedijk, J. The First Solid-Phase Synthesis of a Peptide-Tethered Platinum(II) Complex. *Angew. Chem., Int. Ed.* **2000**, *39* (17), 3096–3099.

- (329) Robillard, M. S.; Valentijn, A. R. P. M.; Meeuwenoord, N. J.; van der Marel, G. A.; van Boom, J. H.; Reedijk, J. The First Solid-Phase Synthesis of a Peptide-Tethered Platinum(II) Complex. *Angew. Chem.* **2000**, *112* (17), 3226–3229.
- (330) Robillard, M. S.; Bacac, M.; van den Elst, H.; Flamigni, A.; van der Marel, G. A.; van Boom, J. H.; Reedijk, J. Automated Parallel Solid-Phase Synthesis and Anticancer Screening of a Library of Peptide-Tethered Platinum(II) Complexes. *J. Comb. Chem.* **2003**, *5* (6), 821–825.
- (331) Robillard, M. S.; van Alphen, S.; Meeuwenoord, N. J.; Jansen, B. A. J.; van der Marel, G. A.; van Boom, J. H.; Reedijk, J. Solid-Phase Synthesis of Peptide-Platinum Complexes Using Platinum-Chelating Building Blocks Derived from Amino Acids. *New J. Chem.* **2005**, *29* (1), 220–225.
- (332) Robillard, M. S.; Davies, N. P.; van der Marel, G. A.; van Boom, J. H.; Reedijk, J.; Murray, V. The Interaction of Peptide-Tethered platinum(II) Complexes with DNA. *J. Inorg. Biochem.* **2003**, *96* (2–3), 331–338.
- (333) Van Zutphen, S.; Robillard, M. S.; van der Marel, G. A.; Overkleeft, H. S.; den Dulk, H.; Brouwer, J.; Reedijk, J. Extending Solid-Phase Methods in Inorganic Synthesis: The First Dinuclear Platinum Complex Synthesised via the Solid Phase. *Chem. Commun.* **2003**, No. 5, 634–635.
- (334) Barragán, F.; Moreno, V.; Marchán, V. Solid-Phase Synthesis and DNA Binding Studies of Dichloroplatinum(ii) Conjugates of Dicarba Analogues of Octreotide as New Anticancer Drugs. *Chem. Commun.* **2009**, No. 31, 4705.
- (335) Guillena, G.; Halkes, K. M.; Rodríguez, G.; Batema, G. D.; van Koten, G.; Kamerling, J. P. Organoplatinum(II) Complexes as a Color Biomarker in Solid-Phase Peptide Chemistry and Screening. *Org. Lett.* **2003**, *5* (12), 2021–2024.
- (336) Aronov, O.; Horowitz, A. T.; Gabizon, A.; Fuertes, M. A.; Pérez, J. M.; Gibson, D. Nuclear Localization Signal-Targeted Poly(ethylene Glycol) Conjugates as Potential Carriers and Nuclear Localizing Agents for Carboplatin Analogues. *Bioconjugate Chem.* **2004**, *15* (4), 814–823.
- (337) Ndinguri, M. W.; Solipuram, R.; Gambrell, R. P.; Aggarwal, S.; Hammer, R. P. Peptide Targeting of Platinum Anti-Cancer Drugs. *Bioconjugate Chem.* **2009**, *20* (10), 1869–1878.
- (338) Mukhopadhyay, S.; Barnés, C. M.; Haskel, A.; Short, S. M.; Barnes, K. R.; Lippard, S. J. Conjugated Platinum(IV)–Peptide Complexes for Targeting Angiogenic Tumor Vasculature. *Bioconjugate Chem.* **2008**, *19* (1), 39–49.
- (339) Abramkin, S.; Valiahdi, S. M.; Jakupec, M. A.; Galanski, M.; Metzler-Nolte, N.; Keppler, B. K. Solid-Phase Synthesis of oxaliplatin–TAT Peptide Bioconjugates. *Dalton Trans.* **2012**, *41* (10), 3001–3005.
- (340) Gaviglio, L.; Gross, A.; Metzler-Nolte, N.; Ravera, M. Synthesis and in Vitro Cytotoxicity of Cis,cis,trans-diamminedichloridodisuccinatoplatinum(IV)–peptide Bioconjugates. *Metallomics* **2012**, *4* (3), 260–266.
- (341) Johnstone, T. C.; Wilson, J. J.; Lippard, S. J. Monofunctional and Higher-Valent Platinum Anticancer Agents. *Inorg. Chem.* **2013**, *52* (21), 12234–12249.
- (342) Kosterlitz, H. W.; Hughes, J. Some Thoughts on the Significance of Enkephalin, the Endogenous Ligand. *Life Sciences* **1975**, *17* (1), 91–96.
- (343) Waterfield, A. A.; Smokcum, R. W. J.; Hughes, J.; Kosterlitz, H. W.; Henderson, G. In Vitro Pharmacology of the Opioid Peptides, Enkephalins and Endorphins. *Eur. J. Pharmacol.* **1977**, *43* (2), 107–116.
- (344) Numa, S. Opioid Peptide Precursors and Their Genes. In *Opioid Peptides: Biology, Chemistry and Genetics*; Udenfriend, S., Meierhofer, J., Eds.; The Peptides - Analysis, Synthesis, Biology; Academic Press: Orlando, Florida, 1984; Vol. 6, pp 1–25.
- (345) Hughes, J.; Smith, T.; Morgan, B.; Fothergill, L. Purification and Properties of Enkephalin — The Possible Endogenous Ligand for the Morphine Receptor. *Life Sciences* **1975**, *16* (12), 1753–1758.

- (346) Hughes, J.; Smith, T. W.; Kosterlitz, H. W.; Fothergill, L. A.; Morgan, B. A.; Morris, H. R. Identification of Two Related Pentapeptides from the Brain with Potent Opiate Agonist Activity. *Nature* **1975**, *258* (5536), 577–579.
- (347) Camerman, A.; Mastropaolo, D.; Karle, I.; Karle, J.; Camerman, N. Crystal Structure of Leucine-Enkephalin. *Nature* **1983**, *306* (5942), 447–450.
- (348) Mastropaolo, D.; Camerman, A.; Camerman, N. Crystal Structure of Methionine-Enkephalin. *Biochem. Biophys. Res. Commun.* **1986**, *134* (2), 698–703.
- (349) Mastropaolo, D.; Camerman, A.; Ma, L. Y. Y.; Camerman, N. Crystal Structure of an Extended-Conformation Leucine-Enkephalin Dimer Monohydrate. *Life Sciences* **1987**, *40* (20), 1995–1999.
- (350) Roques, B. P.; Garbay-Jaureguiberry, C.; Oberlin, R.; Anteonis, M.; Lala, A. K. Conformation of Met5-Enkephalin Determined by High Field PMR Spectroscopy. *Nature* **1976**, *262* (5571), 778–779.
- (351) Picone, D.; D'ursi, A.; Motta, A.; Tancredi, T.; Temussi, P. A. Conformational Preferences of [Leu5]enkephalin in Biomimetic Media. *Eur. J. Biochem.* **1990**, *192* (2), 433–439.
- (352) Marcotte, I.; Separovic, F.; Auger, M.; Gagné, S. M. A Multidimensional 1H NMR Investigation of the Conformation of Methionine-Enkephalin in Fast-Tumbling Bicelles. *Biophys. J.* **2004**, *86* (3), 1587–1600.
- (353) Klee, W. A. Endogenous Opiate Receptors. In *Peptides in Neurobiology*; Gainer, H., Ed.; Current Topics in Neurobiology; Plenum Press: New York, 1977; pp 375–396.
- (354) Goodchild, C. S.; Nadeson, R.; Cohen, E. Supraspinal and Spinal Cord Opioid Receptors Are Responsible for Antinociception Following Intrathecal Morphine Injections. *Eur. J. Anaesthesiol.* **2004**, *21* (03), 179–185.
- (355) Fontaine, J.; Reuse, J. Contractor Responses of the Isolated Colon of the Mouse to Morphine and Some Opioid Peptides. *Br. J. Pharmacol.* **1985**, *85* (4), 861–867.
- (356) Garcia-Garayoa, E.; Schibli, R.; Schubiger, P. A. Peptides Radiolabeled with Re-186/188 and Tc-99m as Potential Diagnostic and Therapeutic Agents. *Nucl. Sci. Tech.* **2007**, *18* (2), 88–100.
- (357) Metzler-Nolte, N.; Schatzschneider, U. Synthesis of Metal-Peptide Bioconjugates. In *Bioinorganic Chemistry: A Practical Course*; Walter de Gruyter, 2009; pp 67–85.
- (358) Kolb, H. C.; Finn, M. G.; Sharpless, K. B. Click Chemistry: Diverse Chemical Function from a Few Good Reactions. *Angew. Chem., Int. Ed.* **2001**, *40* (11), 2004–2021.
- (359) Kolb, H. C.; Finn, M. G.; Sharpless, K. B. Click-Chemie: diverse chemische Funktionalität mit einer Handvoll guter Reaktionen. *Angew. Chem.* **2001**, *113* (11), 2056–2075.
- (360) Huisgen, R.; Szeimies, G.; Möbius, L. 1,3-Dipolare Cycloadditionen, XXXII. Kinetik Der Additionen Organischer Azide an CC-Mehrfachbindungen. *Chem. Ber.* **1967**, *100* (8), 2494–2507.
- (361) Rolf Huisgen. Kinetics and Reaction Mechanisms: Selected Examples from the Experience of Forty Years : Pure and Applied Chemistry. *Pure Appl. Chem.* **1989**, *61* (4), 613–628.
- (362) Rostovtsev, V. V.; Green, L. G.; Fokin, V. V.; Sharpless, K. B. A Stepwise Huisgen Cycloaddition Process: Copper(I)-Catalyzed Regioselective “Ligation” of Azides and Terminal Alkynes. *Angew. Chem., Int. Ed.* **2002**, *41* (14), 2596–2599.
- (363) Rostovtsev, V. V.; Green, L. G.; Fokin, V. V.; Sharpless, K. B. A Stepwise Huisgen Cycloaddition Process: Copper(I)-Catalyzed Regioselective “Ligation” of Azides and Terminal Alkynes. *Angew. Chem.* **2002**, *114* (14), 2708–2711.
- (364) Tornøe, C. W.; Christensen, C.; Meldal, M. Peptidotriazoles on Solid Phase: [1,2,3]-Triazoles by Regiospecific Copper(I)-Catalyzed 1,3-Dipolar Cycloadditions of Terminal Alkynes to Azides. *J. Org. Chem.* **2002**, *67* (9), 3057–3064.
- (365) Kolb, H. C.; Sharpless, K. B. The Growing Impact of Click Chemistry on Drug Discovery. *Drug Discovery Today* **2003**, *8* (24), 1128–1137.
- (366) Meldal, M.; Tornøe, C. W. Cu-Catalyzed Azide–Alkyne Cycloaddition. *Chem. Rev.* **2008**, *108* (8), 2952–3015.

- (367) Click Chemistry: Function Follows Form (Chemical Society Reviews Themed Issue). *Chem. Soc. Rev.* **2010**, 39 (4), 1221–1408.
- (368) Spiteri, C.; Moses, J. E. Copper-Catalyzed Azide–Alkyne Cycloaddition: Regioselective Synthesis of 1,4,5-Trisubstituted 1,2,3-Triazoles. *Angew. Chem., Int. Ed.* **2010**, 49 (1), 31–33.
- (369) Spiteri, C.; Moses, J. E. Kupferkatalysierte Azid-Alkin-Cycloadditionen: regioselektive Synthese von 1,4,5-trisubstituierten 1,2,3-Triazolinen. *Angew. Chem.* **2010**, 122 (1), 33–36.
- (370) Baskin, J. M.; Bertozzi, C. R. Bioorthogonal Click Chemistry: Covalent Labeling in Living Systems. *QSAR Comb. Sci.* **2007**, 26 (11–12), 1211–1219.
- (371) Vollhardt, K. P. C.; Schore, N. E. 13.11: Natürlich vorkommende und physiologisch aktive Alkine. In *Organische Chemie*; Butenschön, H., Ed.; Wiley-VCH Verlag GmbH: Weinheim, 2005; pp 661–663.
- (372) Griffin, R. J. 3 The Medicinal Chemistry of the Azido Group. In *Progress in Medicinal Chemistry*; Ellis, G. P., Luscombe, D. K., Eds.; Elsevier, 1994; Vol. 31, pp 121–232.
- (373) Finn, M. G.; Fokin, V. V. Click Chemistry: Function Follows Form. *Chem. Soc. Rev.* **2010**, 39 (4), 1231–1232.
- (374) Agalave, S. G.; Maujan, S. R.; Pore, V. S. Click Chemistry: 1,2,3-Triazoles as Pharmacophores. *Chem. Asian J.* **2011**, 6 (10), 2696–2718.
- (375) Han, S.-Y.; Kim, Y.-A. Recent Development of Peptide Coupling Reagents in Organic Synthesis. *Tetrahedron* **2004**, 60 (11), 2447–2467.
- (376) Montalbetti, C. A. G. N.; Falque, V. Amide Bond Formation and Peptide Coupling. *Tetrahedron* **2005**, 61 (46), 10827–10852.
- (377) Valeur, E.; Bradley, M. Amide Bond Formation: Beyond the Myth of Coupling Reagents. *Chem. Soc. Rev.* **2009**, 38 (2), 606–631.
- (378) Merrifield, R. B. Solid Phase Peptide Synthesis. I. The Synthesis of a Tetrapeptide. *J. Am. Chem. Soc.* **1963**, 85 (14), 2149–2154.
- (379) Hans, R. H.; Guantai, E. M.; Lategan, C.; Smith, P. J.; Wan, B.; Franzblau, S. G.; Gut, J.; Rosenthal, P. J.; Chibale, K. Synthesis, Antimalarial and Antitubercular Activity of Acetylenic Chalcones. *Bioorg. Med. Chem. Lett.* **2010**, 20 (3), 942–944.
- (380) Fattahi, A.; McCarthy, R. E.; Ahmad, M. R.; Kass, S. R. Why Does Cyclopropene Have the Acidity of an Acetylene but the Bond Energy of Methane? *J. Am. Chem. Soc.* **2003**, 125 (38), 11746–11750.
- (381) Rivara, M.; Patel, M. K.; Amori, L.; Zuliani, V. Inhibition of NaV1.6 Sodium Channel Currents by a Novel Series of 1,4-Disubstituted-Triazole Derivatives Obtained via Copper-Catalyzed Click Chemistry. *Bioorg. Med. Chem. Lett.* **2012**, 22 (20), 6401–6404.
- (382) Walter, W.; Francke, W. 2.6 Alkyne. In *Beyer Walter - Lehrbuch der Organischen Chemie*; S. Hirzel Verlag: Stuttgart, 2004; pp 96–105.
- (383) Larsson, F. C. ; Lawesson, S.-O. Preparation and Alkylation of Substituted  $\beta$ -Hydroxydithiocinnamic Acids. *Tetrahedron* **1972**, 28 (21), 5341–5357.
- (384) Ohsugi, E.; Fujioka, T.; Harada, H.; Nakamura, M.; Maeda, R. Synthetic Studies on Diuretics. 5-(3,3-N,S-Substituted-2-Propenoyl)-2, 3-Dihydro-2-Benzo[b]furan-2-carboxylic Acids. *Chemical & Pharmaceutical Bulletin* **1989**, 37 (5), 1268–1278.
- (385) Chandrasekharam, M.; Singh, O. M.; Ila, H.; Junjappa, H. Reaction of Beta-Oxodithioesters With Propargylamine: A Facile Entry to Novel 2-(Acylalkylidene)-5-(Methylene)Thiazolidines. *Synth. Commun.* **1998**, 28 (16), 3073–3079.
- (386) Ackermann, G.; Jugelt, W.; Möbius, H.-H.; Suschke, H. D.; Werner, G. Elektrolyt-Gleichgewichte Und Elektrochemie. In; Lehrwerk Chemie; VEB Deutscher Verlag für Grundstoffindustrie: Leipzig, 1988; Vol. Lehrbuch 5, p 147.
- (387) Vollhardt, K. P. C.; Schore, N. E. 8.3: Alkohole als Säuren und Basen. In *Organische Chemie*; Butenschön, H., Ed.; Wiley-VCH Verlag GmbH: Weinheim, 2005; pp 331–334.
- (388) Chatt, J.; Guy, R. G.; Duncanson, L. A. 176. Complexes of Acetylenes with platinum(II). Part I. Alkynes. *J. Chem. Soc.* **1961**, 827–834.

- (389) Hiscox, W.; Jennings, P. W. Catalytic Hydration of Alkynes with Zeise's Dimer. *Organometallics* **1990**, *9* (7), 1997–1999.
- (390) Hartman, J. W.; Hiscox, W. C.; Jennings, P. W. Catalytic Hydration of Alkynes with platinum(II) Complexes. *J. Org. Chem.* **1993**, *58* (26), 7613–7614.
- (391) Jennings, P. W.; Hartman, J. W.; Hiscox, W. C. Alkyne Hydration Using Pt(II) Catalysts. *Inorg. Chim. Acta* **1994**, *222* (1–2), 317–322.
- (392) Hintermann, L.; Labonne, A. Catalytic Hydration of Alkynes and Its Application in Synthesis. *Synthesis* **2007**, *2007* (8), 1121–1150.
- (393) Barral, K.; Moorhouse, A. D.; Moses, J. E. Efficient Conversion of Aromatic Amines into Azides: A One-Pot Synthesis of Triazole Linkages. *Org. Lett.* **2007**, *9* (9), 1809–1811.
- (394) Kueh, J. T. B.; Choi, K. W.; Brimble, M. A. Enantioselective Synthesis of C-Linked Spiroacetal-Triazoles as Privileged Natural Product-like Scaffolds. *Org. Biomol. Chem.* **2012**, *10* (30), 5993–6002.
- (395) Pieck, J. C.; Kuch, D.; Grolle, F.; Linne, U.; Haas, C.; Carell, T. PNA-Based Reagents for the Direct and Site-Specific Synthesis of Thymine Dimer Lesions in Genomic DNA. *J. Am. Chem. Soc.* **2006**, *128* (5), 1404–1405.
- (396) Maddani, M.; Prabhu, K. R. A Chemoselective Aerobic Oxidation of Benzylic Azides Catalyzed by Molybdenum Xanthate in an Aqueous Medium. *Tetrahedron Lett.* **2008**, *49* (29–30), 4526–4530.
- (397) Lieber, E.; Rao, C. N. R.; Chao, T. S.; Hoffman, C. W. W. Infrared Spectra of Organic Azides. *Anal. Chem.* **1957**, *29* (6), 916–918.
- (398) Hagler, A. T.; Dauber, P.; Lifson, S. Consistent Force Field Studies of Intermolecular Forces in Hydrogen-Bonded Crystals. 3. The C=O···H-O Hydrogen Bond and the Analysis of the Energetics and Packing of Carboxylic Acids. *J. Am. Chem. Soc.* **1979**, *101* (18), 5131–5141.
- (399) García-Orozco, I.; Ortega-Alfaro, M. C.; López-Cortés, J. G.; Toscano, R. A.; Alvarez-Toledano, C. Synthesis and Characterization of Novel Dinuclear Copper(I) Complexes. Dimerization of [CuL(PPh<sub>3</sub>)<sub>2</sub>] (L = Methyl 3-Hydroxy-3-(p-R-Phenyl)-2-Propenedithioate). *Inorg. Chem.* **2006**, *45* (4), 1766–1773.
- (400) Knorr, R.; Trzeciak, A.; Bannwarth, W.; Gillessen, D. New Coupling Reagents in Peptide Chemistry. *Tetrahedron Lett.* **1989**, *30* (15), 1927–1930.
- (401) König, W.; Geiger, R. Racemisierung Bei Peptidsynthesen. *Chem. Ber.* **1970**, *103* (7), 2024–2033.
- (402) Hammud, H. H.; Holman, K. T.; Masoud, M. S.; El-Faham, A.; Beidas, H. 1-Hydroxybenzotriazole (HOBt) Acidity, Formation Constant with Different Metals and Thermodynamic Parameters: Synthesis and Characterization of Some HOBt Metal Complexes – Crystal Structures of Two Polymers: [Cu<sub>2</sub>(H<sub>2</sub>O)<sub>5</sub>(OBt)<sub>2</sub>(μ-OBt)<sub>2</sub>] · 2H<sub>2</sub>O · EtOH (1A) and [Cu(μ-OBt)(HOBt)(OBt)(EtOH)] (1B). *Inorg. Chim. Acta* **2009**, *362* (10), 3526–3540.
- (403) Papatrifiantafyllopoulou, C.; Diamantopoulou, E.; Terzis, A.; Tangoulis, V.; Lalioti, N.; Perlepes, S. P. High-Nuclearity nickel(II) Clusters: Ni<sub>13</sub> Complexes from the Use of 1-Hydroxybenzotriazole. *Polyhedron* **2009**, *28* (9–10), 1903–1911.
- (404) Zhang, Z.-Q.; Huang, R.-D.; Dong, L.-J.; Xu, Y.-Q.; Yu, L.-Q.; Jiao, Z.-W.; Hu, C.-W. Synthesis, Structures, Luminescence/magnetic Properties of Complexes of the M/1-Hydroxybenzotriazole, M = Cobalt, Nickel, Silver, Zinc and Copper. *Inorg. Chim. Acta* **2009**, *362* (9), 3056–3064.
- (405) Ravindran Durai Nayagam, B.; Jebas, S. R.; Selvarathy Grace, P.; Schollmeyer, D. Chlorido(dimethyl Sulfoxide)(pyridine-2-Thiolato N-Oxide-κ<sup>2</sup>S,O)platinum(II). *Acta Crystallogr., Sect. E: Struct. Rep. Online* **2008**, *64* (7), m975–m976.
- (406) Autorenkollektiv. *Organikum : Organisch-Chemisches Grundpraktikum*, 22. ed.; Wiley-VCH: Weinheim, 2004.
- (407) Rink, H. Solid-Phase Synthesis of Protected Peptide Fragments Using a Trialkoxy-Diphenyl-Methylester Resin. *Tetrahedron Lett.* **1987**, *28* (33), 3787–3790.

- (408) König, W.; Geiger, R. Eine Neue Methode Zur Synthese von Peptiden: Aktivierung Der Carboxylgruppe Mit Dicyclohexylcarbodiimid Unter Zusatz von 1-Hydroxy-Benzotriazolen. *Chem. Ber.* **1970**, *103* (3), 788–798.
- (409) König, W.; Geiger, R. Eine Neue Methode Zur Synthese von Peptiden: Aktivierung Der Carboxylgruppe Mit Dicyclohexylcarbodiimid Und 3-Hydroxy-4-Oxo-3.4-Dihydro-1.2.3-Benzotriazin. *Chem. Ber.* **1970**, *103* (7), 2034–2040.
- (410) Pfeiffer, H.; Rojas, A.; Niesel, J.; Schatzschneider, U. Sonogashira and “Click” Reactions for the N-Terminal and Side-Chain Functionalization of Peptides with [Mn(CO)<sub>3</sub>(tpm)]<sup>+</sup>-Based CO Releasing Molecules (tpm = Tris(pyrazolyl)methane). *Dalton Trans.* **2009**, No. 22, 4292–4298.
- (411) Nonius. *Collect Data Collection Software*; Nonius BV: Delft, The Netherlands, 1998.
- (412) Otwinowski, Z.; Minor, W. Processing of X-Ray Diffraction Data Collected in Oscillation Mode. In *Methods in Enzymology*; Charles W. Carter, J., Ed.; Academic Press, 1997; Vol. 276, pp 307–326.
- (413) Blessing, R. H. Outlier Treatment in Data Merging. *J. Appl. Crystallogr.* **1997**, *30* (4), 421–426.
- (414) Sheldrick, G. M. A Short History of SHELX. *Acta Cryst. allogr., Sect. A: Found. Crystallogr.* **2008**, *64* (1), 112–122.
- (415) Rigaku/MS. *CrystalClear and CrystalStructure*; Rigaku/MS Inc.: The Woodlands, Texas, USA, 2006.
- (416) Spek, A. L. Single-Crystal Structure Validation with the Program PLATON. *Journal of Applied Crystallography* **2003**, *36* (1), 7–13.
- (417) Spek, A. L. Structure Validation in Chemical Crystallography. *Acta Crystallographica Section D Biological Crystallography* **2009**, *65* (2), 148–155.
- (418) Dolomanov, O. V.; Bourhis, L. J.; Gildea, R. J.; Howard, J. A. K.; Puschmann, H. OLEX2: A Complete Structure Solution, Refinement and Analysis Program. *Journal of Applied Crystallography* **2009**, *42* (2), 339–341.
- (419) Rieger, P. Übertragung Spektrofotometrischer Daten von Küvetten Auf Microplates. *Labor-Praxis* **2000**, *24* (5), 72–76.
- (420) Nardone, R. M. Eradication of Cross-Contaminated Cell Lines: A Call for Action. *Cell Biol Toxicol* **2007**, *23* (6), 367–372.
- (421) LGC Standards S.a.r.l. American Type Culture Collection database [http://www.lgcstandards-atcc.org/Products/Cells\\_and\\_Microorganisms/Cell\\_Lines](http://www.lgcstandards-atcc.org/Products/Cells_and_Microorganisms/Cell_Lines) (accessed May 22, 2015).
- (422) Leibniz Institut DSMZ-Deutsche Sammlung von Mikroorganismen und Zellkulturen GmbH. Deutsche Sammlung von Mikroorganismen und Zellkulturen <https://www.dsmz.de/catalogues/catalogue-human-and-animal-cell-lines.html> (accessed May 22, 2015).

---

# SUPPLEMENT

*The following additional information can be found in the supplement:*

<i>Supplement A:</i>	<i>Crystallographic Data</i>
<i>Supplement B:</i>	<i>Protein Interaction - ESI MS Spectral Data</i>
<i>Supplement C:</i>	<i>DNA Interaction</i>
<i>Supplement D:</i>	<i>Bioconjugates</i>
<i>Supplement E:</i>	<i>Media Composition</i>
<i>Supplement F:</i>	<i>Abbreviations</i>
<i>Supplement G:</i>	<i>Digital Media</i>





## SUPPLEMENT A: CRYSTALLOGRAPHIC DATA

Formula used for the calculation of standard deviation and residual values:

$$* \quad S = \left\{ \frac{\sum [w(F_o^2 - F_c^2)]}{(n-p)} \right\}^{0.5}, \quad n = \text{no. of reflections}; p = \text{no. of parameters.}$$

$$** \quad R_1 = \frac{\sum ||F_o| - |F_c||}{\sum |F_o|}$$

$$*** \quad wR2 = \left\{ \frac{\sum [w(F_o^2 - F_c^2)]}{\sum [w(F_o^2)]} \right\}^{0.5}$$

Table S 1 Crystallographic data of compounds **50** and **82**.

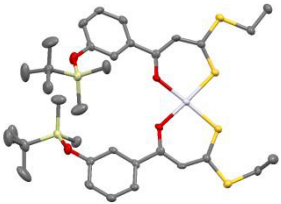
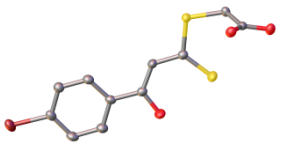
Compound	<b>50</b>	<b>82</b>
		
<b>Empirical formula</b>	C <sub>34</sub> H <sub>50</sub> O <sub>4</sub> PtS <sub>4</sub> Si <sub>2</sub>	C <sub>11</sub> H <sub>9</sub> BrO <sub>3</sub> S <sub>2</sub>
<b>Formula weight [g·mol<sup>-1</sup>]</b>	902.25	333.22
<b>collection T [K]</b>	133(2)	170.0
<b>λ (Mo K<sub>α</sub>) [Å]</b>	0.71073 Å	0.71073
<b>Crystal system</b>	monoclinic	orthorhombic
<b>Space group</b>	P2 <sub>1</sub> /c	P2 <sub>1</sub> 2 <sub>1</sub> 2 <sub>1</sub>
<b>Cell constants</b>		
<b>a [Å]</b>	16.9053(8)	6.2614(2)
<b>b [Å]</b>	11.9274(8)	7.1327(3)
<b>c [Å]</b>	20.3286(12)	27.5023(8)
<b>α [°]</b>	90	90.00
<b>β [°]</b>	106.746(4)	90.00
<b>γ [°]</b>	90	90.00
<b>V [Å<sup>3</sup>]</b>	3925.1(4)	1228.27(7)
<b>Z</b>	4	4
<b>ρ<sub>calcd</sub> [g·cm<sup>-3</sup>]</b>	1.527	1.802
<b>μ [mm<sup>-1</sup>]</b>	3.883	3.678
<b>F(000)</b>	1824	664.0
<b>crystal dimensions [mm]</b>	0.04 × 0.04 × 0.03	0.21 × 0.18 × 0.11
<b>2 θ range [°]</b>	2.52 to 27.46	5.9 to 73.48
<b>index ranges</b>	-21 ≤ h ≤ 19 -15 ≤ k ≤ 12 -21 ≤ l ≤ 26	-9 ≤ h ≤ 9 -8 ≤ k ≤ 11 -42 ≤ l ≤ 42
<b>measured reflections</b>	23843	22844
<b>unique reflections</b>	8605	4878
<b>R<sub>int</sub></b>	0.0703	0.0477
<b>data with I &gt; 2σ(I) / restraints / parameters</b>	8605 / 0 / 418	4878/0/156
<b>Goodness-of-fit on F<sup>2</sup> / S*</b>	1.050	1.093
<b>R1 [I &gt; 2σ(I)]**</b>	0.0441	0.0359
<b>wR2 [I &gt; 2σ(I)]***</b>	0.0825	0.0692
<b>R1<sub>all</sub>**</b>	0.0830	0.0545
<b>wR2 [all data, on F<sup>2</sup>]***</b>	0.0971	0.0841
<b>max./min. residual electron density [e·Å<sup>-3</sup>]</b>	1.839/-1.453	0.58/-0.47

Table S 2 Crystallographic data of compounds **72** and **73**.

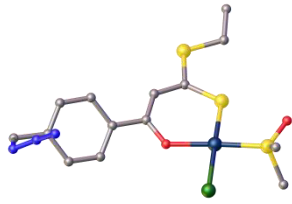
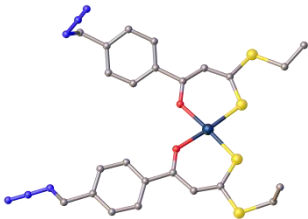
		
Compound	<b>72</b>	<b>73</b>
Empirical formula	C <sub>14</sub> H <sub>18</sub> ClN <sub>3</sub> O <sub>2</sub> PtS <sub>3</sub>	C <sub>24</sub> H <sub>24</sub> N <sub>6</sub> O <sub>2</sub> PtS <sub>4</sub>
Formula weight [g·mol <sup>-1</sup> ]	587,04	751,82
collection T [K]	293	293
λ (Mo K <sub>α</sub> ) [Å]	0.71075	0.71075
Crystal system	monoclinic	triclinic
Space group	P2 <sub>1</sub> /n	P-1
Cell constants		
a [Å]	24.68(3)	11.436(8)
b [Å]	7.408(6)	13.558(10)
c [Å]	24.75(2)	26.982(18)
α [°]	90.00	91.835(9)
β [°]	118.097(12)	94.275(10)
γ [°]	90.00	105.974(9)
V [Å <sup>3</sup> ]	3992(7)	4005(5)
Z	4	2
ρ <sub>calcd</sub> [g·cm <sup>-3</sup> ]	1.925	3.802
μ [mm <sup>-1</sup> ]	7.488	27.023
F(000)	2188.0	3990.0
crystal dimensions [mm]	0.2 × 0.2 × 0.2	0.2 × 0.2 × 0.2
2 θ range [°]	3.2 to 55.14	3.04 to 55.04
index ranges	-31 ≤ h ≤ 32 -9 ≤ k ≤ 9 -32 ≤ l ≤ 32	-14 ≤ h ≤ 14 -17 ≤ k ≤ 17 -35 ≤ l ≤ 35
measured reflections	38244	34466
unique reflections	9144	17736
R <sub>int</sub>	0.1067	0.0716
data with I > 2σ(I) / restraints/ parameters	9144/36/441	17736/0/429
Goodness-of-fit on F <sup>2</sup> / S*	1.081	1.393
R1 [I > 2σ(I)]**	0.0659	0.1040
wR2 [I > 2σ(I)]***	0.1687	0.2496
R1 <sub>all</sub> **	0.0788	0.1284
wR2 [all data, on F <sup>2</sup> ]***	0.1801	0.275
max./min. residual electron density [e·Å <sup>-3</sup> ]	4.23/-4.61	6.68/-9.24

Table S 3 Bond lengths [Å] for compound 50.

Atoms		Bond lengths [Å]	Atoms (continued)		Bond lengths [Å]	Atoms (continued)		Bond lengths [Å]
Pt(1)	O(1)	2.022(4)	Si(2)	C(27)	1.841(7)	C(12)	C(14)	1.535(11)
Pt(1)	O(3)	2.020(3)	Si(2)	C(29)	1.884(6)	C(12)	C(13)	1.536(10)
Pt(1)	S(1)	2.2275(14)	O(1)	C(3)	1.283(7)	C(16)	C(17)	1.512(9)
Pt(1)	S(3)	2.2303(15)	O(2)	C(8)	1.374(6)	C(18)	C(19)	1.388(8)
S(1)	C(1)	1.687(6)	O(3)	C(20)	1.276(7)	C(19)	C(20)	1.395(8)
S(2)	C(1)	1.758(5)	O(4)	C(25)	1.368(7)	C(20)	C(21)	1.507(7)
S(2)	C(16)	1.816(6)	C(1)	C(2)	1.405(8)	C(21)	C(26)	1.385(8)
S(3)	C(18)	1.690(6)	C(2)	C(3)	1.387(8)	C(21)	C(22)	1.393(8)
S(4)	C(18)	1.757(6)	C(3)	C(4)	1.511(8)	C(22)	C(23)	1.389(8)
S(4)	C(33)	1.803(6)	C(4)	C(5)	1.378(8)	C(23)	C(24)	1.374(8)
Si(1)	O(2)	1.662(4)	C(4)	C(9)	1.402(7)	C(24)	C(25)	1.393(8)
Si(1)	C(10)	1.843(6)	C(5)	C(6)	1.385(8)	C(25)	C(26)	1.388(7)
Si(1)	C(12)	1.864(7)	C(6)	C(7)	1.381(8)	C(29)	C(31)	1.507(10)
Si(1)	C(11)	1.868(7)	C(7)	C(8)	1.380(8)	C(29)	C(30)	1.533(9)
Si(2)	O(4)	1.672(4)	C(8)	C(9)	1.381(8)	C(29)	C(32)	1.532(10)
Si(2)	C(28)	1.843(7)	C(12)	C(15)	1.526(9)	C(33)	C(34)	1.529(8)

Table S 4 Bond angles [°] for compound 50.

Atoms	Bond angles [°]	Atoms (continued)	Bond angles [°]
O(1)-Pt(1)-O(3)	80.62(14)	C(7)-C(6)-C(5)	120.2(5)
O(1)-Pt(1)-S(1)	96.81(11)	C(6)-C(7)-C(8)	120.0(6)
O(3)-Pt(1)-S(1)	176.78(11)	O(2)-C(8)-C(7)	118.1(5)
O(1)-Pt(1)-S(3)	177.55(10)	O(2)-C(8)-C(9)	121.3(5)
O(3)-Pt(1)-S(3)	96.93(11)	C(7)-C(8)-C(9)	120.6(5)
S(1)-Pt(1)-S(3)	85.63(5)	C(8)-C(9)-C(4)	119.1(5)
C(1)-S(1)-Pt(1)	108.8(2)	C(15)-C(12)-C(14)	108.1(7)
C(1)-S(2)-C(16)	105.6(3)	C(15)-C(12)-C(13)	109.8(6)
C(18)-S(3)-Pt(1)	108.6(2)	C(14)-C(12)-C(13)	109.0(6)
C(18)-S(4)-C(33)	105.4(3)	C(15)-C(12)-Si(1)	110.2(5)
O(2)-Si(1)-C(10)	111.5(2)	C(14)-C(12)-Si(1)	109.0(5)
O(2)-Si(1)-C(12)	104.5(3)	C(13)-C(12)-Si(1)	110.7(5)
C(10)-Si(1)-C(12)	110.9(3)	C(17)-C(16)-S(2)	114.7(5)
O(2)-Si(1)-C(11)	107.9(3)	C(19)-C(18)-S(3)	128.7(4)
C(10)-Si(1)-C(11)	110.5(3)	C(19)-C(18)-S(4)	114.3(4)
C(12)-Si(1)-C(11)	111.4(3)	S(3)-C(18)-S(4)	117.1(3)
O(4)-Si(2)-C(28)	109.8(3)	C(20)-C(19)-C(18)	129.3(5)
O(4)-Si(2)-C(27)	111.2(3)	O(3)-C(20)-C(19)	126.9(5)
C(28)-Si(2)-C(27)	110.4(4)	O(3)-C(20)-C(21)	114.2(5)
O(4)-Si(2)-C(29)	103.1(2)	C(19)-C(20)-C(21)	118.9(5)
C(28)-Si(2)-C(29)	111.7(4)	C(26)-C(21)-C(22)	119.8(5)
C(27)-Si(2)-C(29)	110.5(3)	C(26)-C(21)-C(20)	118.8(5)
C(3)-O(1)-Pt(1)	129.5(3)	C(22)-C(21)-C(20)	121.4(5)
C(8)-O(2)-Si(1)	131.6(4)	C(23)-C(22)-C(21)	119.5(5)
C(20)-O(3)-Pt(1)	129.5(4)	C(24)-C(23)-C(22)	120.6(5)
C(25)-O(4)-Si(2)	132.0(4)	C(23)-C(24)-C(25)	120.0(5)
C(2)-C(1)-S(1)	129.1(4)	O(4)-C(25)-C(26)	122.7(5)
C(2)-C(1)-S(2)	112.2(4)	O(4)-C(25)-C(24)	117.6(5)
S(1)-C(1)-S(2)	118.8(3)	C(26)-C(25)-C(24)	119.6(5)
C(3)-C(2)-C(1)	128.3(5)	C(21)-C(26)-C(25)	120.3(5)
O(1)-C(3)-C(2)	127.5(5)	C(31)-C(29)-C(30)	109.3(6)
O(1)-C(3)-C(4)	113.8(5)	C(31)-C(29)-C(32)	109.6(6)
C(2)-C(3)-C(4)	118.7(5)	C(30)-C(29)-C(32)	109.3(6)
C(5)-C(4)-C(9)	120.3(5)	C(31)-C(29)-Si(2)	110.7(5)
C(5)-C(4)-C(3)	121.9(5)	C(30)-C(29)-Si(2)	108.9(4)
C(9)-C(4)-C(3)	117.8(5)	C(32)-C(29)-Si(2)	108.9(5)
C(4)-C(5)-C(6)	119.8(5)	C(34)-C(33)-S(4)	108.1(4)

Table S 5 Bond lengths [Å] for compound **72**.

Atoms		Bond lengths [Å]
Pt1	S9	2.196(5)
Pt1	S10	2.262(5)
Pt1	Cl12	2.336(5)
Pt1	O35	2.010(11)
Pt2	S6	2.193(5)
Pt2	S11	2.239(5)
Pt2	Cl13	2.343(5)
Pt2	O0AA	2.002(11)
S6	C31	1.785(13)
S6	C46	1.791(14)
S6	O1	1.467(13)
S7	C18	1.857(16)
S7	C20	1.827(17)
S8	C19	1.699(16)
S8	C27	1.741(19)
S9	C4	1.780(14)
S9	C1	1.778(14)
S9	O2	1.479(13)
S10	C20	1.674(17)
S11	C19	1.715(16)
C18	C34	1.52(2)
C19	C14	1.40(2)
C20	C45	1.35(2)
C25	O35	1.271(16)
C25	C45	1.375(17)

Atoms (continued)		Bond lengths [Å]
C25	C8	1.519(16)
C27	C15	1.51(3)
C44	C11	1.476(18)
C44	C14	1.39(2)
C44	O0AA	1.343(17)
C8	C13	1.44(2)
C8	C2	1.448(17)
C11	C17	1.457(18)
C11	C3	1.369(18)
C13	C5	1.47(2)
C2	C6	1.434(17)
C5	C12	1.427(19)
C6	C12	1.362(17)
C7	C9	1.442(19)
C7	C10	1.375(19)
C7	O0AA	1.50(2)
C12	C1A	1.501(18)
C9	C3	1.391(19)
C10	C17	1.36(2)
C1A	N5	1.55(3)
N1	N5	1.15(2)
N1	N3	1.21(3)
O0AA	O0AA	1.51(2)
O0AA	N4	1.14(2)
N2	N4	1.22(3)

Table S 6 Bond angles [°] for compound **72**.

Atoms			Bond angles [°]	Atoms (continued)			Bond angles [°]
S9	Pt1	S10	89.46(17)	O35	C25	C8	113.9(11)
S9	Pt1	Cl12	90.11(17)	C45	C25	C8	118.0(10)
S10	Pt1	Cl12	176.37(14)	C15	C27	S8	109.8(16)
O35	Pt1	S9	173.5(3)	C25	O35	Pt1	128.8(9)
O35	Pt1	S10	95.8(4)	C14	C44	C11	123.1(12)
O35	Pt1	Cl12	84.9(4)	O0AA	C44	C11	112.0(12)
S6	Pt2	S11	89.88(18)	O0AA	C44	C14	124.6(12)
S6	Pt2	Cl13	89.70(18)	C20	C45	C25	126.1(13)
S11	Pt2	Cl13	178.15(15)	C13	C8	C25	120.5(11)
O0AA	Pt2	S6	173.5(4)	C13	C8	C2	124.0(12)
O0AA	Pt2	S11	95.5(4)	C2	C8	C25	115.4(11)
O0AA	Pt2	Cl13	85.0(4)	C17	C11	C44	119.1(12)
C31	S6	Pt2	110.3(5)	C3	C11	C44	123.2(12)
C31	S6	C46	101.7(8)	C3	C11	C17	117.6(13)
C46	S6	Pt2	109.0(6)	C44	C14	C19	130.5(14)
O1	S6	Pt2	116.9(6)	C8	C13	C5	113.3(14)
O1	S6	C31	109.2(6)	C6	C2	C8	117.8(11)
O1	S6	C46	108.7(7)	C13	C5	C12	122.7(12)
C20	S7	C18	106.1(8)	C12	C6	C2	121.0(12)
C19	S8	C27	107.3(8)	C9	C7	C0AA	120.8(13)
C4	S9	Pt1	111.3(5)	C10	C7	C9	118.0(15)
C4	S9	C1	103.0(9)	C10	C7	C0AA	121.2(13)
C1	S9	Pt1	110.0(5)	C5	C12	C1A	118.3(12)
O2	S9	Pt1	117.6(5)	C6	C12	C5	121.0(13)
O2	S9	C4	108.1(7)	C6	C12	C1A	120.7(14)
O2	S9	C1	105.7(7)	C3	C9	C7	119.4(15)
C20	S10	Pt1	105.9(6)	C17	C10	C7	122.7(14)
C19	S11	Pt2	110.9(5)	C10	C17	C11	119.9(14)
C34	C18	S7	106.4(14)	C12	C1A	N5	115.7(14)
S11	C19	S8	119.5(8)	C11	C3	C9	122.4(14)
C14	C19	S8	114.4(12)	N5	N1	N3	167(2)
C14	C19	S11	125.5(12)	N1	N5	C1A	108.9(17)
S10	C20	S7	115.0(9)	N0AA	C0AA	C7	112.2(14)
C45	C20	S7	111.6(12)	N4	N0AA	C0AA	110.1(19)
C45	C20	S10	133.4(13)	N0AA	N4	N2	160(3)
O35	C25	C45	128.1(11)	C44	O0AA	Pt2	129.2(10)

Table S 7 Bond lengths [Å] for compound **73**.

Atoms		Bond lengths [Å]	Atoms (continued)		Bond lengths [Å]
Pt1	S8	2.229(3)	C59	C7AA	1.56(2)
Pt1	S15	2.244(4)	C64	C94	1.40(2)
Pt1	O2	2.018(9)	C94	C3BA	1.40(2)
Pt1	O3	2.016(9)	C94	C4BA	1.57(3)
Pt2	S9	2.240(4)	C102	C110	1.41(2)
Pt2	S16	2.227(4)	C7BA	C8BA	1.402(17)
Pt2	O1	1.997(10)	C7BA	C8AA	1.493(19)
Pt2	O1AA	1.992(8)	C8BA	C2AA	1.418(17)
Pt3	S10	2.233(4)	C15	C42	1.403(18)
Pt3	S12	2.245(4)	C8AA	C9AA	1.45(2)
Pt3	O0AA	2.035(10)	C8AA	C2BA	1.422(19)
Pt3	O5	2.019(9)	C3AA	C36	1.39(2)
C7	C46	1.392(17)	C3AA	C40	1.54(2)
C7	C3BA	1.31(2)	C3AA	C45	1.36(2)
S8	C5AA	1.714(14)	C9AA	C36	1.39(2)
S9	C5BA	1.684(14)	C2BA	C45	1.38(2)
S10	C2AA	1.680(14)	C40	N35	1.48(2)
S11	C4	1.744(14)	C57	N15	1.64(5)
S11	C6	1.811(13)	O1	C19	1.306(17)
S12	C42	1.693(14)	O2	C32	1.300(15)
S13	C42	1.731(15)	O3	C28	1.252(15)
S13	C29	1.811(13)	C4	C20	1.386(16)
S14	C5AA	1.751(13)	C5	C8	1.388(17)
S14	C10	1.836(14)	C6	C14	1.59(2)
S15	C4	1.726(13)	C5AA	C11	1.384(17)
S16	C5	1.721(14)	C8	C19	1.440(18)
S17	C2AA	1.749(13)	C9	C13	1.52(2)
S17	C18	1.837(14)	C10	C9BA	1.52(2)
S18	C9	1.823(14)	C11	C28	1.453(16)
S18	C5BA	1.764(14)	C12	C30	1.57(2)
S19	C5	1.742(12)	C5BA	C24	1.376(18)
S19	C12	1.858(15)	C16	C23	1.38(2)
O0AA	C6AA	1.241(16)	C16	C38	1.55(2)
O5	C7BA	1.311(15)	C16	C44	1.40(2)
C4AA	C0BA	1.430(18)	C17	C29	1.55(2)
C4AA	C6BA	1.36(2)	C18	C26	1.565(19)
C0AA	C1AA	1.36(2)	C20	C32	1.397(17)
C0AA	C102	1.42(2)	C21	C33	1.44(2)
C0AA	C57	1.57(3)	C21	C41	1.42(2)
C6AA	C49	1.513(19)	C21	C61	1.63(3)
C6AA	C15	1.455(19)	C22	C25	1.41(2)
C1BA	C0BA	1.38(2)	C22	C32	1.512(17)
C1BA	C86	1.38(2)	C22	C34	1.42(2)
C1AA	C81	1.41(2)	C23	C37	1.46(2)
C0BA	C19	1.501(18)	C24	C38	1.37(2)
C27	C46	1.390(19)	C25	C41	1.41(2)
C27	C64	1.39(2)	C7AA	N0AA	1.49(3)
C6BA	C59	1.38(2)	N31	N35	1.24(2)
C46	C28	1.497(17)	N31	N50	1.18(3)
C49	C81	1.43(2)	C33	C34	1.38(2)
C49	C110	1.37(2)	C37	C0CA	1.41(3)
C59	C86	1.42(2)	C38	O1AA	1.282(17)



Atoms (continued)		Bond lengths [Å]
C39	C0CA	1.39(3)
C39	C44	1.39(2)
C0CA	C68	1.54(3)
C4BA	N7	1.77(4)
C61	N18	1.23(4)
C68	N9	1.51(3)

Atoms (continued)		Bond lengths [Å]
N0AA	N1AA	1.14(5)
N8	N9	1.21(3)
N8	N13	1.10(4)
N18	N6	1.39(4)
N2AA	N1AA	1.27(5)
N6	N10	1.35(5)

Table S 8 Bond angles [°] for compound 73.

Atoms			Bond angles [°]
S8	Pt1	S15	88.52(13)
O2	Pt1	S8	174.7(3)
O2	Pt1	S15	96.7(3)
O3	Pt1	S8	96.0(3)
O3	Pt1	S15	175.5(3)
O3	Pt1	O2	78.7(4)
S16	Pt2	S9	87.59(13)
O1	Pt2	S9	175.7(3)
O1	Pt2	S16	96.7(3)
O1AA	Pt2	S9	96.2(3)
O1AA	Pt2	S16	176.2(3)
O1AA	Pt2	O1	79.5(4)
S10	Pt3	S12	88.17(13)
O0AA	Pt3	S10	174.9(3)
O0AA	Pt3	S12	96.9(3)
O5	Pt3	S10	96.6(3)
O5	Pt3	S12	175.2(3)
O5	Pt3	O0AA	78.3(4)
C3BA	C7	C46	128.9(14)
C5AA	S8	Pt1	108.6(4)
C5BA	S9	Pt2	108.1(5)
C2AA	S10	Pt3	109.0(4)
C4	S11	C6	106.4(6)
C42	S12	Pt3	108.7(5)
C42	S13	C29	105.8(7)
C5AA	S14	C10	106.2(6)
C4	S15	Pt1	107.8(4)
C5	S16	Pt2	108.6(4)
C2AA	S17	C18	104.8(7)
C5BA	S18	C9	106.2(7)
C5	S19	C12	105.9(6)
C6AA	O0AA	Pt3	130.0(9)
C7BA	O5	Pt3	130.5(8)
C6BA	C4AA	C0BA	118.2(14)
C1AA	C0AA	C102	122.2(16)
C1AA	C0AA	C57	119.0(17)
C102	C0AA	C57	118.5(16)
O0AA	C6AA	C49	114.6(12)
O0AA	C6AA	C15	128.0(12)
C15	C6AA	C49	117.3(12)
C86	C1BA	C0BA	120.1(14)

Atoms (continued)			Bond angles [°]
C45	C2BA	C8AA	115.5(14)
C9AA	C36	C3AA	119.0(16)
N35	C40	C3AA	110.3(16)
S12	C42	S13	118.2(8)
C15	C42	S12	129.7(12)
C15	C42	S13	112.1(11)
C3AA	C45	C2BA	124.0(16)
C0AA	C57	N15	112(2)
C19	O1	Pt2	131.8(8)
C32	O2	Pt1	127.8(8)
C28	O3	Pt1	132.0(8)
S15	C4	S11	116.8(7)
C20	C4	S11	112.5(10)
C20	C4	S15	130.6(11)
S16	C5	S19	117.0(7)
C8	C5	S16	130.2(10)
C8	C5	S19	112.8(10)
C14	C6	S11	103.9(9)
S8	C5AA	S14	117.1(7)
C11	C5AA	S8	130.8(11)
C11	C5AA	S14	112.1(11)
C5	C8	C19	126.9(12)
C13	C9	S18	108.0(10)
C9BA	C10	S14	109.9(10)
C5AA	C11	C28	125.2(12)
C30	C12	S19	111.3(10)
S9	C5BA	S18	117.4(7)
C24	C5BA	S9	130.6(12)
C24	C5BA	S18	112.0(10)
C23	C16	C38	119.4(14)
C23	C16	C44	121.4(15)
C44	C16	C38	119.1(14)
C26	C18	S17	104.2(10)
O1	C19	C0BA	115.7(11)
O1	C19	C8	125.5(12)
C8	C19	C0BA	118.8(12)
C4	C20	C32	125.5(12)
C33	C21	C61	118.7(16)
C41	C21	C33	121.2(15)
C41	C21	C61	120.0(16)
C25	C22	C32	116.9(12)

Atoms (continued)			Bond angles [°]
C0AA	C1AA	C81	122.5(18)
C4AA	C0BA	C19	114.9(12)
C1BA	C0BA	C4AA	120.6(12)
C1BA	C0BA	C19	124.3(12)
C46	C27	C64	119.4(13)
C4AA	C6BA	C59	121.9(14)
C7	C46	C28	120.6(12)
C27	C46	C7	114.8(12)
C27	C46	C28	124.6(12)
C81	C49	C6AA	121.9(13)
C110	C49	C6AA	117.5(14)
C110	C49	C81	120.6(14)
C6BA	C59	C86	119.1(14)
C6BA	C59	C7AA	124.7(14)
C86	C59	C7AA	116.1(15)
C27	C64	C94	121.7(17)
C1AA	C81	C49	115.9(15)
C1BA	C86	C59	119.8(15)
C64	C94	C3BA	118.9(16)
C64	C94	C4BA	120.8(18)
C3BA	C94	C4BA	120.2(17)
C110	C102	C0AA	115.1(16)
C49	C110	C102	123.5(16)
O5	C7BA	C8BA	125.9(12)
O5	C7BA	C8AA	111.9(11)
C8BA	C7BA	C8AA	122.3(13)
C7BA	C8BA	C2AA	128.0(13)
C42	C15	C6AA	126.7(13)
C9AA	C8AA	C7BA	120.5(12)
C2BA	C8AA	C7BA	118.3(13)
C2BA	C8AA	C9AA	121.3(13)
S10	C2AA	S17	119.4(7)
C8BA	C2AA	S10	129.7(10)
C8BA	C2AA	S17	110.8(10)
C36	C3AA	C40	117.0(15)
C45	C3AA	C36	121.1(15)
C45	C3AA	C40	121.7(15)
C36	C9AA	C8AA	118.9(13)

Atoms (continued)			Bond angles [°]
C25	C22	C34	121.3(13)
C34	C22	C32	121.8(13)
C16	C23	C37	117.5(16)
C38	C24	C5BA	125.9(14)
C22	C25	C41	120.4(15)
N0AA	C7AA	C59	102.8(17)
O3	C28	C46	114.7(11)
O3	C28	C11	127.1(11)
C11	C28	C46	118.1(11)
C17	C29	S13	106.5(9)
N50	N31	N35	176(2)
O2	C32	C20	130.0(11)
O2	C32	C22	111.3(11)
C20	C32	C22	118.7(11)
C34	C33	C21	119.3(16)
C33	C34	C22	119.7(15)
N31	N35	C40	114.4(19)
C7	C3BA	C94	116.2(15)
C0CA	C37	C23	119.1(19)
C24	C38	C16	118.8(13)
O1AA	C38	C16	111.2(12)
O1AA	C38	C24	129.7(13)
C44	C39	C0CA	117.3(19)
C37	C0CA	C68	119(2)
C39	C0CA	C37	122(2)
C39	C0CA	C68	119(2)
C25	C41	C21	118.0(15)
C94	C4BA	N7	107(2)
C39	C44	C16	122.4(17)
N18	C61	C21	110(3)
N9	C68	C0CA	108(2)
N1AA	N0AA	C7AA	108(4)
N13	N8	N9	171(4)
N8	N9	C68	109(3)
C61	N18	N6	126(4)
C38	O1AA	Pt2	128.8(8)
N0AA	N1AA	N2AA	160(6)
N10	N6	N18	162(4)

Table S 9 Bond lengths [Å] for compound **82**.

Atoms		Bond lengths [Å]
Br1	C9	1.895(2)
S1	C3	1.744(2)
S1	C2	1.791(2)
S2	C3	1.671(2)
O3	C5	1.323(3)
C3	C4	1.432(3)
C5	C4	1.375(3)
C5	C6	1.465(3)
C2	C1	1.513(3)

Atoms (continued)		Bond lengths [Å]
C7	C6	1.398(3)
C7	C8	1.386(4)
C11	C6	1.398(3)
C11	C10	1.374(3)
C8	C9	1.395(4)
C9	C10	1.379(3)
C1	O1	1.310(3)
C1	O2	1.217(3)

Table S 10 Bond angles [°] for compound **82**.

Atoms			Bond angles [°]
C3	S1	C2	103.28(11)
S2	C3	S1	122.62(13)
C4	C3	S1	111.32(16)
C4	C3	S2	126.05(17)
O3	C5	C4	122.5(2)
O3	C5	C6	113.5(2)
C4	C5	C6	124.0(2)
C5	C4	C3	126.2(2)
C1	C2	S1	114.44(15)
C8	C7	C6	121.2(2)
C10	C11	C6	120.6(2)

Atoms (continued)			Bond angles [°]
C7	C6	C5	119.4(2)
C11	C6	C5	121.9(2)
C11	C6	C7	118.7(2)
C7	C8	C9	118.3(2)
C8	C9	Br1	119.86(18)
C10	C9	Br1	118.79(19)
C10	C9	C8	121.3(2)
C11	C10	C9	119.8(2)
O1	C1	C2	111.73(19)
O2	C1	C2	124.5(2)
O2	C1	O1	123.7(2)



# SUPPLEMENT B: PROTEIN INTERACTION - ESI MS

## SPECTRAL DATA

### Interaction with horse heart cytochrome c

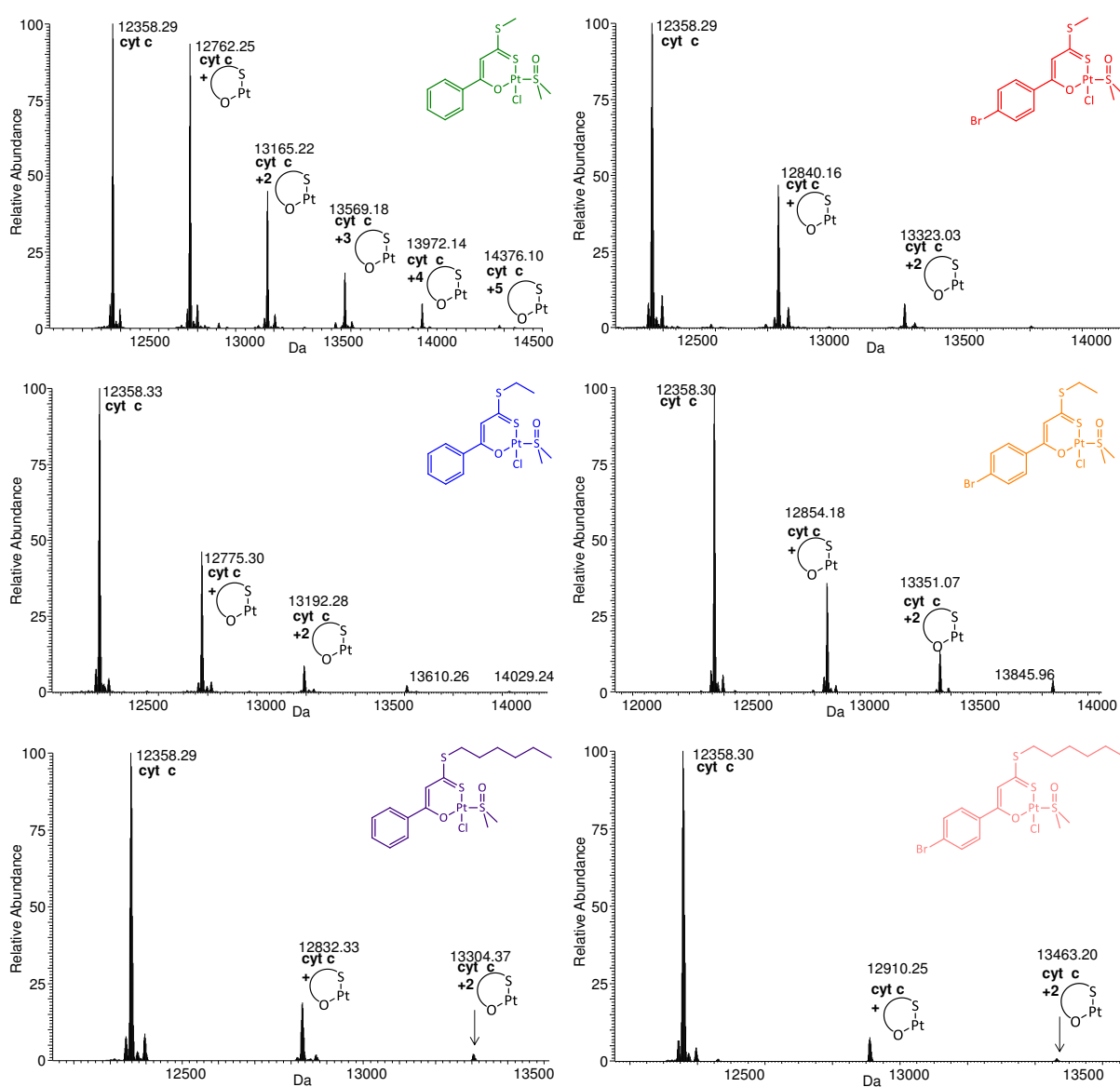


Figure S 1 Deconvoluted ESI MS spectra of cytochrome c incubated with representative H- and *p*-Br- substituted complexes 29, 30, 32, (left) 33, 34, 36 (right).<sup>118</sup>

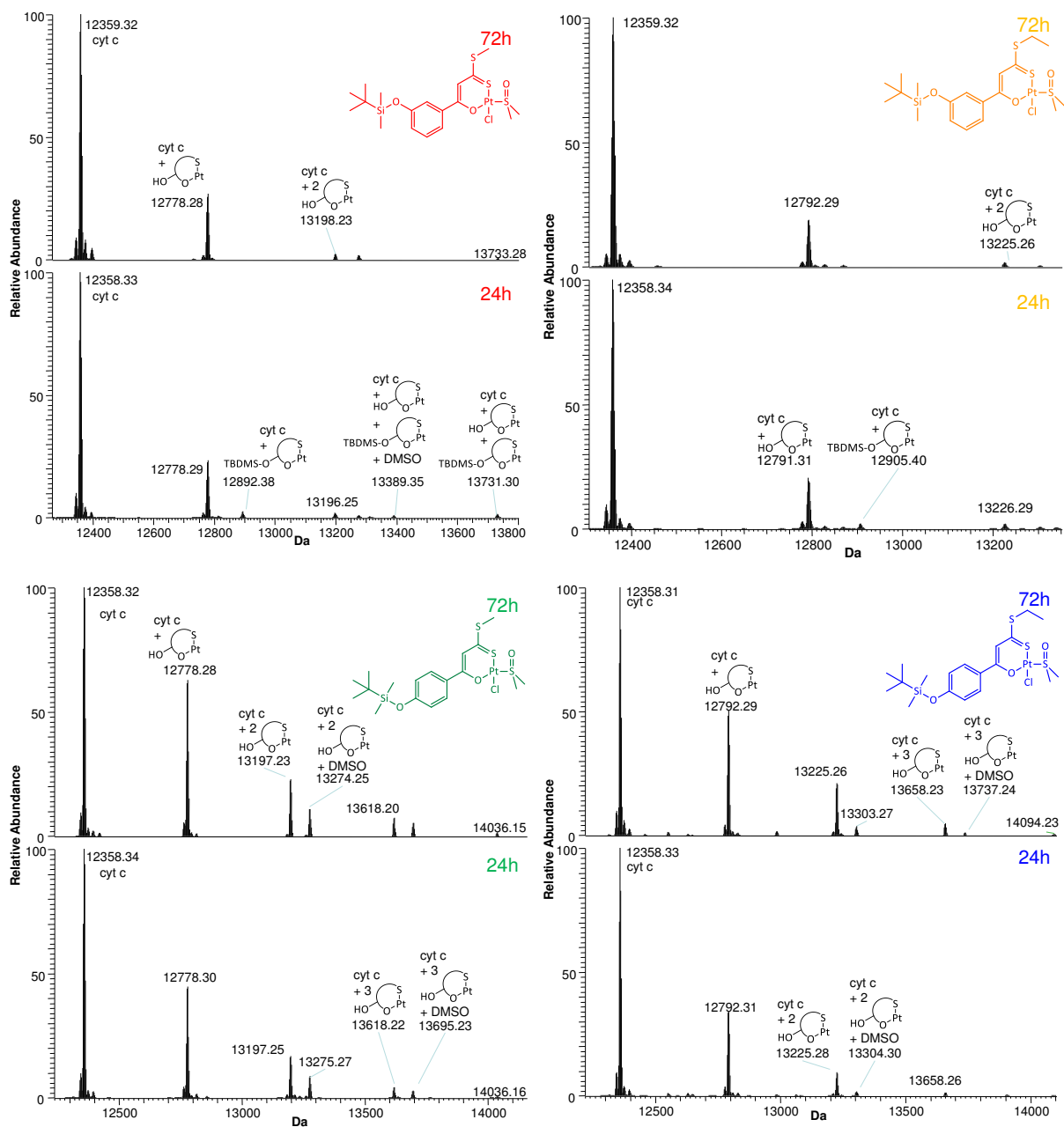


Figure S 2 Deconvoluted ESI MS spectra of cytochrome c incubated with the O-silyl protected compounds **37** (red), **38** (orange), **41** (green), and **42** (blue) for 24 and 72 h.

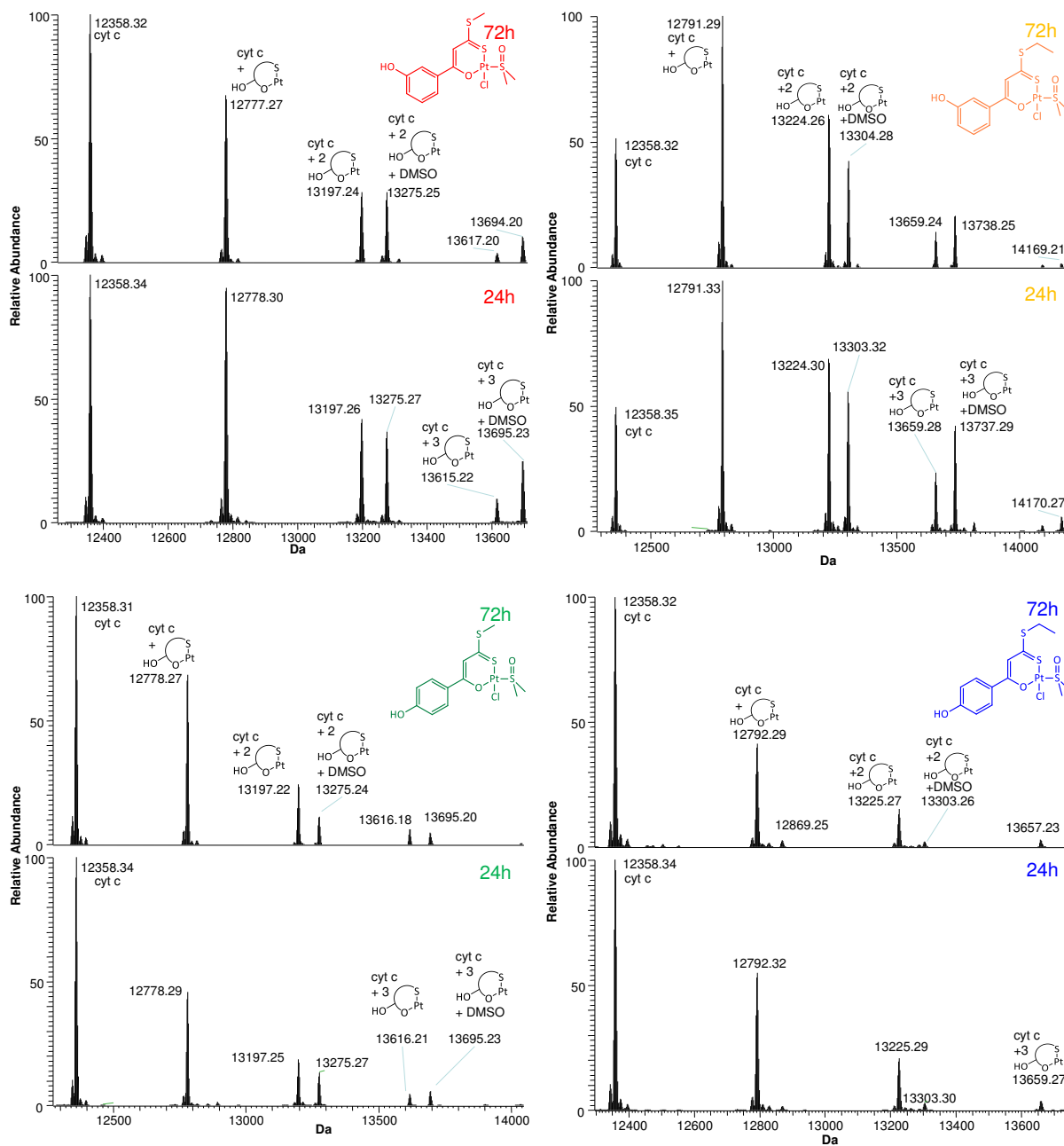


Figure S 3 Deconvoluted ESI MS spectra of cytochrome c incubated with the OH-substituted compounds 45 (red), 46 (orange), 47 (green), and 48 (blue) for 24 and 72 h.

## Interaction with hen egg white lysozyme

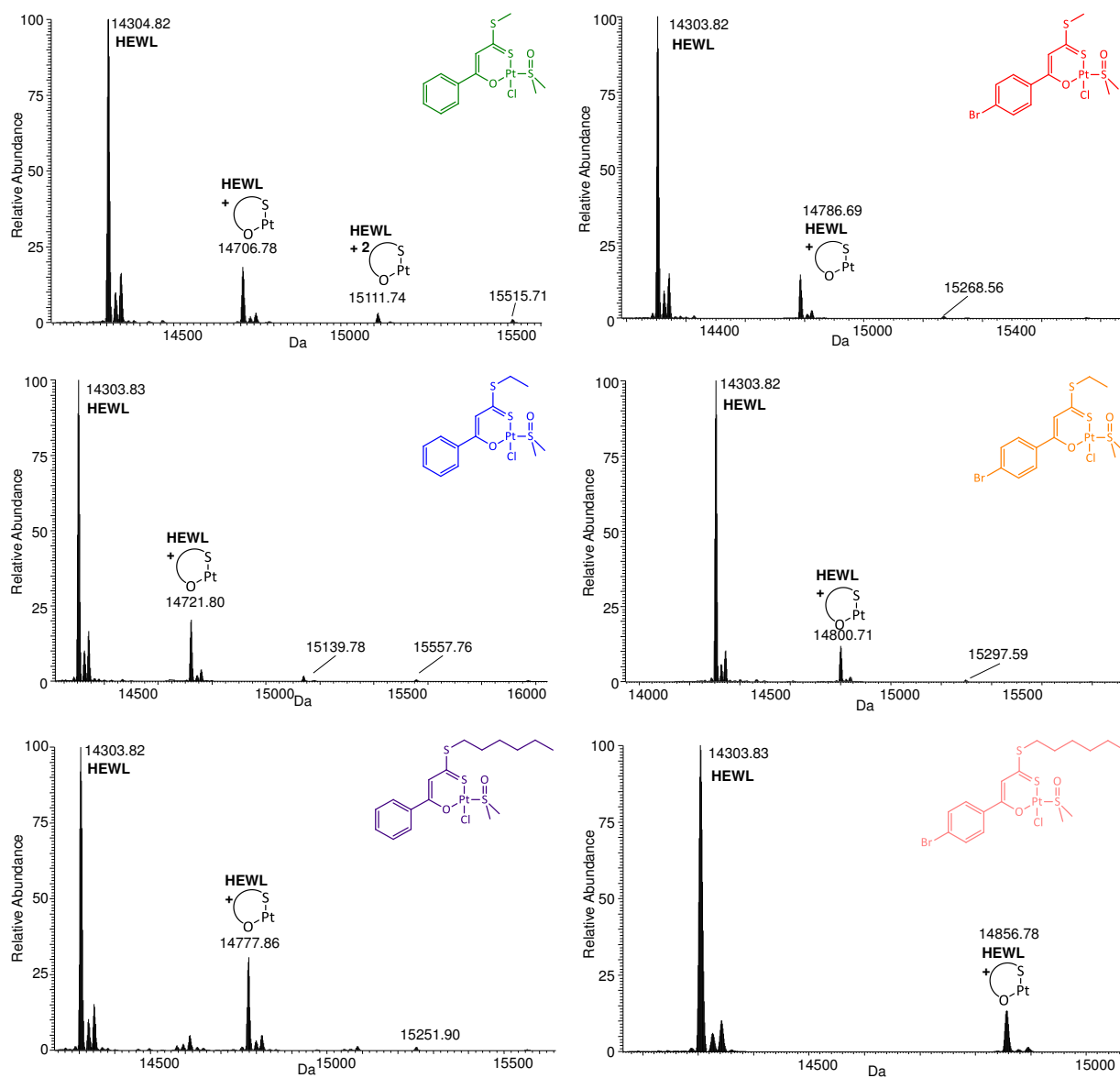


Figure S 4 Deconvoluted ESI mass spectra of H- and *p*-Br derived compounds **29**, **30**, **32** (left), **33**, **34**, **36** (right) after incubation with HEWL in a 3:1 Pt:protein ratio for 72 h.



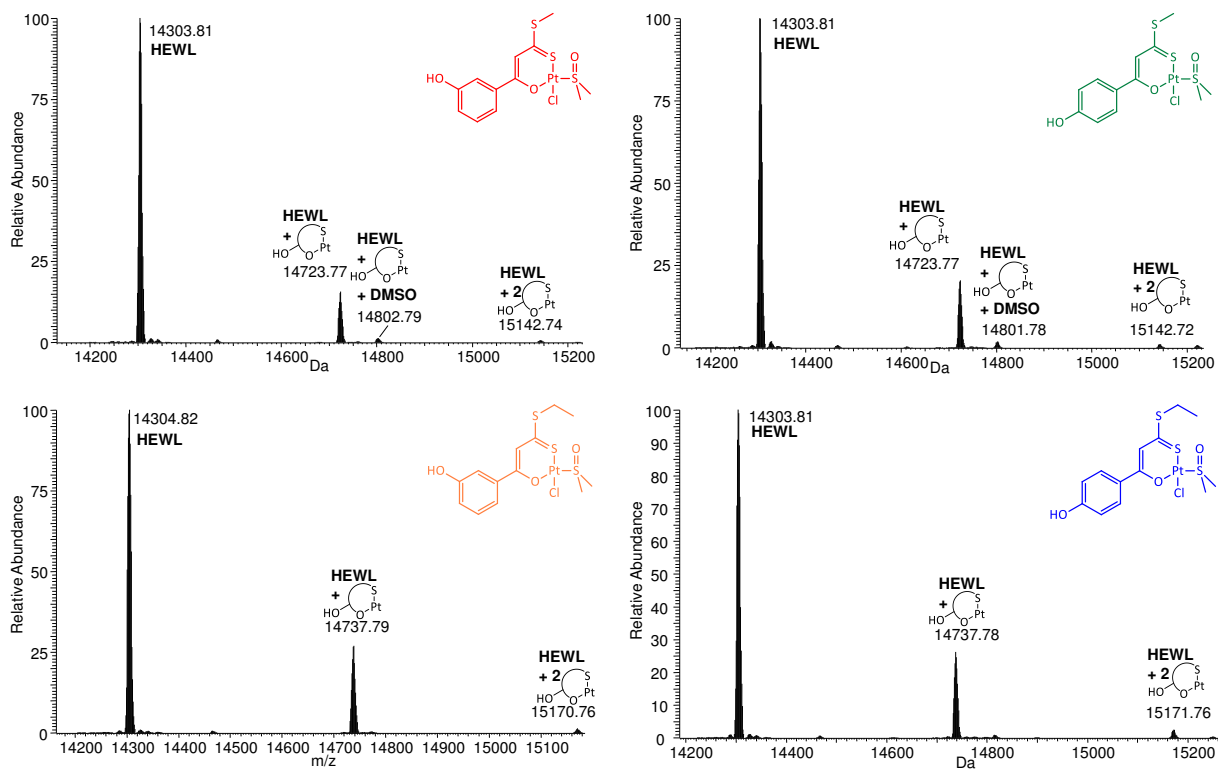


Figure S 5 Deconvoluted ESI MS spectra of HEWL incubated with *m*- and *p*-OH substituted compounds 45-48 for 24h in a 3:1 metal:HEWL ratio at 37 °C using TMAA buffer.

## Interaction with ribonuclease A

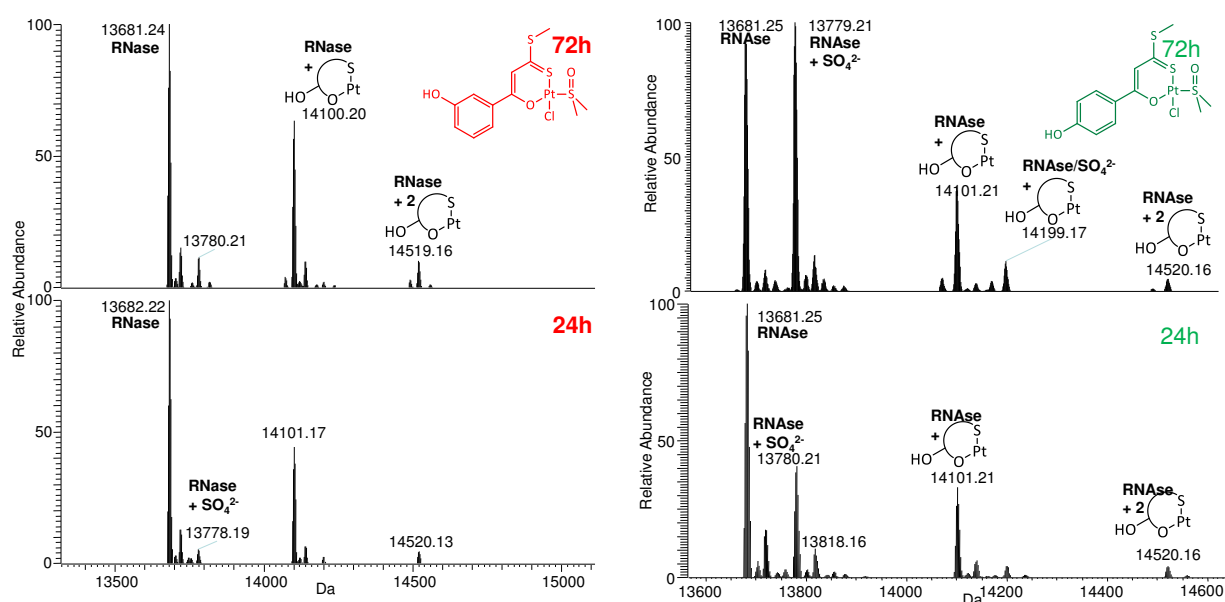


Figure S 6 Deconvoluted ESI MS spectra of RNase A incubated with compounds **45** (left) and **47** (right) for 72h (top) and 24h (bottom) in a 3:1 metal:RNase A ratio at 37 °C using TMAA buffer. Presence of sulfate in the RNase A spectra is intrinsic to the protein and has been observed in other, independent experiments. It does not originate from the actual incubation experiment and was thus neglected.

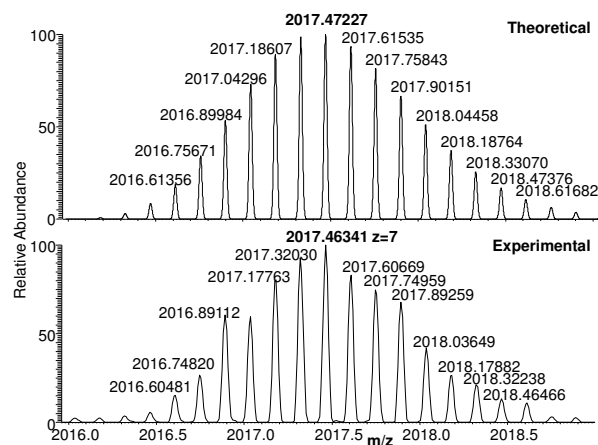


Figure S 7 Multicharged ESI MS spectrum of the monoadduct of cyt c with **46** after 24h incubation (37 °C, TMAA buffer) in a 3:1 Pt:cyt c ratio. Top, theoretical isotopic pattern for  $[(\text{cyt}c)^+ + ((\text{O,S})\text{Pt})^+ + 5\text{H}^+]$  at charge state +7. Bottom, experimental isotopic pattern of the monoadduct at charge state +7. The calculated sum formula is  $[\text{C}_{571}\text{H}_{890}\text{N}_{148}\text{O}_{158}\text{S}_6\text{Fe}_1\text{Pt}_1]^7+$ .

# SUPPLEMENT C: DNA INTERACTION

## Positive ESI MS and UV-vis experiments with 9-methyl guanine

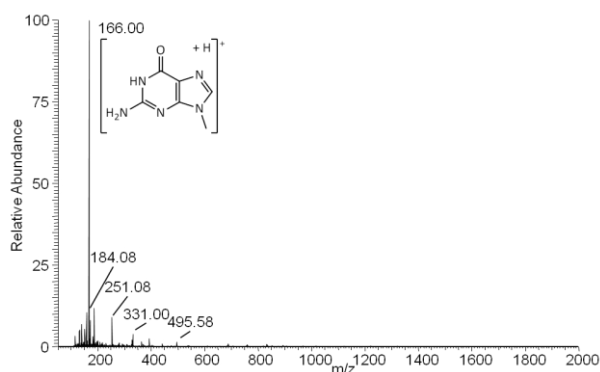


Figure S 8 Positive ESI MS spectrum of free **9-mg** for comparison with the adduct spectra. Spectrum was recorded in

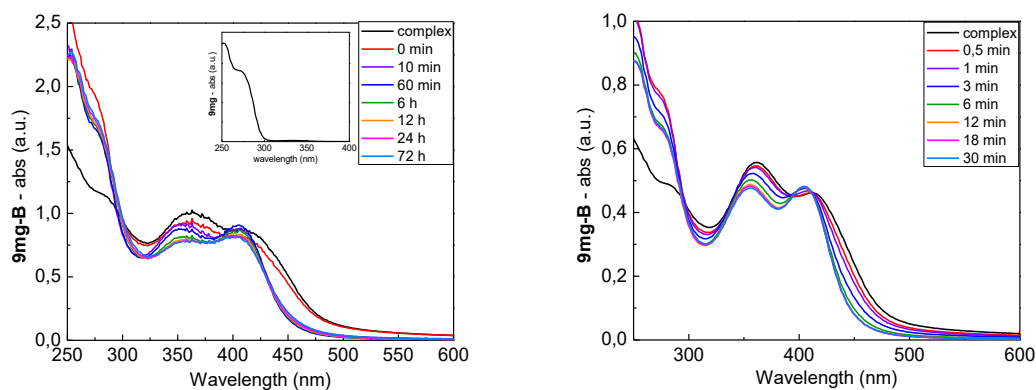


Figure S 9 UV Vis Spectra of the adduct formation between **46** and **9-mg** ( $c = 50\mu\text{M}$ , LC-MS H<sub>2</sub>O), recorded without **9-mg** (black line), and after different time intervals up to 72 h (left) and over 30 min in short intervals (right). Inset: free **9-mg**.

## Negative ESI MS experiments of free ODNs

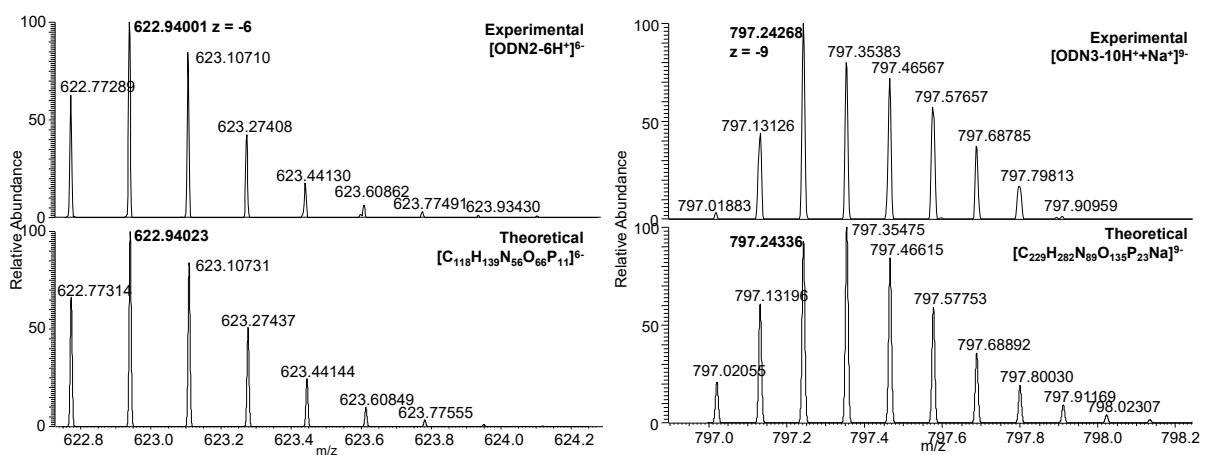


Figure S 10 Comparison of theoretical vs. experimental multicharge isotopic patterns at charge state -6 (ODN2, left) resp. -9 (ODN3, right).

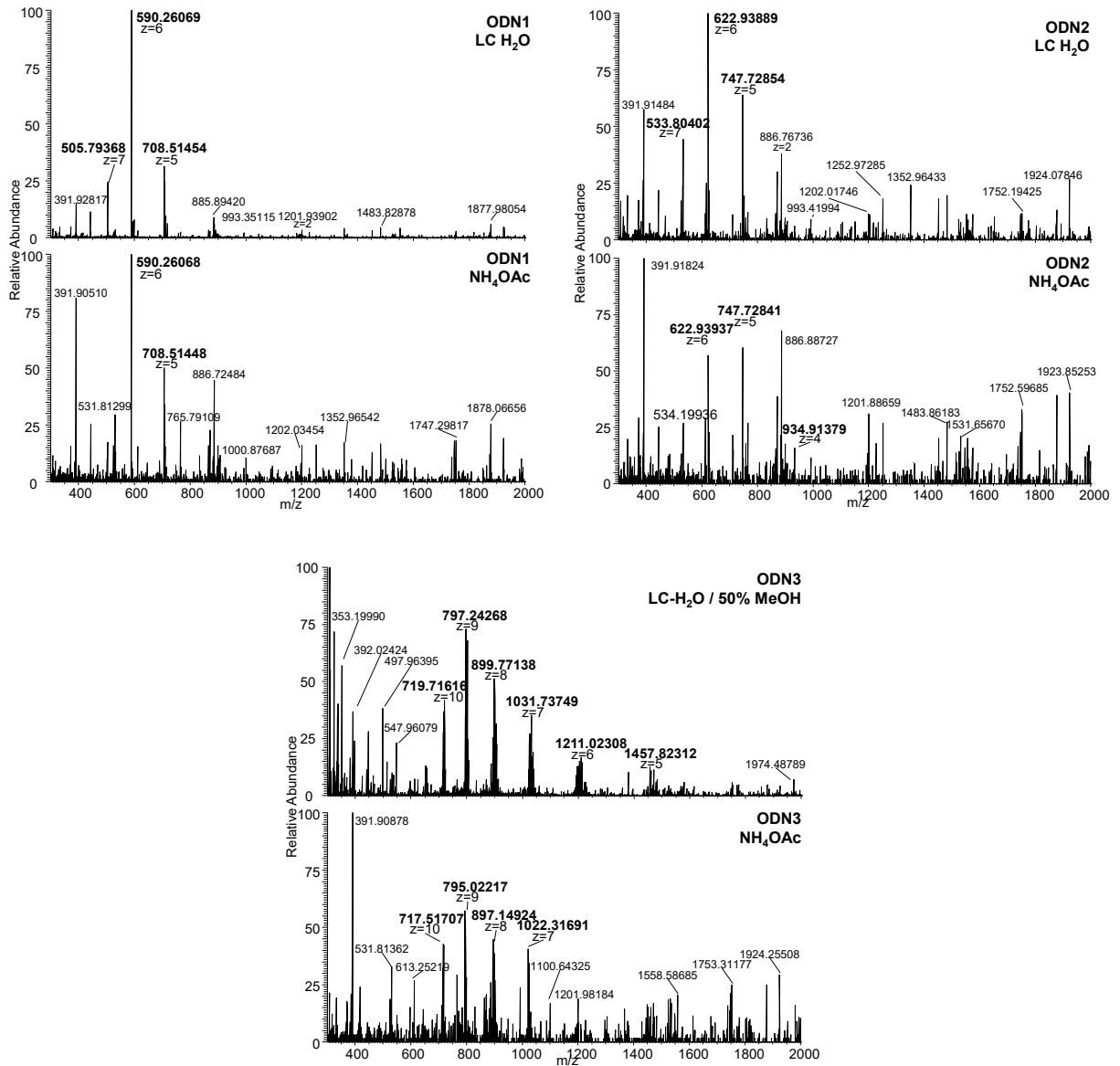


Figure S 11 Multicharged ESI MS spectra of **ODN1** (top left) and **ODN2** (top right) recorded in LC-MS grade water and ammonium acetate. S/N ratio is greatly improved in LC-MS grade water. Below, multicharged ESI MS spectra of **ODN3** recorded in LC-grade water/ 50% MeOH and ammonium acetate. 50% MeOH had to be added directly prior to the experiment in order to acquire reasonable spectra. All Z values are negative.

## Negative ESI MS of ODN adducts

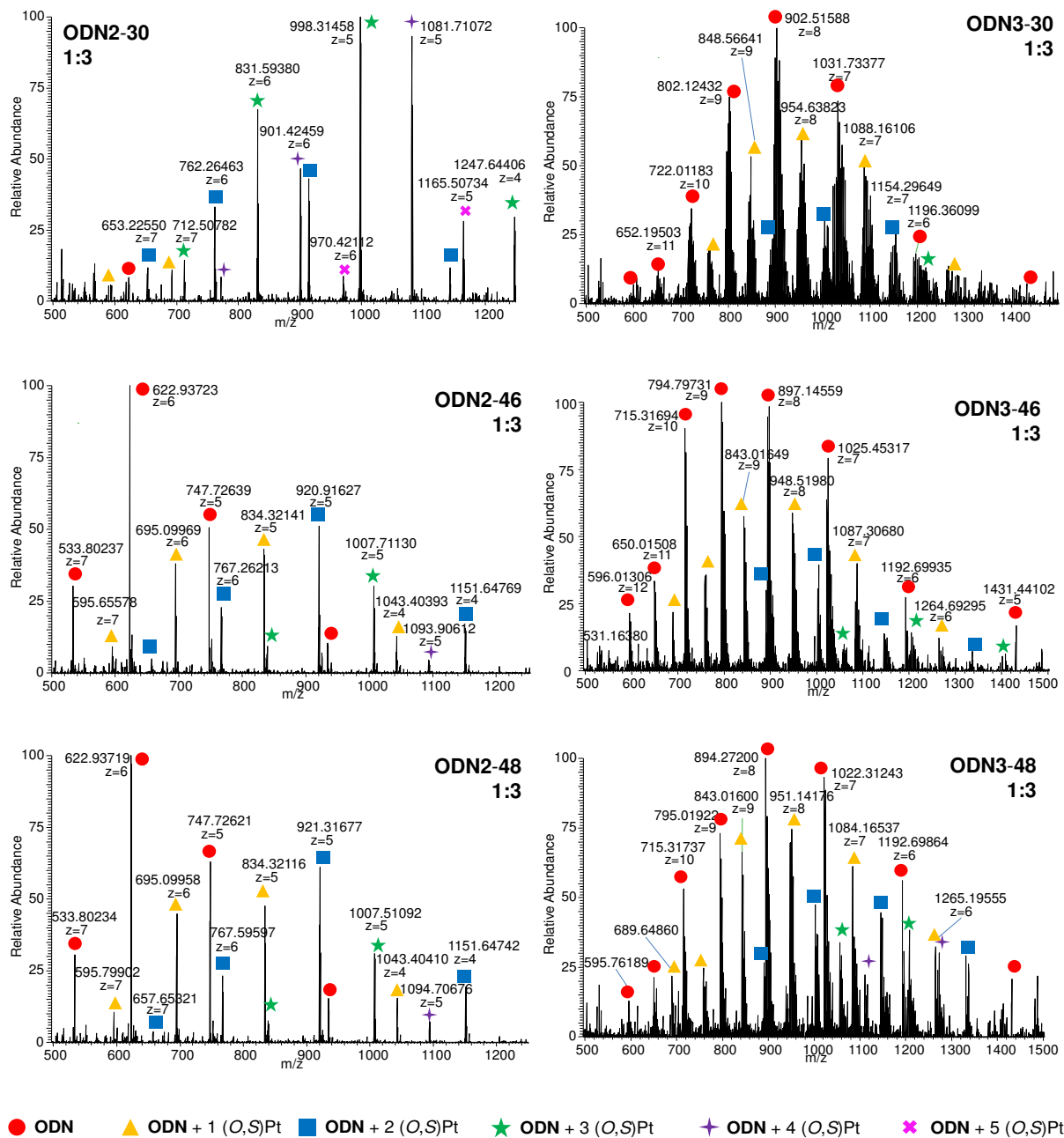


Figure S 12 Adduct spectra of ODN2 (left) and ODN3 (right) with compound 30 (top), 46 (middle) and 48 (bottom), recorded after incubation in LC-MS grade water for 24 h at 37 °C in a 3:1 metal:ODN ratio. c(ODN) was 10 μM. All Z are negative

Table S 11 found mass data in samples of free **ODN1** and respective metal adducts. Signals of free **ODN1** within the adduct spectra are summarized as “free **ODN1**” under the respective sections; adduct peaks are listed separately for both incubation ratios. The reported mass values represent those of the signal with the highest intensity within each experimental isotopic pattern. The number of found Na adducts is reported. Isolated signals for MS<sup>2</sup> experiments are highlighted in red.

ODN1 free	value	Z	Na
	<b>505,94</b>	7	0
	<b>590,26</b>	6	0
	<b>708,51</b>	5	0

ODN1 /30	value	Z	x (O,S)Pt <sup>+</sup>	Na
free ODN1	<b>505,79</b>	7	0	0
	<b>590,26</b>	6	0	0
	<b>708,51</b>	5	0	0
	<b>885,89</b>	4	0	0
1:1	<b>659,92</b>	6	1	0
	<b>791,91</b>	5	1	0
	<b>990,64</b>	4	1	0
1:3	<b>659,92</b>	6	1	0
	<b>729,42</b>	6	2	0
	<b>791,91</b>	5	1	0
	<b>875,51</b>	5	2	0
	<b>958,7</b>	5	3	0
	<b>990,14</b>	4	1	0
	<b>1094,38</b>	4	2	0
	<b>1199,13</b>	4	3	0

ODN1 /46	value	Z	x (O,S)Pt <sup>+</sup>	Na
free ODN1	<b>505,94</b>	7	0	0
	<b>590,26</b>	6	0	0
	<b>708,52</b>	5	0	0
	<b>886,15</b>	4	0	0
1:1	<b>662,59</b>	6	1	0
	<b>795,11</b>	5	1	0
	<b>993,27</b>	4	1	0
1:3	<b>662,59</b>	6	1	0
	<b>795,11</b>	5	1	0
	<b>882,11</b>	5	2	0
	<b>994,14</b>	4	1	0
	<b>1102,63</b>	4	2	0

ODN1 /48	value	Z	x (O,S)Pt <sup>+</sup>	Na
free ODN1	<b>505,86</b>	7	0	0
	<b>590,26</b>	6	0	0
	<b>708,51</b>	5	0	0
	<b>886,84</b>	4	0	0
1:1	<b>662,42</b>	6	1	0
	<b>795,11</b>	5	1	0
	<b>881,90</b>	5	2	0
	<b>1005,97</b>	4	1	2
1:3	<b>567,79</b>	7	1	0
	<b>662,42</b>	6	1	0
	<b>734,58</b>	6	2	0
	<b>795,11</b>	5	1	0
	<b>806,91</b>	6	3	0
	<b>881,70</b>	5	2	0
	<b>968,30</b>	5	3	0
	<b>993,20</b>	4	1	0
	<b>1102,92</b>	4	2	0

Table S 12 Found mass data in samples of free **ODN2** and respective metal adducts. Signals of free **ODN2** within the adduct spectra are summarized as “free **ODN2**” under the respective sections; adduct peaks are listed. The reported mass values represent those of the signal with the highest intensity within each experimental isotopic pattern. The number of found Na adducts is reported.

ODN2 free	value	z	Na
	533,80	7	0
	623,11	6	0
	747,73	5	0
	934,66	4	0

ODN2 / 30	value	z	x (O,S)Pt <sup>+</sup>	Na
Free ODN2	622,94	6	0	0
3:1	593,51	7	1	0
	653,23	7	2	0
	692,77	6	1	0
	712,51	7	3	0
	762,26	6	2	0
	772,36	7	4	0
	831,59	6	3	0
	901,42	6	4	0
	914,52	5	2	0
	970,42	6	5	0
	998,31	5	3	0
	1081,71	5	4	0
	1143,40	4	2	0
	1165,51	5	5	0
	1247,64	4	3	0
	1352,14	4	4	0
	1456,63	4	5	0

ODN2 / 46	value	z	x (O,S)Pt <sup>+</sup>	Na
Free ODN2	533,80	7	0	0
	622,94	6	0	0
	747,73	5	0	0
	934,66	4	0	0
	940,41	4	0	1
3:1	595,66	7	1	0
	657,51	7	2	0
	695,10	6	1	0
	767,26	6	2	0
	834,32	5	1	0
	838,71	5	1	1
	839,76	6	3	0
	920,92	5	2	0
	925,31	5	2	1
	1007,71	5	3	0
	1043,40	4	1	0
	1093,91	5	4	0
	1151,65	4	2	0
	1156,89	4	2	1
	1259,89	4	3	0
	1368,13	4	4	0

ODN2 / 48	value	z	x (O,S)Pt <sup>+</sup>	Na
Free ODN2	533,80	7	0	0
	622,94	6	0	0
	747,73	5	0	0
	934,91	4	0	0
3:1	595,80	7	1	0
	657,65	7	2	0
	695,10	6	1	0
	767,60	6	2	0
	834,32	5	1	0
	839,26	6	3	0
	921,32	5	2	0
	1007,51	5	3	0
	1043,40	4	1	0
	1094,71	5	4	0
	1151,65	4	2	0
	1259,89	4	3	0
	1265,39	4	3	1
	1368,63	4	4	0
Adenine loss	600,76	6	0	-A*
	672,93	6	1	-A*
	721,12	5	0	-A*

\* -A: signals detected of ODN2 after loss of adenine



Table S 13 observed *m/z* values in multicharged spectra of **ODN3** incubated with compound **30**.

<i>ODN3 free</i>				<i>ODN3 / 30 adducts</i>				<i>ODN3 / 30 adducts (continued)</i>					
value	z	Na	*	value	z	x (O,S)Pt+	Na	*	value	z	x (O,S)Pt+	Na	*
650,02	11	0		757,22	10	1	0		1141,74	7	2	0	
652,20	11	1	*	759,11	10	1	1	*	1144,88	7	2	1	
654,19	11	2		761,41	10	1	2		1148,02	7	2	2	
656,19	11	3		763,41	10	1	3		1151,16	7	2	3	
658,19	11	4		765,61	10	1	4		1154,30	7	2	4	*
715,32	10	0		768,01	10	1	5		1157,01	7	2	5	
717,51	10	1		841,24	9	1	0		1160,29	7	2	6	
719,81	10	2		843,57	9	1	1		1163,29	7	2	7	
722,01	10	3	*	846,35	9	1	2		1167,00	7	2	8	
724,11	10	4		848,57	9	1	3	*	1213,01	7	3	4	
726,41	10	5		851,23	9	1	4		1262,19	6	1	0	
728,41	10	6		853,34	9	1	5		1265,86	6	1	1	*
730,90	10	7		855,78	9	1	6		1273,14	6	1	3	
794,91	9	0		858,56	9	1	7		1284,34	6	1	6	
797,35	9	1		890,01	9	2	1		1292,17	6	1	8	
799,90	9	2		946,65	8	1	0		1346,85	6	2	4	
802,12	9	3	*	949,27	8	1	1						
804,68	9	4		952,14	8	1	2						
807,01	9	5		954,64	8	1	3	*					
809,67	9	6		957,51	8	1	4						
812,00	9	7		960,38	8	1	5						
814,56	9	8		963,13	8	1	6						
894,52	8	0		965,76	8	1	7						
897,02	8	1		968,25	8	1	8						
899,89	8	2		971,13	8	1	9						
902,52	8	3	*	998,77	8	2	0						
905,39	8	4		1001,39	8	2	1						
908,14	8	5		1004,14	8	2	2	*					
910,76	8	6		1006,76	8	2	3						
913,76	8	7		1009,76	8	2	4						
916,50	8	8		1012,38	8	2	5						
919,13	8	9		1015,38	8	2	6						
921,88	8	10		1018,00	8	2	7						
1022,31	7	0		1020,63	8	2	8						
1025,00	7	1		1082,17	7	1	0						
1028,59	7	2		1085,31	7	1	1						
1031,73	7	3	*	1088,16	7	1	2	*					
1034,87	7	4		1091,45	7	1	3						
1038,01	7	5		1094,44	7	1	4						
1041,01	7	6		1097,44	7	1	5						
1044,29	7	7		1100,72	7	1	6						
1047,29	7	8		1103,89	7	1	7						
1050,29	7	9		1107,43	7	1	8						
1053,57	7	10		1110,29	7	1	9						
1192,00	6	0											
1196,36	6	1	*										
1200,00	6	2											
1203,69	6	3											
1225,34	6	8											
1431,44	5	0											

\* most abundant peak of series

Table S 14 observed  $m/z$  values in multicharged spectra of **ODN3** incubated with compound **46**. Left, signals belonging to free **ODN3**, right; signals belonging to Pt adducts.

<i>ODN3 free</i>				<i>ODN3 / 46 adducts</i>				
value	z	Na	*	value	z	x (O,S)Pt+	Na	*
596,01	12	0	*	689,65	11	1	0	*
597,68	12	1		691,46	11	1	1	
599,51	12	2		693,65	11	1	2	
650,02	11	0	*	758,61	10	1	0	*
652,19	11	1		760,81	10	1	1	*
654,10	11	2		763,01	10	1	2	
656,10	11	3		765,01	10	1	3	
658,19	11	4		767,41	10	1	4	
715,32	10	0	*	769,30	10	1	5	
717,62	10	1		843,06	9	1	0	*
719,71	10	2		845,35	9	1	1	
722,01	10	3		847,90	9	1	2	
724,31	10	4		850,34	9	1	3	
726,21	10	5		852,45	9	1	4	
794,80	9	0	*	891,24	9	2	0	
797,46	9	1		948,52	8	1	0	*
799,79	9	2		951,39	8	1	1	
802,12	9	3		954,01	8	1	2	
804,57	9	4		956,76	8	1	3	
807,12	9	5		959,14	8	1	4	
894,52	8	0		1002,77	8	2	0	
897,15	8	1	*	1005,51	8	2	1	*
899,89	8	2		1008,01	8	2	2	
902,64	8	3		1010,13	8	2	3	
905,39	8	4		1013,63	8	2	4	
908,01	8	5		1057,52	8	3	0	
1022,17	7	0		1059,64	8	3	1	
1025,45	7	1	*	1062,88	8	3	2	
1028,31	7	2		1065,01	8	3	3	
1031,73	7	3		1068,14	8	3	4	
1034,73	7	4		1084,31	7	1	0	
1037,87	7	5		1087,31	7	1	1	*
1041,15	7	6		1090,59	7	1	2	
1192,70	6	0	*	1093,45	7	1	3	
1196,36	6	1		1096,01	7	1	4	
1200,19	6	2		1099,87	7	1	5	
1203,69	6	3		1146,16	7	2	0	*
1431,44	5	0	*	1148,88	7	2	1	
				1152,30	7	2	2	
				1155,44	7	2	3	
				1158,73	7	2	4	
				1207,87	7	3	0	*
				1210,87	7	3	1	
				1214,30	7	3	2	
				1264,69	6	1	0	*
				1268,69	6	1	1	
				1273,13	6	1	2	

\* most abundant peak of series

Table S 15 observed  $m/z$  values in multicharged spectra of **ODN3** incubated with compound **48**. Left, signals belonging to free **ODN3**, right; signals belonging to Pt adducts.

<b>ODN3 free</b>				<b>ODN3 / 48 adducts</b>				<b>ODN3 / 48 adducts (continued)</b>					
value	z	Na	*	value	z	x (O,S)Pt+	Na	*	value	z	x (O,S)Pt+	Na	*
595,76	12	0		689,65	11		1	0 *	1111,01	8	4	0 *	
650,20	11	0	*	758,81	10		1	0 *	1114,01	8	4	1	
652,00	11	1		761,01	10		1	1	1116,50	8	4	2	
654,00	11	2		762,81	10		1	2	1119,38	8	4	3	
656,00	11	3		764,90	10		1	3	1146,16	7	2	0 *	
658,00	11	4		767,21	10		1	4	1149,30	7	2	1	
715,32	10	0	*	769,10	10		1	5	1152,44	7	2	2	
717,31	10	1		843,02	9		1	0 *	1155,58	7	2	3	
719,81	10	2		845,68	9		1	1	1158,72	7	2	4	
721,81	10	3		848,01	9		1	2	1162,01	7	2	5	
723,61	10	4		850,34	9		1	3	1165,01	7	2	6	
795,02	9	0		852,67	9		1	4	1208,30	7	3	0 *	
797,24	9	1	*	891,24	9		2	0	1211,44	7	3	1	
799,79	9	2		948,77	8		1	0	1214,44	7	3	2	
802,01	9	3		951,14	8		1	1 *	1217,44	7	3	3	
804,45	9	4		954,14	8		1	2	1220,58	7	3	4	
807,01	9	5		956,64	8		1	3	1265,20	6	1	0 *	
894,27	8	0		959,76	8		1	4	1268,52	6	1	1	
897,14	8	1	*	1002,89	8		2	0 *	1269,87	7	4	0	
899,77	8	2		1005,64	8		2	1	1273,12	6	1	2	
902,52	8	3		1008,14	8		2	2	1275,72	6	1	3	
905,26	8	4		1011,01	8		2	3	1279,29	6	1	4	
908,01	8	5		1056,89	8		3	0 *	1337,36	6	2	0 *	
1022,31	7	0		1059,64	8		3	1	1394,01	7	6	0	
1025,60	7	1	*	1062,38	8		3	2					
1028,74	7	2		1065,13	8		3	3					
1031,73	7	3		1084,17	7		1	0 *					
1035,02	7	4		1087,59	7		1	1					
1192,70	6	0		1090,30	7		1	2					
1196,36	6	1	*	1093,30	7		1	3					
1200,19	6	2		1096,87	7		1	4					
1203,02	6	3		1100,01	7		1	5					
1431,64	5	0											

\* most abundant peak of series

**MS<sup>2</sup> of free ODN<sub>1</sub>**

Table S 16 MS<sup>2</sup> fragmentation data for free **ODN<sub>1</sub>**. Found: first peak of signal sets found (at instrument's nominal resolution; 100 000 at *m/z* 400). Calcd: calculated monoisotopic *m/z* value as obtained from Mongo Oligo Mass calculator.\*<sup>292</sup>

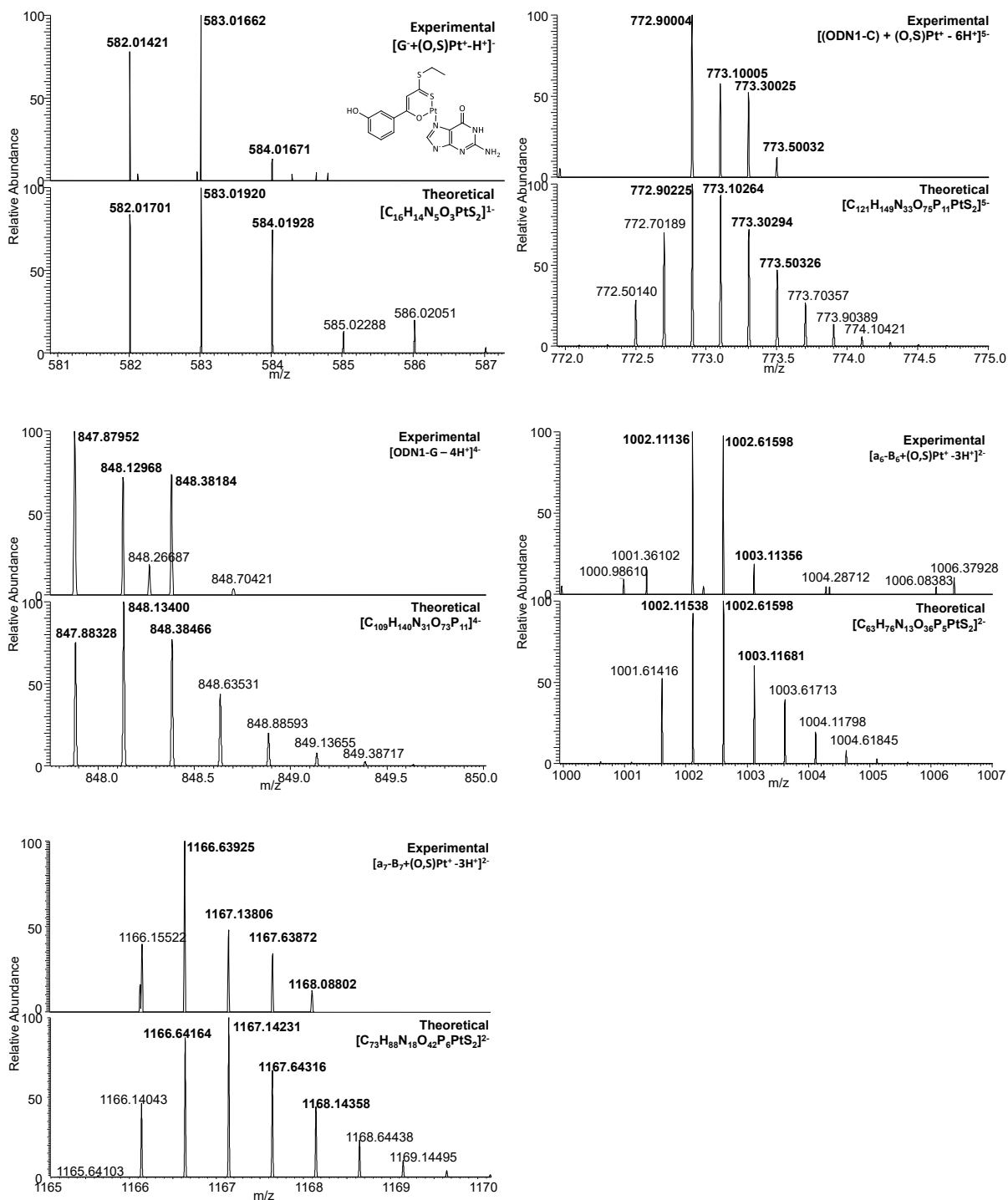
found ( <i>m/z</i> )	calcd ( <i>m/z</i> )	error (ppm)	fragment	<i>z</i>	found ( <i>m/z</i> )	calcd ( <i>m/z</i> )	error (ppm)	fragment	<i>z</i>
<b>297,04330</b>	297,043	-1,01	<b>w<sub>1</sub></b>	-2	<i>(continued)</i>				
<b>306,04852</b>	306,048	-1,70	<b>w<sub>1</sub></b>	-1	<b>675,12018</b>	675,120	-0,27	<b>a<sub>3</sub>-B<sub>3</sub></b>	-1
<b>386,07386</b>	386,074	0,36	<b>a<sub>2</sub>-B<sub>2</sub></b>	-1	<b>683,10339</b>	683,105	2,36	<b>M-TH</b>	-5
<b>395,38959</b>	395,390	1,04	<b>w<sub>4</sub></b>	-3	<b>683,30409</b>	683,306	2,80	<b>M-T</b>	-5
<b>449,06549</b>	449,066	1,14	<b>w<sub>3</sub></b>	-2	<b>685,10010</b>	685,101	1,31	<b>w<sub>9</sub></b>	-4
<b>489,07885</b>	489,079	0,32	<b>a<sub>4</sub>-B<sub>4</sub></b>	-2	<b>686,10394</b>	686,104	0,09	<b>M-CH</b>	-5
<b>490,06927</b>	490,070	1,49	<b>w<sub>8</sub></b>	-5	<b>686,30438</b>	686,306	2,36	<b>M-C</b>	-5
<b>496,73792</b>	496,738	0,16	<b>w<sub>5</sub></b>	-3	<b>689,45032</b>	689,451	0,99	<b>y<sub>7</sub></b>	-3
<b>547,87836</b>	547,879	1,17	<b>w<sub>9</sub></b>	-5	<b>705,10626</b>	705,107	1,05	<b>a<sub>10</sub>-B<sub>10</sub></b>	-4
<b>553,60504</b>	553,606	1,73	<b>y<sub>4</sub></b>	-2	<b>705,62817</b>	705,628	-0,24	<b>y<sub>5</sub></b>	-2
<b>555,24536</b>	555,246	1,15	<b>w<sub>11</sub></b>	-6	<b>741,11909</b>	741,120	1,22	<b>y<sub>10</sub></b>	-4
<b>571,58478</b>	571,586	2,13	<b>M-CH</b>	-4	<b>742,77967</b>	742,782	3,13	<b>a<sub>8</sub>-B<sub>8</sub></b>	-3
<b>571,75262</b>	571,754	2,41	<b>M-C</b>	-4	<b>745,61060</b>	745,611	0,54	<b>w<sub>5</sub></b>	-2
<b>579,76636</b>	579,767	1,10	<b>y<sub>6</sub></b>	-3	<b>761,11139</b>	761,112	0,80	<b>w<sub>10</sub></b>	-4
<b>593,58850</b>	593,589	0,85	<b>w<sub>4</sub></b>	-2	<b>785,62433</b>	785,624	-0,42	<b>a<sub>6</sub>-B<sub>6</sub></b>	-2
<b>595,09393</b>	595,094	0,12	<b>w<sub>1</sub></b>	-1	<b>790,79846</b>	790,80	1,95	<b>y<sub>8</sub></b>	-3
<b>600,41833</b>	600,419	1,12	<b>d<sub>6</sub>-H<sub>2</sub>O</b>	-3	<b>813,38104</b>	813,382	1,18	<b>y<sub>11</sub></b>	-4
<b>606,42206</b>	606,422	-0,10	<b>w<sub>6</sub></b>	-3	<b>817,45337</b>	817,455	1,99	<b>w<sub>8</sub></b>	-3
<b>608,68719</b>	608,688	1,33	<b>w<sub>10</sub></b>	-5	<b>819,17368</b>	819,173	-0,83	<b>y<sub>3</sub></b>	-1
<b>612,83862</b>	612,839	0,62	<b>w<sub>8</sub></b>	-4	<b>844,12954</b>	844,130	0,54	<b>a<sub>9</sub>-B<sub>9</sub></b>	-3
<b>624,69287</b>	624,693	0,21	<b>a<sub>11</sub>-B<sub>11</sub></b>	-5	<b>870,15372</b>	870,154	0,32	<b>y<sub>6</sub></b>	-2
<b>632,84509</b>	632,846	1,44	<b>a<sub>9</sub>-B<sub>9</sub></b>	-4	<b>899,13937</b>	899,139	-0,41	<b>w<sub>3</sub></b>	-1
<b>633,60181</b>	633,602	0,30	<b>a<sub>5</sub>-B<sub>5</sub></b>	-2	<b>950,15021</b>	950,151	0,83	<b>a<sub>7</sub>-B<sub>7</sub></b>	-2
<b>665,10809</b>	665,109	1,37	<b>y<sub>9</sub></b>	-4	<b>979,16504</b>	979,166	0,98	<b>a<sub>4</sub>-B<sub>4</sub></b>	-1
<b>666,49628</b>	666,497	1,08	<b>w<sub>11</sub></b>	-5					

\* Mongo Oligo Mass Calculator gives values with 10<sup>-3</sup> *m/z* accuracy; the high-resolution spectrometer allows data to be given in 10<sup>-5</sup> *m/z* accuracy.

## MS<sup>2</sup> of ODN1-46 monoadduct

Table S 17. Peak assignment for MS<sup>2</sup> data of the **ODN1-46** monoadduct. For fragments without Pt, the found first peak and calculated monoisotopic mass (Mongo Oligo calculator),<sup>292</sup> are listed. For fragments with Pt, the found peak of highest intensity and matching signal of calculated isotopic pattern (Xcalibur software) is listed.

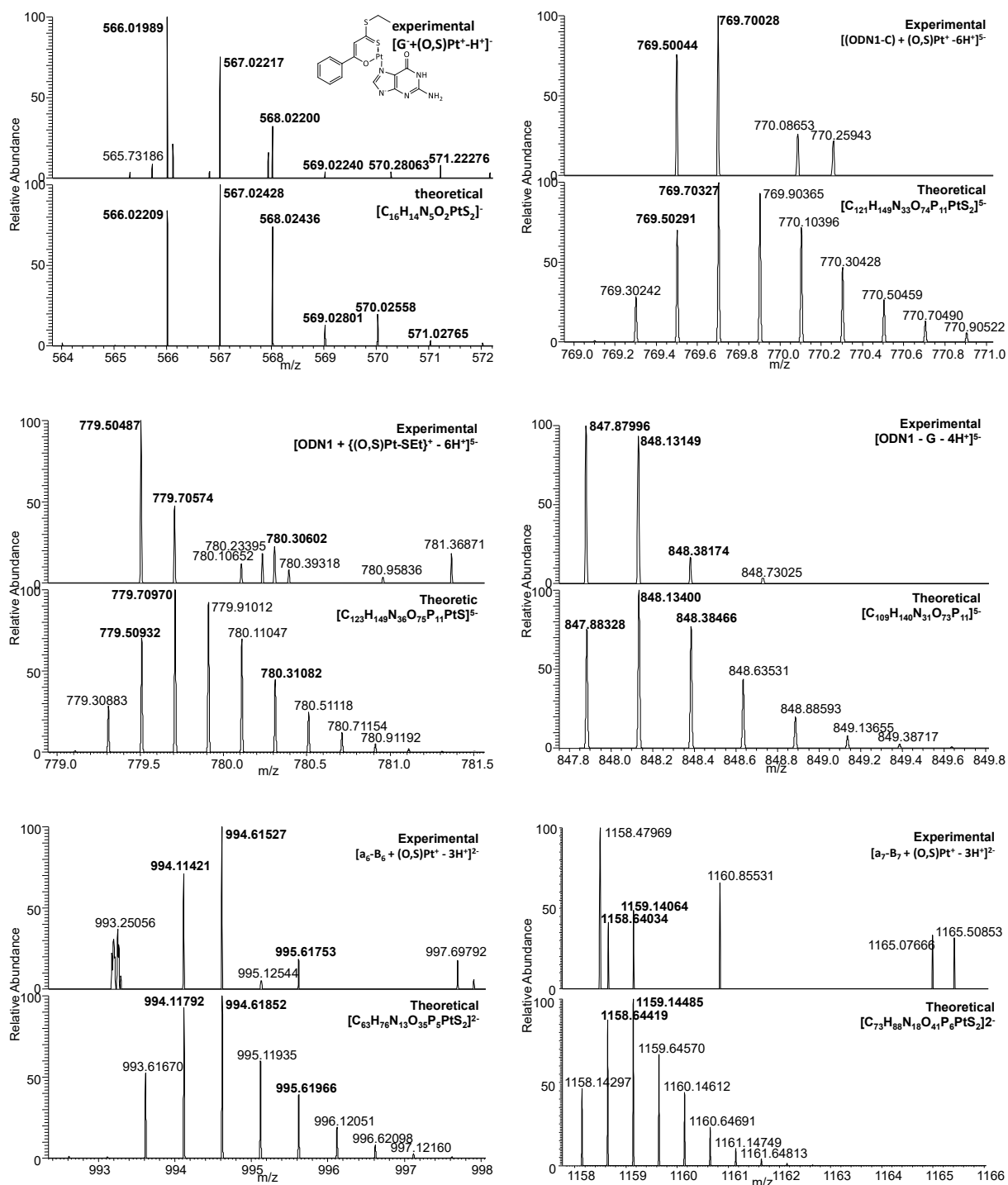
found (m/z)	calcd (m/z)	error (ppm)	assignment	z
449,06520	449,066	1,78	w <sub>3</sub>	-2
489,07811	489,079	1,82	a <sub>4</sub> -B <sub>4</sub>	-2
496,73756	496,738	0,89	w <sub>5</sub>	-3
582,01421	582,01701	4,81	[G <sup>-</sup> + (O,S)Pt <sup>+</sup> -H <sup>+</sup> ] <sup>-</sup>	-1
595,09280	595,094	2,02	w <sub>2</sub>	-1
606,42143	606,422	0,94	w <sub>6</sub>	-3
633,09664	633,098	2,15	a <sub>7</sub> -B <sub>7</sub>	-3
745,61051	745,611	0,66	w <sub>5</sub>	-2
772,90004	772,90225	2,86	[ODN1 - C + (O,S)Pt <sup>+</sup> -6H <sup>+</sup> ] <sup>5-</sup>	-5
785,62387	785,624	0,17	a <sub>6</sub> -B <sub>6</sub>	-2
847,87952	847,88328	4,43	ODN1-GH	-4
870,15378	870,154	0,25	y <sub>6</sub>	-2
899,13919	899,139	-0,21	w <sub>3</sub>	-1
910,13626	910,137	0,81	w <sub>6</sub>	-2
950,14898	950,151	2,13	a <sub>7</sub> -B <sub>7</sub>	-2
979,16491	979,166	1,11	a <sub>4</sub> -B <sub>4</sub>	-1
1002,11127	1002,11538	4,01	[(a <sub>6</sub> -B <sub>6</sub> ) + (O,S)Pt <sup>+</sup> -2H <sup>+</sup> ] <sup>2-</sup>	-2
1166,63925	1166,64164	2,05	[(a <sub>7</sub> -B <sub>7</sub> ) + (O,S)Pt <sup>+</sup> -3H <sup>+</sup> ] <sup>2-</sup>	-2

Figure S 13 Experimental vs. theoretical isotopic patterns of diagnostic fragments of the **ODN1-46** monoadduct after CID.

## MS<sup>2</sup> of ODN1-30 monoadduct

Table S 18. Peak assignment for MS<sup>2</sup> data of the **ODN1-30** monoadduct. For fragments without Pt, the found first peak and calculated monoisotopic mass (Mongo Oligo calculator),<sup>292</sup> are listed. For fragments with Pt, the found peak of highest intensity and matching signal of calculated isotopic pattern (Xcalibur software) is listed.

found (m/z)	calcd (m/z)	error (ppm)	assignment	z
392,30934	392,308	-3,42	a <sub>6</sub> -B <sub>6</sub>	-4
449,06517	449,066	1,85	w <sub>3</sub>	-2
496,73746	496,738	1,08	w <sub>5</sub>	-3
566,01989	566,02209	3,89	[G <sup>-</sup> + (O,S)Pt <sup>+</sup> - H <sup>+</sup> ] <sup>-</sup>	-1
606,42082	606,422	1,95	w <sub>6</sub>	-3
612,83783	612,839	1,91	w <sub>8</sub>	-4
633,09702	633,098	1,55	a <sub>7</sub> -B <sub>7</sub>	-3
745,61053	745,611	0,63	w <sub>5</sub>	-2
769,50044	769,50291	3,21	[ODN1 - C + (O,S)Pt <sup>+</sup> - 6H <sup>+</sup> ] <sup>5-</sup>	-5
779,50487	779,50932	5,71	[ODN1 + {(O,S)Pt-SEt} <sup>+</sup> - 6H <sup>+</sup> ] <sup>5-</sup>	-5
847,87996	847,88328	3,92	[ODN1 - G - 4H <sup>+</sup> ] <sup>4-</sup>	-4
870,15479	870,154	-0,91	y <sub>6</sub>	-2
899,13796	899,139	1,15	w <sub>3</sub>	-1
910,13624	910,137	0,83	w <sub>6</sub>	-2
950,14911	950,151	1,99	a <sub>7</sub> -B <sub>7</sub>	-2
979,16632	979,166	-0,33	a <sub>4</sub> -B <sub>4</sub>	-1
994,11421	994,11792	3,73	[(a <sub>6</sub> -B <sub>6</sub> ) + (O,S)Pt <sup>+</sup> - 2H <sup>+</sup> ] <sup>2-</sup>	-2
1158,64034	1158,64419	3,32	[(a <sub>7</sub> -B <sub>7</sub> ) + (O,S)Pt <sup>+</sup> - 3H <sup>+</sup> ] <sup>2-</sup>	-2

Figure S 14 Experimental vs. theoretical isotopic patterns of diagnostic fragments of the **ODN1-30** monoadduct after CID.



### MS<sup>2</sup> of ODN1-30 bisadduct

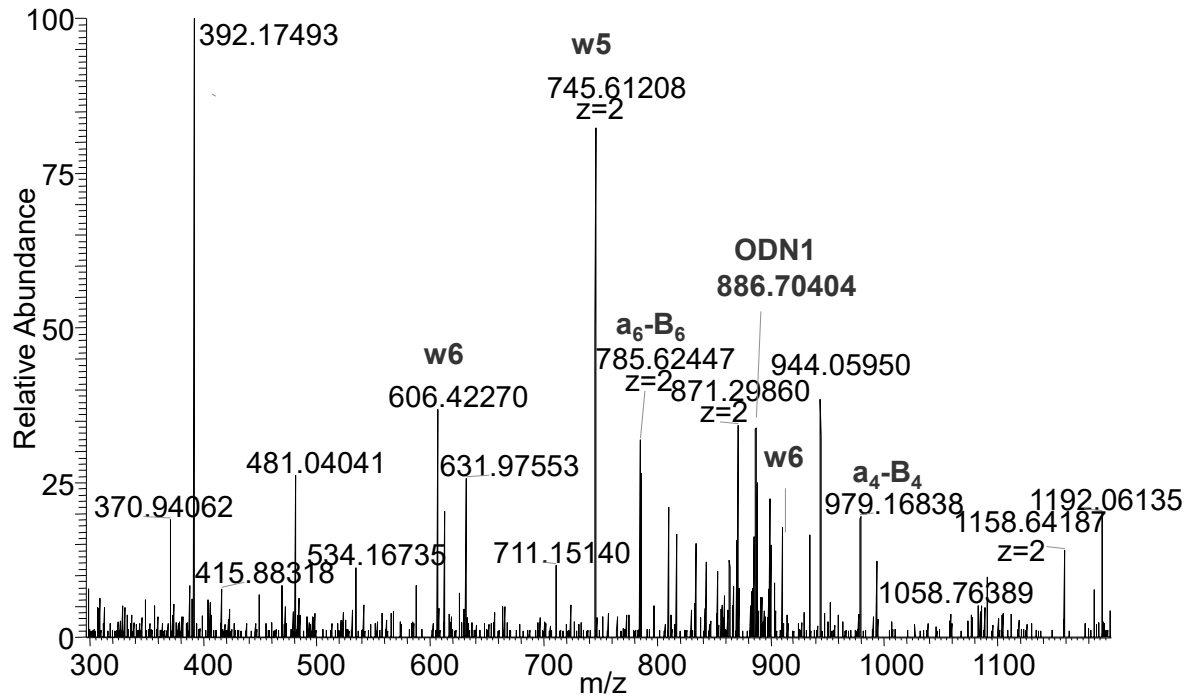


Figure S 15 Multicharged MS<sup>2</sup> spectrum of the **ODN1-30** bisadduct. Only few fragments could be assigned, no Pt-containing peaks could be identified with certainty.



## SUPPLEMENT D: BIOCONJUGATES

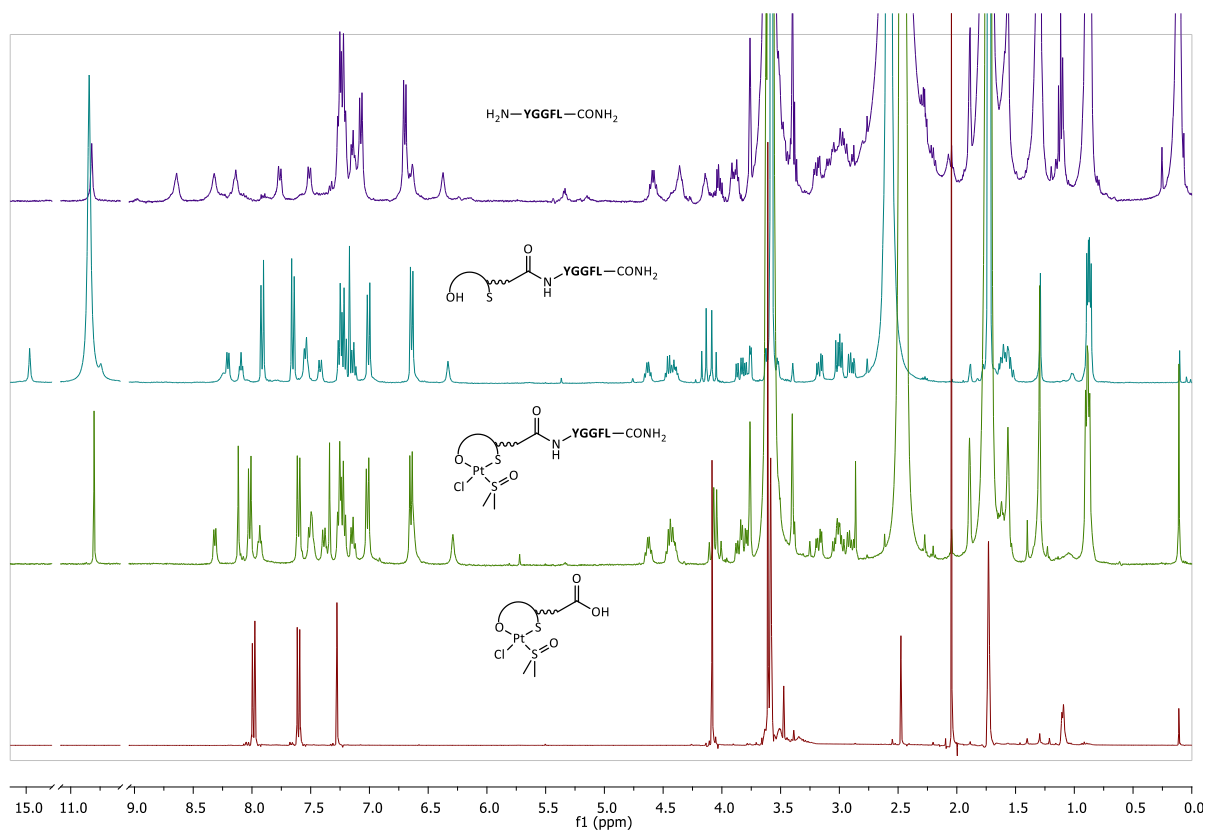


Figure S 16 Overlay of <sup>1</sup>H NMR spectra of Leu<sup>5</sup>-Enk **75** (top/violet), ligand **84** (second, petrol), complex **85** (third, green) and small-molecule complex **83** (bottom, red). All spectra were recorded in THF-d<sub>8</sub>. Due to low sample quantity resp. low solubility, signals in the aliphatic region are partially obscured by the solvent residual signals.

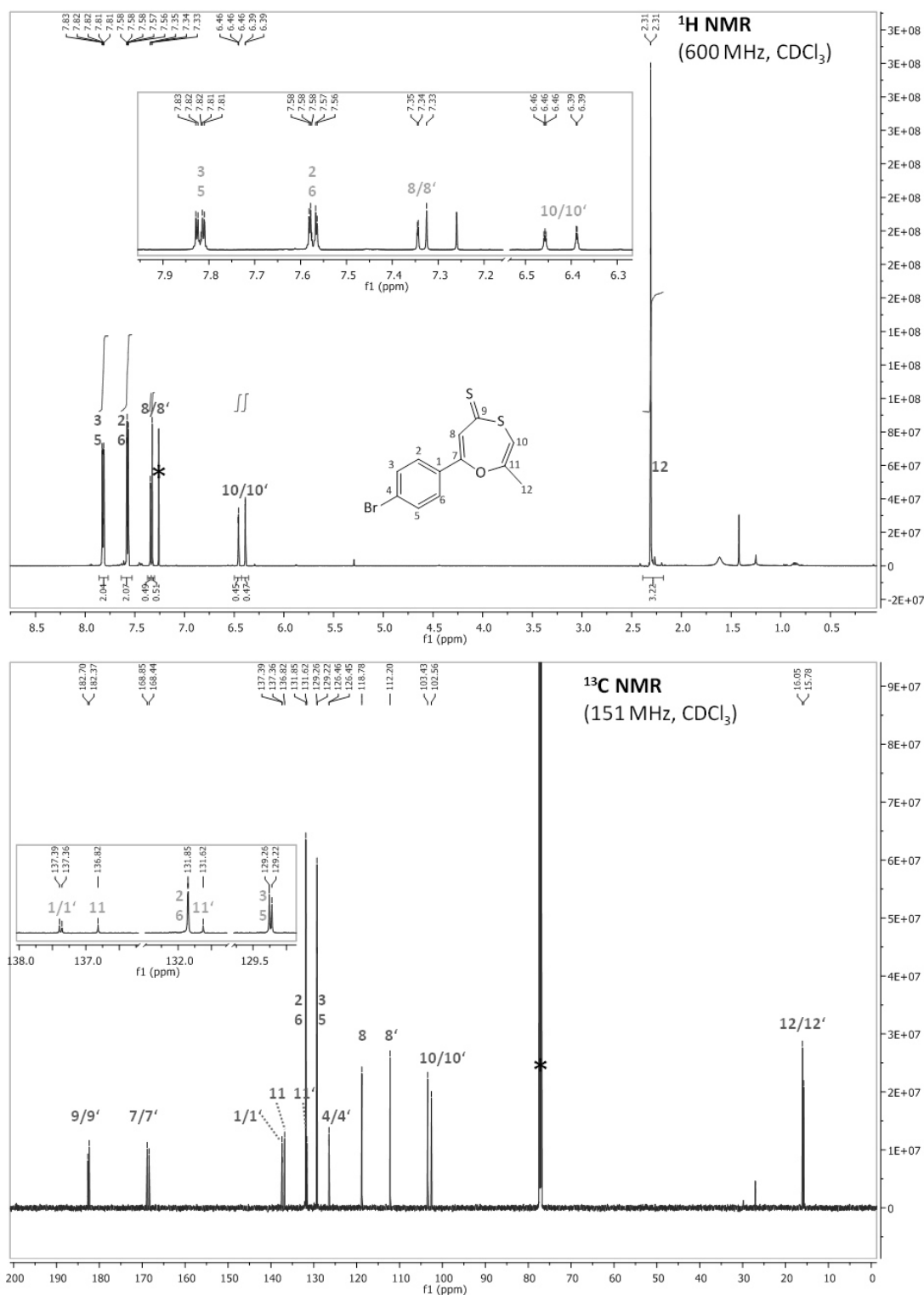


Figure S 17  $^1\text{H}$  and  $^{13}\text{C}$  NMR spectra of the rearranged product **58** of the one-pot ligand synthesis attempt of **57**. The proposed structure and signal assignment are given in the figure. Spectra were recorded at 298 K in  $\text{CDCl}_3$  on a 600 MHz spectrometer. \* marks solvent residual signals.

## SUPPLEMENT E: MEDIA COMPOSITION

### DPBS

Dulbecco's Phosphate-Buffered Saline (DPBS), without calcium, magnesium, phenol red

Supplier: Gibco®, Catalog number 14190-086

Components	M [g/mol]	x [mg/L]	mM
Potassium Chloride (KCl)	75.0	200.0	2.6666667
Potassium Phosphate monobasic (KH <sub>2</sub> PO <sub>4</sub> )	136.0	200.0	1.4705882
Sodium Chloride (NaCl)	58.0	8000.0	137.93103
Sodium Phosphate dibasic (Na <sub>2</sub> HPO <sub>4</sub> ·7H <sub>2</sub> O)	268.0	2160.0	8.059702

### Trypsin-EDTA

Trypsin-EDTA (0.05%), with phenol red

Supplier: Gibco®, Catalog number 25300-054

Components	M [g/mol]	c [mg/L]	mM
<i>Inorganic Salts</i>			
Potassium Chloride (KCl)	75.0	400.0	5.3333335
Potassium Phosphate monobasic (KH <sub>2</sub> PO <sub>4</sub> )	136.0	60.0	0.44117647
Sodium Bicarbonate (NaHCO <sub>3</sub> )	84.0	350.0	4.1666665
Sodium Chloride (NaCl)	58.0	8000.0	137.93103
Sodium Phosphate dibasic (Na <sub>2</sub> HPO <sub>4</sub> ·7H <sub>2</sub> O)	268.0	90.0	0.33582088
<i>Other Components</i>			
D-Glucose (Dextrose)	180.0	1000.0	5.5555553
EDTA 4Na 2H <sub>2</sub> O	416.2	200.0	0.4805382
Phenol Red	398.0	10.0	0.025125628
Trypsin	23800.0	500.0	0.021008404

**DMEM**

DMEM (Dulbecco's Modified Eagle Medium), high glucose (4.5 g), GlutaMAX™ Supplement

Supplier: Gibco®; Catalog number 61965-026

<b>Components</b>	<b>M [g/mol]</b>	<b>x [mg/L]</b>	<b>mM</b>
<i>Amino Acids</i>			
Glycine	75.0	30.0	0.4
L-Alanyl-Glutamine	217.0	862.0	3.9723501
L-Arginine hydrochloride	211.0	84.0	0.39810428
L-Cysteine	313.0	48.0	0.15335463
L-Histidine hydrochloride-H <sub>2</sub> O	210.0	42.0	0.2
L-Isoleucine	131.0	105.0	0.8015267
L-Leucine	131.0	105.0	0.8015267
L-Lysine hydrochloride	183.0	146.0	0.7978142
L-Methionine	149.0	30.0	0.20134228
L-Phenylalanine	165.0	66.0	0.4
L-Serine	105.0	42.0	0.4
L-Threonine	119.0	95.0	0.79831934
L-Tryptophan	204.0	16.0	0.078431375
L-Tyrosine disodium salt dihydrate	261.0	104.0	0.39846742
L-Valine	117.0	94.0	0.8034188
<i>Vitamins</i>			
Choline chloride	140.0	4.0	0.028571429
D-Calcium pantothenate	477.0	4.0	0.008385744
Folic Acid	441.0	4.0	0.009070295
Niacinamide	122.0	4.0	0.032786883
Pyridoxal hydrochloride	204.0	4.0	0.019607844
Riboflavin	376.0	0.4	0.0010638298
Thiamine hydrochloride	337.0	4.0	0.011869436
i-Inositol	180.0	7.2	0.04
<i>Inorganic Salts</i>			
Calcium Chloride (CaCl <sub>2</sub> ) (anhyd.)	111.0	200.0	1.8018018
Ferric Nitrate (Fe(NO <sub>3</sub> ) <sub>3</sub> ·9H <sub>2</sub> O)	404.0	0.1	2.4752476E-4
Magnesium Sulfate (MgSO <sub>4</sub> ) (anhyd.)	120.0	97.67	0.8139166
Potassium Chloride (KCl)	75.0	400.0	5.3333335
Sodium Bicarbonate (NaHCO <sub>3</sub> )	84.0	3700.0	44.04762
Sodium Chloride (NaCl)	58.0	6400.0	110.344826
Sodium Phosphate monobasic (NaH <sub>2</sub> PO <sub>4</sub> ·H <sub>2</sub> O)	138.0	125.0	0.9057971
<i>Other Components</i>			
D-Glucose (Dextrose)	180.0	4500.0	25.0
Phenol Red	376.4	15.0	0.039851222

## SUPPLEMENT F: ABBREVIATIONS

The following abbreviations were used in this monograph:

( <i>O,S</i> )	$\beta$ -hydroxo dithiocinnamic ester unit	COSY	Correlation Spectroscopy
$\tilde{\nu}$	wave number [ $\text{cm}^{-1}$ ] (in IR)	Cp	cyclopentadiene; cyclopentadienyl
$\mu\text{W}$	microwave	ctDNA	calf thymus desoxyribonucleic acid
9-mg	9-methyl guanine	CuAAC	copper-catalyzed 1,3-dipolar azide-alkyne cycloaddition
Å	Angström	cyt c	cytochrome c
aa	amino acid	d	doublet
AA	azidoacetic acid	DACH	diaminocyclohexane
abs.	absorbance [a.u.]	DAPI	4',6-diamidino-2-phenylindole
AIBN	azobisisobutylnitril	DCM	dichloromethane
Apaf	apoptotic protease activating factor	dd	doublet of a doublet (in NMR)
approx.	approximately	decomp.	decomposition
arom	aromatic	DEI	direct electron ionization (in MS)
ATR	attenuated total reflection	D'PEA	diisopropyl ethylamine
b	broad (in IR and NMR)	DMEM	Dulbecco's Modified Eagle's Medium
Bcl-2	B-cell lymphoma 2	DMF	dimethylformamide
bf	bright field	DMSO	dimethyl sulfoxide
bp	base pair	DNA	desoxyribonucleic acid
BSA	bovine serum albumin	DPBS	Dulbecco's Phosphate-Buffered Saline
Bu	butyl	dt	doublet of a triplet (in NMR)
calcd.	calculated	<i>e.g.</i>	<i>exempli gratia</i> (latin: for example)
CD	circular dichroism		
CDDP	<i>cis</i> -diammine dichlorido platinum(II)		
CID	collision-induced dissociation		

EA	ethyl acetate	HSQC	Heteronuclear Single Quantum Coherence Spectroscopy
EDTA	ethylenediamine tetraacetate	<i>i.e.</i>	<i>id est</i> (latin: that is)
EI MS	electron impact mass spectrometry	ICP-OES	inductively coupled plasma optical emission spectrometry
Enk	enkephalin	IP3	inositol trisphosphate
EPR	Enhanced Permeability and Retention	IR	infrared
eq.	equivalent	IRMPD	infrared-multiphoton dissociation
ER	endoplasmatic reticulum	<i>J</i>	coupling constant [Hz]
ESI	electrospray ionization	KO <sup>t</sup> Bu	potassium- <i>tert</i> -butoxylate
Et	ethyl	LC	liquid chromatography
Et <sub>2</sub> O	diethyl ether	LPPS	liquid phase peptide synthesis
FAB	fast atom bombardment (in MS)	m	medium (in IR) multiplet (in NMR)
FAB	fast atom bombardment	<i>m</i> -	<i>meta</i> - (stereodescriptor)
FCS	fetal calf serum	<i>m/z</i>	ratio of mass to charge
FGP	functional group pair	MALDI	matrix-assisted laser desorption ionization
Fmoc	Fluorenylmethoxycarbonyl	M <sub>av</sub>	molar mass - average mass
FTICR	fourier transform ion cyclotron resonance	Me	methyl
FTIR	fourier transformation infrared spectroscopy	MeOH	methanol
GP	general procedure	M <sub>mono</sub>	monoisotopic mass
GSH	glutathione (L-γ-glutamyl-L- cysteinyl-glycine)	mp.	melting point
h	hours	mQ	Millipore
HEWL	hen egg white lysozyme	MS	mass spectrometry
Hex	hexyl	MT	metallothionein
HMBC	Heteronuclear Multiple Bond Correlation Spectroscopy	MTT	3-(4,5-dimethylthiazol-2-yl)- 2,5-diphenyltetrazolium bromide
HMG	High Mobility Group	NaH	sodium hydride
HOBt	1-Hydroxybenzotriazol	NBS	N-bromo succinimide
HPLC	high pressure liquid chromatpgraphy	<sup>n</sup> Bu <sub>4</sub> NOH	tetrabutylammonium hydroxide
HSAB	hard and soft acids and bases	NCE	normalized collision energy
		NER	nucleotide excision repair



NH <sub>4</sub> OAc	ammonium acetate	SAR	structure-activity-relationships
NMR	nuclear magnetic resonance	SCLC	small cell lung cancer
NSCLC	non-small cell lung cancer	SD	standard deviation
N <sup>TA</sup>	nitrogen atom of triazol unit	SPPS	solid phase peptide synthesis
OAc	acetate	SRS	solvent residual signal (in NMR)
ODN	oligodesoxinucleotide	t	triplet (in NMR)
ODN	oligodeoxynucleotide	<i>T</i>	temperature [°C or K]
<i>p</i> -	<i>para</i> - (stereodescriptor)	TBAF	tetrabutyl ammonium fluoride
PA	pentinoic acid	TBDMS	<i>tert</i> -butyl dimethylsilyl
PB	Phosphate buffer	TBTU	<i>N,N,N',N'</i> -Tetramethyl- <i>O</i> - (benzotriazol-1-yl)uronium tetrafluoroborate
PBS	Phosphate-Buffered Saline	<sup>t</sup> Bu	<i>tert</i> -butyl
Ph	phenyl	TES	triethylsilane
PI	Propidium Iodide	TFA	trifluoro acetic acid
<i>P</i> <sub>o/w</sub>	octanol-water partition coefficient	THF	tetrahydrofuran
ppm	parts per million	TLC	thin layer chromatography
r.t.	room temperature	TMAA	tetramethyl ammonium acetate
resp.	respectively	UV	ultraviolet
R <sub>f</sub>	retention faktor	UV-vis	UV-visible
RNA	ribonucleic acid	vs	very strong (in IR)
RNase	Ribonuclease	w	weak (in IR)
<i>rp</i> -HPLC	reversed phase high pressure liquid chromatpgraphy	w/	with
rpm	rotations per minute	w/o	without
s	strong (in IR) singlet (in NMR)	δ	chemical shift [ppm]
		λ	wave length

Amino acids were abbreviated using either the three- or one-letter code; nucleobases were abbreviated using the one-letter code:

<b>amino acid</b>	<b>three-letter code</b>	<b>one-letter code</b>
<b>tyrosine</b>	Tyr	Y
<b>phenylalanine</b>	Phe	F
<b>methionine</b>	Met	M
<b>leucine</b>	Leu	L
<b>histidine</b>	His	H
<b>glycine</b>	Gly	G
<b>glutamic acid</b>	Glu	E
<b>cysteine</b>	Cys	C
<b>aspartic acid</b>	Asp	D

<b>nucleobase</b>	<b>one-letter code</b>
<b>adenine</b>	A
<b>cytosine</b>	C
<b>guanine</b>	G
<b>thymine</b>	T
<b>uracil</b>	U

## **SUPPLEMENT G: DIGITAL MEDIA**

On the provided CD, the following media are made available:

Crystallographic data of compounds 50, 72, 73, and 80 (res-files)

Manuscripts that have been prepared during the PhD project (PDF format)



---

# ACKNOWLEDGEMENT

I would like to express my deepest gratitude to all those who have supported me during my PhD work:

First, I wish to thank Professor Wolfgang Weigand for his supervision, for offering me the opportunity to carry on the work I started as a diploma student, and for making it possible for me to independently push forward all those different research subjects. Furthermore, I would like to thank him for introducing me into the COST D39, later CM1105, networks. It has given me some of the most valuable scientific and personal experiences to get into contact with so many different international researchers on such a high-level, yet friendly and open scientific platform. Also, I thank him for “letting me go” in many different ways: for letting me go to international meetings, for letting me go abroad for scientific missions, and in the end also for letting me go to follow my heart and finish my PhD work away from my home institution.

A significant part of my research has been carried out in laboratories other than the institute of inorganic and analytical chemistry at university of Jena. In this context, it is of special importance for me to thank Professor Luigi Messori at university of Florence for his hospitality during several research stays. His sharp mind and special way of putting together pieces of a scientific puzzle have taught me a lot about research and writing.

During my last year of PhD work, I was kindly hosted by Professor Nils Metzler-Nolte at the university of Bochum. A very special thanks to him, who made it not only possible for me to relocate to Bochum, but also opened up for me a completely new research field and provided me with the tools to perform biological work and synthesis at the same time. When I came, I truly never thought that it would become another year of intensive research before I finally finished up!

I furthermore feel very grateful for the fruitful collaborations with scientists I unfortunately haven't met in person until now: Professor Enrico Mini (Florence), Professor Daniela Montesachio (Naples), Dr. Antonello Merlino (Naples) and their co-workers that have shared my interest in this new compound class and offered to shed light on their mode of actions with each ones' special expertise. It has been a great experience for me and I learned a lot from these different approaches.

Not only the PI's of the research groups I worked in have contributed a lot to my research, also the colleagues always played an important part.

First, thanks is owed to my colleagues in Jena with whom I have spent many hours of discussions and conversations in scientific and less scientific contexts. Special thanks to the "hen coop", which wasn't all chicken in the end. Thanks is also owed to the research students and bachelor candidates that have worked with me during my time in Jena. Many of the research results they produced haven't made it into this thesis, but have laid a fundament to projects that wouldn't have been possible without their efforts and interest in what our group was doing: Stefanie Wolfram, Matthias Hartlieb, Theresia Palenta, Ruiqi Liu, Nora Nowak, Marcel Ritter, and especially Jana Hildebrandt, who taught me that it is not always wise to trust in the good and scientific integrity of all persons.

Also in Jena, a big "thank you" goes to Dr. Joachim Clement, Nadine Rüdiger and all colleagues at the IZKF. I was welcomed warmly and supported deeply when I took my first steps in cell culturing in their labs. Thank you for the great time and fruitful discussions.

In Florence, the co-workers of Professor Luigi Messori changed as I returned one more, one last, and one very last time to conduct my experiments, all always welcomed me sincerely and helped in so many ways. I have met great scientists there, and some have grown to be dear friends over time. Angela, Chiara, Federica, Lara, Tiziano: Thank you. One person deserves particular respect: Elena Michelucchi at CISM, who patiently recorded ESI mass spectra over and over again, always gave good advices and spent hours with me discussing, simulating, e-mailing back-and-forth ideas, doubts, questions. Without her help, most of the work presented here wouldn't exist.

In Bochum, again I was greeted warmly by the colleagues of the chair of inorganic chemistry I. "Hood hopping" was made possible, I always found someone to bother with practical and theoretical questions or to help me out when I had to run for daycare closing time. Special thanks is owed to Martin Strack and Jack Slootweg, who taught me a lot about peptide chemistry. Also, Annegret Knüfer and Sandra Bobersky shall feel thanked for their support in- and outside of the cell culture lab. All others whose name remains unmentioned should feel thanked as well: It has been a pleasure to work in this friendly and professional atmosphere.

Of course, no PhD project can be accomplished without money. I am grateful for the PhD scholarship I was granted by the Carl-Zeiss-Stiftung, which even made it possible for me to interrupt my work to have a proper maternity leave. I was very lucky to be granted a second PhD scholarship by Studienstiftung des deutschen Volkes, who initially accepted me for non-material benefits and even granted me financial support when funding by Carl-Zeiss-Stiftung ended.

However, there was a time when no foundation could support me, as I was forced to interrupt my PhD work due to pregnancy. If it hadn't been for Professor Matthias Westerhausen, I would have been left with nothing during that time. He offered me a position, knowing that I could never fulfill any scientific tasks in the lab for him. I am deeply grateful for this act of benevolence which made this time so much more bearable for me.

Travelling to Florence has been made possible by the DAAD, who funded a Vigoni project for exchange between the Weigand and Messori labs. Two other stays have been made possible by COST actions D39 and CM1105; Within both I was granted to execute a short term scientific mission (STSM) to Florence.

Furthermore, both COST actions funded several attendances to meetings and conferences, which truly enriched my scientific perspective. At this point, also members of the COST actions are gratefully acknowledged for the interesting meetings and for the always helpful and inspiring atmosphere. It felt like family.

Speaking of which: My family is owed an enormous hug and a thank you that cannot be described with words. I cannot imagine where I would stand today without the loving support of my parents, grandparents, sister and all other relatives that have helped me in so many different ways during the last years. It is a wonderful feeling to know you are there.

The last thank you is reserved for the two most important persons in my life, Greta and Ulf. You bring so much trouble – but a lot more joy to my life; I don't want to miss any minute. Thank you for loving me the way I am and bearing me during these very unpleasant last months of my PhD project.





---

# CURRICULUM VITAE

## Personal details

*Name* Carolin Mügge  
*Date/Place of birth* 10.12.1985 in Leipzig / Germany  
*Home Address* Semperstr. 87, 44801 Bochum / Germany  
*Home institutional Address* Institute of Inorganic and Analytical Chemistry – Friedrich-Schiller-University Jena,  
Humboldtstraße 8, 07743 Jena / Germany  
*Marital status* unmarried,  
1 daughter (born 2011)



## Academic track record

since July 2015 Ruhr-University Bochum,  
research fellow with Jun.-Prof. Dr. R. Kourist / Junior Research Group for  
Microbial Biotechnology

Oct. 2009 – June 2015 Friedrich-Schiller-University Jena, research for PhD project  
title of thesis “Metal Complexes with Sulfur Ligands as Cytotoxic Agents”  
(supervision: Prof. Dr. W. Weigand)

Sept. 2009 Friedrich-Schiller-University Jena, Diploma in chemistry  
title of thesis: Platinum(II) Complexes with Sulfur-containing Ligands as  
Possible Cytotoxic Substances (supervision: Prof. Dr. W. Weigand)

Oct. 2004 - Sept. 2009 Friedrich-Schiller-University Jena, student  
subject: chemistry-diploma

May 2004 Carl-Zeiss-Gymnasium Jena, Abitur

## External research experience during PhD work

Oct 2014	University of Florence, Group of Prof. Dr. L. Messori COST-based short term scientific mission (STSM) Grant No. COST-STSM-CM1105-131014-050336
May 2014 – June 2015	Ruhr-University Bochum, research associate with Prof. Dr. N. Metzler-Nolte
Jan 2014	University of Florence, Group of Prof. Dr. L. Messori DAAD-Vigoni-based collaboration project Project No. 54668125
Sept 2012	University of Florence, Group of Prof. Dr. L. Messori DAAD-Vigoni-based collaboration project Project No. 54668125
March – April 2010	University of Florence, Group of Prof. Dr. L. Messori COST-based short term scientific mission (STSM) Grant No. COST-STSM-ECOST-D39-250310-000000

## Awards, fellowships

<i>Fellowships</i>	Feb. 2007 – Sept. 2009	Studienstiftung des deutschen Volkes: fellowship
	June 2010 – July 2014	Carl-Zeiss-Stiftung: PhD fellowship
	July 2010 – May 2015	Studienstiftung des deutschen Volkes: PhD fellowship
<i>Awards</i>	June 2010	Selected for attendance of the 60 <sup>th</sup> Nobel Laureate Meeting
	Nov 2010	Scholarship of Einstein Foundation to attend the „Einstein Young Scholars Programme“ / 2 <sup>nd</sup> Falling Walls Conference in Berlin

## Conference attendances, further training

<i>Oral Presentation</i>	22.09.- 23.09.2009	COST Action D39 whole Meeting, Debrecen, HU
<i>Oral Presentation</i>	22.06.-26.06.2010	EUROBIC10, Thessaloniki, GR
<i>Attendance</i>	27.06.-02.08.2010	60 <sup>th</sup> Nobel Laureate Meeting (Interdisciplinary), Lindau, DE
<i>Attendance</i>	08.11.2010	2 <sup>nd</sup> Falling Walls Conference, Berlin; DE
<i>Oral Presentation</i>	30.04.2011	3 <sup>rd</sup> Postgraduate Symposium on Cancer Research, Dornburg / Jena, DE
<i>Oral Presentation</i>	24.-26. 02.2013	COST Action CM1105 WG 1+5 Joint Meeting, Gronigen, NL
<i>Poster</i>	27.04.2013	5 <sup>th</sup> Postgraduate Symposium on Cancer Research, Dornburg/Jena, DE
<i>Poster/ Participation</i>	12.-19.05.2013	2013 Chemistry of Metals in Biological Systems Summer School, Louvain-La-Neuve, BE
<i>Oral Presentation</i>	09.-10.09.2013	COST Action CM1105 Whole Action Meeting “1 <sup>st</sup> International Symposium on Functional Metal Complexes that Bind to Biomolecules”, Barcelona, ES
<i>Oral Presentation</i>	02.-04.03.2014	10. Koordinationschemie-Tagung, Kaiserslautern, DE
<i>Oral Presentation</i>	28.-29.04.2014	COST Action CM1105 WG5 Expert Meeting, Madrid, ES
<i>Oral Presentation</i>	22.-23.08.2014	COST Action CM1105 Whole Action Meeting “2 <sup>nd</sup> International Symposium on Functional Metal Complexes that Bind to Biomolecules”, Zurich, CH
<i>Attendance</i>	09.06.2015	ChromForum Bonn

Jena,

---

Carolin Mügge



---

# LIST OF CONFERENCE PRESENTATIONS

- C. Mügge**, C. Rothenburger, A. Beyer, C. Gabbiani, A. Casini, L. Messori, W. Weigand, *Sulfur-Containing Platinum(II) Complexes as Potentially Anticancer Active Substances*.  
COST Action D39 Meeting, 22.-23.09.2009.
- C. Mügge**, C. Gabbiani, H. Görls, E. Michelucci, I. Landini, S. Nobili, E. Mini, L. Messori, W. Weigand, *Platinum(II) Complexes with Sulfur Donors for Anticancer Therapy: Biologic Activity and Protein Binding*.  
EUROBIC10, 22.-26.06.2010.
- C. Mügge**, R. Liu, N. Rüdiger, E. Michelucci, J. H. Clement, W. Weigand, *Remarkable Activity of Platinum Complexes with Sulfur containing Ligands*. 3<sup>rd</sup> Postgraduate Symposium on Cancer Research, 30.04.2011.
- C. Mügge**, L. Messori, W. Weigand, *Antiproliferative Properties and Biomolecular Interactions of Platinum(II) Complexes with O,S Bidentate Ligands*.  
COST Action CM1105 WG 1+5 Joint Meeting, 24.-26. 02.2013.
- C. Mügge**, E. Michelucci, F. Boscaro, C. Gabbiani, L. Messori, W. Weigand, *Selective Binding of Diphosphane Platinum(II) Dichlorides to Cytochrome c – Insights Into Reactions of Metallodrugs with Proteins*.  
5<sup>th</sup> Postgraduate Symposium on Cancer Research, 27.04.2013.
- C. Mügge**, R. Liu, H. Görls, C. Gabbiani, E. Michelucci, N. Rüdiger, J. H. Clement, L. Messori, W. Weigand, *Platinum(II) Compounds with O,S Bidentate Ligands – Antiproliferative Activity and Biomolecular Interactions of New Drug Candidates*.  
2013 Chemistry of Metals in Biological Systems Summer School, 12.-19.05.2013.
- C. Mügge**, N. Nowak, M. Ritter, H. Weiss, W. Weigand, *O,S-Chelate Platinum Complexes: Novel Derivatives for the Functionalization of Potent Antiproliferative Compounds*.  
1<sup>st</sup> International Symposium on Functional Metal Complexes that Bind to Biomolecules, 09.-10.09.2013.

- C. Mügge**, H. Görls, E. Michelucci, J. H. Clement, L. Messori, W. Weigand *Platinum(II) Complexes with Ligands Based on a O,S-Chelating Moiety for the Development of Anticancer-Active Compounds.*  
10. Koordinationschemie-Tagung, 02.-04.03.2014.
- C. Mügge**, N. Nowak, H. Weiss, W. Weigand, *Metal Complexes of O,O and O,S- Chelating Ligands – Functionalization for Better Drug Targeting.*  
COST Action CM1105 WG5 Expert Meeting, 28.-29.04.2014.
- C. Mügge**, W. Weigand, *Recent Results on Biological Active Platinum Complexes from Jena Lab.*  
2<sup>nd</sup> International Symposium on Functional Metal Complexes that Bind to Biomolecules, 22.-  
23.08.2014

---

## LIST OF PUBLICATIONS

- C. Mügge, C. Rothenburger, A. Beyer, H. Görls, C. Gabbiani, A. Casini, E. Michelucci, I. Landini, S. Nobili, E. Mini, L. Messori, W. Weigand, *Structure, Solution Chemistry, Antiproliferative Actions and Protein Binding Properties of Non-Conventional Platinum(II) Compounds with Sulfur and Phosphorus donors*. *Dalton Trans.* **2011**, 40, 2006-2016.
- C. Mügge, E. Micheucci, F. Boscaro, C. Gabbiani, L. Messori, W. Weigand, *Reactions of Metallodrugs with Proteins: Selective Binding of Phosphane-Based Platinum(II) Dichlorides to Horse Heart Cytochrome c Probed by ESI MS coupled to Enzymatic Cleavage*. *Metallomics* **2011**, 3, 987-990.
- C. Mügge, R. Liu, H. Görls, C. Gabbiani, E. Michelucci, N. Rüdiger, J. H. Clement, L. Messori, W. Weigand, *Novel Platinum(II) Compounds with O,S Bidentate Ligands: Synthesis, Characterisation, Antiproliferative Properties and Biomolecular Interactions*. *Dalton Trans.* **2014**, 43, 3072–3086.
- A. Martin, C. Mügge, D. L. Gin, B. Donnio, W. Weigand, *Stabilizing Effects of Combined Trifluoromethyl Groups and Semifluorinated Side Chains on the Thermotropic Liquid Crystal Behavior of  $\beta$ -Enaminoketone Ligands and their Bischelate Pd<sup>II</sup>Complexes*. *Eur. J. Inorg. Chem.* **2014**, 32, 5609-5617.
- C. Mügge, T. Marzo, L. Massai, J. Hildebrandt, N. Metzler-Nolte, L. Messori, W. Weigand, *Platinum(II) Complexes with O,S Bidentate Ligands: Biophysical Characterization, Antiproliferative Activity and Crystallographic Evidence of Protein Binding*. *Inorg. Chem.* **2015**, accepted
- C. Mügge, D. Musumeci, E. Michelucci, F. Porru, T. Marzo, L. Massai, L. Messori, W. Weigand, D. Montesarchio, *Elucidating the Reactivity of Pt(II) Complexes with (O,S) Bidentate Ligands Towards DNA Using Various Model Systems and Analytical Techniques*. Manuscript in preparation.





---

# DECLARATION OF AUTHORSHIP

I, Carolin Mügge, herewith declare that this thesis and the work presented herein is my own and has been generated by me as a result of my own original research.

I confirm that:

1. This work was done mainly while in candidature for a research degree at Friedrich-Schiller University Jena.
2. Where I have consulted the published work of others, this is always clearly attributed.
3. Where I have quoted from the work of others, the source is always given.
4. I have acknowledged all main sources of help
5. Where the thesis is based on work done by myself jointly with others, I have made clear exactly what was done by others and what I have contributed myself.
6. Parts of this work have been published in peer-reviewed journals as specified in Pg. 325.

Ich erkläre, dass ich die vorliegende Arbeit selbständig und unter Verwendung der angegebenen Hilfsmittel, persönlichen Mitteilungen und Quellen angefertigt habe.

Jena,

---

Carolin Mügge